Cranfield
UNIVERSITY

School of Engineering

PhD Thesis

Maria Luisa Parra Saldivar

HEAT AND MASS TRANSFER BEHAVIOURS OF BUILDING MATERIALS AND STRUCTURES

Supervisors: Prof. W.Batty and Prof. D.Greenhalgh

March 2005

This thesis is submitted in partial fulfilment for the degree of
Doctor of Philosophy

Abstract

Heat storage as a means to respond to the requirements for improved energy efficiency motivated this study. The objective was to evaluate the impact of thermal energy storage systems in dwellings under Mexican climatic conditions. In the first part of this work thermal behaviors of adobe traditional architecture is discussed; in the second part a latent heat storage system using phase change materials (PCMs) is proposed and assessed.

The high thermal mass structural elements of adobe traditional architecture have been characterized as heat wave modulators. Nevertheless, the moisture content in these structures also plays a significant role as a means for heat storage and potentially enhancing thermal lag. The objective of this part of the study was to assess the scope of existing coupled heat and mass transport models regarding water contained latent heat storage on porous structures.

The significant contribution of latent heat storage recognized in adobe structures, led to the study of a solar-thermal storage system using (PCMs).

The objective of this part of the study was twofold: 1) Enhance the existing computational models on the Stephan problem by considering the effect of regional variations (weather conditions imposed) on the boundary conditions. 2) Evaluate the impact of the solar-thermal system proposed when applied in dwellings in view of regional variations under Mexican weather conditions.

Solar-thermal storage systems independent of the structure offer the possibility to be applied to existing buildings as well as new constructions. The proposal is a storage element that constitutes internal blinds in windows. The computational model of the Stephan problem was solved with the enthalpy method. Simulations were run under different sets of climatic conditions. For the first time the main factors for promoting system's optimisation, when gathered in a single comparison study, provided a more general insight on system's performance. Experimental work was also carried out regarding the charging of the heat storage unit by heat gains other than direct radiation, and the storage unit's performance as insulator. A large-scale solar simulator was constructed.

Statistical analysis of experimental results showed interesting findings including: The important role that internal heat gains play on the charging of the latent heat storage unit proposed. A larger effect on the discharging ratio was found with lower air temperatures than with faster air flow rates. The faster discharging rate tests also released slightly more energy. PCM volume was found to be the most critical factor on system performance. The importance of providing the means to discharge the total quantity of heat stored was pointed out. For the cooling mode, elements to enhance discharging might be required. For system control, thermal insulation was found to be an effective measure when the discharging is required to occur over a longer period. The multiple PCM unit was found to be more efficient during the charging process (storing more energy) than units containing a single PCM. Nevertheless the single PCM unit performed better for cooling than the multiple PCM unit. The question was raised as to what extent PCM thermal conductivity actually influences system's performance.

The thermal storage system proposed in this study reduced the heating system energy consumption requirements for an experimental room by 28.6%.

CHAPTER 1

INTRODUCTION

"Nothing is rich but the inexhaustible wealth of nature". Ralph Waldo Emerson

Mexico towards sustainable development

Despite the fact that Latin America's regions own relatively abundant natural resources their profligate use is causing environmental deterioration and their scarcity. The efficiency in handling the environment in developing countries depends on their cultural adjustment to the economic development [1.1] process. Latin American nations have often distanced themselves from sustainable [1.2] alternatives, because the immediate principal goal of development policy is not subsistence (life preservation), but economic growth, where the exploitation of natural resources has had an important role.

Mexico is attempting to support domestic industrialisation to encourage greater economic autonomy, so that in the long term it may become self-sufficient. Additional costs to promote system's efficiency are considered to be too high, and the long pay off time of such investments makes them even more expensive. Consequently, such investments rarely occur. Environmental protection in Mexico, since the 1970's has mainly been reduced to two concerns: pollution and public health. Regarding energy conservation, the country's main preoccupation is the future of the petroleum reserves.

Conventional economic development is more interested in the processes involved in the short term exploitation of resources rather than in the examination of the long term potential of natural resources when applied to

---

1.1 *"Development is any and all kinds of activities or processes that increase the capacity of people or the environment to meet human needs or improve the quality of human life" Trzyna, T. C. (1995). A sustainable world : defining and measuring sustainable development.*

1.2 *"Sustainable development goal is to improve and maintain the well-being of people (meeting their needs having a large range of choices and opportunities to fulfil their potential) and ecosystems (maintaining their quality and diversity and thus their potential to adapt to change and provide a wide range of choices and opportunities to the future)" Ibid.*

development. The substitution of oil for other fuels (natural gas, coal, nuclear, and renewable sources) is subject to technical, socio-economic and environmental constraints. This excessive exploitation of fossil fuels is also observed in the rest of the world. Petroleum and gas started to be used a few years before the Second World War, nowadays, oil provides more than half of the world's energy.

In Mexico an environmental movement of social origin has been attempting to integrate two perspectives. First, an awareness of the struggle of the poor to secure the necessities of life and second, a greater environmental consciousness among a small fraction of the more privileged and educated people (Redclift 1987).

Appraisal of energy resources and energy utilization in Mexico

The first law of thermodynamics presents the foundation for all quantitative accounts of energy[1.3]. From the energy generation from fuels to the eventual energy discharge into the environment, energy conversion has an important role. Energy is fundamental to the current perceptions of human quality of life. Along the energy processing path, all possible means to use the energy throughout the cycle should be deployed.

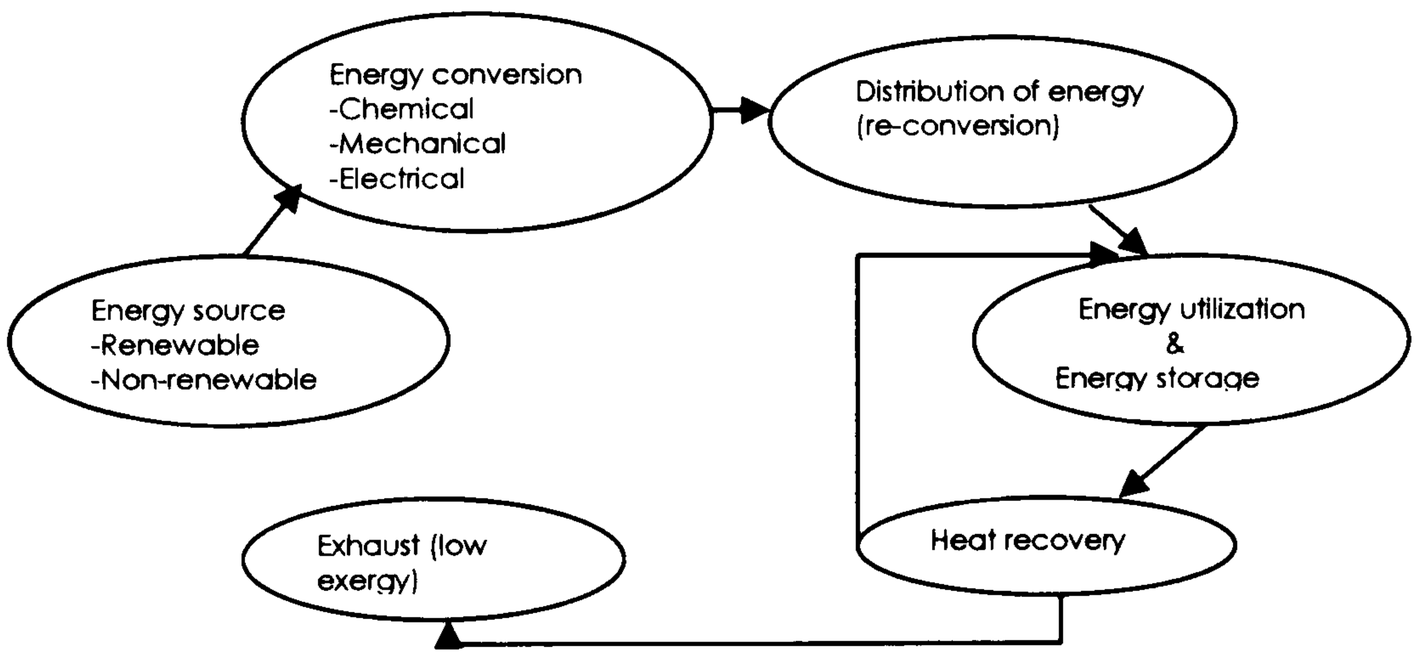

Figure 1.1 The energy process diagram

The efficiencies of each energy source, their distribution and their conversion steps have to be estimated to establish means to attain equilibrium between the primary fuel consumption and the useful exergy[1.4] obtained.

Structure of energy sources

[1.3] "The difference of energy between any two states is to be found from the sum of the heat and the work required bringing a system by any convenient process from the one state to the other" Bridgman, P. W. (1943). The nature of thermodynamics, Cambridge, Mass : Harvard university press.

[1.4] Exergy is the available extractable energy

Mexico has a surface area of 1.958.201 km^2, and a population of 96.807.451 (1997 census); 76% of which is urban population, and the remaining 24% is rural population (1997 census) (Instituto Nacional de Estadistica)

Mexican proven petroleum reserves are estimated to be about 58 000 millions of barrels, while natural gas reserves reach 852 000 millions of cubic meters. Mexico has the 9th largest petroleum reserves in the world, and the fourth largest natural gas reserves in the American continent.

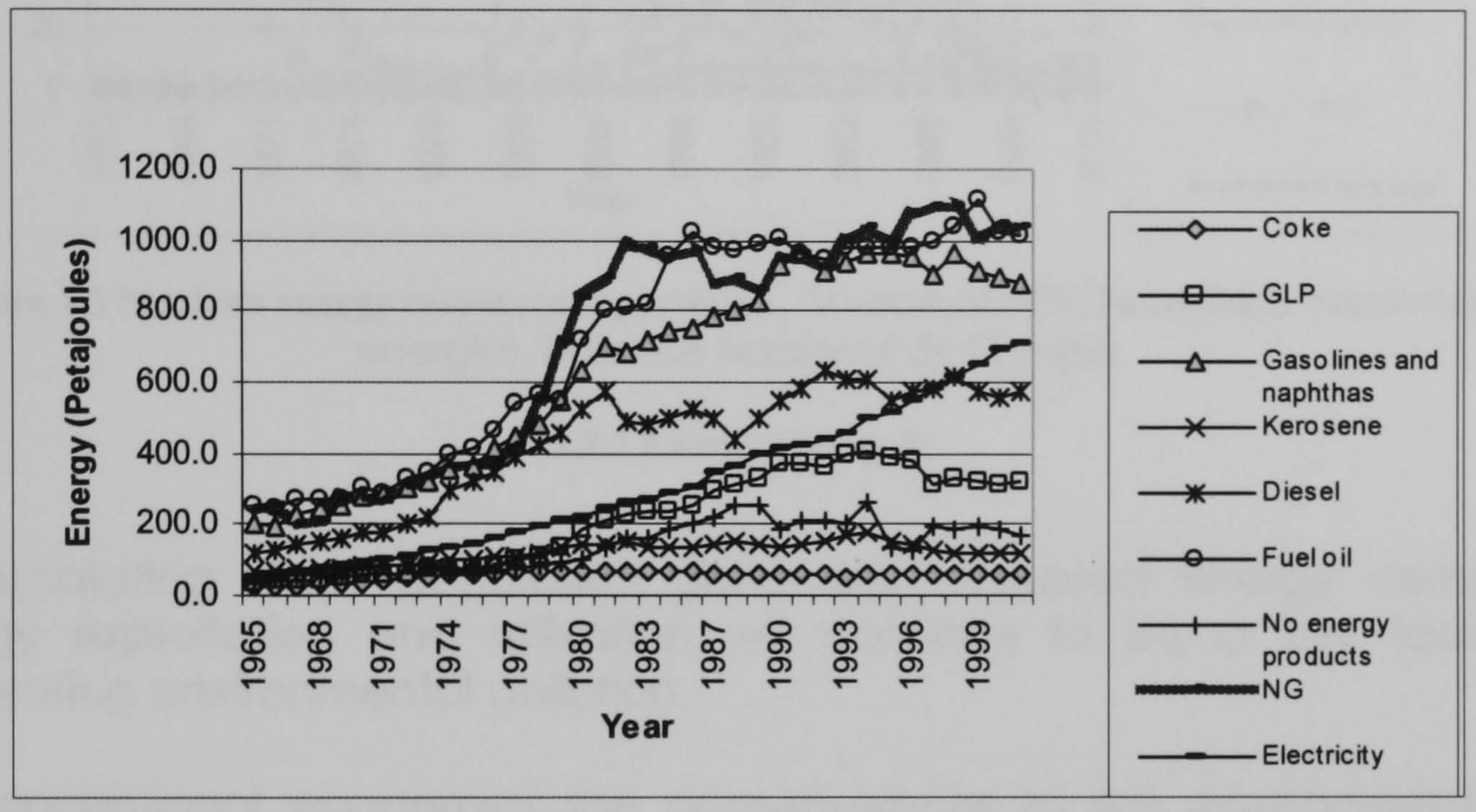

Figure 1.2: Mexican Energy production, excluding renewable energy. Information . Source: SENER(Secretaria Nacional de energia), Balance Nacional de Energía. (1 Petajoule is the same as one million gigajoules)

Fossil fuels are the principal source of energy in Mexico due to their low cost. Mexico occupies the 21st. position in fossil fuel reserves in the world. The zenith of Mexican oil production[1.5] was reached in 2002 (Paez 2004). If consumption continues at the present rate, Mexico will deplate its petrol reserves by the second half of the 21st century. (Redclift 1987)
Consequently, Mexican society must be prepared for a post-petroleum era, proceeded by a vital adaptation period. During this period the last petrol reserves might be vital. That is, at that stage, exporting more than half of the national oil and gas production might be inappropriate, e.g. compare figures 1.2 and 1.3.

[1.5] a Gaussian shaped curve, called Hubert curve

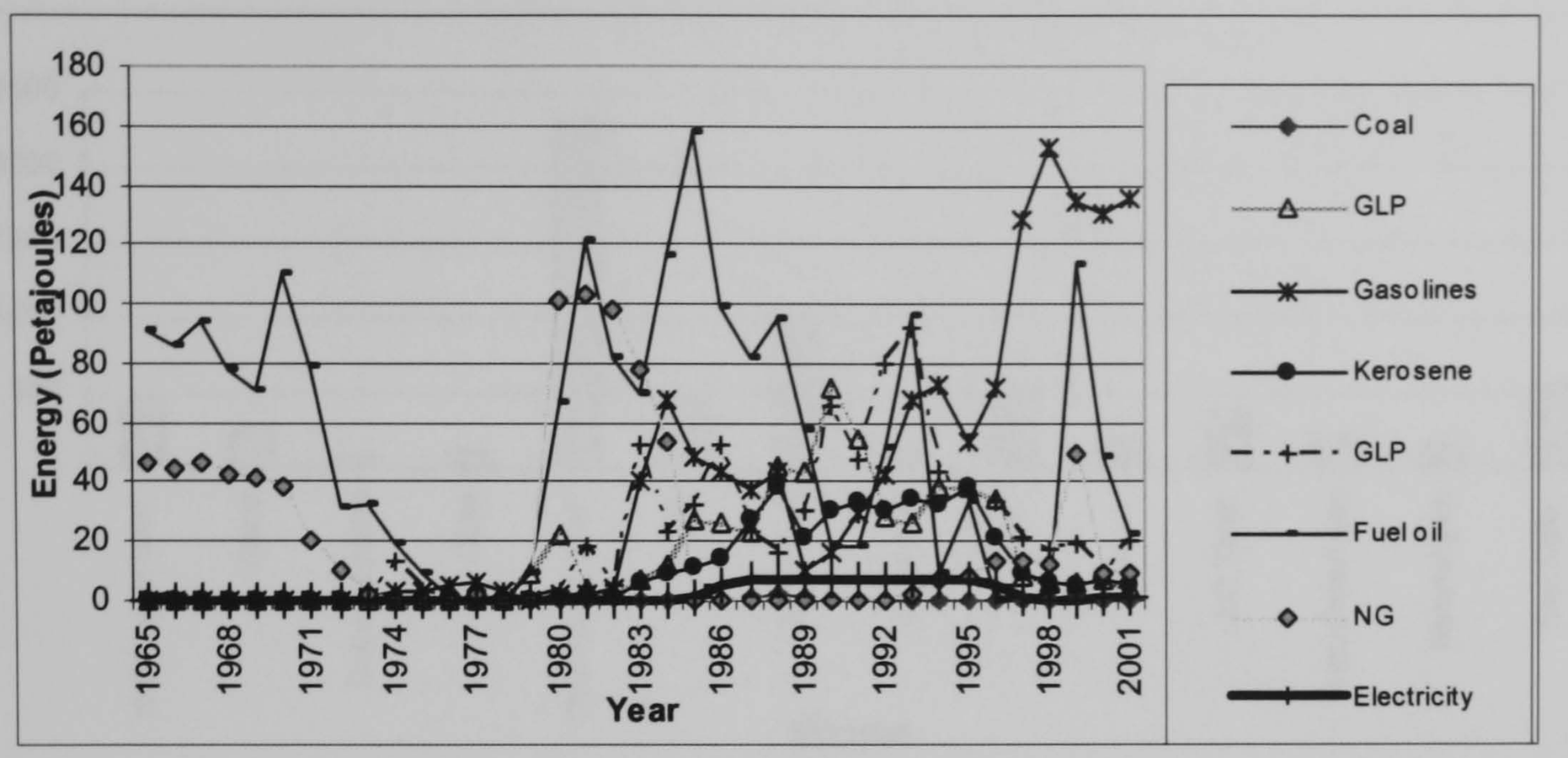

Figure 1.3 Mexican energy resources exportation. Source: SENER(Secretaria Nacional de energia), Balance Nacional de Energía.

1.2.2 Energy Demand:

An escalating world population generates increased energy demands. Energy exploitation and utilisation will continue to be a key factor in generating environmental pollution.

In conventional economics the consequences to the environment and ecosystems of fossil fuel exploitation continue to be misunderstood because their costs and the cost of their impacts are incorporated as part of the pricing structure and so remain hidden (B.E.S.T 2003). This encourages extreme energy utilization, over-exploitation of natural resources, and damage to biodiversity.

In the next 10 years, the energy source that will have the most significant use in Mexico is natural gas[1.6]. The national demand will provoke a deficit of this fuel source that will need to be covered by imports, which will represent 23.7% of the total demand (Gutierrez 2001).

[1.6] Now a days, there is a World wide tendency to utilize natural gas as the primary energy source. One factor that has impelled this tendency is the development of gas turbines to generate electrical energy. Another important factor is their thermal efficiency and low environmental impact.

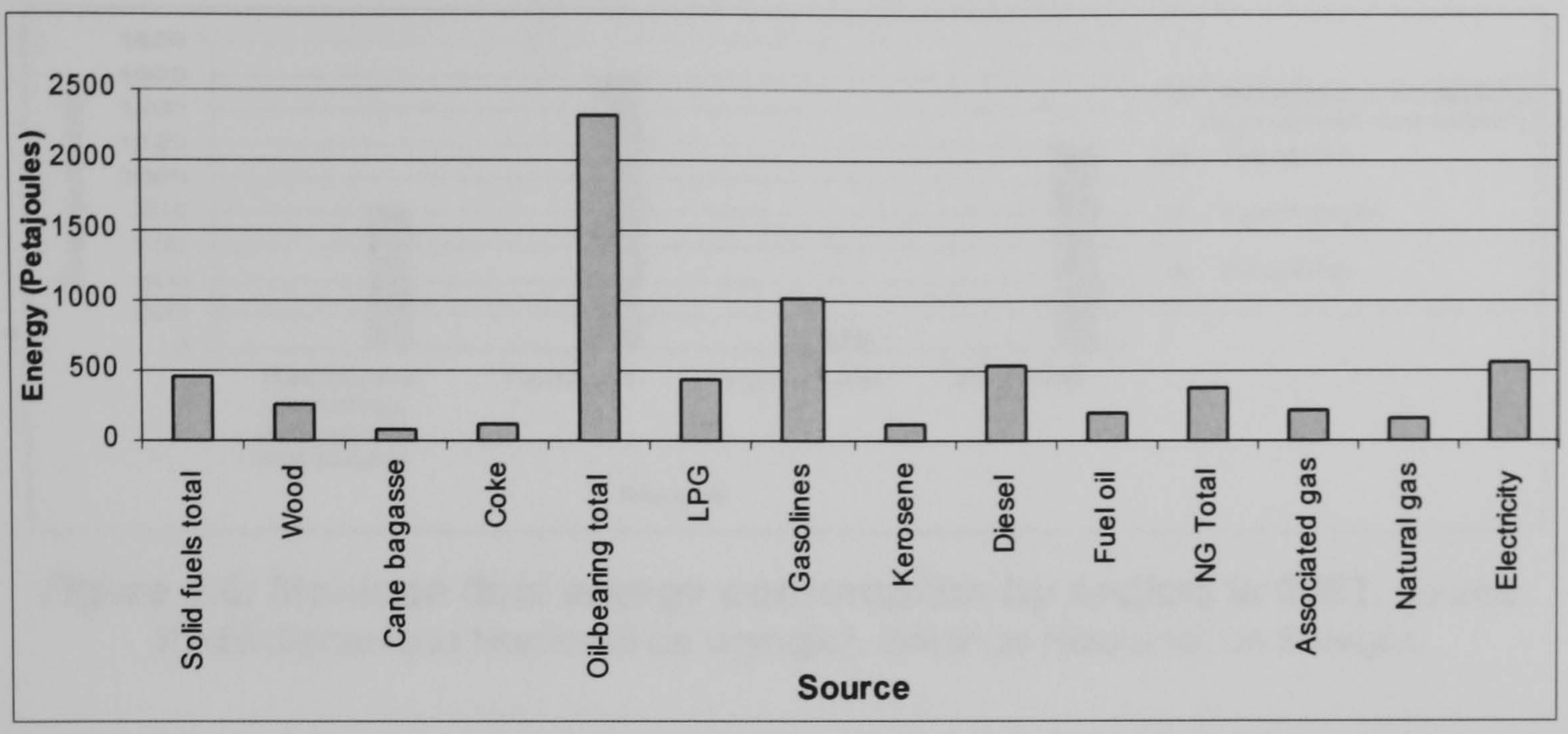

Figure1.4: Mexican total energy consumption 2001. Source: SENER(Secretaria Nacional de energia), Balance Nacional de Energía.

The structure of national consumption of energy distinguishes 2 parts: the energy production sector and the final consumer sector.

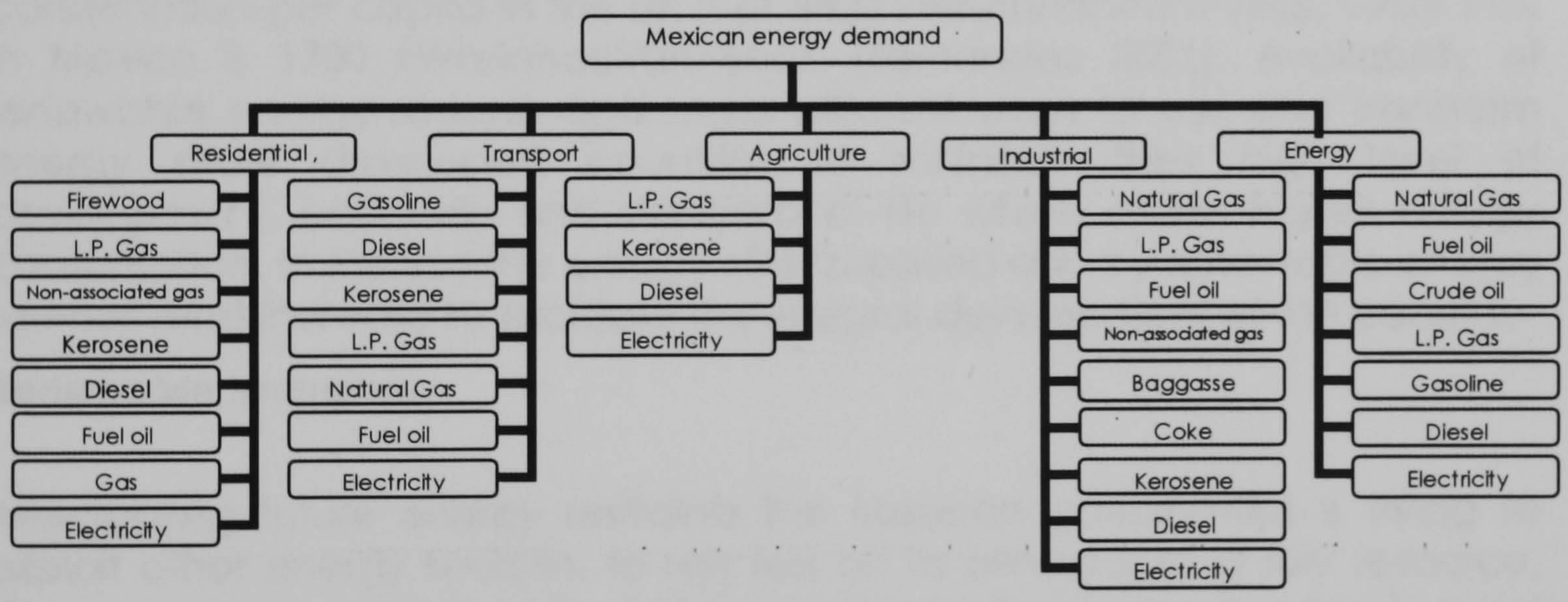

Figure 1.5: Mexican energy demand, final consumer sectors

(Garibaldi 2002)

The final consumer category is divided into 4 sectors. The main consumer sector of energy consumption is the transport sector, followed by the industrial sector, then the residential, commercial and public sector and finally the agricultural sector. This tendency will be maintained depending on the type of technology each sector uses.

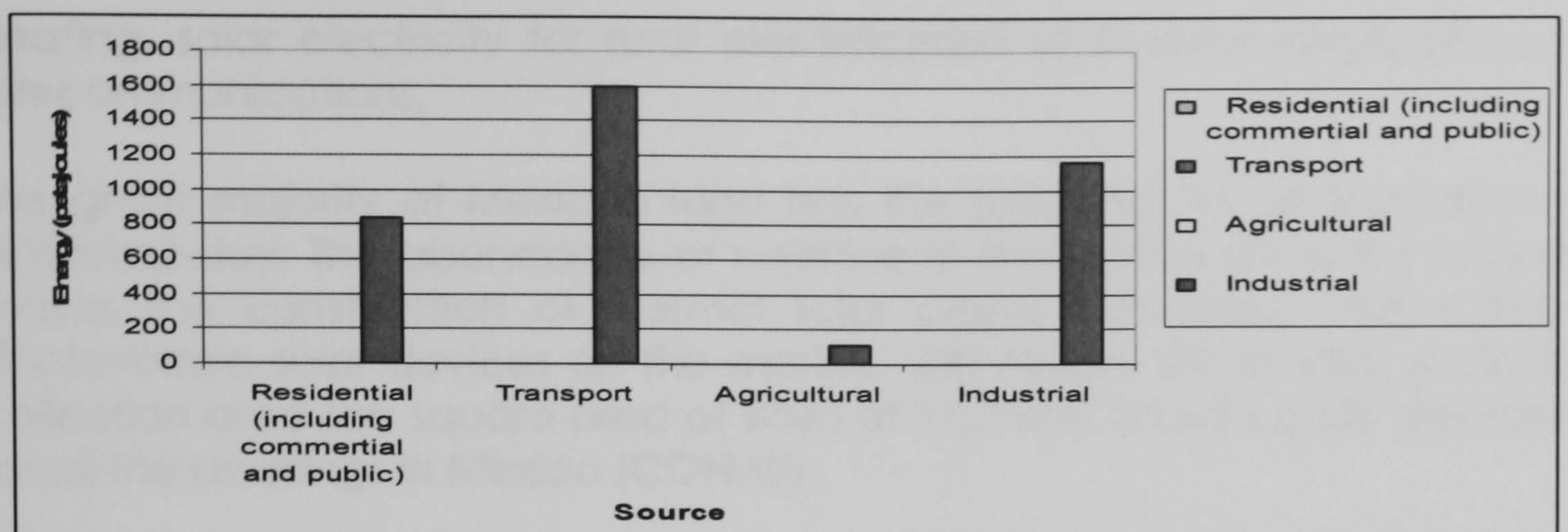

Figure 1.6: Mexican final energy consumption by sectors in 2001. Source: SENER(Secretaria Nacional de energia), Balance Nacional de Energía.

In Mexico the electrical consumption is low and the electrical power distribution infrastructure is weak, the latter reflects a setback dating from the petroleum expansion era.

The developed nations consume energy at a rate that is one or two orders of magnitude greater than that of the developing countries. Electrical consumption per capita in the UK is of 5800 kWh/inhabitant-year; while that in Mexico is 1700 kWh/inhabitant-year. (Fernandez 2001). Availability of renewable energy sources and more efficient ways to use and transform energy allow developed countries to maintain their high level of development, economy and standard of life which allows higher energy consumption. In Mexico the energy offer supplied also by renewable energy sources must increase to facilitate the integral development of the country.

Renewable energies:

Anticipating future energy restraints the Mexican government is trying to exploit other energy sources, to rely less on its principal fossil fuel resource. However, the mechanisms to enrich modern technologies bearing in mind sustainability remain largely unexplored.

There is no question regarding the necessity for economic growth, the real issue is to know how to grow sustainably. Renewable energy emerges as a promising answer to solve the conflict between economic growth and the conservation of resources. Mexico has a high potential in renewable energies. At present, Mexico has access to nearly 10,500 MWs of renewable energy . Hydraulic and thermal energy renewable resources are the more developed with 9,679 and 837 MWs of generation respectively. Little progress has been achieved regarding wind and photovoltaic based solar energy based electricity generation (CONAE).

Around 12 MW of solar energy and 5,7 MWs of wind energy are installed. Solar energy has been applied mainly on solar-thermal installations for water

heating, solar electricity for rural electrification and some applications in telecommunications.

The great majority of Mexican land has the potential for an insolation of 5kWh/m2-day. The abundance of sunshine in the northwest of the country makes the construction of thermal solar plants appealing. With current photovoltaic solar devices on the market, 200 millions m^2 of solar radiation collection area (an square area of sides of 14.2 km) could supply electricity for all the dwellings in Mexico (CONAE) .

Regarding biomass, waste disposal is a major problem. The metropolitan areas generates 800 tons of solid waste each day, of which only 75% is collected (Redclift 1987). The estimated generation of solid waste in Mexico is about 90 thousand tons per day. This could generate around 150 MW of electricity.

Waste from the forest, agriculture, wood industry, food industry, sugar cane bagasse(waste pulp), livestock dung, could be important energy sources. The potential generation of electricity (through cogeneration plants) from these energy sources is greater than 4 thousand gigawatt-hours per year.

Regarding geothermal energy Mexico occupies the third place in the world in electrical generation, with an installed capacity of 855 megawatts (CONAE)

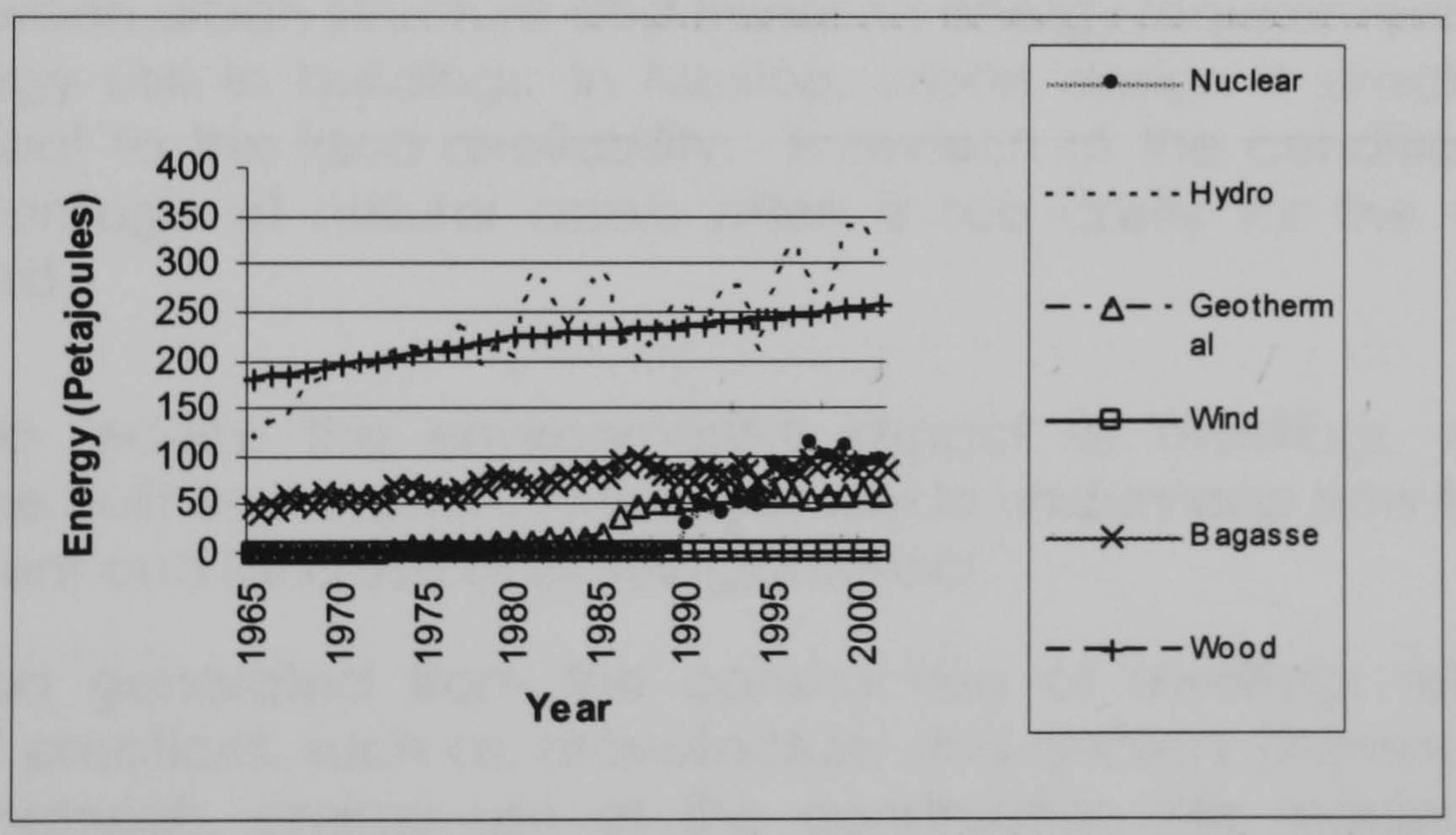

Figure 1.7: Mexican primary energy production, renewable energy sources.

Source: SENER(Secretaria Nacional de energia), Balance Nacional de Energía.

It has been estimated that there is a potential for additional 17,000 MWs of energy produced from other renewable sources such as hydraulic, mini-hydraulic, wind and solar energy (Secretaria de Energia).

Stronger encouragement of renewable energy production would allow the electrical generation on a massive scale via distributed energy generation

delivered by a national grid. This would also reduce the atmospheric emissions and environmental impact.

It is desirable to increase the installed capacity for energy production to consumption per capita up to 4000 kWh/habitant-year in 2030. Because of the Mexican geographic situation, weather conditions, and ecosystems, about 88% of this could come from renewable sources: 16% could be provided by geothermal and hydrothermal systems, 20.8% by wind , 22.4% by solar and 28.8% by biomass(Fernandez 2001).

The use of alternative energy sources pays for employment not fuels, promotes appropriate technology and industry, encourages the economic, social and regional development, protects the ecology and allow for sustainable development.

Energy efficiency in dwellings

The use of solar energy in dwellings has great potential for reducing energy consumption and CO_2 emissions. The main systems involved in the urbanisation process are:

a) Travel and transport: Physical segregation of activities, established in part by the density and in part by the distribution of different land uses, seems to be the most important aspect in the relationship between urban structure and transport energy requirements.
b) Energy use in buildings: In Mexico, urban design is practically only subject to the land availability. A revision of the conditions to take advantage of natural assets often is too costly for the country to afford.

In order to reduce the environmental impact of dwellings, as well as improve the built environment, it is necessary to understand how the design, refurbishment and land use of buildings interact.

Air pollution generated from the construction of dwellings relates to a number of practices, such as: manufacture and delivery (transportation) of building materials, energy use at the construction site (equipment), the generation and removal of damaged materials, and the profligate use of energy during the building's operation. In order to reduce the environmental impact of buildings it is necessary to optimize the use of renewable and non-renewable resources by recycling, reusing, and by reducing conventional energy use.

The secretary of the environment and natural resources (SEMARNAT) in Mexico has expressed his concern for the high consumption of energy that heating and air conditioning systems represent in the states of the north of the country. Insulation of walls and windows and any means to reduce

consumption are recommended. A variation of one degree Celsius in the set point temperatures in buildings can imply a consumption reduction of 6%.

Renewable energy technologies emerge as a promising answer to solve the conflict between economic growth and the conservation of resources. Solar energy is a suitable renewable energy technology to be applied in Mexico. Solar energy in Mexico has been applied mainly to solar-thermal installations for water heating and solar electricity.

One of the major drawbacks on the utilization of solar energy is the discontinuous and unmatched availability of solar energy with the immediate demand. A possible solution to this is solar energy storage. Technology on heat storage needs to move forward to offer less expensive and less complex systems.

Heat Storage

When fuels are transformed to generate energy, the first form of energy occurring as a result of that transformation is heat energy and it is also the final form of energy that is disposed at the end of the energy cycle, including all the energy conversion processes. Low temperature thermal energy is a low quality energy form. Its conversion into higher quality energy is limited by the Carnot efficiency[1.7]. A more comprehensive energy processing strategy could be achieved through conversion methods that are able to make use of heat energy from sources that have only low exergy, generally achieved through energy cascading.

Besides the use of the simultaneous thermal energy production and utilisation during energy conversion processes, the use of solar radiation as an energy source has gained much attention. Solar energy can be used to provide hot water, to produce electricity, and to heat, cool, and illuminate buildings. The interest in this energy source has allowed the development of a range of renewable energy technologies. Hydraulic energy, energy from crude oil, biomass and the wind all have a common origin: Solar energy. However, this solar energy has generally been stored for periods ranging from a few weeks or months to millions of years.

The problem with the availability of instantaneous solar energy is that it is discontinuous and often out of phase with the immediate demand for energy. Storage systems are involved in the energy processing cycles when energy demand and supply are not balanced. Energy storage[1.8] also has an essential role in energy preservation.

[1.7] The maximum amount of work available in a thermodynamic operation is generally governed by the Carnot efficiency

[1.8] Energy may be stored as mechanical energy, kinetic energy, chemical energy and thermal energy.

Thermal energy can be stored in three ways:

1) Sensible heat: by causing the temperature of a material to increase or decrease by virtue of the heat capacity and density (if volume is important) of the storage medium.

2) Latent heat: by virtue of the latent heat of the change of phase[1.9] of the medium, the temperature of the medium remains more or less constant (Garg et al. 1985)

3) Heat of reversible thermo-chemical reaction: The energy supplied by solar heating on a reservoir starts a chemical reaction. The physical separation of the chemical components (caused by the reaction) prevents the usual reverse reaction during cooling: the stored energy can be released at any chosen time. (Brousseau and Lacroix 1996)

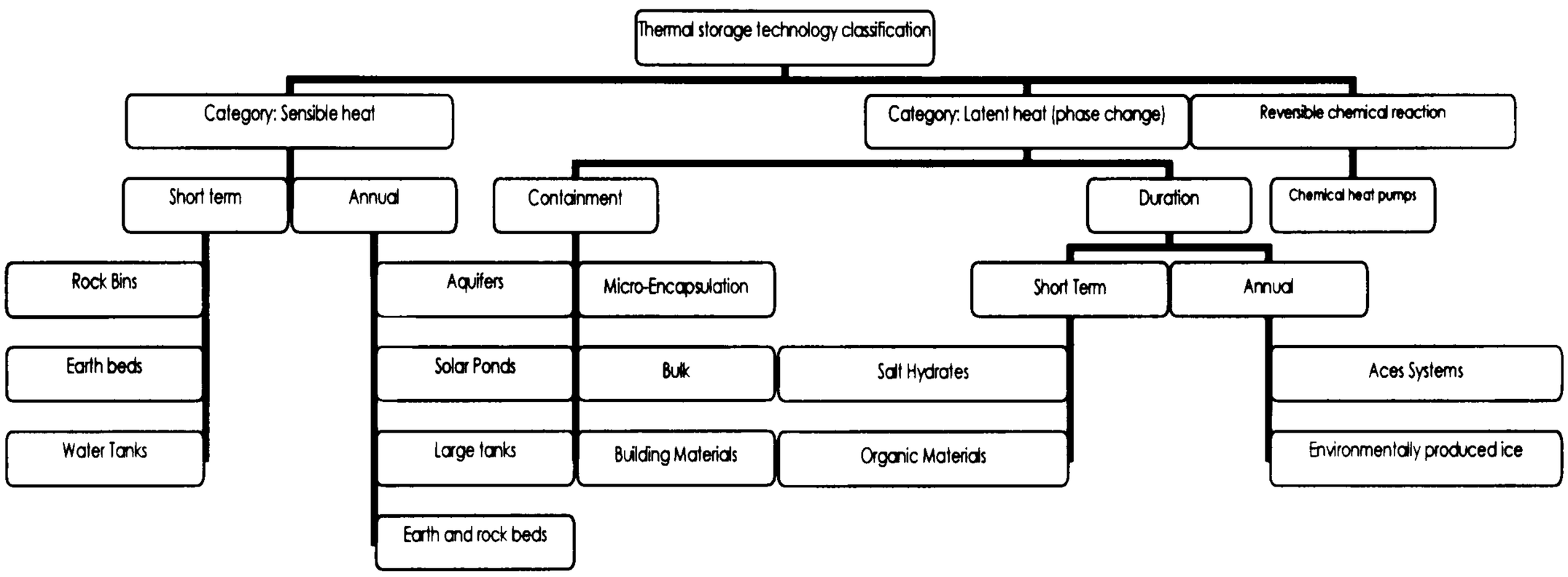

Figure 1.8 Thermal storage technology classification *(Garg et.al. 1985)*

Solar energy has great potential as an alternative source of energy in Mexico. Some regions in Mexico have the world's highest average annual insolation. So far, in Mexico solar energy already satisfies the requirements in some dwellings, mainly in rural communities, that lack mains distributed electricity. A house can be self-sufficient, regarding the external supply of energy from utility companies, by using solar energy collection systems and designing dwelling architecture for passive heating and cooling. This contributes to reduce dependency on fossil fuel based energy sources.

Solar energy is not a universal solution by which all energy necessities can be satisfied. Solar energy contributes modestly as another energetic possibility. However, a realistic strategy would be to consider it as a serious option while taking account of its technological deficiencies, actual economical disadvantages and the longer-term advantages. The two main disadvantages in the utilization of solar energy are: 1) High cost of solar

---

1.9 The latent heat of transformation and the temperature at which the phase change occurs are important for system control.

systems compared with conventional systems and 2) Its maintenance implications (Tonda 1993) However, the high capital costs of such systems generally reduce with time as they come to be manufactured in greater quantities. Additionally, in rural regions the costs of connection to electricity and gas supply grids are costly and often hidden or ignored when economic comparisons are made.

The effective application of solar energy often depends on the interest given to its technological development by government agencies. Mexican solar investigation includes principally the study of plane solar panels, solar ponds and solar photovoltaic cells. Thus, so far direct solar radiation has been converted mainly into heat (photothermal conversion) and to electricity (photovoltaic conversion).

However, the building infrastructure of cities and urban areas act as unintentional solar energy collectors. A study for the heat storage flux density in buildings in Mexico City was undertaken by Oke. The peak storage flux conducted into the buildings and ground of urban areas was studied in relation to the net solar radiation. The convective flux to the air from the building surfaces almost always reaches its maximum in the afternoon. Nevertheless, fully 58% of the total daytime net radiation is stored in the urban fabric, compared to 38% convected to the lower atmosphere. At night the hourly heat release from this solar energy storage is large: ensemble hourly average values range from about -120W/ m^2 just after sunset to about -90W/m^2 near sunrise. Individual hourly values can be in excess of -130W/m^2 as stated by Oke. The relative convective sensible heat/ net radiation is likely to increase with the fraction of the surface covered by built impervious surfaces. Energy balance measurements near the centre of Mexico City in the dry season show an environment dominated by sensible heat storage, with large amounts of heat stored in the building fabric by day and released by night. (Oke et al. 1999)

Aims of the research

The development of solar-based technologies still requires research. For example, it is necessary to design solar heat storage systems at lower costs and for them to be simple to operate, efficient and long lasting.

This study has the objective of achieving a better understanding of the potential of thermal energy storage in Mexican climatic conditions for the application to buildings and building systems. High thermal mass structures constructed from clay as used in rural communities, and phase change materials (PCM's) used in a photo-thermal storage system for existing and new building structures have been studied in this project.

Both alternatives are interesting from the environmental perspective. The raw materials used in earth construction already form part of the ecosystem. Adobe construction has a long history in Mexico and is well understood at

an intuitive level in the context of traditional buildings and lifestyles. However, how this technique may be applied to modern buildings and lifestyles is less clear. The roles of liquid water and water vapour in the thermal behaviour of adobe systems are being studied. Although some research has been carried out by Hugo Houben, the introduction of modern materials such as thermal insulants in adobe walls is not well understood yet.

The objective of the part of the study regarding adobe structures was to assess the scope of existing coupled heat and mass transport models regarding water contained latent heat storage.

The substantial role played by latent heat storage on the thermal behaviour of adobe structures, led to the study of a solar-thermal storage system using Phase Change Materials

The objective of the PCM part of the study was twofold: 1) Enhance the existing computational models on the Stephan problem by considering the effect of regional variations (weather conditions imposed) on the boundary conditions. 2) Evaluate the impact of the solar-thermal system proposed when applied in dwellings in view of regional variations under Mexican weather conditions. This original research approach to the application of thermal storage for climatic regions in Mexico was the basis for this project.

The investigation was carried out both as an experiment and via mathematical modelling of the blind system.

Three experiments were carried out to achieve the objectives considered for the PCM part of the project. Experiment one for the computer model validation. Experiment two for the optimization and performance evaluation of the system proposed. Experiment three for an assessment of the impact of the application of the system proposed.

The proposal was a storage element that constituted internal blinds in windows. In this location the storage unit may take advantage of incident solar radiation. This location also provides the opportunity to fluctuate the mass flow rate of the heat transfer fluid (air) without the use of additional electro-mechanical means.

The experimental unit consisted of a single and a series of encapsulated PCMs contained in aluminium tubes . The tubes form a blind which acts as a heat exchanger with the atmospheric air as the working fluid as well as experiencing direct thermal irradiation.

The PCM's working temperature was chosen to keep the chamber at a comfort temperature between 22 and 25 °C. The objective of achieving a temperature modulation to maintain the environmental conditions within comfortable temperature ranges (achieving temperature differences of 6°C for the extreme conditions) was attained.

The study included experimental investigations for two sets of Mexican climatic conditions. The climatic conditions for two states within Mexico, at extreme latitudes, and during extreme seasons[10], were simulated. The dominant temperatures for each location and season determined the chosen PCM melting temperature range required for the change of phase of the material. In this way the temperature at which storage commenced and the subsequent heat release occurred were controlled.

The amount of energy stored/released and the rate of energy transfer was also studied as well as the efficiency of the system and its potentiality as an alternative energy for indoor thermal comfort under Mexican weather conditions was explored.

The possibility of providing dwellings with means to modulate the heat wave effect would represent economical and energetic savings for the country. It would also provide thermal comfort to Mexican houses without compromising the future of natural resources.

References

B.E.S.T. (2003). "Good for the environment, good for the economy." Building environmental science and technology.

Bridgman, P. W. (1943). *The nature of thermodynamics*, Cambridge, Mass : Harvard university press.

Brousseau, P., and Lacroix, M. (1996). "Study of the thermal performance of a multi-layer PCM storage unit." *Energy Conversion and Management*, 37(5), 599-609.

CONAE. "Energias renovables." Comision Nacional para el Ahorro de Energia. http://www.conae.gob.mx/wb/distribuidor.jsp?seccion=1,August 2005

Fernandez, J. L. (2001). "Alternativas energeticas para Mexico." FICA.

Garg, H. P., Mullick, S. C., and Bhargava, A. K. (1985). *Solar thermal energy storage*, D. Reidel ;
Sold and distributed in the U.S.A. and Canada by Kluwer Academic Publishers, Dordrecht ; BostonHingham, MA.

Garibaldi, J. (2002). "Experiencias mexicanas con los modelos bottom top." Secretaria de energia. Direccion general de informacion y estudios energeticos.

Gutierrez, G. (2001). ""Reflecciones sobre el uso de energeticos primarios" IV congreso de la asociacion Mexicana de Ecoomia Energetica."

---

[10] Two cities, one at a high and the other at a low latitude during winter and summer were considered for the simulation.

Instituto Nacional de Estadistica, G. e. I. I., Mexico. "Informacion Estadistica, Mexico."

Oke, T. R., Spronken-Smith, R. A., Jauregui, E., and Grimmond, C. S. B. (1999). "The energy balance of central Mexico City during the dry season." *Atmospheric Environment*, 33(24-25), 3919-3930.

Paez, A. (2004). "Reservas de hidrocarburos, para 13 años: Calderón." Diario el Universal, Jueves 12 febrero 2004.

Redclift, M. R. (1987). *Sustainable development : exploring the contradictions*, Methuen, London ; New York.

Secretaria de Energia, M. "Energias Renovables, Mexico." http://www.energia.gob.mx/wb2/Sener/Sene_Seminario_Energias_2005, August 2005

Tonda, J. (1993). *El oro solar y otras fuentes de energia*, Fondo de Cultura Económica, México, D.F.

Trzyna, T. C. (1995). *A sustainable world : defining and measuring sustainable development*.

CHAPTER II

HEAT STORAGE

"The goal of sustainable development is to meet the needs of the present without compromising the ability of future generations to meet their needs"

CHAPTER II

The quality of building performance depends on its ability to satisfy fundamental human needs, such as safe shelter, services facilities, and comfort. The most outstanding consequences of design on building performance can be observed in the areas of structural safety, functionality and hygro-thermal and energy performance of buildings.

Second stage performance assessment areas are fire safety, internal air quality, lighting, acoustics, and general operation of buildings and components. Durability and long-term functionality are often considered last. Means to predict long term performance of building materials need further development (Becker 1999).

This project is concerned with the effects of modifying the thermal behaviours of building materials on the energy consumption of buildings.
The quantities of energy used to maintain the environmental condition within a building significantly depends upon the thermal performance of the

structural materials employed. When taking advantage of the stored energy within the building materials to control the indoor environment, energy consumption (dependence on mechanical means) may be reduced.

The hygrothermal behaviour of materials has an effect on the general performance of structures. Understanding the hygrothermal behaviour of building components helps to prevent damage to or excessive heat loss or gain through structures.

Structural damage can be caused by internal stresses originating from mechanical strains due to thermal and hydrodynamic expansion. If the material strength is exceeded fissures appear and in the worst cases shear failure results in detachment (IBP 2003).

On the other hand, thermal behaviour of building structures (and therefore thermal comfort, which is a function of both temperature and humidity) is necessarily altered by the simultaneous phenomenon of moisture transport and heat transfer to and from the indoor environment and the building structural components.

Additionally, the storage of heat and moisture is an interesting option in building integrated systems for heating/cooling load shifting. As moisture is absorbed, the heat of absorption is captured by thermal energy storage.

Review on the hygrothermal behaviour and heat storage of Adobe building structures

Rural buildings and houses in particular, are mostly constructed from locally available materials. Adobe[2.1] brick has been commonly used in many regions of the world. Little energy is used in fabricating the bricks and in climatic regions where they have been used traditionally they have provided a basic standard of thermal comfort for low rates of energy consumption.

It was established by the Zuni Indians (Alva 2001), that the high thermal capacity of earth meant that it could store much of the heat it absorbed during the day, thus keeping the interior of a dwelling constructed from earth relatively cool during the day. Later, when the outside temperature had dropped at night the walls would emit the heat stored during the day into the building interior. The physical mass and specific heat capacity of the adobe material are considered to be key factors in its ability to moderate temperature swings in buildings.
The ability of soil to transmit heat strongly depends on its water content, which will vary with the degree of saturation; more highly saturated soil will conduct heat at a greater rate (Rees, Zhou et al. 2001).

2.1 Adobe is a construction technique that uses soil (a mixture of clay, sand and water), stabiliser and binder, as raw materials that are mixed and moulded to form sun-dried porous blocks.

Philip and De Vries (De Vries 1987) demonstrated that the rate of energy consumption is more strongly correlated to variations in soil conductivity than to the presence/absence of thermal insulation within the construction elements of adobe structures.

Additionally, the water contained within adobe has latent heat effects, which modify both the thermal conductivity and thermal capacity of the material. Current investigations have shown that clay's reversible hydration-dehydration processes make them also good chemical heat accumulators (Sadek and Mekhamer 2000).

As water plays such an important role on the thermal behaviour of the adobe construction system, mass transfer within the walls needs to be reviewed.

Porous Material

Adobe bricks are porous[2.2] building materials; their thermodynamic behaviour is similar to that of soils, due to the presence of clay in the mixture and to their porous structure.

Understanding the transient thermal and hydrodynamic processes in building elements requires some fundamental knowledge about the storage and transport features of these processes on building materials, as shown in figure 2.1.

2.2 Porosity refers to volume fraction of void space. This void space can be actual space filled with air or space filled with both water and air.

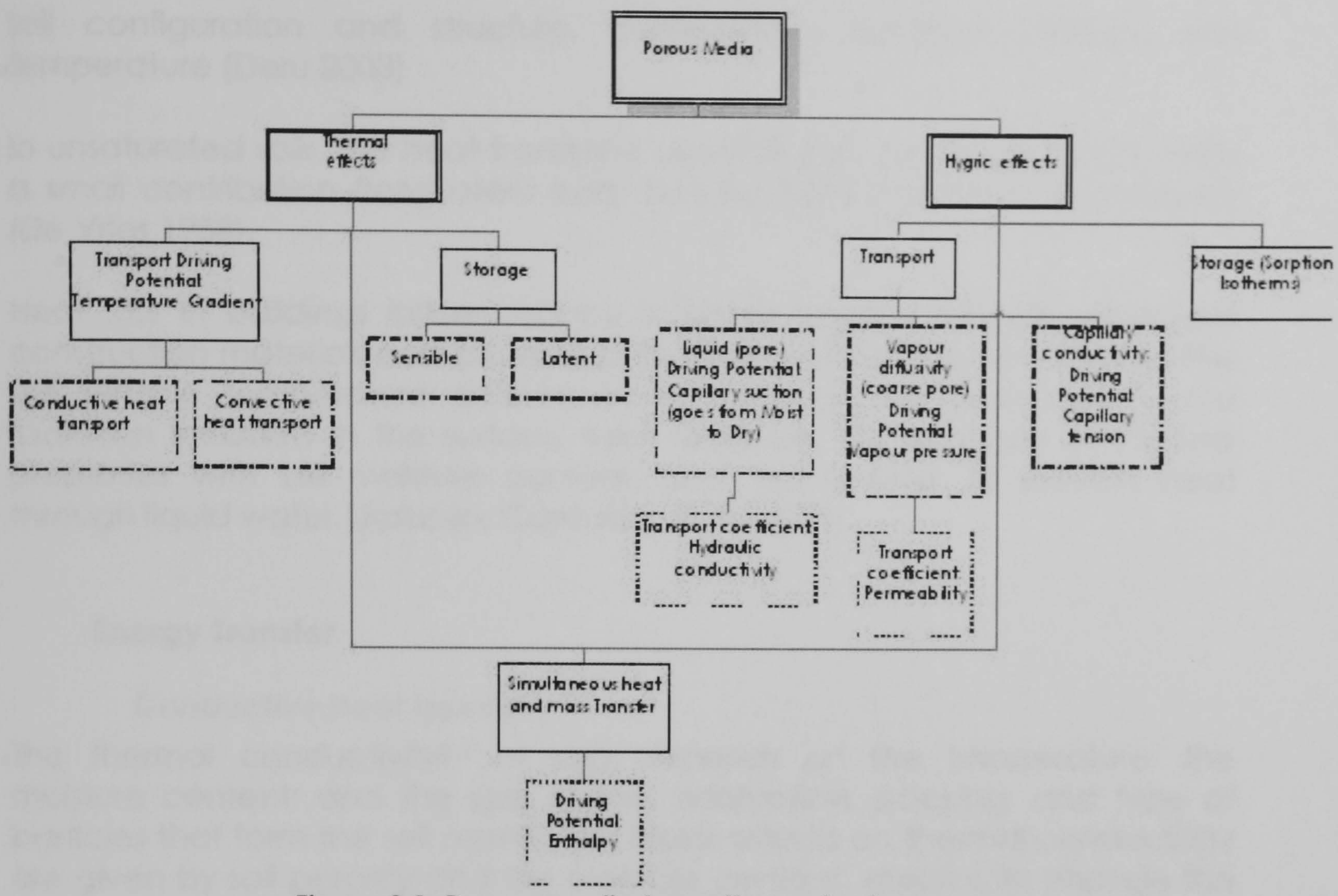

Figure 2.1: Porous media hygrothermal scheme

Thermal Effects

Porous media can be regarded as an arrangement of solid and gaseous phases.

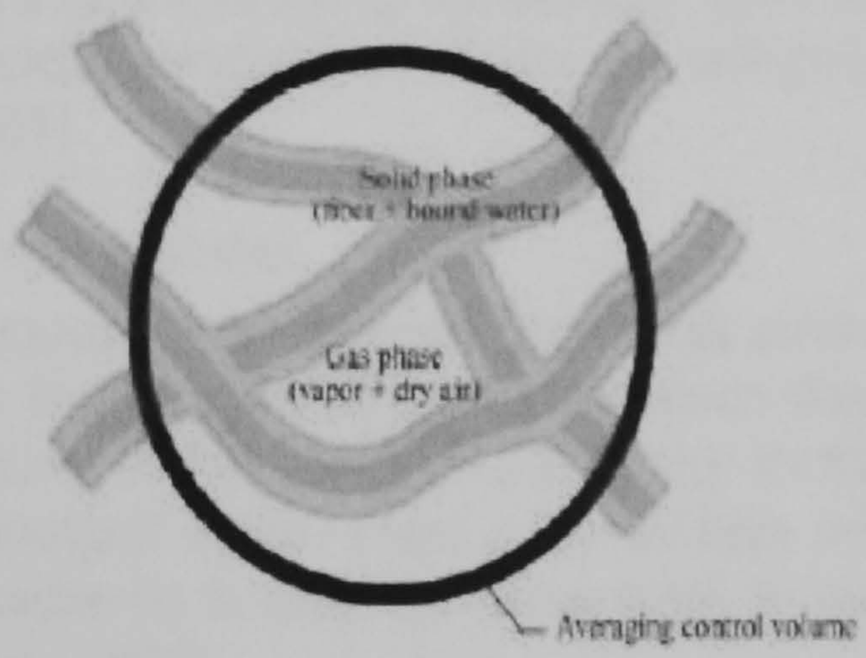

Figure 2.2: Schematic diagram of the two dimensional structure of porous media (Barker, Song et al.)

Due to its form and structure, heat transfer in soils takes place through several paths. These include: conduction (through the soil particles, water, and air); latent heat transfer (through the evaporation-condensation cycles of the water present in the material); sensible heat transfer (by water vapour and liquid diffusion and convection); and radiation (in the air-filled pores). The relative significance of the various heat-transfer terms depends on the

soil configuration and structure, composition, moisture content and temperature (Deru 2003)

In unsaturated soils, the heat transfer is controlled by pure conduction, with a small contribution from latent heat transfer (due to vapour movement) (De Vries 1958).

Heat loss in buildings influenced by moisture transfer through soil-based construction materials can be related to three main concurrent effects: The soil surface temperature difference affected by the evaporation and radiation included in the surface heat balance; The variation of thermal properties with soil moisture content; and the transfer of sensible heat through liquid water (Janssen, Carmeliet et al. 2004).

Energy Transfer

Conductive heat transfer

The thermal conductivity[2.3] of soils depends on the temperature; the moisture content; and the size, shape, orientation, packing, and type of particles that form the soil matrix. The major effects on thermal conductivity are given by soil porosity and the moisture content, which can change the thermal conductivity significantly (Deru 2003)

The effective thermal conductivity[2.4] is limited by the contact resistance between the soil particles. Therefore, reducing this resistance raises thermal conductivity. Thermal resistance is reduced by providing better contact between soil grains (e.g. increasing its density and reducing its porosity by compression), and adding moisture[2.5] to a dry soil provides another path for heat flow (Farouki 1981).

Convective heat transfer

In the heat transfer equation for porous materials such as soils, the governing term in most cases is the conduction, apart from the case when there is a large stream of moisture at the surface (i.e. rain). In this case the convective term can be the principal term. Free convection within soils taking place from temperature gradients is only considerable in soils having particle sizes larger than 8 mm (Deru 2003)

Storage

2.3 "The rate at which heat energy flows across a unit area of soil due to a unit temperature gradient" (Farouki 1981).

2.4 The net overall thermal conductivity of porous material, present in the solid phase and in the gas confined in the solid. Effective thermal conductivity of air is based on physical considerations like the diffusivity of the water vapour in air and the enthalpy of phase change.

2.5 Gases are insulators, and when moisture levels increase (approaching to saturation), gases are replaced with higher thermally conductive moisture. (Deru M 2003)

Heat is stored as a result of temperature increments[2.6], but it can also be stored from changes in water pressure[2.7], through the sensible and latent heats associated with the liquid phase (Janssen, Carmeliet et al. 2004).

Thermal energy can be stored in three ways: 1) sensible heat (via temperature change of the medium acting through the storage medium heat capacity,) 2) latent heat (via the latent heat of transformation of the medium, the temperature of the medium remains more or less constant during heat transfer) and 3) Heat of reversible thermo-chemical reaction (Brousseau and Lacroix 1996).

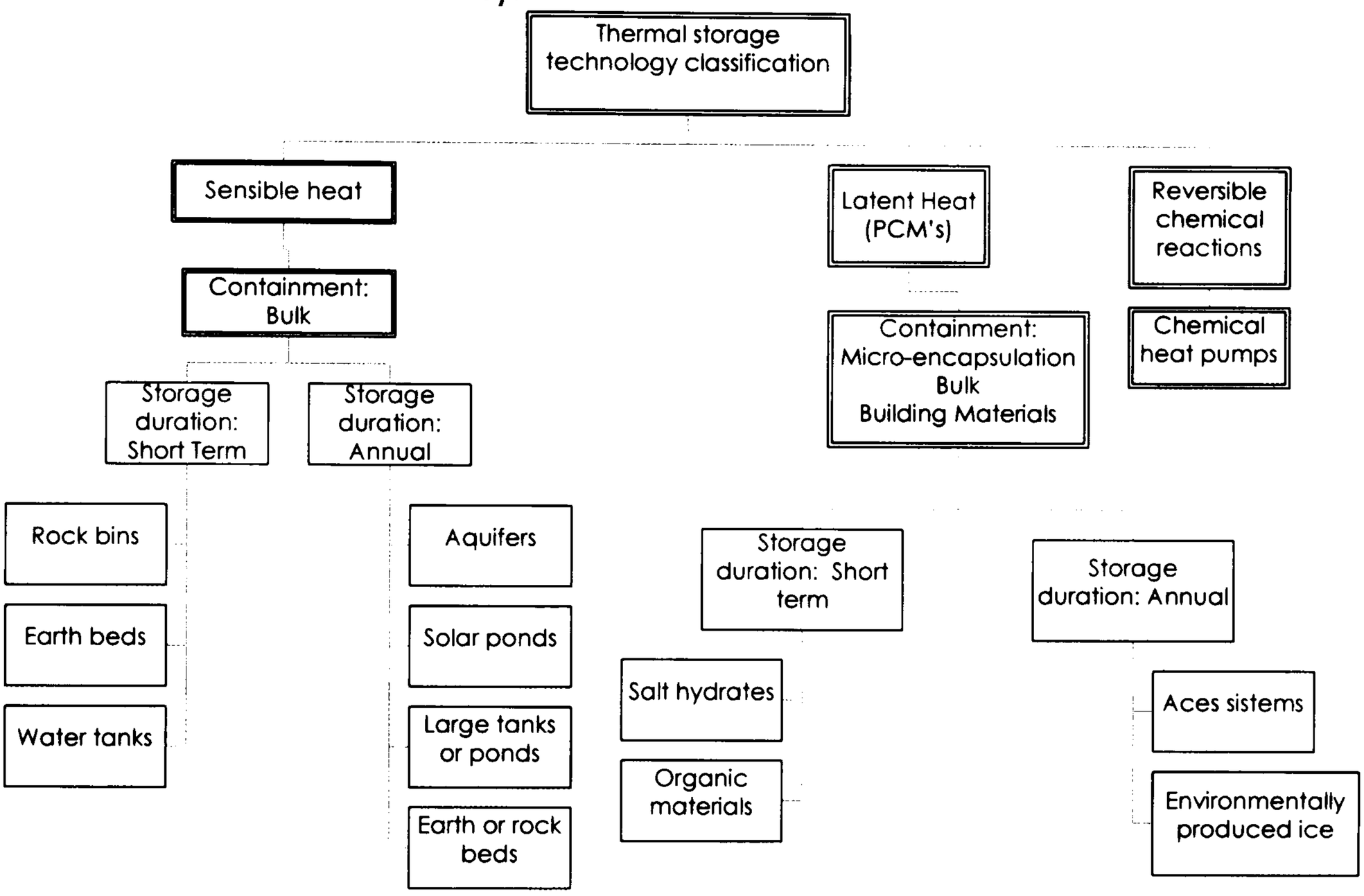

Figure 2.3: Thermal storage technology classification. (Brousseau and Lacroix 1996).

Sensible heat transfer and storage:

Moisture transfer and/or moisture storage result in a parallel transfer and/or storage of sensible and/or latent heat.

During the charging or discharging of sensible heat storage, the temperature of the medium changes (varying its heat content). Altering the state of the moisture contained within the soil causes the storage or dissipation of heat. Soil thermal conductivity and thermal capacity are highly dependent on soil moisture content.

2.6 Thermal energy storage in a solid occurs when its temperature increases with time (Myers, 1971)

2.7 The capillary or matric potential (moisture content) corresponds to the soil water pressure head (h)

Thermal capacity variations are less evident than the moisture related thermal conductivity variations. Nevertheless the heat capacity values of porous materials when transforming from the dry to the wet state can double or triple. (Janssen, Carmeliet et al. 2004)

Latent heat transfer and storage

Along with the energy transferred through the porous building structures, condensation-evaporation processes occur as a consequence of the moisture transport. These processes can be associated with the release or adsorption of substantial amounts of heat.

Thermo chemical process

Solar chemical heat pipes are solar energy converters which use high-temperature collected solar energy in a solar reactor as an endothermic reversible reaction. The chemical heat pipe may then be transported to the site where the energy is needed and the exothermic reverse reaction is performed, giving up as much process heat as was stored from the solar energy. They are then sent back to the solar reactor to be recharged and for the cycle to be repeated. (Steinfeld and Palumbo 2001)

Evaporation

When structures start to dry, the evaporation of the surface water results in heat loss in the form of latent heat (liquid water evaporates on the hot side, absorbing the latent heat of vaporization). This loss of heat causes the surface temperature to drop. The cooler surface temperature compared to the deeper layers of the building element drives the heat flux from the interior towards the surface (Gayo, De Frutos et al. 1996).

Condensation[2.8]

Diffusion is induced by the vapour pressure gradient causing liquid water evaporation and movement[2.9]; latent heat of vaporization is released on the other side of the pore, where vapour condenses.

Hydrodynamic Effects

Moisture Transport

An important aspect of the description of building elements is their moisture behaviours. Water and water vapour transport and storage affects a structures thermal performance, degradation rate and durability. The water

---

2.8 The lower the air temperature, the less water vapour is required for the air to become saturated. The temperature at which saturation occurs is the DEW POINT; once is reached, condensation will occur.

2.9 The saturation (or equilibrium) vapour pressure is a measure of the maximum mass of water vapour per unit volume before condensation occurs.

movement[2.10] is influenced by its inherent properties such as thermal conductivity, porosity, solubility, etc and by external conditions (climate).

Moisture in porous media can be transported by thermo-capillary forces and vapour diffusion.

Vapour diffusion[2.11] is most important in large pores, whereas liquid transport[2.12] takes place at pore surfaces, in crevices and small capillaries. (Kunzel and Kiessl 1996). Both moisture transport mechanisms are independent and must be differentiated for the modelling of this phenomenon. The flow via vapour diffusion and liquid transport may be in the same or in opposite directions (Bomberg 1974).

Damping process (stages of saturation)

-Molecular adsorption: the dry surfaces of the pores adsorb vapour
-Water vapour diffusion: this occurs across a vapour pressure gradient caused by condensation in micro-pores.
-Transport in series: capillary condensation generates still water drops.
-Parallel transport: Absorbed layer in capillaries is thick enough to start local flow of water.
-Unsaturated water flow: The layer of water absorbed by the capillary walls becomes thick enough to start a flow of liquid water.
-Saturated water flow: Air bubbles entrapped inside the larger micro-pores are surrounded by the flowing water[2.13]. This kind of flow starts at capillary saturation (Bomberg 1974)

Drying process

A moisture content gradient practically does not exist at the very first moment of drying. On the exterior surfaces the energy required to drive the drying process may be provided both by solar irradiation and/or by the difference in temperature between the surface and the ambient environment causing heat to be transferred to the surface[2.14]. This causes evaporation and sets up the potential differences that start the moisture transport processes.

Eventually, insufficient liquid water will exist close to the surface for liquid migration to occur. Consequently, liquid water can no longer move through the material[2.15], and the moisture that subsequently migrates to the surface does so as water vapour[2.16].

2.10 Initiated by forces called driving potentials
2.11 Its driving potential is the partial vapour pressure
2.12 Its driving force is capillary suction.
2.13 A direct air transfer is no longer possible
2.14 Free water evaporates from the surface
2.15 Water from the larger pores is lost
2.16 Water is lost from the fine pores or cells. Absolute dryness is never attained in actual buildings

The drying rate is determined by: a) Environmental factors such as ambient temperature, air velocity, temperature difference between the surface and the adjacent air, vapour concentration in air and b) Parameters for internal moisture transfer such as temperature gradient in the layer adjacent to the dried surface, vapour pressure differences, moisture content, moisture content gradient, initial moisture content, and geometry of the dried material.

Capillary conductivity, driving potential: capillary tension

Capillary conduction is established under capillary moisture conditions (e.g. when driving rain occurs). Capillary tension is the driving force arising from the surface tension of the water in the meniscus at the boundary between water and pore-air.
The driving force in the liquid phase corresponds to a particular vapour pressure in the gas phase. Thus vapour pressure can be used as driving potential for capillary conduction.

Capillary conductivity: Equilibrium humidity in the pore

When solving mass transfer problems, usually phase equilibrium is considered to exist at the interface, despite the way that the mathematical boundaries[2.17] are chosen. As for heat transfer similarity conditions, contiguous phases are assumed to have the same temperature at the boundary. That is, thermal equilibrium between adjoining phases is considered. For mass transfer the same velocity is assumed at the interface for the adjacent phases.

Vapour Diffusivity transport (coarse pore)

The water vapour driving potential is the vapour pressure (which depends upon the temperature[2.18]). Permeability[2.19] (μ) is used as the transport coefficient. The vapour pressure is proportional to the vapour density[2.20] at a given temperature, and so the vapour diffusion equation can be written in terms of the vapour density.

Fick's law[2.21] is typically used to simulate diffusion in porous materials with the vapour pressure as the driving potential. Fick's law says that the diffusion flux

---

[2.17]The boundaries of the mass transfer systems are either the phase interfaces or arbitrarily chosen average conditions within the phases.

[2.18]The vapour pressure of any pure substance is characteristic of that substance and of its temperature.

[2.19] Vapour permeability or moisture permeability, is the total flux including moisture transport both in the liquid and the vapour state. The 'differential moisture permeability' relates the total flux of moisture to the pressure gradient across a differential thickness of material; it is a function of the relative humidity (Galbraith).

[2.20] Density of a gas, expressed as the mass of a given volume of the gas divided by the mass of an equal volume of a reference gas (such as hydrogen or air) at the same temperature and pressure

[2.21] The principle that a substance put into solution will tend to diffuse towards constant concentration throughout the solution.

is equal to the water concentration potential gradient[2.22] multiplied by a constant or diffusion coefficient. The diffusion coefficient is dependent upon the water content of the material

$$J = -D\frac{\partial C}{\partial x}$$ **Equation 2.1: Fick's law of diffusion**

J= Flux or rate of diffusion (atoms /m2/s)
D= Coefficient of diffusion (m2/s)
$\frac{\partial C}{\partial x}$ = Concentration gradient (atoms/m4)

The "moisture" coefficient of diffusion translates the action of the thermal movement in the overall transfer of moisture. It fluctuates with humidity (moisture content) and temperature (De Freitas, Abrantes et al. 1996)

Vapour pressure, water vapour driving potential

The amount of or rate at which water is absorbed by a material depends on its pore pressure. The initial moisture migration is larger in the regions with higher temperature, where the saturated vapour pressure is larger. The free pores in the regions close to the lower temperature zones are then likely to be saturated and condensation will occur. Now water migration will be governed by the hydraulic pressure differences produced by saturated vapour pressure at the borders of the saturated section (England and Khoylou 1995)

Liquid Transport (pore)

At high moisture contents, moisture transport is dominated by liquid transport. The liquid flow that originated in the smallest pores when the adsorbed water film was sufficiently thick becomes a complete liquid flow. When a constant liquid phase wraps the whole pore structure and locks the free air path, the knick point[2.23] of the water intake process, occurs.

The liquid water driving potential is the capillary pressure[2.24] and the transport coefficient is the hydraulic conductivity[2.25]. The hydraulic conductivity in unsaturated soil depends on the soil and fluid properties, moisture content, and temperature (Deru 2003)

[2.22] Differences in potential energy of water between one point and another give rise to the tendency of water to flow within the soil.

[2.23] Knick point: an abrupt change of gradient in the profile of a stream(M. Bomberg)
[2.24] Capillary pressure: the difference between pressures of phases, in this case air and water, and is assumed to be a function of saturation (Hassanizade)
[2.25] Hydraulic conductivity: the proportionality factor (L t^{-1}) relating water flux density to a hydraulic gradient. It is highly dependent on wetness for a given set of soil conditions.

Limited experimental measurements[2.26] show that, the diffusion coefficient for liquids varies appreciably with concentration(Pel, Brocken et al. 1996)

Storage

As the moisture content and the vapour density are subject to both matric head[2.27] and temperature, moisture storage can take place from changes in both the matric head and temperature (Janssen, Carmeliet et al. 2004) Matric head is a potential associated with the attraction of solid surfaces for water surface tension related to the adsorptive forces and is sometimes called capillary potential. In saturated soil the matric potential is zero

To model water storage, the moisture retention function is used. In the next figure the representation of the water retention function of a building material is shown. The function has three parts: a) the sorption isotherm up to 95% RH, b)the capillary moisture range and the c) over saturated moisture range, where the water retention function is a vertical line at 100% r.h.(Kunzel and Kiessl 1996). A capillary-active material exposed to water will adsorb this water up to free saturation (at RH=100%). The saturation vapour pressure is reduced in the smaller capillaries, with this, some condensation takes place, and the moisture equilibrium is increased. The maximum water content is greater than free saturation (due to air trapped in pores) and is determined by the porosity[2.28].

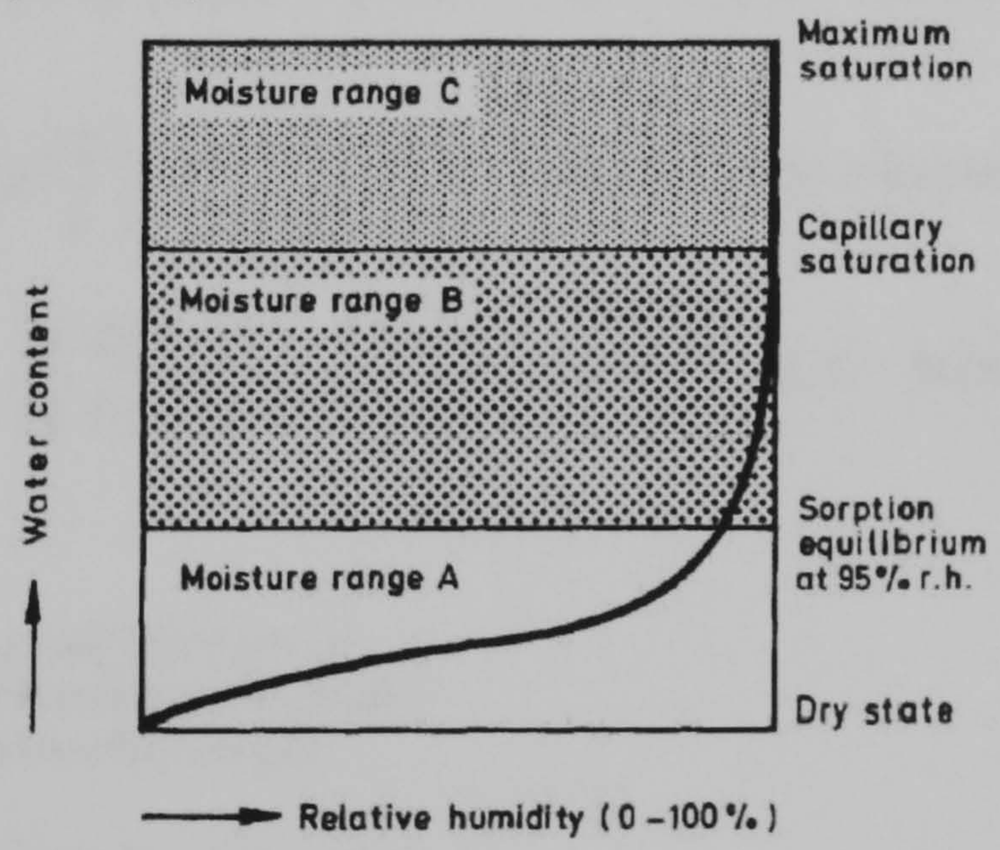

Figure 2.4: Schematic representation of the water retention function of hygroscopic, capillary(Kunzel and Kiessl 1996)

2.26 Moisture content methods are: the electrical moisture meters, coloured indicator papers, hygrometers (BRE 163) Moisture concentration profiles determined by Nuclear Magnetic Resonance (NMR) (Pel, 1996)

2.27 Describes the water pressure in "metres water column" instead of the more common capillary pressure in "Pascal"

2.28 Porosity [m^3/m^3], determines the maximum water content (by water density multiplication 1000 kg/m^3). The porosity can be estimated from the true density and the bulk density: $Porosity = 1 - \rho_{bulk} / \rho_{true}$

The hygroscopic moisture storage is represented by the material sorption curves.

Simultaneous heat and mass transfer

Coupled heat and mass transfer through porous media takes place in important engineering processes such as production processes, drying, food processing and chemical engineering applications. Tiles and bricks drying up to equilibrium moisture content is a crucial process, which comprises problems of heat and mass transfer, to and from the porous solid (Suresh, Murugesan et al. 1999)

Temperature gradients cause redistribution of moisture. If two regions in a wall are maintained at different temperatures so that there is a flux of heat, thermally driven moisture and/or vapour flows are induced. Moisture is forced to start redistributing as concentration gradients are generated inside the specimen at a rate that is proportional to the local vapour pressure gradients. The flow continues until the total energy balance is equalised.

Each moisture flow creates a temperature gradient and vice-versa[2.29] (Bomberg 1974). Initial mass flow rates are thus greatest where the temperature gradients and hence the vapour pressure gradients are greatest.

$$\rho(Cp + \lambda Cp_{w}) \frac{\partial T}{\partial t} = \frac{\partial}{\partial x}\left(k \frac{\partial T}{x}\right) + h_{v} \frac{\partial}{\partial x}\left(\frac{\delta}{R_{v}} \frac{\partial p}{\partial x}\right)$$

Equation 2.2: Heat transport and storage

$$\rho_{w} \frac{\partial u}{\partial \phi} \cdot \frac{\partial \phi}{\partial t} = \frac{\partial}{\partial x}\left(\rho_{w} D_{w} \frac{\partial u}{\partial \phi} \frac{\partial \phi}{\partial x}\right) + \frac{\partial}{\partial x}\left(\frac{\delta}{Rv} \frac{\partial p}{\partial x}\right)$$

Equation 2.3: Moisture Transport and storage

D_w= Liquid Transport coefficient (m^2/s)
Cp= Specific heat of the material (J/kgK)
Cp_w= Specific heat of water (J/kgK)
λ = Liquid Fraction
h_v= Evaporation enthalpy of water (J/kg)
p= Water vapour partial pressure (Pa)
u = Water content (m^3/m^3)
δ = Water vapour diffusion coefficient in air (kg/msPa)
T= Temperature (°C)
k= Heat conductivity of moist material (W/mK)
R_v= Vapour diffusion resistance factor of dry material
ρ_{w} = Density of water (kg/m^3)
ϕ = Relative humidity (IBP 2003)

2.29 An effect called the Dufour effect is the tendency towards the generation of a temperature gradient in conjunction with mass transfer arising from a concentration gradient.

On the left-hand sides of both equations are the storage terms. Heat storage includes the heat capacity of the moisture in the material and the heat capacity of the dry material. Moisture storage is depicted by the derivative of the moisture storage function (retention curve).

On the right-hand side of equations 2.2 and 2.3 are the transport terms. In equation 2.2 these relate to the heat transport and the moisture-dependent thermal conductivity and vapour enthalpy[2.30]. Moisture transport is described by equation 2.3 and includes liquid transport and vapour diffusion[2.31]. Liquid transport, which exhibits only fairly minor temperature dependence, takes place through surface diffusion and capillary conduction[2.32]. Conversely, vapour diffusion, is clearly influenced by the temperature profile[2.33]. Equation 2.2 and Equation 2.3 must be solved for every part of the envelope individually.

The complexity in modelling simultaneous heat and moisture transport is attributable to: (i)The pore system, which is already complicated; (ii) A highly non-linear character: (iii)diffusion coefficients that may be variable and (iv) hysteresis effects. The process gradients are non linear and accounting for the heat of evaporation in the energy balance is a problem, as there is no way to measure vapour and liquid flows separately (only the total flow can be measured).

Dimensionless correlations for mass transfer

For constant mass diffusivity values and similar boundary conditions exist; the expressions, equations and correlations for mass transfer are analogous to those of heat transfer (their solutions are similar) (Gupta and Srinivasan 1978)

2.30 Vapour enthalpy heat transport (called latent heat effect) is due to water evaporating in one place and thus absorbing latent heat from this place, then diffusing to a different place, condensing there and releasing latent heat. Moisture phase change includes latent heat effects and changes in thermal and hydraulic properties

2.31 Both due to a gradient of relative humidity

2.32 Both due to a gradient of relative humidity

2.33 Since the saturation vapour pressure increases exponentially with temperature

Dimensionless heat transfer group	Dimensionless mass transfer group	Interpretation
Nusselt Number $Nu = \frac{hL}{k_f}$	Sherwood number $Sh = \frac{h_m L}{D_m}$	Dimensionless temperature gradient at the heat/mass transfer boundary
Prandtl Number $\Pr = \frac{C_p \mu}{k} = \frac{v}{\alpha}$	Schmidt Number $Sc = \frac{\mu}{\rho \cdot D_m} = \frac{v}{D_m}$	Ratio of the momentum and thermal/mass diffusivities. If Sc/Pr=1 heat and mass transferred lead to equal temperature and composition profiles
Peclet Number $Pe = \frac{VL}{\alpha} = \mathrm{Re}_L \Pr$	Peclet Number $Pe = \frac{VL}{D_m}$	Relates the forced convection of a system to its heat conduction

Table 2.1: Heat and mass transfer analogous dimensionless correlations

Where:
h = Convection heat transfer coefficient (W/m^2K)
L= Characteristic length (m)
k_f = Fluid thermal conductivity (W/mK)
C_p= Specific heat (J/kgK)
μ =Viscosity (kg/sm)
v = Kinematic viscosity (m2/s)
α = Thermal diffusivity (m^2/s)
V= fluid velocity (m/s)
Re= Reynolds number based con characteristic length
D_m= Mass diffusivity (m^2/s)
ρ = Density (kg/m^3)
h_m= Diffusion rate (m/s)

The Lewis relation

Dimensionless heat and mass transfer coefficients are equal at a given Re (for a particular case of $D_m = \alpha$). That is, the analogy is valid for air and water vapour at low mass transfer rates, $\alpha / D_m = 1 \therefore D_m = \alpha$. For other gas mixtures the ratio of thermal to vapour diffusivity may differ from unity.

$$\frac{h_m l}{D} = f(\mathrm{Re}, Sc) \qquad \text{And} \qquad \frac{h\, l}{k} = f(\mathrm{Re}, \Pr)$$

As $D_m = \alpha$ then, $Sc = v/D_m = v/\alpha = \Pr$

$$\therefore \frac{h_m l}{D_m} = \frac{hl}{k} \qquad \therefore h_m = h\frac{D_m}{k} \quad \text{and} \quad h = \frac{kh_m}{\alpha} = \frac{kh_m}{\frac{k}{\rho Cp}} = h_m \rho Cp$$

$$\therefore h_m = \frac{h}{\rho Cp}$$

that is $\frac{h}{h_m \rho Cp} = 1$ **Equation 2.4: Lewis relation** (Welty 1974)

The ratio of thermal to molecular diffusivity α/D is known as the Lewis number (Bennet and Myers 1984). It is a measure of the comparative rates of diffusion of energy and mass in a system. For practical purposes it can be assumed to be unaffected by temperature variation.
For turbulent flow, the Lewis relation is valid, even if $\alpha/D \neq 1$, since the macroscopic mixing action comprised in the eddy diffusion is the same for heat and mass transfer, overwhelming any molecular diffusion. Lewis relation is only valid for $\alpha/D = 1$ in laminar flow (ASHRAE, Elmahdy et al. 2000)

Enthalpy, Driving Potential for simultaneous heat and moisture transfer

The driving potential for the simultaneous transfer of heat and mass in air-water vapour mixtures is to a close approximation enthalpy[2.34]. The enthalpy of air and water vapour mixtures is represented by

$$h_{aw} = Cp_{ha} t_a + h_{fw} HR_a \qquad \text{(Hasan and Siren 2002)}$$

where
Cp_{ha}= Specific heat capacity of humid air (kJ/kgK)
t_a= Air temperature (°C)
h_{fw}= Latent heat of evaporation of water (kJ/kg)
HR_a= Humid ratio of moist air at air temperature (kg water/kg dry air)

For these mixtures the flows of mass and energy takes place from the bulk water to a boundary, and then from the boundary to the neighbouring air mass. Each interface resistance to these flows results in gradients in enthalpy[2.35], humidity ratio and temperature.

Merkel's theory[2.36] establishes that the overall heat transfer in air-water vapour mixtures is directly proportional to the enthalpy gradient[2.37]. Namely, as the ambient wet bulb temperature is augmented, the enthalpy driving force is decreased. That is, for a lower driving force more heat transfer area or more air are required (Daeil Aqua Co.)

In the Elmahdy and Mitalas (ASHRAE, Elmahdy et al. 2000) approach for heat and mass transfer in moist air, the total energy transfer rate is considered to be proportional to the enthalpy difference between the free stream air and saturated air at the temperature of the surface (Zhou and W.)

2.34 Enthalpy: Is equal to the difference in the heat transfer into the system and the work done by the system. The work and heat transfer depend on the process used to change the state.
2.35 The heat flux to the materials in a pore causes a change in the enthalpy (Harris, Kendall T. 2001)
2.36 Concept of heat transfer in evaporative cooling tower performance developed by Markel in 1925
2.37 Enthalpy gradient: The difference between the enthalpy of saturated air at the water temperature and the enthalpy of air at the point of contact with water.

Clays as chemical heat accumulators

Chemical heat accumulators (CHA) are systems in which low and middle temperature heat can be stored and recovered. Dehydration is a physical reaction commonly used for heat accumulation, as a consumption of 2260 kJ/kg is required for the evaporation of water[2.38]. A high heat of vaporisation value, is given by the hydrogen bonding in the liquid water[2.39]. Reversible hydration-dehydration reactions are suitable for several applications.

CHA systems consist of two components

1) Inert porous matrices: the host materials of diverse types, e.g. silica gels, alumina, polymeric, carbonaceous, or metallic porous substances.

   The matrix comprises the supporting framework for the energy accumulating material and provides the diffusion path. According to its internal shape, the matrix might assist heat and mass transfer.

2) The chemical heat storing substance (CSS), for the dehydration of water molecules is impregnated into the matrix pores.
   Most interest has been shown in three CSS inorganic materials: crystalline hydrates of simple salts, hydroxides, and zeolites.
   The main disadvantage of crystalline hydrates of simple salts, as contained in clay, is a limited mass transfer rate[2.40].

Heat accumulation and recovery:
An external source provides heat for the dehydration process. Where water vapour pressure differences exist, water by an endothermic reaction changes state from liquid water-to-water vapour by absorbing heat energy[2.41]. Heat of evaporation is removed from the body of water. This energy is stored in the desiccant as the water evaporates. For the recovery of this stored energy, water vapour is added, and the reaction is reversed. That is, as the vapour condenses in the porous matrix and heat of condensation is given off (Tahat, Babus'Haq et al. 1995); (Levitskij, Aristov et al. 1996)

In the case of adobe walls, the system is called "open" because the available source of water vapour is ambient air.

The main thermodynamic parameters for energy accumulation are:
1) Enthalpy change during the reaction (which exhibits the specific energy storage capacity of the system)

2.38 That is, for the liberation of the water molecule chemically bounded
2.39 For water to evaporate, the polymer chains must be split into individual molecules
2.40 Due to the inhibited utilization of diffuse crystalline hydrate particles, given by their fluidization.
2.41 As water is vaporised, the polymer chains must be broken up into individual molecules.

2) Transition temperature, which represents the system operating temperature (Levitskij, Aristov et al. 1996)

Clays are characterized by particles having a diameter of 0.004 mm; having a chemical composition of Aluminium oxide (Al_2O_3), Silicon dioxide (SiO_2) and Magnesium (Mg) and Iron (Fe) hydrosilicates; having a layered structure; being highly porous and in most cases having the capacity to absorb ions from a solution[2.42] and release the ions later when conditions change (Foley 1999). In the case of montmorillonite clay for example, it is able to absorb as much water as 7±10 times of its volume.

Smectites (montmorillonite) are swelling clays, consisting of segmented layers of minerals formed by negatively charged sheets. The layers are closely adhered by a charge-balancing interlayer of cations such as calcium, magnesium, or sodium.

Clays thus meet one of the most important requirements for energy accumulation, water absorption. Clays swell[2.43] as they absorb water, and being able to operate in a reversible hydration/dehydration mode, they contract[2.44] reacting to changes in temperature and humidity.
As water hydrogen bonds penetrate through the clay's layers an exothermic reaction occurs[2.45].

Simulations

In previous research carried out by the author, the influence of various factors on the dynamic response of the thermal performance of adobe constructions was assessed. However further research was needed to include the effects of wetting due to rain and the absorption/desorption of water vapour due to changes in the relative humidity. In this project the moisture transport of these structures was studied in order to evaluate the effect of moisture content on the latent heat storage.

WUFI-pro 3.3.1 Commercial software was used for the hygrothermal analysis of the building envelope. Next some generalities about the software, and data required for the calculations are given.

The WUFI simulation model is a one-dimensional transient heat and mass transfer model which can be used to assess the heat and moisture

---

2.42 Water molecules are strongly attracted to clay mineral surfaces
2.43 Interlayer swelling', or intra-crystalline swelling of Montmorillonite for example depends on the type of clay and the type of cation.
2.44 Hydration and dehydration can vary the thickness of a single clay particle by almost 100 percent.
2.45 When the interlayer cations in montmorillonite become hydrated, large hydration energy is evolved.

distributions for specific multi-layered building material and climatic conditions.

In the calculation of heat transport, WUFI takes into account: thermal conduction, enthalpy flows through moisture movement with phase change, short-wave solar radiation.
The vapour transport mechanisms included in WUFI are: vapour diffusion, solution diffusion.
The liquid transport mechanisms taken into account are: capillary conduction, surface diffusion.
The boundary conditions for each time step are expressed in terms of meteorological data (temperature, relative humidity, driving rain, radiation), since in building physics these are the relevant parameters specifying the conditions at surfaces exposed to natural weather.

With WUFI it is possible to calculate the temporal evolution of the temperature and moisture fields in the building component.

Data required:

Material WUFI data required:

Basic Values
1900 kg/m3 Bulk density
0.30 m3/m3 Porosity
1800 J/kgK Heat Capacity
0.5-2.5 W/mK Thermal conductivity
28 Diffusion resistance

Table 2.2: Basic material WUFI data required.

Optional data:
The moisture storage function describes the amount of moisture taken up by the building material if it is exposed to air with a specific relative humidity (RH). Since the relation between RH and moisture content is largely temperature independent; the RH is an important and unique related parameter when describing the moisture content of a material.

Moisture storage function

No.	RH	Water Content (kg/m3)
1	0	0
2	0.5	20
3	0.65	30
4	0.8	50
5	0.9	70
6	0.93	120
7	0.95	180
8	0.99	210
9	1	250

Table 2.3: Adobe moisture storage function

The liquid transport coefficient for suction describes the capillary uptake of water when the absorbing surface is fully wetted.
The liquid transport coefficient for redistribution (DWW) describes the spreading of the absorbed water when the wetting is finished.

Liquid transport coefficient , suction

No.	Water Content (kg/m3)	DWS
1	0	0
2	10	1.50E-10
3	250	1.50E-07

Table 2.4: Adobe Liquid transport coefficient for suction

Liquid transport coefficient , redistribution

No.	Water Content (kg/m3)	DWW
1	0	0
2	10	1.50E-10
3	250	1.50E-08

Table 2.5: Adobe liquid transport coefficient, redistribution

Thermal conductivity, moisture dependent

No.	Water Content (kg/m3)	Thermal conducti
1	0	0.5
2	20	0.5
3	40	1.0
4	60	1.5
5	80	2.0
6	100	2.5
7	110	2.5
8	250	2.5

Table 2.6: Adobe Thermal conductivity moisture dependent

Water vapour diffusion resistance factor, mositure dependent

No.	RH	Miu value
1	0	7.0

Table 2.7 Adobe water vapour diffusion resistance factor, moisture dependent

The material was divided in 3 layers, each one starting with a different moisture content to observe wetting and drying of the wall. The heat losses/ gains varied accordingly with the corresponding thermal conductivity

Initial moisture content (kg/m3) in each layer

Layer	Option 1	Option 2
Exterior	250	60
Central	80	20
Interior	60	0

Table 2.8: Adobe initial moisture content for experimental set up

Climate WUFI data required to perform the calculations:

The location selected was Mexicali, Baja California, a Mexican province with the most extreme weather conditions found in Mexico:

Month	Day No.	Hours	Rain (lt/m^2hr)	Radiation (W/m^2)	Exterior T(°C)	Exterior RH (%)	Interior T(°C)	Interior RH (%)
Januay	30	744	4	557	12.3	68	17	50
February	60	1416	2.5	740	14.8	68	19	50
March	90	2160	15	617	17.1	69	20	51
April	120	2880	5	539	20.7	72	22	54
May	151	3624	1	535	24.7	74	25	56
June	181	4344	0	529	29.5	77	31	59
July	212	5088	0	538	29.5	78	32	60
August	243	5832	0	543	32.6	78	33	60
September	273	6552	2	622	29.7	76	31	58
October	304	7296	2.5	604	23.8	74	26	56
November	334	8016	4	502	17.1	72	20	54
December	365	8760	2.5	474	12.8	69	17	51

Figure 2.5: Baja California climate data

Surface transfer coefficients WUFI data required:

Heat transfer resistance: Heat transport is effectuated by several transport mechanisms: heat conduction through the air adjacent to the surface, convective transport by air flows, and emission of long-wave radiation. In the context of building physics modelling of all these phenomena is not complicated. For the temperature and flow situations encountered, a simple proportionality with a constant coefficient is usually adequate (heat transfer coefficient). The heat transfer coefficient consists of convective heat transfer coefficient and radiative heat transfer coefficient. WUFI employs the heat transfer resistance, which is simply the reciprocal of the heat transfer coefficient.

The thermal conductivity of adobe porous walls is moisture dependent. For higher water content, higher thermal conductivity implies lower resistance, the resistance values used range from 0.4 W/mKfor saturated walls, to 2 W/mK for dry walls (Rees2001)

The temperature dependent (also moisture dependent) thermal conductivity values were set up in the material data base, the initial water content set to saturation/dry conditions (for higher/lower thermal conductivity) the weather and interior conditions imposed would define the drying or wetting process. It was possible to observe some "material" temperature changes when varying the surface heat resistance (that, as mentioned before the WUFI uses to reflect the actual thermal conductivity).

Short-wave Radiation Absorptivity (s.r.a.): indicates the fraction of the total (i.e., long- and short-wave) solar radiation incident on the component surface which is absorbed. WUFI calculates the radiation load vertical to the surface from the data in the climate file, multiplies it - if positive - by the s.r.a. and applies the result as a heat source to the component. (If the radiation load computed from the climate data is negative, it is multiplied by the long-wave radiation emissivity.) For dark lime stone 0.6 and for oil paint green light 0.5 were the values used.

Long-wave Radiation Emissivity: during a clear night, radiation cooling may lead to a considerable drop in temperature at the component surface, due to emission of long-wave radiation. It can therefore be useful to treat this effect with more attention than is possible by the general radiation component in the heat transfer coefficients. The values used were 0.9 for dark limestone, and 0.95 for oil paint.

Vapour diffusion thickness: A surface coating e.g. paint coats, impede water vapour diffusion. Instead of including a separate, often extremely thin layer in the component assembly, the effect of the coating on water vapour transport can be taken into account by only applying a separate diffusion resistance at the surface. Adobe traditional surface coatings are mud plaster, lime plaster, white wash, stucco, paints (oil base, resin, emulsion) Portland cement washes, coatings of plant extracts, and coatings of fresh animal blood. The values used for the simulations were oil paint sd_value=1.5, and no coating

Initial conditions WUFI data required :

The temperature and the moisture field must be initialised with constant temperature across the component. The temperature values used were 12 and 32 °C for a hot summer and cold winter respectively. The moisture load was varied between high and low values.

Testing:

An experimental design described in appendix C illustrates the tests carried out. Also in this appendix are shown the results of such simulations.

Results:

Latent heat: The water condensing in the adobe wall must be able to dry out (moisture must not accumulate over time). Increased moist favours heat losses.

According to WUFI, the latent heat effects can be negligible depending on the heat source or sink when water condenses or evaporates. The hygrothermal simulations carried out in WUFI usually don't depend very sensitively on the precise values of the heat conductivities, so the difference may be negligible.

In the simulations carried out it was found that the factor with higher effect on the final moisture content was the weather conditions, followed by the heat resistance (and therefore the thermal conductivity) and the initial moisture content. Wall thickness, orientation, hygrothermal conditions, interior moisture load, and vapour diffusion thickness and radiation (absorption-emission values) had a lesser effect, in the order listed.

The effects of the enthalpy change (from water change of phase) of earth walls don't affect interior air temperature. The one dimensional WUFI software version used calculates a building component under given exterior and interior boundary conditions. Only uses this temperature as a constant boundary condition to obtain temperatures and humidity at the material's nodes (including the material boundary node). That is, the solution is not given as a marching problem (with heat transferred from the interior wall to the interior air altering the interior air temperature), but rather as a boundary value problem.

So, the question of determining the influence of the building components on the room climate by build-up in moisture, moisture and temperature buffering can't be answered with this software. And at the moment to the best knowledge of a WUFI employee, you cannot find any other software which could calculate this problem.

By varying the surface heat resistance it was possible to observe some material temperature changes, but for the same case including and excluding the latent heat of fusion and evaporation no change was found in the resulting surface temperature evolution, or heat flux. That is, heat transport calculations do take into account enthalpy flows through moisture movement with phase change (increased or reduced moisture content) by applying the corresponding moisture dependent thermal conductivity. But

WUFI hygrothermal simulations are only slightly affected by these heat conductivities. Also no latent heat storage is taken into account in the heat transfer computation. Materials with moisture dependent thermal conductivities have an important effect on the heat transport, as was observed in (Parra-Saldivar 2000). Also the latent heat storage modify significantly the heat flux balance, and hence should have a clear effect on the heat transport calculations.

Nevertheless, enthalpy flows modify moisture distribution within the material, as latent heat is taken into account for the moisture movement.

In this work it is proposed to improve this model by taking into account the latent heat storage/release due to the water change of phase for the heat transfer.

This can be solved by following a similar methodology as that was used to evaluate the PCM's heat storage. With the material surface temperature (initial boundary value), obtained with the heat flux balance on the boundary, and with the water vapour temperature profile obtained from the WUFI coupled heat and mass transfer, the temperature coefficients for the nodes are formed. The finite differences are solved to determine liquid fractions (amount of water changing state). Then the energy stored is calculated using the temperature-water vapour correlation. When the material has completely dried out or is completely saturated, according to the interactive weather conditions, the cycle starts again.

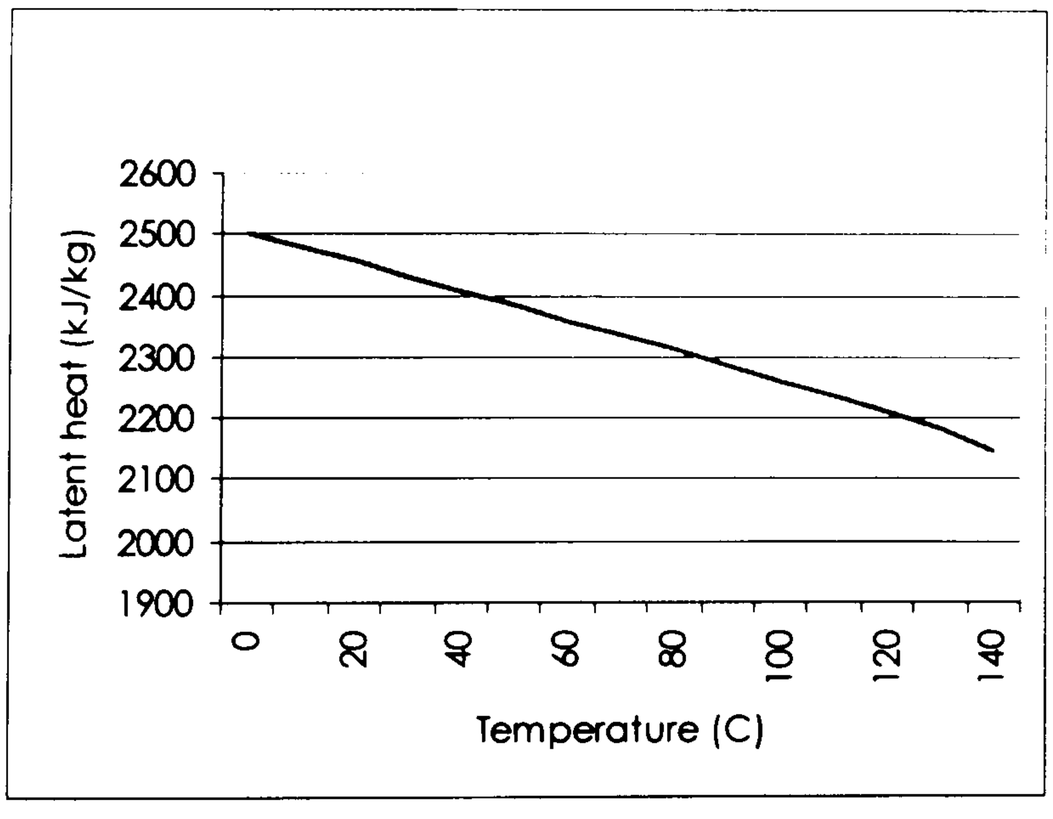

Figure 2.6: Latent heat of saturated steam

$$Est = WC * V_{wall} DH \quad \text{.....Equation 2.5}$$

where

Est= Energy stored (kJ)
WC= Water content (obtained from WUFI) kg/m3

V_{wall}= Wall volume, that in this case was set to 2.64m^3, used just for comparative purposes
DH= Enthalpy differencial (kJ/kg)

As an example, from the simulations shown in appendix 2.B , tests 2 and 3 were picked for the following analysis as to have reached the lowest and highest moisture content.

During the day peak hours the water vapour contained in the wall changes phase and releases the latent heat for vaporization (latent heat stored). Later in the evening, when the interior moisture conditions start to add up, and water vapour condenses, the wall starts to store heat again. (see Figure 2.7)

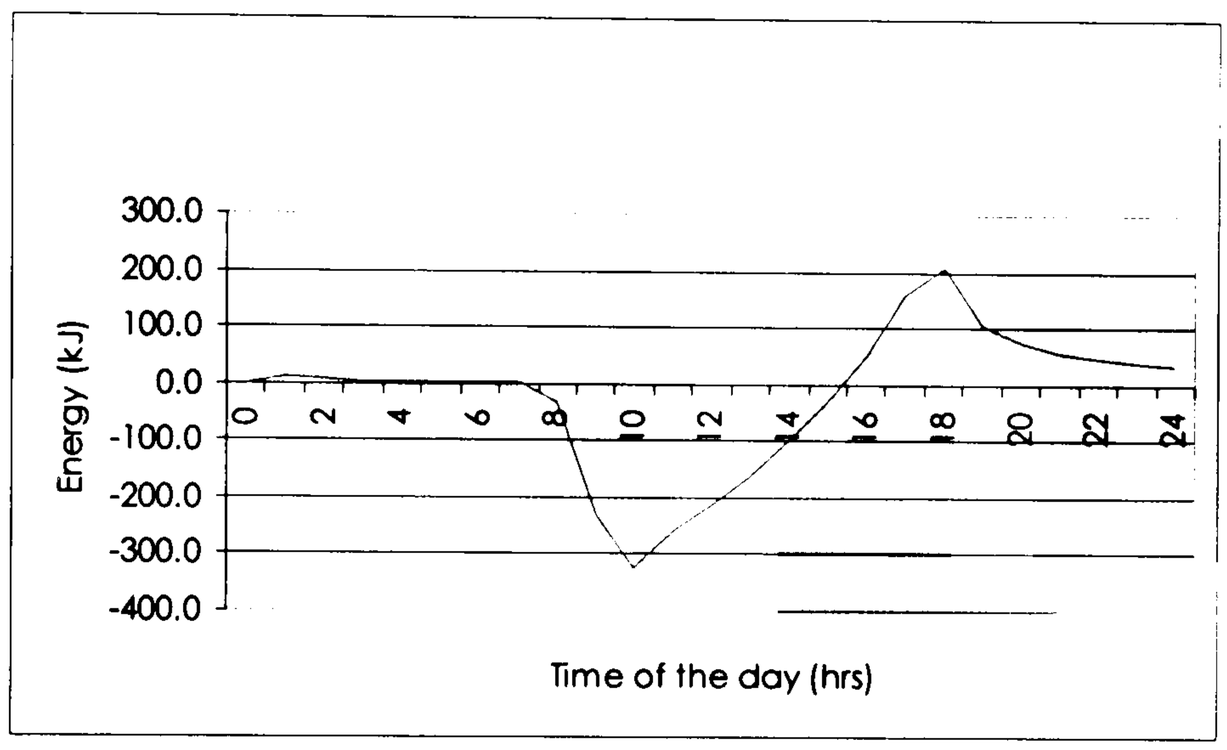

Figure 2.7: Energy stored/released evolution according to the water content, run 2

As we can observe from Figure 2.8, due to the initial conditions set for experiment three, in which a low initial air temperature is considered, provide the oscillatory behaviour of the heat released during the day. Nevertheless, the final energy stored is still larger than that obtained with run 2 conditions.

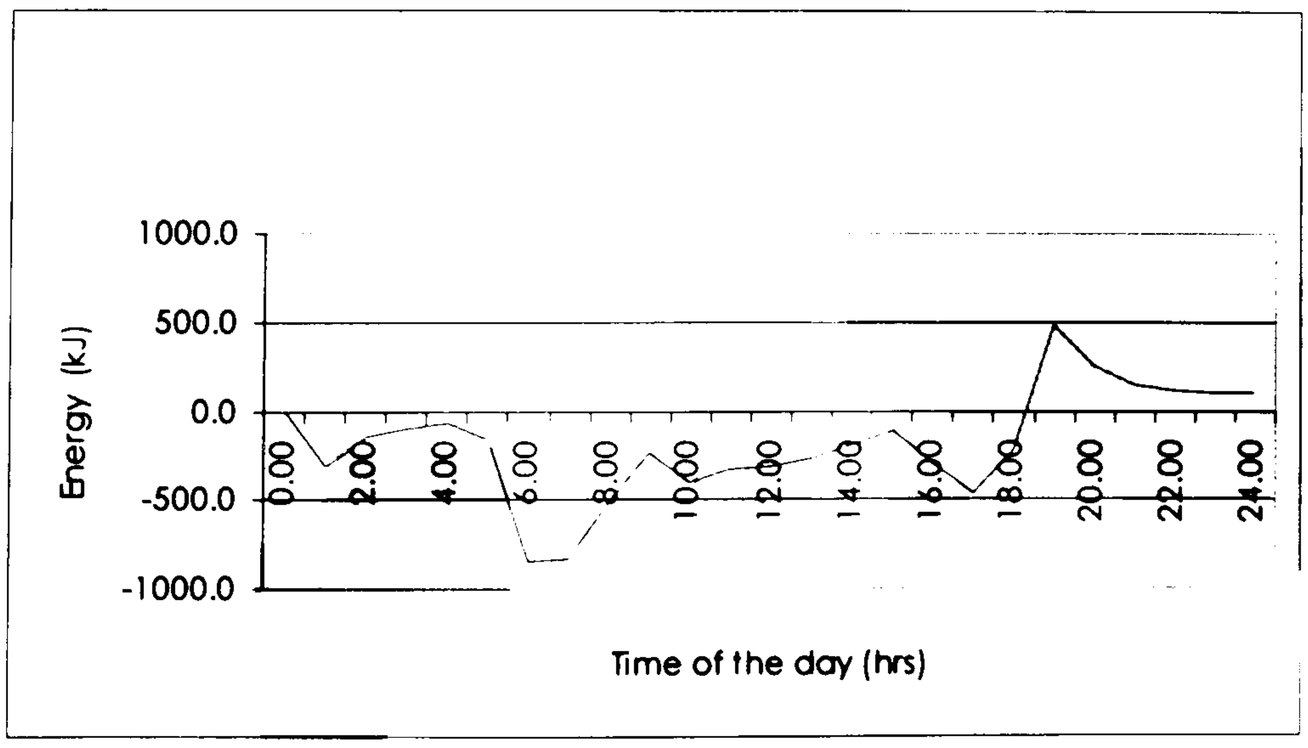

Figure 2.8: Energy stored/released evolution according to the water content, run 3

The largest amount of moisture is attained on the exterior layer (leftmost peak) of the wall, and it is there where the largest amount of energy is stored as we can observe in the next figure.

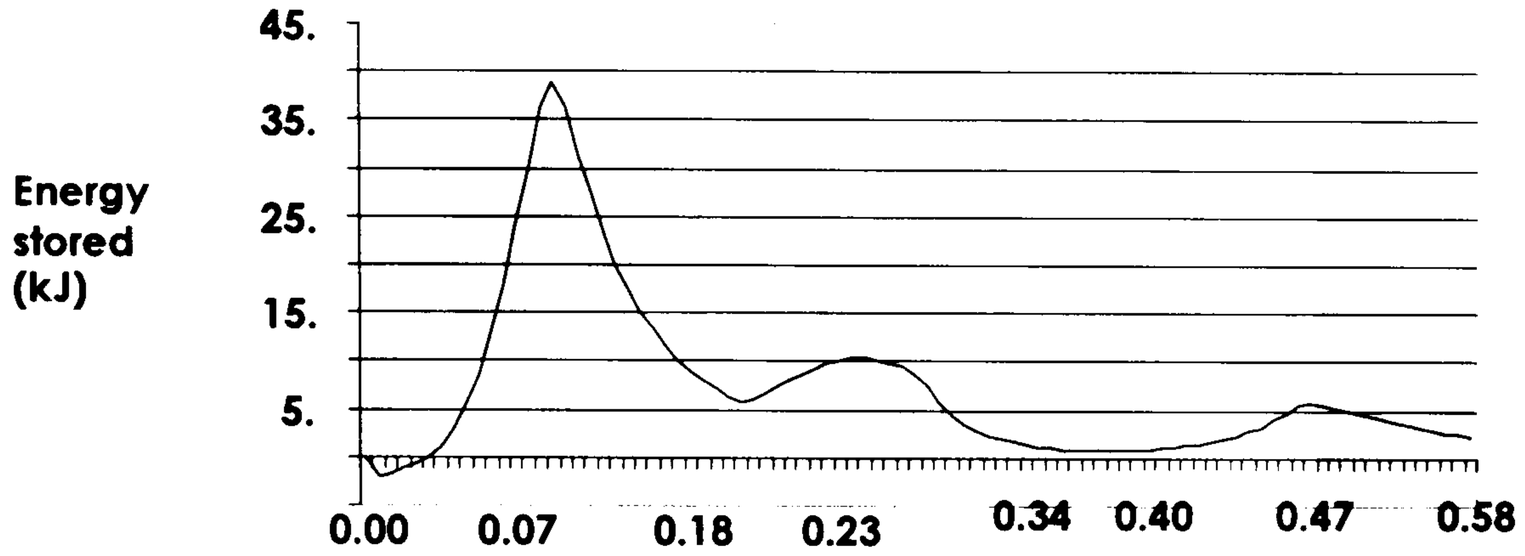

Figure 2.9: Energy stored profile according to the water content, on the 21st. of January at 0 hrs, run 2

As discussed for the previous graph, the wall layer facing the exterior stores the largest amount of energy as it was considered to initially have larger moisture content. As the conditions for this test are set for summer, high interior air temperature allows the lost of some of the moisture, and thus the release of some of the energy stored.

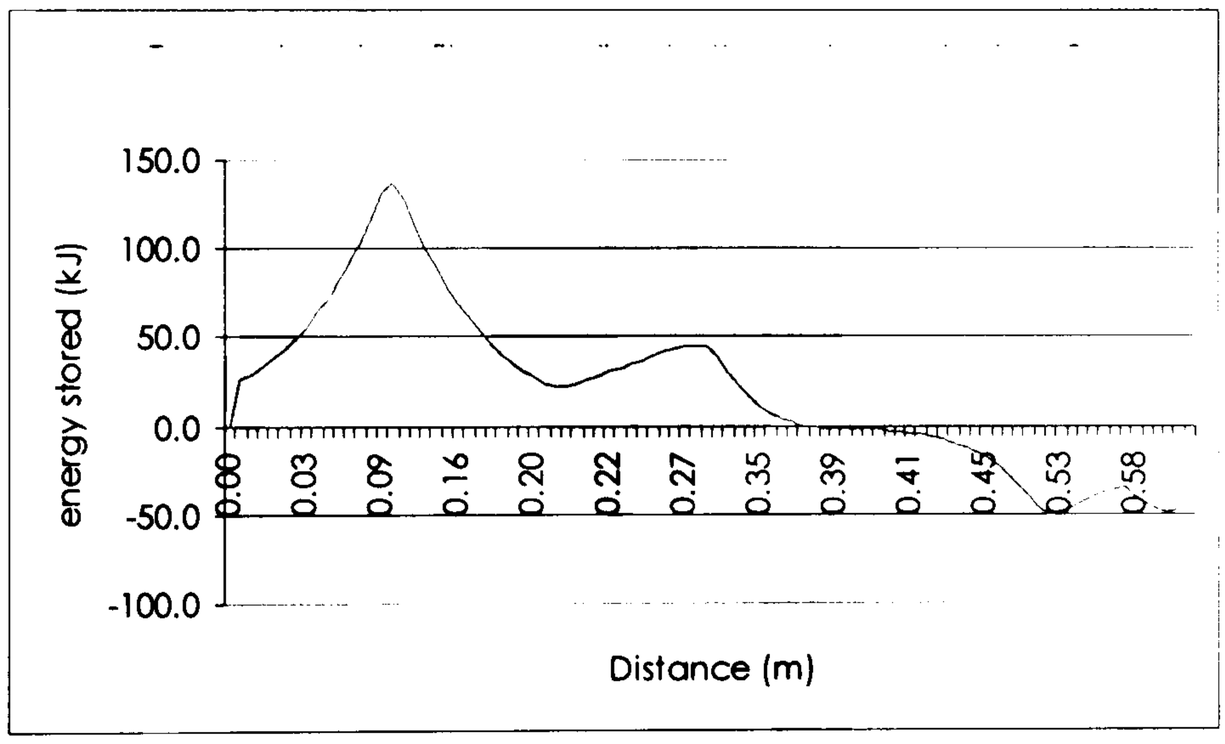

Figure 2.10: Energy stored/released profile according to the water content, on the 21st. of June at 0 hrs. ,run 3

The change in moisture content within the material shows that some of the contained water has been lost by evaporation or was acquired by condensation or capillary suction. Certainly the test with higher initial moisture content (run3) stores/releases more energy.

With the energy profile and the energy evolution (given in kJ), it is possible to obtain W/m^2, flux which must be included in the balance. Then, the material temperature must be affected by the heat added or subtracted for the water change of phase.

The construction of a building is responsible for a large percentage of the final energy demand, considering its later demolition the environmental impact is even higher. For example, the cement industry is responsible for more than half the CO_2 emissions in the industrial sector. The residues production of the construction sector is higher than the residues production on the urban sector.

Adobe constructions allow the reduction of CO_2 production as the bricks are sun dried. Adobe walls can be demolished producing a lot less environmental issues than ordinary buildings. Adobe walls high thermal mass and latent heat storage allow the modulation of the heat wave by passive means, reducing the size of heating and cooling power required.

Concluding notes regarding the adobe section

Adobe building systems for dwellings offer several advantages both structurally and thermally.

Structurally, as adobe walls are more homogeneous than the alternative brick and mortar systems commonly used in Mexico, joint failures are better endured. That is, adobe walls have a better weight bearing capacity and elasticity. The durability of the structure depends mainly on its water impermeability. Deterioration mainly originates due to shrinkage, thermal expansion and erosion associated to the presence of water, and salts intake.

On the other hand heat energy can be stored as sensible heat, latent heat, and chemical/physical reaction within adobe walls. The thermal behaviours of all three systems are strongly dependent on the hydration/dehydration of the clay, and the crystallization of the dissolved salts. Some of the main advantages of using clay for thermal storage are its porosity and large water absorption capacity.

Salts may be transferred into masonry by rising damp or due to its hygroscopic nature by ion attraction[2.46] to the surface of the clay, from the atmosphere and including organic molecules (Foley 1999). Stress produced by the accumulated salt crystals strongly affects the adobe brick's tensile strength.

Clay stabilization methods used so far, including the use of asphalt, concrete, lime, etc. intend to prevent the absorption of water, for improved structural behaviour. According to the Mexican building codes 2.5% maximum absorbed humidity is allowed.

[2.46] Related to the charged surface of clay

However, using water for thermal storage presents many advantages. For every degree of temperature difference, water absorbs and releases more heat than a number of substances. Because of the hydrogen bonding in liquid water, when changing phase from liquid to vapour (for chemical heat accumulation), the latent heat of vaporisation is fairly high. Furthermore, water is non-corrosive, non-toxic and is an inert chemical substance (Tahat, Babus'Haq et al. 1995)

The main disadvantage of an open system such as adobe for maintaining thermal comfort in a building is that its performance depends strongly on weather and ambient conditions. Sensible and latent energy transfers require a heat source or sink for setting up a temperature difference which would trigger heat and mass transfer, an increased heat capacity and a change of phase. But in particular, the fact that water is the central element for the changes that occur means that lacking its absorption by the wall would make the system thermally much less efficient.

Although adobe walls have a long tradition, and are accepted in many countries as a vernacular form of building, they are rarely utilised in the construction of modern cities. Many reasons may exist for this situation, but the variability of materials used for adobe construction, the need for nearby local sources of clay and a lack of large-scale manufacture means that adobe remains a largely rural expression of traditional building. Consequently, most current urban buildings will use concrete or other manufactured construction materials such as fired-clay bricks and tiles. To the construction industry these materials have predictable and reliable structural performance properties and so are preferred to adobe. These materials may provide designers with considerable thermal mass for sensible heat storage, but they lack the versatility of adobe materials

In non-adobe structures, heat storage systems that are independent of the structural element would be more versatile, as they could be applied as retrofit to old or as design elements in new buildings and they would be more suitable for current urban conditions. The application of such independent systems and their maintenance would not require major structural modifications to existing buildings. Independent thermal storage systems lend themselves to standardized industrial production.
For these reasons, structurally independent heat storage systems, based on sensible and/or latent energy storage for thermal comfort in dwellings, were considered for development and subsequently analysed.

That is, after the simulations were carried out, when I looked at adobe the important contribution of latent heat storage to the total energy stored draw my attention to systems based mainly on latent heat storage. Among these systems phase change materials offer several advantages as explained in the following section.

Latent heat storage using Phase Change Materials

Passive energy storage systems, typically aim to offer short-term energy storage with no fossil fuel derived external energy sources or mechanical means being used. In buildings the structural fabric collects and stores solar energy as sensible heat by taking advantage of their heat capacity, and consequently, restraining large interior temperature swings as the exterior temperatures increase or decrease.

But sensible heat storage has some disadvantages. It requires large massive or highly dense structures to generate the thermal mass effect. The price for such weight requirements can have important detrimental consequences. Sometimes extra insulation is required since thermal energy is lost as the amount of the stored thermal energy increases the material temperature. Energy cannot be stored or released at a constant temperature and may not be stored or released at useful times. The dense thermal-mass elements need to be supported and this may increase construction costs.

Latent heat storage is an attractive alternative to sensible heat storage. The so-called "phase change materials" (PCM's) undergo a change of state by absorbing and releasing heat at around their melting points in a generally isothermal process[2.47]. With the correct choice of PCM the indoor temperature may be maintained within a small range appropriate for human comfort, and this is also convenient for system control. Smaller volumes and masses for absorbing energy are required for the equivalent quantities of energy storage based on sensible heat[2.48].

However, their generally low thermal conductivity delays the heat storage process. To solve this, fins and high thermal conductivity containers can be used to increase the heat transfer rate. Also a holding structure or an encapsulation technique is required to handle the PCM volume change during solidification and drainage during melting. All these represent extra-cost in the production of such systems (Bader 2002). Regional variations have also to be taken into account. That is, the correct transition temperature and hence the PCM applied have to be designed for each climate region. Their application in building fabrics with no encapsulation can present hazardous conditions, bad odour and complications in controlling the system performance, and contamination.

[2.47] Interior air temperature remains constant

[2.48] The latent heat of most materials are large compared to their heat capacity. For example, in the case of water, 80 times as much energy is required to MELT one kg. of ICE as to raise the temperature of one kg of WATER by 1°C. This means that a much smaller weight and volume of material is needed to store a certain amount of energy

In this part of the chapter a small preface is given on the PCM thermal transition stages, their classification, and their application for industrial processes and dwellings. As this project is concerned with dwellings the system's efficiency, manufacture and the actual incorporation and utilization of PCM energy saving systems in domestic scale buildings are discussed.

Thermal transition stages of the PCM

Differential Scanning Calorimetry is a technique used to study the thermal transitions[2.49] of polymers. Using a Differential Scanning calorimeter (DSC) it is possible to measure the latent heat of fusion, the specific heat and the melting temperature of a polymer (Sharma, Buddhi et al. 1999)

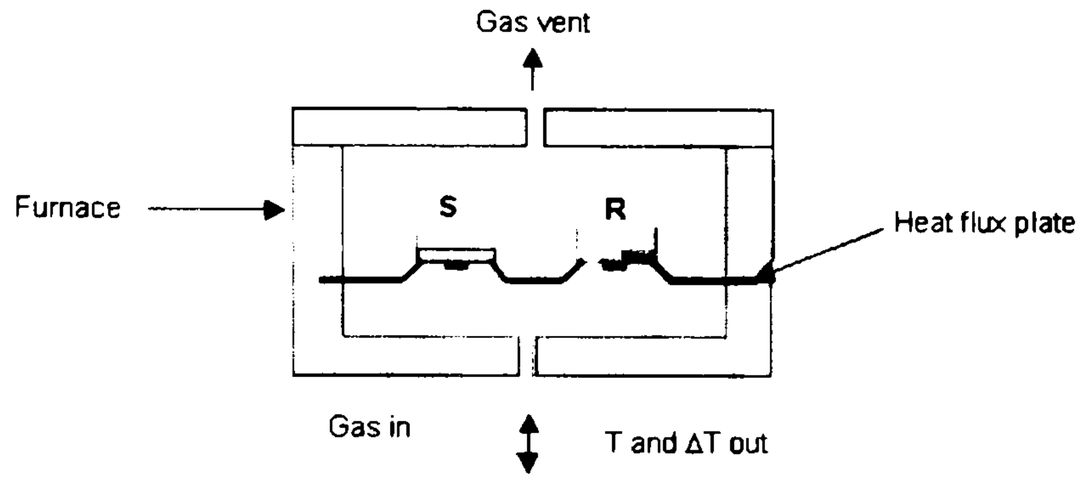

Figure 2.11: Schematic of a DSC chamber (S: sample pan, R: reference pan)

A schematic of a DSC is shown in Figure 2.11 where the sample (solid polymer) and the reference (empty) pan are heated at the same time and at a constant rate. A number of transitions can take place as the polymer sample is heated or cooled:

Glass transition[2.50]: The polymer absorbs heat and undergoes a change in its heat capacity; it is able to take in more heat with smaller rises in temperature.

Crystallisation[2.51]: When the polymers have gained enough energy to form crystalline arrangements, heat is released. The heat required in the sample pan to keep the temperature of the sample pan rising is reduced.

Melting: if heating continues beyond the polymer's crystallisation temperature another transition called melting is attained. When the polymer's melting temperature is reached the polymer crystals start to disintegrate, that is: they melt (by absorbing heat).

The first order transition[2.52] is reached and the polymer's temperature won't increase until the crystals have melted[2.53]. This means that the sample

---

2.49 Thermal transitions: changes that take place in a polymer when it is heated

2.50 During the glass transition only a change in the heat capacity takes place; there is no heat stored or discharged. As there is no latent heat involved it is called a second order transition (DPSUSM)

2.51 The rate of crystallisation or solidification restrains the rate at which thermal energy can be withdrawn from the PCM storage

(polymer) pan will require more heat in order to both melt the crystals and keep the temperature rising at the same rate as that of the reference pan[2.54]. When the polymer has melted completely, its temperature will increase for a second time, at a lower rate (DPSUSM 2003)

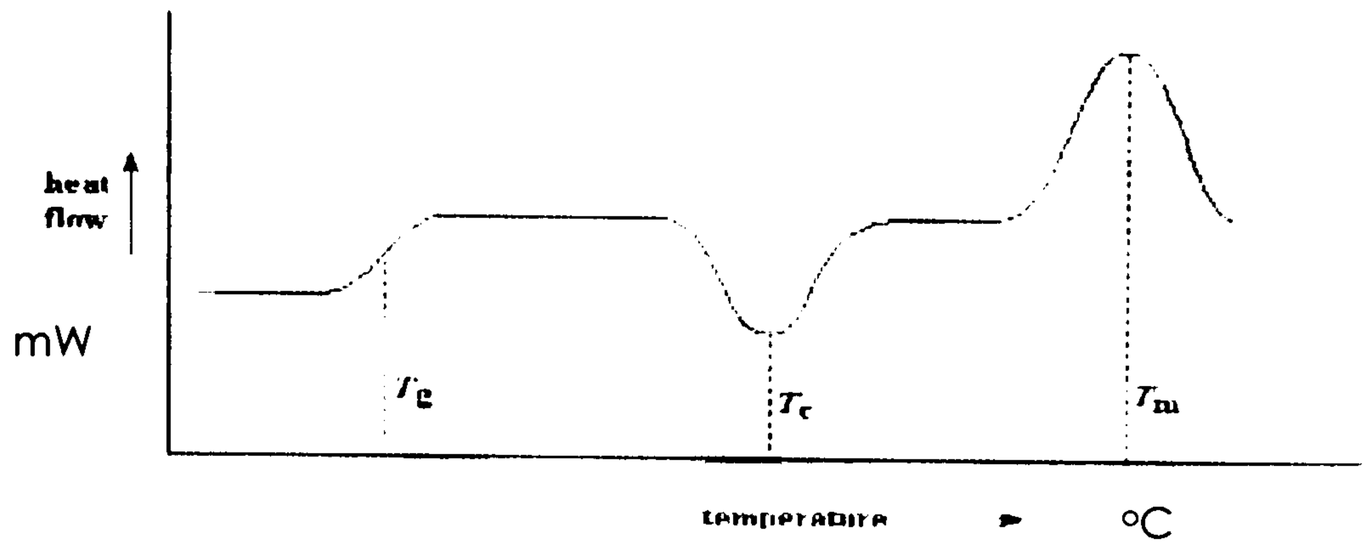

Figure 2.12: DSC schematic plot of the thermal transition stages of a typical polymer based PCM (DPSUSM 2003)

PCM's Classification

PCM materials can be derived from a number of different sources.

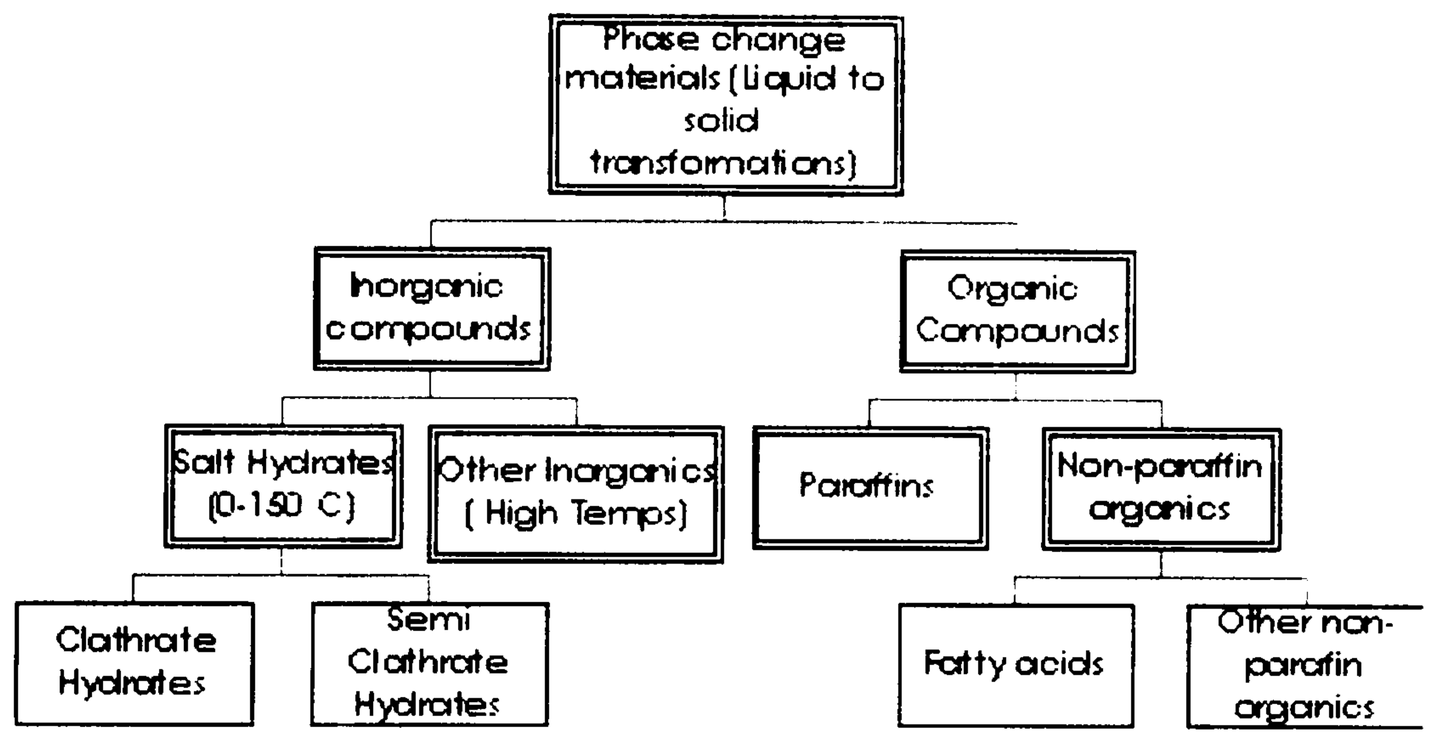

Figure 2.13: PCM's liquid to solid transformations classification scheme

Inorganic compounds: include

- *Salt hydrates*[2.55]

Advantages:

[2.52] Any transformation occurring due to heat (melting, freezing, boiling, condensation) which has a change both in its heat capacity and latent heat involved, is called: first order transition.
[2.53] The temperature rising stops because melting requires energy. All the energy supplied at the polymer's melting point is undertaken for the melting, and none of it goes into increasing the temperature, this heat is called the latent heat of melting.
[2.54] The temperature holds steady despite that heat is added to the polymer, until the polymer has melted entirely.
[2.55] Salts chemically combined with water and form hydrates, i.e. sodium sulfate Decahydrate (Glauberis salt), calcium chloride hexahydrate, etc.

1) They have high volumetric storage densities due to their high latent heat and density
2) Have relatively high thermal conductivity
3) Are better economic choices for commercial development
4) Not flammable
5) Large range of melting points (between 0 and 120 °C)
6) Have the most appropriate chemistry to base research into stable, consistent and reliable energy storage

Drawbacks:

1) Supercooling[2.56] during solidification: A solid structure can't develop without a nucleus to trigger the crystallisation. The liquid phase is sustained until the dynamical arrest[2.57] temperature is reached, then the liquid solidifies into an amorphous non-crystalline solid. Supercooling can be prevented by including nucleating agents or by assisting nucleation by rough container surfaces.

2) Incongruent melting[2.58]: If not enough hydrated particles are formed to dissolve the solid present, the solid, which is denser, descends to the bottom of the container. A substantial part of the settled salt is unable to come into contact with water for rehydration into the crystalline form, resulting in irreversibility of the process (Garg, Mullick et al. 1985)

3) Phase segregation When a material has incongruent melting (i.e. complete melting is not achieved) the density discrepancies among the solid and liquid phases will produce segregation, resulting in changes in the chemical composition of the material (Garg, Mullick et al. 1985). To prevent phase segregation it is possible to use thickening agents, encapsulate[2.59] the PCM's and use rotating storage devises.

4) Corrosion: Some hydrates may be very corrosive , which limits the types of materials that can be used to contain them and often excludes metal containers.

5) Encapsulation methods have presented difficulties (originating distortion on the chemical structures and consequently unreliable heat control).

2.56 Is the cooling of a liquid until transition temperature (freezing point) without the transition occurring (solidification).
2.57 Also called gellation or jamming, is the 'transition' of a liquid to a 'solid-like' but non-crystalline substance, by modifying some physically relevant parameter (as temperature, density, pH, etc). Molecules or particles basically halt their movement.
2.58 The property exhibited when a solid does not simply melt, but reacts and decomposed to form another solid plus liquid neither of which has the composition of original solid.
2.59 The macro-encapsulation of PCM's can refrain large phase separations, boost the heat transfer rate, and offer a self supporting structure for the PCM. Salt/ceramics is PCM micro-encapsulation within the pores of a ceramic matrix.

- *Other inorganics*

- Salt mixtures: *Eutectics*[2.60] perform in a similar way to congruent melting salt hydrates (Hasnain 1998)

- Metals and Alloys

Organic Compounds

- *Paraffins*[2.61]

Advantages:

1) Have high heat of fusion[2.62] : Due to its high internal energy more energy is stored in small volumes.
2) Negligible super cooling
3) Self nucleating
4) No phase segregation
5) Chemically inert and stable
6) Commercially available at sensible prices

Drawbacks:

1) Low thermal conductivity: High thermal conductivities allow small temperature gradients for storing and releasing energy[2.63] (Hasnain 1998)

2) Undergo large volume changes during phase transition (which is in the order of 10%) (Farid, Khudhair et al. 2004)

3) Pure paraffin waxes are expensive, hence only technical grade[2.64] paraffins can be used for latent heat storage and these tend to have extended melting temperatures.

4) Flammable: Serious potential fire-hazards are present as paraffins remain flammable in normal atmospheric conditions. It has been suggested to constrain the PCM wallboard saturation to 20% and treat the PCM with insoluble fire retardant. (Lawrence Berkely)

- *Non-paraffin organics*
- Fatty acids[2.65]:

[2.60] Are mixtures of two or more crystalline substances which have a lower melting point than that of any of its constituents.
[2.61] A group of high molecular weight alkane hydrocarbons referred to as methane series or as paraffins, obtained by fractional distillation from petroleum. Their melting points range between 6 to 80 °C
[2.62] Latent heat of fusion: is the heat required (supplied) to melt a substance. The latent heat of freezing is the energy released by a substance when it solidifies
[2.63] Metal matrix structures and fillers can be used to enhance thermal conductivity
[2.64] Technical grade paraffins are mixtures of many hydrocarbons and therefore, have a melting temperature RANGE, rather than a sharp melting point .(Hasnain, 1998)
[2.65] Derived by the hydrolysis of the ester linkages in a fat or biological oil (both of which are triglycerides), with the removal of glycerol

1) Are highly available as by-products of various industrial processes. Fatty acids, such as capric, lauric, palmitic and stearic, are found in abundance in animal fats as well in cotton seeds, corn, soya, coco, and palm oils.
2) Their melting ranges are suitable for building applications.
3) Because of the protected carboxyl group they are chemically stable, and not affected by normal temperatures and climatic conditions
4) In addition they are non-toxic and moderately fire safe.

- Alcohols, glycols and polyhydric alcohols

PCM's selection criteria

The following selection criteria are regarded as important when considering the application of PCms:

- Suitability for the required range of melting and freezing: The transition range temperature for charging and discharging must meet the intended operating temperature.
- Large latent heat of transformation
- Suitable density: High enough for containment of heat storage in smaller volumes and low enough for the holding structure bearing limitations.
- High specific heat and thermal conductivity: for high heat storage system capacity
- Little or no super cooling
- Chemical stability: to minimize the detriment of system performance, and hazardous conditions.
- Melting/freezing point congruency
- Low vapour pressure at room temperature
- Availability and low price
- Compatibility with building fabrics
- Feasibility to control volume changes during phase change: Low encapsulation cost

(Feldman, Banu et al. 1995)

Phase Change Materials applications

According to the application (operating temperature required), the PCM studies are classified in two groups:

Industrial PCM thermal storage applications:

Requirements for comfort have increased over the years. Demand for hot food (pizza, coffee), cold food products (ice cream); comfortable homes, offices, and factories make claims for better heating and cooling systems. Effective management of thermal energy can also respond to other practical uses such as feet warming when it is cold; freeing the roadways of

ice; and, keeping vaccines at the right temperature to be safe and effective.

Following some commercial uses of PCMs will be listed. In some cases data is available, but it is presented only for illustrative purposes, that is, there is no reference of scientific proof provided by the manufacturers.

Low temperature applications:

The main PCMs employed have been inorganic salt mixtures, such as sulphates of magnesium sodium, and potassium; sodium, ammonium, calcium, or magnesium Chlorides (Tomlinson.J). The companies that manufacture the PCM container systems (cold packs[2.66] and cooling gels, metal containers, etc) keep confidential the information on the specific PCM used. Nevertheless shipping and storage containers (using a wide variety of PCM's) for all types of applications and temperatures are offered. Some examples are given next.

Low temperature applications:	Application	PCM Type
Low-temperature storage for food preservation and transportation	cold accumulators (cooling plates) for food refrigeration (temperature should be kept between 0° to 4°C).	Low temperature melting salt mixtures packed in metal containers (McGuffey 1947).
Biomedical and biological carrying systems:	temperature-sensitive pharmaceutical products (such as vaccines, protein-based drugs, etc) must be kept frozen when transported. Human parts transportation (e.g. cornea) should be maintained in a specific temperature range of 2-8oC	The standard approach is to use thermal packaging (polyfoam), which includes a –15°C melting point PCM, which keeps products below –10°C for five days.A commercial PCM product called Phase 5 can be used for the required temperature range.
Heat Sinks for electronics and enclosures	Made of channels or pin fins that incorporate phase change materials using only passive cooling means for cooling (natural convection and radiation heat transfer modes) (J. Marongiu and J. Marongiu)	
Body-cooling systems (clothing and Outerwear)	To remove metabolic heat from the body and to block heat exchange with the outer environment. Mainly used for exposure to elevated environmental temperatures (in occupations ranging from deep mining to aerospace industries).	Solid carbon dioxide or dry ice with a solid to gas transformation utilising a latent heat of vaporization of 547 kJ/kg, and a cooling capacity of 682 kJ/kg when used to cool humans.
To decrease swelling in patients	Sports doctors and hospital institutions use cool packs consisting of low temperature PCM stabilized in a super cool state and a nucleating material. The breaking of a seal that divides the two materials causes their mixing, resulting in crystallization, cooling occurs as proc. progresses.	

Table 2.9: PCM low temperature applications. (McGuffey 1947), (J. Marongiu and J. Marongiu),(Schutte, Klerk et al. 2002)

[2.66] Commercially available cold packs contain a small quantity of ammonium nitrate, which is separated from water by a thin membrane. When the pack is struck with the palm of the hand, the membrane breaks and the salt dissolves in the water, producing an endothermic chemical reaction, thereby providing cooling. Based on solubility and enthalpy of reaction, ammonium nitrate has great potential for use in endothermic cooling systems (Matesa, 2001).

High temperature applications

For warmers and products to keep things warm/hot the main PCM's used are hydrated salts with melting temperatures ranging from 29 to 89 °C, as well as paraffin and synthetic waxes with melting temperatures from 0 to 148.9 °C (TEAP)

High temperature applications:	Application	PCM Type
Portable warming containers, and hot plates for food warming	food can be maintained at around 60 °C for serving in restaurants, and food delivery	Hydrate salt called TH 58 °C (TEAP),PCM properties: latent heat of 80.7 W-h/L, solid sensible heat of 1.12 W-h/L °C , liquid sensible heat of 1.63 W-h/L °C , and a useful temperature range from 55°C to 61°C PCM (additives are used for stability after cycling).
Thermos flasks (hot bottle):	Consisting of acetic acid sodium salt (sodium acetate, with melting point 300 °C) and sodium thiosulphate (with a density of 1.528 g/ml and a melting point 48C) mixed with fine sand, gravel and metals. The PCM contained on the cavity wall surrounding the bottle is fragmented along the surface when shaken, to release the nucleating agents and activate crystallisation. A flask to heat baby's milk is also on the market (ideas patented by Crooker. H.L, and Othmer. D.F)	
Cold weather clothing	The original idea (patented by Mauleos and Davy) was a suit designed to be used by divers, explorers and aviators. This is used for survival clothing (extreme sports, police and military).	It contained lithium hydride (with density of 0.82 g/ml, and melting temperature of 680 °C) with water circulating round the suit by a heat exchanger. Currently, microcapsules containing paraffin, are used to thermo-regulate body temperature. Feldman patented rescue bags with a rubber sponge saturated with an inorganic salt hydrate with a melting point between 28 - 45 oC
Therapeutic pads	Originally, sodium metaborate, a silvery soft waxy metallic element of the alkali metal group was used, currently sodium sulphate (Glauber's salt, with a density of 1.46 g/ml melting point at 32 °C) is used for hot packs. Heat packs have a higher melting point than the cool packs. The heat generated will last 2 to 3 hours depending on the size, insulation and external conditions. The crystallization is triggered by a bending a stainless steel button inside the vinyl pack.	
Solar dynamic power system spacecraft	The energy stored is used for the operation of a heat engine in orbital eclipse periods. This idea was proposed to be used in aircrafts as a cylindrical receiver placed at the focal plane of a solar concentrator.According to Frysinger & Sliwkowski a PCM was used in the Apollo 15 space program to release the heat load from the computers, electrical equipment and the Rover Vehicle (Vener 1997)	Canisters operating with high-temperature PCM's are used for efficient storage of thermal energy. Lithium fluoride is suitable for its high heat of fusion, appropriate melting point (998 oC) and long-term stability (Kerslake and Jacqmin 1991).
Piping	Oil piping efficiency depends on its flow consistency, which is depends on the temperature conditions to which it is exposed. In locations where temperatures reduce the optimum flows (for instance deep sea), PCM can be incorporated to provide an efficient and steady flow of oil at all times (TEAP)	

Table 2.10: PCM high temperature applications. (TEAP), (Kerslake and Jacqmin 1991),(Vener 1997)

PCM applications in dwellings

The main purpose for utilising PCMs in dwellings is to use off-peak electrical energy space heating/cooling. The PCM transition range temperature for charging and discharging will depend on the location (weather conditions). The weather conditions in human settlements range from extreme cold at -50°C (during winter in the in north-eastern Siberia) to extreme hot at +50°C (daytime summer temperatures in the Sahara). An ideal thermal storage system in the heating mode for a cold climate would be fully charged in 7 hours maximum, and discharged during the rest of the day, and vice versa in the cooling mode(Scalat, Banu et al. 1996).

Fundamental theoretical and experimental studies are available in the literature concerning latent heat storage/discharge. A range of PCM systems existing as either bare formats, e.g. wallboards where the PCM is contained within the pore matrix of the material, and encapsulated formats in cylinders, spheres and flat geometries (P. Brousseau) have been studied. Heat exchanger proposals range from coils, cans, and disks either surrounded by or containing heat transfer fluids (Neeper 2000). Next some applications in buildings are considered.

PCM applications in dwellings	Generalities	
Thermal storage batteries	First used in trial house named "The Dover House" proposed by Dr. Maria Telkes in 1946. According to Frysinger & Sliwkowski glass panels collecting solar radiation passed the heat energy collected (by circulating heated air) to metallic drums filled with Glauber's Salt with a potential heat storage capacity of 11MJ (representing 12 days heating load). Initially successful the stand-alone system provided an indoor temperature of 21 °C, but failed after 3 years. According to Lane, in later attempts to improve the performance nucleation and thickening agents, borex and sodium silicate were added to the Glauber's salt, as well as corrosion inhibitors such as chromate (Vener 1997). El-Dessouky studied a double-pipe heat exchanger containing either paraffin wax grade 116 or calcium chloride hexahydrate. Banaszek proposed spiral heat exchanger. Air passed through a concentric spiral passage surrounding one that contains paraffin wax PPW-20.	
Encapsulated PCM's	Application	PCM Type
PCM radiant warming system encapsulated in a conical shaped container	A system called TEA29 provides floor warming, giving a floor surface temperature between 24°C and 26°C (maximum suggested for walking comfort) in order to provide an interior room air temperature of 20°C	Water heated in a roof solar panel is pumped through pipes to the thermal storage bank. The under-floor thermal bank absorbs or releases heat when exposed to temperature variations above or below 21°C. The PCM used is a mineral salt composition with a melting point of about 29°C. The PCM is injected into the thermo-formed capsules of high density polyethylene PVC. The capsules are then hermetically sealed with an aluminium faced polyethylene PVC/polyester cover strip (J. Marongiu and J. Marongiu)
Roof/ceiling PCM-insulation encapsulated in tiles	This system consists of two PCM pouches moulded inside fibreglass-reinforced polymer concrete tiles. Glauber's salt is used providing 920kJ latent heat storage capacity. Typical applications include floor constructions within sun rooms, ceilings, bench tops and window seats (Vener 1997). TEAP manufactures a PCM and insulation system for roof/ceiling applications, to increase the effective R-value performance in buildings. TH24 / TH 29 hydrated salt with a latent heat of 79 Wh/L are used. Heat transferred to the building interior is reduced by 75%, thus load requirements, and air conditioning system running costs drop (TEAP). Tiles could also be used in paving materials to reduce night time icing on bridges and overpasses, whilst also minimizing surface damage from freeze-thaw cycling (EERE)	
Panels encapsulating PCM's (for a wide range of applications)	A panel that uses 8.4 kg of calcium chloride hexahydrate (melting temperature of 27°C) encapsulated by a rotational moulding process inside a low density polyethylene structure, is available on the market. The thermal storage capacity provided is 1.6MJ (Vener 1997)	
PCM integrated by encapsulation within cavities in building fabrics	These systems incorporate the PCM's within a timber stud, masonry cavity wall construction, behind a single glazed screen or mounted within a sun room behind glazing. Their purpose is to provide thermal storage by maximizing the use of the structural elements by using them as PCM containers i.e. they hold considerable quantities of PCM	
Heat storage, distribution, insulation and shading by PCM encapsulated in rotating rods	A module contains a chain of PCM filled rods with a total capacity of 2MJ. The rods are rotated by automatic controls, displaying either a black surface (for radiation absorption) in the heat-storage mode; or a reflective surface (for heat rejection in summer) covered with insulation (for heat retention) during night time. Heat released from rods is spread into the room by fans (Vener 1997)	
PCM encapsulated in spheres (for a wide range of applications):	TEAP has attained encapsulation of a range of PCM's from -31°C to 89°C in spherical, cylindrical and micro-encapsulation shapes. Spherical capsules of Polypropylene have 75 mm outside diameter, are 1.2mm thick, and weight 210 grams approximately (175 grams of PCM per Ball). Micro-encapsulation is valuable in the building product industry for concrete, wallboard and fiberglass insulation (TEAP)	
Impregnated drywalls	Feldman studied wallboard impregnation with esters of fatty acids. The thermal characteristics of some Methyl Palmitate- Methyl Stearate mixtures alone and loaded in wallboard can be found in Feldman, Banu et al. 1995	
Heat pumps	It is possible to decrease the cost of heat pumps, and increase their efficiency by incorporating thermal storage in the system. The required heat pump size is reduced, and the heat pump is allowed to operate at lower condensing temperatures. As the heat pump size is reduced, it will run for longer periods (to satisfy a given load), reducing the on/off cycling losses (Esen 2000)	
Air Heating Systems	As PCMs can be placed in any container shape. The latent heat storage of the unit is lightweight compared with a sensible storage system, and its storage capacity is larger (RUBITHERM)	
Boiler	Electricity consumption, CO_2 emissions and thermal losses can be reduced by using a PCM hot water system	The PCM used is an hydrated salt TH 89 with high density of storage: 70 kWh/m^3 , and it is encapsulated in plastic tubes (RUBITHERM)

Table 2.11: PCM dwellings applications. (Vener 1997), (El-Dessouky and Al-Juwayhel 1997), (Banaszek, Domanski et al. 1999), (J. Marongiu and J. Marongiu), (Vener 1997), (TEAP), (EERE), (Esen 2000), (RUBITHERM), (RUBITHERM)

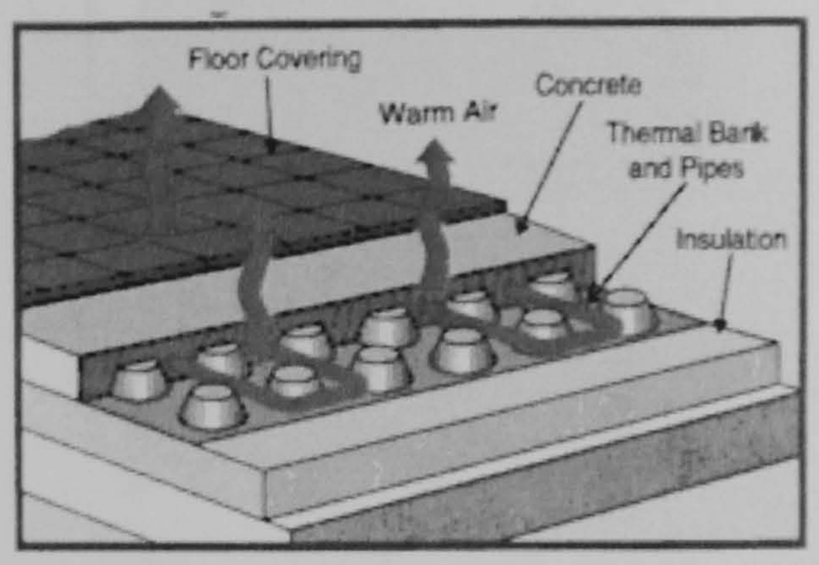

Figure 2.14: Conically shaped PVC encapsulated PCM and HTF in tubular container heat exchanger for floor radiant warming (TEAP)

Methods for drywall or wallboard PCM incorporation

1) By using pellets of high-density polyethylene (HDPE) filled with melted paraffin, merged in wet gypsum and compressed in sheet form(Garg, Mullick et al. 1985)

2) Saturating the wallboard by immersing conventional wallboard into containers of constant temperature melted wax. The PCM in the liquid phase is held by surface tension in the pores of the supporting material (Scalat, Banu et al. 1996).

The porosity of the host material, determines the amount of PCM that can be contained within the capillary structure. Depending on the desired saturation (PCM absorption) the immersion time varies up to 10 minutes for about 30% of composite weight absorbed PCM. (Feustel and Stetiu 1995).

Regarding volume changes during phase change, paraffins undergo a 10% reduction in volume on crystallisation (Farid, Khudhair et al. 2004). The joint effect of capillary forces of the host material and cross-linking additives will prevent leakage of the PCM, even if in the liquid phase. Available air spaces (within pores) allow for solidification expansion, and the change of phase goes unnoticed.

Wallboard immersion can achieve a higher storage capacity than the wax filled pellets added to wallboard (Feustel and Stetiu 1995)

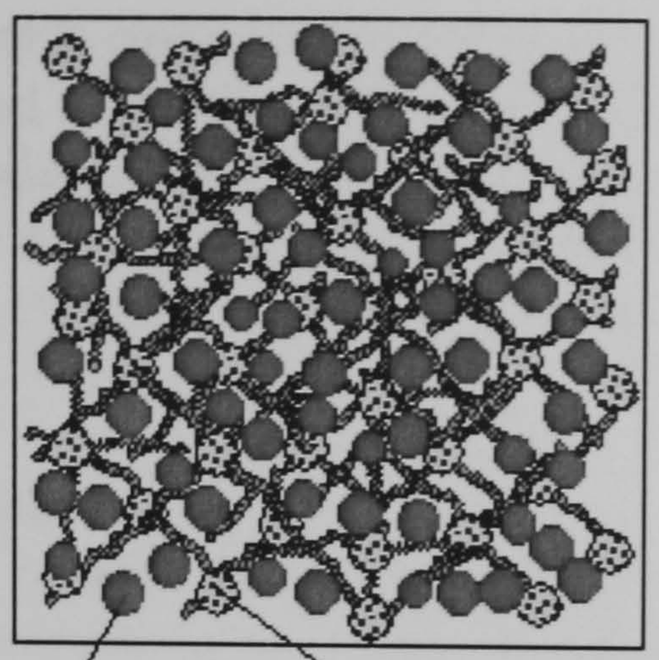

Figure 2.15: PCM gel like behaviour when PCM is in liquid state in a wood fibre or gypsum board (RUBITHERM)

Charging and discharging a PCM unit for building applications.

The amount of energy and the rate at which it can be passively absorbed and released is influenced by:

- PCM thermal conductivity (and diffusivity)
- Air Velocity
- PCM latent heat of fusion
- Melt temperature (or the temperature range over which the melt occurs)
- PCM specific heat
- PCM viscosity (Hamdan and Elwerr 1996)

According to Velraj one of the major drawbacks of latent heat storage is the PCM's undesirable low thermal conductivity, which slows down the heat transfer process for energy storage and release (Velraj, Seeniraj et al. 1999)

Previous observations have shown that air velocity control is especially critical for heat storage/release in locations where a large range of temperatures takes place. Recommended charging velocities are in the 4-5 m/s range while those for the cooling mode must be about 1.5 m/s (Lee, Hawes et al. 2000). Heat storage is insensitive to variations in heat transfer coefficient if latent heat storage, depending on the transition temperature, occurs outside room temperature variation range (Neeper 2000)

One of the major advantages of latent heat storage is the large total energy densities associated with most PCMs. A proper selection of the PCM (melting point) in relation to its application is crucial for the maximum exploitation of this asset.

Depending on the type of application, heat transfer might need to be enhanced either for charging, discharging or both. For example

discharging enhancement is desired when heat is available at a continuous rate for a longer time, and it needs to be discharged in a shorter time, as in domestic hot water applications. On the other hand in discontinuous processes (such as waste heat recovery) where a vast quantity of heat is to be stored in a short time, charging enhancement is required (Velraj, Seeniraj et al. 1999)

Charging/discharging rates:
In order to select the proper PCM transition range temperature, it is necessary to know the temperatures under which the system will operate. If the PCM is inside the building envelope (as for example interior wallboard wall), the average temperature of the system is the same as the average room temperature. If the PCM is also exposed to the exterior (as for example an exterior wallboard wall), the system's temperature is a mean value between the average room and average outdoor temperatures.

When the PCM melting temperature equals the system's temperature in the actual conditions, the system operates at its maximum capacity, for heat storage. When the room temperature starts differing from the melt temperature, the energy storage is reduced. Once the room temperature decreases below the melting temperature, the inverse process is started, and the energy stored is released. Although the total latent capacity of the wallboard is unchanged, the daily energy storage can be severely reduced if the room temperature is markedly different from the PCM transition temperature; since the room temperature prevents the phase transition from taking place (Neeper 2000).

When the system is heated by solar radiation, a melt temperature between 1-3°C above the room temperature is considered to be the optimal (Peippo, Lund et al. 1999).

Efficiency of a PCM thermal storage unit.

The main parameters for thermal storage system design (to define suitable storage system type and capacity) are:

i) Heating or cooling energy requirements
ii) Diurnal temperature ranges for the year
iii) Heat energy sources available
iv) Regarding the heat transfer fluid (HTF) supply (i.e. air) to define the way in which it is to be heated/cooled, humidified/ dehumidified, delivered and returned (Lee, Hawes et al. 2000)

The efficiency[2.67] of a storage system can be defined by

[2.67] Ratio of the effective or useful output to the total input in any system

- The first law efficiency (i.e. energy analysis, conservation law): This estimates the total energy stored in a system which can be recovered (Dincer 2002)
- Second law efficiency (i.e. thermodynamic entropy law): Shows how well available energy is used. Optimal thermal designs (for useful work storage, rather than energy storage) given by the attenuation of entropy generation were first studied by Bejan (Bejan 1996). Bejan evaluated entropy generation numbers[2.68] for only the thermal energy storage process. The point of maximum entropy generation number presents the condition of minimum second law effectiveness. (El-Dessouky and Al-Juwayhel 1997)
- Exergy[2.69] analysis is derived from both, the conservation of mass and energy principles, and the Second Law of thermodynamics. It integrates the concept of growing thermodynamic unavailability by taking into account the quality (availability) of the recovered energy (Bascetincelik, ozturk et al. 1999). Krane (Krane 1987) adapted and completed the second law analysis of Bejan to simulate the complete storage–removal cycle of a storage system. Exergy analysis can reveal whether or not and by how much it is possible to design more efficient energy systems by reducing the inefficiencies in existing systems.(Dincer 2002)

To estimate the efficiency of design and operating parameters of a heat storage system, it is necessary to specify:

- Thermophysical properties of the heat transfer surface
- Thermophysical properties of the storage materials and the heat transfer fluid
- Operating fluid inlet temperatures during the cycling process (heat supply and recovery) (El-Dessouky and Al-Juwayhel 1997)

The total energy stored in a latent heat thermal storage unit is a complex function of the PCM (its volume; its properties, specially the melt temperature of the PCM and the temperature range over which melting occurs) of the heat transfer surfaces, and of the casting materials as well as of the temperature changes (maximum and minimum operating temperatures) (Brousseau and Lacroix 1996);(Banaszek, Domanski et al. 1999); (Neeper 2000)

Design of energy storage systems is in general case-specific, as the regional variations (temperature differentials), method of construction (heat losses and gains of materials used, size of the building and room distribution) and occupancy schemes play a crucial role in the performance of the system. To have an idea of how different parameters have been optimized and applied for a more favourable design in previous research, the next cases are presented:

2.68 The degraded exergy (availability) divided by the total energy input to the cycle

2.69 Is the available, extractable energy. It can only be consumed or destroyed (due to irreversibilities in any process)

The time taken for the whole PCM to melt is one of the crucial factors for a heat storage system design.
In the heating mode, for a cold climate it is considered desirable (with regard to efficiency) to have a thermal storage system which is capable of being completely charged over a period of 7 hours and have the capacity to discharge heat over a period of up to 16 hours. That is, thermal and geometric parameters including the PCM selection must bring about a system compatible with the total daylight time. (Esen, Durmu et al. 1998); (Scalat, Banu et al. 1996)

Effect of mass flow rate:

To evaluate the performance of a PCM wallboard in a practical operating schedule, Scalat tested minimum charging/discharging times (8°C temperature change in less than 7 hours). By introducing hot or cold air it was possible to adjust the charging or discharging rate. (Scalat, Banu et al. 1996)
Lee carried out heating and cooling tests in Canada to assess the correlation between the saturation time and the air velocity. He observed that for flow velocity of 3 m/s, the charging time was about 20% longer than the expected 8 hrs while the discharging time was 7% shorter than the required 14 hrs at 2 m/s. For Canadian-like weather conditions charging velocities must be in the range of 4-5 m/s, while those for the cooling mode must be about 1.5 m/s. As air velocity is governed by the diurnal environmental temperature, air velocity control is largely significant for all seasons in areas that go through a large temperature range (Lee, Hawes et al. 2000). According to Neeper boosting the convective heat transfer coefficient raises the diurnal storage for a melting temperature near the average room temperature. (Neeper 2000)

Effect of PCM operating temperature:

In a heating dominant climate (as that of Canada), satisfactory indoor winter temperatures may range from 18 to 22°C. In a cooling dominant climate, (as that of Mexico), the ideal PCM would have a melting- freezing interval in the range 22-26°C and a latent heat of at least 120 J/g. An efficient utilization of a PCM melting-freezing range and optimization of latent heat storage released, depends on an appropriate PCM selection for each type of application.(Feldman, Banu et al. 1995)

In the Esen heat storage system the CCHH (calcium chloride hexahydrate) stores heat energy at a faster rate compared to paraffin, paraffin wax, and SSDH (sodium sulphate decahydrate)(Esen, Durmu et al. 1998)

Neeper concluded that the maximum diurnal energy storage takes place at a PCM melting temperature near the average room temperature in most

cases. He also inferred that diurnal energy storage drops if the phase change transition takes place over a range of temperatures[70]. He also confirmed that PCMs exhibiting wide transition widths provide less than optimal storage. That is, if the transition is wide (of 4°C or more) or if the melt temperature is far from average room temperature, even raising the heat transfer coefficient can have minimal effect. (Neeper 2000)
(Neeper 2000)

Effect of PCM volume:

Esen considered a system with cylindrical latent heat storage tanks in two modes: mode1: containing PCM and with heat transfer fluid parallel to it and mode 2: pipes containing the heat transfer fluid are embedded in the PCM. In mode 2 as the total PCM volume in the tank increases, the thickness of the pipe wall augments the melting time, which is consequently extended. (Esen, Durmu et al. 1998). He also stated in other work that the thickness of the pipe walls should be thinner if a lot of pipes with small radius are used. (Esen, 1994).

Encapsulation and heat exchanger elements:

In most cases, the system effectiveness improves as the specified heat transfer area increases. Regarding encapsulation materials, Esen's study showed that metals are better PCM containers than PVC[2.71](Esen 2000)
Concerning the effect of boundary conditions, Neeper claimed that, if the melt temperature is optimal, a wallboard on the exterior wall stores slightly more energy than the wallboard on the interior wall, possibly because the exterior wallboard can release more energy at night.(Neeper 2000)

The boundary conditions imposed on the wall of the PCM container are important aspects defining the transition from natural convection to the pure conduction mechanism of heat transfer. Natural convection in the liquid phase during solidification can lead to delaying or eventually interrupting the solidification process. Ismail et al. concluded that the transition time is determined by the difference between the wall temperature and the initial temperature of the liquid PCM. They also confirmed that natural convection only takes over during the initial stages of the process.(Ismail and Goncalves 1999).

According to the container shape and boundary conditions imposed during the heating or cooling of a system from both sides, a pattern of free convection can appear near walls, but remaining solid or still liquid at the

---

2.70 An hypothesis of this work is that multiple PCM cells having multiple melting points (transitions occur within a "range" of environmental temperatures) might improve the efficiency of the system
2.71 polyvinyl chloride

core. (Banaszek, Domanski et al. 1999) For this reason, heat enhancement might be of crucial importance when optimising a heat storage system.

Heat transfer enhancement: Sparrow et al. observed that the use of fins can delay the commencement of natural convection during solidification.(Ismail and Goncalves 1999). For the melting process, Costa proposed a system with fins which increased the melt fraction about four times in comparison to the system without fins. (Costa, Buddhi et al. 1998). Sasaguchi et al. also confirmed that the heat flux in finned tubes is much larger than that for bare tubes.(Ismail and Goncalves 1999)

Heat transfer fluid: El-Dessouky studied the effect of the operating fluid inlet temperature in the heat recovery and storage processes for a system using either air or water as the heat transfer fluid.
The second law effectiveness improved with the increase of operating fluid inlet temperature in the heat recovery process and with the decrease of the fluid inlet temperature in the heat storage process.
Lower second law effectiveness was found for a system using air compared to the systems using water. The water inlet temperature in the heat recovery process had a very small impact on the entropy generation number. (El-Dessouky and Al-Juwayhel 1997)
A plastic greenhouse tested by Bascetincelik raised its total and net energy efficiencies with the increasing the inlet temperature of the heat transfer fluid.(Bascetincelik, ozturk et al. 1999)

Geometry: The melting time of the encapsulated PCM is a crucial parameter when sizing and the shaping the container, as it must match to the total daily insolation. According to Zivcobvic a cylindrical container melting time is nearly twice that of a rectangular one.(Zivkovic and Fujii 2001)
Banaszek presented a vertical spiral heat exchanger concluding that the outermost PCM channel didn't work efficiently(thermal energy stored dropped. This was caused by the fact that in the last PCM channel only 'one-side' heat transfer took place between both media.

Although the charging/discharging periods for improved efficiency depend on the specific conditions of the system application, in this study, for the assessment of factors effect on the system response, faster total charging and total discharging of the system is desired. For this reason the rectangular shape was chosen for this study.

Concluding notes regarding the PCM section

PCM's have been selected to be studied in the heat storage system proposed due to: their versatility[2.72], availability[2.73], low maintenance requirements, negligible CO_2 emissions, noiseless operation, and because they have no requirements for mechanical or electrical systems, and they operate effectively with solar energy as heat source.

Encapsulation of the PCM seemed to be wise for the system, as a better control of the storage operation is possible; hazards due to ambient interactions are reduced; the change of volume (when changing phase) is contained; maintenance is simpler and system location is more flexible.

The PCM latent heat storage system described in the previous chapter designed to operate under Mexican weather conditions.

Suitable PCM's for the required operating conditions were analysed on a differential scanning calorimeter (DSC) to determine some of their properties and to examine their stability and thermal behaviour under imposed conditions. The encapsulating material must be compatible with the chosen PCM's, inexpensive, and of low weight. The encapsulation method must also be economical, and straightforward, in order to reduce the inconveniences on adopting the system. As solar radiation is the heat source, the storage system must be located so that it is exposed to solar radiation. However the system is required to interact and respond according to the building interior conditions and for this reason must be located on the interior of the building envelope[2.74].

The major factors affecting the rate of heat transfer for storage system efficiency (as PCM volume, insulating elements, multiple PCM systems, etc) were tested experimentally. This information is useful to determine the main factors establishing the system's behaviour when particular weather conditions are imposed.

The hypothesis of controlling the rate and amount of energy stored by specific system settings is assessed by carrying out an experiment where heat fluxes were measured. The impact of the LHSS on the conservation of thermal environmental conditions is evaluated by comparing air temperatures and surface temperatures of the chamber fitted with the PCM blind and the chamber fitted with the ordinary (empty)blind.

Subsequently the results obtained from the theoretical model (where the same boundary and initial conditions as those on the experiment were imposed) are compared with the experimental findings

---

2.72 Large range of operating temperatures

2.73 Low price availability and reduced ecological load is also possible if PCM's used are obtained form recycled products or derivatives of other industrial processes.

2.74 If the system was placed on the exterior, it would rather be performing as an insulator, as none of the stored energy would be provided to the interior, but lost to the exterior

Regarding the numerical assessment of this heat storage system, a model for the moving boundary problem is developed. The model is based on imposed constant boundary conditions to develop the temperature and enthalpy evolution of the PCM. With this methodology the heat transfer flux could be evaluated and compared with experimental data.

In the following chapters a theoretical section will cover a literature review on the numerical analysis of the Stephan problem, the development of the computational model and analysis of the results. One section will cover the DSC experimental testing of the PCM, the testing of the actual heat storage system (experiment carried out according to the experimental design) and a statistical comparative study.

Appendix 2.A: Thermophysical properties of clays

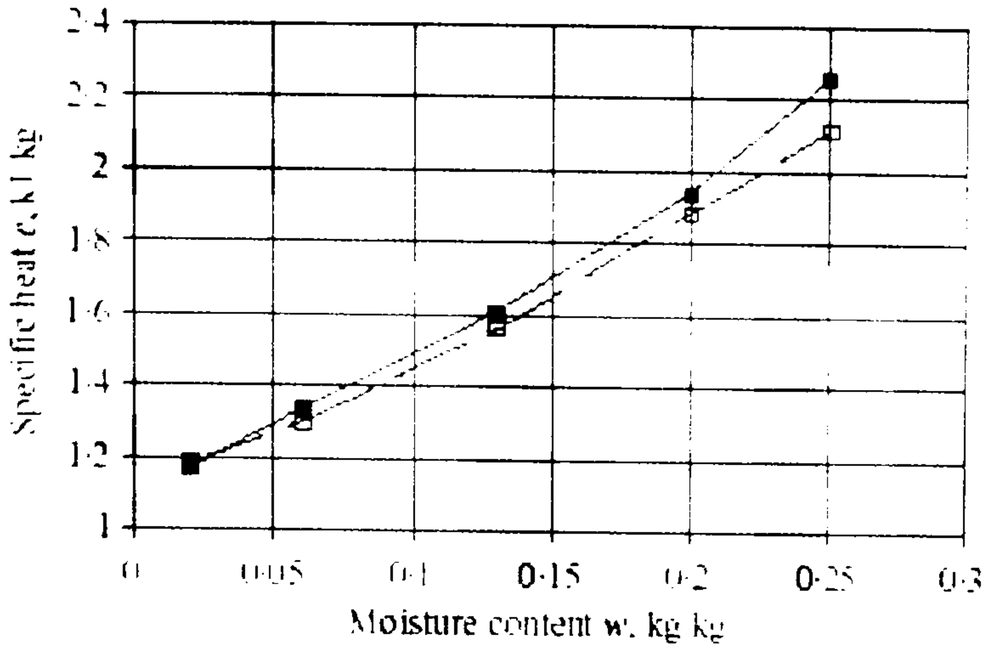

Figure 2.16: Observed ( ) and predicted ( ) specific heat as a function of moisture content for a clay soil at a bulk density of 1300 kg/m³ (Abu-Hamdeh 2003)

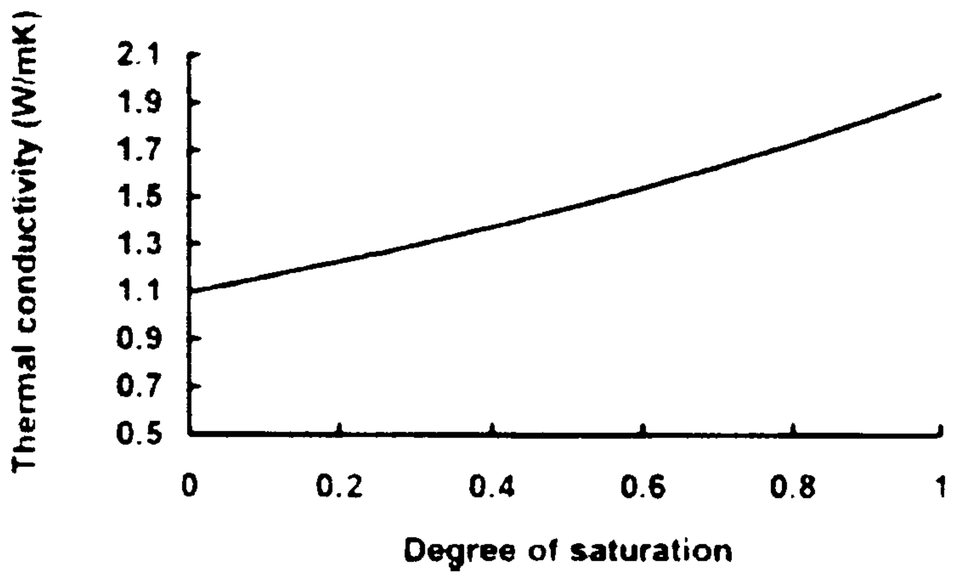

Figure 2.17: Thermal conductivity of clay soils vs degree of saturation (Rees, Zhou et al. 2001)

Name	Classification	Particle Volumetric Content			Porosity	Bulk Density	Sat. Hydraulic Conductivity
		Sand	Silt	Clay		(kg/m³)	(m/s)
Solar Village Clay (Hampton 1989)	bentonitic clay	0.158	0.40	0.442	0.550	1.260	1.51-6
Yolo Light Clay (Moore 1939)	clay loam	0.238	0.45	0.312	0.495	1.320	1.23E-7
River Rock Sandy Clay Loam	sandy clay loam	0.56	0.16	0.28	0.381	1.120	5.7E-5
Bighorn Sandy Loam	sandy loam	0.77	0.10	0.13	0.381	1.400	5.01 -5 *
Loamy Sand (Noborio et al. 1996)	loamy sand	0.835	0.07	0.09	0.396	1.602	1.455E-5

* Estimated value of saturated hydraulic conductivity

Table 2.12: Classification, porosity, bulk density and saturated hydraulic conductivity of some soils (Deru 2003)

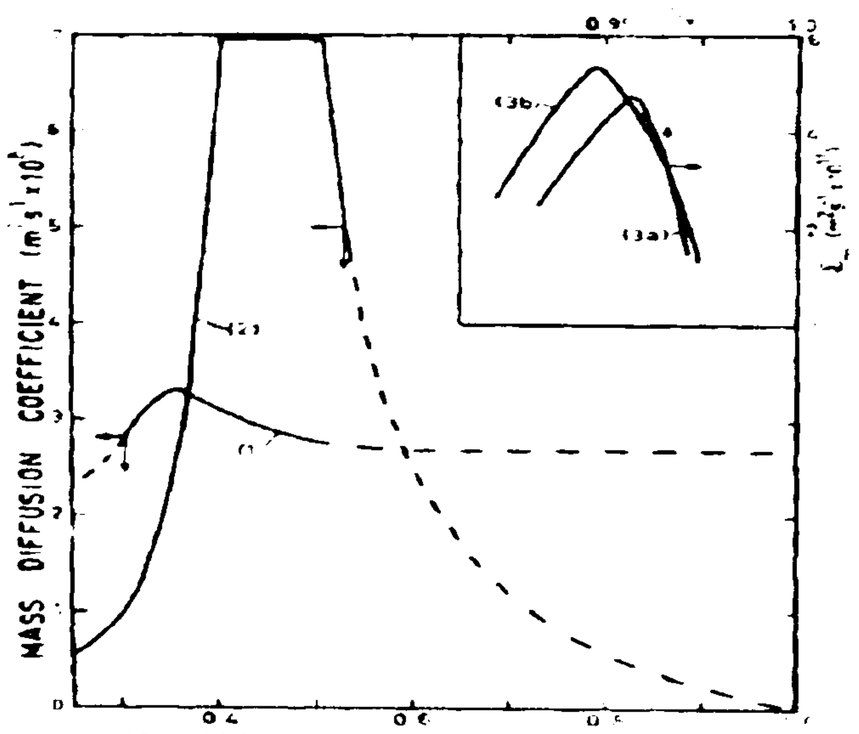

Figure 2.18: Mass diffusion coefficient at high moisture contents for clays: 1) Hyde clay, 2) Kibushi clay, 3) Bentonite clay paste, a) run1, b) run 2 (Evans and Keey 1975)

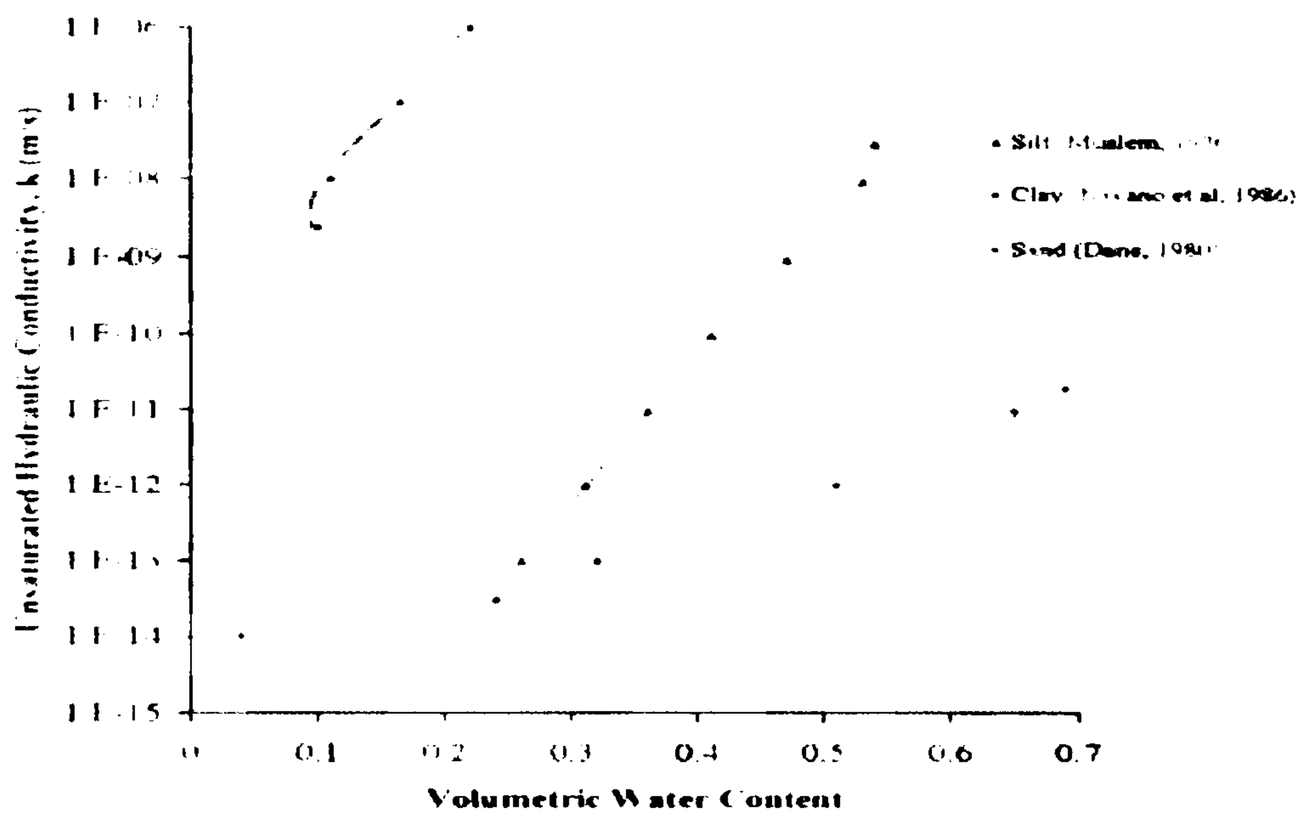

Figure 2.19: Typical hydraulic conductivity- water content relationship (Rees, Adjali et al. 2000)

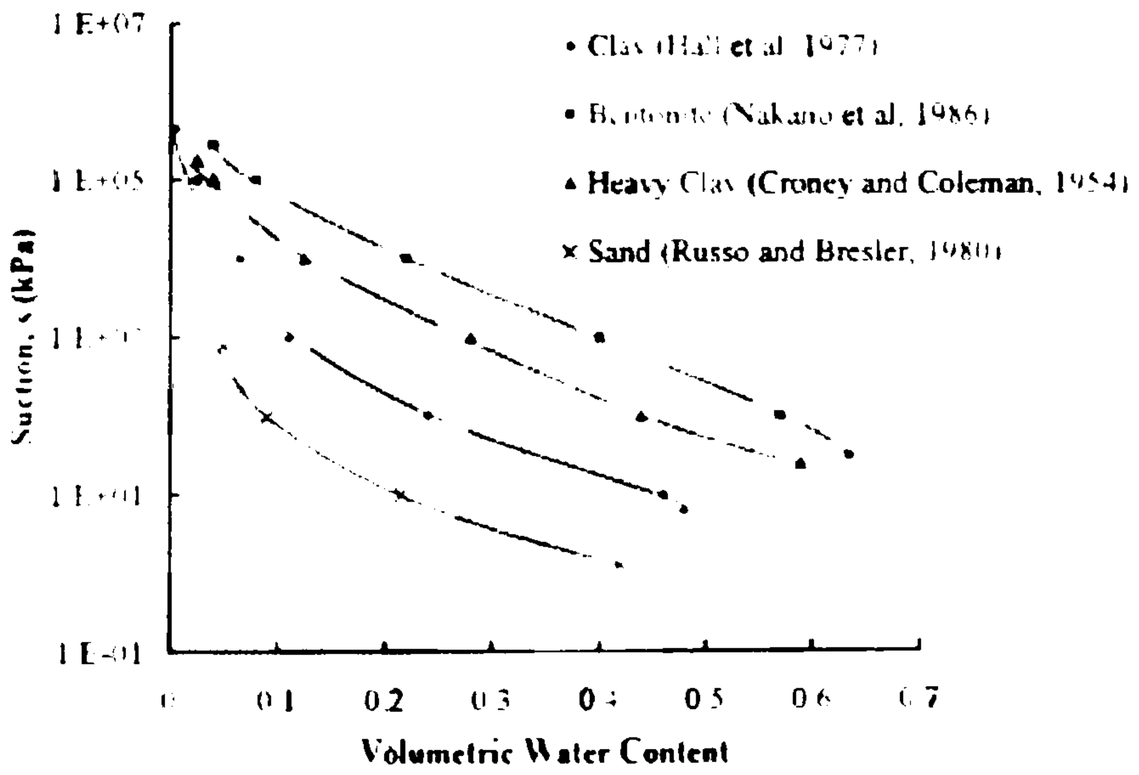

Figure 2.20: Typical water retention curves (suction curves) (Rees, Adjali et al. 2000)

Appendix 2B: Adobe coupled heat and moisture transfer simulations using the one dimensional commercial software WUFI.

Experimental design

Tests carried out:

Run (test)	Resistance and moisture content (MC)	Orient ation	Sd val & radiation absorptivity & emissivity	Wall thickness (cm)	Weather	Hygrothermal conditions	Interior moisture load
1	Low res. ; high MC	South	No Coating; Lime stone	60	Hot summer	Including enthalpy	Low
2	Low res. ; high MC	South	No Coating; Lime stone	30	Cold winter	Excluding enthalpy	High
3	Low res. ; high MC	North	Oil paint; Oil paint	60	Hot summer	Excluding enthalpy	High
4	Low res. ; high MC	North	Oil paint; Oil paint	30	Cold winter	Including enthalpy	Low
5	High res.; low MC	South	Oil paint; Oil paint	60	Cold winter	Including enthalpy	High
6	High res.; low MC	South	Oil paint; Oil paint	30	Hot summer	Excluding enthalpy	Low
7	High res.; low MC	North	No Coating; Lime stone	60	Cold winter	Excluding enthalpy	Low
8	High res.; low MC	North	No Coating; Lime stone	30	Hot summer	Including enthalpy	High

Run 1

Water Content [kg/m³]

Layer/Material	Start of Calc.	End of Calc.	Min.	Max.
Exterior layer	250,00	144,64	144,64	250,00
Middle layer	80,00	122,26	80,00	132,25
Interior layer	60,00	42,01	34,53	60,00

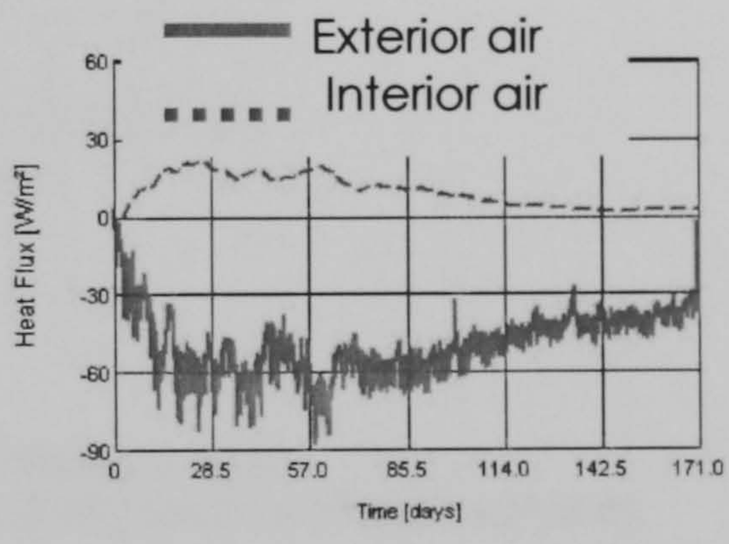

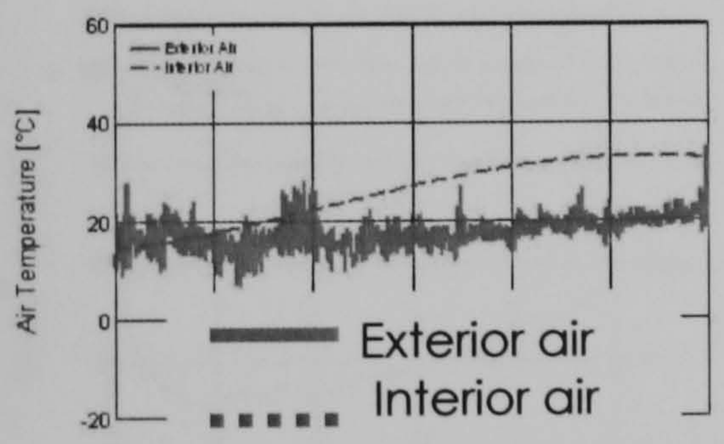

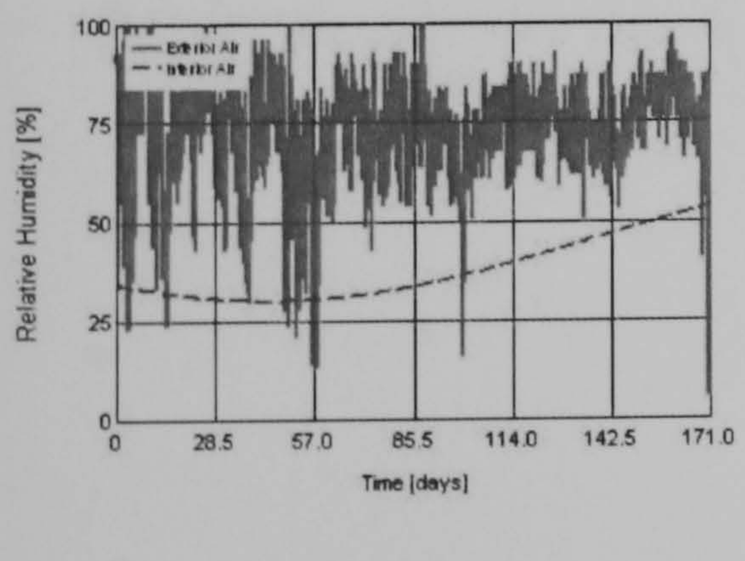

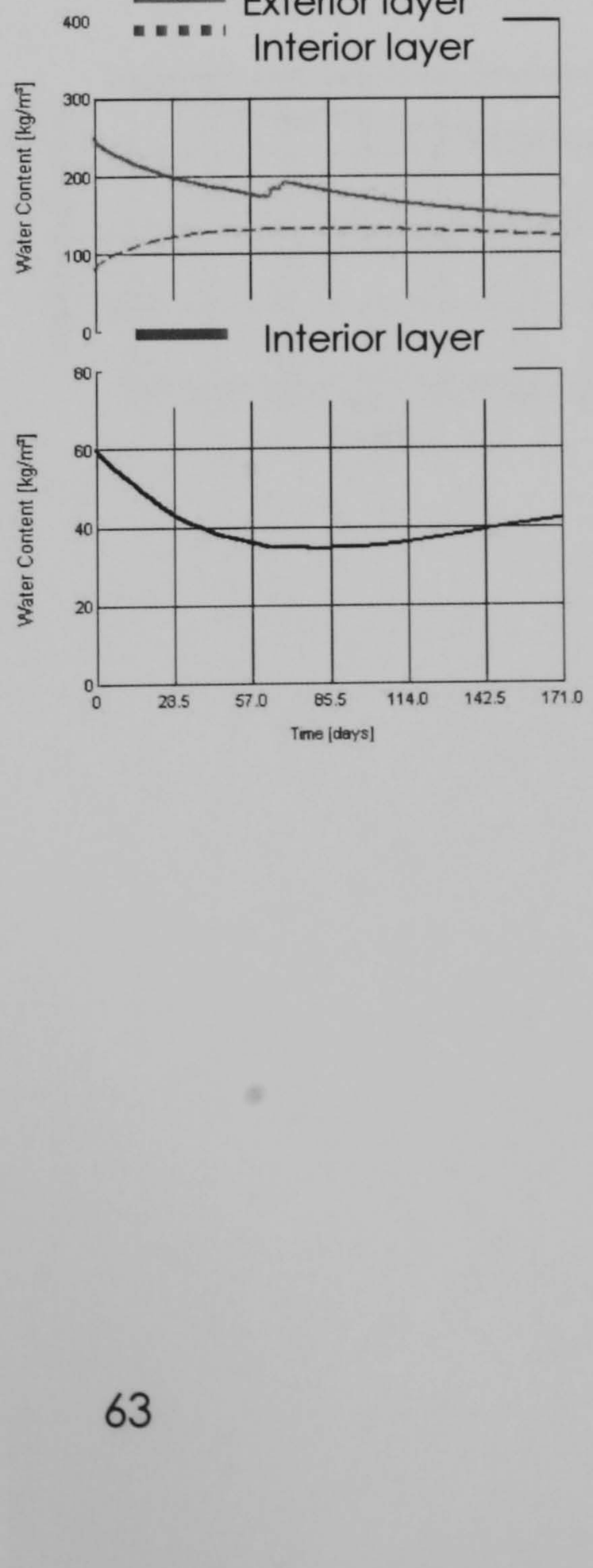

First day simulation
Last day simulation

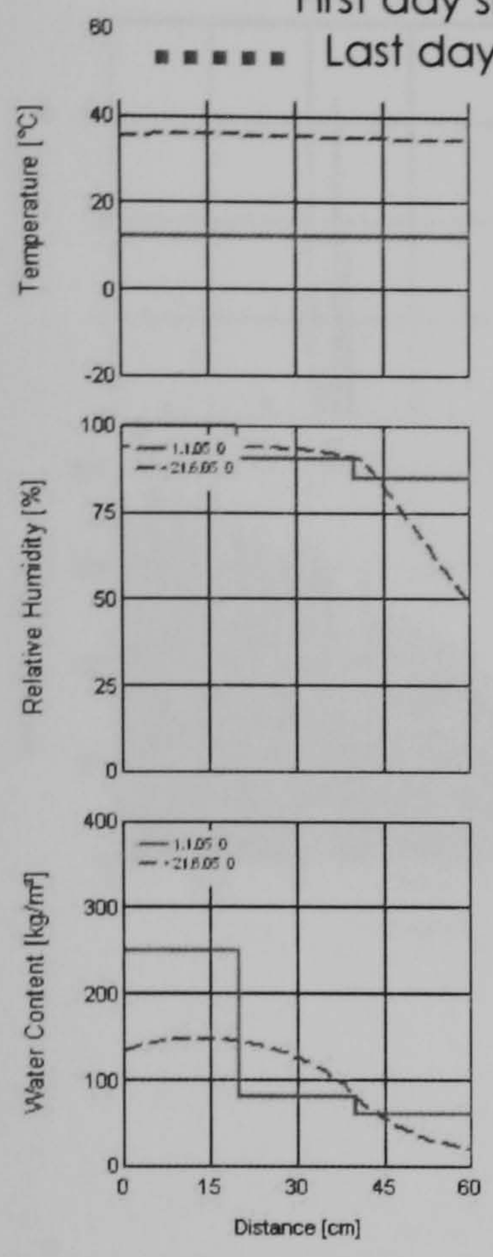

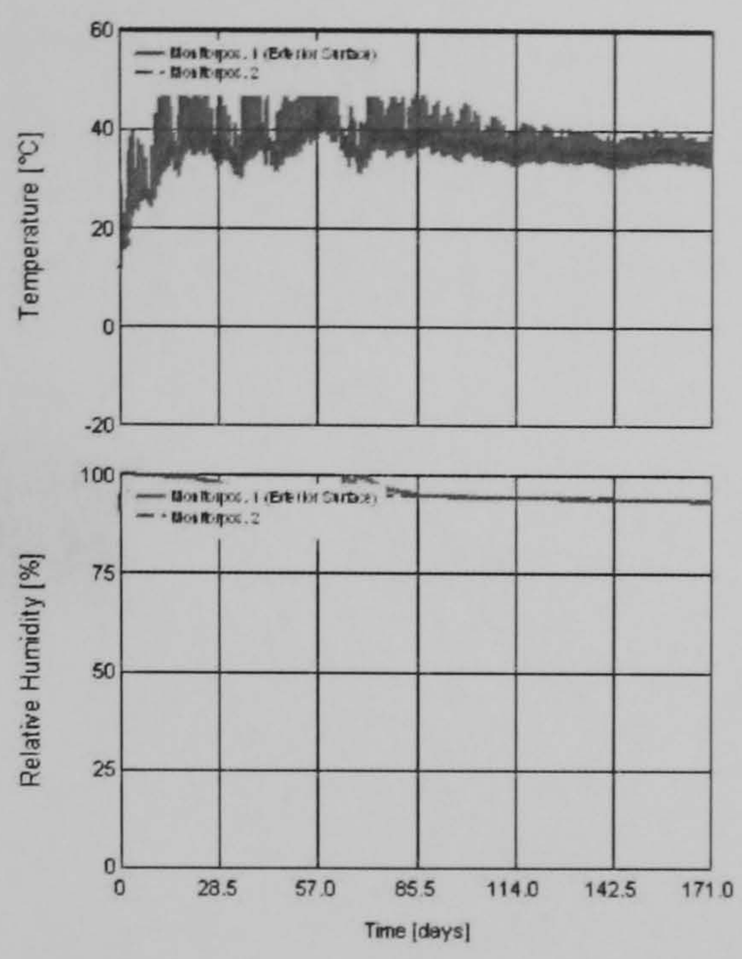

Monitoring point 1 (exterior surfac
Monitoring point 2

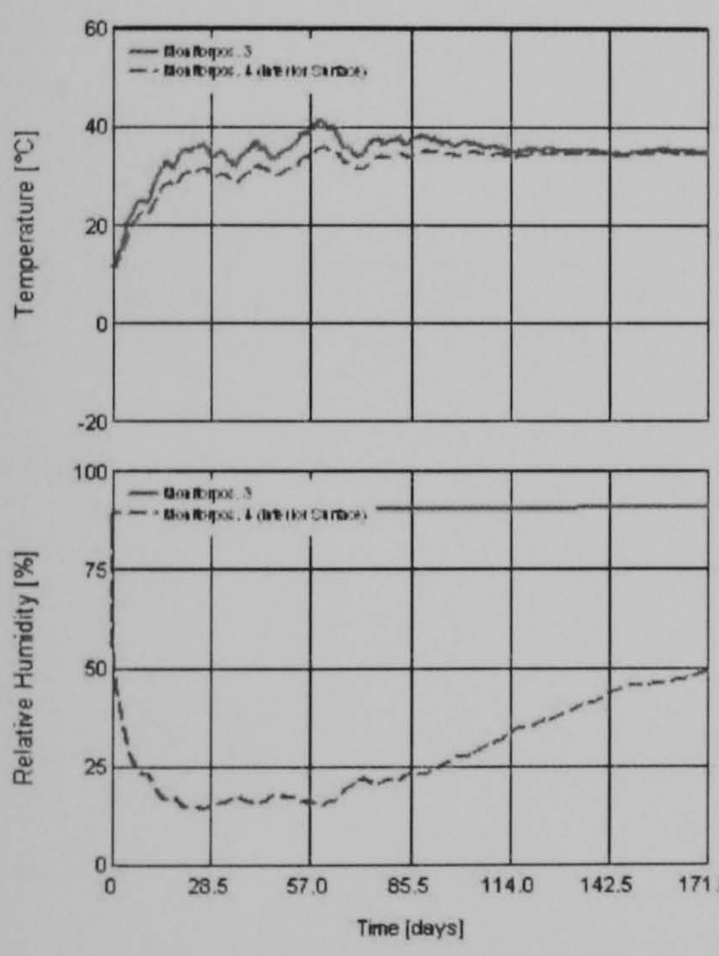

Monitoring point 3
Monitoring point 4 (interior surface)

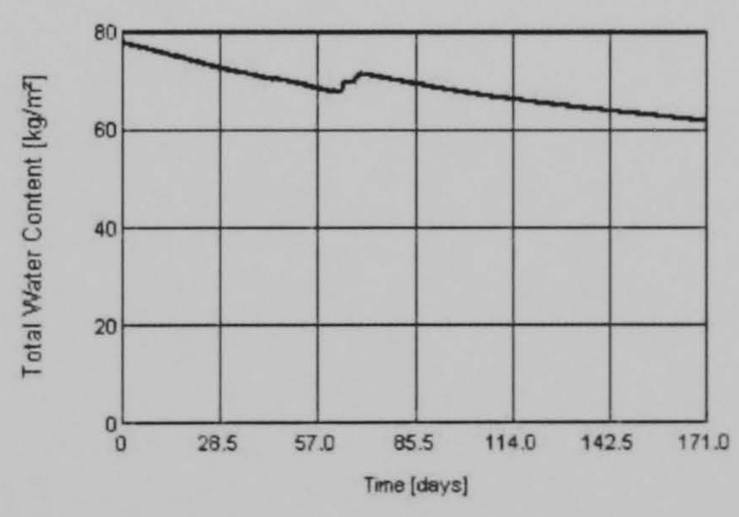

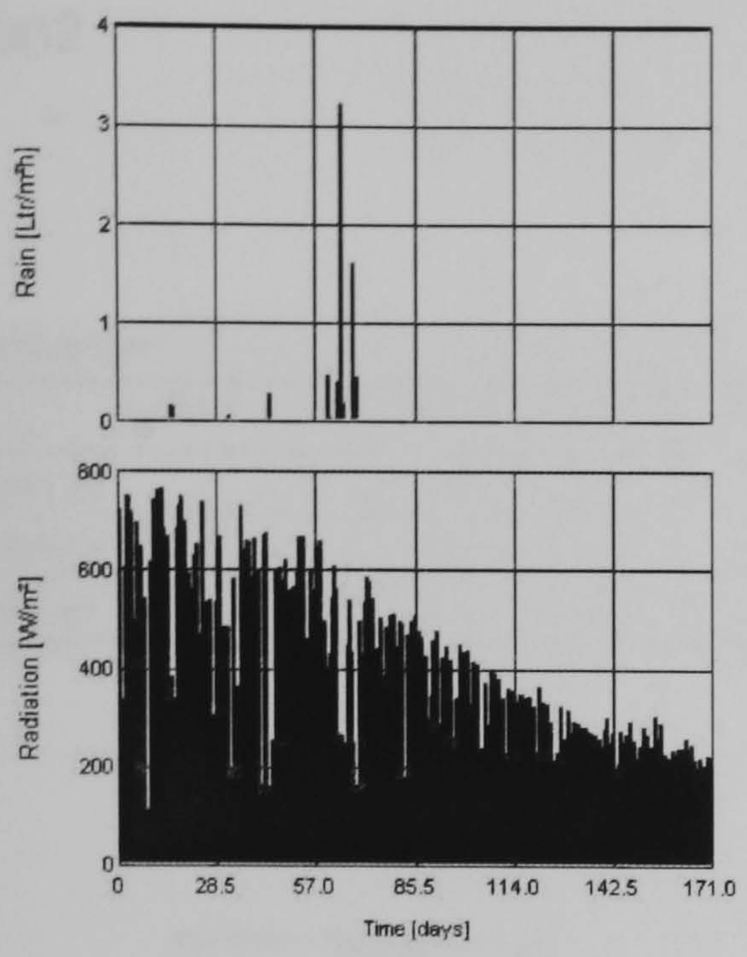
Rain [Ltr/m²h]
4
3
2
1
0
800
600
400
200
0
Radiation [W/m²]
0
28.5
57.0
85.5
114.0
142.5
171.0
Time [days]

Run2

Water Content [kg/m²]

Layer/Material	Start of Calc	End of Calc.	Min.	Max.
Exterior Layer	250,00	3,95	3,07	250,00
Central Layer	80,00	5,48	5,22	112,67
Interior Layer	60,00	6,87	6,37	60,00

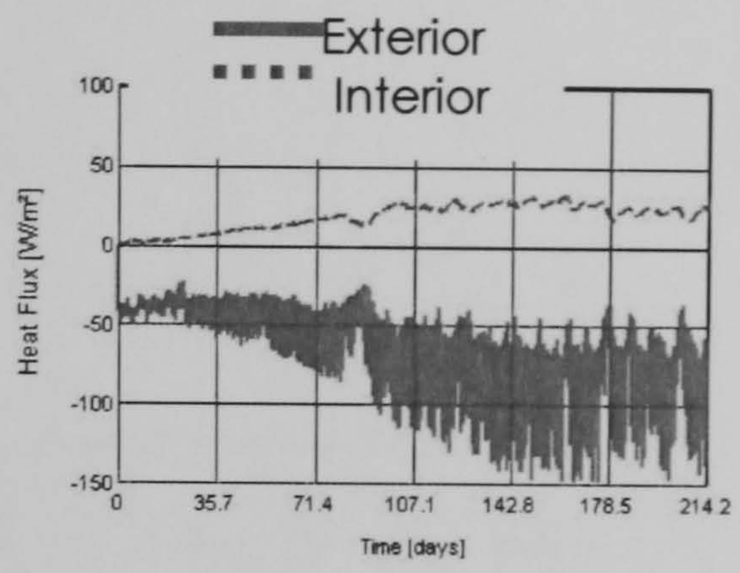

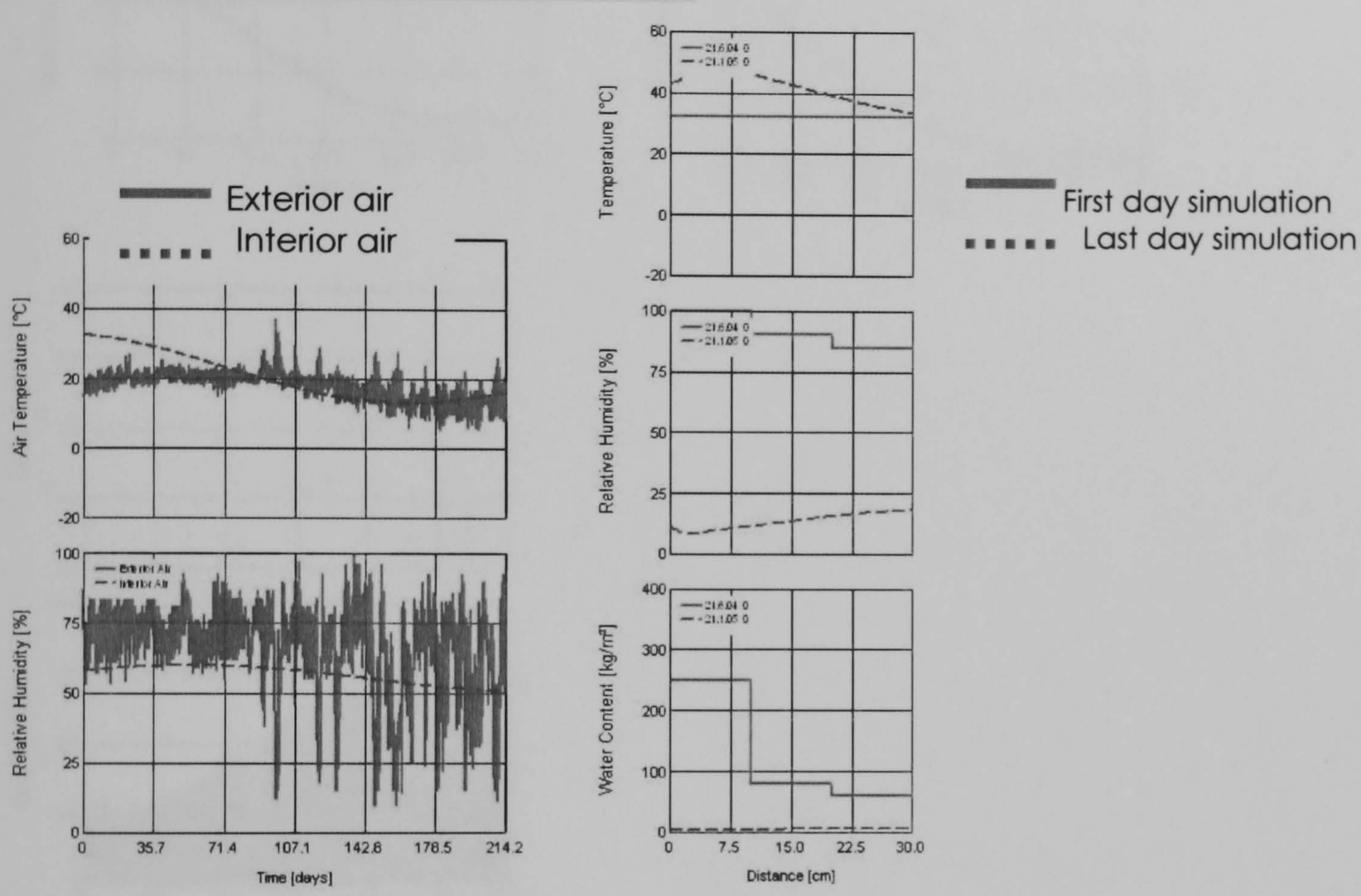

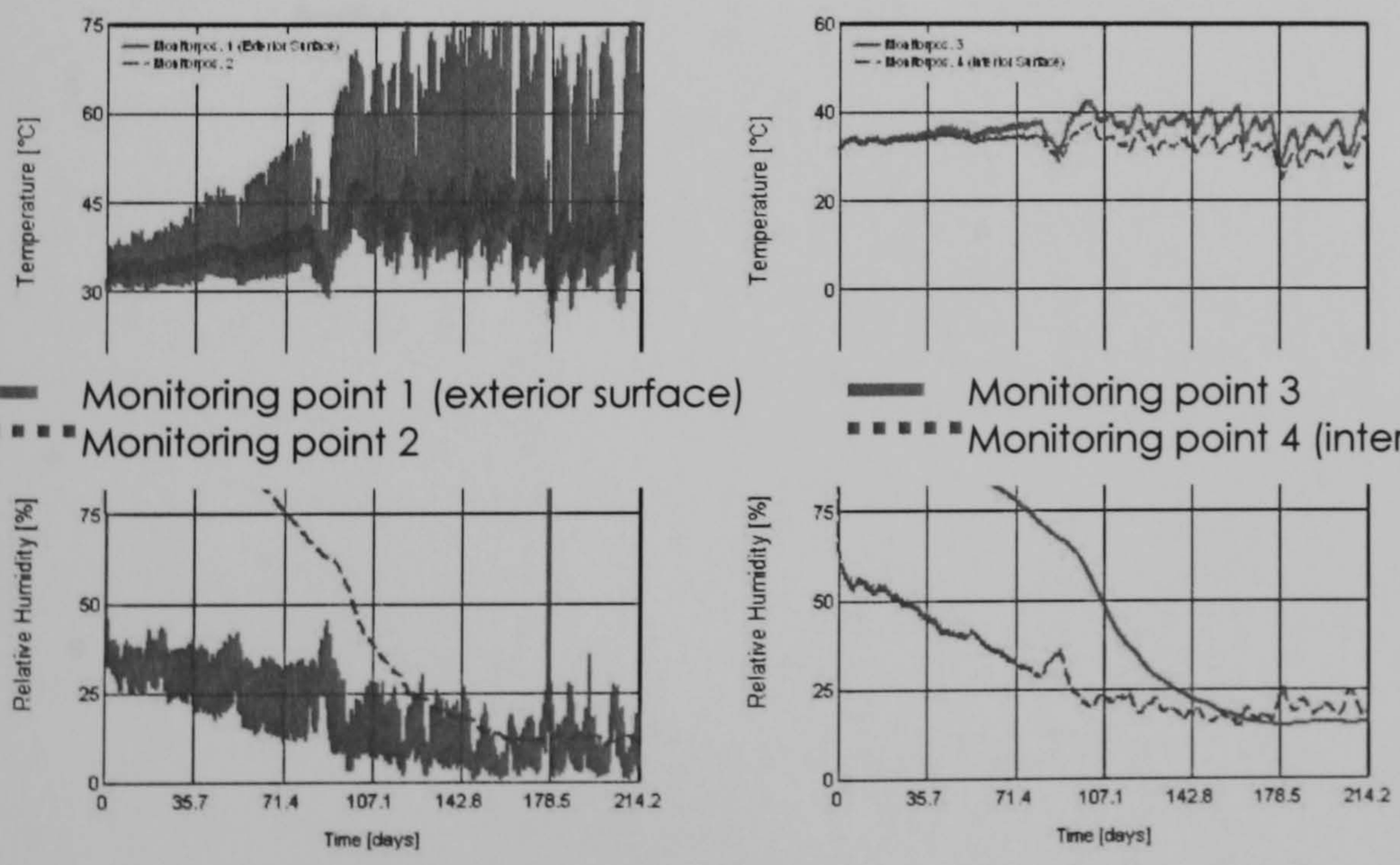

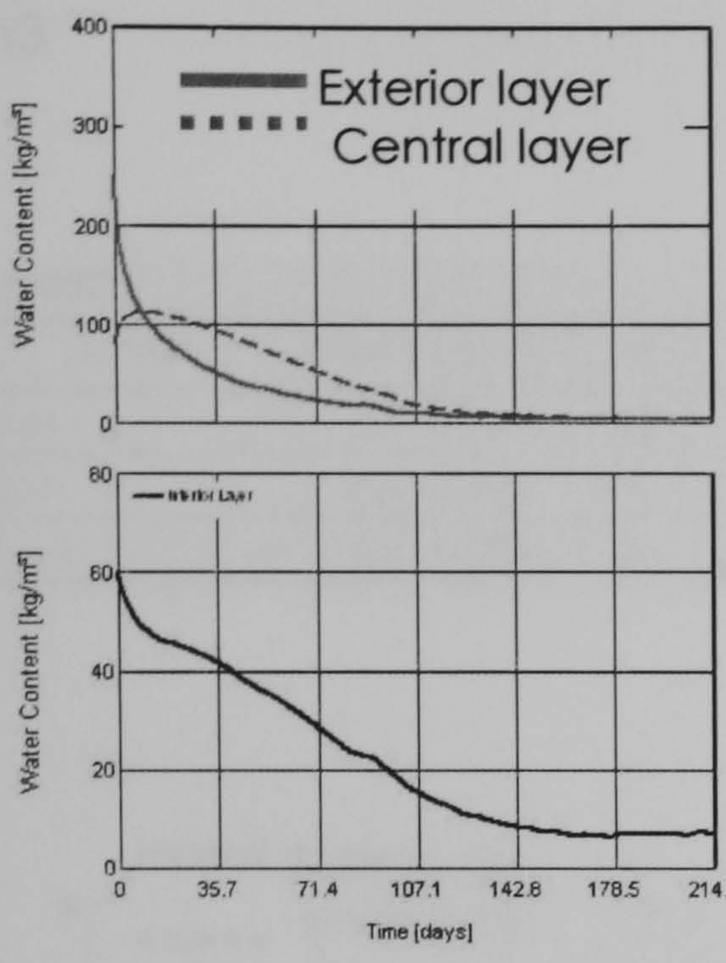
Exterior layer
Central layer
Water Content [kg/m²]
400
300
200
100
0
Interior Layer
Water Content [kg/m²]
80
60
40
20
0
0
35.7
71.4
107.1
142.8
178.5
214.2
Time [days]

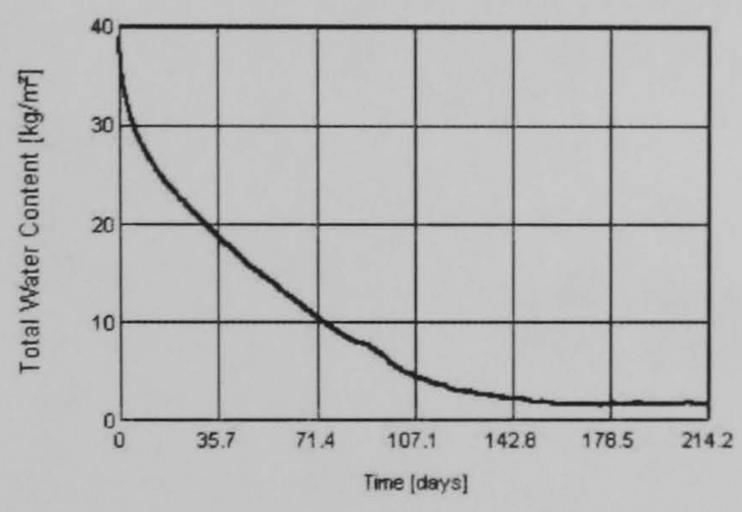
Total Water Content [kg/m²]
40
30
20
10
0
0
35.7
71.4
107.1
142.8
178.5
214.2
Time [days]

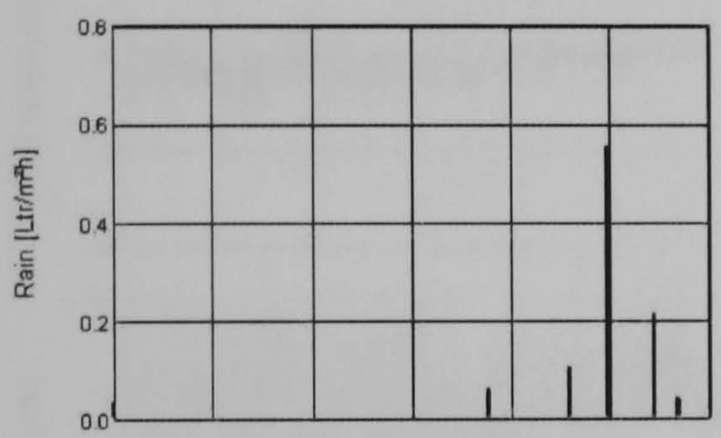
Rain [Ltr/m²h]
0.8
0.6
0.4
0.2
0.0

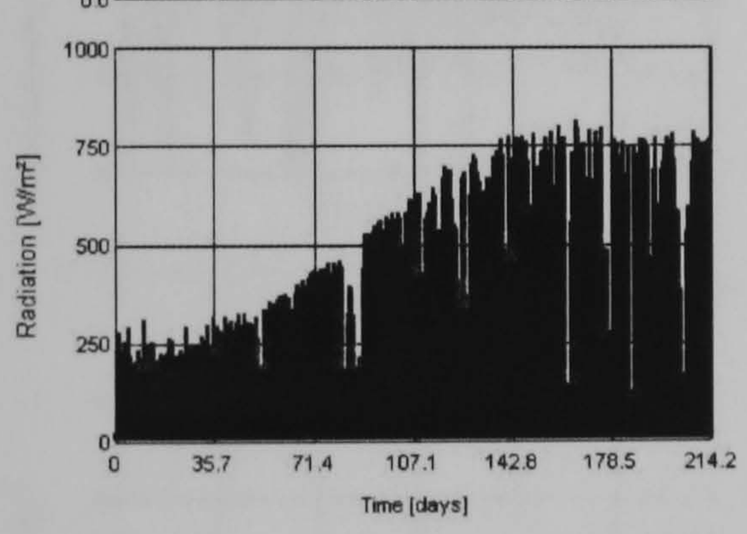
Radiation [W/m²]
1000
750
500
250
0
0
35.7
71.4
107.1
142.8
178.5
214.2
Time [days]

Run3

Water Content [kg/m³]

Layer/Material	Start of Calc.	End of Calc.	Min.	Max.
Exterior Layer	250,00	163,06	163,06	250,00
Central Layer	80,00	136,24	80,00	138,34
Interior Layer	60,00	62,24	50,15	62,24

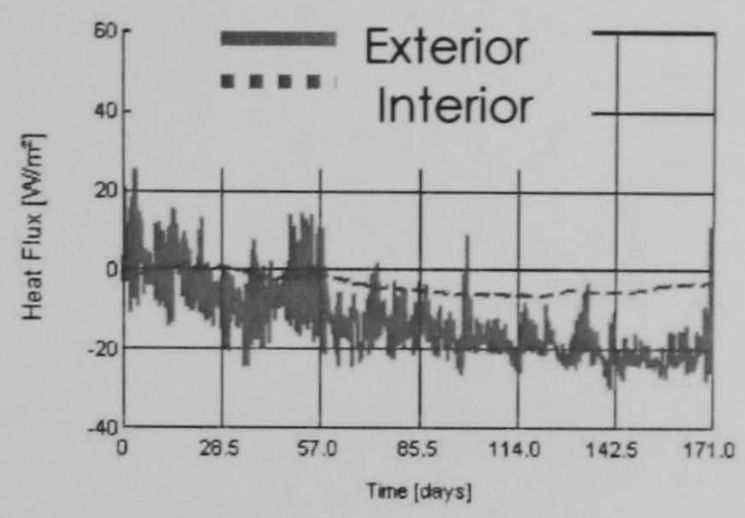

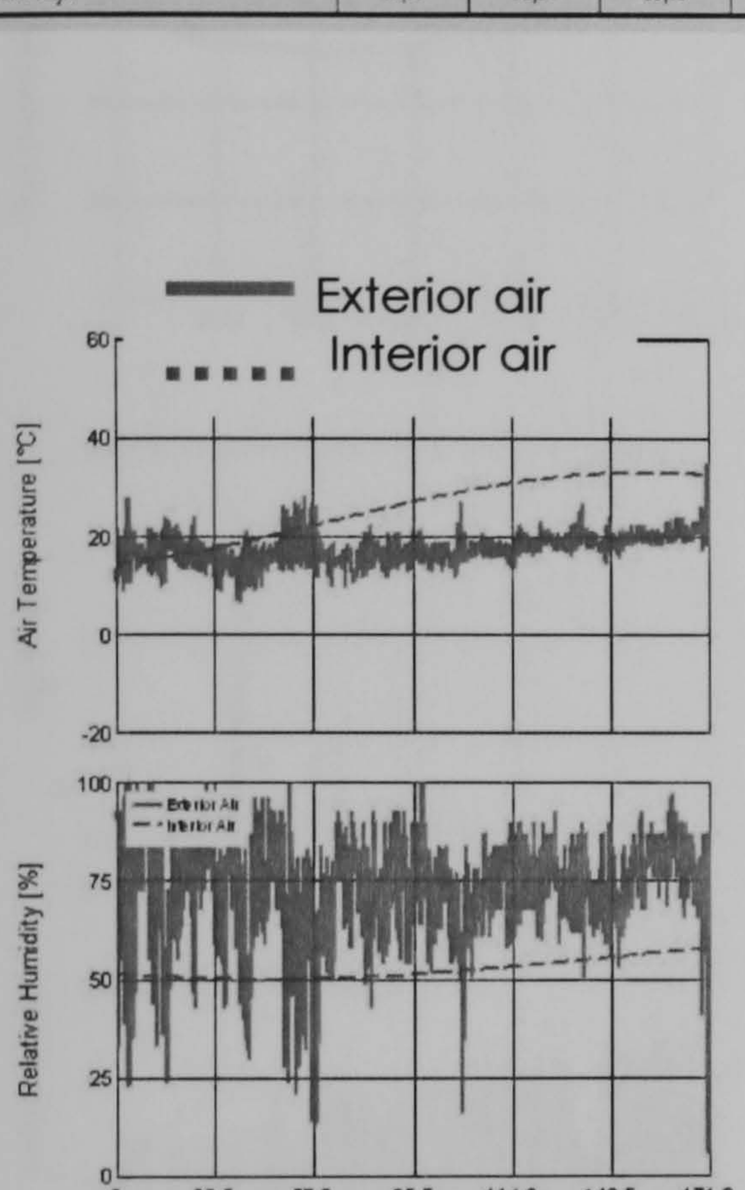

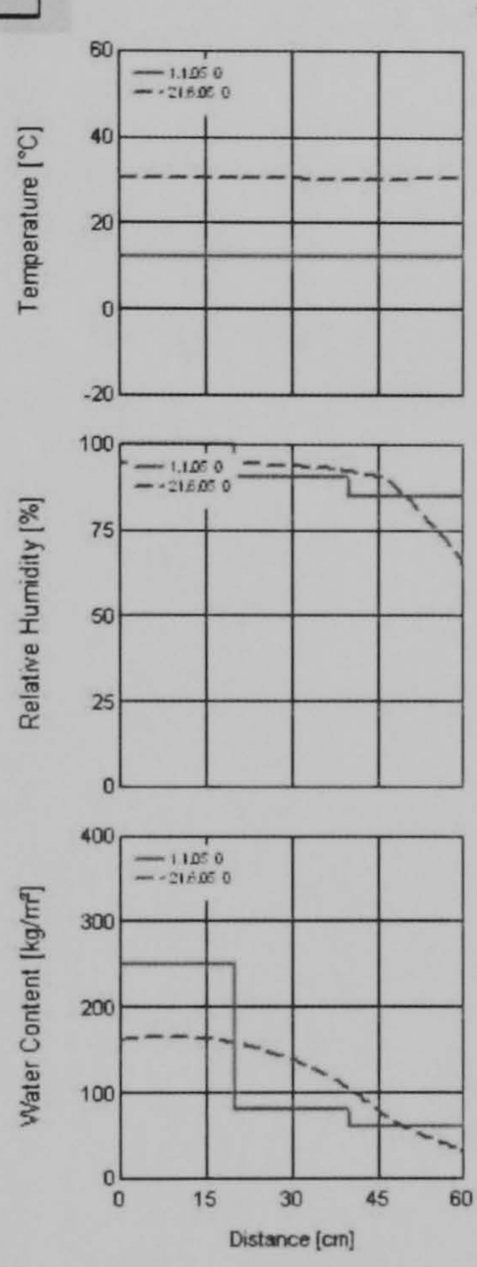

First day simulation
Last day simulation

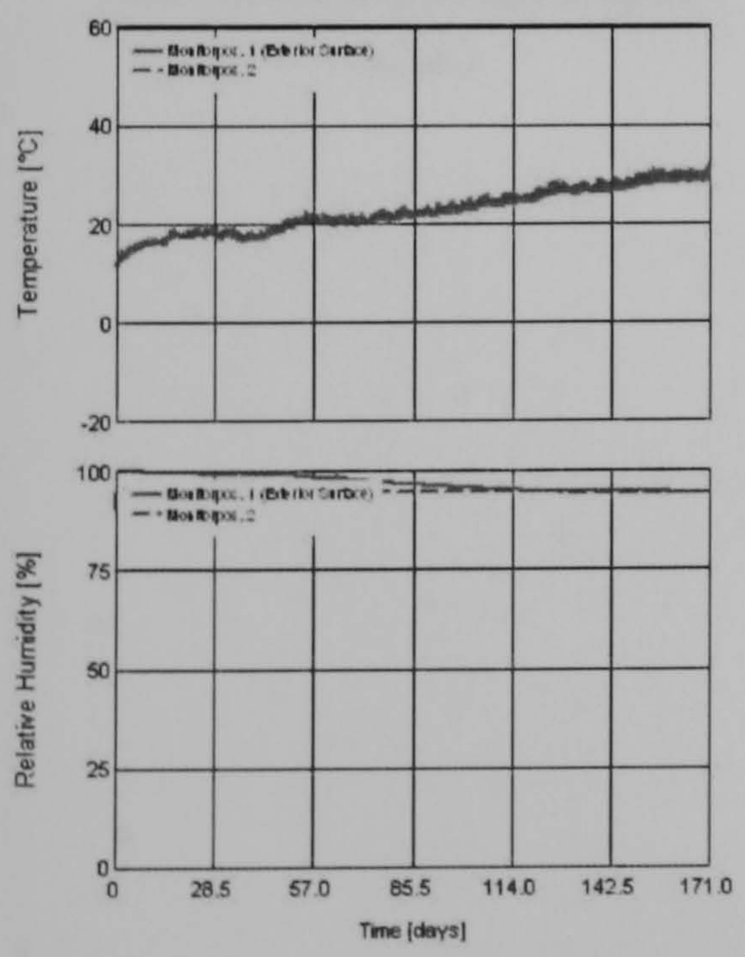

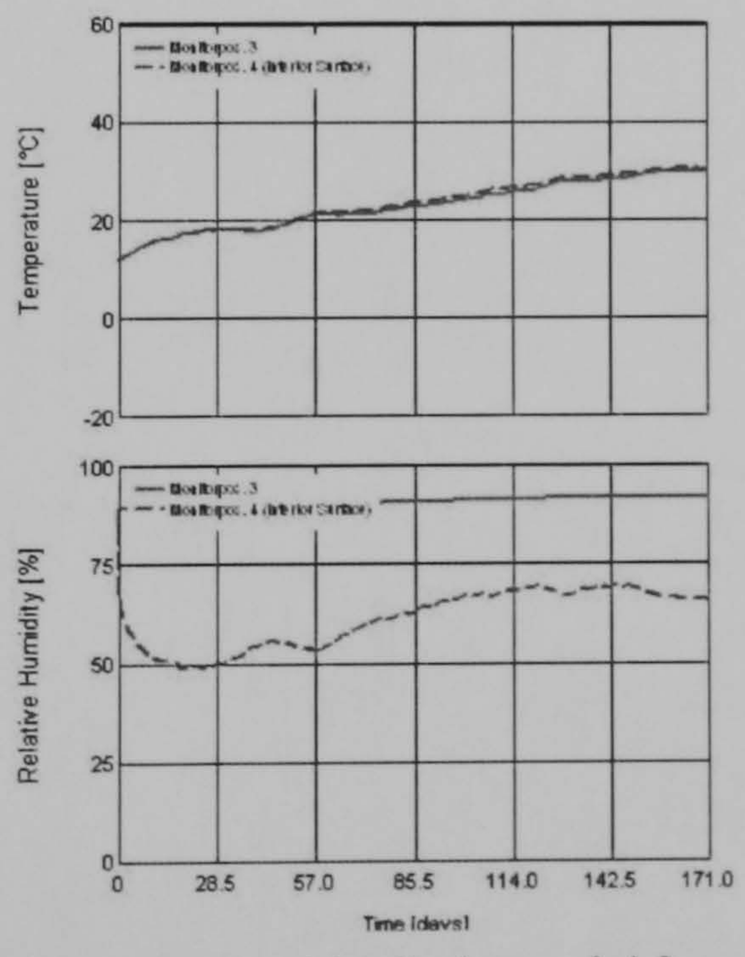

Monitoring point 1 (exterior surface)
Monitoring point 2

Monitoring point 3
Monitoring point 4 (interior surface)

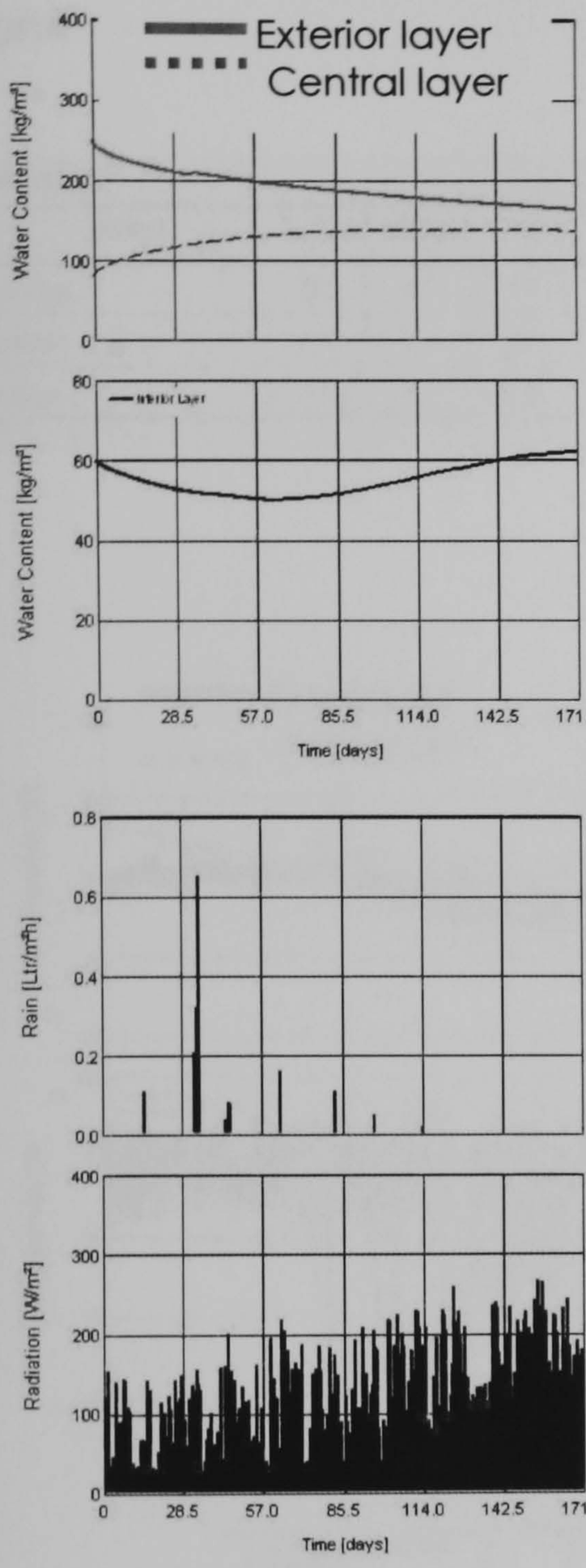
Exterior layer
Central layer
Water Content [kg/m²]
400
300
200
100
0
Water Content [kg/m²]
80
60
40
20
0
0
28.5
57.0
85.5
114.0
142.5
171.0
Time [days]
Rain [Ltr/m²h]
0.8
0.6
0.4
0.2
0.0
Radiation [W/m²]
400
300
200
100
0
0
28.5
57.0
85.5
114.0
142.5
171.0
Time [days]

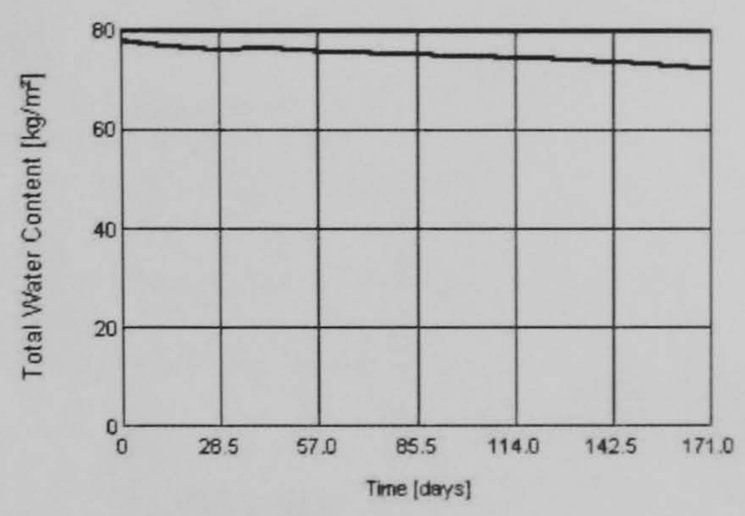
Total Water Content [kg/m²]
80
60
40
20
0
0
28.5
57.0
85.5
114.0
142.5
171.0
Time [days]

Run4

Water Content [kg/m²]

Layer/Material	Start of Calc.	End of Calc.	Min.	Max.
External Layer	250,00	116,27	116,27	250,00
Central Layer	80,00	97,48	80,00	136,17
Interior layer	60,00	40,32	40,32	63,22

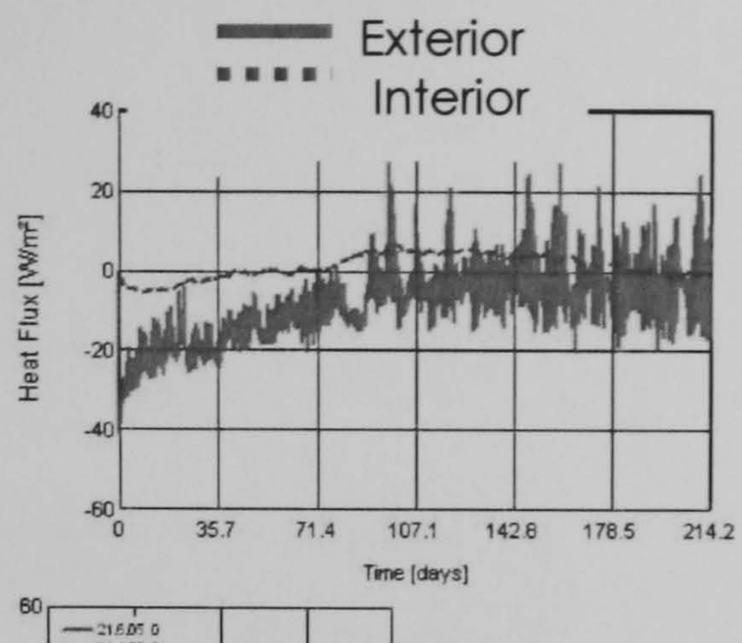

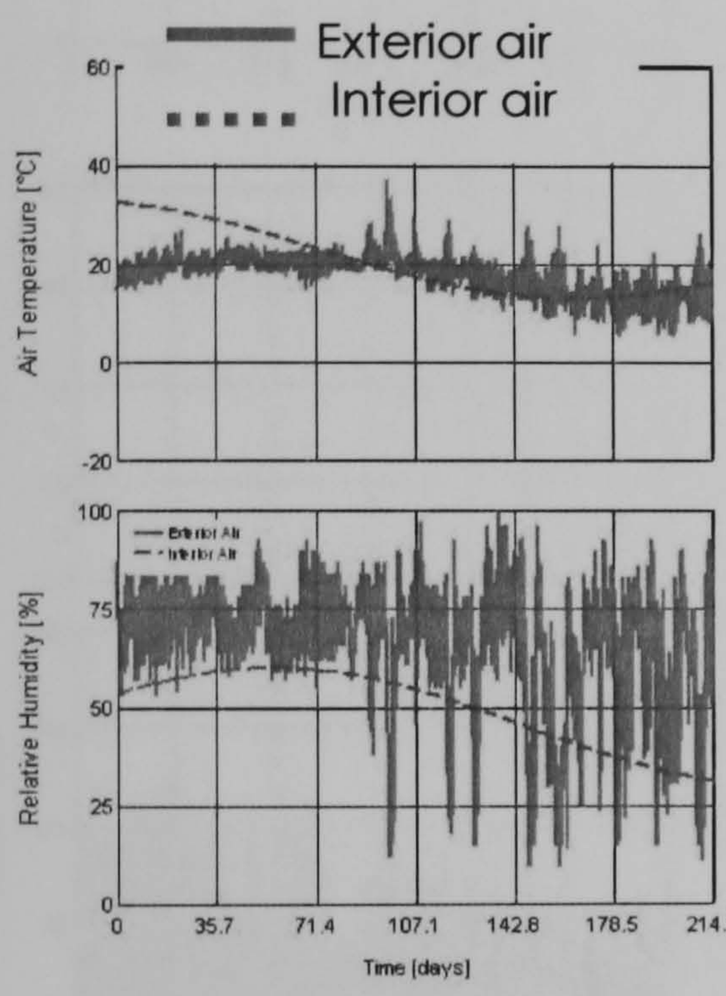

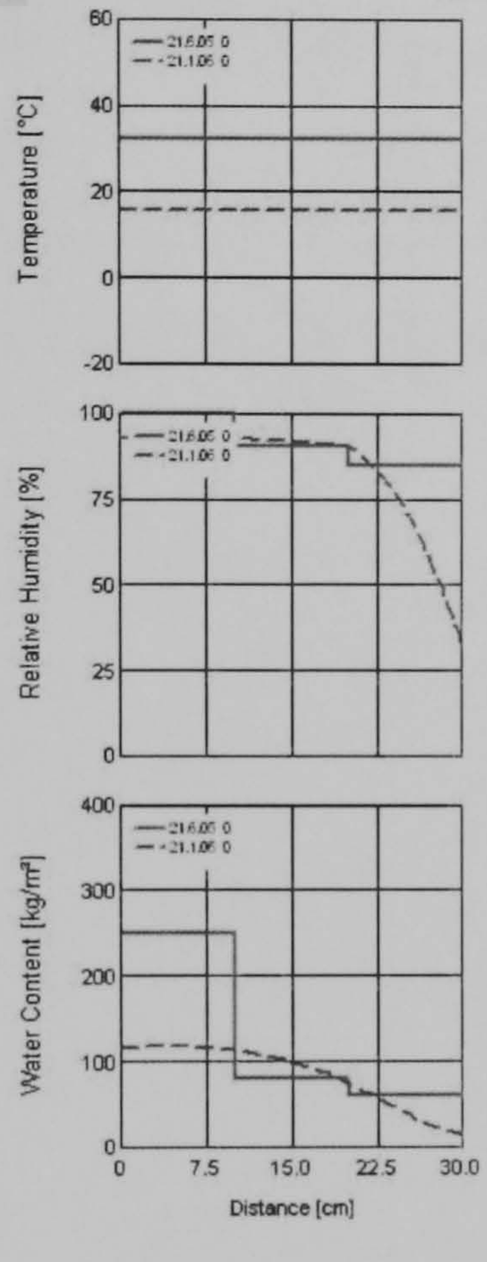

First day simulation
Last day simulation

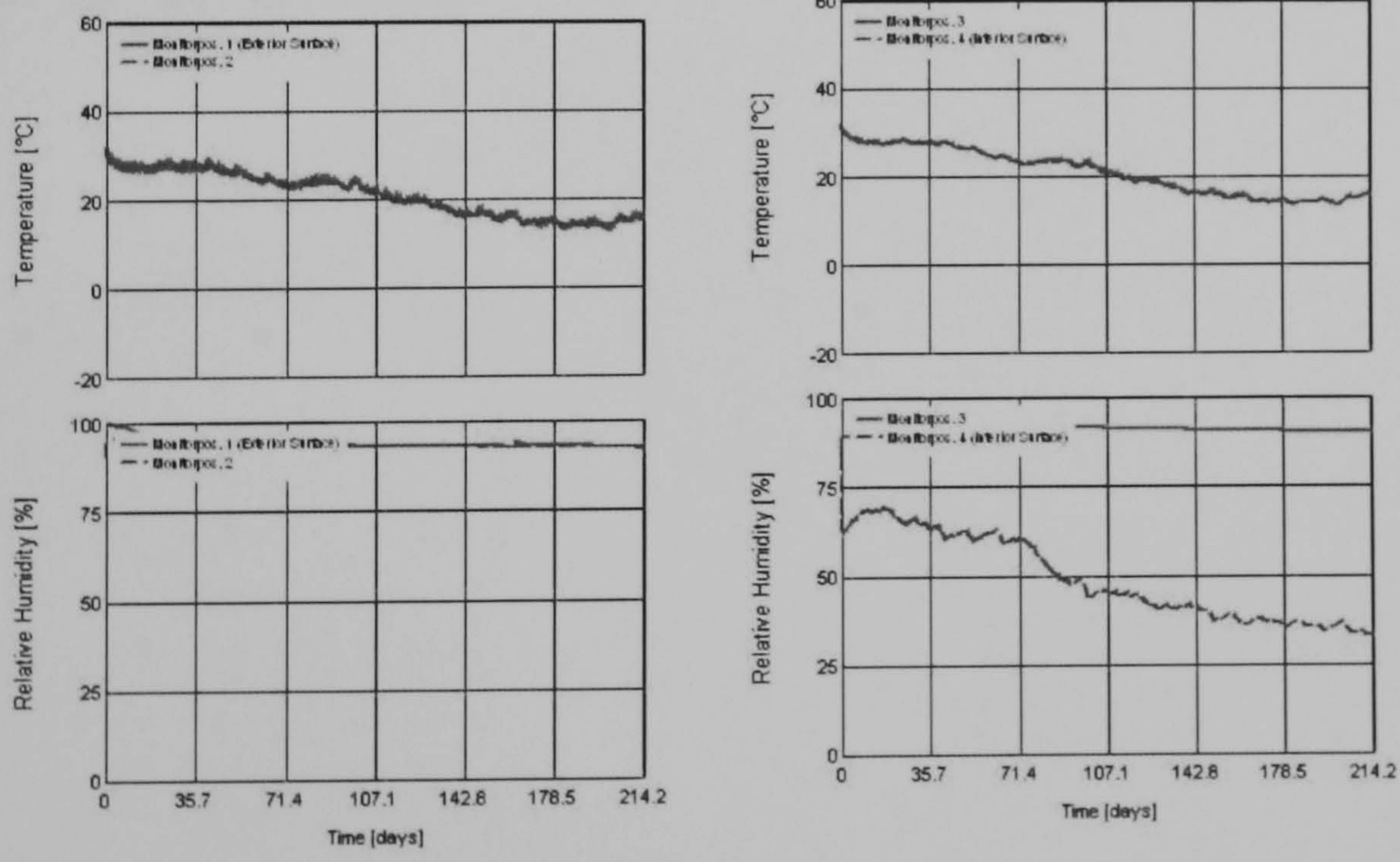

Monitoring point 1 (exterior surface)
Monitoring point 2

Monitoring point 3
Monitoring point 4 (interior surface)

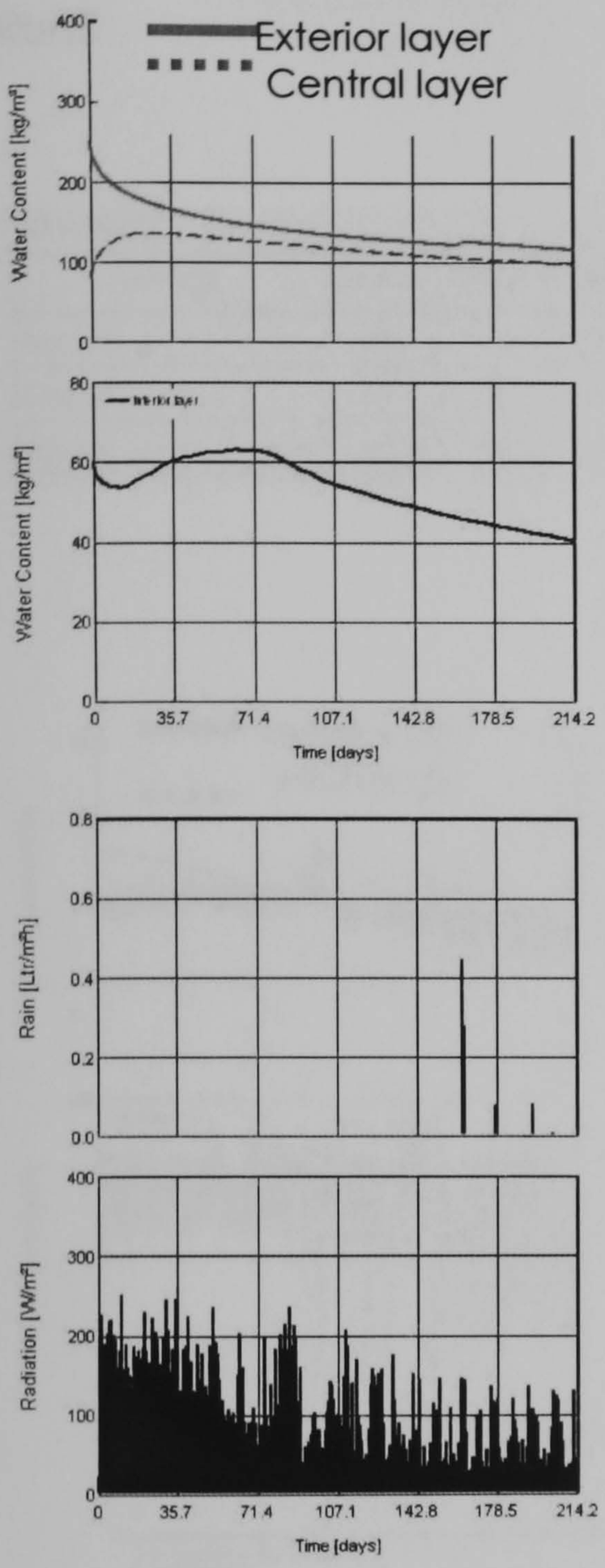
Exterior layer
Central layer
Water Content [kg/m²]
400
300
200
100
0
Water Content [kg/m²]
80
60
40
20
0
0
35.7
71.4
107.1
142.8
178.5
214.2
Time [days]
Rain [Ltr/m²h]
0.8
0.6
0.4
0.2
0.0
Radiation [W/m²]
400
300
200
100
0
0
35.7
71.4
107.1
142.8
178.5
214.2
Time [days]

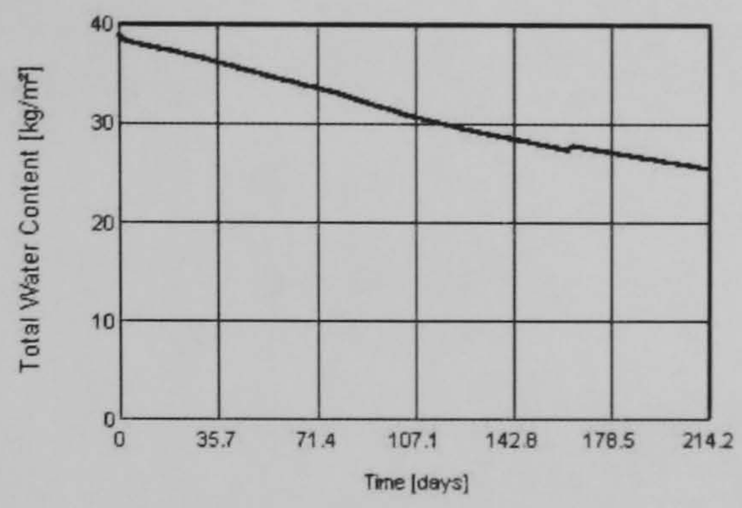
Total Water Content [kg/m²]
40
30
20
10
0
0
35.7
71.4
107.1
142.8
178.5
214.2
Time [days]

Run5

Water Content [kg/m²]

Layer/Material	Start of Calc.	End of Calc.	Min.	Max.
Exterior Layer	60,00	15,27	15,27	60,00
Central Layer	20,00	17,40	17,40	25,85
Interior Layer	0,00	12,44	0,00	17,25

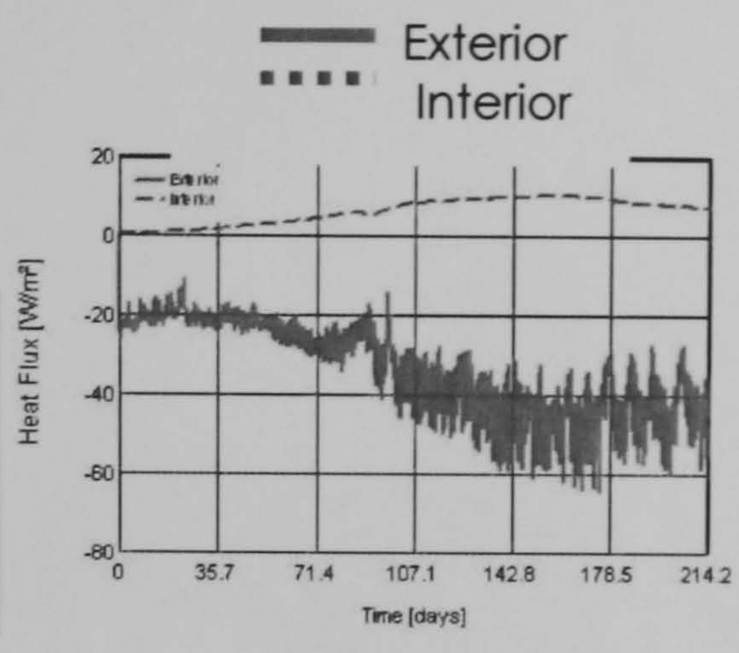

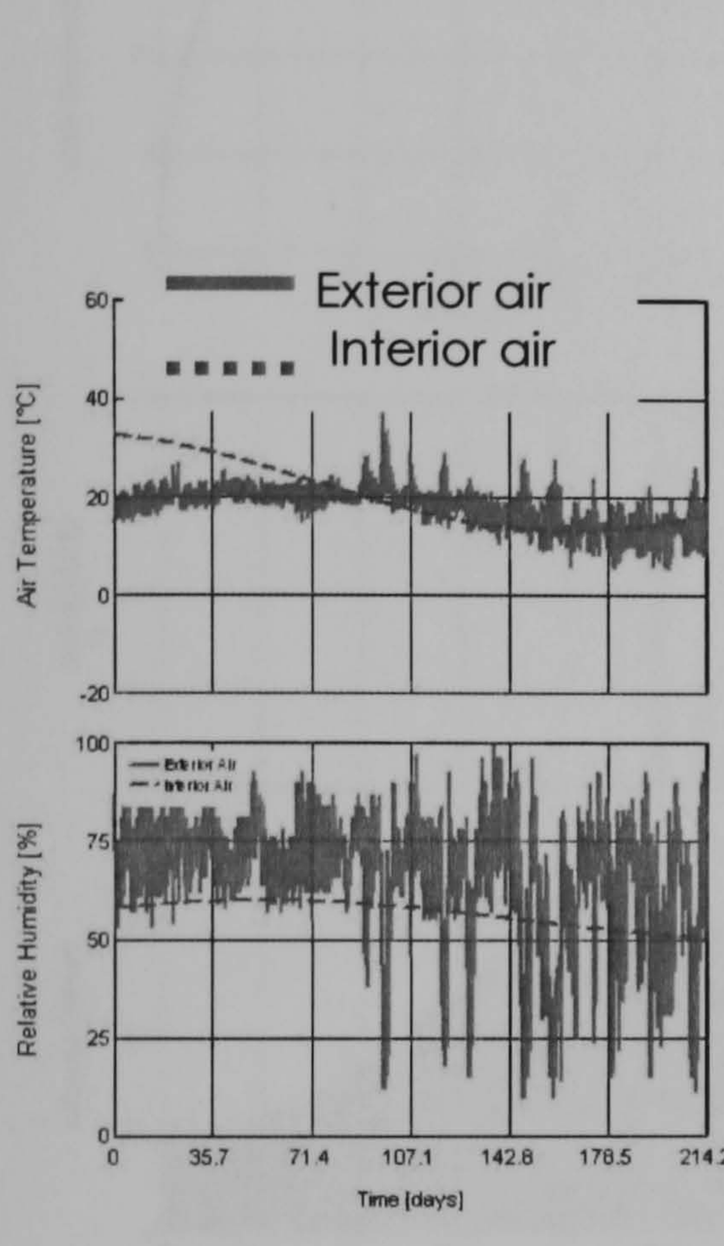

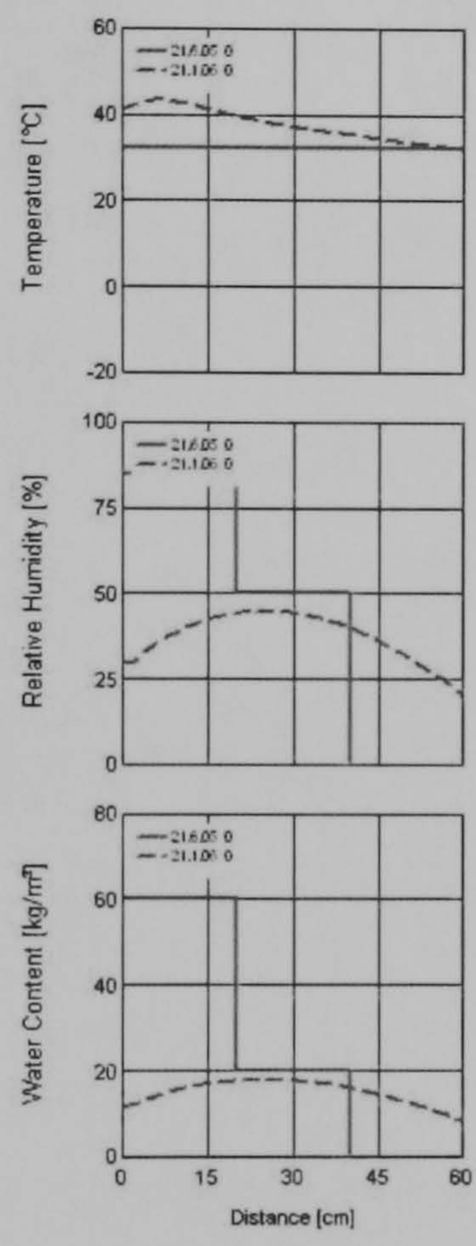

First day simulation
Last day simulation

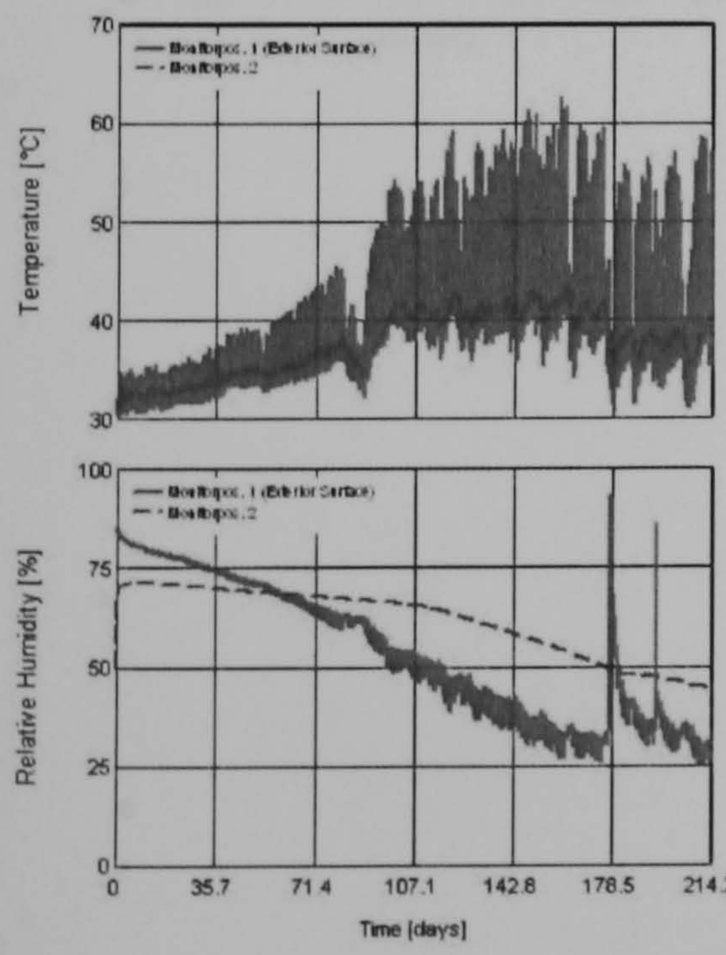

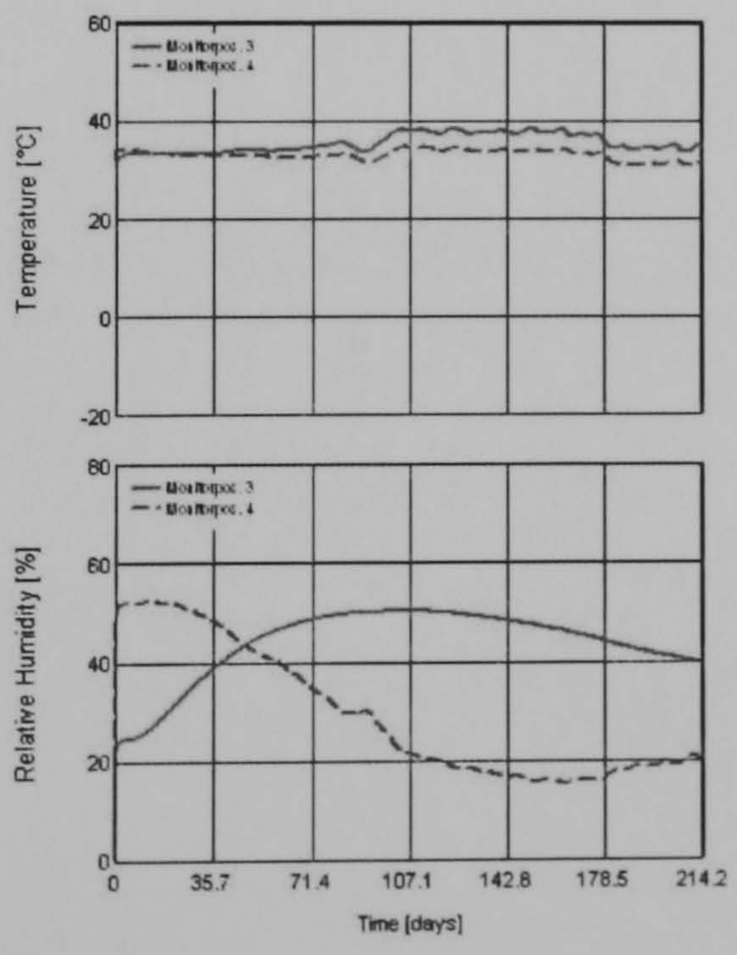

Monitoring point 1 (exterior surface)
Monitoring point 2

Monitoring point 3
Monitoring point 4 (interior surface)

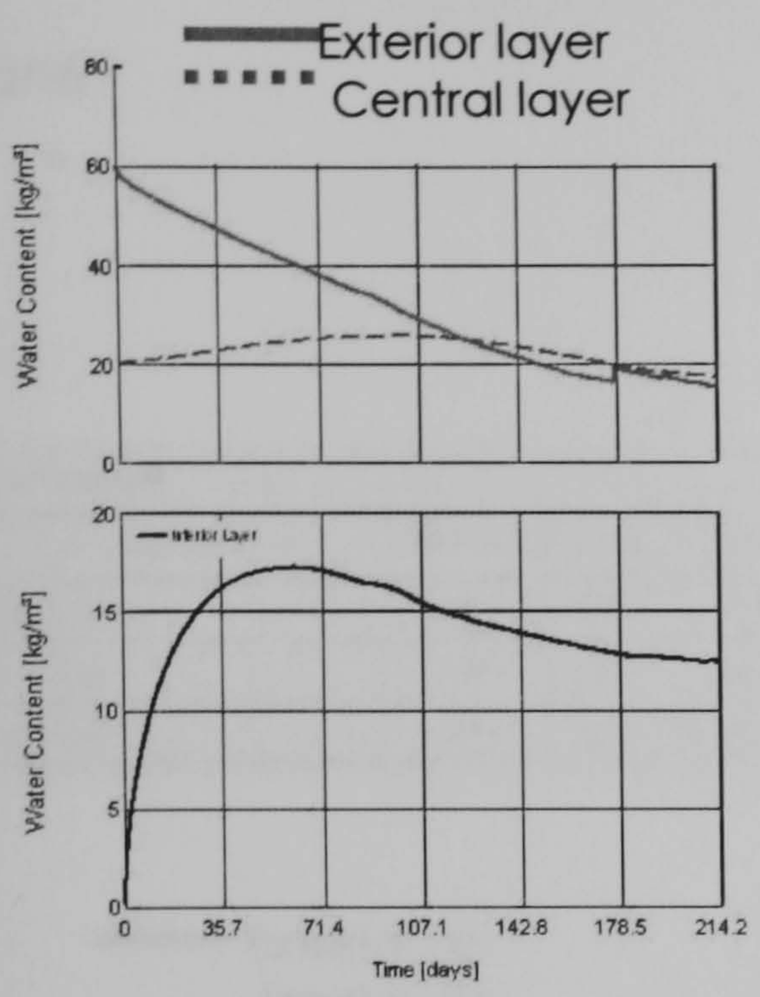
Exterior layer
Central layer
Water Content [kg/m²]
60
40
20
0
Interior Layer
15
10
5
0
0
35.7
71.4
107.1
142.8
178.5
214.2
Time [days]

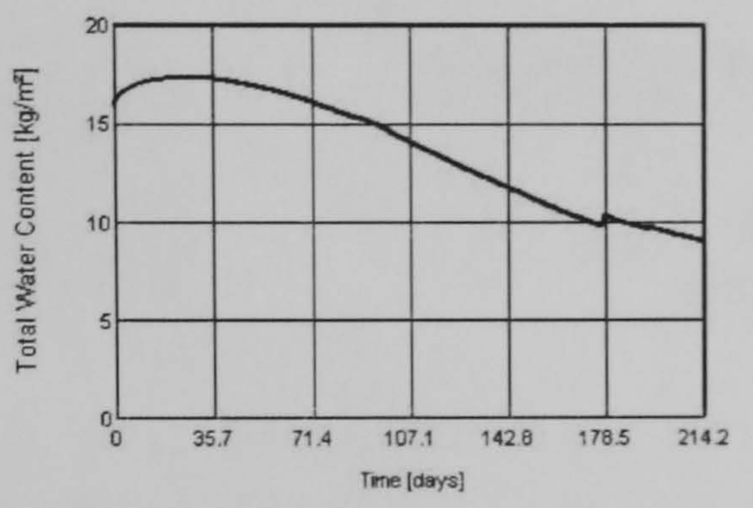
Total Water Content [kg/m²]
20
15
10
5
0
0
35.7
71.4
107.1
142.8
178.5
214.2
Time [days]

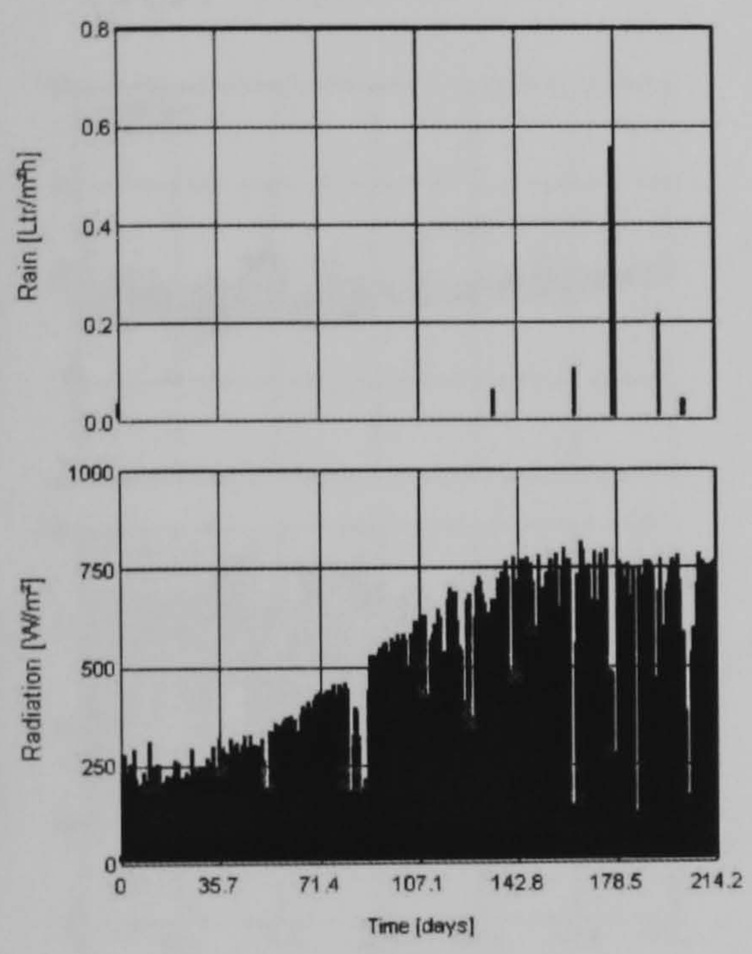
Rain [Ltr/m²h]
0.8
0.6
0.4
0.2
0.0
Radiation [W/m²]
1000
750
500
250
0
0
35.7
71.4
107.1
142.8
178.5
214.2
Time [days]

Run6

Water Content [kg/m²]

Layer/Material	Start of Calc.	End of Calc.	Min.	Max.
Exterior Layer	60,00	19,93	18,96	71,83
Central Layer	20,00	20,50	16,72	24,47
Interior Layer	0,00	19,86	0,00	19,86

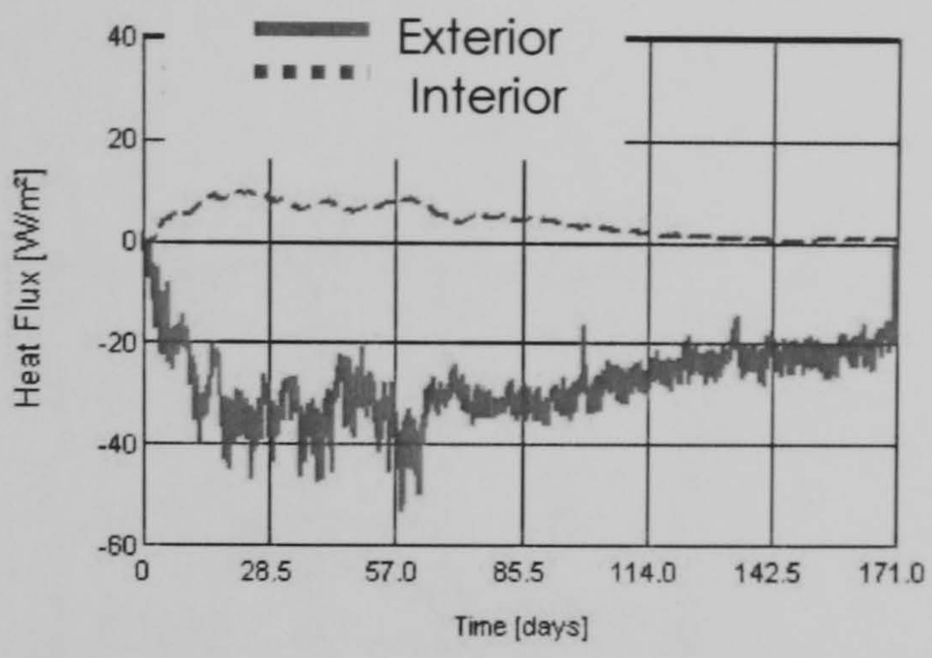

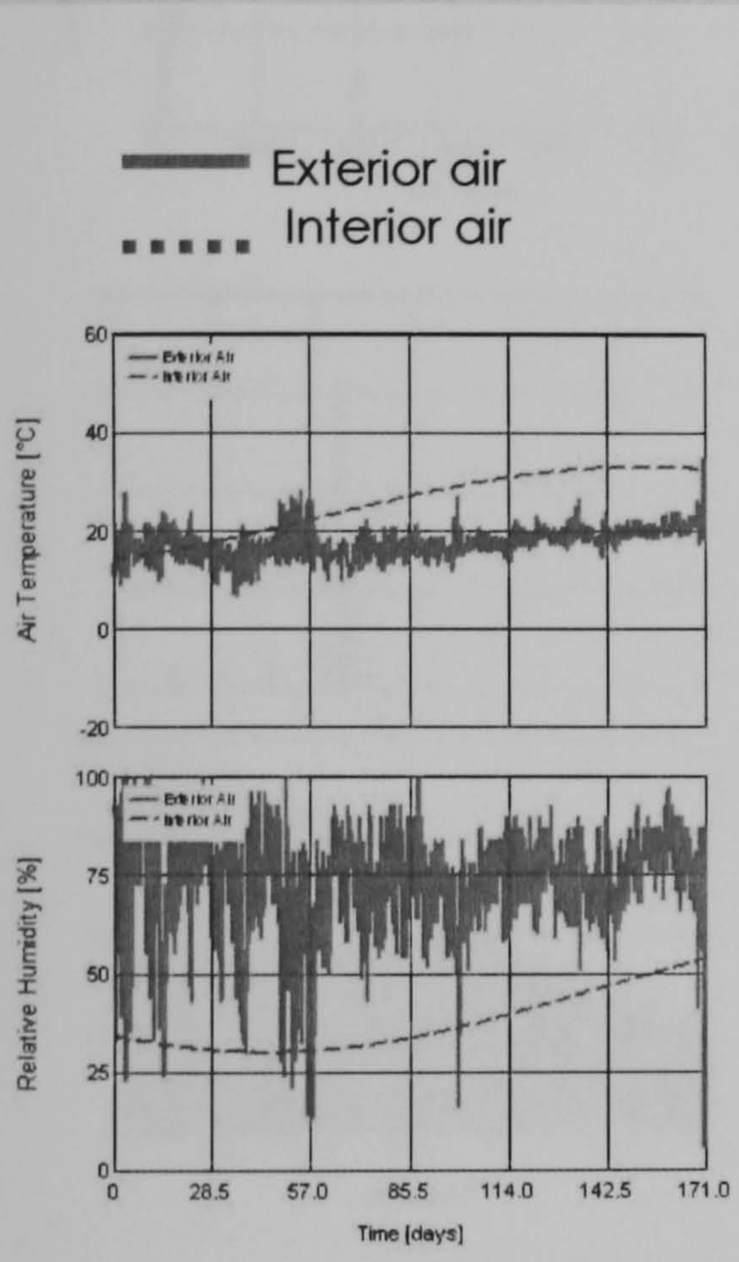

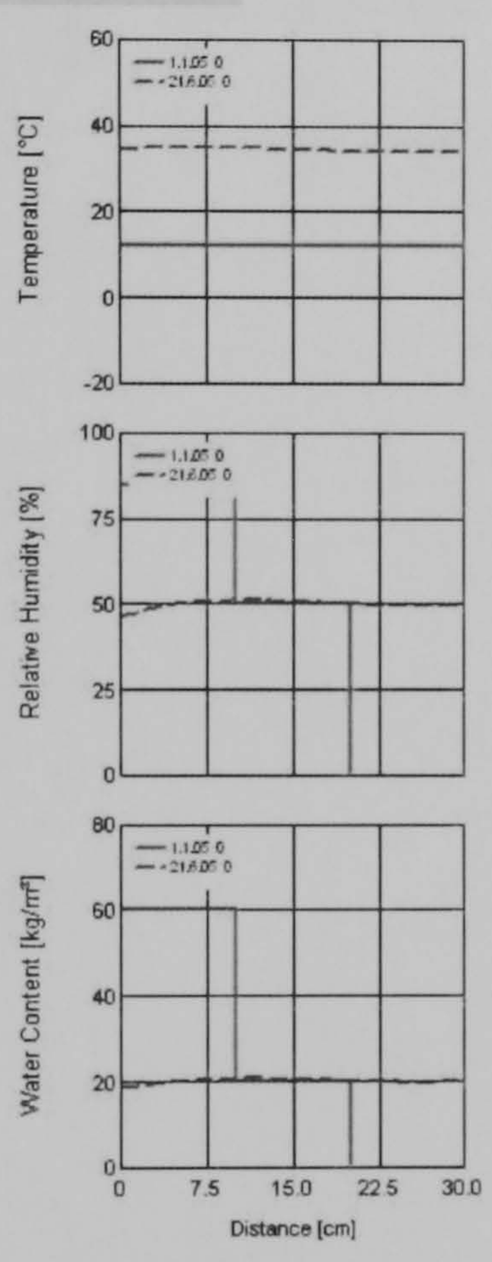

First day simulation
Last day simulation

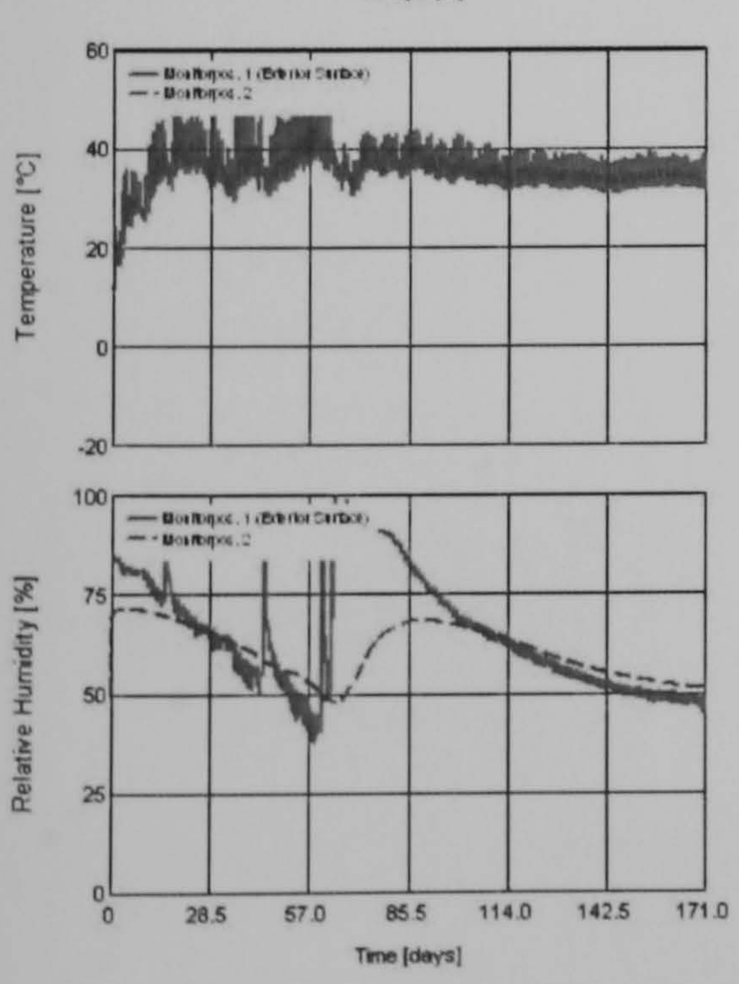

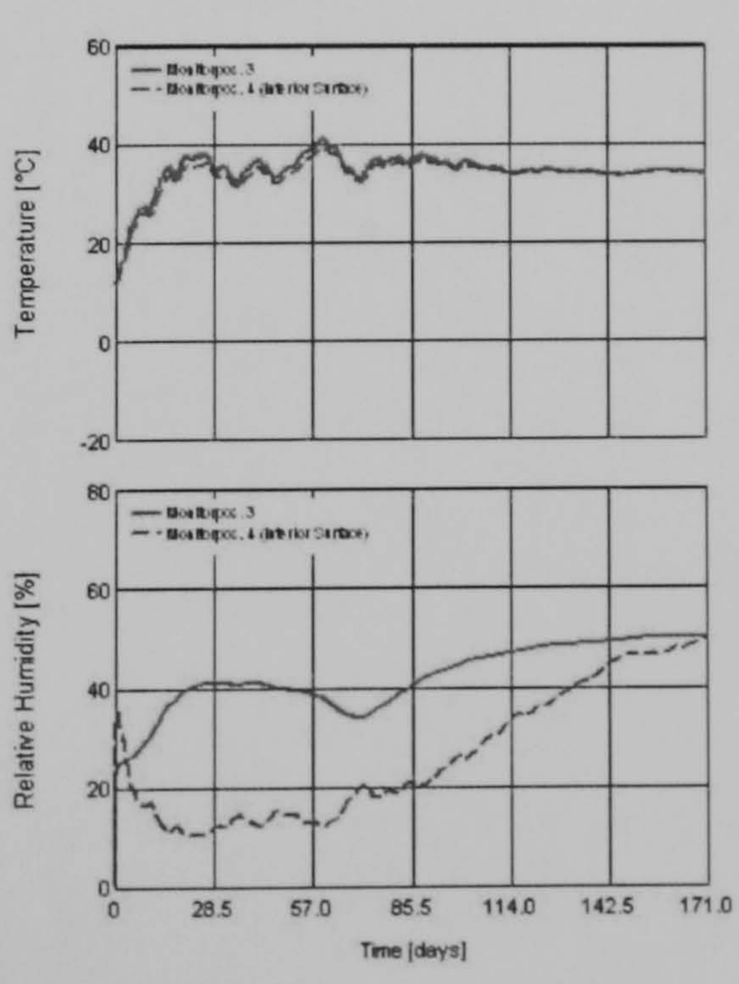

Monitoring point 1 (exterior surface)
Monitoring point 2

Monitoring point 3
Monitoring point 4 (interior surface)

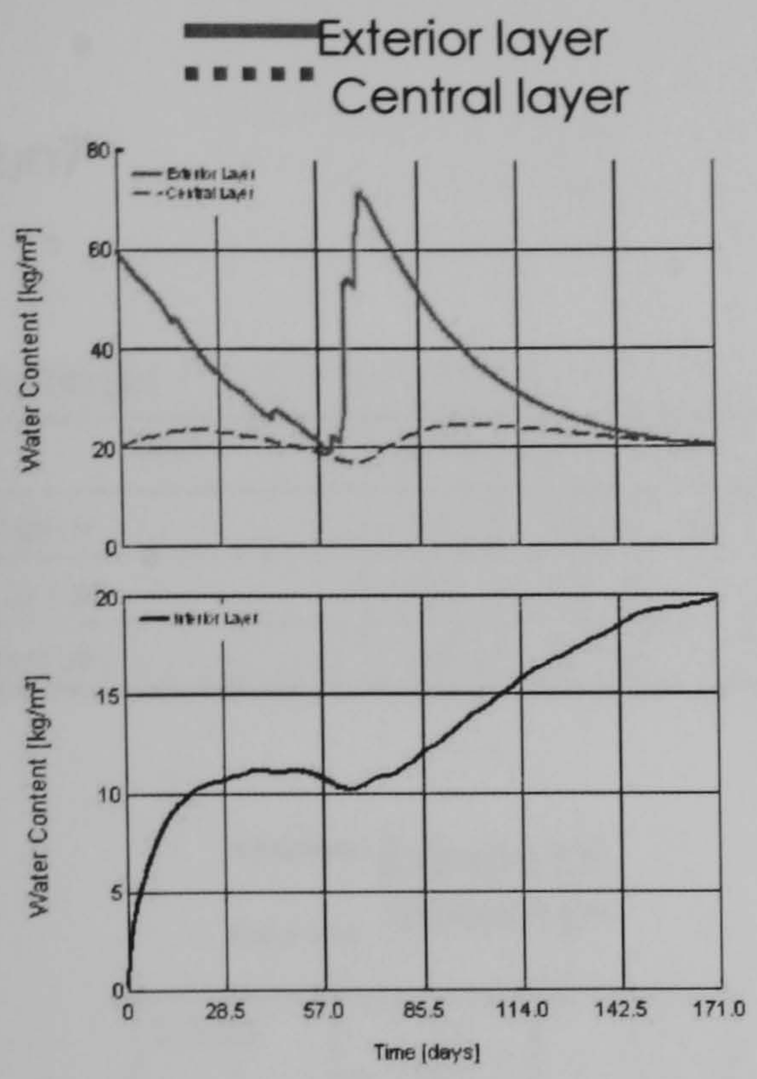
Exterior layer
Central layer
Water Content [kg/m²]
60
40
20
0
Water Content [kg/m²]
20
15
10
5
0
0
28.5
57.0
85.5
114.0
142.5
171.0
Time [days]

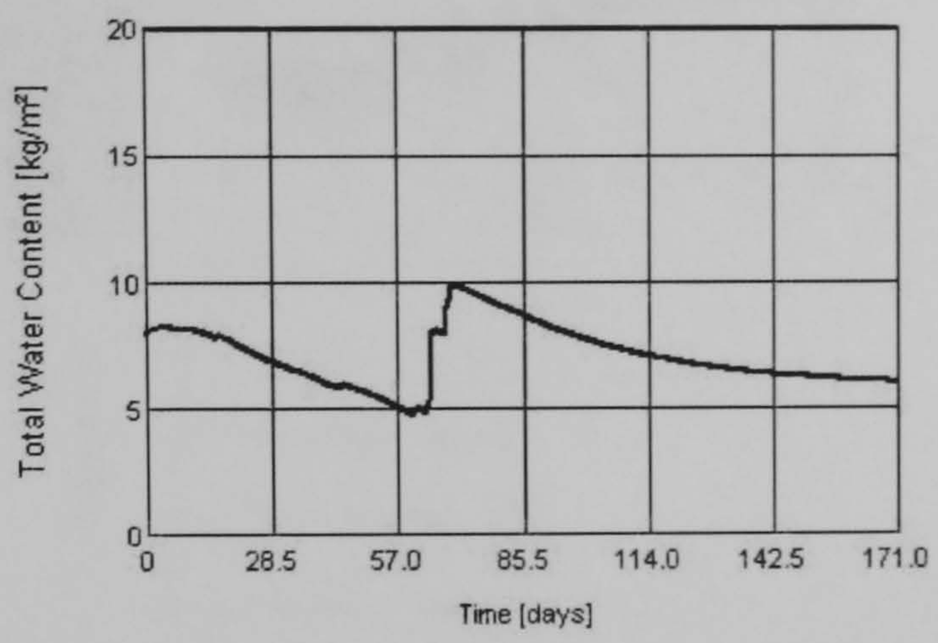
Total Water Content [kg/m²]
20
15
10
5
0
0
28.5
57.0
85.5
114.0
142.5
171.0
Time [days]

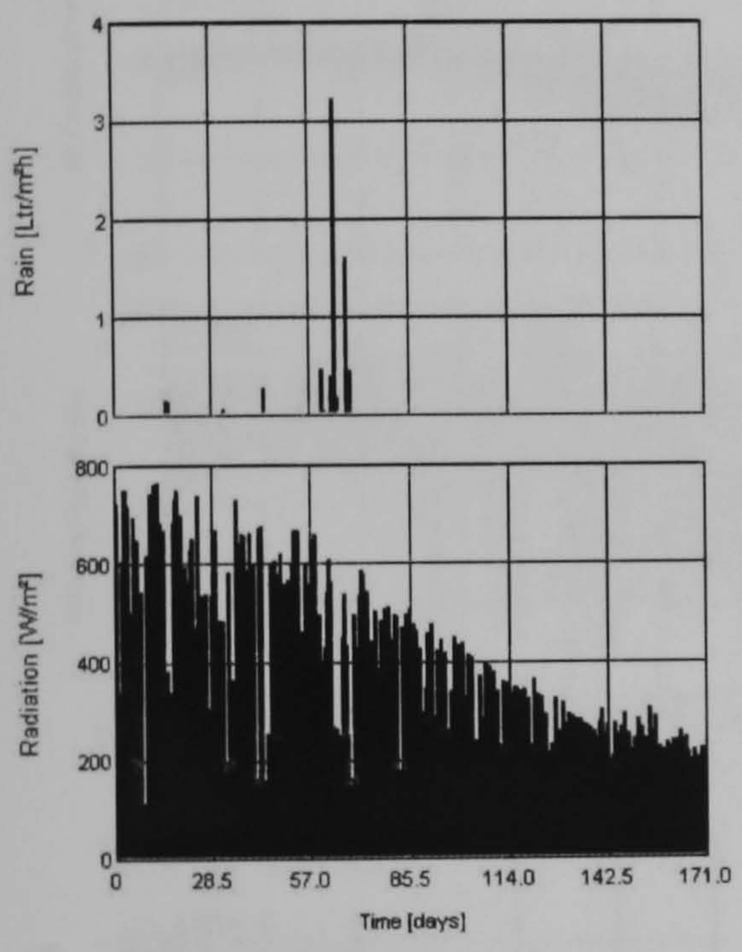
Rain [Ltr/m²h]
4
3
2
1
0
Radiation [W/m²]
800
600
400
200
0
0
28.5
57.0
85.5
114.0
142.5
171.0
Time [days]

Run7

Water Content [kg/m³]

Layer/Material	Start of Calc.	End of Calc.	Min.	Max.
Exterior Layer	60,00	15,93	14,62	60,00
Central Layer	20,00	15,74	15,74	22,72
Interior Layer	0,00	13,27	0,00	16,24

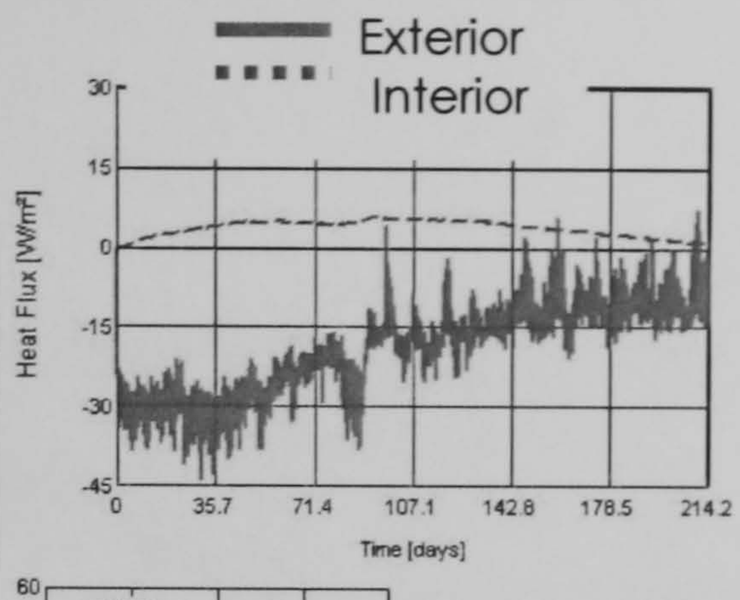

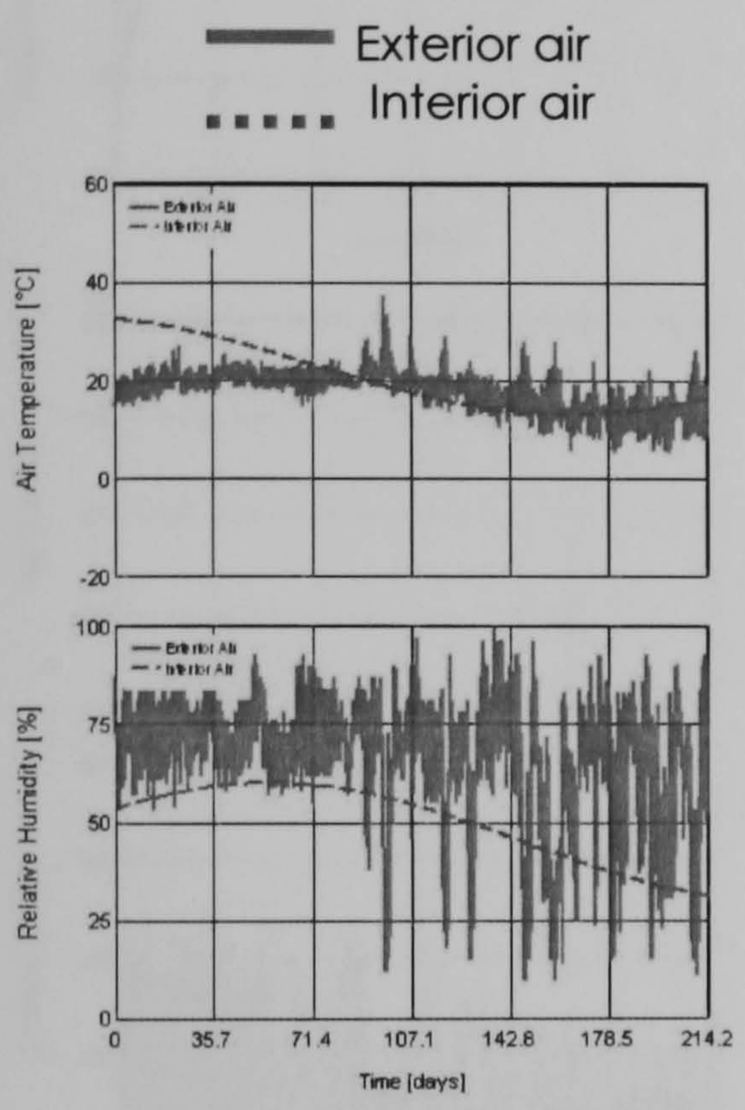

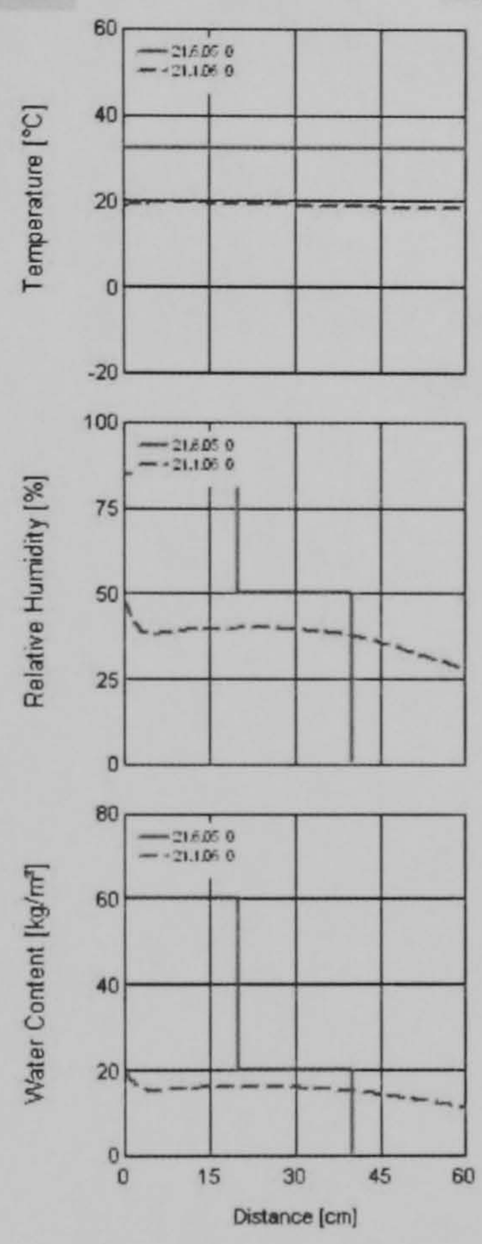

First day simulation
Last day simulation

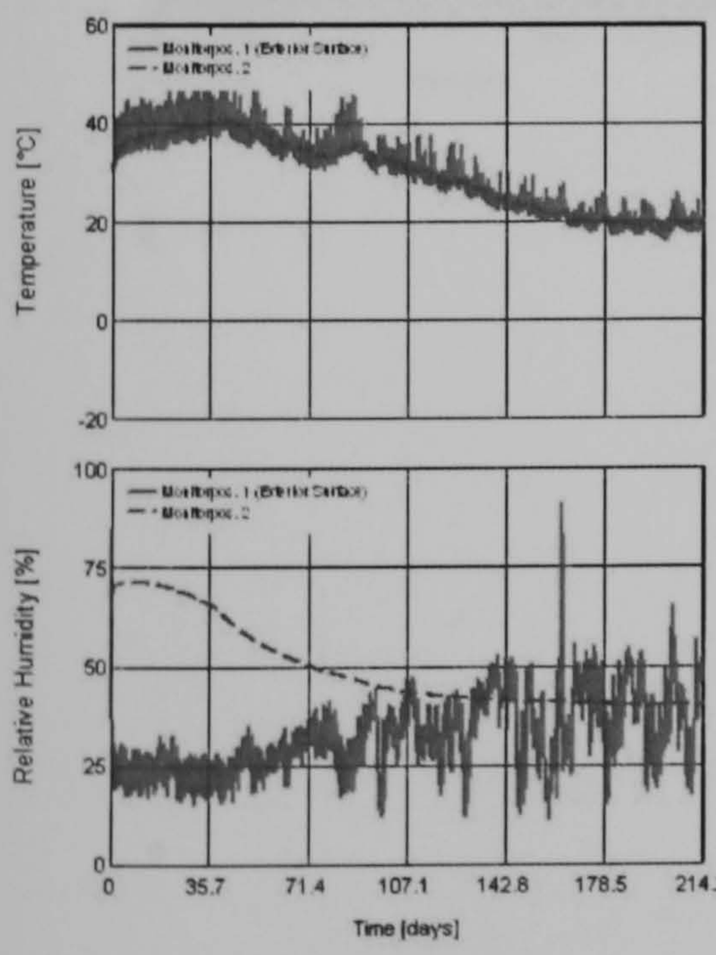

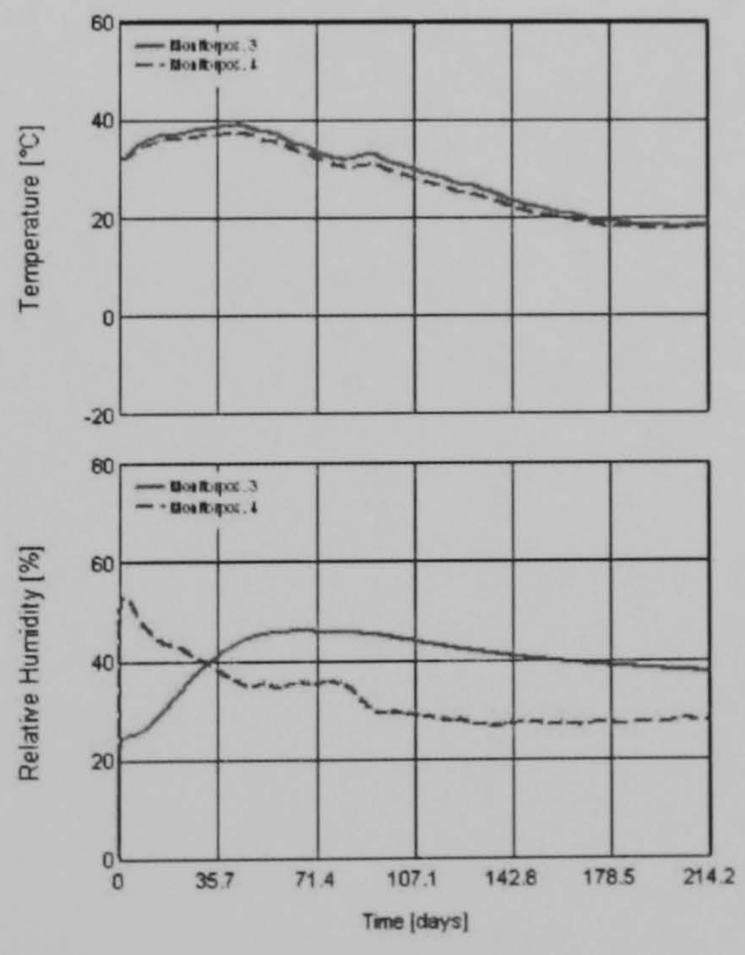

Monitoring point 1 (exterior surface)
Monitoring point 2

Monitoring point 3
Monitoring point 4 (interior surface)

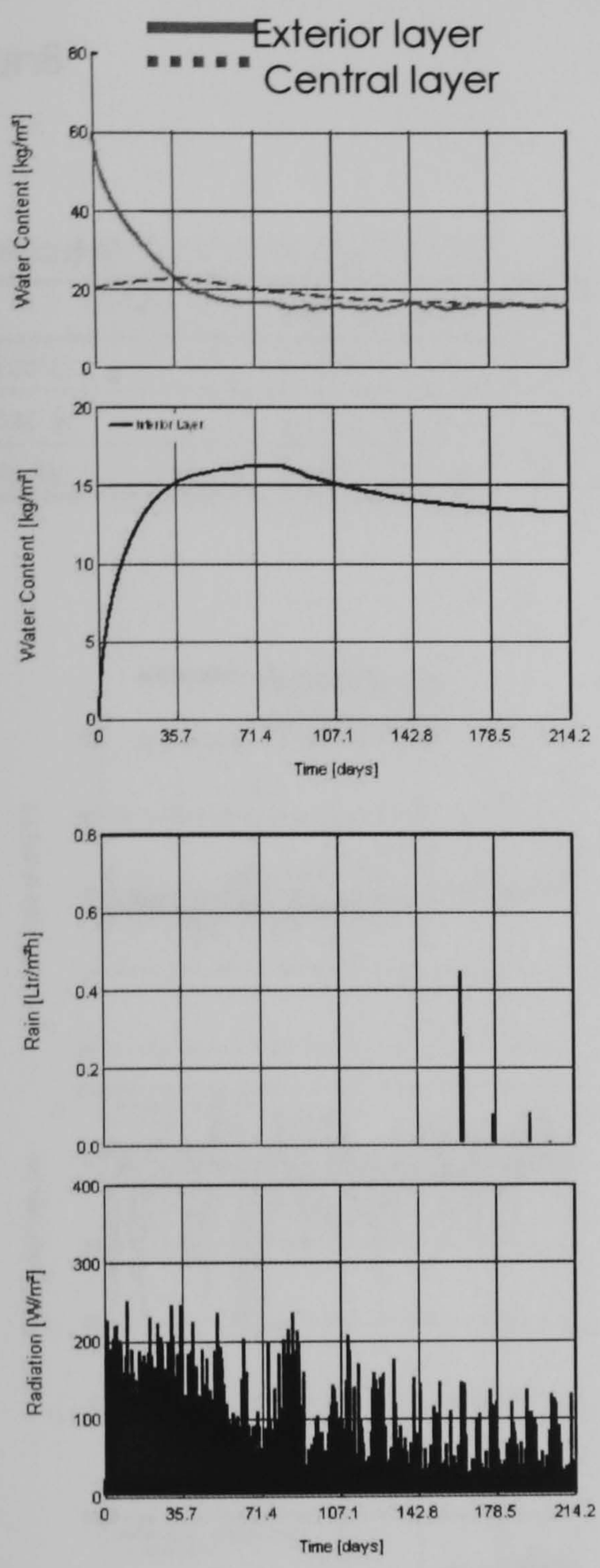
Exterior layer
Central layer
Water Content [kg/m²]
60
40
20
0
Interior Layer
15
10
5
0
35.7
71.4
107.1
142.8
178.5
214.2
Time [days]
Rain [Ltr/m²h]
0.8
0.6
0.4
0.2
0.0
Radiation [W/m²]
400
300
200
100

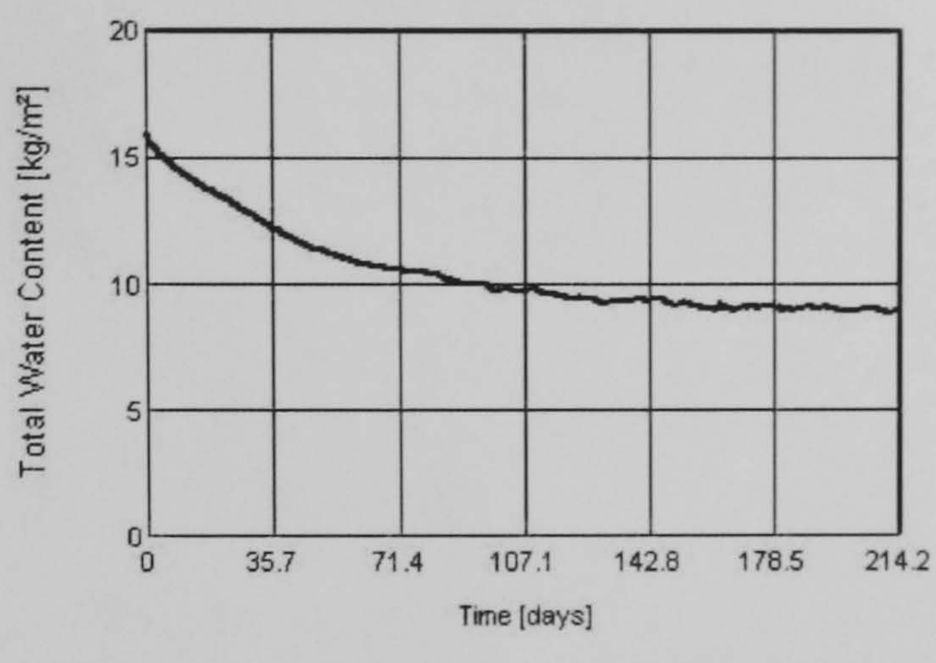
Total Water Content [kg/m²]
20
15
10
5
0
0
35.7
71.4
107.1
142.8
178.5
214.2
Time [days]

Run8

Water Content [kg/m³]

Layer/Material	Start of Calc.	End of Calc.	Min.	Max.
Exterior Layer	60,00	9,41	9,41	60,00
Central Layer	20,00	12,57	12,57	23,68
Interior Layer	0,00	14,34	0,00	19,01

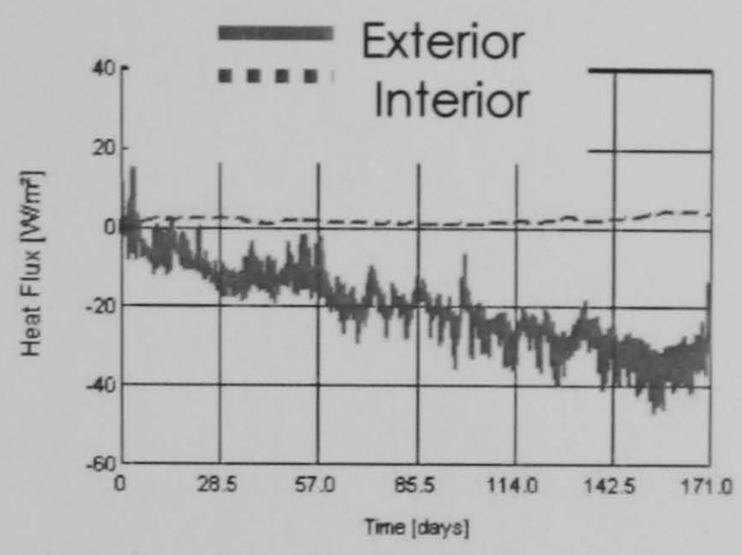

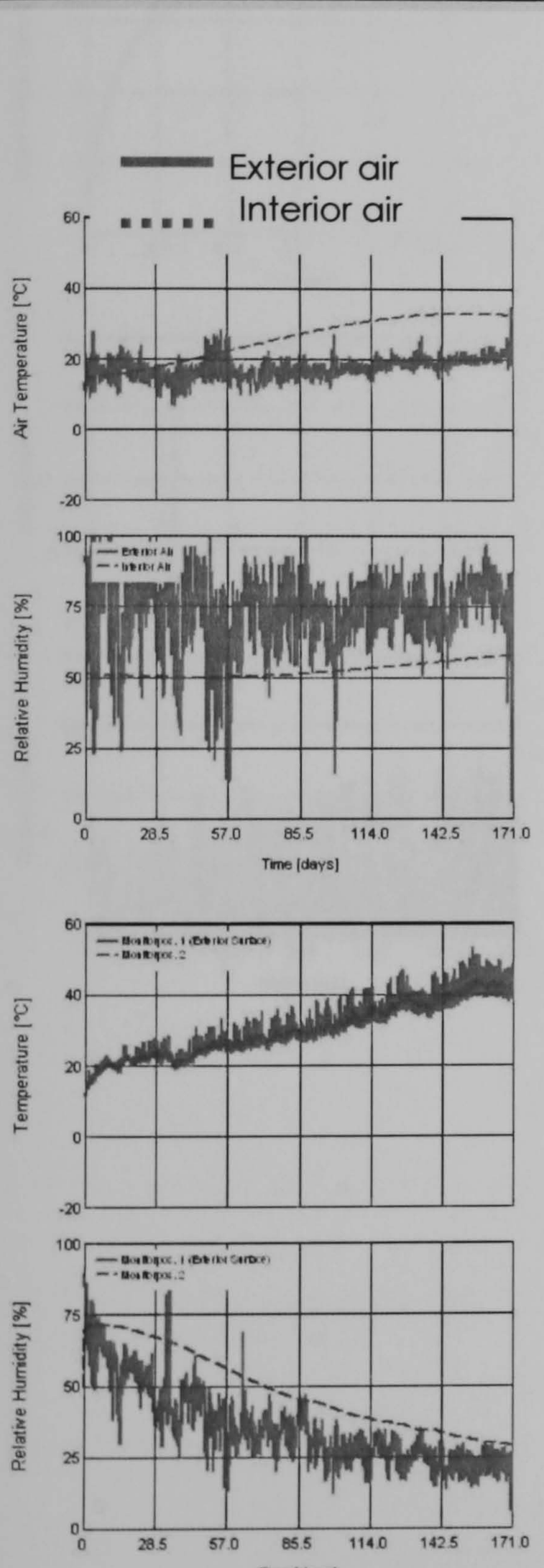

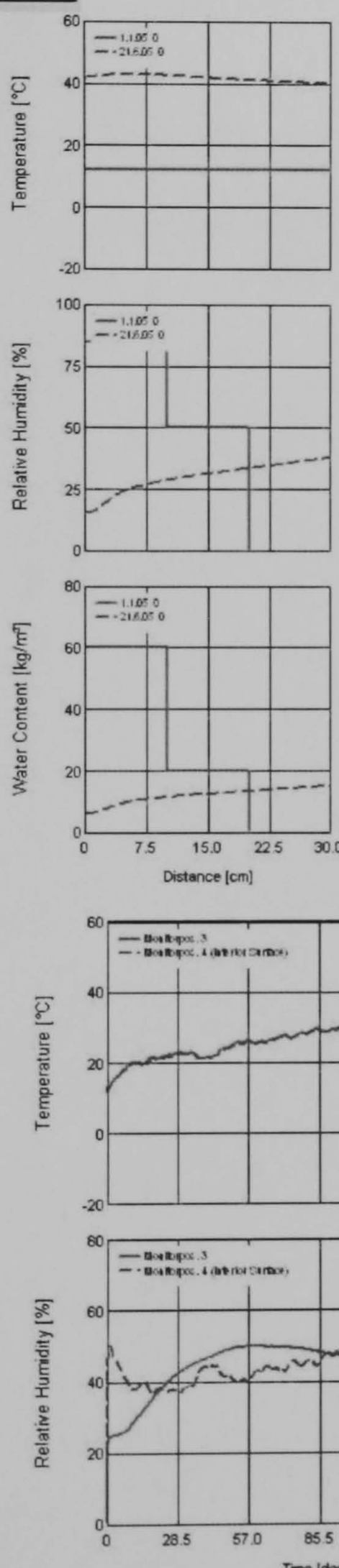

First day simulation
Last day simulation

Monitoring point 1 (exterior surface)
Monitoring point 2

Monitoring point 3
Monitoring point 4 (interior surface)

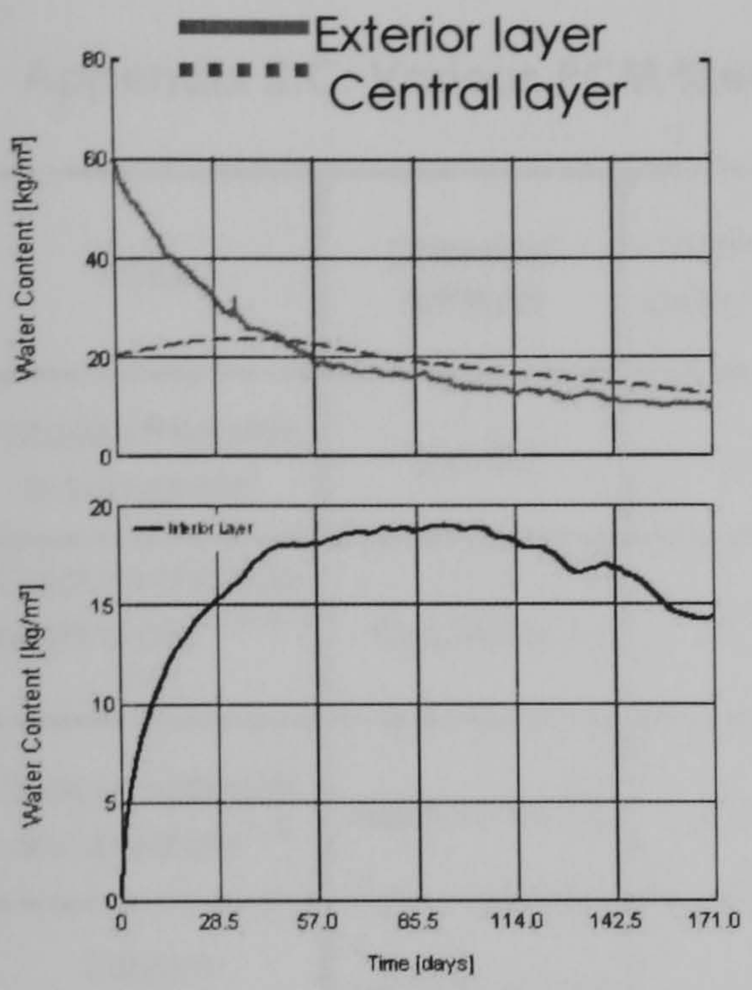
Exterior layer
Central layer
Water Content [kg/m³]
80
60
40
20
0
Interior Layer
Water Content [kg/m³]
20
15
10
5
0
0
28.5
57.0
85.5
114.0
142.5
171.0
Time [days]

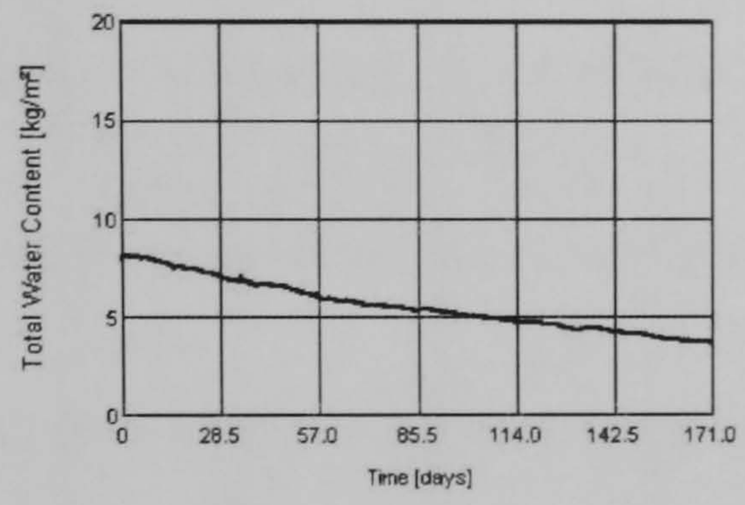
Total Water Content [kg/m²]
20
15
10
5
0
0
28.5
57.0
85.5
114.0
142.5
171.0
Time [days]

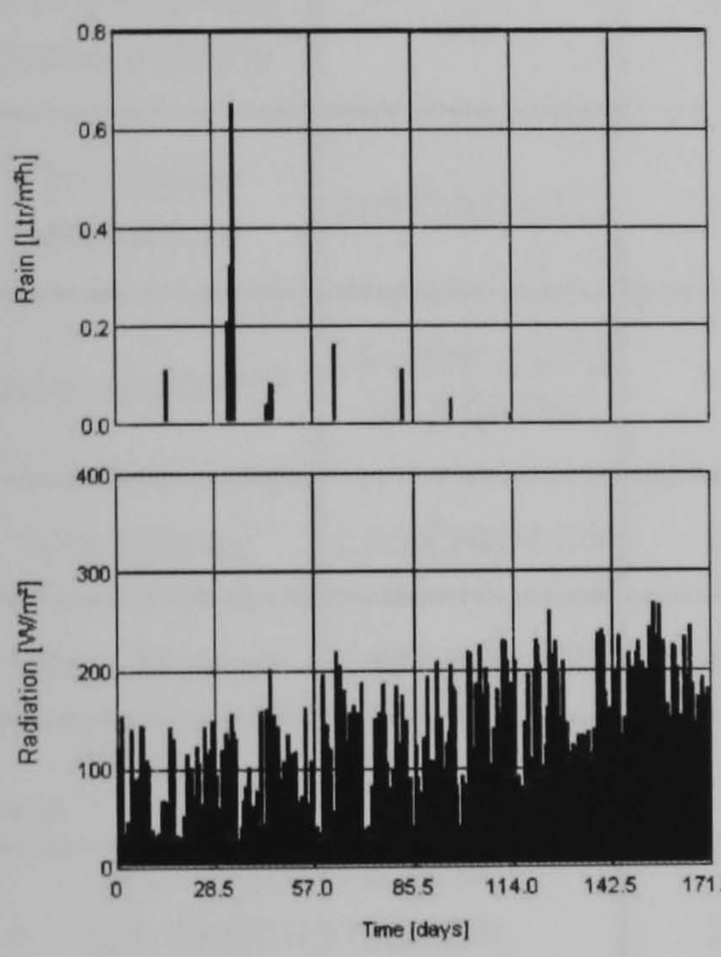
Rain [Ltr/m²h]
0.8
0.6
0.4
0.2
0.0
Radiation [W/m²]
400
300
200
100
0
0
28.5
57.0
85.5
114.0
142.5
171.0
Time [days]

Appendix 2.C: Various PCM thermal properties and prices

PCM	Chemical formula	Melting point(°C)	Density (kg/m^3)	Specific heat ($kJ/kg°K$)	Thermal conduct ($W/m°K$)	Enthalpy (kJ/kg)	Aldrich Prod. num	Price
Potassium flouride tetrahydrate[1]	KF4H2O	18.5	-	-	-	231	-	-
Calcium chloride hexahydrate[3,14,15,16,21,22]	CaCl26H2O	29.7	1680(s)1500(l)	1.25(s)2.13(l)	0.624(s)0.454(l)	200	21110	£15/kg
Sodium sulphate decahydrate[1,15]	Na2SO410H2O	32.4	1485	2	0.15(s)0.3(l)	254	71971	£8.90/kg
Sodium orthophosphate dodecahydrate[1]	Na2HPO412H2O	35	-	-	-	281	-	-
Zinc nitrate hexahydrate[1]	Zn(NO3)26H2O	36.4	2065	-	-	147	96482	£114.97/kg
Butyl stearate[1,24]	CH3(CH2)16COO(CH2)3CH3	19	861	-	-	140	B5720	£15.30/lt
1-dodecanol[1]	CH3(CH2)11OH	26	800	-	0.14	200	44381-6	£42.6/kg
1-tetradecanol[1]	CH3(CH2)12OH	38	823	-	0.136	205	T960-0	£21.4/kg
Paraffin wax[1,6,7,8,9,13,14,15,17]	CH3(CH2)n(CH3)..	20 | 60	786	2.04/2.89	0.14(s)0.277(l)	141 | 266	Pot Hille	£8.86/kg
45% CH3(CH2)8COOH 55% CH3(CH2)10COOH 45/55 capric-lauric acid[1]		21	*	*	*	143	*	*
Propyl palmitate[1]	CH3(CH2)12COOC3H7	19	-	-	-	186	-	-
73.5% C10 H20 O2 26.5% C10 H26 O2 73.5/26.5 capric-myristic acid[1]		21.4/23.5	*	*	*	152	*	*
75.2% C10 H20 O2 24.8% C16 H32 O2 75.2/24.8 Capric acid-Palmitic[1]		22.1/23.5	*	1.83(s)2.15(l)	0.185	152	*	*
62.6% C12 H24 O2 37.4% C14 H26 O2 62.6/37.4 Lauric-myristic acid[1]		31.8/32.6	*	*	*	156	*	*

PCM	Chemical formula	Melting point(°C)	Density (kg/m^3)	Specific heat (kJ/kg°K)	Thermal conduct (W/m°K)	Enthalpy (kJ/kg)	Aldrich Prod. num	Price
64% C12 H24 O2 36% C16 H32 O2 64/36 Lauric-palmitic acid[1,15]		33	*	*	*	165	*	*
75.5% C12 H24 O2 24.5% CH3(CH2)16CO2H 75.5/24.5 Lauric-stearic acid[1,15]		37	*	*	*	171	*	*
61.5% C10 H20 O2 38.5% C10 H24 O2 61.5/38.5 capric-lauric acid[1,15]		18.5	*	*	*	132	*	*
Myristic-palmitic[1]	-	39.8	-	-	-	165	-	-
Myristic-stearic[1]	-	44	-	-	-	181	-	-
Palmitic-stearic[1,15,26]	-	50.4	-	-	-	179	-	-
Lauric[1,15,33]	C12H24O2	41.3/43/45	870	1.76(s), 2.27(l)	1.6	178/211	61620	£12.30/kg
Capric[1,2,15]	C10H20O2	31¦33	886	2.09	0.17	153	W23264	£18/lt
Myristic[1,15,33]	C14H26O2	52.1	844	2.26	0.1-0.2	187/204	70082	£17.30/kg
Palmitic[1,15,31,33]	C16H32O2	54.1-64	0.942(s) 0.862(l)	2.20(l) 1.70(s)	0.16	183/203	76122	£23.3/kg
Stearic[1,7,15,26,27,33,34]	CH3(CH2)16CO2H	64.5/70	845	2.07(l) 1.90(s)	0.1-0.2	196/203	17536	£12/kg
Capric-stearic[1]	-	26.8	-	-	-	160	-	-
olefins, isoparaffins, n-paraffins[2,11,12,14,18,25]	-	4.5¦68	817¦930	2.1¦2.5	0.15¦0.21	153¦244	-	-
Water	H2O	0	917(l) 998(s)	2.09(s) 4.18(l)	2.2(s) 0.69(20°C)	333	-	-
Salt: Potassium fluoride tetrahydrate[2]	FK · 4H2O	18.5	1455	1.84(s) 2.39(l)	-	231	-	-
Salt: Calcium chloride hexahydrate[2,3,9]	CaCl2 · 6H2O	29.7	1710(s)1 496(l)	1.45(s)	-	171	21111	£24.70/kg
Salt:Sodium sulfate decahydrate[2,14]	Na2O4S · 10H2O	32.4	1485(s)	1.93(s)	0.544	254	71971	£10.50/kg

PCM	Chemical formula	Melting point(°C)	Density (kg/m^3)	Specific heat (kJ/kg°K)	Thermal conduct (W/m°K)	Enthalpy (kJ/kg)	Aldrich Prod. num	Price
Salt: Sodium phosphate dibasic dodecahydrate[2]	HNa2O4P · 12H2O	35	1520(s) 1442(l)	1.7(s) 1.95(l)	0.514(s) 0.476(l)	281	71663	£21.20/kg
Salt: Zinc nitrate hexahydrate[2]	N2O6Zn · 6H2O	36.4	2065	1.34(s) 2.2.6(l)	-	147	96482	£27.50/kg
Salt: Sodium thiosulfate pentahydrate[2, 23]	Na2O3S2 · 5H2O	48	1730(s)- 1670(l)	1.46(s) 2.39(l)	-	201	S8503	£24/kg
Salt:Barium hydroxide octahydrate[2]	H2BaO2 · 8H2O	78	2180(s)	1.17	-	267	217573	£36.8/kg
Salt: Magnesium chloride hexahydrate[4,15]	Cl2Mg · 6H2O	58/116	1570(s) 1450(l)	2.25(s) 2.61(l)	0.704(s) 0.570(l)	132/168	63033	£29.60/kg
Eutectic[2]:Sodium sulfate(13%), Sodium chlorate(13%), Potassium chlorate (16%), Water(40%)	Na2O4S(31%) ClNaO3(13%) ClKO3(16%) H2O(40%)	4	-	-	-	234	71963, 71368, 60124	£11/kg, £54.2/kg £42.9/kg
Eutectic[2]:Calcium chloride(48%), Sodium chlorate(4.3%),Potassium chlorate (0.4%), Water(47.3%)	CaCl2(48%) ClNaO3(4.3%) ClKO3(0.4%) H2O(47.3%)	26.8	-	-	-	-	383155 71368 60124	- £54.2/kg £42.9/kg
Eutectic[2]: Calcium nitrate tetrahydrate(67%), Magnesium nitrate hexahydrate(33%)	CaN2O6 · 4H2O(67%), MgN2O6 · 6H2O(33%)	30	-	-	-	136	21194 63084	£53.4/kg £31.5/kg
Eutectic2: Propionamide (25.1%), Palmitic acid (74.9%)	-	50	-	1.96(s) 2.40(l)	-	192	-	-

PCM	Chemical formula	Melting point(°C)	Density (kg/m^3)	Specific heat (kJ/kg°K)	Thermal conduct (W/m°K)	Enthalpy (kJ/kg)	Aldrich Prod. num	Price
Eutectic[2]:Magnesium nitrate hexahydrate(53%in mol%), Magnesium chloride hexahydrate(47%)	MgN2O6·6H2O(53%), Cl2Mg·6H2O(47%)	59.1	-	1.34(s) 3.16(l)	-	144	63084 63033	£31.5/kg £29.60/kg
Eutectic[2]:Magnesium nitrate hexahydrate(53%in mol%), Aluminum nitrate nonahydrate(47%)	MgN2O6·6H2O(53%), AlN3O9·9H2O(47%)	61	-	-	-	148	63084 31154	£31.5/kg £29.9/kg
Eutectic[2]: Lithium nitrate(27% in mol%), Hydroxylammonium nitrate(68%), Ammonium chloride(5%)	LiNO3(27%) H4N2O4(68%) ClH4N(5%)	81.6	-	-	-	111	13023 438235 09724	£54.4/kg - £16.9/kg
Methyl Palmitate(93-95%), Methyl Stearate(7-5%) [5]	-	23|26.5	-	-	-	180	-	-
Acetamide[7]	CH3CONH2	81	-	1.98	-	241	160	£68.2
Shaped-stabilized paraffin[10]	-	53.8	-	-	-	121.4	-	-
Sodium thiosulphate pentahydrate[15]	Na2O3S2·5H2O	48	-	-	-	200	-	-
Sodium phosphate dibasic dodecahydrate[15]	HNa2O4P·12H2O	34|37	-	-	-	265	71663	£21.20/kg
Sodium carbonate decahydrate[15]	CNa2O3·10H2O	32|36	-	-	-	247	71366	£12.80/kg

PCM	Chemical formula	Melting point(°C)	Density (kg/m^3)	Specific heat ($kJ/kg°K$)	Thermal conduct ($W/m°K$)	Enthalpy (kJ/kg)	Aldrich Prod. num	Price
Eutectic[15]:Sodium sulfate(32.5%), water(41.4%), Sodium chlorate(6.66%), Ammonium chloride(6.16%)	Na2O4S(32.5%) H2O(41.4%), NaCl(6.66%), ClH4N(6.16%)	13	-	-	-	146	71963 - 71368 09724	£11/kg £54.2/kg £16.90/kg
Eutectic[15]: Magnesium nitrate hexahydrate(61.5%),Ammonium nitrate(38.5%)	MgN2O6· 6H2O(61.5%), H4N2O3(38.5%)	51	-	-	-	131.3	63084 09889	£31.5/kg, £40.70/kg
Eutectic[15]: Magnesium nitrate hexahydrate(58.3%),Magnesium chloride hexahydrate(41.7%)	MgN2O6· 6H2O(58.3%),Cl 2Mg· 6H2O(41.7%)	58	-	-	-	106	63084 63033	£31.5/kg, £29.60/kg
Eutectic [15]: Calcium chloride hexahydrate+ Calcium bromide hexahydrate	CaCl26H2O	14	-	-	-	140	21110 -	£15/kg -
1,1,1-Tris(hydroxymethyl) ethane[19]	C5H12O3	81 (solid-solid transforma tion)	1193 1118	2.75	0.36|0.34	193	93340	£21.40/kg
Polyethylene glycol[20]	-	34	1100(l) 1120s)	2.26	0.188	150.5	-	-
Neopentyl glycol[19]	-	43 (solid-solid transforma tion)	1046 984	2.76	0.25|0.21	131	-	-
Manganese nitrate hexahydrate[25]	Mn(NO3)2·6H2 O	-	-	-	-	-	-	-

PCM	Chemical formula	Melting point(°C)	Density (kg/m^3)	Specific heat ($kJ/kg°K$)	Thermal conduct ($W/m°K$)	Enthalpy (kJ/kg)	Aldrich Prod. num	Price
TME tetrahydrate (PCM30) [25]	C5H12O3·4H2O	-	-	-	-	-	93340	£21.40/kg
Oleic acid [26]	C18H34O2	-4 ¦ 16	-	-	-	75.5	75096	£16.30/lt
(0-100%) C12 H24 O2 (100-0%) C16 H32 O2 Lauric-palmitic acid[28]		32.13-63.28	-	-	-	146.5 ¦ 202	-	-
(65mol%) CH3(CH2)8COOH (35 mol%) CH3(CH2)10COOH 65/35 capric-lauric acid[29]		18	894.9(l) 900(s)	2.24(l) 1.97(s)	0.139(l) 0.143(s)	140	-	-
(65mol% capric +35mol%lauric)+Pentadecane proportions:90:10, 70:30, 50:50		10.2 ¦ 13.3	827 ¦ 883 (l), 850 ¦ 900 (s)	2.42 ¦ 2.89(l), 2.08 ¦ 2.44(s)	-	142.2 ¦ 157.8	-	-
Pentadecane[29]	C15H32	9.6	727(l) 776(s)	3.53(l) 3.08(s)	0.15(l) 0.182(s)	168	76510	£300/lt
Neopentylglycol[30]	-	43	-	-	-	130	-	-
Methyl stereate[32]	CH3(CH2)16CO2CH3	37.8	-	-	-	240	-	-
Methyl palmitate[32]	CH3(CH2)14CO2CH3	29	-	-	-	215	-	-

"-" : Not available "*" data for individual elements forming part of the mixture presented elsewhere in the table; "/" separating different values presented in literature; " ¦ " separating a range of values. Superindex indicates source of information

For materials with no available information on density and specific heat, according to (Hasnain 1998), for organic PCM this values are around 2kJ/kg specific heat andaround 800 kg/m3 density. For organic PCM also 2kJ/kg specific heat, and 1600 kg/m3 density

1: (Kelly 1999), 2: (Abhat,1983), 3:(Yanadori 1989), 4:(Choi 1992), 5:(Feldman 1995B), 6: (Brousseau 1996), 7:(Sharma 1999), 8:(Tayeb 1996), 9:(El-Dessouky 1997), 10: (Inaba 1997), 11:(Leong 1997), 12: (Leong 1997B), 13:(Bo 1998), 14:(Essen, 1998), 15:(Hasnain 1998), 16:(Carlsso 1980), 17: (Banazec 1999), 18(Tan 1999), 19:(Wang 1999), 20(Wang 1999B), 21:(Bajnoczy 2000), 22:(ESen 2000), 23:(Hadjieva 2000), 24:(Lee 2000), 25:(Domanski 2000), 26(Cedeno 2001), 27:(Sari 2001), 28: (Zhang 2001), 29:(Dimaano 2001),30:(Dincer 2002), 31:(Sari 2002), 32:(Nikolic 2003), 33:(Sari 2003), 34:(Buddhi 1999)

Appendix 2.D: PCM Related experimental work

Ref	Geom	PCM	Experiment	General Features
(Cardinale and Vacca)		Salt hydrates (SSDH) & Paraffins	Trombe walls containing PCM	
(Goff)	Fats and oils (beef tallow and soybean oil), Palmitic and stearic acid			
(Hawes, Banu et al.)		Wallboard k, α	Gypsum Impregnated wallboard & Impregnated concrete block	Wall length to depth is short, doesn't require mechanical means for heat exchange. Thermal inertia reduces thermostat switching
(Jahns)	Paraffinic hydrocarbons, fatty acids and fatty alcohols preferred for use in buildings for zero solubility in water. Salt hydrates may wash out in moist climate			Advantages and disadvantages of encapsulated and impregnated PCM (advantage of thermal mass). Focuses in microcapsules
(Kelly)	Salt hydrates, organic PCMs, Fatty acids, PCM combinations, concrete-PCM			Latent and sensible storage, economic viability, energy storage. Capric acid phase diagram
(McCoy)		Sodium acetate trihydrate		Crystallization, super cooling, hot pack
(R.Domanski and Jaworski)		Waxes, n-alkanes & salt hydrates	PCM properties investigation stand. *DSC* curves	Measurement of properties: Cp, TM, H, and relation T-H for not-pure substances (larger samples) stability after cycling. Allows to observe superheating and sub-cooling. Thermal history of material influences enthalpy changes vs Temperature
(Szwedowska-Kotlinska and Wolna)		Sodium sulfate decahydrate	Sealed glass pipes with mineral fibres (to avoid irrevers) and SSDH	SSDH disadvantages: incongruent melting, supercooling, decay of prop with cycling
(Cohen 1979)		Paraffin, Glauber's salt	Test facility apparatus for testing various TES units to asses potential	Optimization of energy storage system. PET program, accuracy of instruments. Economics of tets. Industrial space heating using waste heat, instrumentation, calibration curves
(Carlsson and Wettermark 1980)	Cylindrical	Calcium chloride hexahydarte	Polyethylane container app. With tube heat exchanger to determine heat transfer properties	Describes experimental rig. Explains observed phenomenon
(Hale and Viskanta 1980)	Rectangular	Freezing and melting from above and below photographic observations		Describes experimental rig and test procedure. Dimensionless graphs

Ref	Geom	PCM	Experiment	General Features
(Abhat 1983)	Properties of: Paraffins, fatty acids, inorganic salt hydrates & eutectic compounds		Thermal Analysis and DSC,(advantages & disadvant) thermal cycling	PCMs compatibility with construction materials. Explains incongruent melting and super-cooling in different PCMs. Nucleating agents
(Lane 1986)	Simple and complex geometries		PCM thermophysical prop & selection, nucleation, cycling, encapsulation, TES performance.	
(Yanadori and Masuda 1989)	cylindrical	Properties CCHH	Cylindrical PCM container with vertical pipe inserted	Measures heat transfer rates in the melting liquid layer section. Describes exp.rig
(Choi and Kim 1992)	Circular tube	Properties Magnesium chloride hexahydrate	Finned and unfinned tube	Describes rig, uses cylindrical pyrex glass. Effect of inlet temp. and air flow rate
(Feldman, Banu et al. 1995(B))		Properties Methyl Palmitate-Methyl-Stearate	Impregnated wallboard, DSC,	Describes DSC, explains curves
(Tayeb 1995)		Organic-inorganic mixtures (Glouber's salt & stearic acid	Hot water solar collector feeding a network heat exchanger inside a PCM container	Advantages and drawbacks of organic and inorganic PCM. Effect of HTF flow rate on energy extraction, cycle time, effect of nucleating agent
(Arderius, Lara et al. 1996)?	tube		Glass tube full with PCM	Determines thermal coeffiecients (k, H, density)
(Brousseau and Lacroix 1996)		Properties paraffin wax	Polypropyle container Multipass PCM. Embedded with heat source for storage, flow of HTF for recovery	
(Domanski and Fellah 1996)			Two storage units in series with air as HTF	System's efficiency calculation (first and second law), exergy analysis (entropy generation)
(Feldman and Banu 1996)			DSC (description), gypsum wallboard	Reproducibility of PCM thermal characteristics in wallboard, effects of cycling. Use of internal heat gain which would otherwise be wasted. Table for PCM selection
(Gong and Mujumdar 1996)	Tube with HTF surrounded by external coaxial cylinder made up of segments with PCM various TM.		Enhanced heat transfer rate by use of Multiple PCMs. Bibliography first multilayer slab, and exergy efficiency increase multiple PCM. Effect of flow rate , of inlet temp, and of duration on energy charge and discharge	

Ref	Geom	PCM	Experiment	General Features
(Scalat, Banu et al. 1996)			Full scale room lined with PCM wallboard. DSC for PCm selection	Procedure for fabricating wallboard, and exp. description . Rapid thermal charge-discharge. Heating and cooling mode room temp. performance. VOC's
(Tayeb 1996)		Paraffin wax, inorganic salts and metals	Metal slags and chips are placed in solar collectors connected to in-out HTF. Wax is also mixed with metallic materials. Effect of HTF on energy extraction, effect of solar intensity on solar efficiency	
(Athienitis, Liu et al. 1997)		Full outdoor test room Gypsum board impregnated with PCM		
(El-Dessouky and Al-Juwayhel 1997)		Paraffin wax and CCHH	PCM contained in the annulus of a double-pipe heat exch. HTF: air or water flows inside smaller tube	
(Inaba and Tu 1997)		Shaped stabilized paraffin (solid-solid treansf)	Transient hot wire method(k) DSC, water calorimenter (cp), volume expansiometer (density)	No need for encapsulation. Measures prop. k, H, density, Cp. Paraffin shaped stabilized consists of paraffin as dispersed material and a high density polyethylene as supporting material. Shows variation of k, density, Cp with temperature
(Leong and Tan 1997)	Rectangular enclosure	(n-paraffins) n-hexadecane and n-octadecane	Inverse heat conduction technique. One wall has a milled copper plate with cold water flowing. Other walls plexiglass (looks at effects of convection in solidification). Effect of aspect-ratio, wall temp in interface	
(Leong and Tan 1997B)	Rectangular enclosure	n-hexadecane		Initial liquid superheat and aspect ratio on freezing. Rig is the same as previous paper. Dimensionless correlations
(Syed, Kumar et al. 1997)		Form-stable silane graft copolymer a polysiloxane (aqualink)		PCM selection criteria chart. Solid-solid transformation PCM. Evaluates thermophysical prop. and performance of TES unit under different operating cond. Feasibility of using PCM
(Banu, Feldman et al. 1998)	PCM wall board DSC , and large scale thermal testing: two identical adjacent rooms			
(Bo, Gustafsson et al. 1998)	Paraffin waxes and their binary mixture: tetradecane, pentadecane, hexadecane	DSC , melting and freezing point, thermal stability, volume expansion		
(Esen, Durmu et al. 1998)	Tanks wher PCM (CCH, paraffin, SSDH, p-wax) is packed in cylinders and HTF flows parallel & pipes containing HTF immersed in PCM		Geometric design (cylinders)	

Ref	Geom	PCM	Experiment	General Features
(Hasnain 1998)		Properties of various PCMs	Review sensible and latent heat storage (classification, problems, prop, etc) for space and water heating. LHTES heat exchanger systems	
(Lacroix and Duong 1998)	Single layer (compared with multi-pass) LHES with embedded electrical heat source. Describes rig, exp. Layout diagram. Rough surface and wire coil inserts to increase Heat trans. Restored energy efficiency. Thermal energy per unit volume			
(Banaszek, Domanski et al. 1999)	spiral	Paraffin wax	Exp. Rig descript. Two side heating or cooling by working fluid: air. Temp. history of the media, changes of vol enthalpy, amount of energy stored, & temporal vol fraction. Charging and discharging process	
(Gong, Devahastin et al. 1999)	Rectangular cavity		Container inversion for convection enhancement of PCM in rect. Cavity with vertical isothermally heated wall. Validation of mathematical model	
(Ismail, Quispe et al. 1999)	Parallel plate	Ice bank	Influence of geometrical and operational parameters in performance of ice bank. Exp. Validation. Effectiveness and heat transfer units (NTU). Energy stored, interface position, and complete sol. time in terms of PCM temp., wall temp. and gap between plates	
(Sharma, Buddhi et al. 1999)		Prop. Stearic acid, acetamide & paraffin wax	Accelerated thermal cycle test. DSC.	Thermal system undergoes 1 cycle per day. Electric hot plate with temp. controller . PCM inside stainless steel container
(Tan and Leong 1999)	Rectangular enclosure	Prop. n-hexadecane	PCM heated on vertical copper wall at constant rate. Thermoelectric cooler for rate heat extraction control	Natural convection in the liquid is negligible under constant heat rate. Plexiglass was used for visualisation. Description of rig.
(Velraj, Seeniraj et al. 1999)	Internal fins, lessing rings (suitable for solidification enhancement)and molten paraffin added to tube with water to create steam bubbles (for heat transfer melting enhancement). Exp. Rig description			
(Wang, Chen et al. 1999)	Spherical, cyclindrical & flat plate	Pentacrythritol, trimethyloletane, neopentil glycol		Homogeneous phase change process (HPCP) (any PCM component starts and ends PC simultaneously and rate is identical
(Wang, Amiri et al. 1999B)	Rectangular	Polyethylene glycol	Flat plate heat pipe heated vertical wall in rect.enclosure	Describes regimes during melting. Describes rig

Ref	Geom	PCM	Experiment	General Features
(Bajnoczy, Palffy et al. 2000)	Calcium chloride crystal hydrates which crystallize in 2 different hydrate forms with different TM		Phase diagram process described. Transparent PVC tube with PCM and seeding crystal with inserted electrically heated plate, and air as HTF. Takes into account solar radiation	
(Esen 2000)	cylinder	Prop.Calcium chloride hexahydrate	Storage tank linked to a solar powered heat pump system	
(Hadjieva, Stoykov et al. 2000)	Cylindrical autoclaved	sodium thiosulphate pentahydrate)	DSC, & TA	Wallboard composite porous concrete impregnated salt hydrate system. Optical transmittance
(Lee, Hawes et al. 2000)		Butyl Stearate and a commercial paraffin	DSC, Macro-scale tests in concrete blocks impregnated with 2 PCM	Desirable charging times. Effect of air velocity in control rates of heat storage and discharge. Describes rig (air conditioning system for heating and cooling). Design parameters
(Neeper 2000)	Wallboard subjected to diurnal variation of temp. but not to radiation. Guidelines for selecting PCM. Energy storage depends on. Maximum energy storage calculation. Transfer coefficients			
(R.Domanski, Rebow et al. 2000)	Cube chaped cavity	Manganese, Nitrate Hexahydrate, TME tetrahydrate, n-octadecane		Transient natural convection (velocity field and shape & location of phase front) of solidifying and melting of PCMs. Describes rig
(Cedeno, Prieto et al. 2001)	Pure fatty acids (palmitic, stearic, oleic) and their binary and ternary mixtures		DSC(explains graph and how H is obtained)	Explains amorphous, solid-solid phase transition previous to solid-liq. Thermal cycle transitions flow diagram.
(Py, Olives et al. 2001)	Tubes and spherical hollow nodules		Paraffin (Paraffin waxes (TM=80C &-9C) & hexadecane) /porous-Compress Expanse natural Graphite matrix (CENG). 'k' measurement. Saturation curves, Increased k	
(Sari and Kaygusuz 2001)		Prop. Stearic acid (high transmisivity)	Transition times, temp range and propagation of interface & effect of heat flow on PCM stability, effect of inlet water temp. Describes rig. DSC behaviour different than large amounts PCM. Overall storage efficiency.	
(Zhang, Zhang et al. 2001)		Binary systems of fatty acids (lauric, palmitic & stearic)	DSC & infrared spectroscopy.	Fatty acids have no super-cooling due to their character of crystallization and self nucleation.
(Dimaano and Watanabe 2002)		Capric-lauric (obtained from vegetable and animal oils)and pentadecane	DSC Fatty acids advantages. Storage system temp. to achieve dehumidification. Describes rig. Efficiency test for heat storage. Rates of charging and discharging. 2 melting peaks reveal heterog & longer solid	

Ref	Geom	PCM	Experiment	General Features
(Dincer and Rosen. 2002)	Latent heat storage generalities, nucleation and super-cooling. Flow chart of LHS system develop. Vol required for latent heat storage. Prop measuring techniques (DSC) Types of crystallization. Charging & discharging heat flow. Binary phase diagrams. Solid-liquid transformation PCM classification & PCM families. Inorganic compounds prop.			
(Jamies on 2002)	T-OPAL 'thermo-optical polymer' in crystalline form (cool days) transmits light, in hot days undergoes phase transition reflecting more light than transmitted. The glass has been patented by Fraunhofer Institute			
(Sari and Kaygusuz 2002)	Palmitic acid		Cylindrical tube-in-heat exchanger. Includes transition times, temp range and propagation and heat flow rate characteristics. Describes rig. DSC graph. Calculate heat losses to the ambient. Solidification curves. Effect of inlet HTF temp. Flow rate of HTF. Vertical and horizontal position of tube. Heat fraction and effectiveness of HE	
(EERE 2003)			Phase change drywall	Salts, paraffin, fatty acids advantage disadvantages s. Drywall manufacturing ways
(Nikolic, Marinovic-Cincovic et al. 2003)		Fatty acid esters(methyl stearate, methyl palmitate, cetyl stearate, cetyl palmitate and their binary mix		Gypsum and bricks PCM simple immersion & high density polyethylene pellets encapsulation. DSC.
(Sari and Kaygusuz 2002)	Pyrex cylindrical capsules	Stearic, palmitic, myristic & lauric	DSC, PCM thermal cycling stability & corrosion of metals (stainless steel, aluminum, carbon steel & copper). Palmitic & myristic more suitable long term. Explains reduction of thermal stability	
(Sari and Kaygusuz 2003)	Stearic, palmitic, myristic and lauric acid		Cylindrical pyrex capsules filled with PCM & set into thermostatic chamber. After cycling DSC test	Thermal reliability or stability(cycling) for industrial grade TM. DSC. A change of TM between 0.26-7.87°C and H between -1%-27.7%
(Bo 2004)		Tetradecane, hexadecane and binary mixtures		(thesis) Cool thermal energy, PCM Phase diagrams, methods for prop evaluation, commercial feasibility (stability)
(Buddhi and Sharma 1999)		Stearic acid	Measurements of effect of temperature and thickness on transmittance of solar radiation through PCM. It can be used a s a transparent insulating material. Describes rig	

References

Abu-Hamdeh, N. H. (2003). "Thermal Properties of Soils as affected by Density and Water Content." Biosystems Engineering **86**(1): 97-102.

Alva, B. A. The conservation of earthen architecture, The Getty conservation Institute Newsletter. **2004**.

ASHRAE, A. H. Elmahdy, et al. (2000). A Simple Model for Cooling and Dehumidifying Coils for Use in Calculating Energy Requirements for Buildings.

Bader, M. (2002). Microencapsulated Paraffin in Polyethylene for Thermal Energy Storage. Department of Chemical & Material Engineering School of Engineering. New Zealand, The University of Auckland: 78.

Banaszek, J., R. Domanski, et al. (1999). "Experimental study of solid-liquid phase change in a spiral thermal energy storage unit." Applied Thermal Engineering **19**(12): 1253-1277.

Barker, R. L., G. Song, et al. Modeling of Thermal Protection Outfits for Fire Exposures, NTC Project: F01-NS50 (formerly S01-NS02, I01-S02). **2004**.

Bascetincelik, A., H. H. ozturk, et al. (1999). "Energetic and exergetic efficiency of latent heat storage system for greenhouse heating." Renewable Energy **16**(1-4): 691-694.

Becker, R. (1999). "Research and development needs for better implementation of the performance concept in building." Automation in Construction **8**(4): 525-532.

Bejan, A. (1996). Entropy generation minimization : the method of thermodynamic optimization of finite-size systems and finite-time processes. Boca Raton, CRC Press.

Bennet, C. O. and J. E. Myers (1984). Momentum, Heat and Mass Transfer. New York, McGraw-Hill.

Bomberg, M. (1974). Moisture flow through porous media. Lund Institute of technology. Sweden.

Brousseau, P. and M. Lacroix (1996). "Study of the thermal performance of a multi-layer PCM storage unit." Energy Conversion and Management **37**(5): 599-609.

Costa, M., D. Buddhi, et al. (1998). "Numerical simulation of a latent heat thermal energy storage system with enhanced heat conduction." Energy Conversion and Management **39**(3-4): 319-330.

Daeil Aqua Co., L. Heat & Mass Transfer Fundamental, Cooling Tower Technical Site of Daeil Aqua Co., Ltd.

Cooling Tower Engineers, Operators and Purchasers. August **2004**.

De Freitas, V. P., V. Abrantes, et al. (1996). "Moisture migration in building walls--Analysis of the interface phenomena." Building and Environment **31**(2): 99-108.

De Vries, D. A. (1958). "Simultaneous Transfer of Heat and Moisture in Porous Media." **39**(5): 909-915.
De Vries, D. A. (1987). "The theory of heat and moisture transfer in porous media revisited." International Journal of Heat and Mass Transfer **30**(7): 1343-1350.
Deru, M. (2003). A Model for Ground-Coupled Heat and Moisture Transfer from Buildings, National Renewable Energy Laboratory
1617 Cole Boulevard Golden, Colorado 80401-3393 NREL is a U.S. Department of Energy Laboratory Operated by Midwest Research Institute • Battelle • Bechtel
Contract No. DE-AC36-99-GO10337. **2004**.
Dincer, I. (2002). "On thermal energy storage systems and applications in buildings." Energy and Buildings **34**(4): 377-388.
DPSUSM (2003). Differential scanning calorimetry, Department of Polymer Science University of Southern Mississippi. **2004**.
EERE, E. E. a. R. E. Phase Change Drywall.
El-Dessouky, H. and F. Al-Juwayhel (1997). "Effectiveness of a thermal energy storage system using phase-change materials." Energy Conversion and Management **38**(6): 601-617.
England, G. L. and N. Khoylou (1995). "Moisture flow in concrete under steady state non-uniform temperature states: experimental observations and theoretical modelling." Nuclear Engineering and Design **156**(1-2): 83-107.
Esen, M. (2000). "Thermal performance of a solar-aided latent heat store used for space heating by heat pump." Solar Energy **69**(1): 15-25.
Esen, M., A. Durmu, et al. (1998). "Geometric design of solar-aided latent heat store depending on various parameters and phase change materials." Solar Energy **62**(1): 19-28.
Evans, A. A. and R. B. Keey (1975). "Definition and variation of diffusion coefficients when drying capillary-porous materials." The Chemical Engineering Journal **10**(1): 135-144.
Farid, M. M., A. M. Khudhair, et al. (2004). "A review on phase change energy storage: materials and applications." Energy Conversion and Management **45**(9-10): 1597-1615.
Farouki, O. T. (1981). Thermal Properties of Soils. USA, CRREL U.S. Army, Cold Regions Research and Engineering Laboratory, Hanover, NH.
Feldman, D., D. Banu, et al. (1995). "Development and application of organic phase change mixtures in thermal storage gypsum wallboard." Solar Energy Materials and Solar Cells **36**(2): 147-157.
Feustel, H. E. and C. Stetiu (1995). "Hydronic radiant cooling -- preliminary assessment." Energy and Buildings **22**(3): 193-205.
Foley, N. K. (1999). Environmental Characteristics of Clays and Clay Mineral Deposits, U.S. Geological Survey (USGS).

Garg, H. P., S. C. Mullick, et al. (1985). Solar thermal energy storage, Dordrecht ; Boston : D. Reidel ; Hingham, MA : Sold and distributed in the U.S.A. and Canada by Kluwer Academic Publishers.

Gayo, E., J. De Frutos, et al. (1996). "A mathematical model simulating the evaporation processes in building materials: Experimental checking through infrared thermography." Building and Environment **31**(5): 469-475.

Gupta, V. and J. Srinivasan (1978). Heat and mass transfer. New Delhi, Tata McGraw Hill.

Hamdan, M. A. and F. A. Elwerr (1996). 'Thermal energy storage using a phase change material." Solar Energy **56**(2): 183-189.

Hasan, A. and K. Siren (2002). 'Theoretical and computational analysis of closed wet cooling towers and its applications in cooling of buildings." Energy and Buildings **34**(5): 477-486.

Hasnain, S. M. (1998). "Review on sustainable thermal energy storage technologies, Part I: heat storage materials and techniques." Energy Conversion and Management **39**(11): 1127-1138.

Hasnain, S. M. (1998). "Review on sustainable thermal energy storage technologies, Part II: cool thermal storage." Energy Conversion and Management **39**(11): 1139-1153.

IBP, F. I. f. B. P. (2003). WUFI (Wärme und Feuchte Instationär) Transient Heat and Moisture Transport. Holzkirchen, Branch Institute Holzkirchen.

Ismail, K. A. R. and M. M. Goncalves (1999). 'Thermal performance of a pcm storage unit." Energy Conversion and Management **40**(2): 115-138.

J. Marongiu, M. and M. J. Marongiu PCM Thermal Solutions. August 2004

Janssen, H., J. Carmeliet, et al. (2004). 'The influence of soil moisture transfer on building heat loss via the ground." Building and Environment **39**(7): 825-836.

Kerslake, T. W. and D. A. Jacqmin (1991). Experiments With Phase Change Thermal Energy Storage Canisters For Space Station Freedom. 26th Intersociety Energy Conversion Engineering Conference,, Boston, Mass., August 4-9, 1991, NASA.

Krane, R. J. (1987). "A Second Law analysis of the optimum design and operation of thermal energy storage systems." International Journal of Heat and Mass Transfer **30**(1): 43-57.

Kunzel, H. M. and K. Kiessl (1996). "Calculation of heat and moisture transfer in exposed building components." International Journal of Heat and Mass Transfer **40**(1): 159-167.

Lee, T., D. W. Hawes, et al. (2000). "Control aspects of latent heat storage and recovery in concrete." Solar Energy Materials and Solar Cells **62**(3): 217-237.

Levitskij, E. A., Y. I. Aristov, et al. (1996). ""Chemical Heat Accumulators": A new approach to accumulating low potential heat." Solar Energy Materials and Solar Cells **44**(3): 219-235.
McGuffey, O. S. (1947). Cooling plates. U.S Patent 2, 416,015. USA.
Neeper, D. A. (2000). "Thermal dynamics of wallboard with latent heat storage." Solar Energy **68**(5): 393-403.
Peippo, K., P. D. Lund, et al. (1999). "Multivariate optimization of design trade-offs for solar low energy buildings." Energy and Buildings **29**(2): 189-205.
Pel, L., H. Brocken, et al. (1996). "Determiination of moisture diffusivity in porous media using moisture concentration profiles." International Journal of Heat and Mass Transfer **39**(6): 1273-1280.
Rees, S. W., M. H. Adjali, et al. (2000). "Ground heat transfer effects on the thermal performance of earth-contact structures." Renewable and Sustainable Energy Reviews **4**(3): 213-265.
Rees, S. W., Z. Zhou, et al. (2001). "The influence of soil moisture content variations on heat losses from earth-contact structures: an initial assessment." Building and Environment **36**(2): 157-165.
RUBITHERM, G. Innovative PCM's and thermal technology. August 2004
Sadek, O. M. and W. K. Mekhamer (2000). "Ca-montmorillonite clay as thermal energy storage material." Thermochimica Acta **363**(1-2): 47-54.
Scalat, S., D. Banu, et al. (1996). "Full scale thermal testing of latent heat storage in wallboard." Solar Energy Materials and Solar Cells **44**(1): 49-61.
Schutte, P., C. d. Klerk, et al. (2002). Body-cooling systems, CSIR Mining Technology, Safety in Mines Research Advisory Committee.
Sharma, S. D., D. Buddhi, et al. (1999). "Accelerated thermal cycle test of latent heat-storage materials." Solar Energy **66**(6): 483-490.
Steinfeld, A. and R. Palumbo. Encyclopedia of physical science & technology, Solar Thermochemical Process Technology, R. A. Meyers Ed Academic press. **2004**.
Suresh, H. N., K. Murugesan, et al. (1999). Drying of porous material using finite element method. Second International Conference on CFD in the minerals and process industies, CSIRO, Melbourne, Australia.
Tahat, M. A., R. F. Babus'Haq, et al. (1995). "Design feasibility of an intermittent domestic energy store." Applied Energy **51**(3): 277-290.
TEAP PCM energy efficiency, TEAP energy.August 2004
Velraj, R., R. V. Seeniraj, et al. (1999). "HEAT TRANSFER ENHANCEMENT IN A LATENT HEAT STORAGE SYSTEM." Solar Energy **65**(3): 171-180.
Vener, C. (1997). PHASE CHANGE THERMAL ENERGY STORAGE. School of The Environment , Building Surveying. Brighton, University of Brighton.
Welty, J. R. (1974). Engineering heat transfer. New York.

Zhou, X. and R. W. Numerical solution in model of chilled water cooling coils (for single counter cross-flow tube with fins). August 2004

Zivkovic, B. and I. Fujii (2001). "An analysis of isothermal phase change of phase change material within rectangular and cylindrical containers." Solar Energy **70**(1): 51-61.

CHAPTER III

NUMERICAL ANALYSIS OF THE MOVING BOUNDARY PROBLEM

"There is inherent in nature a hidden harmony that reflects itself in our minds under the image of simple mathematical laws. That then is the reason why events in nature are predictable by a combination of observation and mathematical analysis. Again and again in the history of physics this conviction, or should I say this dream, of harmony in nature has found fulfilments beyond our expectations". Hermann Weil

Chapter III: Numerical analysis of the moving boundary problem

Melting and solidification processes have been part of human life since the Neolithic period. This can be observed in solid-liquid processes in nature -, in the thawing and solidification of the polar ice caps influencing environmental conditions; in tectonic movements influenced by molten rocks when volcanic activity occurs. From the first development of technology when metals were manufactured as tools and weapons to the flourishing metallurgical industries of the present, solid-liquid processes have accompanied human evolution and civilization through history.(Sarler 1995)

The better understanding and modelling of the phenomenon of melting and solidification is crucial for future industrial development and for modelling natural processes

In this project solid-liquid phase change applied to latent heat storage is of particularly interest. Fundamental experimental and numerical studies on

heat transfer during melting and solidification of PCM encapsulated in cylinders, spheres, and flat geometries have been published. Some other publications have reported the main drawbacks of latent heat storage systems. The efficiency of different storage units have been investigated, as well as PCM's cycling. Numerical methods to solve the heat transfer equations for steady or unsteady, one-dimensional, multidimensional, parabolic or elliptic flow have been developed. (Minkowycz, Sparrow et al. 1988)

In this project a mathematical model for specific systems designed to be applied under Mexican-like weather conditions are intended to provide a tool to analyse the suitability and economics of a latent storage system in view of regional climatic variations. This original research approach to the application of thermal storage for climatic regions in Mexico will be the basis for this project.

For the first time the main factors for promoting system's optimization are gathered in a single comparison study. The effects of individual factors on the efficiency of a thermal storage system and its contribution to energy saving is evaluated by running computer model simulations under different sets of climatic conditions. With the information gathered it should be possible to establish means to control the system i.e. to have extended discharging time for its application in cold regions and shorter for hot regions.

Solid-liquid phase transformations

Joseph Black proved that solid-liquid phase change thermal processes could not be interpreted on the basis of sensible heat transfer only. Therefore, he introduced the expression and the concept of latent heat. (Sarler 1995)

Latent heat storage is a non-linear event which depends on the progress of the boundary between phases when a state transformation of the PCM occurs. Heat transfer problems of evolving moving phase change occurring at a constant temperature are called Stefan[3.1] problems.

Stefan explored the solid-liquid phase change in a series of works[3.2]. This part of his work comprised problems such as diffusional transport of material in a reaction zone or experimental and theoretical aspects of evaporation.

[3.1] Jozef Stefan was born in Slovenia in 1835 and died in 1893 in Vienna. (Sarler, 1995)
[3.2] On some problems in the theory of heat conduction, On the theory of ice formation, particularly on ice formation in the Arctic seas, On inter-diffusion of acid and basic compounds, Experiments on evaporation and on evaporation and dissolution as diffusion processes, On the theory of ice formation. (Sarler, 1995)

The work on the mathematical modelling of solid-liquid transformations has been focused on: approximate analytical methods and numerical techniques.(Sarler 1995)

Describing the problem presented

A transient[3.3], conduction controlled[3.4], heat transfer problem is presented. It is of the moving boundary[3.5] (boundary-value[3.6]) type and requires the solution of a parabolic equation.
The heat equation is a nonlinear[3.7], second order[3.8], partial differential equation[3.9] for which the dependent variable specified on the boundary[3.10] is the temperature (Dirichlet condition).
The analysis requires the solution of the unsteady heat conduction equation. The parabolic heat diffusion equation governing the unsteady heat conduction problem of the temperature variation with time and space in one dimension:

$$\frac{\partial^2 T}{\partial x^2} = \frac{1}{\alpha}\frac{\partial T}{\partial T}$$

Equation 3.1: Unsteady one dimensional heat conduction governing equation

In two dimensions:

$$\frac{\partial T}{\partial t} = \alpha\left(\frac{\partial^2 T}{\partial x^2} + \frac{\partial^2 T}{\partial y^2}\right)$$

Equation 3.2: Unsteady two dimensional heat conduction governing equation

Where

α = thermal diffusivity= $\frac{k}{\rho c_p}$ (m^2/s)

T= temperature (K)
t= time (s)

3.3 The solution of the parabolic PDE, provides the variation of temperature with both time and special coordinates
3.4 Convection effects due to density changes at the phase interface or density variations in the liquid phase are neglected
3.5 Associated with time-dependent problems; the position of the boundary has to be determined as a function of time and space (Crank, 1984)
3.6 Problems in which the solution of a differential equation has to satisfy certain conditions on the boundary of a prescribed domain
3.7 Thermal analysis is intrinsically nonlinear, as thermal conductivity is a function of temperature. As phase change is involved, and the location of the phase front is not known up front, a linear problem can become nonlinear.
3.8 Two boundary conditions are required
3.9 Function of two independent variables: time and space
3.10 The boundary conditions specify the heat flow or the temperature at the boundaries of the region. Boundary conditions can be classified into: Dirichlet (temperature specified at the boundary), Newman(heat flux specified at the boundary), and mixed boundary condition

Melting and solidification problems are non-linear in the mathematical sense due to the presence of a moving interface (boundary) between the two phases associated with the discharge of latent heat. It is not possible to forecast the position or the velocity of the interface. A discussion regarding the penetration rate of the phase change interface can be found in(Ma and Wang 1995). In some cases, temperature dependent thermophysical properties add to the complexity of the mathematical analysis.(Rabin and E.Korin 1993)

Two steps will be followed for the solution of the heat transfer equation

1) Obtain a system of ordinary differential equations (ODE) to approximate the behaviour of the heat equation;
2) Solve the systems of ordinary differential equations by an approximate numerical technique.(Myers 1971)

The reformulation of this problem (to obtain the ODE) is in general considered as an integral part of the numerical method.(Cryer)
Tracing the moving phase change boundary is required for the numerical solution of phase change problems. The continuously moving interface can be tracked across a region described by a set of points. Several methods have been proposed to overcome this difficulty. (Voller and Cross 1981)

Moving boundary problems numerical solution classification

Phase change moving boundary problems numerical solutions can be classified into two groups depending on the techniques applied. (Ketkar 1999; Sampath and Zabaras 1999). A comparison of accuracy attained by various numerical techniques is presented in(AliAbadi and Ortiz 1998)

1) Multiple domain methods:

Independent conservation equations applied for each phase are coupled (governing equations are solved in two domains of different phases)(Clavier, Arquis et al. 1994) with suitable boundary conditions at the freezing/melting boundary. The moving interface is explicitly and accurately tracked on a deforming grid. (Sampath and Zabaras 1999)

1.1) Front tracking methods: The moving boundary problems are handled by relocating the node points of the mesh to follow the fluid, generating a Lagrangian[3.11] frame of reference (Voller and Swaminathan 1990). This method explicitly tracks the phase front (moving interface) on a deforming grid by an explicit energy balance at a phase front. The problem is worked

---

[3.11] Lagrangian of a dynamical system, named after Joseph Louis Lagrange, is a functional of the dynamical variables which concisely describes the equations of motion of the system.

out in its original form, that is, the unknown boundary has to be explicitly approximated throughout the computation (Cryer). The position of the phase front is explicitly tracked and the condition on the moving boundary is imposed. The two grids[3.12] (solid and liquid)are updated to the next iteration, and the consequent overall mesh movement is calculated from the actual iteration time to the subsequent iteration time using the updated grids and the grids at the actual iteration time[3.13] (Sampath and Zabaras 1999).

It is possible to use a numerical method in which the position of the moving boundary is computed on a fixed grid on the space-time domain at each time step. The boundary will be in general between two grid points at any given time (fixed finite difference grid). Its main drawback is the loss of accuracy associated with unequal space intervals near the boundary.
Alternatively, the grid itself has to be deformed in some way (modified grids with variable time step[3.14], or with variable space grid, and adaptive meshes with finite element[3.15])

A spreadsheet simulation of the front tracking method for one dimensional Stefan problem is presented in (Kharab 1997)

1.2) Analytical transformation: Occasionally it is feasible to completely transform the problem, finding for example an equivalent integral equation(Cryer). Even though Stefan-type problems are fundamentally non-linear (because of the condition on the boundary) linearity often exists in each of the domains on either side of the boundary and the integral equation method is still functional. These techniques have been principally developed to resolve one dimensional steady-state partial differential equations, such as the Laplace equation(Cryer)

The heat balance integral method (HBIM), proposed by Goodman, employed finite difference methods on a deforming grid which changes as the phase front moved. A specific temperature profile was assumed, then the heat equation is integrated over a suitable interval to acquire a set of heat-balance integral equations. The equations are then solved to find the movement of the phase boundary. The technique offers a way to track the phase front in a one dimensional problem. The method was improved by

---

3.12 The energy equation is then solved separately in each phase with temperature prescribed to be the melting temperature on the interface.
3.13 Given the solid and liquid phase grids at any iteration during the solution process and the interface update velocity (Sampath and Zabara, 1999)
3.14 Such that the moving boundary coincides with a grid line in space at each time level
3.15 Bernnerot and Jamet used a space grid which was adapted at each time step to construct quadrilateral finite elements in space and time for the non-rectangular grid (Crank,1984)

Bell by sectioning the dependent variable (temperature), and assuming a linear profile in every section.(Caldwell and Chan 2000)

The application of front tracking methods (also called temperature based formulations, as they use temperature as the dependent variable) is limited to a-priori assumed sharp interfacial surfaces and the Stefan condition at the interface between the phases (latent heat energy jump condition) has to be satisfied. Problems with multiple phase changes, those with mushy regions and problems with phase changes occurring over a temperature range can't be solved by using this method. (Ketkar 1999)

1.3) Front Fixing methods: An alternative to tracking the moving front is to fix it by a suitable choice of new space coordinates. The idea is that the solution of a more complicated problem can be simplified by using a simple domain. Therefore the unknown domain is mapped onto a fixed domain. (Cryer) A transformation of variables can be adopted, so that the moving boundary is always on a grid line, or is fixed in the transformed domain (Crank 1984).

A well known method for solving fixed-boundary problems is the method of lines[3.16] : The basic idea is to discretize the time variable. As a result the partial differential equation is replaced by a sequence of one dimensional steady-state (free-boundary problem) partial differential equations (unknown boundary problem[3.17])(Cryer). Srinivas et al. presented a mathematical technique combining the method of lines and the enthalpy method (Srinivas and Allen 1998)

To fit the shape of an original curved-shaped region with body fitted coordinates, the original coordinate system is transformed into a new system such that the curved boundaries become coordinate lines (a fixed rectangular domain).(Crank 1984)

Another version of the front fixing methods is the isotherm migration method. In a one dimensional time-dependent heat flow problem, the temperature can be interchanged with the space variable, so that the solution evaluates either the traditional time dependence of temperature at chosen values of the space variable; or the space variation with temperature and time, so that a specified temperature moves through the medium, in other words, the isotherms migrate. Crank extended the method to the solution of general heat flow problems in two space dimensions with a partial transformation of variables, later a complete transformation was proposed.

3.16 Meyer developed the method in relation to moving boundary problems (Crank, 1984)

3.17 In the solution of unknown boundary problems (UBP) one obtains a solution of the governing differential equation which satisfies one boundary condition and contains a parameter, and then chooses this parameter so as to satisfy the remaining boundary conditions (Cryer)

(Crank 1984). The isotherm (as the phase front) is used as the dependent variable. This transformation results in a more complex equation and frequently results in a singularity initially.(Caldwell and Chan 2000). Ilken argued that it is possible to find an analytical solution for one dimensional phase change problem in a semi-infinite slab by using relations (found by regression analysis) between isotherms for conduction with or without phase change to find the interface position.(Ilken and Gunerhan 1996)

An alternative solution when the state of the system is conveniently characterised by the position of the interface (sharp phase front) is the Arbitrary Lagrangian-Eulerian (ALE) approach: The moving boundary is handled by fitting the new free surface, but using a mesh smoothness condition to regulate the movement of interior nodes. The velocity difference between fixed and transformed meshes appears as a convective velocity in the equations (Voller and Swaminathan 1990)

The main drawback of the front-fixing and front-tracking methods is that the necessary mathematical algorithms to suitably adjust the mesh are usually very complex. Their implementation is frequently complicated, they are computationally demanding and can rarely be simply integrated into other conventional numerical codes based on fixed grid points.(Xu and Naterer 2001)

2) Fixed domain transformation

Solid-liquid regions do not need to be considered independently; instead conservation laws are imposed globally, regardless of the phase[3.18].(Ketkar 1999) An essential feature in the development of fixed grid methods is the characterization of the local liquid volume fraction, which is determined according to the nature of the change of state(cooling rate, solidification speed and nucleation).(Voller and Swaminathan 1990)
These methods have the benefit of easier numerical implementation. (Xu and Naterer 2001)

2.1) The enthalpy formulation:

The governing equation is broken up into latent and sensible components. The enthalpy accounts for the latent heat absorption/liberation at the interface, thus preventing the need to explicitly implement the interface temperature condition. The numerical solution can be carried out on a space grid that remains fixed through out the calculation[3.19].

3.18 A single region formulation eliminates the need for separate conservation equations at the freezing front (Sampath, Zabaras, 1999)
3.19 A weak or generalised solution is defined on a known fixed domain

The temperature values in the implicit finite difference form of the governing equation are substituted by the enthalpy values only for nodal sub-volumes containing both the solid and liquid phases. (Implicit representation of the phase interface is obtained[3.20] without modifications of the spatial grid[3.21]) (Cryer; Date 1991). Since the energy equation is the same for both phases, the position of the interface need not to be tracked explicitly. A drawback of the method is that the temperature on the phase-change node is held at the melting temperature[3.22]. This generates temperature and heat flux histories which exhibit a step-like or wavy pattern. (Date 1991)

Despite the possible wavy pattern, this method has been shown to be successful when solving phase change evolutionary partial differential equations[3.23] such as the Stefan problem.

The two essential mathematical ideas of the method are:

a) A new independent variable, the enthalpy[3.24], is introduced; being a multi-valued function of the liquid fraction. (Cryer) The flux condition expressing the conservation of heat and release of latent heat is automatically satisfied across the phase front. The change of phase is realized as a jump discontinuity in the enthalpy.(Caldwell and Chan 2000)

b) A differential equation of the enthalpy is derived. A particularly important aspect of the enthalpy method is that it is able to handle so-called mushy regions[3.25] (Cryer)

A number of ways to implement the numerical scheme exist:

a) Source-based methods: the governing equation is reformulated in terms of a single unknown variable with the non-linear latent heat effects "isolated" in a source term[3.26] or a coefficient.(Swaminathan and V.R.Voller 1992). In the numerical model the latent heat may be released according to the fraction solidified, as calculated at a specific temperature from the phase diagram. (Lally, Biegler et al. 1990). A numerical method involving a moving heat source using a reformulated enthalpy technique is presented in (Nehad 1995)

3.20 The phases and the interface are determined later from the solution
3.21 The initial spatial discretization mesh doesn't change
3.22 Surrounding the phase change node the nodal temperature is held constant till the interface crosses the control volume
3.23 This unknown boundary problem is called Moving-boundary problem
3.24 The latent heat evolution is accounted for in the governing equation by the definition of the enthalpy
3.25 These are regions in which the material being considered consists of a mixture of two phases
3.26 That is, including the latent heat as an enthalpy or a source term.

b) Apparent heat capacity methods: the heat produced by the change of phase is taken into account in the energy balance equation written at fixed computation nodes.(Clavier, Arquis et al. 1994; Kim, Lee et al. 2000) The latent heat is accounted for using a heat capacity that varies strongly with temperature(Lally, Biegler et al. 1990)

Drawbacks of the method:

In the case of a narrow melting range or isothermal phase change the numerical solution obtained oscillates strongly when the Stefan number is small(Clavier, Arquis et al. 1994) It is possible to develop the method to a strong enthalpy formulation by eradicating the wavy pattern. This can be done in 3 ways:

1) The time step can be iteratively estimated such that the entire control volume liberates the latent heat of the control volume (node-jumping scheme) this can not be extended to multidimensional problems.
2) Refine the mesh, so that the time over which the phase-change temperature is held becomes very small, and the essentially wavy solution appears smooth
3) Generalize the H-T relationship in such a way that no book-keeping is required.(Date 1991)

Estimating the heat flux across the boundary of phase change cells and the distance between the phase front and the centre of neighbouring cell an effective conduction length to mitigate the oscillatory behaviour of the enthalpy method is obtained in (Kim and Anghaie 2001)

Other drawbacks of the method are: the complex calculation of liquid fraction updates and the fact that the temperature field within the PCM is not calculated explicitly but via enthalpy-temperature correlation. In previous work a method has been proposed that introduces a slight modification to the enthalpy method, which enables decoupling of temperature and liquid fraction fields.(Zivkovic and Fujii 2001).

Ockendon published a simplified compendium of moving boundary problems solution techniques including the weak solution, heat source term, and integral formulation.

Method selected

The choice of one of these approaches is mainly determined by the physics of the solid-liquid phase transition. As paraffin is included as one of the PCM's in this study, and as its interface is not clearly defined (mushy zone) a front tracking approach is difficult to apply.

The numerical algorithm in this work is not original as it is based on the modified enthalpy formulation presented Voller and used by (Zivkovic and Fujii 2001). However the non-linear temperature-enthalpy relation of the substances and the temperature dependent properties as heat capacity and thermal conductivity used are original contributions. Additionally functions were build in the model to apply the weather data (as air temperature, irradiation and mass flow rate) as input conditions, in order to evaluate the system performance under different climatic conditions.

The enthalpy method was selected, having the following advantages:

1) The governing equation is similar to the single phase equation
2) The method does not require explicit treatment of the conditions on the phase change boundary (cf. Carslaw and Jaeger, 1959), i.e. there is no need for tracking the phase change boundary throughout the phase change domain.(Zivkovic and Fujii 2001). There is no condition to be satisfied at the solid-liquid interface as it automatically obeys the interface condition.
4) The enthalpy formulation allows a mushy zone between the two phases

The complexity of the Stefan Problem modelling arises from two aspects:

A) Non-linearity: The governing equation is non-linear in that it contains two related but unknown variables (temperature and enthalpy).
B) Moving boundary: Change of the PCM properties due to a phase change. That is, a time-dependence of position, profile and slope of the solid-liquid interface

The physics of the phenomenon and the complexity of its modelling

The role of PCM temperature in the simulation:

As it was explained earlier, the phase transformation taking place either over a temperature range or at a discrete temperature is an important piece of information when choosing a solution methodology. The phase transformation of some solution combinations (as some binary alloy systems and some eutectic mixtures) takes place over a temperature range (non-isothermally). The solid-liquid interface is typically irregular. This region is often called a 'mushy zone'. (Sampath and Zabaras 1999). On the other hand, the change of phase of a pure substance generally occurs at a fixed temperature point (isothermally) generating sharp phase front. For pure substances, the specific heat capacity is infinite at the melting point, and the difference equation does not hold at the solid liquid interface, but has to be written separately in the liquid and solid regions. (Minkowycz, Sparrow et al. 1988)

Temperature evolution of the PCM also plays an important role when defining the material's thermodynamic and transport properties. The temperature dependence of the enthalpy, thermal conductivity, density and heat capacity has been the subject of vast investigation. In the improved enthalpy method presented by Fikiin all non-linearities brought about by the temperature dependence of the thermophysical coefficients are eliminated by introducing a functional relationship among the volumetric specific enthalpy and the Kirchhoff function. Potential inaccuracies originated by 'jumping' of the corresponding specific heat capacity peak at the maximum of the latent heat effect are removed. (Fikiin 1996). Sassi used an exact location equation called the Moknine relation to account for the discontinuity at the moving boundary, thus eliminating the nonlinearity due to the a priori unknown interface position. The technique proposed is independent of geometry and independent of the nonlinearity due to variation of thermophysical data(Sassi and Raynaud 1998).

An integrated solar collector described by Rabin assumes temperature dependent thermophysical properties and time dependent meteorological parameters and applies an effective thermal conductivity (Rabin, Bar-Niv et al. 1995)

Heat capacity

Heat capacity is an intense function of temperature (due to the effect of heat of fusion)(Lally, Biegler et al. 1990). With the enthalpy function H, heat capacities at constant pressure are readily obtainable. The heat capacity varies from a low value at the solid or liquid state to a maximum value at the melting temperature. An effective heat capacity can be used to consider the latent heat in the phase region. Farid used a delta function[3.27] to express the effective heat capacity variation within the phase region[3.28]. The Dirac function was also applied, among other authors by Bonacina (Bonacina, Comini et al. 1973).The area of the triangle approximating the delta function should be equal to the latent heat of melting of the PCM. Care should be taken when a very narrow delta function is assumed, as a large number of space partitions are required. If small partitions are used a fast interface motion would be induced as an important part of the latent heat would be lost.

The variation of the effective heat capacity in the two phase region is fully described by the following equations: (Farid, Hamad et al. 1998)

$$Cp_e = Cp_s + \left(\frac{Cp_m - Cp_s}{Tm - Tm_{start}}\right) * (T - Tm_{start}) \quad \text{for } Tm_{start} \prec T \prec Tm$$

Equation 3.3: Effective heat capacity for a node temperature between the PCM beginning of melting and the PCM melting temperature

---

[3.27] An important property of the *The Dirac Delta Function* is that whenever any function is integrated against it, the result is the value of the function at time t=0. The integral of the delta function is 1.

[3.28] Assuming melting range of 2-4 °C

$$Cp_e = Cp_m - \left(\frac{Cp_m - Cp_l}{Tm_{end} - Tm}\right) * (T - Tm) \quad \text{for } Tm \prec T \prec Tm_{end}$$

Equation 3.4: Effective heat capacity for a node temperature between the PCM melting temperature and the PCM end of melting temperature

$$Cp_m = \frac{2h - 2(Cp_l - Cp_s)(Tm_{end} - Tm) + Cp_s(Tm - Tm_{start}) + Cp_l(Tm_{end} - Tm)}{Tm_{end} - Tm_{start}}$$

Equation 3.5: Effective heat capacity for a node at the melting temperature

Where
Cp_e= Effective heat capacity (kJ/kg°C)
Cp_s= Heat capacity solid state (kJ/kg°C)
Cp_m= Heat capacity during melting (kJ/kg°C)
T= Temperature (°C)
Tm= Melting temperature (°C)
Tm_{start} = Temperature at the beginning of melting (°C)
Tm_{end} = Temperature at the end of melting (°C)
H= Latent heat of melting (kJ/kg)

An effective heat capacity calculated from the rate of energy addition to a micron size PCM sphere was calculated from the rate of energy addition to the sphere and the rate of change of average sphere temperature is presented in (Bowman and Brown 1998)

Enthalpy

Enthalpy[3.29] is a state function, (depends only on the current state of the system) defined to account for the heat evolved (or absorbed) by a system[3.30].

A source-based enthalpy method can handle phase change problems specified by an explicit liquid fraction-temperature relationship.
In this method the governing equation is reformulated in terms of a single unknown variable with the non-linear latent heat effects "isolated" in a source term or a coefficient.(Swaminathan and V.R.Voller 1992). This method is discussed in more detail later in the chapter.

3.29 Enthalpy is the total internal energy of a system at constant pressure. It is measured by examining what happens to the surroundings of the system. These changes are termed enthalpy change.
3.30 The changes in enthalpy are related to changes in free energy. All the thermodynamic properties of a system may be expressed in terms of the free energy and its derivatives. Free energy change is strongly dependent on temperature.

Density

When density differences in solid and liquid states exist, a force imbalance on the solid is set. During the melting process a denser solid continuously moves downward as melting develops and consequently creates a flow field within the liquid.

To incorporate the effect of solid-liquid density change Asako calculated a mass source included as a source term in the continuity equation. Regarding the effect of density change, he found that the melt thickness decreases with increasing solid/liquid density ratio. The solid velocity increases with time at the first stage and then decreases after it reaches a maximum value., the volume ratio decreases almost linearly with time because of melting. The effect of density change on the melt thickness, solid velocity and on the volume of solid PCM to its initial volume is small. (Asako and M.Faghi 1999).

The effects of solid-liquid density difference and transverse convection in close-contact melting phenomenon occurring between a phase change material and an isothermally heated flat surface has been studied by Yoo. The melting process was described as follows: The liquid melt formed along the solid–liquid boundary fills the gap, flows towards the ends, and is ultimately forced out through the end openings. The simultaneous actions of melting and solid descending motion develop a descending flow that has its maximum velocity at the melting front, diminishing as it goes across the liquid film, and finally disappears on the heated surface. It is, the density difference that influences the solid downward velocity.(Yoo, Hong et al. 1998)

In the case studied in this project, the density variation caused by the difference between solid and liquid is within relatively narrow limits.

Thermal conductivity

Thermal conductivity is a strong function of the dependent variable (temperature). Difficulties on modelling arising due to a rapidly changing or discontinuous temperature-dependent conductivity can be prevented by using the Kirchhoff transformation[3.31].(Crank 1984; Lally, Biegler et al. 1990; Voller and Swaminathan 1990; Voller 2001) Fikiin suggested an enhanced enthalpy method that introduced the non-linearities, originated by the temperature dependence of the thermophysical coefficients in a functional relationship relating the volumetric specific enthalpy and the Kirchhoff function (Fikiin 1996)

[3.31] Defined as $\upsilon = \int_0^U K(\zeta)d\zeta$

In the present study the density and the thermal conductivity are considered constant but different in the solid and melt regions.

Hysteresis

Latent heat is only found during first-order phase transformations[3.32]. These transformations can exhibit hysteresis. Molecules change properties during heat transfer (via a potential field or a higher temperature increment) and it is this change that causes hysteresis[3.33].

The distinguishing characteristic of a phase transition is an abrupt sudden change in one or more physical properties, in particular the heat capacity with a small change in a thermodynamic variable such as the temperature. That is, the previous history of the system plays a role in the current evolution rate.

It has been difficult to develop an adequate theory to characterise hysteresis in systems of differential equations. In previous work some forms of hysteresis have been modelled. Formal operators inserted in problems for partial differential equations have worked well when dealing with hysteresis nonlinearities.

Little et al. presents in his paper the model problem of a parabolic diffusion equation coupled to hysteresis. (Little and Showalter 1995)

Effect of natural convection within the melt:

As it was discussed in chapter two, a phase transformation starts given the presence of a driving force: activation energy and temperature. These two determine whether a phase is stable or a transformation is possible, and at what rate.

In the case of solidification a transformation starts by nucleation of the new phase in which a critical activation energy is needed. The nuclei will grow, often through diffusion, until the old phase is replaced.
In some cases, convection during freezing can be induced during the release of latent heat and during the density change[3.34] upon freezing. The thermal and solutal setting in the region of the solid-liquid solidification boundary can be altered by convection in the liquid. (Sampath and Zabaras 1999).

3.32 During first order phase transitions, a system either absorbs or releases a fixed (and typically large) amount of energy. First order phase transitions include the solid/liquid/gas transitions.
3.33 Is a property of physical systems that do not instantly follow the forces applied to them, but react slowly, or do not return completely to their original state: that is, systems whose states depend on their immediate history.
3.34 Buoyancy force caused by thermal gradients in the liquid

At the initial stage of the solidification, a lower wall temperature and a higher liquid superheat develop a large temperature gradient[3.35] on the phase front. This is indicative of natural convection in the liquid, which according to previous studies has been identified in the surrounding area of the phase front only. The phase front's temperature gradient decreases with time as the temperature in the liquid homogenizes, and as the flow velocities are reduced. That is, convection in the liquid weakens with time. (Duan, Tan et al. 2002)

According to Zhang the effect of buoyancy in the course of solidification can be neglected. (Zhang, Su et al. 2001).

At the beginning of the melting process, the heat transfer within the liquid phase is controlled by conduction. This has been established as a horizontal interface and has been observed according to previous research (Hernandez-Guerrero, Aceves et al. 1999). A slight transition stage follows and as the melt volume grows, natural convection starts playing a more significant role. A subsequent irregular interface is produced.(Hamdan and Elwerr 1996) (Zhang, Su et al. 2001).

The problem of computing the behaviour of phase change systems is already complicated as the moving interface is non-linear and the thermophysical properties for each phase are different(Costa, Buddhi et al. 1998). Nevertheless, and although no exact theory has been developed the effect of natural convection of the PCM in the melt region can be included in the conduction equation by applying an effective thermal conductivity for the liquid. For a confined rectangular container heated from its vertical wall this can be done by using the relation proposed by Berkovsky and Polevikov. (Costa, Buddhi et al. 1998)

$$\frac{k_{eff}}{k_l} = NU$$

Equation 3.6: Effective thermal conductivity

where

if $2 \prec \frac{L}{s(t)}$

$$Nu = 0.22\left(\frac{\mathrm{Pr}}{0.2+\mathrm{Pr}}Ra\right)^{0.28}\left(\frac{L}{s(t)}\right)^{0.25}$$

Equation 3.7: Nusselt number for an enclosed rectangular container heated from its vertical wall, with length to interface position with time ratio larger than two

---

3.35 A phase front with a larger slope indicates strong convection in the liquid region, while a phase front with a lesser slope indicates weak convection in the liquid.(Duan, Tan et al. 2002)

if $1 \prec \frac{L}{s(t)} \prec 2$

$$Nu = 0.18\left(\frac{\mathrm{Pr}}{0.2+\mathrm{Pr}}Ra\right)^{0.29}$$

Equation 3.8: Nusselt number for an enclosed rectangular container heated from its vertical wall, with length to interface position with time ratio between one and two

k_{eff} = Effective thermal conductivity (w/mK)

k_l =Liquid thermal conductivity (w/mK)

Nu = Nusselt number

Pr= Prandlt number

Ra= Rayleigh number

L= length (m)

s= Interface position (m)

t= Time (s)

Coupled heat and mass transfer taking place in moving boundary problems coupled with an exothermic heat of mixing induces a fast rise of temperature around the moving boundary which produces an enhanced convective flow in the liquid (Hu and Argyropoulos 1996). A conduction controlled melting process in a rectangular enclosure was investigated to predict the melted fraction in(Hamdan and Elwerr 1996). A computational technique considering various boundary conditions i.e. conduction, convection and radiation alone or in combination and these are presented in the paper (Rabin and E.Korin 1993).

Due to the above mentioned complexity of the problem numerous analytical solutions presented so far have ignored convection in the melt region. That is, the solid-liquid interface has been treated as a vertical one.(Hamdan and Elwerr 1996)

Meteorological parameters:

The sole simulation of actual transient environmental conditions (including solar spectra, temperatures, humidity, air changes per hour) requires total commitment. The objective in this study is not to attain an accurate reproduction of environmental conditions, but to assess the magnitude and reliability of the relations between variables for optimum LHSS performance. To achieve this objective it is possible to consider constant environmental conditions.

In the case where solar irradiation is lessen due to overcastted conditions the system performance is assessed according to a specific test considering the charging of the unit by solely interior heat gains and available diffuse radiation.

Nevertheless I would like to explain that average cloudiness in Baja California (BC) one of the Mexican regions considered for the experimental and numerical work ranges from 0.32 (in December)to 0.44 (in august) being 1 a hundred percent cloudy, the cloudiness in this region is low.

Assumptions made for the computer model

1.- Constant meteorological parameters
2.-Thermal conductivity of the PCM in the direction of the Heat transfer fluid (HTF) flow is ignored. The influence of conduction within the PCM can be ignored for low convective heat transfer coefficients (such are those when air is used as the HTF) and relatively short containers (from 200 to 400 mm). Furthermore, a previous study of a similar experiment has shown that no significant improvement of the results is obtained if the conduction within the PCM is accounted for. (Zivkovic and Fujii 2001)
3.-The effects of natural convection within the melt are negligible and can be ignored.
4.-The PCM behaves ideally, i.e. such phenomena as property degradation and super-cooling are not accounted for.
5.- The PCM is assumed to have a definite melting point (isothermal phase change).
6.-Thermophysical properties of the PCM are different for the solid and liquid phases but are independent of temperature.
7.-The PCM is homogeneous and isotropic.
8.- Thermal resistance across the wall of the container is neglected.
9.-Lateral sides of the rectangular container are well insulated, i.e. heat transfer occurs only on sides x=0 and x= (cf. Fig. 1)
10.- Heat transfer within the PCM is conduction controlled. (Effects of natural convection within the melt can be ignored for the conditions investigated)
11.- The PCM is initially in the solid phase for melting and in the liquid state for solidification
12.- The PCM is homogenous and isotropic.

Defining the latent heat storage system prototype for modelling

The unit modelled has been designed to improve the aspects of the design that have been shown in previous research to influence the performance of the heat storage unit.

When designing a heat storage unit, it is necessary to determine its mode of operation. This depends on the type and capacity of thermal storage (including container material wall thickness and geometry), amount of heating and cooling energy required (to determine the unit dimensions), diurnal temperature ranges for the year (to determine the PCM properties to

be applied) and available source of energy to be exploited (to determine boundary conditions).

An evaluation of the heating and cooling loads for a house with five inhabitants on an average day in winter and summer in the region with greater requirements (more extreme weather conditions) was obtained from the software Thermal Assessment Simulation (TAS) and is presented in appendix 3.B.

Source of energy

Heat sources imposed to dwellings, as solar radiation, radiators, and other incidental sources as grills, ovens, lights, equipment and even occupants.

Heat radiated through roofs provides a high contribution to heat gains and losses in dwellings due to their surface area and the time during which they are exposed to solar radiation. If the storage unit is to be placed on the exterior of an already existing roof, it will act only as heat modulator (the stored heat won't be released to the interior when the exterior temperature drops; only a small part will be transmitted as sensible heat and the rest will be exhausted to the exterior).

For the present study the application of the storage system as blinds for windows is proposed. The location was chosen so as to take advantage of solar radiation (direct and diffuse) and of indoor heat gains.

Solar direct and diffuse radiation data for a vertical surface in two different regions in Mexico (Mexicali, Tuxtla-Gutierrez, and Ciudad-Victoria) have been determined and are shown in appendix 3.C.

Heat Transfer Fluid (HTF)

The HTF characterizes the way of collecting the energy stored, its transportation, and diffusion for its final delivery at the point of use. In the present study air has been chosen as the HTF. Air changes per hour in a room create sufficient air movement for the heat transfer process. No mechanical device is required to carry out the heat exchange process. The average speed of the air supplied was in the order of 1.5m/s. In the chapter regarding experimentation this is examined in more detail.

Container

Encapsulated PCM was preferred to the use of a wallboard matrix hosting the PCM. This was due to the unpredictability of the wallboard system, as correct soaking time for PCM absorption is dependent on the variable porosity paths of the matrix, the PCM exposure to external conditions makes it subject to deterioration, unknown rate of evaporation (reduction of the PCM would also decrease its performance), it might represent a fire risk, and for organic PCMs their decomposition may cause bad odour and contamination that might attract insects and bugs. Moreover, the

composite PCM wallboard has only a fraction of the PCM contained in the same dimensions encapsulated PCM unit (Rudd 1993). On the other hand construction of the Latent Heat Energy Storage (LHES) unit in single containers with packed PCM, has many advantages as it enables modular assembly and is also very economic from the point of view of mass production. For all these reasons it has been decided to use an encapsulated unit for this study.

An important factor on the failure of first packed PCM products was the underestimated importance of the testing of the PCM encapsulant. The thermal conductivity and the potential for corrosion of the container have to be assessed.

A mixture of sodium sulphate and sodium chloride water and additives contained in a polypropylene tube showed the important and negative effect of a low thermal conductivity container on the heat transfer according to (Kurklu, Wheldon et al. 1996) .

Among the good thermal conductors, hexaloy silicon carbide is a suitable option, for corrosive storage media but it is expensive. High density polypropylene is a good candidate for containing the PCM also but seems to be readily available in commercial retailer stores only in low density sheet presentation. The material finally selected was aluminium, which is light, not expensive and a good conductor of heat. The corrosion resistance of aluminium varies widely depending on alloy, environment, PCM material and design. A clean aluminium surface is reactive and will react spontaneously with water or air and form aluminium oxide. This oxide is very stable and has in addition a very good adhesion to the metal surface and thus protects aluminium from corrosion or further oxidation. Fatty acids may react with aluminium if the conditions are unfavourable. Fatty alcohols may corrode or react with aluminium, the attack may be insignificant if the water content or temperature is favourable.(Alubook)

Initially it was proposed to use internal metallic dishcloth in order to improve PCM thermal conductivity and reduce the chance for phase segregation to occur. Difficulties on the building of such probes made it unfeasible to include this element in the tests.

Geometry

Regarding the container shape, Farid presented a mathematical model using vertical cylinders filled with different melting PCM temperatures(Farid and Kanzawa 1989). A semi-infinite slab and a long prism was used in (Rabin and E.Korin 1993) model. Cylindrical geometries were used in the enthalpy method modelled by (Rose 1993). Fikiin used for his quasi-one-dimensional formulation an infinite slab, infinite cylinder, and a sphere(Fikiin 1996). A rectangular enclosure containing PCM was presented in (Hamdan and Elwerr 1996). A solar assisted cylindrical energy storage tank was

investigated by (Esen and Ayhan 1996). The melted fraction in a rectangular enclosure heated from one side is presented in (Hamdan and Elwerr 1996). A flat plate coated with paint containing micron size spheres of phase change material is presented in (Bowman and Brown 1998). A concentric cylinder performance was analysed by (Yimer and Senthil 1998). Tanks where the PCM is packed in cylinders and the HTF flows parallel to it, and tanks where pipes containing the fluid are embedded in the PCM are compared in (Esen, Durmu et al. 1998). In addition the most favourable geometric design of the storage unit was presented. Homogeneous phase change process[3.36] (HPC) is shown to reduce the melting time for a sphere, a cylinder and a flat plate (Wang, Chen et al. 1999). Banazec presented a paraffin wax-air spiral storage unit (Banaszek, Domanski et al. 2000). Bibliography on different shape energy storage units can be found in (Brousseau and Lacroix 1996)

In general, previous studies have shown that cylindrical, spiral and spherical containers have slower melting rate than those of rectangular dimension. Zivkovic concluded that a rectangular container requires nearly half of the melting time in comparison with a cylindrical container (Zivkovic and Fujii 2001).

As explained earlier the rectangular shape was selected for this study to have shorter charging and discharging processes, as faster rates are considered to improve system's performance.

The cell model is expected to represent one of the multiple cells that constitute the LHSS (latent heat storage system). Two rectangular aluminium tubes of two different dimensions are used as the PCM container:

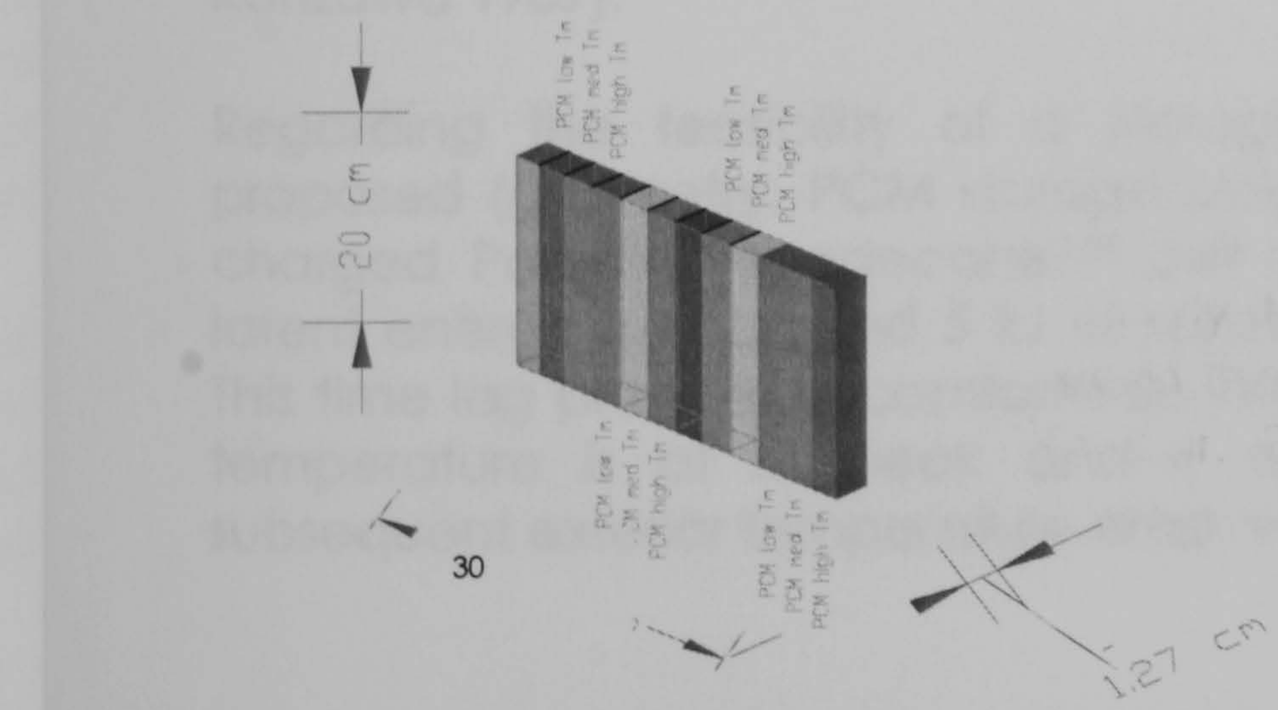

Figure 3.1: Complete storage unit

Figure 3.2: Storage cell

[3.36] Any component of the PCM starts and ends its phase change simultaneously(has no obvious interface in the PCM), and the phase change rate of every component is identical and remains constant during the phase change process (Wang, Chen et al. 1999)

PCM

An inadequate choice of PCM was an important factor on the failure of early PCM products. As mentioned in the previous chapter, the candidate PCM should have: high latent heat of fusion, high thermal conductivity, high density, thermal stability during repeated cycles[3.37], low volume change, exhibit no super cooling, be non-corrosive, non-toxic and non-flammable and have a melting temperature in the desired range.

An accurate determination of the transition zone at fusion and at freezing is crucial for the optimal design of a latent thermal energy storage unit, as the transition zone of the PCM must correspond the intended operating temperature.

In previous research it was concluded that the energy stored drops rapidly as the melt temperature diverges from average room temperature. In the case of heating by direct solar radiation the most advantageous diurnal storage takes place with a melt temperature of one to three degree Celsius above room temperature.(Peippo, Kauranen et al. 1991).

In order to decide on which PCMs to employ for this study, information about their melting temperature, density, specific heat, thermal conductivity, enthalpy and price were required.

A comparison of the variation of energy storage with time for four different PCMs is presented in (Esen and Ayhan 1996). The idea of multiple PCMs used in a single storage unit has been studied previously. Vertical cylinders filled with different melting PCM temperatures were found to have higher heat transfer rates than single PCM units in the study carried out by(Farid and Kanzawa 1989).

Regarding the feasibility of a storage system with the characteristics proposed (geometry, PCM storage properties, weather conditions), a fully charged Paraffin hexadecane[3.38] cell unit[3.39] , can store around 11kJ of latent energy and around 5 kJ of sensible energy in a period of 3.5 hours. This time lag provides a comfortable interior temperature when the exterior temperature is at its peak and is adequate to compensate for the subsequent exterior temperature drop, when this energy will be released.

3.37 For instance, the initial thermal storage capacity was observed to reduce over a number of fusion/crystallisation cycles, due to the use of chemicals that didn't have congruent melting, resulting in PCM segregation.

3.38 Enthalpy (H)= 236 kJ/kg, Heat capacity (Cp)=2.200 kJ/kgK, Thermal conductivity (k)=0.45 W/mK, Density (ρ)=870 kg/m^3, Volume of one cell unit= (0.2x.3x.0254)=1.52x10^{-3}m3

3.39 A cell can be of volume 1.029×10^{-4} or 6.4516×10^{-5}

Three PCM substances were selected due to their appropriate melting point for the required weather conditions and their large enthalpy values, and those were: paraffin hexadecane, tetradecanol, and a fatty acid mixture of capric and palmitic acid. After a preliminary testing with a Differential Scanning Calorimeter (DSC) of the thermal properties and behaviours of the substances the capric acid was selected to verify the results of the computer model. Details of the DSC testing are included in the chapter regarding experimental work. See appendix 2.C and 2.D for further details regarding PCM properties literature survey.

The highest melting temperature PCM was placed next to a medium melting temperature PCM and this one next to a low melting temperature PCM which was again next to the highest melting temperature PCM. It would be interesting in further work to test the performance of the system under different melting point PCM arrangements.

Boundary conditions

The heat storage unit is exposed to simulated solar radiation. An independent calculation evaluates the air temperature inside the chamber reached with the given radiation received (sol-air temperature). The condition for the moving boundary problem imposed at the irradiated wall is that of convection. The edges of the unit are insulated.

The heat flux at the external collector surface is defined by the irradiation data obtained from the weather data for three regions at different latitudes in Mexico.
The basic weather data and the calculation for the direct and diffuse radiation for the variation of incidence angle are included in appendix 3.C.

Mathematical model

The code for the computer model was written on C language.

The Governing equation

Discrete temperature and enthalpy equations

The integral form of the energy equation $\left(\frac{dH}{dt} = -\int_A \vec{q}\vec{n}dA\right)$[3.40] is converted to a series of algebraic equations for the enthalpies and temperatures at discrete points. The representation of the nodes for the volume discretization is as follows:

[3.40] Where $\vec{q} = -k\nabla T$ or $\vec{q} = h(T_\infty - T)$ or $q = \varepsilon\sigma(T_\infty^4 - T^4)$; $\vec{n}$=outward pointing vector at the bounding surface; dA=Elemental area on the bounding surface

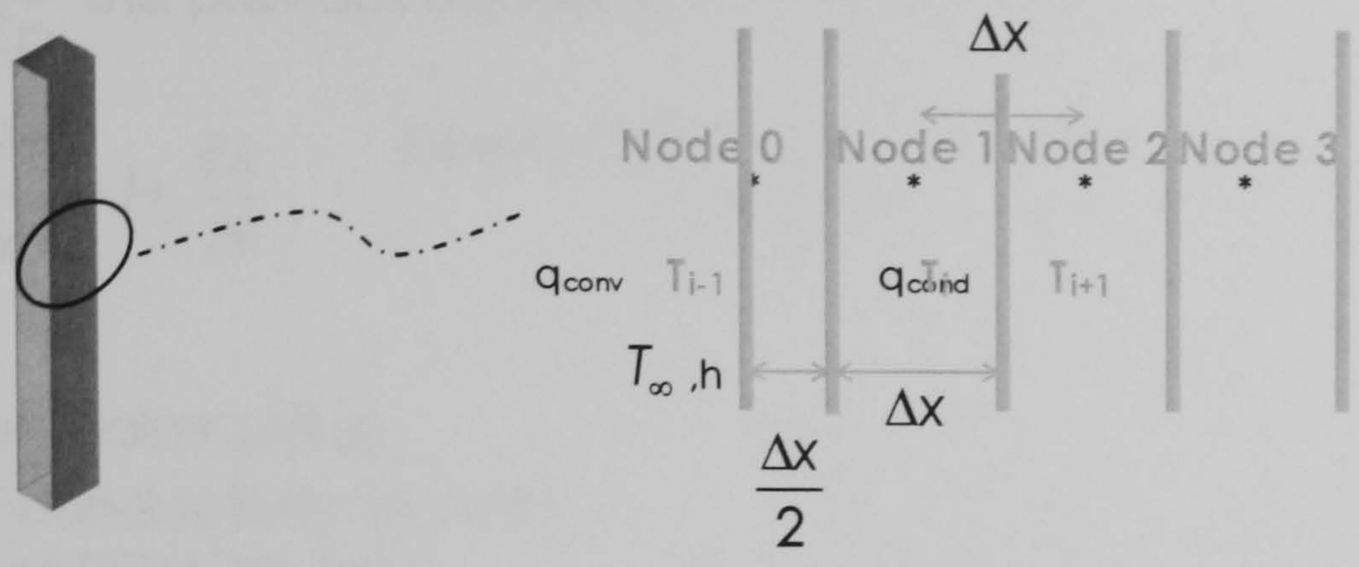

Figure 3.3: Control volume grid system

where "i" is the space coordinate of the nodes in the direction parallel to the flow. A discretised form of the energy equation is acquired for every volume.

A slightly modified enthalpy method was used for the modelling. The temperature and the liquid fraction fields are decoupled, following the next procedure.

Breaking up the total enthalpy into sensible and latent heat components:

$$H_T = H_s + H_l * \lambda$$

$$\frac{\partial H_s}{\partial t} = \frac{\partial H_T}{\partial t} - \frac{\partial H_L}{\partial t}$$

Where
H_s= Sensible enthalpy
H_l=Latent enthalpy
λ = Liquid fraction
From the definition of sensible enthalpy $\left(H_s = \int_{Tm(PCM)}^{T_{PCM}} Cp dT \right)$:

$$\frac{\partial H_s}{\partial t} \equiv Cp \frac{\partial T_{PCM}}{\partial t}$$

From Equation 3.1, $\frac{\partial T_{PCM}}{\partial t} = \alpha \frac{\partial^2 T}{\partial x^2}$

The governing equation for unsteady heat transfer and conduction controlled isothermal phase change, according to the boundary conditions given by the moving boundary

$$\frac{\partial H_T}{\partial t} = Cp\,\alpha \frac{\partial^2 T}{\partial x^2} - H_l \frac{\partial \lambda}{\partial t}$$

As $\alpha = \frac{k}{\rho Cp}$ the previous equation can be written:

$$\frac{\partial H_T}{\partial t} = \frac{k}{\rho}\frac{\partial^2 T}{\partial x^2} - H_l \frac{\partial \lambda}{\partial t}$$

Equation 3.9: Heat transfer and phase change governing equation

Where

H_T = Total enthalpy (J/kg)

k= Thermal conductivity (W/mK)

ρ=Density of PCM (kg/m^3)

Finite differences are used to solve the Partial Differential Equations (PDE). The discretization domain for one dimensional phase change problem would be:

For Internal Nodes

The two main approaches used to obtain the difference approximations to the conduction terms are: 1) writing simple difference approximations by direct inspection of the physical energy balance for the element, 2) Using a Taylor series expansion of the variables to obtain higher-order approximations. For internal nodes the second option is applied and for external nodes the physical energy balance is used

The left hand side of Equation 3.9 substituted by a simple backward time-difference ratio for the nodal enthalpy stands for the mass-averaged enthalpy of the matter in the volume:

$$\frac{\partial H}{\partial t} = \frac{H_{i,j} - H_{i,j-1}}{\Delta t}$$

Representing the derivative on first element of the second term of the difference Equation 3.9 (which is a second derivative of temperature in space) by a central difference ratio:

$$\frac{\partial^2 T}{\partial x^2} = \frac{T_{i+1} - T_i}{\Delta x} - \frac{T_i - T_{i-1}}{\Delta x} = \frac{T_{i+1} - 2T_i + T_{i-1}}{\Delta x^2}$$

The derivative on the second element of the second term of Equation 3.9 represented by a backward difference in time:

$$\frac{\partial \lambda}{\partial t} = \frac{\lambda_{i,j} - \lambda_{i,j-1}}{\Delta t}$$

Equation 3.9 can be written:

$$\frac{H_{i,j} - H_{i,j-1}}{\Delta t} = \frac{k}{\rho \Delta x^2}(T_{i-1} - 2T_i + T_{i+1}) - H\frac{\lambda_{i,j} - \lambda_{i,j-1}}{\Delta t}$$

Equation 3.10: Discretized moving boundary problem governing equation

Where "j" denotes the discrete time levels (periods)
A set of linear equations in the unknown enthalpies is outlined by the finite difference equations. Nevertheless the liquid fraction source term value is not known a priori and an iterative technique is required to go forward one time step in the solution(Voller 1990)

Case 1: As stated in the assumptions, before the change in conditions, the unit is at a uniform temperature T_o . If the control volume is fully solid there is no liquid fraction:

$$\frac{\partial \lambda_{(i)}}{\partial t} \equiv 0$$

For an interior node in a one dimensional problem, using a uniform square grid, the governing equation reduces to the single-phase ordinary heat diffusion equation (Equation 3.1):

$$\frac{\partial T_{PCM(i)}}{\partial t} = \frac{k}{\rho c \Delta x^2}(T_{i-1} - 2T_i + T_{i+1})$$

Discretizing the first term, the backward difference in time :

$$\frac{(T_{ij} - T_{i,j-1})}{\Delta t} = \frac{k}{\rho Cp \Delta x^2} T_{i-1} - \frac{2k}{\rho Cp \Delta x^2} T_i + \frac{k}{\rho Cp \Delta x^2} T_{i+1}$$

Multiplying by Δt :

$$T_{ij} - T_{i,j-1} = \Delta t \frac{k}{\rho Cp \Delta x^2} T_{i-1} - \frac{2k}{\rho Cp \Delta x^2} \Delta t T_i + \frac{k}{\rho Cp \Delta x^2} \Delta t T_{i+1}$$

Using the Fourier number (Fo) definition:

$$\frac{k}{\rho Cp \Delta x^2} = \frac{\frac{k}{\rho Cp}}{\Delta x^2} = Fo = \frac{\alpha}{\Delta x^2} \Delta t$$

The backward difference ends up being:

$$T_{ij} - T_{i,j-1} = FoT_{i-1,j} - 2FoT_{ij} + FoT_{i+1,j}$$

Applying implicit[3.41] method for solving the differences:

$$T_{i,j-1} = -FoT_{i-1,j} + 2FoT_{i,j} - FoT_{i+1,j} + T_{ij}$$

Rearranging:

$$T_{i,j-1} = -FoT_{i-1,j} + (2Fo + 1)T_{i,j} - FoT_{i+1,j}$$

Equation 3.11: Evaluation of temperature profile (interior nodes) from the governing equation of single-phase ordinary heat diffusion

Case 2 : If melting or freezing occurs at the node, the liquid fraction lies between zero and one.

$$\lambda(T) = \begin{cases} 1 \\ 0 \end{cases}$$

3.41 Implicit method is not as accurate as ıethod, but numerical oscillations will never appear (no matter how lc taken)

From the definition of the liquid fraction

$$\begin{array}{ll} 1 & \text{if } T_{PCM} > T_m \\ 0 & \text{if } T_{PCM} < T_m \end{array}$$

Mushy zone:

When the melting temperature is reached, the PCM temperature stays constant $\Delta T = 0$. With no change of temperature, there is no change in enthalpy, that is:

If $T_i = Tm$ then $\frac{\partial H}{\partial t} = 0$ and substituting in Equation 3.10:

$$H\frac{\lambda_{i,j} - \lambda_{i,j-1}}{\Delta t} = \frac{k}{\rho \Delta x^2}(T_{i-1} - 2T_i + T_{i+1})$$

And the liquid fraction at a node in the mushy zone:

$$\lambda_{i,j} = \frac{k}{H\rho\Delta x^2}\Delta t(T_{i-1} - 2T_i + T_{i+1}) + \lambda_{i,j-1}$$

Equation 3.12: Equation for updating the liquid fraction

For exterior node

Heat conduction dominates the heat flow at the boundary of the element; thus the difference expressions at the boundary don't include enthalpies but only temperatures at the actual node and neighbouring nodes. The energy balance incorporates terms reflecting the boundary conditions.(Minkowycz, Sparrow et al. 1988)

To derive the equation for a surface node with convection and one dimensional transient conduction, an energy balance was applied.

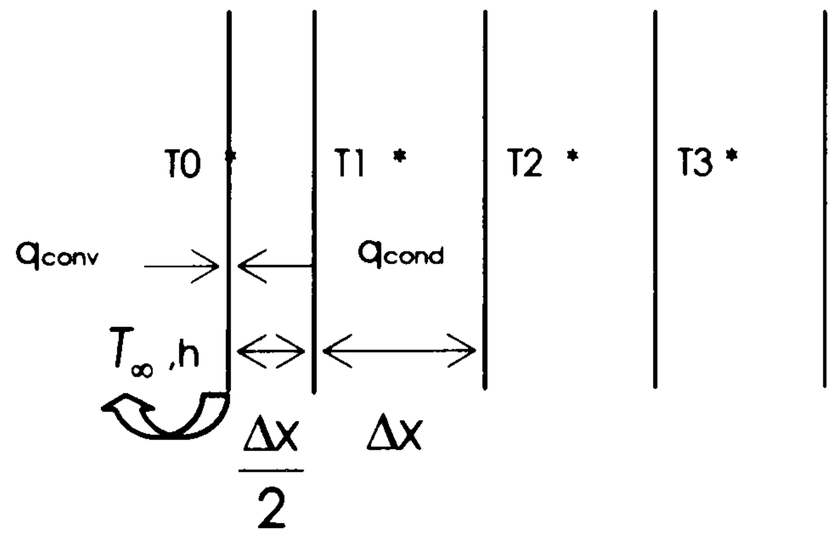

$$\rho CpA\frac{\Delta x}{2}\frac{(T_{i,j} - T_{i,j-1})}{\Delta t} = \frac{kA}{\Delta x}(T_{i+1,j} - T_{i,j}) - hA(T_\infty - T_{i,j})$$

Multiplying by $\frac{2\Delta t}{\rho CpA\Delta x}$

$$T_{i,j} - T_{i,j-1} = \frac{kA}{\Delta x}\frac{2\Delta t}{\rho CpA\Delta x}(T_{i+1,j} - T_{i,j}) - hA\frac{2\Delta t}{\rho CpA\Delta x}(T_\infty - T_{i,j})$$

As $Fo = \frac{\alpha}{\Delta x^2}\Delta t$

$$T_{i,j-1} = -2Fo(T_{i+1,j}) + 2Fo(T_{i,j}) + T_{i,j} - \frac{h}{\rho Cp}\frac{2\Delta t}{\Delta x}(T_\infty - T_{i,j})$$

$$T_{i,j-1} = (1+2Fo)T_{i,j} - \frac{h}{\rho Cp}\frac{2\Delta t}{\Delta x}(T_\infty - T_{i,j}) - 2Fo(T_{i+1,j})$$

Equation 3.13: Temperature equation for surface node exposed to cooling convection

And to obtain the one-dimensional enthalpy difference equation, a balance is also applied:

$$\rho CpA\frac{\Delta x}{2}\frac{(\lambda_{i,j} - \lambda_{i,j-1})}{\Delta t} = \frac{kA}{\Delta x}(T_{i+1,j} - T_{i,j}) - hA(T_\infty - T_{i,j})$$

Multiplying by $\frac{2\Delta t}{\rho CpA\Delta x}$

$$\lambda_{i,j} - \lambda_{i,j-1} = \frac{kA}{\Delta x}\frac{2\Delta t}{\rho CpA\Delta x}(T_{i+1,j} - T_{i,j}) - hA\frac{2\Delta t}{\rho CpA\Delta x}(T_\infty - T_{i,j})$$

$$\lambda_{i,j} = \lambda_{i,j-1} + \frac{2k\Delta t}{\rho Cp\Delta x^2}T_{i+1,j} - \frac{2k\Delta t}{\rho Cp\Delta x^2}T_{i,j} - \frac{2h\Delta t}{\rho Cp\Delta x}T_\infty - \frac{2h\Delta t}{\rho Cp\Delta x}T_{i,j}$$

$$\lambda_{i,j} = \lambda_{i,j-1} - \frac{2h\Delta t}{\rho Cp\Delta x}T_\infty + 2Fo(T_{i+1,j}) - \left(2Fo + \frac{2h\Delta t}{\rho Cp\Delta x}\right)T_{i,j}$$

Equation 3.14: Liquid fraction equation for convectively cooled one dimensional phase change problem

The temperature and enthalpy equations presented are applied to all the nodes in the mesh in order to obtain the temperature field, and to calculate the liquid fractions, so as to evaluate the latent heat evolution and heat flux. The convective heat transfer coefficient (forced convection) for the given mass flow rate is calculated as shown in appendix 3.D.

Evaluation of the net heat flux and the air temperature inside the chamber reached with the given radiation received was evaluated following the procedure also presented in appendix 3.D.

Solution of the nonlinear difference equations

The unknown enthalpy distribution is described by the set of nonlinear[3.42] nodal equations. The iterative method used to solve the equations in this study was the nonlinear Gauss-Seidel iterative method

Nonlinear Gauss-Seidel iterative method:

3.42 Equations are nonlinear because the nodal enthalpies as well as the nodal temperatures have to be determined and the relation between enthalpy and temperature is nonlinear.

Given an initial temperature distribution, and the computed heat transfer coefficient and the sol-air temperature[3.43] the temperature coefficients of the phase change governing equation are calculated for the first time step for each node of the grid. At every time step, the calculation goes across the grid. The vector formed with the coefficients is fed to the Gauss-Seidel iterative method and the set of temperatures are stored.

It is essential to keep in mind that the temperature of a two-phase node in a pure substance stays at the melting point as long as the enthalpy of the node remains between the solid and liquid enthalpy values.(Minkowycz, Sparrow et al. 1988)

With these temperatures and the initialized values of the liquid fraction, and the Phase Transition(PhT), Beginning of Melting (BM), Melted Completely (MC), Beginning of Solidification (BS), Completely Solid (CS) variables, the liquid fraction for each node is calculated and stored.

These variables assist in determining the conditions (solid, liquid or mushy) of previous node condition to define the actual node condition and the final liquid fraction update, and call for a new iteration until the node has completely changed phase.

The updated liquid fraction, the temperature of the nodes, and the initial energy content are used to calculate the energy stored at each period. The energy stored depends on the evolution of the liquid fraction formed. It can contain an initial energy stored, sensible liquid part, sensible solid part and latent energy, depending on the liquid fraction condition ($\lambda \leq 0$, $0 \prec \lambda \prec 1$, $\lambda \geq 1$)

The change in enthalpy was evaluated with the updated liquid fraction and the non-linear temperature-enthalpy relation of the substance occupying the volume element, which was obtained from the DSC. The iterations will continue until the total number of periods (according to the duration of the test) is completed. Results of temperature, liquid fraction, heat fluxes, energy stored, are printed

Calculating subsidiary results

One important advantage of the enthalpy method is that calculations of parameters such as the total energy content, position of the moving boundary or boundary between phases, and surface heat flux distributions, are not needed for marching ahead with the enthalpy calculations(Minkowycz, Sparrow et al. 1988)

[3.43]Is the temperature inside the chamber that accounts for the received irradiation from the lamps, and the injected air.

Fluxes: From the surface temperature, the heat fluxes are calculated by using the surface boundary conditions as in a single-phase heat conduction problem. The temperatures reached at the surfaces are obtained as a result of the Gauss-Seidel iterative method which was fed with the temperature coefficients evaluated with the liquid fraction calculation.

Liquid fraction: The overall masses in the solid-phase and liquid-phase nodes are calculated independently by adding the values of the corresponding nodes and multiplying the total by the density of the specific phase. The nodal enthalpy of the two phase nodes is a volume average of the solid and liquid fractions. The fractions are added up and then included in the respective totals from the single-phase zones.

Location of moving boundary: The interface passes though the grid nodes. As it was mentioned earlier, the nodes liquid fraction (solid and liquid portions) lies between zero and a hundred percent and can be evaluated. Nevertheless from the fragmented areas it is not possible to generate a two dimensional curve for the following reason.

The interface is not tracked in the enthalpy method. At the melting point the temperature at the node is held constant despite what portion of the volume is frozen or molten. Earlier we have spoken about the waviness of the interface shape given by this method. In order to apply some degree of smoothing in calculating the interface shape: The total added volume of the nodes that are fully solid and the portions of the two phase nodes are summed accumulatively. A curve is fitted to the data, and differentiating the smoothed curve with respect to the space variable (say x) yield a smooth curve y(x) (Minkowycz, Sparrow et al. 1988)

Choice of step size

The enthalpy method is able to calculate accurately the melting/freezing rates even with fairly coarse grids. Regarding the time step, the idea is to have small enough steps so that the change of phase of each node is completed in many steps in time. It is necessary to avoid stepping from one phase to another. If the spatial grid is finer to improve accuracy, the time step should be consequently reduced due to the presence of the moving boundary (Minkowycz, Sparrow et al. 1988)

Verification of results

A straightforward test that runs well with the enthalpy method is as follows. At regular periods of time the products of the enthalpies and volumes of all the nodes are calculated and added to obtain the energy content in the substance. Simultaneously, the total heat transfer rate is computed and

recorded as a function of time. These total heat transfer rates are integrated over time[3.44], and the result is compared against the change of energy content calculated earlier. If the difference is more than a few percent there are at least four possible sources of error to consider: (Minkowycz, Sparrow et al. 1988)

1.- The step sizes in time or space are too large

2.- The finite difference representations of the boundary conditions are inaccurate

3.-The iterations were terminated prematurely

4.- There is a program error

Flow diagram of the phase change model

The flow diagram is presented in appendix 3.A. A pseudo code is presented in appendix 3.E , showing the algorithm of the main functions for the program

---

3.44 This can be done by using either the trapezoidal rule or Simpson's rule

Appendix 3.A: Program flow diagram

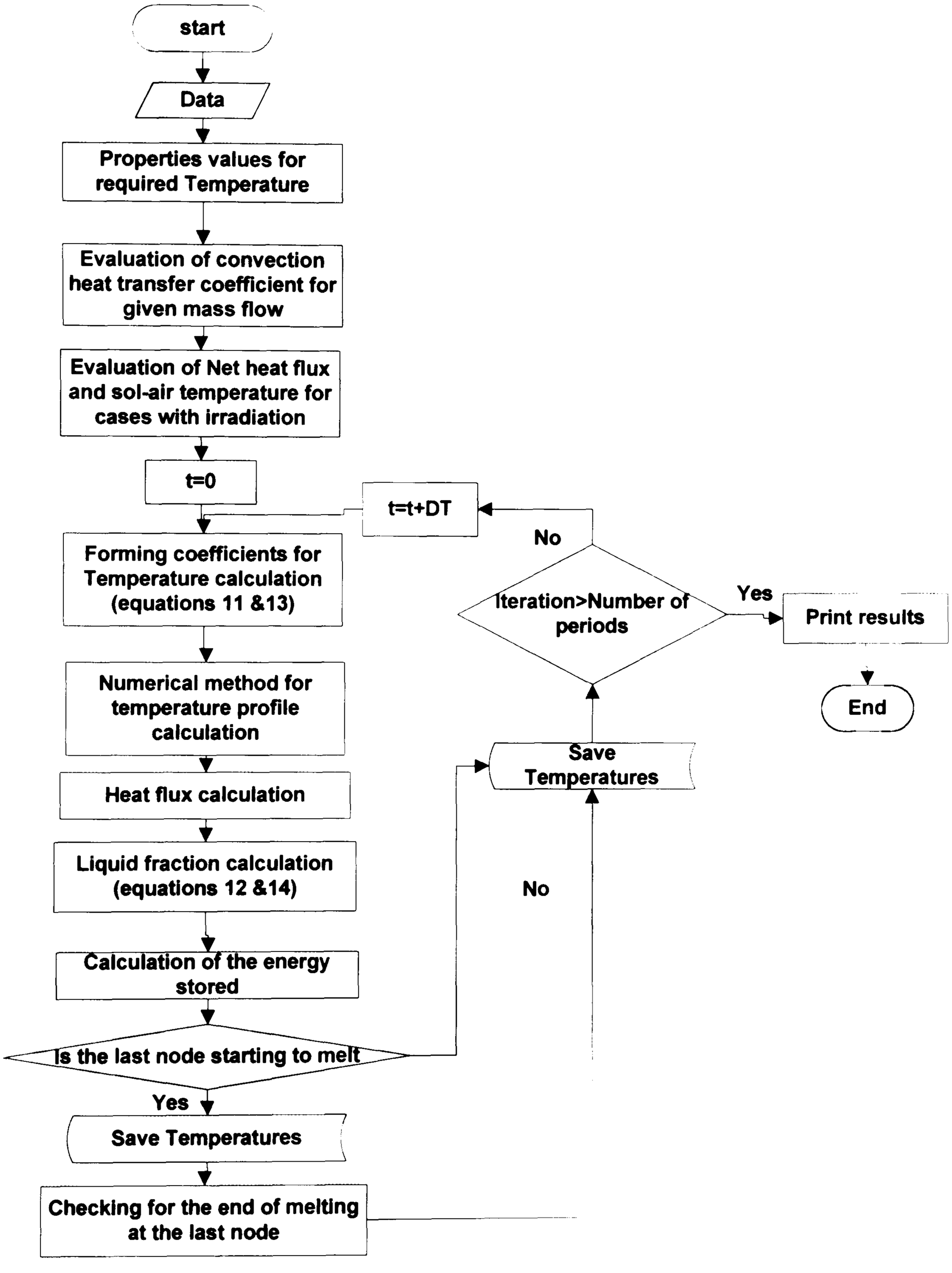

Appendix 3.B : Heating and cooling energy loads for the dwellings derived from TAS software simulations

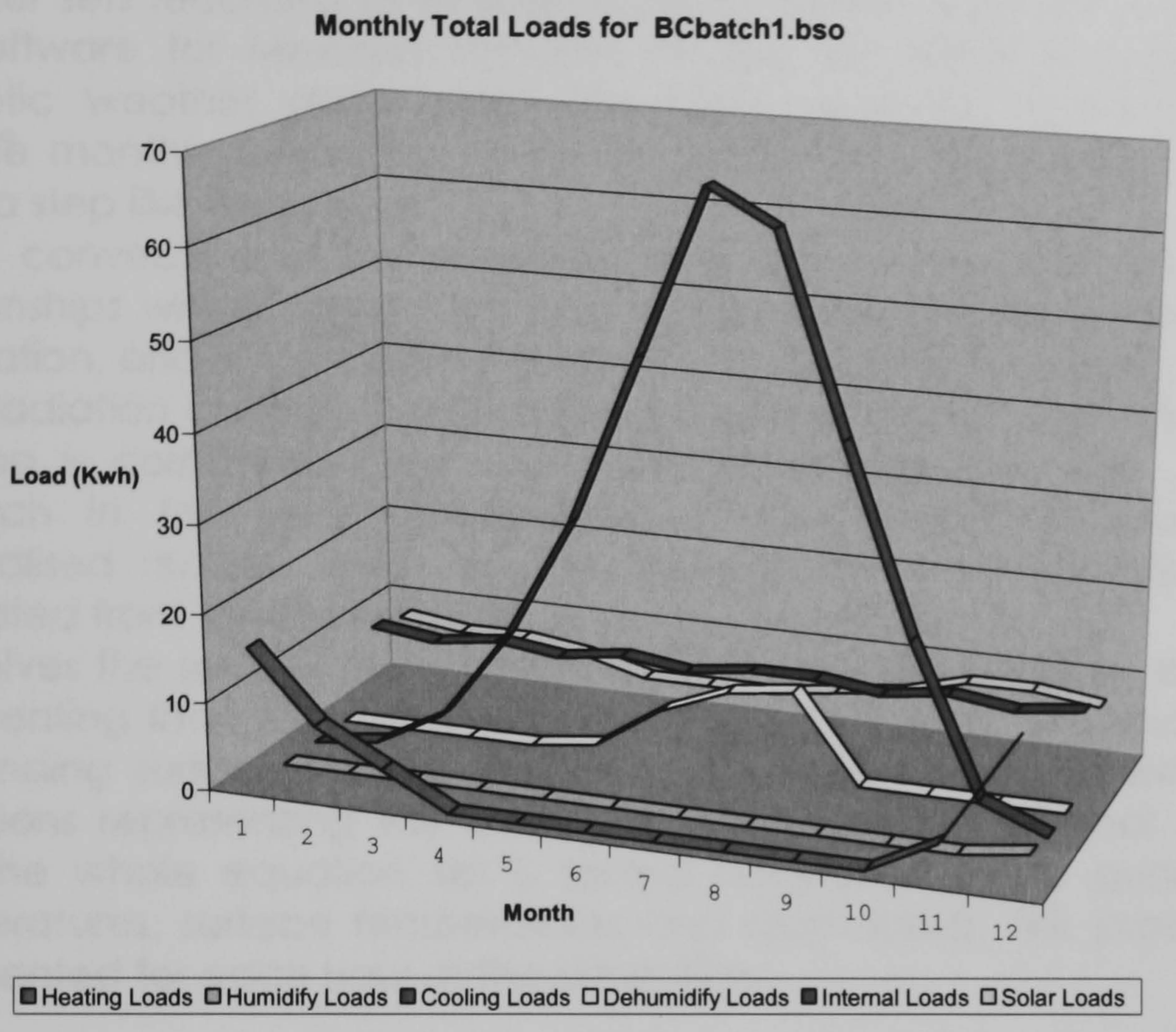

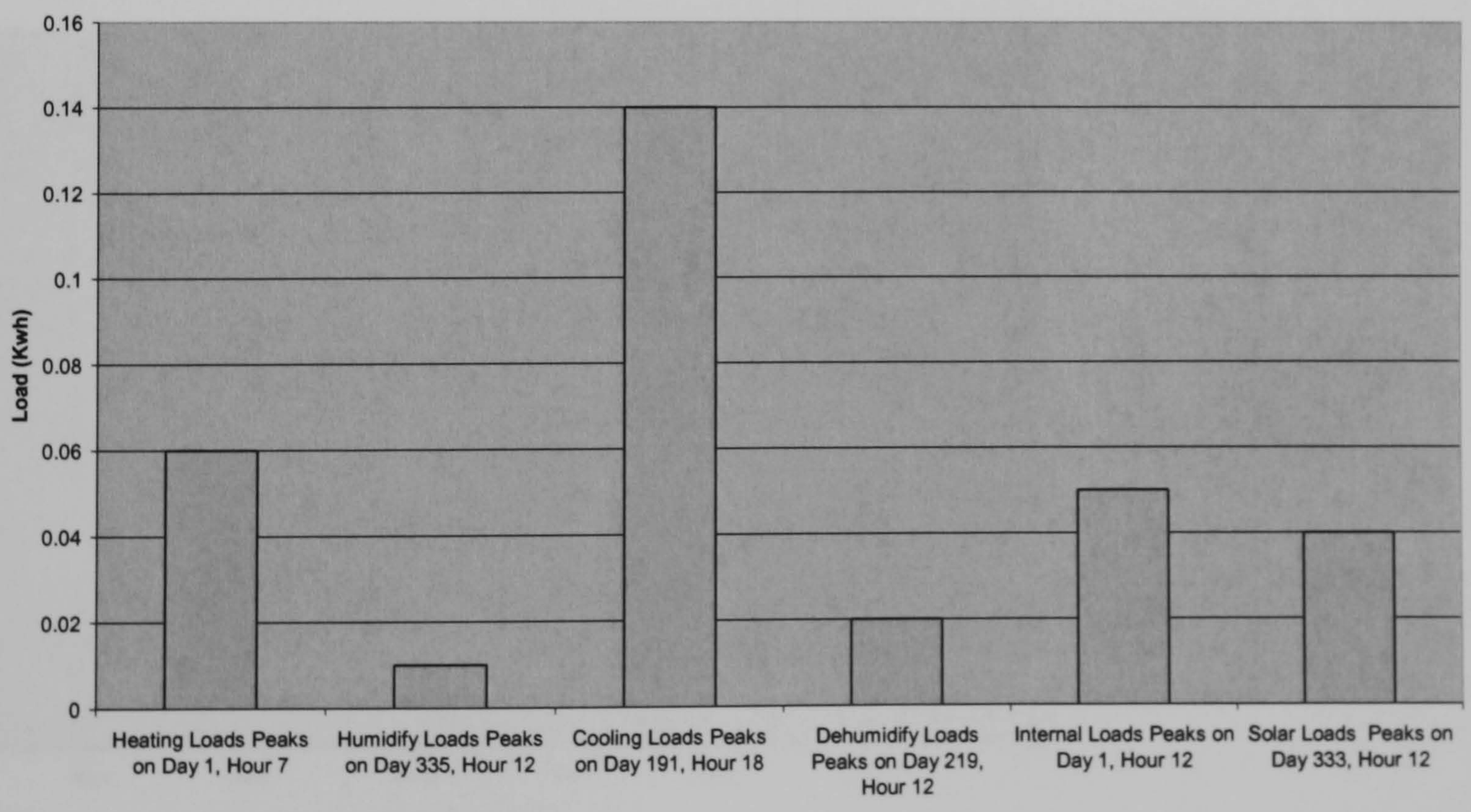

To assess the environmental performance of the building TAS was fed with the required weather parameters for the simulation. Historic weather sets recorded at sufficiently short periods were not available in this software for Mexican latitudes. It was necessary to generate a synthetic weather data (using the CIBSE weather synthesis), which provide monthly averages. This is the reason why the following graphs show a step like behaviour.

In TAS convection at the building surfaces is treated using theoretical relationships which relate heat flow to temperature difference, surface orientation, and in the case of external convection wind speed.

Solar radiation absorbed, reflected and transmitted by each element of building is computed from solar data on the weather file. A lot of research in the solar energy field is concerned with developing generalised models which enable the weather characteristics to be estimated from minimum inputs.

TAS solves the sensible heat balance for a zone by setting up equations representing the individual energy balances for the air and each of the surrounding surfaces. These equations are then combined with further equations representing the energy balances at the external surfaces, and the whole equation set is solved simultaneously to generate air temperatures, surface temperatures and room loads. This procedure is represented for each hour of the simulation.

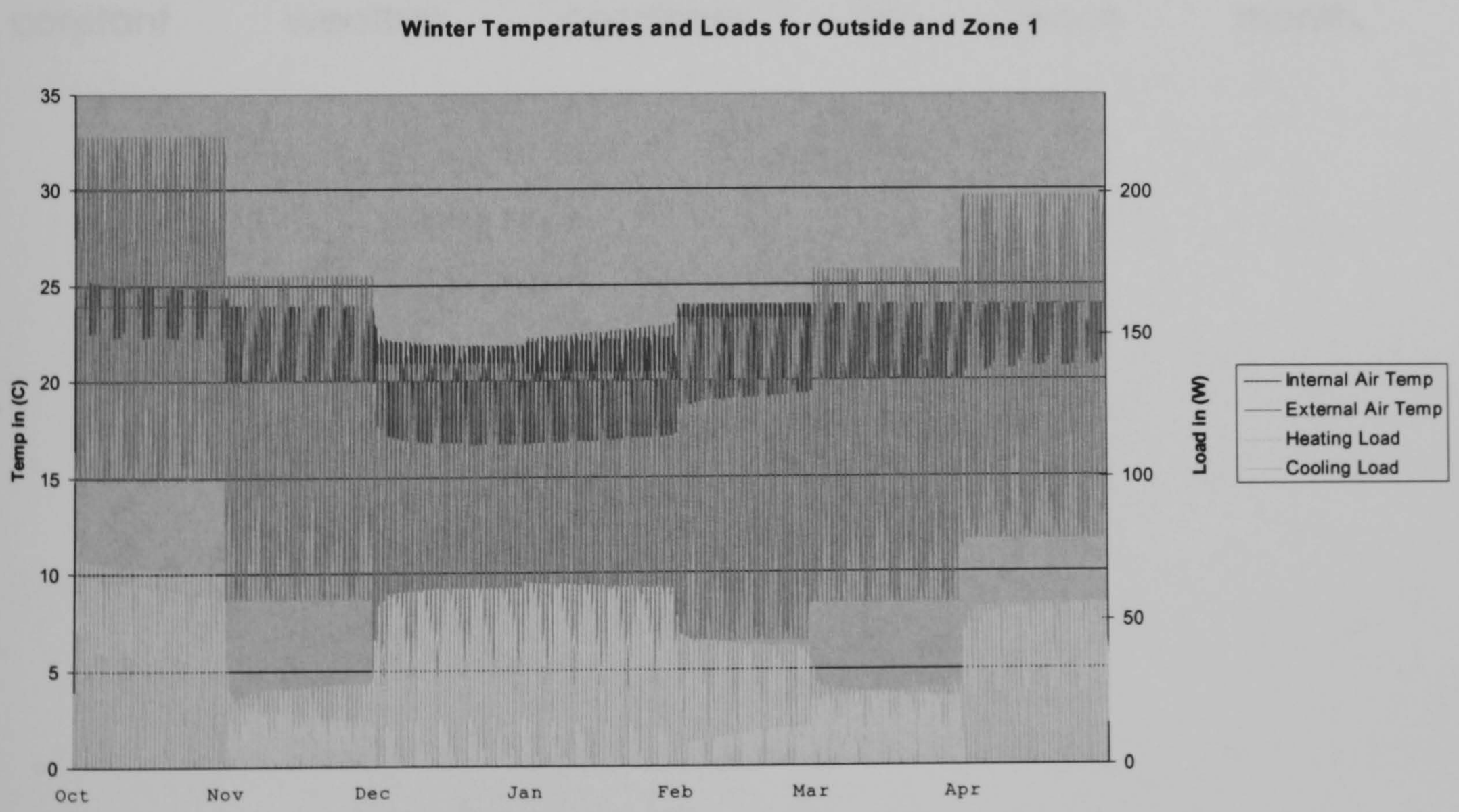

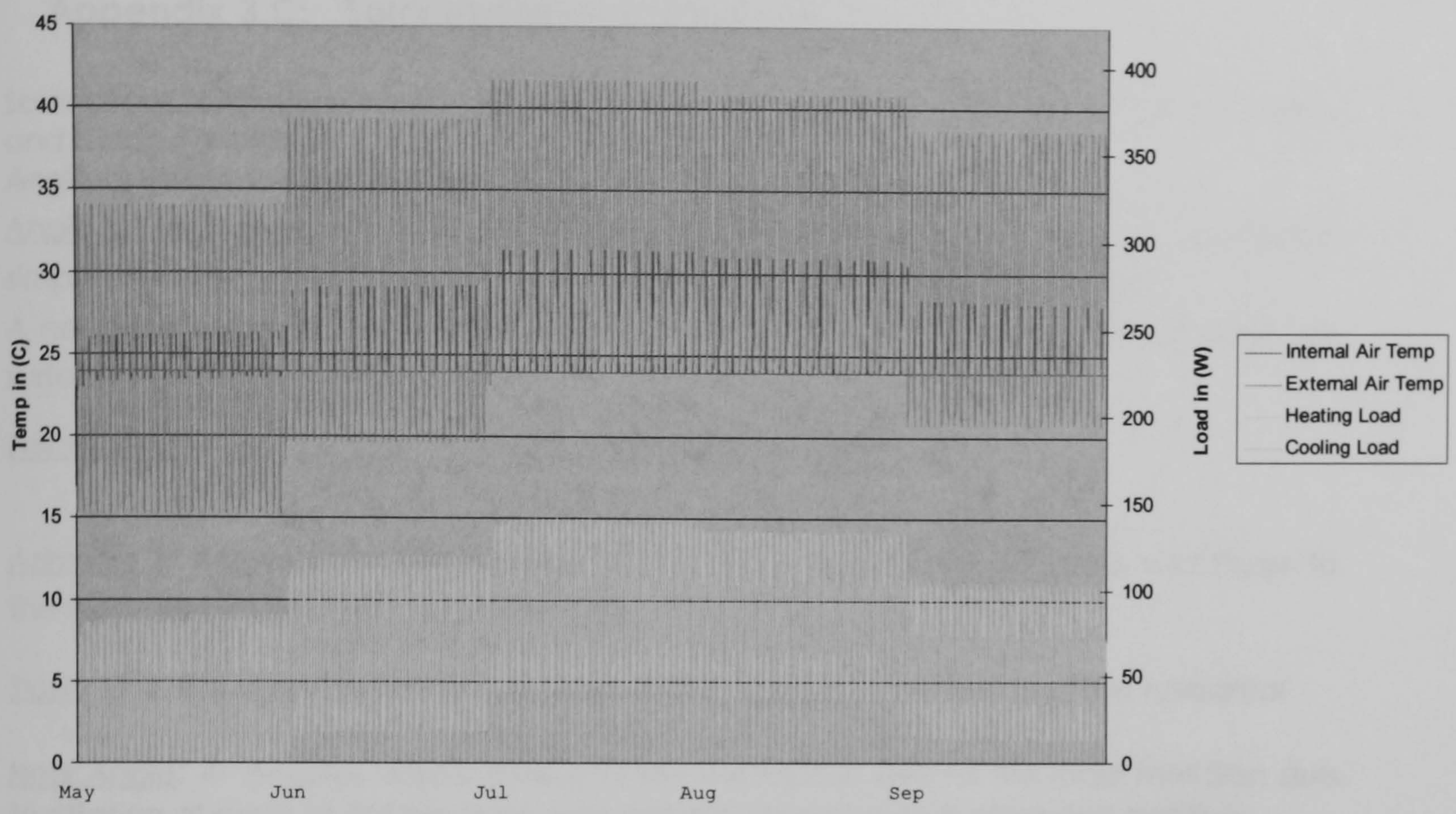

The stepped like temperatures are due to the use of synthetic weather data on the TAS simulations. This type of weather date considers constant weather conditions for each month.

Appendix 3.C: Solar radiation calculation

Solar direct and diffuse radiation data for a vertical surface in Mexicali, Tuxtla-Gutierrez, and Ciudad-Victoria

Angle of Incidence calculation

Angle of Incidence: $\beta = 90^o$ and if facing south: $\gamma = 0^o$, so we end up having the simplified form: $$Cos\theta = Sin\phi\, Cos\delta\, Cos\omega - Cos\phi\ Sin\delta$$

A negative value of $Cos\theta$ indicates that θ >90° and the sun's rays do not strike the surface

Declination: $$\delta = 23.45 Sin\left(360 * \frac{284 + n}{365} \right)$$

Azimuth: γ Angles subtended to the east of the meridian are negative and those to the west are positive; with zero due south

Slope β is the angle between the plane of the surface of interest and the horizontal

Hour Angle: ω Angular displacement of the sun east or west of the local meridian due to rotation of earth at 15° per hour: with morning negative and afternoon positive.
i.e. 12-hour= number of hours difference *15

a) Correction for the difference in longitude between the observer's meridian location and the meridian on which the local time is based and has a constant value.

$$Solar\ Time = Local\ Time + 4(L_{st} - L_{loc}) + E - D$$

And L_{loc} is the longitude of the location in question in degrees west . The longitude values are measured west of Greenwich (Jan F. Kreider)
E is the value for the day of the year obtained from the equation of time

b) Correction that takes into account the perturbations of earth's rate of rotation, expressed by the equation of time.

$$E = (9.87 * Sin(2 * B)) - (7.5 * Cos(B)) - (1.5 * Sin(B)) \qquad \text{in minutes}$$

Average angle= 360°/365.24 days in a year =0.986° per day

$$B = \frac{360(n - 81)}{364}$$

CIBSE METHOD FOR RADIATION CALCULATION

1) For a particular latitude, date and time of day, the solar altitude and the angle of incidence onto a surface of given slope and orientation are uniquely determined.
For obtaining solar altitude and azimuth angles for the average day of each month (considered to be the 21st. of each month, CIBSE) table A2.23 was used.
The values to interpolate corresponding to the regions mentioned are as follows:
- Mexicali Baja-California (BC): latitude = 32.25°
- Tuxtla-Gutierrez, Chiapas (CH): latitude = 16.75°
- Ciudad-Victoria, Tamaulipas (Tmps): latitude = 23.73°

The interpolated values obtained are:

Baja California

Month	hour	6	7	8	9	10	11	12	13	14	15	16	17	18
Jan-21	altitude	0	1.5	13.3	23.0	31.0	36.8	38.8	36.8	31.0	23.0	13.3	1.5	0
	azimuth	0	115.0	123.3	133.5	146.5	162.3	180.0	197.8	213.5	226.5	236.8	245.0	0
Feb-21	altitude	0	6.8	18.5	29.3	39.0	45.8	47.8	45.8	39.0	29.3	18.5	6.8	0
	azimuth	0	107.3	116.3	126.5	140.8	158.5	180.0	201.5	219.3	233.5	243.8	252.8	0
Mar-21	altitude	0	12.8	25.5	37.3	48.0	55.8	58.8	55.8	48.0	37.3	25.5	12.8	0
	azimuth	90	98.3	106.5	117.8	132.0	152.8	180.0	207.3	228.0	242.3	253.5	261.8	270
Apr-22	altitude	6.3	19.0	31.8	44.5	56.3	66.0	70.8	66.0	56.3	44.5	31.8	19.0	6.3
	azimuth	80.0	87.3	94.8	105.0	117.8	140.8	180.0	219.3	242.3	255.0	265.3	272.8	280.0
May-22	altitude	10.5	23.3	36.0	48.0	60.8	72.3	78.8	72.3	60.8	48.0	36.0	23.3	10.5
	azimuth	72.3	79.5	86.0	93.5	104.3	125.0	180.0	235.0	255.8	266.5	274.0	280.5	287.8
Jun-21	altitude	12.3	24.3	37.0	49.8	62.0	74.5	82.5	74.5	62.0	49.8	37.0	24.3	12.3
	azimuth	69.3	76.5	83.0	89.5	98.5	116.0	180.0	244.0	261.5	270.5	277.0	283.5	290.8
Jul-23	altitude	10.5	23.3	36.0	48.0	60.8	72.3	78.8	72.3	60.8	48.0	36.0	23.3	10.5
	azimuth	72.3	79.5	86.0	93.5	104.3	125.0	180.0	235.0	255.8	266.5	274.0	280.5	287.8
Aug-22	altitude	6.3	19.0	31.8	44.5	56.3	66.0	70.8	66.0	56.3	44.5	31.8	19.0	6.3
	azimuth	80	87.3	94.8	105.0	117.8	140.8	180.0	219.3	242.3	255.0	265.3	272.8	280
Sep-22	altitude	0	12.8	25.5	37.3	48.0	55.8	58.8	55.8	48.0	37.3	25.5	12.8	0
	azimuth	90	98.3	106.5	117.8	132.0	152.8	180.0	207.3	228.0	242.3	253.5	261.8	270
Oct-22	altitude	0	6.8	18.5	29.3	39.0	45.8	47.8	45.8	39.0	29.3	18.5	6.8	0
	azimuth	0	107.3	116.3	126.5	140.8	158.5	180.0	201.5	219.3	233.5	243.8	252.8	0
Nov-22	altitude	0	1.5	13.3	23.0	31.0	36.8	38.8	36.8	31.0	23.0	13.3	1.5	0
	azimuth	0	115.0	123.3	133.5	146.5	162.3	180.0	197.8	213.5	226.5	236.8	245.0	0
Dec-21	altitude	0	0.0	10.3	20.3	28.0	33.8	35.8	33.8	28.0	20.3	10.3	0.0	0
	azimuth	0	88.5	126.25	136.25	148.5	163.25	180	196.75	211.5	223.75	233.75	181.5	0

CHIAPAS

Day	Hour	6	7	8	9	10	11	12	13	14	15	16	17	18
Jan-21	altitude	0	7.3	20.3	32.0	42.6	50.3	53.3	50.3	42.6	32.0	20.3	7.3	0
	azimuth	0	113.4	119.7	128.1	140.1	157.7	180.0	202.3	220.0	232.0	240.3	246.7	0
Feb-21	altitude	0	10.7	24.3	37.3	49.6	58.6	62.3	58.6	49.6	37.3	24.3	10.7	0
	azimuth	0	105.4	110.7	119.1	130.8	150.4	180.0	209.6	229.3	241.0	249.3	254.7	0
Mar-21	altitude	0	14.7	28.7	42.7	56.0	67.6	73.3	67.6	56.0	42.7	28.7	14.7	0
	azimuth	90	94.4	99.1	105.8	116.5	136.8	180.0	223.2	243.6	254.3	261.0	265.7	270
Apr-22	altitude	3.4	17.4	32.0	46.0	60.7	74.7	84.6	74.7	60.7	46.0	32.0	17.4	7.25
	azimuth	78.4	82.4	86.1	89.8	95.2	106.0	180.0	254.1	264.9	270.3	274.0	277.7	281.7
May-22	altitude	5.7	19.4	33.4	47.4	61.4	75.4	86.8	75.4	61.4	47.4	33.4	19.4	5.7
	azimuth	70.4	73.7	76.1	77.8	78.2	73.7	0.0	286.4	281.9	282.3	284.0	286.3	289.7
Jun-21	altitude	6.7	19.7	33.7	47.4	60.7	74.1	83.4	74.1	60.7	47.4	33.7	19.7	6.7
	azimuth	67.4	70.7	72.4	73.1	71.8	62.6	0.0	297.4	288.2	286.9	287.6	289.3	292.7
Jul-23	altitude	5.7	19.4	33.4	47.4	61.4	75.4	86.8	75.4	61.4	47.4	33.4	19.4	5.7
	azimuth	70.4	73.7	76.1	77.8	78.2	73.7	0.0	286.4	281.9	282.3	284.0	286.3	289.7
Aug-22	altitude	3.4	17.4	32.0	46.0	60.7	74.7	84.6	74.7	60.7	46.0	32.0	17.4	3.4
	azimuth	78.4	82.4	86.1	89.8	95.2	106.0	180.0	254.1	264.9	270.3	274.0	277.7	281.7
Sep-22	altitude	0	14.7	28.7	42.7	56.0	67.6	73.3	67.6	56.0	42.7	28.7	14.7	0
	azimuth	90	94.4	99.1	105.8	116.5	136.8	180.0	223.2	243.6	254.3	261.0	265.7	270
Oct-22	altitude	3.5	15.2	28.9	41.2	52.8	59.7	61.2	55.5	45.8	32.8	19.8	7.2	0
	azimuth	0	105.4	110.7	119.1	130.8	150.4	180.0	209.6	229.3	241.0	249.3	254.7	0
Nov-22	altitude	0	7.3	20.3	32.0	42.6	50.3	53.3	50.3	42.6	32.0	20.3	7.3	0
	azimuth	0	113.4	119.7	128.1	140.1	157.7	180.0	202.3	220.0	232.0	240.3	246.7	0
Dec-21	altitude	0	6.3	19.0	30.6	40.6	47.3	50.3	47.3	40.6	20.0	19.0	6.3	0
	azimuth	0	117.0	122.7	131.1	143.1	159.7	180.0	200.3	217.0	229.0	238.0	243.0	0

Tamaulipas

Day	Hour	6	7	8	9	10	11	12	13	14	15	16	17	18
Jan-21	altitude	0	4.5	16.8	27.8	37.0	44.0	46.3	44.0	37.0	27.8	16.8	4.5	0
	azimuth	0	114.0	121.7	131.5	143.5	160.5	180.0	199.5	216.5	228.5	238.3	246.0	0
Feb-21	altitude	0	9.3	21.5	33.8	44.8	52.3	55.3	52.3	44.8	33.8	21.5	9.3	0
	azimuth	0	113.5	113.5	123.2	136.2	155.2	180.0	204.8	223.8	236.8	246.5	254.0	0
Mar-21	altitude	0	14.0	27.3	40.5	52.5	62.0	66.3	62.0	52.5	40.5	27.3	14.0	0
	azimuth	90	95.7	103.2	112.0	124.7	146.5	180.0	213.5	235.3	248.0	256.8	264.3	270
Apr-22	altitude	4.7	18.0	32.0	46.0	59.3	71.8	78.3	71.8	59.3	46.0	32.0	18.0	4.7
	azimuth	79.0	84.5	90.2	96.7	107.0	126.7	180.0	233.3	253.0	263.3	269.8	275.5	281.0
May-22	altitude	7.7	21.5	34.7	48.0	62.0	75.3	86.3	75.3	62.0	48.0	34.7	21.5	7.7
	azimuth	71.0	76.5	81.0	85.5	90.7	100.2	134.3	259.8	269.3	274.5	279.0	283.5	289.0
Jun-21	altitude	9.5	21.7	35.7	48.7	62.7	76.0	87.5	76.0	62.7	48.7	35.7	21.7	9.5
	azimuth	68.0	73.5	77.2	80.7	84.5	80.5	134.3	272.1	275.5	279.3	282.8	286.5	292.0
Jul-23	altitude	7.7	21.5	34.7	48.0	62.0	75.3	86.3	75.3	62.0	48.0	34.7	21.5	7.7
	azimuth	71.0	76.5	81.0	85.5	90.7	100.2	134.3	259.8	269.3	274.5	279.0	283.5	289.0
Aug-22	altitude	4.7	18.0	32.0	46.0	59.3	71.8	78.3	71.8	59.3	46.0	32.0	18.0	4.7
	azimuth	79.0	84.5	90.2	96.7	107.0	126.7	180.0	233.3	253.0	263.3	269.8	275.5	281.0
Sep-22	altitude	0	14.0	27.3	40.5	52.5	62.0	66.3	62.0	52.5	40.5	27.3	14.0	0
	azimuth	90	95.7	103.2	112.0	124.7	146.5	180.0	213.5	235.3	248.0	256.8	264.3	270
Oct-22	altitude	0	9.3	21.5	33.8	44.8	52.3	55.3	52.3	44.8	33.8	21.5	9.3	0
	azimuth	0	106.0	113.5	123.2	136.2	155.2	180.0	204.8	223.8	236.8	246.5	254.0	0
Nov-22	altitude	0	4.5	16.8	27.8	37.0	44.0	46.3	44.0	37.0	27.8	16.8	4.5	0
	azimuth	0	114.0	121.7	131.5	143.5	160.5	180.0	199.5	216.5	228.5	238.3	246.0	0
Dec-21	altitude	0	3.5	14.8	25.8	35.0	40.3	43.3	40.3	35.0	25.8	14.8	3.5	0
	azimuth	0	117.7	124.7	133.7	146.5	161.7	180.0	198.3	213.5	226.3	1816.0	242.3	0

2) Basic Direct irradiance (I_{bb}): Using the values for latitude obtained for each hour for the specific average day of each month, interpolate the irradiance values for zero wall solar azimuth over a vertical surface, obtaining next values.

Basic Direct Irradiation value interpolated from values for Vertical surfaces (W/m2) BC

Month/Hour	6	7	8	9	10	11	12	13	14	15	16	17	18
Jan-21	0	63	461.25	609	640	634.75	628.75	634.75	640	609	461.25	63	0
Feb-21	0	269.5	561	637.75	628	589	573	589	628	637.75	561	269.5	0
Mar-21	0	448.75	626.5	633.25	571	491.75	458.75	491.75	571	633.25	626.5	448.75	0
Apr-22	262.5	569	640	599	486.25	364	298.75	364	486.25	598	640	569	262.5
May-22	392.5	611	637	571	434.875	276.25	178.75	276.25	434.875	571	637	611	392.5
Jun-21	436.25	619	634	557	418	242.5	120	242.5	418	557	634	619	436.25
Jul-23	392.5	611	637	571	434.875	276.25	178.75	276.25	434.875	571	637	611	392.5
Aug-22	252.5	569	640	598	486.25	364	298.75	364	486.25	598	640	569	252.5
Sep-22	0	448.75	626.5	633.25	571	491.75	458.75	491.75	571	633.25	626.5	448.75	0
Oct-22	0	269.5	561	637.75	590	589	573	589	590	637.75	561	269.5	0
Nov-22	0	63	461.25	408	640	599.75	553.75	599.75	640	408	461.25	63	0
Dec-21	0	0	386.25	587	500	640	476.25	572.5	500	587	386.25	0	0

Basic Direct Irradiation value interpolated from values for Vertical surfaces (W/m2) Chiapas

Month/Hour	6	7	8	9	10	11	12	13	14	15	16	17	18
Jan-21	0	288.2	587.4	640.0	609.4	552.3	519.3	552.3	609.4	640.0	587.4	288.2	0
Feb-21	0	396.3	619.4	633.1	558.2	460.4	670.4	475.1	558.2	633.1	619.4	396.3	0
Mar-21	0	496.3	636.0	609.1	489.6	342.4	261.3	342.4	489.6	609.1	636.0	496.3	0
Apr-22	140.7	542.6	640.0	587.0	436.2	240.3	86.4	240.3	436.2	587.0	640.0	542.6	304.5
May-22	233.8	574.6	640.0	576.2	426.8	229.8	52.0	229.8	426.8	576.2	640.0	574.6	233.8
Jun-21	267.8	580.2	640.0	576.2	435.6	249.3	105.6	249.3	435.6	576.2	640.0	580.2	267.8
Jul-23	233.8	574.6	640.0	576.2	426.8	229.8	52.0	229.8	426.8	576.2	640.0	574.6	233.8
Aug-22	140.7	542.6	640.0	587.0	436.2	240.3	86.4	240.3	436.2	587.0	640.0	542.6	140.7
Sep-22	0	496.3	636.0	609.1	489.6	342.4	261.3	342.4	489.6	609.1	636.0	496.3	0
Oct-22	0	508.2	636.6	618.1	524.8	448.9	428.8	495.1	604.8	640.0	581.0	283.1	0
Nov-22	0	288.2	587.4	640.0	609.4	654.6	590.1	654.6	609.4	640.0	587.4	288.2	0
Dec-21	0	254.2	568.2	640.0	621.4	577.0	654.6	577.0	621.4	585.0	568.2	254.2	0

Basic Direct Irradiation value interpolated from values for Vertical surfaces (W/m2) Tamaulipas

Month/Hour	6	7	8	9	10	11	12	13	14	15	16	17	18
Jan-21	0	189.34	533.19	483.34	633.95	600.90	584.84	600.90	520.56	483.34	533.19	189.34	0
Feb-21	0	354.64	496.03	640.00	596.43	530.03	497.03	530.03	596.43	640.00	496.03	354.64	0
Mar-21	0	480.00	447.78	621.95	527.41	417.78	360.36	417.78	527.41	630.94	447.78	480.00	0
Apr-22	199.33	553.00	640.00	608.00	453.21	283.57	185.95	283.57	453.21	608.00	640.00	553.00	199.33
May-22	303.36	496.97	640.00	571.00	418.00	231.19	59.68	231.19	418.00	571.00	640.00	496.97	303.36
Jun-21	362.73	481.99	637.76	565.03	407.93	220.00	40.13	220.00	407.93	565.03	637.76	481.99	362.73
Jul-23	303.36	496.97	640.00	571.00	418.00	231.19	59.68	231.19	418.00	571.00	640.00	496.97	303.36
Aug-22	199.33	553.00	640.00	587.00	453.21	283.57	185.95	283.57	453.21	587.00	640.00	553.00	199.33
Sep-22	0	480.00	447.78	621.95	527.41	417.78	360.36	417.78	527.41	621.95	447.78	480.00	0
Oct-22	0	354.64	496.03	640.00	596.43	654.88	497.03	530.03	596.43	640.00	496.03	354.64	0
Nov-22	0	189.34	533.19	483.34	633.95	600.90	584.84	600.90	633.95	483.34	533.19	189.34	0
Dec-21	0	147.34	499.05	343.34	450.56	623.38	605.38	623.38	450.56	343.34	499.05	147.34	0

It was necessary to use ASHRAE design manual to evaluate the basic diffuse solar radiation, as no calculation for this element was found on the CIBSE guide.

3) For the calculation of basic diffuse solar radiation (I_{db}), a simplified general relation found in ASHRAE F27.8 this reads: $$I_{db} = CI_{bb}F_{ss}$$

Where

C =is the diffuse factor, this constant for the ASHRAE equation was obtained from "Solar Energy Engineering", by Jui Sheng Hsieh:

Month	C (Dimensionless)
Jan	0.058
Feb	0.6
March	0.071
April	0.097
May	0.121
June	0.134
July	0.136
August	0.122
Sept	0.092
Oct	0.073
Nov	0.063
Dec	0.057

I_{bb} = Is the calculated Basic Direct (beam) radiation

F_{ss} = is the angle factor between the surface and the sky, i.e. the fraction of short-wave radiation emitted by the sky that reaches the tilt surface (dimensionless) Its value is 0.5 for vertical surfaces

The Basic Diffuse solar radiation values obtained are:

Diffuse Radiation BC

Month/Hour	6	7	8	9	10	11	12	13	14	15	16	17	18
Jan-21	0.0	1.8	13.4	17.7	18.6	18.4	18.2	18.4	18.6	17.7	13.4	1.8	0.0
Feb-21	0.0	80.9	168.3	191.3	188.4	176.7	171.9	176.7	188.4	191.3	168.3	80.9	0.0
Mar-21	0.0	15.9	22.2	22.5	20.3	17.5	16.3	17.5	20.3	22.5	22.2	15.9	0.0
Apr-22	0.0	27.6	31.0	29.1	23.6	17.7	14.5	17.7	23.6	29.0	31.0	27.6	12.7
May-22	23.7	37.0	38.5	34.5	26.3	16.7	10.8	16.7	26.3	34.5	38.5	37.0	23.7
Jun-21	29.2	41.5	42.5	37.3	28.0	16.2	8.0	16.2	28.0	37.3	42.5	41.5	29.2
Jul-23	26.7	41.5	43.3	38.8	29.6	18.8	12.2	18.8	29.6	38.8	43.3	41.5	26.7
Aug-22	15.4	34.7	39.0	36.5	29.7	22.2	18.2	22.2	29.7	36.5	39.0	34.7	15.4
Sep-22	0.0	20.6	26.8	29.1	26.3	22.6	21.1	22.6	26.3	29.1	26.8	20.6	0.0
Oct-22	0.0	9.8	20.5	23.3	21.5	21.5	20.9	21.5	21.5	23.3	20.5	9.8	0.0
Nov-22	0.0	2.0	14.5	12.9	20.2	18.9	17.4	18.9	20.2	12.9	14.5	2.0	0.0
Dec-21	0.0	0.0	11.0	16.7	14.3	18.2	13.6	16.3	14.3	16.7	11.0	0.0	0.0

Diffuse Radiation

Month/Hour	6	7	8	9	10	11	12	13	14	15	16	17	18
Jan-21	0.0	8.4	17.0	18.6	17.7	16.0	15.1	16.0	17.7	18.6	17.0	8.4	0.0
Feb-21	0.0	118.9	185.8	189.9	167.5	138.1	201.1	142.5	167.5	189.9	185.8	118.9	0.0
Mar-21	0.0	17.6	22.6	21.6	17.4	12.2	9.3	12.2	17.4	21.6	22.6	17.6	0.0
Apr-22	6.8	26.3	31.0	28.5	21.2	11.7	4.2	11.7	21.2	28.5	31.0	26.3	14.8
May-22	14.1	34.8	38.7	34.9	25.8	13.9	3.1	13.9	25.8	34.9	38.7	34.8	14.1
Jun-21	17.9	38.9	42.9	38.6	29.2	16.7	7.1	16.7	29.2	38.6	42.9	38.9	17.9
Jul-23	15.9	39.1	43.5	39.2	29.0	15.6	3.5	15.6	29.0	39.2	43.5	39.1	15.9
Aug-22	8.6	33.1	39.0	35.8	26.6	14.7	5.3	14.7	26.6	35.8	39.0	33.1	8.6
Sep-22	0.0	22.8	29.3	28.0	22.5	15.8	12.0	15.8	22.5	28.0	29.3	22.8	0.0
Oct-22	0.0	18.5	23.2	22.6	19.2	16.4	15.7	18.1	22.1	23.4	21.2	10.3	0.0
Nov-22	0.0	9.1	18.5	20.2	19.2	20.6	18.6	20.6	19.2	20.2	18.5	9.1	0.0
Dec-21	0.0	7.2	16.2	18.2	17.7	16.4	18.7	16.4	17.7	16.7	16.2	7.2	0.0

Diffuse Radiation — Tamaulipas

Month/Hour	6	7	8	9	10	11	12	13	14	15	16	17	18
Jan-21	0.0	5.5	15.5	14.0	18.4	17.4	17.0	17.4	15.1	14.0	15.5	5.5	0.0
Feb-21	0.0	106.4	148.8	192.0	178.9	159.0	149.1	159.0	178.9	192.0	148.8	106.4	0.0
Mar-21	0.0	17.0	15.9	22.1	18.7	14.8	12.8	14.8	18.7	22.4	15.9	17.0	0.0
Apr-22	9.7	26.8	31.0	29.5	22.0	13.8	9.0	13.8	22.0	29.5	31.0	26.8	9.7
May-22	18.4	30.1	38.7	34.5	25.3	14.0	3.6	14.0	25.3	34.5	38.7	30.1	18.4
Jun-21	24.3	32.3	42.7	37.9	27.3	14.7	2.7	14.7	27.3	37.9	42.7	32.3	24.3
Jul-23	20.6	33.8	43.5	38.8	28.4	15.7	4.1	15.7	28.4	38.8	43.5	33.8	20.6
Aug-22	12.2	33.7	39.0	35.8	27.6	17.3	11.3	17.3	27.6	35.8	39.0	33.7	12.2
Sep-22	0.0	22.1	20.6	28.6	24.3	19.2	16.6	19.2	24.3	28.6	20.6	22.1	0.0
Oct-22	0.0	12.9	18.1	23.4	21.8	23.9	18.1	19.3	21.8	23.4	18.1	12.9	0.0
Nov-22	0	6.0	16.8	15.2	20.0	18.9	18.4	18.9	20.0	15.2	16.8	6.0	0.0
Dec-21	0	4.2	14.2	9.8	12.8	17.8	17.3	17.8	12.8	9.8	14.2	4.2	0.0

4) By applying radiation correction factors the basic irradiances can be further converted to design irradiances appropriate to the radiation climates at particular localities. This is done by applying a height correction factor and direct and diffuse radiation correction factors. The equation that correlates them in order to determine the design radiation data is:

For direct radiation: $$I_{bD} = k_a k_b I_{bb}$$

For diffuse radiation: $$I_{dD} = k_a k_d I_{db}$$

Where:

I_{bD} = Beam design radiation
I_{dD} = Diffuse design radiation
k_a = Height correction factor
k_b = Beam radiation factor (direct radiation factor)
I_{bb} = Beam basic irradiance (direct) (W/m²)
k_d = Diffuse radiation factor
I_{db} =Diffuse basic irradiance (W/m²)

The height correction factor depends on solar altitude and the height and the height of the locality above sea level. In order to apply the values for height correction proposed in CIBSE the regions altitudes are:

- Mexicali Baja-California (BC): altitude = 10 masl (meters above sea level)
- Tuxtla-Gutierrez, Chiapas (CH): altitude = 528 masl
- Ciudad-Victoria, Tamaulipas (Tmps): altitude = 321 masl

Values for k_a must be interpolated from fig. FA2.2. A height correction factor of unity may be assumed, irrespective of solar altitude for heights between 0 and 300 m (as is the case of BC)

Radiation factors should be taken from table FA.30

The design direct radiation values are:

Design direct irradiance (W/m2) (IDd) — Baja California

Month/Hour	6	7	8	9	10	11	12	13	14	15	16	17	18
Jan-21	0	69.3	507.4	669.9	704.0	698.2	691.6	698.2	704.0	669.9	507.4	69.3	0
Feb-21	0	296.5	617.1	701.5	690.8	647.9	630.3	647.9	690.8	701.5	617.1	296.5	0
Mar-21	0	493.6	669.2	696.6	628.1	540.9	504.6	540.9	628.1	696.6	669.2	493.6	0
Apr-22	288.8	625.9	704.0	658.9	534.9	400.4	328.6	400.4	534.9	657.8	704.0	625.9	288.8
May-22	431.8	672.1	700.7	628.1	478.4	303.9	196.6	303.9	478.4	628.1	700.7	672.1	431.8
Jun-21	479.9	680.9	697.4	612.7	459.8	266.8	132.0	266.8	459.8	612.7	697.4	680.9	479.9
Jul-23	431.8	672.1	700.7	628.1	478.4	303.9	196.6	303.9	478.4	628.1	700.7	672.1	431.8
Aug-22	277.8	625.9	704.0	657.8	534.9	400.4	328.6	400.4	534.9	657.8	704.0	625.9	277.8
Sep-22	0	493.6	669.2	696.6	628.1	540.9	504.6	540.9	628.1	696.6	669.2	493.6	0
Oct-22	0	296.5	617.1	701.5	649.0	647.9	630.3	647.9	649.0	701.5	617.1	296.5	0
Nov-22	0	69.3	507.4	448.8	704.0	659.7	609.1	659.7	704.0	448.8	507.4	69.3	0
Dec-21	0	0.0	424.9	645.7	550.0	704.0	523.9	629.8	550.0	645.7	424.9	0.0	0

Design direct irradiance (W/m2) (IDd) Chiapas													
Month/Hour	6	7	8	9	10	11	12	13	14	15	16	17	18
Jan-21	0	288.2	419.99	416.00	380.88	339.63	316.74	339.63	380.88	416.00	419.99	288.20	0
Feb-21	0	344.74	427.39	405.18	343.29	280.84	405.58	289.81	343.29	405.18	427.39	344.74	0.00
Mar-21	0	392.04	422.91	383.73	298.63	205.44	155.44	205.44	298.63	383.73	422.91	392.04	0.00
Apr-22	140.7	412.38	416.00	363.94	263.92	142.95	50.98	142.95	263.92	363.94	416.00	412.38	299.93
May-22	233.8	416.59	422.40	354.36	258.20	135.55	30.42	135.55	258.20	354.36	422.40	416.59	233.80
Jun-21	265.1	417.74	419.20	354.36	263.51	147.06	62.83	147.06	263.51	354.36	419.20	417.74	265.12
Jul-23	233.8	416.59	422.40	354.36	258.20	135.55	30.42	135.55	258.20	354.36	422.40	416.59	230.29
Aug-22	140.7	412.38	416.00	363.94	263.92	142.95	50.98	142.95	263.92	363.94	416.00	412.38	140.70
Sep-22	0	392.04	422.91	383.73	298.63	205.44	155.44	205.44	298.63	383.73	422.91	392.04	0.00
Oct-22	0	442.13	439.22	395.58	322.72	273.80	259.42	301.98	371.92	409.60	400.89	246.30	0.00
Nov-22	0	288.20	419.99	416.00	380.88	402.59	359.98	402.59	380.88	416.00	419.99	288.20	0.00
Dec-21	0	254.20	409.10	419.20	391.48	357.74	402.59	357.74	391.48	418.28	409.10	254.20	0.00

Design direct irradiance (W/m2) (IDd) Tamaulipas													
Month/Hour	6	7	8	9	10	11	12	13	14	15	16	17	18
Jan-21	0	189.336	287.92	251.34	326.49	306.46	298.27	306.46	268.09	251.34	287.92	189.34	0
Feb-21	0	196.82	260.41	329.60	304.18	270.32	253.49	270.32	304.18	329.60	260.41	196.82	0.00
Mar-21	0	259.20	232.85	317.20	268.98	213.07	183.78	213.07	268.98	321.78	232.85	259.20	0.00
Apr-22	199.3	295.86	329.60	310.08	231.14	144.62	94.83	144.62	231.14	310.08	329.60	295.86	199.33
May-22	171.4	263.40	329.60	291.21	213.18	117.91	30.44	117.91	213.18	291.21	329.60	263.40	171.40
Jun-21	217.6	253.04	325.26	288.17	208.04	112.20	20.47	112.20	208.04	288.17	325.26	253.04	217.64
Jul-23	171.4	263.40	329.60	291.21	213.18	117.91	30.44	117.91	213.18	291.21	329.60	263.40	171.40
Aug-22	199.3	295.86	329.60	299.37	231.14	144.62	94.83	144.62	231.14	299.37	329.60	295.86	199.33
Sep-22	0	259.20	232.85	317.20	268.98	213.07	183.78	213.07	268.98	317.20	232.85	259.20	0.00
Oct-22	0	196.82	260.41	329.60	304.18	333.99	253.49	270.32	304.18	329.60	260.41	196.82	0.00
Nov-22	0	189.34	287.92	251.34	326.49	306.46	298.27	306.46	326.49	251.34	287.92	189.34	0.00
Dec-21	0	147.34	271.98	180.25	232.04	317.92	308.74	317.92	232.04	180.25	271.98	147.34	0.00

The design diffuse radiation values are:

Design diffuse irradiance (W/m2) (IDd) Baja California													
Month/Hour	6	7	8	9	10	11	12	13	14	15	16	17	18
Jan-21	0.0	1.6	12.0	15.9	16.7	16.6	16.4	16.6	16.7	15.9	12.0	1.6	0.0
Feb-21	0.0	72.8	151.5	172.2	169.6	159.0	154.7	159.0	169.6	172.2	151.5	72.8	0.0
Mar-21	0.0	14.3	20.0	20.2	18.2	15.7	14.7	15.7	18.2	20.2	20.0	14.3	0.0
Apr-22	0.0	24.8	27.9	26.1	21.2	15.9	13.0	15.9	21.2	26.1	27.9	24.8	11.5
May-22	21.4	33.3	34.7	31.1	23.7	15.0	9.7	15.0	23.7	31.1	34.7	33.3	21.4
Jun-21	26.3	37.3	38.2	33.6	25.2	14.6	7.2	14.6	25.2	33.6	38.2	37.3	26.3
Jul-23	24.0	37.4	39.0	34.9	26.6	16.9	10.9	16.9	26.6	34.9	39.0	37.4	24.0
Aug-22	13.9	31.2	35.1	32.8	26.7	20.0	16.4	20.0	26.7	32.8	35.1	31.2	13.9
Sep-22	0.0	18.6	25.9	26.2	23.6	20.4	19.0	20.4	23.6	26.2	25.9	18.6	0.0
Oct-22	0.0	8.9	18.4	21.0	19.4	19.3	18.8	19.3	19.4	21.0	18.4	8.9	0.0
Nov-22	0.0	1.8	13.1	11.6	18.1	17.0	15.7	17.0	18.1	11.6	13.1	1.8	0.0
Dec-21	0.0	0.0	9.9	15.1	12.8	16.4	12.2	14.7	12.8	15.1	9.9	0.0	0.0

Design diffuse irradiance (W/m2) (IDd) Chiapas													
Month/Hour	6	7	8	9	10	11	12	13	14	15	16	17	18
Jan-21	0	18.39	26.80	26.54	24.30	21.67	20.21	21.67	24.30	26.54	26.80	18.39	0.00
Feb-21	0	227.53	282.07	267.42	226.57	185.36	267.68	191.28	226.57	267.42	282.07	227.53	0.00
Mar-21	0	30.62	33.03	29.97	23.32	16.04	12.14	16.04	23.32	29.97	33.03	30.62	0.00
Apr-22	15.01	44.00	44.39	38.83	28.16	15.25	5.44	15.25	28.16	38.83	44.39	44.00	32.00
May-22	31.12	55.45	56.22	47.17	34.37	18.04	4.05	18.04	34.37	47.17	56.22	55.45	31.12
Jun-21	39.08	61.58	61.79	52.23	38.84	21.68	9.26	21.68	38.84	52.23	61.79	61.58	39.08
Jul-23	34.98	62.32	63.19	53.01	38.63	20.28	4.55	20.28	38.63	53.01	63.19	62.32	34.45
Aug-22	18.88	55.34	55.83	48.84	35.42	19.18	6.84	19.18	35.42	48.84	55.83	55.34	18.88
Sep-22	0	39.67	42.80	38.83	30.22	20.79	15.73	20.79	30.22	38.83	42.80	39.67	0.00
Oct-22	0	35.50	35.27	31.77	25.91	21.99	20.83	24.25	29.87	32.89	32.19	19.78	0.00
Nov-22	0	19.97	29.11	28.83	26.39	27.90	24.95	27.90	26.39	28.83	29.11	19.97	0.00
Dec-21	0	15.94	25.65	26.28	24.55	22.43	25.24	22.43	24.55	26.23	25.65	15.94	0.00

Design diffuse irradiance (W/m2) (IDd) Tamaulipas													
Month/Hour	6	7	8	9	10	11	12	13	14	15	16	17	18
Jan-21	0	12.08	18.37	16.04	20.83	19.55	19.03	19.55	17.10	16.04	18.37	12.08	0.00
Feb-21	0	129.90	171.87	217.54	200.76	178.41	167.30	178.41	200.76	217.54	171.87	129.90	0.00
Mar-21	0	20.24	18.19	24.77	21.01	16.64	14.35	16.64	21.01	25.13	18.19	20.24	0.00
Apr-22	21.27	31.57	35.17	33.09	24.66	15.43	10.12	15.43	24.66	33.09	35.17	31.57	21.27
May-22	22.81	35.06	43.87	38.76	28.37	15.69	4.05	15.69	28.37	38.76	43.87	35.06	22.81
Jun-21	32.08	37.30	47.94	42.48	30.67	16.54	3.02	16.54	30.67	42.48	47.94	37.30	32.08
Jul-23	25.64	39.40	49.31	43.57	31.89	17.64	4.55	17.64	31.89	43.57	49.31	39.40	25.64
Aug-22	26.75	39.70	44.23	40.18	31.02	19.41	12.73	19.41	31.02	40.18	44.23	39.70	26.75
Sep-22	0	26.23	23.56	32.10	27.22	21.56	18.60	21.56	27.22	32.10	23.56	26.23	0.00
Oct-22	0	15.80	20.91	26.47	24.43	26.82	20.35	21.71	24.43	26.47	20.91	15.80	0.00
Nov-22	0	13.12	19.95	17.42	22.63	21.24	20.67	21.24	22.63	17.42	19.95	13.12	0.00
Dec-21	0	9.24	17.05	11.30	14.55	19.93	19.36	19.93	14.55	11.30	17.05	9.24	0.00

5) Global radiation values are:

Global radiation BC

Month/Hour	6	7	8	9	10	11	12	13	14	15	16	17	18
Jan-21	0 0	70.9	519.4	685.8	720.7	714.8	708 0	714 8	720.7	685.8	519.4	70.9	0.0
Feb-21	0 0	369.2	768.6	873.7	860.4	806.9	785.0	806 9	860 4	873.7	768.6	369.2	0.0
Mar-21	0 0	508.0	709.2	716.8	646.3	556.6	519.3	556.6	646.3	716.8	709.2	508 0	0 0
Apr-22	288 8	650.7	731.9	685.0	556.1	416.3	341.7	416.3	556.1	683.9	731.9	650 7	300.2
May-22	453.1	705.4	735.4	659.2	502.0	318.9	206.4	318.9	502.0	659.2	735.4	705 4	453 1
Jun-21	506.2	718.2	735.6	646.3	485.0	281.4	139.2	281.4	485.0	646.3	735.6	718.2	506.2
Jul-23	455.8	709.5	739.7	663.0	505.0	320.8	207.6	320.8	505.0	663.0	739.7	709.5	455.8
Aug-22	291.6	657.1	739.1	690.6	561.6	420.4	345.0	420.4	561.6	690.6	739.1	657.1	291 6
Sep-22	0.0	512.2	715.1	722.8	651.7	561.3	523.6	561.3	651.7	722.8	715.1	512.2	0 0
Oct-22	0.0	305.3	635.5	722.5	668.4	667.2	649.1	667.2	668.4	722.5	635.5	305.3	0 0
Nov-22	0.0	71.1	520.5	460.4	722.1	676.7	624.8	676.7	722.1	460.4	520.5	71.1	0 0
Dec-21	0.0	0.0	434.8	660.8	562.8	720.4	536.1	644.4	562.8	660.8	434.8	0.0	0 0

Global CH

Month/Hour	6	7	8	9	10	11	12	13	14	15	16	17	18
Jan-21	0	306.6	446.8	442.5	405.2	361.3	337.0	361.3	405.2	442.5	446.8	306 6	0.0
Feb-21	0.0	572.3	709.5	672.6	569.9	466.2	673.3	481.1	569.9	672.6	709.5	572.3	0.0
Mar-21	0.0	422.7	455.9	413.7	321.9	221.5	167.6	221.5	321.9	413.7	455.9	422.7	0.0
Apr-22	155.7	456.4	460.4	402.8	292.1	158.2	56.4	158.2	292.1	402.8	460.4	456.4	331.9
May-22	264.9	472.0	478.6	401.5	292.6	153.6	34.5	153.6	292.6	401.5	478.6	472.0	264.9
Jun-21	304.2	479.3	481.0	406.6	302.3	168.7	72.1	168.7	302.3	406.6	481.0	479.3	304.2
Jul-23	268.8	478.9	485.6	407.4	296.8	155.8	35.0	155.8	296.8	407.4	485.6	478.9	264.7
Aug-22	159.6	467.7	471.8	412.8	299.3	162.1	57.8	162.1	299.3	412.8	471.8	467.7	159.6
Sep-22	0.0	431.7	465.7	422.6	328.8	226.2	171.2	226.2	328.8	422.6	465.7	431.7	0.0
Oct-22	0.0	477.6	474.5	427.3	348.6	295.8	280.3	326.2	401.8	442.5	433.1	266.1	0.0
Nov-22	0.0	308.2	449.1	444.8	407.3	430.5	384.9	430.5	407.3	444.8	449.1	308.2	0.0
Dec-21	0.0	270.1	434.8	445.5	416.0	380.2	427.8	380.2	416.0	444.5	434.8	270.1	0.0

Global Tmps

Month/Hour	6	7	8	9	10	11	12	13	14	15	16	17	18
Jan-21	0.0	201.4	306.3	267.4	347.3	326.0	317.3	326.0	285.2	267.4	306.3	201.4	0.0
Feb-21	0.0	326.7	432.3	547.1	504.9	448.7	420.8	448.7	504.9	547.1	432.3	326.7	0.0
Mar-21	0.0	279.4	251.0	342.0	290.0	229.7	198.1	229.7	290.0	346.9	251.0	279.4	0.0
Apr-22	220.6	327.4	364.8	343.2	255.8	160.1	105.0	160.1	255.8	343.2	364.8	327.4	220.6
May-22	194.2	298.5	373.5	330.0	241.6	133.6	34.5	133.6	241.6	330.0	373.5	298.5	194.2
Jun-21	249.7	290.3	373.2	330.6	238.7	128.7	23.5	128.7	238.7	330.6	373.2	290.3	249.7
Jul-23	197.0	302.8	378.9	334.8	245.1	135.5	35.0	135.5	245.1	334.8	378.9	302.8	197.0
Aug-22	226.1	335.6	373.8	339.5	262.2	164.0	107.6	164.0	262.2	339.5	373.8	335.6	226.1
Sep-22	0.0	285.4	256.4	349.3	296.2	234.6	202.4	234.6	296.2	349.3	256.4	285.4	0.0
Oct-22	0.0	212.6	281.3	356.1	328.6	360.8	273.8	292.0	328.6	356.1	281.3	212.6	0.0
Nov-22	0.0	202.5	307.9	268.8	349.1	327.7	318.9	327.7	349.1	268.8	307.9	202.5	0.0
Dec-21	0.0	156.6	289.0	191.6	246.6	337.9	328.1	337.9	246.6	191.6	289.0	156.6	0.0

Appendix 3.D: Evaluation of convection heat transfer coefficient for a given mass flow rate over a flat plate with forced convection, net heat flux and sol-air temperature

The mean fluid temperature in Celsius: $T_{mf} = \frac{T_{sw} + T_{ach}}{2}$

T_{ach}= Air temperature inside the chamber (°K)
T_{sw}= Surface temperature of the cell wall (°K)

The air density for each specific day using barometric pressure $\rho_{bar} = \frac{P_{day}}{RT_{air}}$

R= Gas constant=287
T_{air}= Air temperature (°K)
P_{day}= Barometric pressure that day (kPa[45])

Air velocity at given mass flow rate inside the chamber $V_{air} = \frac{\dot{m}}{\rho}$

Define number of time intervals $Np = \frac{T_{Lenght}}{DT}$ and space interval $Dx = \frac{L/2}{nN}$

T_{Lenght}= Total time length
DT= Time interval
L= Unit total length
nN= number of nodes

At the trailing edge of the plate critical Reynolds number $\mathrm{Re}_L = \frac{(V_{air} * L)}{\nu}$

ν = kinematic viscosity (m^2/s)
For flow over a flat plate critical Re=$5x10^5$

For laminar flow of a fluid with $\mathrm{Pr} \succ 0.6$, the local Nusselt number at which x=L can be estimated by: $Nu_L = 0.332\mathrm{Re}_L^{1/2}\,\mathrm{Pr}^{1/3}$

And the convective heat transfer coefficient $h = \frac{Nu_L k}{L}$

The average Nusselt number $\overline{Nu} = cRa^n\left(\frac{H}{D_{w-g}}\right)^{-1/9}$

Where
H= window height

And the Rayleigh number: $Ra\,\frac{g\beta(T_s - T_\infty)D_{w-g}^{\ 3}}{\nu\alpha}$

g=Gravitational acceleration constant=9.81 m/s^2
β = Volumetric thermal expansion coefficient (1/°K)
T_∞ =Air temperature (°K)

---

[45] 1bar=10^5Pa=10^2kPa

D_{w-g}= Distance between the unit wall and the glass
And c=0.20, n=0.25 for $Ra_L<2x10^5$
c=0.071 n=0.33 for $Ra_L>2x10^5$

The average convection heat transfer coefficient: $\bar{h} = \frac{N\bar{u}k}{D_{w-g}}$

The heat flux for convection: $q_{conv} = \bar{h}(T_{ach} - T_s)^{n+1}$

Evaluation of the net heat flux and sol-air temperature.

$$q_{net} = \tau_g I\left(\frac{1}{1-\rho_{rw}\rho_{rg}}\right) - \rho_{rg}\tau_g I\left(\frac{1}{1-\rho_{rg}\rho_{rw}}\right) - q_{conv} - \frac{\sigma\left(T_{sw}^4 - T_{sg}^4\right)}{\frac{1-\varepsilon_w}{\varepsilon_w} - \frac{1}{1} - \frac{1-\varepsilon_g}{\varepsilon_g}}$$

where:

τ_g = glass transmisivity

I= Irradiation received (W/m^2)

ρ_{rw} =Cell wall reflectivity

ρ_{rg} =glass reflectivity

σ =Stefan Boltzmann constant=$5.67x10^{-8}$

T_{sg}= Glass surface temperature

ε_w = Wall emissivity

ε_g = Glass emissivity

The outside surface resistance combining convective and radiative heat transfer:

$$R_{so} = \frac{1}{(\varepsilon h_r + hc)}$$

Where

Convection and radiation coefficients: $hc = 5.8 + 4.1V_{air}$ and $hr = 4\sigma T_{swall}^3$

The sol-air temperature is given by: $T_{sa} = \left[(\alpha_{ra} q_{net}) - (\varepsilon_a I_c)\right] R_{so} + T_{ach}$

The interior resistance $R_{si} = \frac{1}{1.2\varepsilon hr + hc}$

Where

Convection coefficient $hc_i = \left[\left(1.5\left(\frac{\Delta T}{Wall\,Height}\right)^{1/4}\right)^6 + \left(1.23(\Delta T)^{1/3}\right)^6\right]^{1/6}$

The heat flux in the cell surface facing the chamber: $HF_b = \frac{k}{\Delta x}(T_b - T_a) + \frac{(T_\infty - T_b)}{R_{si}}$

The heat flux in the cell surface facing the window:

$HF_a = \frac{T_\infty - T_{sa}}{Rsi}$

Appendix 3.E: Modelling pseudo code

//

Temperature coefficients 'a', and 'b', to form matrix

//

Initialization (λ [46], PhT[47], BM[48], MC[49], BS[50], CS[51])

Function: Temperature coefficients for the **boundary** node in the **heating** mode (eq.13)

if ($BM_{i,j}$ is false)

$$a_{i-1,j} = (1 + 2Fo) + \left(\frac{2\Delta t}{\Delta x}\frac{h}{\rho Cp}\right)$$

$$a_{i,j} = (-2Fo)$$

$$b_{i,j} = T_{i,j-1} + \left(\frac{2\Delta t}{\Delta x}\frac{h}{\rho Cp}\right)T_{\infty}$$

Solid state properties are applied

end if

else

if ($BM_{i,j}$ is true and $MC_{i,j}$ is false)

During phase transition, node temperature remains at TM

if ($T_{i,j-1}$ >TM)

$T_{i,j-1}$ =TM

end if

$a_{i,j} = 1$

$b_{i,j} = TM$

As phase transition occurs, respective control variable: Phase Transition is set to true

$PhT_{i,j}$ =true

end if

else

if ($BM_{i,j}$ is true and $MC_{i,j}$ is true)

$$a_{i-1,j} = (1 + 2Fo) + \left(\frac{2\Delta t}{\Delta x}\frac{h}{\rho Cp}\right)$$

$$a_{i,j} = (-2Fo)$$

$$b_{i,j} = T_{i,j-1} + \left(\frac{2\Delta t}{\Delta x}\frac{h}{\rho Cp}\right)T_{\infty}$$

Liquid state properties are applied

end if

---

[46] Liquid fraction
[47] Phase Transition
[48] Beginning of Melting
[49] Melted completely
[50] Beginning of Solidification
[51] Completely Solid

Function: Temperature coefficients for the **boundary** node in the **cooling** mode (eq.13)

if (BS[1]is false)

$$a_{i-1,j} = (1 + 2Fo) + \left(\frac{2\Delta t}{\Delta x}\frac{h}{\rho Cp}\right)$$

$$a_{i,j} = (-2Fo)$$

$$b_{i,j} = T_{i,j-1} + \left(\frac{2\Delta t}{\Delta x}\frac{h}{\rho Cp}\right)T_{\infty}$$

Liquid state properties are applied

end if

else

if (BS[1] is true and $CS_{i,j}$ is false)

During phase transition, node temperature remains at TM

if ($T_{i,j-1}$>TM)

$T_{i,j-1}$=TM

end if

$a_{i,j} = 1$

$b_{i,j} = TM$

$PhT_{i,j}$=true

end if

else

if (BS[1] is true and $CS_{i,j}$ is true)

$$a_{i-1,j} = (1 + 2Fo) + \left(\frac{2\Delta t}{\Delta x}\frac{h}{\rho Cp}\right)$$

$$a_{i,j} = (-2Fo)$$

$$b_{i,j} = T_{i,j-1} + \left(\frac{2\Delta t}{\Delta x}\frac{h}{\rho Cp}\right)T_{\infty}$$

Solid state properties are applied

end if

Function: Temperature coefficients for the **inner** node in the **heating** mode (eq.11)

for all interior nodes

if ($BM_{i,j}$ is false)

Melting has not started

$$a_{i-1,j} = -Fo$$

$$a_{i,j} = (1 - 2Fo)$$

$$a_{i+1,j} = -Fo$$

$$b_{i,j} = T_{i,j-1}$$

Solid state properties are applied

end if

end for

for all interior nodes

if ($BM_{i,j}$ is true and $MC_{i,j}$ is false)

if ($T_{i,j-1} \succ TM$)

$T_{i,j-1} = TM$

end if

$a_{i,j} = 1$

$b_{i,j} = TM$

Only after the previous control volume has melted completely the successive control volume may commence with melting:

if ($MC_{i,j-1}$ is true)

As phase transition occurs, respective control variable: Phase Transition is set to true

$PhT_{i,j}$ =true

end if

end if

end for

for all interior nodes

if ($BM_{i,j}$ is true and $MC_{i,j}$ is true)

Node completely melted, node temp. may increase above TM

$a_{i-1,j} = -Fo$

$a_{i,j} = (1-2Fo)$

$a_{i+1,j} = -Fo$

$b_{i,j} = T_{i,j-1}$

Liquid state properties are applied

end if

end for

Function: Temperature coefficients for the **inner** node in the **cooling** mode (eq.11)

for all interior nodes

if ($BS_{i,j}$ is false)

Melting hasn't started

$a_{i-1,j} = -Fo$

$a_{i,j} = (1-2Fo)$

$a_{i+1,j} = -Fo$

$b_{i,j} = T_{i,j-1}$

Liquid state properties are applied

end if

end for

for all interior nodes

if ($BS_{i,j}$ is true and $CS_{i,j}$ is false)

if ($T_{i,j-1} \leq TM$)

$T_{i,j-1} = TM$

end if

$a_{i,j} = 1$

$b_{i,j} = TM$

Only after the previous control volume is completely solid the successive control volume may commence with solidifying:

if ($CS_{i,j-1}$ is true)

$PhT_{i,j}$ =true

end if

end if

end for

for all interior nodes

if ($BS_{i,j}$ is true and $CS_{i,j}$ is true)

Material is completely solid, it's temp. may decrease below TM

$a_{i-1,j} = -Fo$

$a_{i,j} = (1-2Fo)$

$a_{i+1,j} = -Fo$

$b_{i,j} = T_{i,j-1}$

Liquid state properties are applied

end if

end for

//

Calculation of Liquid Fractions

//

Function: Evaluate the liquid fraction at the **boundary node** during the **heating** mode

if ($PhT_{i,j}$ is true)

Phase transition occurs; the liquid fraction has to be updated (eq.14)

$$\lambda_{i,j} = \lambda_{i,j-1} + \frac{2h\Delta t}{\rho Cp\Delta x} T_\infty + 2Fo\left(T_{i+1,j}\right) - \left(2Fo + \frac{2h\Delta t}{\rho Cp\Delta x}\right) T_{i,j}$$

end if

if ($MC_{i,j}$ is true)

The control volume has melted completely

$$\lambda_{i,j} = 1$$

end if

if ($PhT_{i,j}$ is false and $MC_{i,j}$ is false)

Previous condition prevails

$$\lambda_{i,j} = \lambda_{i,j-1}$$

end if

Function: Evaluate the liquid fraction at the **boundary node** during the **cooling** mode

if ($PhT_{i,j}$ is true and $\lambda_{i,j} \succ 0$)

$$\lambda_{i,j} = \lambda_{i,j-1} - \frac{2h\Delta t}{\rho Cp\Delta x} T_\infty + 2Fo\left(T_{i+1,j}\right) - \left(2Fo + \frac{2h\Delta t}{\rho Cp\Delta x}\right) T_{i,j}$$

end if

if ($CS_{i,j}$ is true or $\lambda_{i,j} \leq 0$)

The control volume is completely solid

$$\lambda_{i,j} = 0$$

end if

if ($PhT_{i,j}$ is false and $CS_{i,j}$ is false)

$$\lambda_{i,j} = \lambda_{i,j-1}$$

end if

Function: Evaluate the liquid fraction at the **inner node** during the **heating** mode (eq. 12)

for all inner nodes

if ($PhT_{i,j}$ is true)

$$\lambda_{i,j} = \frac{k}{H\rho\Delta x^2}\Delta t\left(T_{i-1} - 2T_i + T_{i+1}\right) + \lambda_{i,j-1}$$

end if

if ($MC_{i,j}$ is true)

The control volume has melted completely

$$\lambda_{i,j} = 1$$

end if

if ($PhT_{i,j}$ is false and $MC_{i,j}$ is false)

$$\lambda_{i,j} = \lambda_{i,j-1}$$

end if

end for

Function: Evaluate the liquid fraction at the **inner node** during the **cooling** mode

for all inner nodes

if ($PhT_{i,j}$ is true and $\lambda_{i,j} > 0$)

$$\lambda_{i,j} = \lambda_{i,j-1} - \frac{k}{H\rho\Delta x^2}\Delta t\left(T_{i-1} - 2T_i + T_{i+1}\right)$$

end if

if ($CS_{i,j}$ is true or $\lambda_{i+1,j} \leq 0$)

$$\lambda_{i,j} = 0$$

end if

if ($PhT_{i,j}$ is false and $CS_{i,j}$ is false)

$$\lambda_{i,j} = \lambda_{i,j-1}$$

end if

end for

//

Checking for the start of melting during Heating and for the start of solidification during Cooling

//

Function: Checking for the Beginning of Melting (BM); during the **heating** mode

do

t=t+DT

for all nodes

Necessary condition for the start of melting: Solid control volume and Melting Temperature (TM) reached

if ($\lambda_{i,j} \leq 0$ and $T_{i,j} \geq TM$)

$BM_{i,j}$ = true

end if

end for

Due to move of phase front, calculation is repeated for the next time step until no node is starting to melt

While (BM[last node] is false and Iteration Number (IN)<= Number of periods (Np))

Function: Checking for the Beginning of Solidification (BS); during the **cooling** mode

do

t=t+DT

for all nodes

Necessary condition for the start of melting: Liquid control volume and Fusion Temperature (TM) reached

if ($\lambda_{i,j}$ is 1 and $T_{i,j} \leq TM$)

$BS_{i,j}$ =true

else $BS_{i,j}$ =false

End for

Loop as long as a node is starting to solidify

While (BS[last node] is true and Iteration Number (IN)<= Number of periods (Np))

//

Checking for the END of MELTING

//

Function: Checking if the node has melted completely (MC); during the **heating** mode

do

t=t+DT

for all nodes

Once the material has gone through the process of transition, then when the liquid fraction reaches 100%, the material has melted completely

if ($PhT_{i,j}$ is true and $\lambda_{i,j} \geq 1$)

$MC_{i,j}$=true

end if

end for

Due to move of phase front, calculation is repeated for the next time step until all the nodes have melted completely

while(MC[last node] is true and Iteration Number (IN)<= Number of periods (Np));

Function: Checking if the node is completely solid (CS); during the **cooling** mode

do

t=t+DT

for all nodes

Once the material has gone through the process of transition, then when the liquid fraction reaches 0%, the material is totally solid

if ($PhT_{i,j}$ is true and $\lambda_{i,j} \leq 0$)

$CS_{i,j}$=true

end if

end for

Due to move of phase front, calculation is repeated for the next time step until all the nodes are completely solid

while(CS[last node] is false and Iteration Number (IN)<= Number of periods (Np))

References

AliAbadi, M. H. and E. L. Ortiz (1998). "Numerical treatment of moving and free boundary value problems with the tau method." Computers & Mathematics with Applications **35**(8): 53-61.

Alubook, I. k. a. a. Guide-lines for the use of Aluminium with foods and chemicals. 2004

Asako, Y. and M.Faghi (1999). "Effect of density change on melting of unfixed rectangular phase-change material under low gravity environment." Numerical heat transfer, part A **36**: 825-838.

Banaszek, J., R. Domanski, et al. (2000). "Numerical analysis of the paraffin wax-air spiral thermal energy storage unit." Applied Thermal Engineering **20**(4): 323-354.

Bonacina, C., G. Comini, et al. (1973). "Numerical solution of phase-change problems." International Journal of Heat and Mass Transfer **16**(10): 1825-1832.

Bowman, W. J. and D. A. Brown (1998). Heat capacity model for a mixture containing a phase change material. Utah & Ohio, Brigham Young University & Air force research laboratory: AIAA-98-2764.

Brousseau, P. and M. Lacroix (1996). "Study of the thermal performance of a multi-layer PCM storage unit." Energy Conversion and Management **37**(5): 599-609.

Caldwell, J. and C.-C. Chan (2000). "Spherical solidification by the enthalpy method and the heat balance integral method." Applied Mathematical Modelling **24**(1): 45-53.

Clavier, L., E. Arquis, et al. (1994). "A fixed grid method for the numerical solution of phase change problems." International Journal for Numerical Methods in Engineering **37**: 4247-4261.

Costa, M., D. Buddhi, et al. (1998). "Numerical simulation of a latent heat thermal energy storage system with enhanced heat conduction." Energy Conversion and Management **39**(3-4): 319-330.

Crank, J. (1984). Free and moving boundary problems. Brunel, Clarendon press Oxford.

Cryer, C. W. Numerical Methods for Free and Moving Boundary Problems. 1978

Date, A. W. (1991). "A strong enthalpy formulation for the Stefan problem." International Journal of Heat and Mass Transfer **34**(9): 2231-2235.

Duan, Q., F. L. Tan, et al. (2002). "A numerical study of solidification of n-hexadecane based on the enthalpy formulation." Journal of Materials Processing Technology **120**(1-3): 249-258.

Esen, M. and T. Ayhan (1996). "Development of a model compatible with solar assisted cylindrical energy storage tank and variation of

stored energy with time for different phase change materials." Energy Conversion and Management **37**(12): 1775-1785.
Esen, M., A. Durmu, et al. (1998). "Geometric design of solar-aided latent heat store depending on various parameters and phase change materials." Solar Energy **62**(1): 19-28.
Farid, M. M., F. A. Hamad, et al. (1998). "Melting and solidification in multi-dimensional geometry and presence of more than one interface." Energy Conversion and Management **39**(8): 809-818.
Farid, M. M. and A. Kanzawa (1989). "Thermal performance of a heat storage module using PCM's with different melting temperatures: Mathematical modeling." Transactions of the ASME **111**: 152-157.
Fikiin, K. A. (1996). "Generalized numerical modelling of unsteady heat transfer during cooling and freezing using an improved enthalpy method and quasi-one-dimensional formulation." International Journal of Refrigeration **19**(2): 132-140.
Hamdan, M. A. and F. A. Elwerr (1996). "Thermal energy storage using a phase change material." Solar Energy **56**(2): 183-189.
Hernandez-Guerrero, A., S. M. Aceves, et al. (1999). "Modeling of the charge and discharge processes in energy storage cells." Energy Conversion and Management **40**(15-16): 1753-1763.
Hu, H. and S. A. Argyropoulos (1996). "Mathematical modeling and experimental measurements of moving boundary problems associated with exothermic heat of mixing." International Journal of Heat and Mass Transfer **39**(5): 1005-1021.
Ilken, Z. and H. Gunerhan (1996). "An investigation about the relations between the results of heat conduction problems with and without phase change." International Communications in Heat and Mass Transfer **23**(6): 899-905.
Ketkar, S. P. (1999). Numerical thermal analysis. New York, ASME.
Kharab, A. (1997). "Spreadsheet simulation of the moving boundary of the one-phase Stefan problem." Computer Methods in Applied Mechanics and Engineering **145**(3-4): 217-225.
Kim, S. and S. Anghaie (2001). "An effective conduction length model in the enthalpy formulation for the stefan problem." International Communications in Heat and Mass Transfer **28**(6): 733-741.
Kim, S., B. Lee, et al. (2000). "A front-layer predictor-corrector algorithm with pseudo newton-rapson method for the phase change heat conduction problems." International Communications in Heat and Mass Transfer **27**(7): 1003-1012.
Kurklu, A., A. Wheldon, et al. (1996). "Mathematical modelling of the thermal performance of a phase-change material (PCM) store: Cooling cycle." Applied Thermal Engineering **16**(7): 613-623.
Lally, B., L. Biegler, et al. (1990). "Finite difference heat-transfer modeling for continuous casting." Metallurgical transactions B **21B**: 761-770.

Little, T. D. and R. E. Showalter (1995). "The Super-Stefan problem." International Journal of Engineering Science **33**(1): 67-75.

Ma, J. and B.-X. Wang (1995). "the penetration rate of solid-liquid phase-change heat transfer interface with different kinds of boundary conditions." International Journal of Heat and Mass Transfer **38**(11): 2135-2138.

Minkowycz, W. J., E. M. Sparrow, et al. (1988). Handbook of numerical heat transfer. New York, Wiley (A Wiley-Interscience publication, John Wiley and sons inc).

Myers, G. E. (1971). Analytical methods in conduction heat transfer. New York, McGraw-Hill.

Nehad, A.-K. (1995). "Enthalpy technique for solution of stefan problems: Application to the keyhole plasma arc welding process involving moving heat source." International Communications in Heat and Mass Transfer **22**(6): 779-790.

Peippo, K., P. Kauranen, et al. (1991). "A multicomponent PCM wall optimized for passive solar heating." Energy and Buildings **17**(4): 259-270.

Pham, Q.T. "Comparison of General Purpose Finite Element Methods for the Stefan problem". http://www.ceic.unsw.edu.au/staff/Tuan_Pham/fedist.pdf, August 2005

Rabin, Y., I. Bar-Niv, et al. (1995). "Integrated solar collector storage system based on a salt-hydrate phase-change material." Solar Energy **55**(6): 435-444.

Rabin, Y. and E.Korin (1993). "An efficient numerical solution for the multidimensional solidification (or melting) problem using a microcomputer." International Journal of Heat and Mass Transfer **36**(3): 673-683.

Rose, M. E. (1993). "An enthalpy scheme for Stefan problems in several dimensions." Applied Numerical Mathematics **12**(1-3): 229-238.

Rudd, A. F. (1993). Phase-Change Material Wallboard for Distributed Thermal Storage in Buildings, Published in the ASHRAE Transactions: Research, Volume 99, Part 2, paper #3724. American Society of Heating Refrigeration and Air-Conditioning Engineers, Atlanta, GA, 1993.

Sampath, R. and N. Zabaras (1999). "An object oriented implementation of front tracking finite element method for directional solidification process." International Journal for Numerical Methods in Engineering **44**: 1227-1265.

Sarler, B. (1995). "Stefan's work on solid-liquid phase changes." Engineering Analysis with Boundary Elements **16**(2): 83-92.

Sassi, M. and M. Raynaud (1998). "Solution of the moving-boundaries problems." Numerical heat transfer, part B **34**: 271-286.

Srinivas, S. S. and R. M. Allen (1998). "Method of lines and enthalpy method for solving moving boundary problems." International Communications in Heat and Mass Transfer **25**(4): 531-540.
Swaminathan, C. R. and V.R.Voller (1992). "A general enthalpy method for modelling solidification processes." Metallurgical transactions B **23B**: 651-663.
Voller, V. and M. Cross (1981). "Accurate solutions of moving boundary problems using the enthalpy method." International Journal of Heat and Mass Transfer **24**(3): 545-556.
Voller, V. R. (1990). "Fast implicit finite-difference method for the analysis of phase change problems." Numerical heat transfer, part B **17**: 155-169.
Voller, V. R. (2001). "Numerical treatment of rapidly changing and discontinuous conductivities." International Journal of Heat and Mass Transfer **44**(23): 4553-4556.
Voller, V. R. and C. R. Swaminathan (1990). "Fixed grid techniques for phase change problems: A review." International Journal for Numerical Methods in Engineering **30**: 875-898.
Wang, J., G. Chen, et al. (1999). "Theoretical study on a novel phase change process." International journal of energy research **23**.
Xu, R. and G. F. Naterer (2001). "Inverse method with heat and entropy transport in solidification processing of materials." Journal of Materials Processing Technology **112**(1): 98-108.
Yimer, B. and K. Senthil (1998). "Experimental and analytical phase change heat transfer." Energy Conversion and Management **39**(9): 889-897.
Yoo, H., H. Hong, et al. (1998). "Effects of transverse convection and solid-liquid density difference on the steady close-contact melting." International Journal of Heat and Fluid Flow 19(4): 368-373.
Zhang, Y., Y. Su, et al. (2001). "A general model for analyzing the thermal performance of the heat charging and discharging processes of latent heat thermal energy storage systems." Transactions of the ASME 123: 233-236.
Zivkovic, B. and I. Fujii (2001). "An analysis of isothermal phase change of phase change material within rectangular and cylindrical containers." Solar Energy 70(1): 51-61.

CHAPTER IV

LATENT HEAT STORAGE EXPERIMENTAL APPROACH

"No amount of experimentation can ever prove me right; a single experiment can prove me wrong" Albert Einstein

Chapter IV: Latent Heat Storage Experimental approach

The experimental part of this work has three main objectives. To validate the computer model presented in the previous chapter by considering the impact of the assumptions made for the physical phenomenon simplification. To optimize and evaluate the performance of the system proposed and to explore the properties and behaviour of the PCMs selected.

Firstly the concept of the heat storage unit is presented, and the experimental rig described. The parametric study, heat transfer enhancement features for system optimization and the energy storage/retrieval, melting/freezing processes for system performance are assessed by an experiment labelled "2". The same experimental rig and testing methodology are used for the computer model validation. The experimental approach can be summarised as explained below.

Experimental approach

The experimental approach carried out was summarized on the scheme showed in figure 4.1. The heat storage unit proposed is a storage element that constitutes internal blinds in windows. The performance of this unit was

tested in experiment 2. The computer model was validated with a special experiment designed for this purpose (experiment 1), but also data obtained from experiment 2 was used to validate the model. Before the performance of the whole system containing PCM was tested, the bared material was submitted to thermal analysis.

Once the concept of the heat storage system was developed, the experimental apparatus for its testing was designed. The rig involved an insulated chamber to keep the unit under controlled conditions; a solar simulator which design process is described in the chapter; a heat exchanger and chiller for temperature control inside the chamber; and finally gauges, meters and logger for data acquisition.

The simulation models were defined according to the number of variables considered by using experimental design. Besides the computer model validation experiment 1 was designed to assess the heat storage charging/discharging behaviour, with and without radiation during cold and hot days and nights and during winter and summer nights in each province (using the lowest interior and exterior air temperatures).

Earlier investigations on elements to boost the efficiency of latent heat storage systems (LHSS) established the variables for the assessment of the overall thermal performance of the system proposed (experiment 2). These variables are: Temperature ranges, PCM melting temperature, PCM volume, surface container insulation, mass flow rate of the heat transfer fluid (HTF), and the charging (heating) and discharging (cooling) mode. The methodology to carry out the experiments was also described.

The approaches for the assessment of the system's performance include the variation of energy stored/extracted with the variation of dependable variables, the application of insulation on the encapsulated unit, and its efficiency mostly determined by its charging ratio.

Regarding the material investigation, all the process for the selection of PCMs to be tested was illustrated. The melting-freezing characteristics considered for the testing were explored on the differential scanning calorimeter DSC test. With the DSC thermal analysis the PCM thermal properties were evaluated and its stability, crystallization, supercooling, superheating, phase segregation assessed. Means to enhance the heat transfer rate (when rapid charging/discharging is required) are proposed.

Concerning long term behaviour, previous studies on the performance of organic and inorganic PCMs after cycling consider the reliability of the material's long-term behaviour as good.

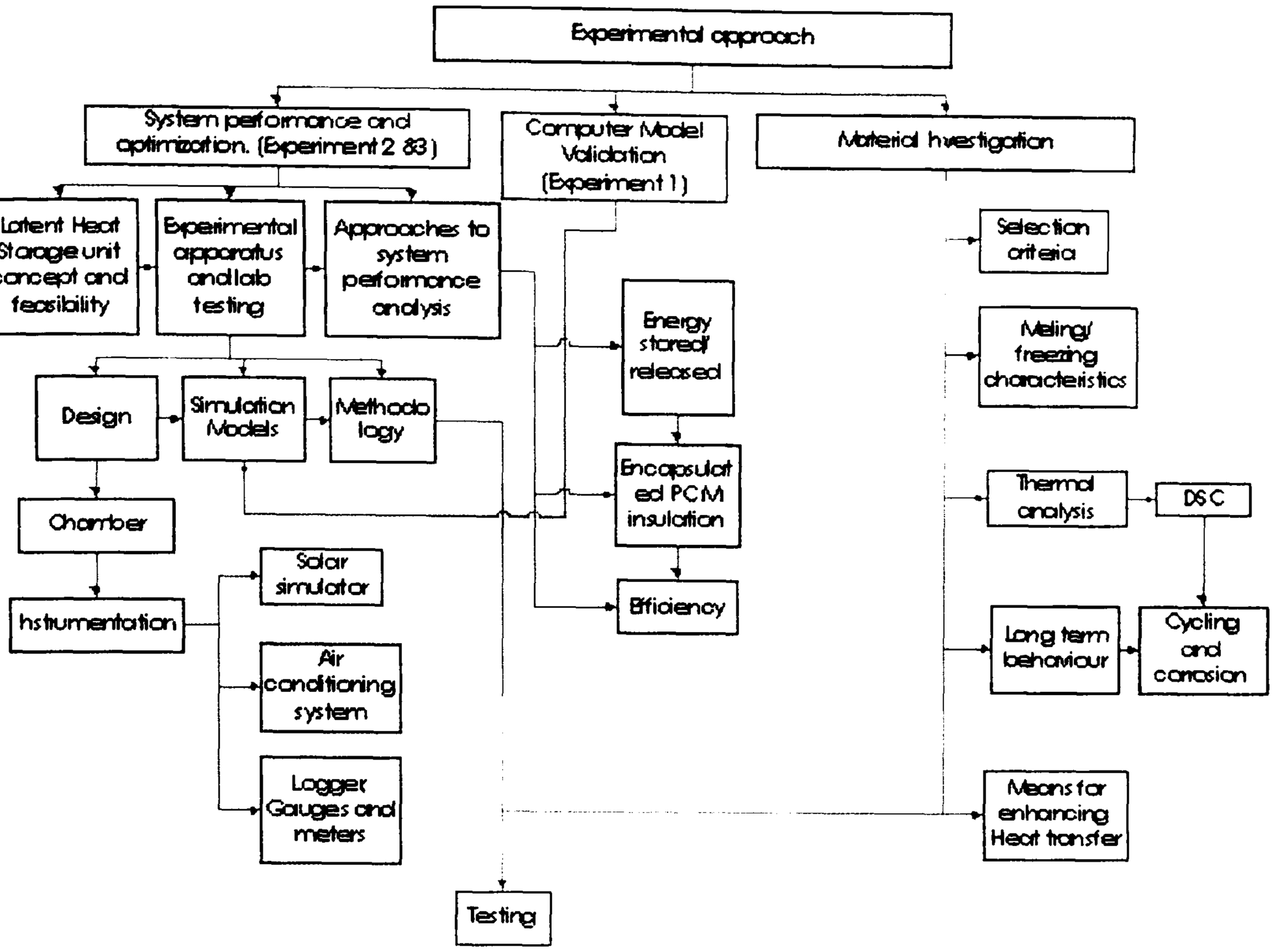

Figure 4.1: Experimental approach diagram

System Performance and optimisation

Latent heat storage unit concept

The heat storage system intends to improve temperature control for thermal comfort (decreasing the risk of overheating by reducing temperature fluctuations), play a role on energy savings (as it is a passive mechanism for thermal comfort) and reduce heating system power to mitigate thermal comfort operating costs (minimizing cycling by attaining larger thermal stability and downsizing equipment by reducing heating load requirements).

The approach is a storage element that constitutes internal blinds in windows. Three major characteristics for promoting the unit's efficiency were taken into account in its design.

1) Ensure the material's complete melting in a satisfactory time interval by choosing suitable physical geometry, dimensions and source of heat. Solar radiation and internal heat gains are the heat sources. The intensity of the irradiation was supplied according to solar irradiation data for two Mexican provinces. The heat gains were evaluated by a simulation run with TAS in these same Mexican provinces in a dwelling assuming 5 inhabitants. Insulation and PCM volume contained were considered variables associated to the charging/retrieval rate control, so these were variables tested in experiment 2.

2) Maximize the exploitation of the energy source and the thermal energy stored. Storage units placed on the roof have been studied previously(Vener 1997). The main advantage of a roof storage unit is the amount of irradiation received and time during which the roof is exposed to it. But this system mainly works as a heat moderator; the stored energy is actually not used inside the building envelope, but lost to the atmosphere. Other studies focused on PCM wallboards have shown the system's ability to store/retrieve energy for indoor's thermal comfort, but can only absorb a small amount of PCM by volume (a board can contain about 25% by weight proportion of PCM). For these reasons the PCM was encapsulated and the storage unit operated as an internal window blind. This location provides at the same time an opportunity to vary the mass flow rate of the heat transfer fluid (air) without the use of additional electro-mechanical means. The effect of air velocity variation on the storage retrieval process is analysed in experiment 2.

3) Improve the PCM's low thermal conductivity by enclosing the PCM in contact with metallic tube containers and by using multiple PCMs. Using an infinite number of PCMs provides an increase of exergy[4.1] compared to a single PCM system(Gong and Mujumdar 1997). The adjacent wall of the contact metallic tubes containing PCMs with different melting temperatures could work as a hot/cold plate modifying the heat transfer rate for the whole unit. In this work it is suggested that if this modulation is understood, the various PCMs arrangement can be used as a passive mean to control the heat flow rate for energy storage/delivery. These are also variables tested in experiment 2.

Original aspects of this experimental work include the application of internal heat gains[4.2], temperature, irradiation and air changes per hour for Mexican like weather conditions. In order to evaluate the energy stored in the LHSS containing PCM operated under Mexican conditions, the room temperature used in the experiment had to be comparable to that expected in a real building(Neeper 2000). Another original contribution is the radiation simulation with a large scale solar simulator using lamps to reproduce irradiation fluxes given in Mexican provinces for the assessment of a latent heat storage system for dwellings. Finally some PCM thermal properties (as enthalpy-temperature relationship, and temperature dependent thermal conductivity and heat capacity) not found in readily available literature are an original contribution

---

[4.1] The maximum amount of work potential (in energy units) of a system in relation to the surrounding environment. The exergy of a system is that part of the system's energy that is available to do work. Due to the limitations of the first and second laws of thermodynamics, the exergy of a system depends on the surrounding environment.
[4.2] contribution expected from occupants, lights, among other sources depending on the nature of the occupancy

The heat storage unit: is formed by twelve rectangular aluminium tubes. The size of the tubes was chosen only for experimental practical purposes, it reproduces neither a real size window blind nor a scale of it. A low temperature PCM was contained in a tube next to a medium temperature PCM and the later next to a high temperature PCM; which was then next to a low temperature PCM. This arrangement was selected in order to assist the charging/ discharging by the contact between the different PCM melting temperatures contained in the aluminium tubes. It would be interesting to assess if a different arrangement would have an effect on the performance of the system.

Environmental conditions within a building envelope can not be scaled, as the complex interrelation of the weather parameters (humidity, solar radiation, ambient temperature, wind, cloud cover, ground temperature) present non-linear behaviours. For this study it was not possible to build a real scale dwelling for testing due to economical reasons. Nevertheless, the proposed experiment allows the characterization of the correlation between variables. The presence/ absence/ variation of each factor provides and understanding of the thermal behaviours of the unit under varied circumstances.

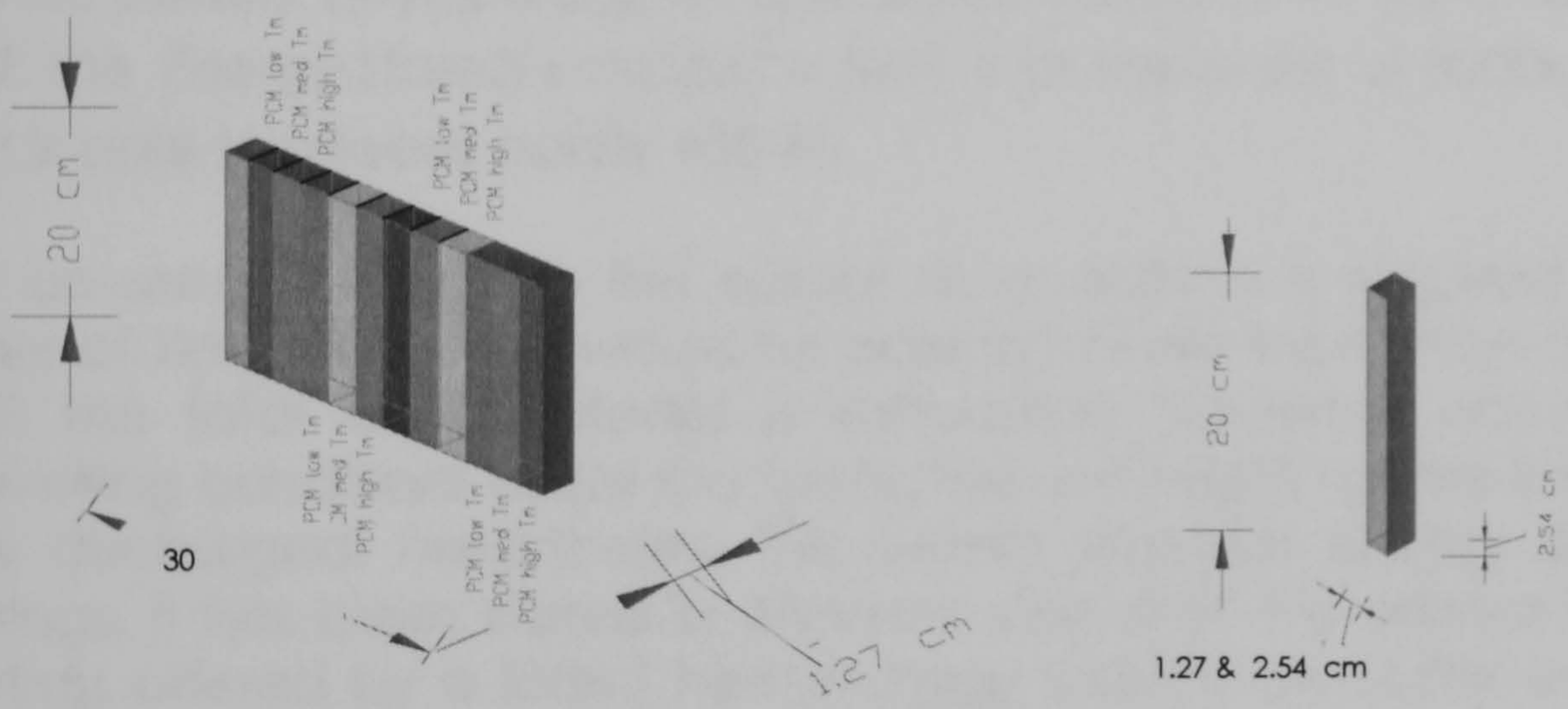

Figure 4.2: The storage unit and cell dimensions

The system operation: the unit was to experience conditions similar to those existing in a real operating window blind. The PCM charging process was carried out by supplying either hot air inside the chamber or constant heat flux by irradiation through the window or both. The loads applied reproduced solar irradiation and interior heat gains inside a building envelop. For the retrieval process cold air supplied to the chamber reproduced the envelope heat losses and air changes. The mass flow rate applied is within the range for natural convection, no mechanical means for the heat exchange are required as the length to depth ratio of the cell is small. All conditions were kept constant for the duration of each process that lasted for about 5-7 hours (total discharging or charging time). Gauges for measuring the irradiated flux to the window, heat flux at the front and back surface of the storage element, mass flow rate, temperature inside the

chamber, temperature of the PCM, and wall temperatures recorded data was saved in a logger.

The simulation of the transient weather conditions (solar spectrum, temperatures, etc.) is a complex task, requires a complete study on its own, or the holding of specialized equipment and it is out of the reach of this study. The correlations and magnitude between variables characterized under specific conditions can be found by applying constant weather conditions as handled in this study.

Preliminary viability assessment:

Even though the present study is not dealing with either full or scaled size units for testing, a rough estimation of the expected energy stored of the full size unit proposed is evaluated here to assess the system's real contribution to thermal loads.

The real window size considered an area of 0.5x0.5m and was 0.0254m in depth for PCM volume. The unit is fully charged and Paraffin hexadecane is used as PCM , with the following properties in the liquid state: Enthalpy (H)= 236 kJ/kg; Heat capacity (Cp)=2.200 kJ/kgK ; Thermal conductivity (k)=0.45 W/mK; Density (ρ)=870 kg/m^3; and liquid fraction $\lambda = 1$ for a totally charged unit. the $Energy\ Stored = mCp\Delta T + \lambda mH$ is of the order of 3200kJ. That is, the unit is able to release nearly 400 W.

For an area of 2.4x2.4m the output of a radiator is required to be of the order of 1kW, so the unit would be able to handle more than 1/3 of the load until the total energy stored is exhausted. However, according to the prevailing conditions inside the room, the unit might not be fully charged or fully discharged; nevertheless the system provides energy and economy savings. It has been stated in previous work that the annual direct energy savings offered by a latent heat storage system are of the order of 15% in temperate weather conditions. (Kelly 1999)

Experimental apparatus and laboratory testing

Design

The chamber

The enclosed thermally controlled space in which the blind was exposed to the experimental parameters consists of a polyethylene insulation board container with a double glazed window. The window has a suitable area to allow full exposure of the storage unit front wall surface. The container was designed to allow enough pressure and temperature differential for applying the recommended air velocity for ventilation in buildings. Attached and connected to the chamber are: the frame to hold the storage unit, the tube for inducing mass flow (which connects to the heat

exchanger) and some heat flux gauges. The chamber's window front is exposed to irradiation received from the solar simulator.

The polyethylene used for the container is a celotex insulation board, which is a low density rigid foam board with an approximate weight of 2.10 kg/m^2 of surface, a thermal conductivity k = 0.032W/mKand with a tri-laminate foil finish on one surface. The mean thickness of the board was chosen to be 70mm to achieve a Thermal transmission value (U-value) of 0.45 W/m^{2}K for the wall sections.

The chamber was constructed in three sections. The bottom part is a rectangular polyethylene enclosure 30 cm in height with a circular opening connected to the tube feeding the incoming airflow from the heat exchanger. Thermocouples to measure the incoming air temperature were fitted. This section was connected to the upper section by a diffuser[4.3]. The central section contained the window and holds the blind. Thermocouples were fitted to measure the air temperature inside the chamber in the section facing the blind. The pyranometer was fitted on the exterior of this section facing the solar simulator. Finally the upper container section was bell-shaped (as an air extractor) in order to allow a more uniform air temperature reading at the top of this section. Right at the crown of the last section was placed the anemometer. The schemes of the container are shown in appendix 4A. A clearer diagram of the next figure can be found in appendix 4A.

[4.3] a lamina with small distributed perforations

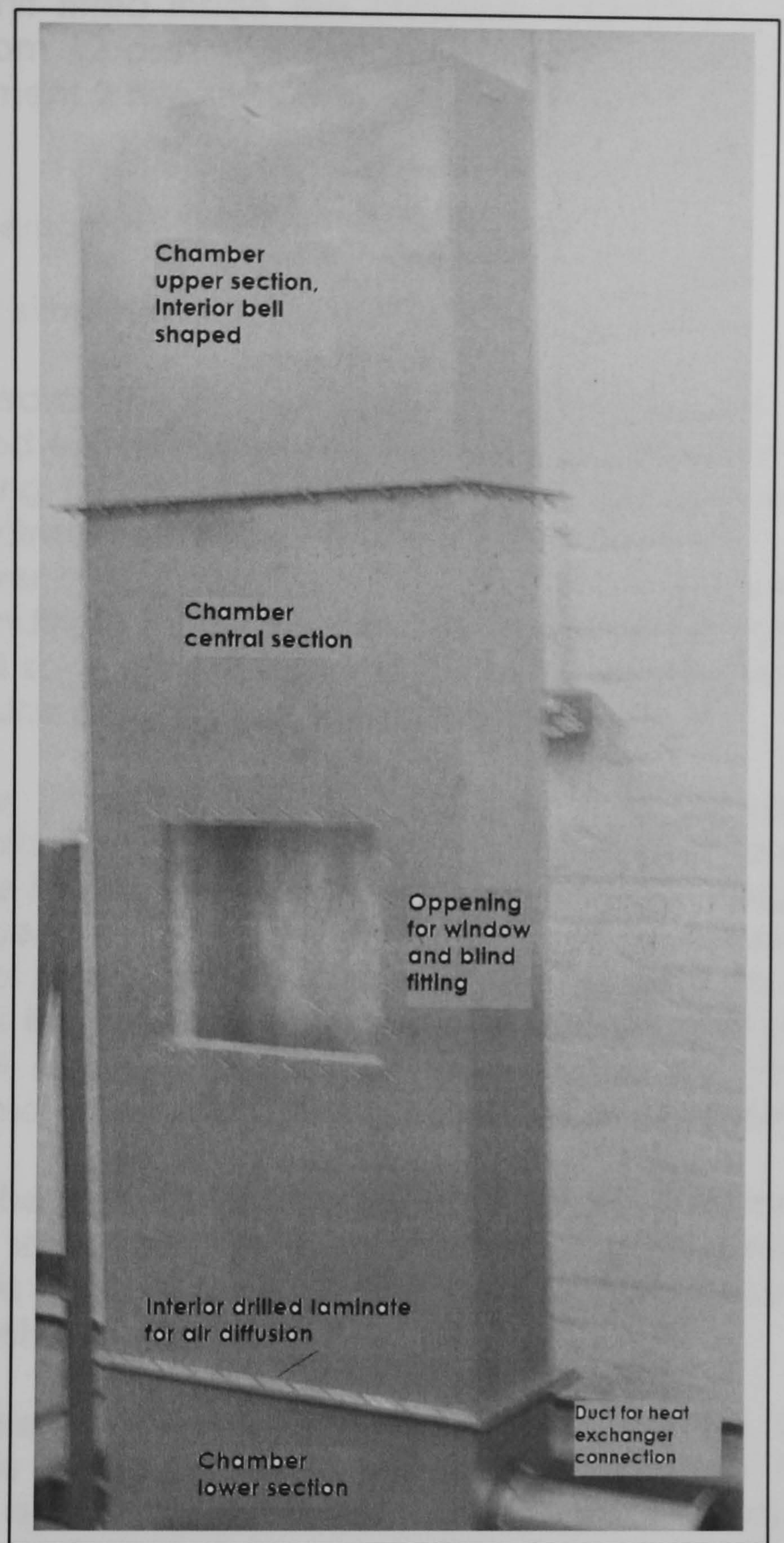

Figure 4.3: Chamber

The losses through the window are minimized by the double glazed window made of two 300x400x6mm panes of glass with an air space of 6mm between them.

The temperature conditions inside the box were maintained constant and supplied by a heat exchanger fed by a chiller with heating and cooling modes of operation. The temperature band of variation was 1 ^{c}C.

The storage unit fitted inside the chamber facing the window and was constructed from 12 assembled rectangular aluminium alloy tubes 22 cm long. In experiment 2 two sizes of tubes were used: 1"x1/2"x16swg and 1"x1 ½"x16swg.

Instrumentation

Solar simulator

In previous research the charging process of latent heat storage units has been performed experimentally by imposing a constant thermal current to the surface using thermoelectric devices and heat sources or by exposing the unit to direct solar irradiation. Solar simulators offer significant advantages over outdoor exposure, because of the unpredictable variation of weather conditions (noise factors). Also research via outdoor exposure is limited to local solar conditions whereas research using a solar simulator is able to reproduce any location's solar conditions.

The Oriel Solar Simulator uses light sources with different spectra and irradiance distribution to provide a close spectral match to the solar spectrum. Since the solar spectra depend on so many variables[4.4], standard spectra have been developed to provide a basis for theoretical evaluation of the effects of solar radiation and as a basis for simulator design. The only problem is that this simulator is extremely expensive and its irradiation only covers a small area (output ranges from 2x2 to 8x8 inches collimated beam), as it is mainly used for photobiology and photochemistry.

To the best of the author's knowledge this is the first time that radiation from a large scale solar simulator using lamps has been used to reproduce irradiation fluxes given in Mexican provinces for the assessment of a latent heat storage system for dwellings.

Although constant irradiation values were applied when running the tests, the next figure gives an idea about the irradiation profile during a representative day in the dwelling simulated by the Thermal Assessment Simulator. The modified bell shape irradiation profile for horizontal surfaces to an "M" shaped profile is due to the fact that the surface is vertical and facing south, and at noon the beams are exactly above the wall.

4.4 Solar radiation reaching the earth's surface varies significantly with location, atmospheric conditions (including cloud cover, aerosol content, and ozone layer condition), time of day, earth/sun distance and solar rotation and activity.

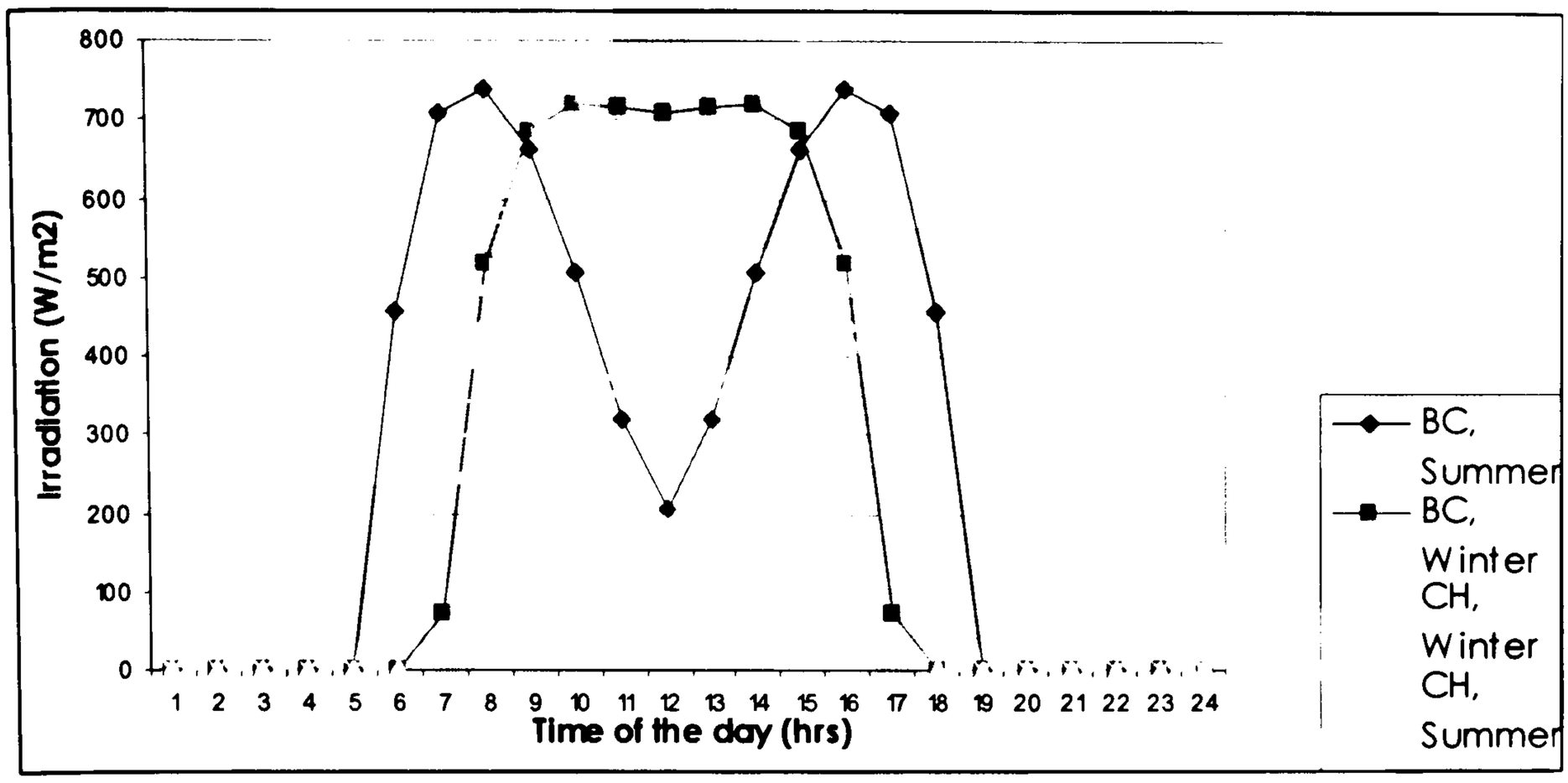

Figure 4.4:Average day solar radiation on a vertical wall at two different seasons and two different regions in Mexico

Where BC stands for Baja California, and CH for Chiapas.

Xenon arc lamps provide the closest spectral match to solar spectra available from any artificial source. But, even if the lamp current is constant the light output of many xenon lamps varies with electrode erosion, gas adsorption, and aging; plus arc lamps have sharp peaks, and in this study a continuous irradiation is required.

Important wavelengths in solar energy go from ultraviolet to near infrared range, that is, from $0.3\,\mu m$ to $2.5\,\mu m$.

On the other hand Quartz Tungsten Halogen[4.5] Lamps (QTH) flux is smooth, continuous and recommended for large targets. The lamps used for the solar simulation were 50 mm diameter Dichroic[4.6] mirror 50 W QTH lamp mounted in an elliptical dichroic glass reflector. A flat diffusing glass was selected for the reflector to allow for total radiation (spectral irradiation) as the radiation flux was measured[4.7]. These lamps provide a close spectral match to solar spectra[4.8] with a usable wavelength range of $0.24 \prec \lambda \prec 2.7\ \mu m$ [4.9]

[4.5] Halogen gas removes the evaporated tungsten from the filament that deposits in the bulb (reducing the output light), and returns it to the filament

[4.6] Dichroic reflector is made of faceted glass, coated with a dichroic film that reflects visible light and transmits infrared energy through the back of the lamp. 80% of the lamps heat passes behind through the dichroic mirror without being reflected. This makes light cooler and safer

[4.7] The irradiation flux was measured by a Pyranometer

[4.8] See appendix 4.D

[4.9] See appendix 4.D

Nevertheless, the brightest tungsten lamps operate at colour temperatures of 3200K (the solar spectrum between 5600-6000 K). The low UV and shortwave visible output prevents an efficient match in these key regions. For this reason Oriel's solar simulator is fitted with filters that allow the modification of the tungsten lamp spectrum. In our simulator it wasn't possible to adapt the filters as their design requires specialized knowledge of the vertical optical thickness of the standard atmosphere and calibration of the optical thickness tilt.

The output intensity levels from the lamps can be varied without significant spectral changes by moving the lamp position. Dimming the lamp voltage is not recommended as the total output is reduced, and the peak wavelength shifts slightly. A change in wavelength, even if it is done within the solar spectra, must be avoided as it is not a variable in this study. Then, to vary the irradiation values, the solar simulator position was adjusted. In previous research it was demonstrated that it is possible to reduce the magnitude of the lamps output in this way by more than 80 %(LOT-Oriel 1993)

Lamps intensity monitoring, preliminary test

It was necessary to screen the intensity of a QTH lamp as data from the manufacturer was not available. At the same time the impact of the lamp position in surface flux uniformity was assessed.

A 0.50x0.60 m metallic frame with rotational axis of mobile x,y and z coordinates, driven by a crank handle was used to move a QTH lamp held by a metallic post joined to the axis. The lamp was moved over a matrix of points over a surface of 54cm^2. Each point was 2 cm apart from each other. The intensity of the lamp's flux was measured in each point at 4 different distances.

Once the output ranges of the radiation received from that "one" lamp for orthogonal planes at different distances was obtained, the data was used to model the beam interaction over the irradiated surface by adding the effects of 31 lamps in different arrangements. In the Table 4.1 the leftmost column shows the number and position of the lamps. On the right columns the received radiation uniformity over the surface obtained from the simulation is shown. The pseudocode for the simulation is presented in appendix 4.B, the results of the lamps intensity monitoring test are shown in appendix 4.C.

From this preliminary monitoring test it was found that the most uniform radiation was given by the "all lamps ON"- arrangement[4.10] at the most distant position. On the other hand an uneven distribution flux was found

---

[4.10] Observe that the lamps are arranged on a zigzag distribution

with the same lamp arrangement for the closest position. The zigzag arrangement gave a satisfactory uniformity for all the distances. For this reason the solar simulator was designed to hold the lamps in the arrangement shown in figure 4.6:

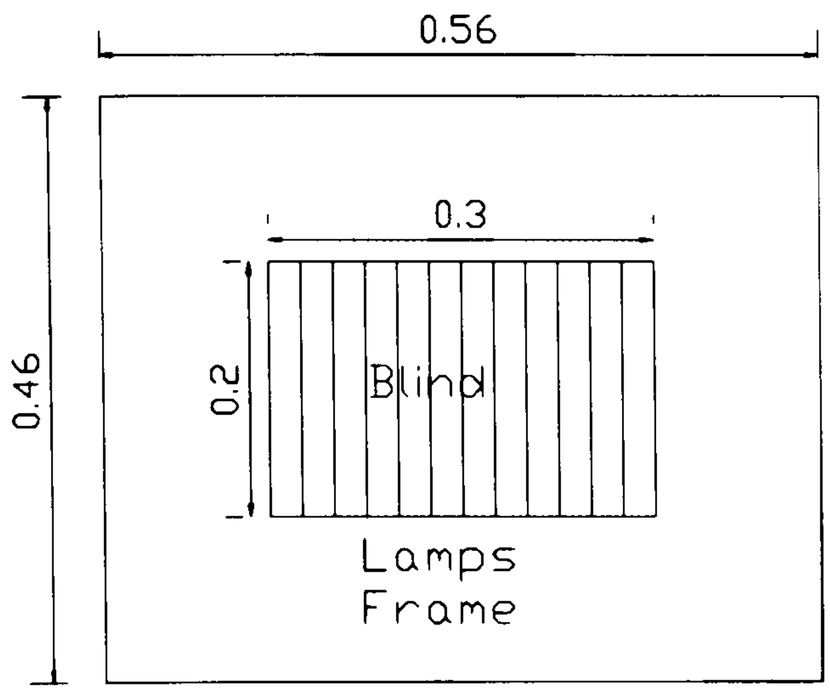

Figure 4.5: Solar simulator frame, Front

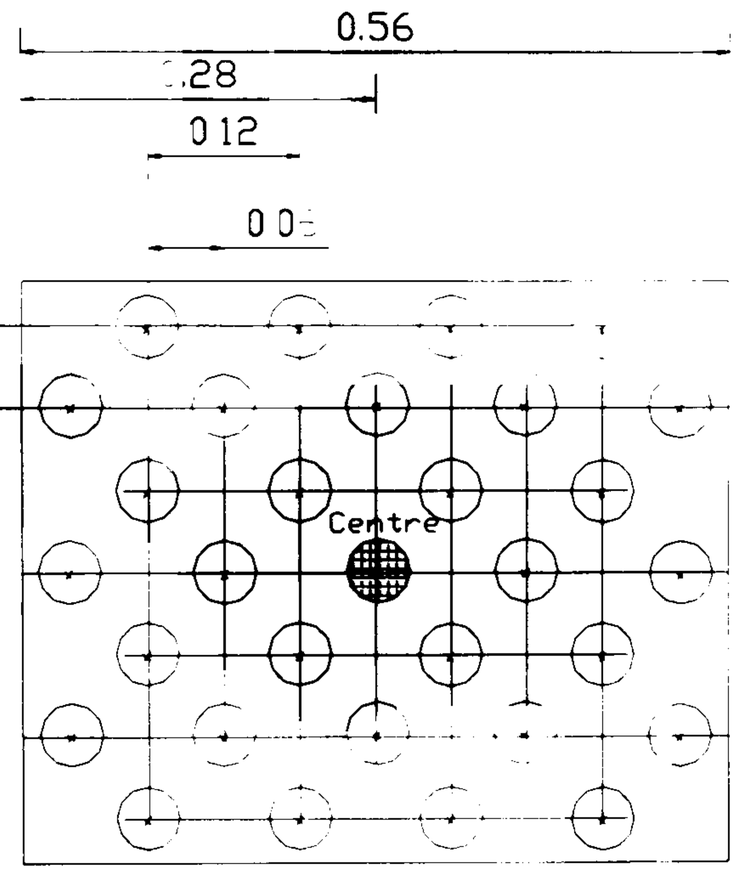

Figure 4.6: Lamps distribution

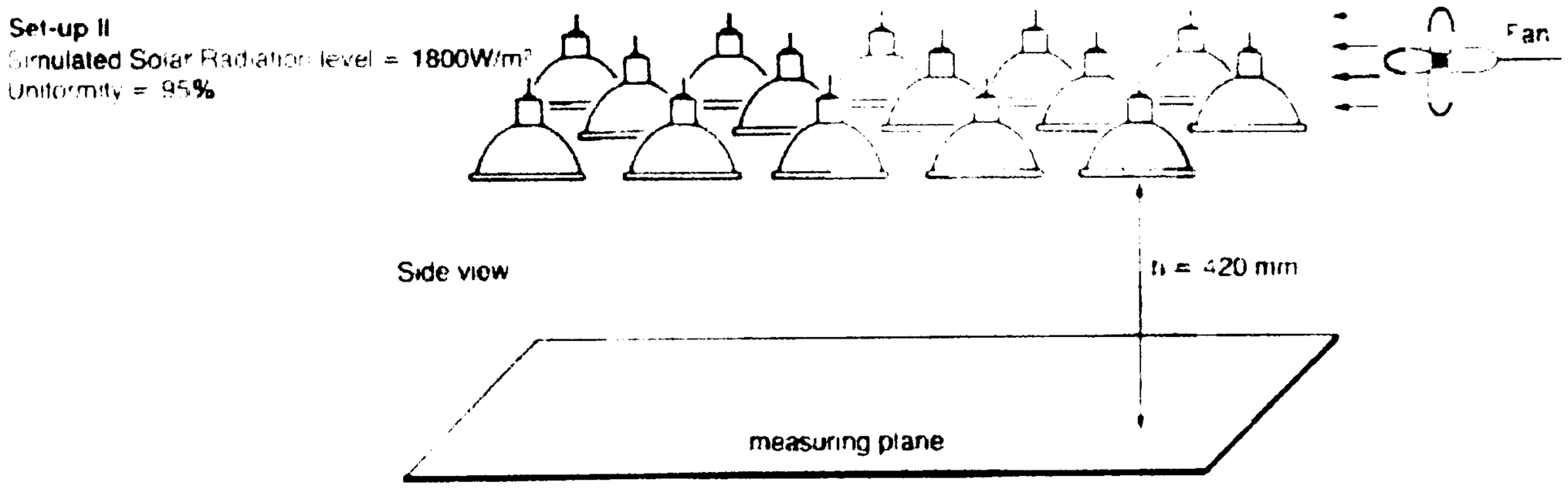

The selected arrangement is similar to a solar simulator sold by Philips:

Figure 4.7: Philips Solar simulator, lamps distribution, lateral view

For intensity levels other than those obtained at the 4 distances presented, the values can be interpolated from the data. The irradiation intensity data for the two Mexican provinces studied for each season (7 different irradiation intensities for summer, and 6 for winter) was considered to set the solar simulator distances. The intensity levels interpolated for a range of distances, set to achieve the required irradiation are shown in Table 4.1

BC Summer							
	Flux 1	Flux 2	Flux 3	Flux 4	Flux 5	Flux 6	Flux 7
Flux Required	456	710	740	663	505	321	208
Highest flux to interpolate	514	771	771	771	514	514	362
Lowest Flux to interpolate	307	656	656	656	307	307	100
Distance for highest flux	49	21	21	21	76	49	74
Distance for lowest flux	76	32	32	32	49	76	93
Distance value required	56	27	24	31	75	74	107
BC Winter							
	Flux 1	Flux 2	Flux 3	Flux 4	Flux 5	Flux 6	
Flux Required	71	519	685	720	714	708	
Highest flux to interpolate	255	656	771	771	771	771	
Lowest Flux to interpolate	-46	514	32	656	656	656	
Distance for highest flux	87	32	21	21	21	21	
Distance for lowest flux	110	49	32	32	32	32	
Distance value required	113	48	22	26	26	27	
CH Summer							
	Flux 1	Flux 2	Flux 3	Flux 4	Flux 5	Flux 6	Flux 7
Flux Required	269	479	486	407	297	156	35
Highest flux to interpolate	410	514	514	514	432	322	227
Lowest Flux to interpolate	165	307	307	307	195	45	-84
Distance for highest flux	68	49	49	49	65	79	91
Distance for lowest flux	86	76	76	76	100	100	115
Distance value required	87	53	53	63	83	102	118
CH Winter							
	Flux 1	Flux 2	Flux 3	Flux 4	Flux 5	Flux 6	
Flux Required	307	447	443	405	361	337	
Highest flux to interpolate	440	514	514	514	514	514	
Lowest Flux to interpolate	205	307	307	307	307	307	
Distance for highest flux	65	49	49	49	49	49	
Distance for lowest flux	81	76	76	76	76	76	
Distance value required	82	58	58	63	69	72	

Table 4.1: Solar simulator-target area distance values interpolated to achieve the required irradiation

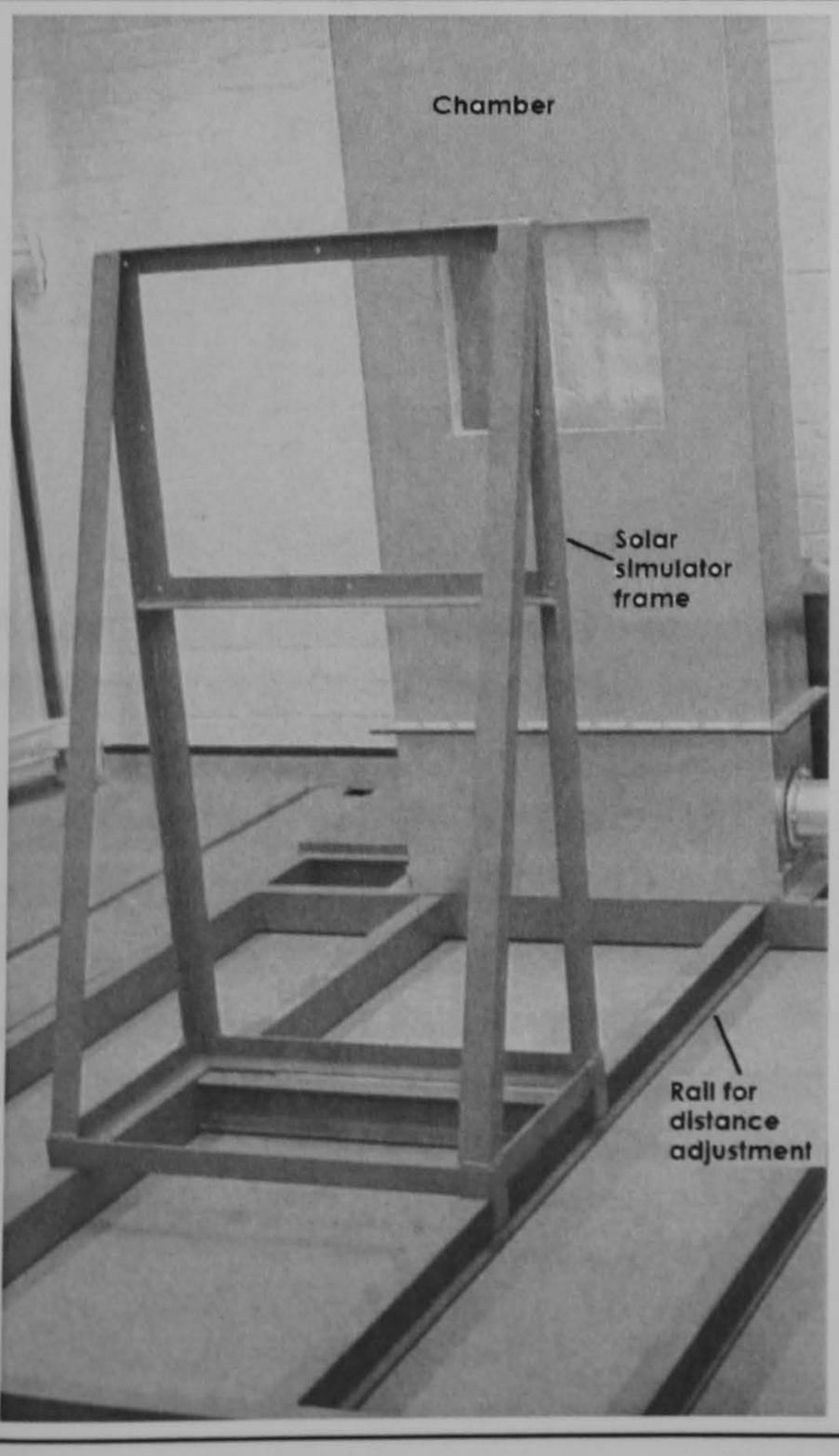

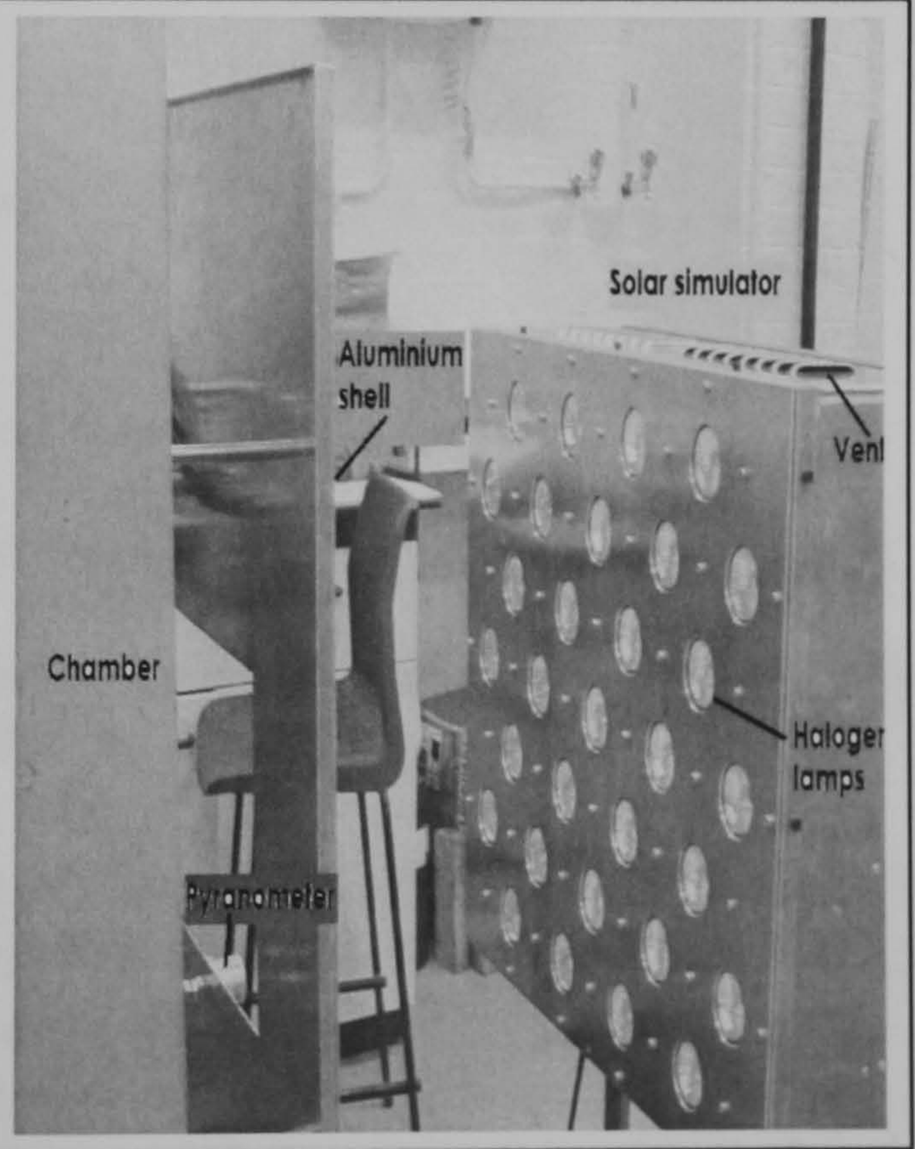

To the left **Figure 4.8: Solar simulator frame and rail** To the right **Figure 4.9: Solar simulator**

Air Conditioning:

Thermal Analysis System (TAS) transient modelling was used to determine the heat loads and then the given interior air temperatures to be simulated. TAS set up equations representing individual energy balances for the air and each of the surrounding surfaces. The energy balance is influenced by building form and orientation, climatic conditions (exterior air temperature, solar gains, wind velocity), internal conditions (lights, equipment, occupants) building element's properties, infiltration, ventilation and air movement.

The individual energy balances are then combined with additional equations representing the energy balances at the external surfaces and the whole equation set is solved simultaneously to generate interior air temperatures, surface temperatures and room loads. As the interior air temperature arises as a result of the energy balance, it is by applying the interior air temperature given by the TAS simulation that the internal heat gains/losses are simulated inside the experimental chamber.

Although a constant temperature value was applied when running the tests, the next figure gives an idea on the temperature fluctuation (ranges) during a representative day in the dwelling as simulated by TAS.

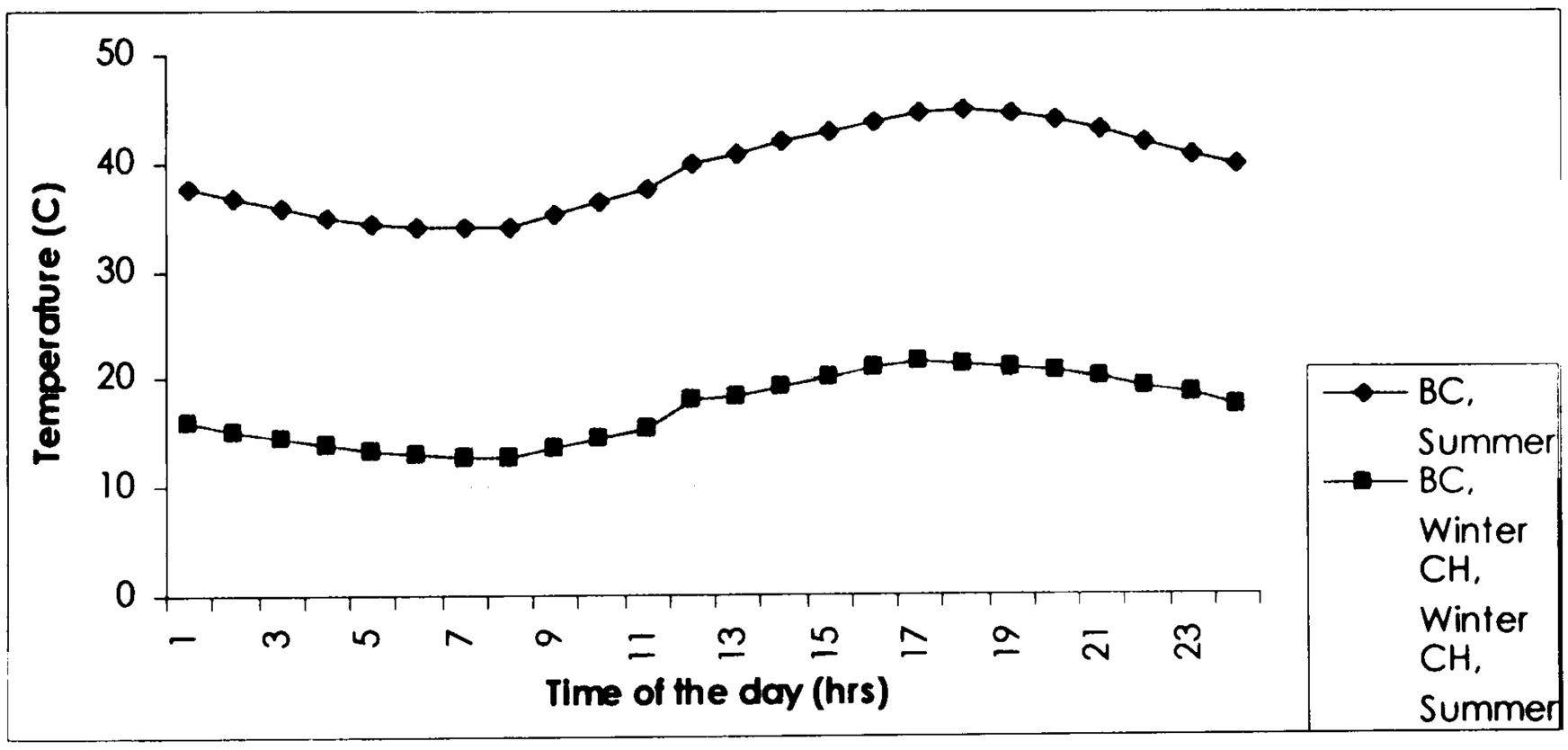

Figure 4.10: Interior air temperature profiles of representative days at two different seasons and in two different Mexican regions

For the TAS simulation a 16x10m one storey dwelling was modelled. A comfortable temperature was considered to range between 19 to 23°C. Room humidity was considered between 40 to 70%. The estimated required air changes per hour were 1.5. The dwelling was assumed to be occupied by 5 members with sensible and latent heat emissions of 80 and 60 W respectively per person during the day and 75 and 40 W respectively during the night.

Once this information was obtained the next step was to determine the heating/cooling system that best satisfied the requirements. The most common systems are forced-circulation hot/cold water, forced circulation hot/cold air, forced circulation steam and electrical resistance heaters[4.11]. Energy conversion units[4.12] convert some of the energy in fuels into heat energy which is transferred to a working fluid. The working fluid circulates to the various terminal units, where the heat is transferred to the space(Clifford 1990). The forced circulation hot/cold air was chosen, for having the further advantage of simultaneously providing the possibility of simulating the mass flow rate in the experimental chamber to represent existing air changes per hour in the dwelling.

The mass flow rate to be applied depends on the maximum air velocity for thermal comfort within the dwellings. Velocities of 2 and 3m/s were used in previous work aiming to evaluate the effect of air velocity in respect to rates of latent heat storage and discharge control in concrete.
The monthly average wind speed for the two Mexican provinces target of this study ranges between 1.8 to 4.3 m/s:

wind speed(m/s)	Jan	Feb	Mar	Apr	May	June	July	Aug	Sep	Oct	Nov	Dec
BC	3.9	3.8	3.8	4	4.1	4.3	3.9	4.3	4	3.8	3.5	3.4
CH	1.8	2.2	2.2	2.0	1.9	2.0	2.0	2.0	2.2	2.6	2.3	2.0

Table 4.2: Wind speed in the two Mexican provinces selected for simulation

The air velocity probable impact on occupants up to 1m/s can be considered still comfortable according to (EFFICIENCY 2003).

The ISO 7730 recommends that for moderate thermal environments with light mainly sedentary activity during cooling, the mean air velocity should be less than 0.25 m/s, whilst in winter it should be less than 0.15 m/s. No minimum velocity is suggested, since it is likely that sufficient air movement will be generated by other means (CIBSE 2001).

The area of the floor diffuser[4.13] delivering the incoming air into the box is 0.05m^2. The maximum volume flow rate required, taking into account a maximum air velocity 0.15m/s, ($\dot{v} = vel * A$) is then 7.55x10^{-3} m^3/s; and the corresponding maximum mass flow rate for that velocity ($\dot{m} = Vel * \rho_{air} * A$) is 9.1410^{-3} kg/s (where ρ_{air} =1.219 kg/m3)

4.11 The electrical energy converted into heat energy is delivered directly to the space by radiation and convection (Clifford, 1990)
4.12 The space heater located within the space burns a fuel such as coal, gas, oil or wood and some of the released energy is delivered by radiation and convection directly to the space to be heated (Clifford, 1990)
4.13 The laminate contains 28 holes of 6mm diameter

A hot wire anemometer was used to measure the air flow rate through the box. For that purpose it was necessary to calibrate the anemometer, which provides velocity values to match the required mass flow rate. Details on the calibration are shown in appendix 4.E.

A finned-tube heat-transfer coil for forced convection cooling and heating of air was used to set up the interior air temperature. These heat exchangers are compact and easy to be installed. The cooling was accomplished with chilled water circulating through the coil tubes, while heating was accomplished by circulating hot water through the coil tubes. The components were specified according to the temperature range, and air mass flow required to be supplied to the chamber. Details of these calculations can be found in appendix 4.F.

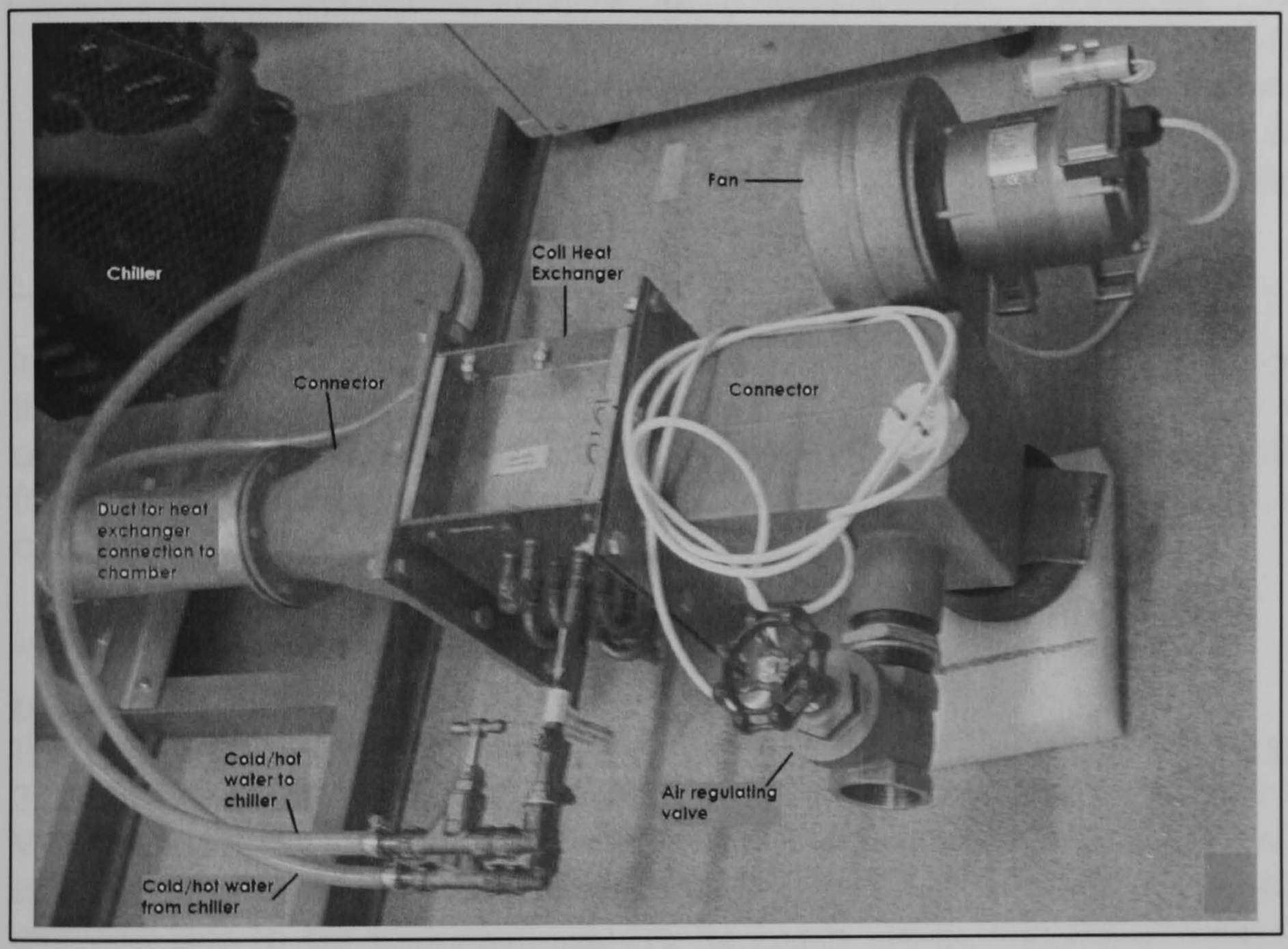

Figure 4.11: Fan, heat exchanger, chiller duct and diffuser connections to the lower chamber section

The cooled/heated air from the heat exchanger achieved the required mass flow rate (for the given pressure gradient) when supplied to the chamber by using a fan regulated by a valve. The required heat transfer rate for cooling during a required time interval was evaluated as shown in appendix 4F.

The standard air volume of the unit was of 0.014m^3/s, and was sized to cope with a duty of 0.5 kW for cooling the air inside the chamber down to 9°C. The water flowed inside the 0.4mm thick copper tubes at 0.03 l/s. The

dimensions of the duct were 150x156x185 mm; with an inlet and outlet connection of ¾". The fin material was aluminium.

The cold-hot water was supplied to the heat exchanger by a chiller. The chiller used was a CONAIR CHURCHILL Type 05/CTCV Chiller/thermo circulator. The chiller maintained the desired pre set flow temperature in the range -3°C to 45°C. Max flow rate 15 litres/min. Cooling capacity 1.3kw. with R12 refrigerant. The control panel had cooling on/off; under temperature and over temperature warning lamps.

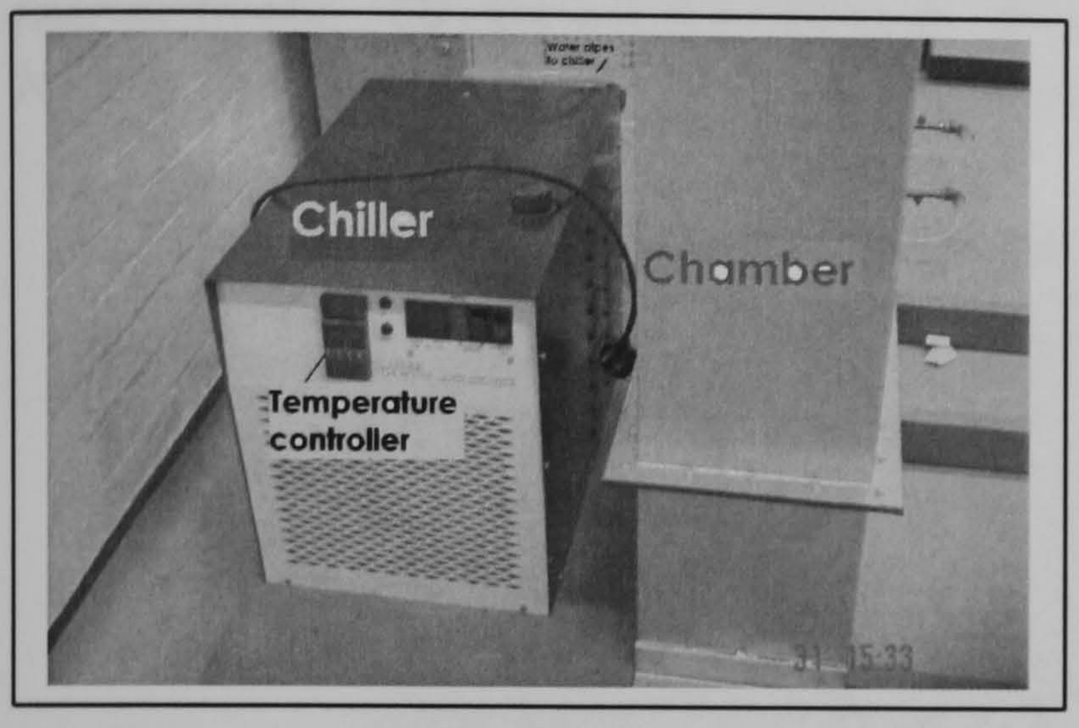

Figure 4.12: Chiller

The chiller was supplied with CAL temperature controller model 9900, supply 230 V at 50-60 Hz. Proportional Integral differential (PID) heat-cool operation. It was not equipped with remote set point[4.14].

In order to reach the lowest air temperature to be supplied to the chamber the chiller had to circulate water at -3°C. This caused the formation of ice on the feeding tubes which after several hours were blocked with the formed ice. To overcome this problem antifreeze liquid was injected to the circulating water

Logger and Gauges:

Logger

The experimental events were recorded by a programmable delta-T logger 3.03 data logger with 4 LAC1(analogue signals)cards, powered either by 12 V mains adaptor or 12 V external battery. The software LS2 Win allows the specification of the sensors connected, the frequency to record data and allowed files to be exported directly to excel. Data was transferred by an RS232 serial port. The logger can record data from up to 56 sensors, using 15 channel mode for 4 cards (terminal groups) and 1 precision resistor per card. The memory fitted (IC1 and IC8 with 32 k ram) stores 16384 timed readings (each reading requires 2 bytes).

In channels 1, 16, 31 and 46 were connected precision resistors[4.15] . In channel 2 the pyranometer also referred to as solarimeter. In channels 3 to 21 were connected thermometers for PCM temperature measurement (these are also referred in this work as internal blind or internal cell

---

4.14 If sensor can provide a remote set point input to the controller its possible to download data to the computer at determined intervals

4.15 For high accuracy performance

thermometers). Channels 6 to 14 measured the PCM temperature of 3 cells at 3 different heights; the remaining 9 cells (out of the 12 cells forming the blind) contained only one thermometer. Channels 22, 24 and 26 were connected to the heat fluxometers on the blind surface facing the window (labelled 4, 5 and 6 "a"). In channels 23, 25 and 27 were connected the heat fluxometers on the blind surface facing the chamber (labelled 4, 5 and 6 "b"). In channels 28 to 34 were connected the blind surface thermometers also called external blind thermometers. Channels 28, 29 and 30 were connected to the cell surface facing the window of cells 9, 8 and 7 respectively. Channels 32, 33 and 34 were connected to the cell surface facing the chamber of cells 7, 8 and 9 respectively.

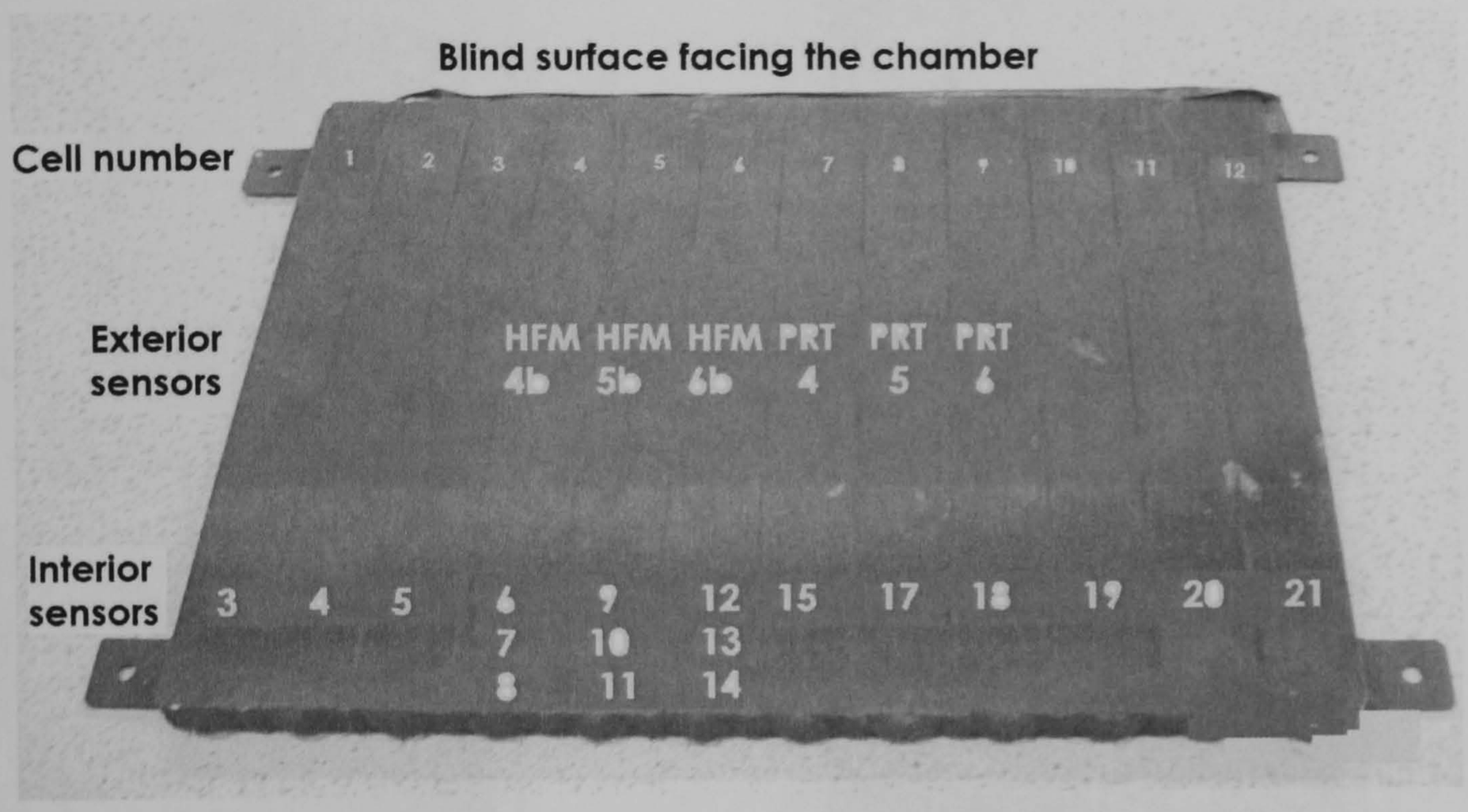

Figure 4.13 Blind surface facing the chamber sensors location

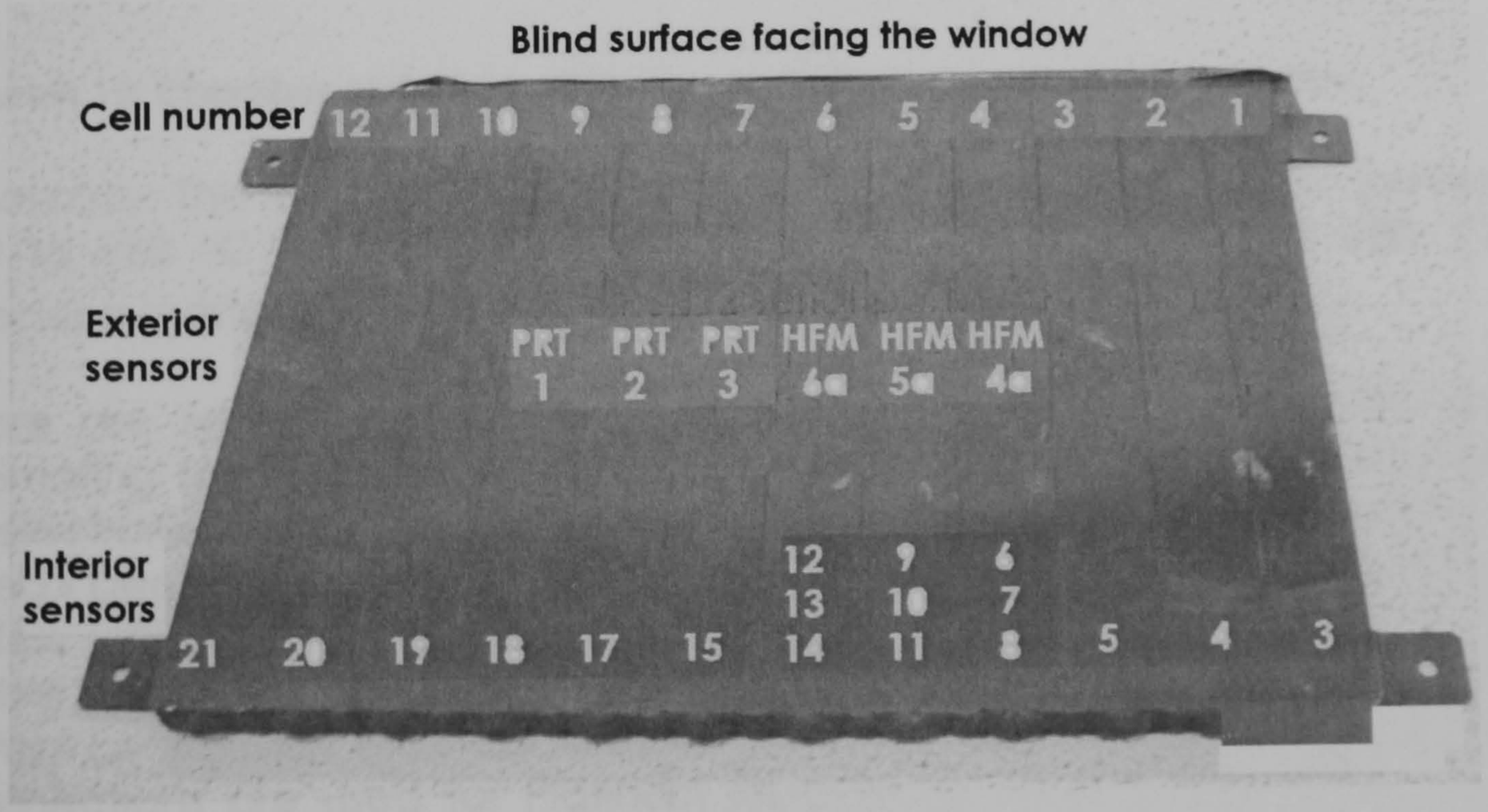

Figure 4.14: Blind surface facing the window sensors location

Channels 35 to 47(except 46) were connected to air temperature thermometers inside the chamber. In the chamber upper section were placed thermometers 1 to 4. In the central section of the chamber were placed thermometers 5-10. Thermometers to measure the inlet air temperature from the heat exchanger were placed in the lower part of the chamber. Channels 48 and 49 were connected to thermometers for exterior air temperature measurement. The anemometer was connected to channel 50.

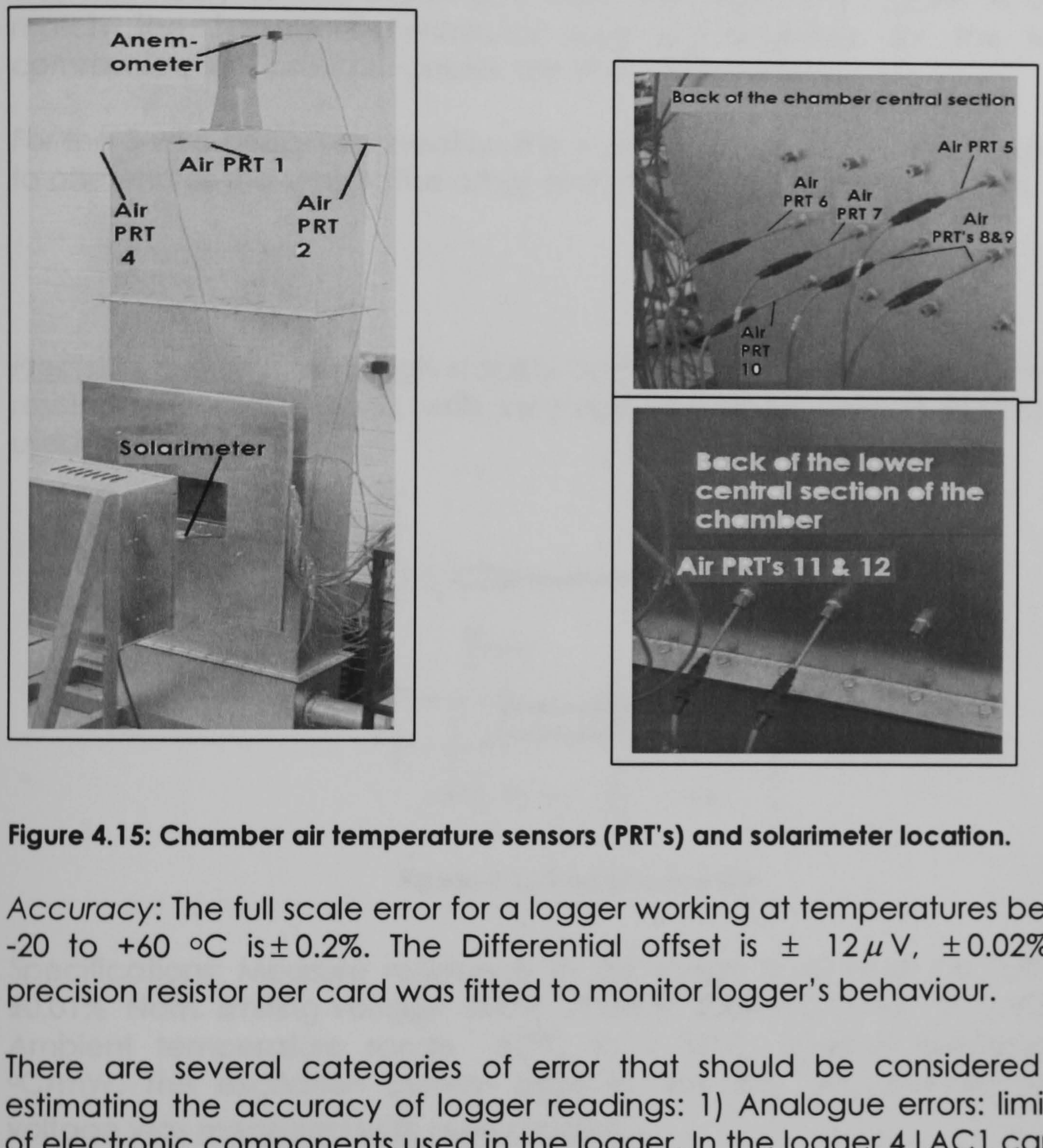

Figure 4.15: Chamber air temperature sensors (PRT's) and solarimeter location.

Accuracy: The full scale error for a logger working at temperatures between -20 to +60 °C is ± 0.2%. The Differential offset is ± 12 μV, ± 0.02%. One precision resistor per card was fitted to monitor logger's behaviour.

There are several categories of error that should be considered when estimating the accuracy of logger readings: 1) Analogue errors: limitations of electronic components used in the logger. In the logger 4 LAC1 cards are fitted. Depending on the wire connexion schemes fitted the accuracy differs (although not the logging configuration). 2) Cabling errors: due to cable resistance are smaller with 2-wire measurements. Only one of the sensor connection wires contributes to cable resistance error. 3-wire bridge connections are used for Platinum Resistance Thermometers (PRT). In this category are also included the inherent accuracy of sensors. 3) Arithmetic errors: due to approximations made by the logger when it performs

calculations and stores data. 4) Sampling errors: can be minimized by careful attention to sensor installation.

Connections:

The Delta-T logger records data from sensors and stores it in its own memory. The logger communicates to a computer by an RS232 cable. Five communication options are implemented on the logger's D connection. It was necessary to find which pins were carrying which signals in order to match the female D-connector style implemented for the logger's communication, as RS232 cables are not standardized.

For the 3-wire bridge connection the + and – terminals are wired separately to one end of the sensor. The other end of the sensor returns to earth.

Sensors:

Precision resistors: Very high stability and very high precision bulk metal foil resistors with radial leads, with very high tolerance resistors RS92AN were used.

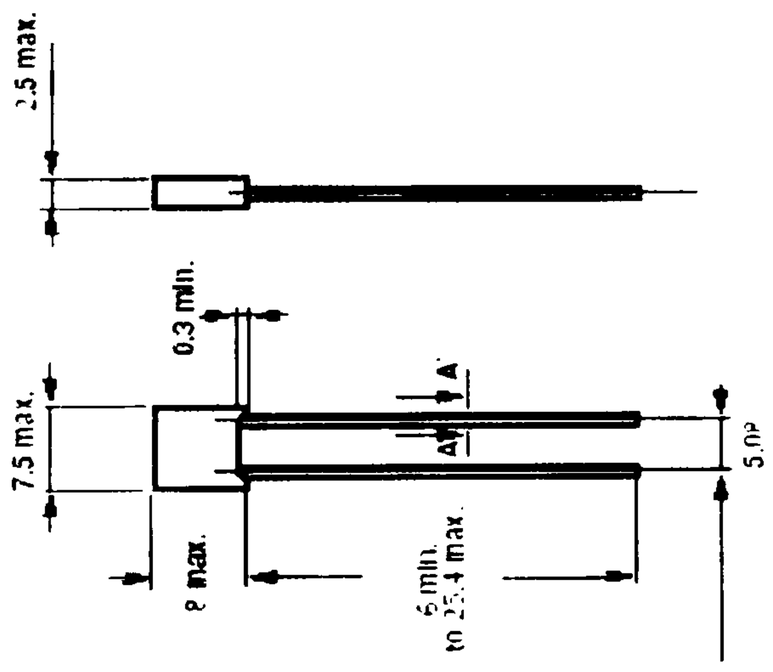

Figure 4.16 Precision resistor

Specifications: Measure resistance in the range 0 to 10.48 kΩ,Tolerance ±0.01% Nom. limiting voltage 200V , Stability 2000 h 0.1W at 70°C ±0.005%, Ambient temperature range -55°C to +125°C. Thermal resistance 0.14 °C/mW. The excitation current applied was 200 μA, and the resulting voltage was measured with auto-ranging.

Thermometers

Platinum resistance thermometers (PRT) were considered preferable to thermocouples[4.16] for the performance for precision temperature

---

4.16 With thermocouples errors can arise from measurements of the cold junction temperature

measurements. Their output is stable over long periods of use. PRT's temperature response is highly linear and repeatable. PRTs have positive temperature coefficient, i.e. resistance increase as temperature rises. The PRT works on the principle of resistance through a fine platinum wire as a function of temperature[4.17].

Specifications: The PRT used was PT1000, supplied by Rhopoint, with a nominal resistance at 0°C of 1000 Ω. The operating temperature range is between -50 to 750 °C. The temperature tolerance is ±1.28°C. The response time at 90 °C in air at 1 m/s is 8 s maximum. The maximum applied current is 3A.
To maintain the PRTs position, the thermocouples were placed in small stainless steel tubes 4 mm diameter, drilled in the desired positions, as suggested by(Wang, Amiri et al. 1999B)

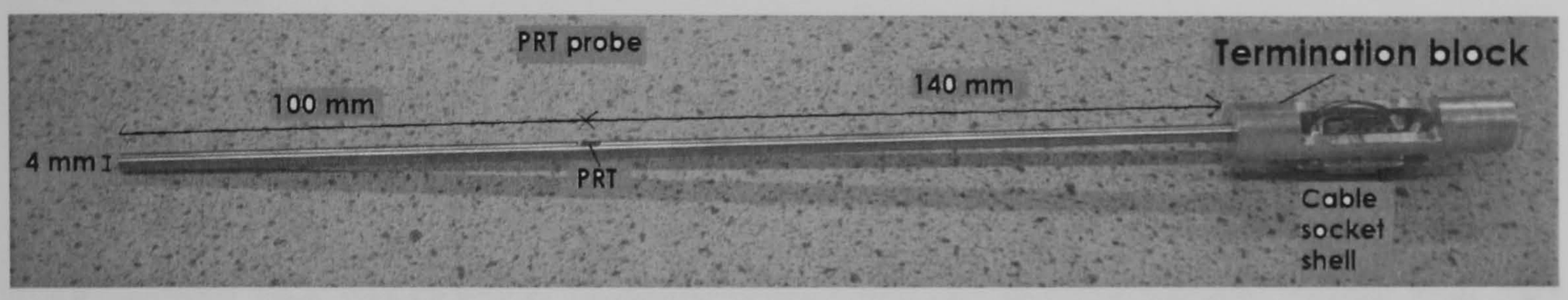

Figure 4.17: PRT probe

Accuracy:
The PRT uses the current from the logger. The electrical measurement excitation current is 2000 μA, auto-range; that is a voltage across PRT of 0.2Volts at 0°C. The logger will be measuring a voltage of 2V (V=RI = 1000 Ω x2000 μA). According to the logger's manual, the voltage reading for analogue accuracy should be set to the range 3, which is a voltage reading accuracy of ±262 mV and a resolution of 64 μA. (DeltaT)

Errors due to cable resistance are minimized with 2-wire measurements (only one of the sensor connections contributes to cable resistance error) , bridge technique

---

4.17 The resistance of the platinum resistor changes with temperature; this enables temperature to be measured by measuring the electrical resistance.

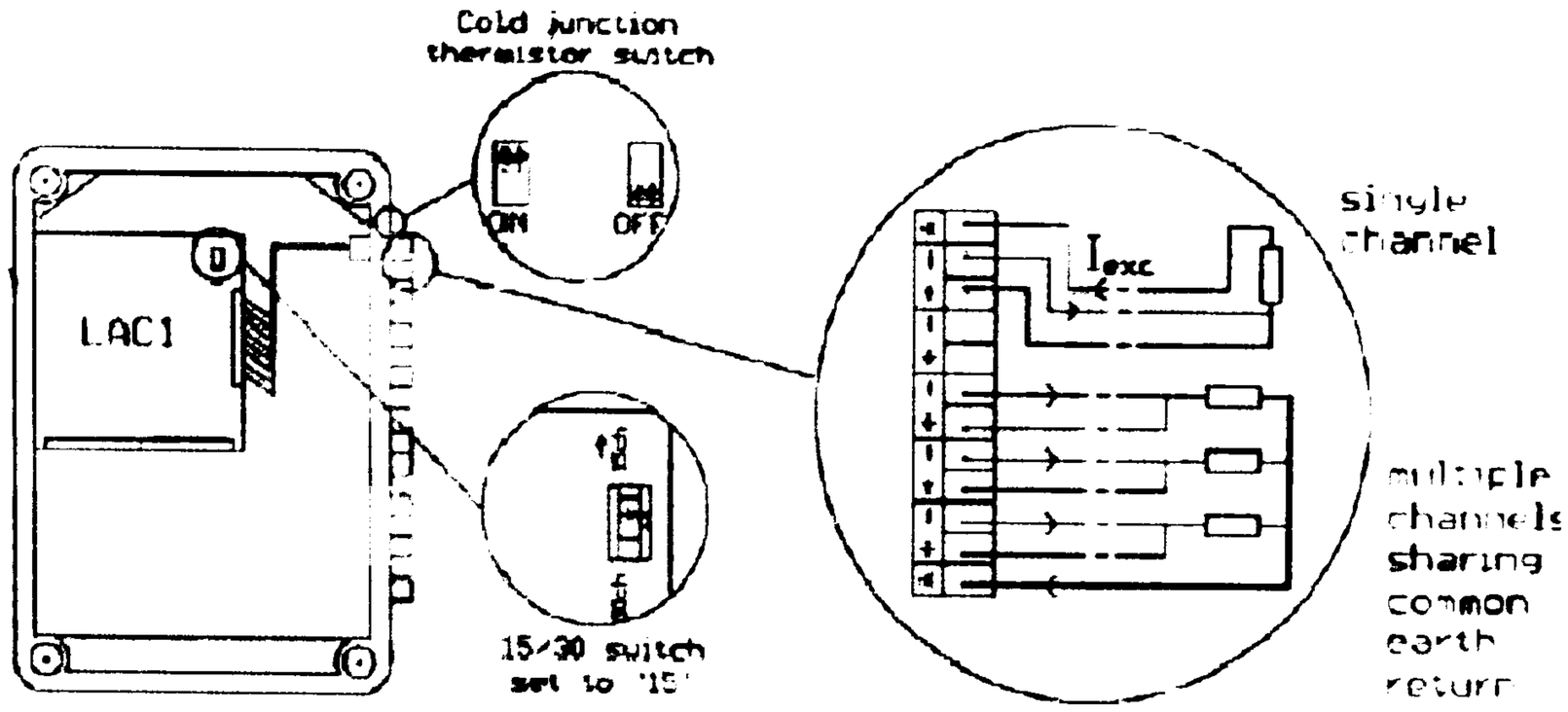

Figure 4.18: PRT connection to the logger: 3-wire resistance (DeltaT)

Error Analysis
Voltage contribution: With a voltage of 2V, the maximum error is 2V x 0.07% (full scale logger error) =1.4mV, expressed in Ω, this is 1.4mV / 2000μA = 0.7Ω. *Resistance contribution:* 1000Ω x 0.05% (error applied to resistance reading) = 0.5Ω. *Total maximum error:* = 0.7Ω + 0.5Ω = 1.2Ω

Converting the resistance reading error into a temperature: Using the PRT tables from the manufacturer for a 1000 Ω PRT, the change in resistance over a 100°C change in temperature is 3.851 Ω/°C. Then the resolution of 0.5Ω, maximum logger error for this sensor is 0.13°C.

For the logger software transformation to engineering units with a measurement range from 0 to 176.96 °C the next linearization table was used:

°C	0	25	50	75	100	125	150	175
ohms	990	1097.3	1194	1289.8	1385	1479	1573	1666

Table 4.3 PRT linearization table for engineering units transformation

Heat flux sensor:

A micro foil heat flux sensor was used for the measurement of heat transfer through the blind. This heat flux meter allows precision measurement of radiation, convection and conduction through any surface material. It is easy to attach to curved or flat surfaces. The way it works is: when heat flows into or out of the transducer surface, a small temperature difference develops across the thermal resistance of the transducer thermopile. Each of the thermocouple pair of the thermopile produces a voltage proportional to the heat flux.

A problem experimented during the use of this sensor was that after several tests the sensor detached from the blind and that the wire welding to the thermopile detached as well. The sensor was replaced and the test redone.

When only one sensor (among the 6 present) failed sporadically (jumped voltage reading) the test was not repeated.

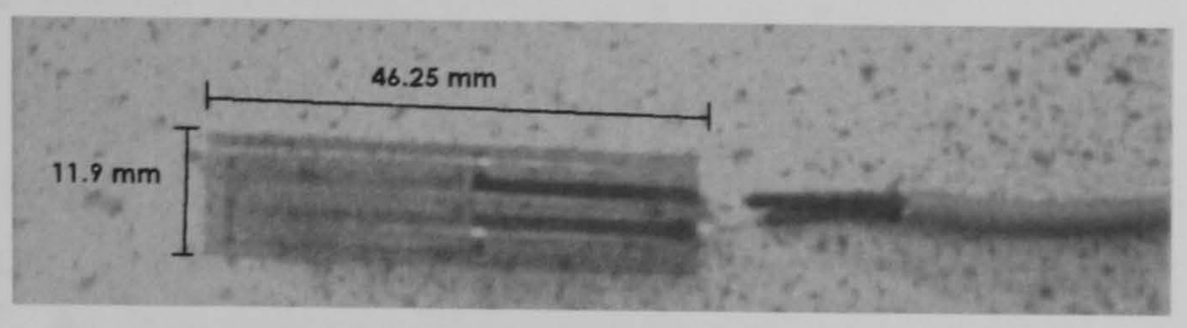

Figure 4.19: Heat flux sensor

Specifications: Nominal sensitivity =0.82 μV/(W/m^2). Maximum heat flux=95 kW/m^2. Response time= 0.6 s. Thermal capacitance=400 J/(m^2-°C). Maximum operating temperature= 150 °C. Not required power supply. Signal output = DC, voltage auto-range. For readings up to 50 W/m^2 the voltage range is ±4mV [4.18], classified as 1 in the logger.

Connection to logger:

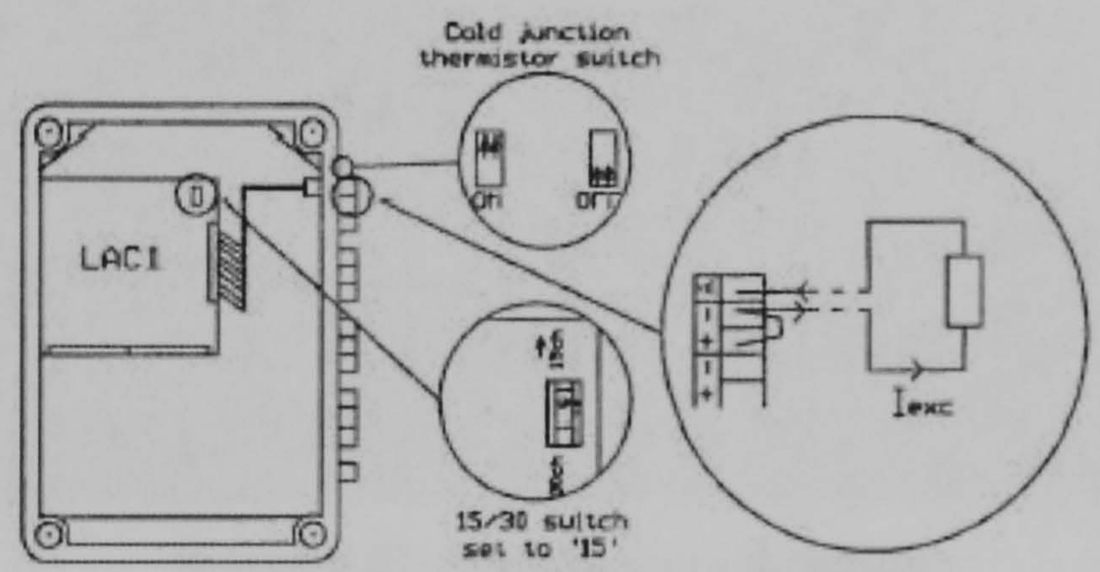

Figure 4.20 Heat flux sensor connection to logger (DeltaT)

For the logger software transformation to engineering units with a measurement range from -4 to 4 kW/m^2, the next linear conversion equation was used: $HF\left(\frac{W}{m^2}\right)=\frac{input(\mu V)}{sensitivity\left(\mu V/(W/m^2)\right)}$, that is, the linear conversion using factor and offset: $kW/m^2=\frac{0+mV}{0.82}$

Solarimeter or Payranometer:

Measures total energy of global solar radiation per unit area (direct and diffuse) received from the whole hemisphere. The sensor is based upon a silicon photo detector which is housed within a weather proof and anodized aluminum body. Mode of operation: a temperature gradient between a hot and a cold junction of a thermopile results in a linear electromotive

---

[4.18] That is, 4000 μV /82 μV /(W/m^2) is 48 W/m^2 ≈ 50 W/m^2

force (V) output (which was read by a data logger) that is proportional to the magnitude of irradiance. The voltage output is then converted into watts per square meter (W/m2)(CASELLA CEL 2004)

Homogeneous irradiation from the solar simulator is considered (validated by the previous study described in the "Lamps intensity monitoring, preliminary test". As the solarimeter was located over the aluminium shell[4.19], the irradiation received was 10 cm behind the actual solarimeter reading. For this reason a preliminary solarimeter readings calibration was done. The solarimeter was gripped in the window frame, behind the glass where the reading was required.

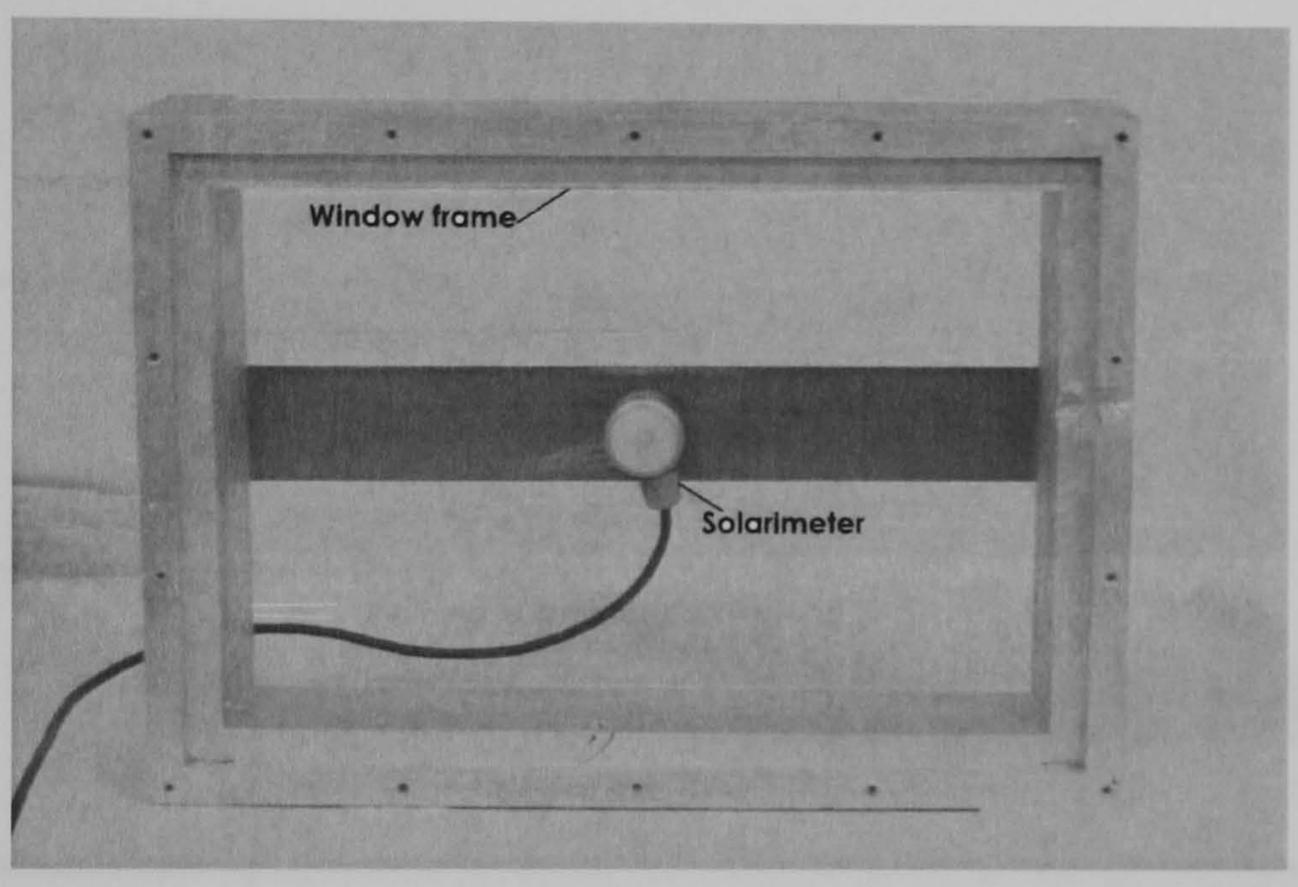

Figure 4.21: Solarimeter calibration

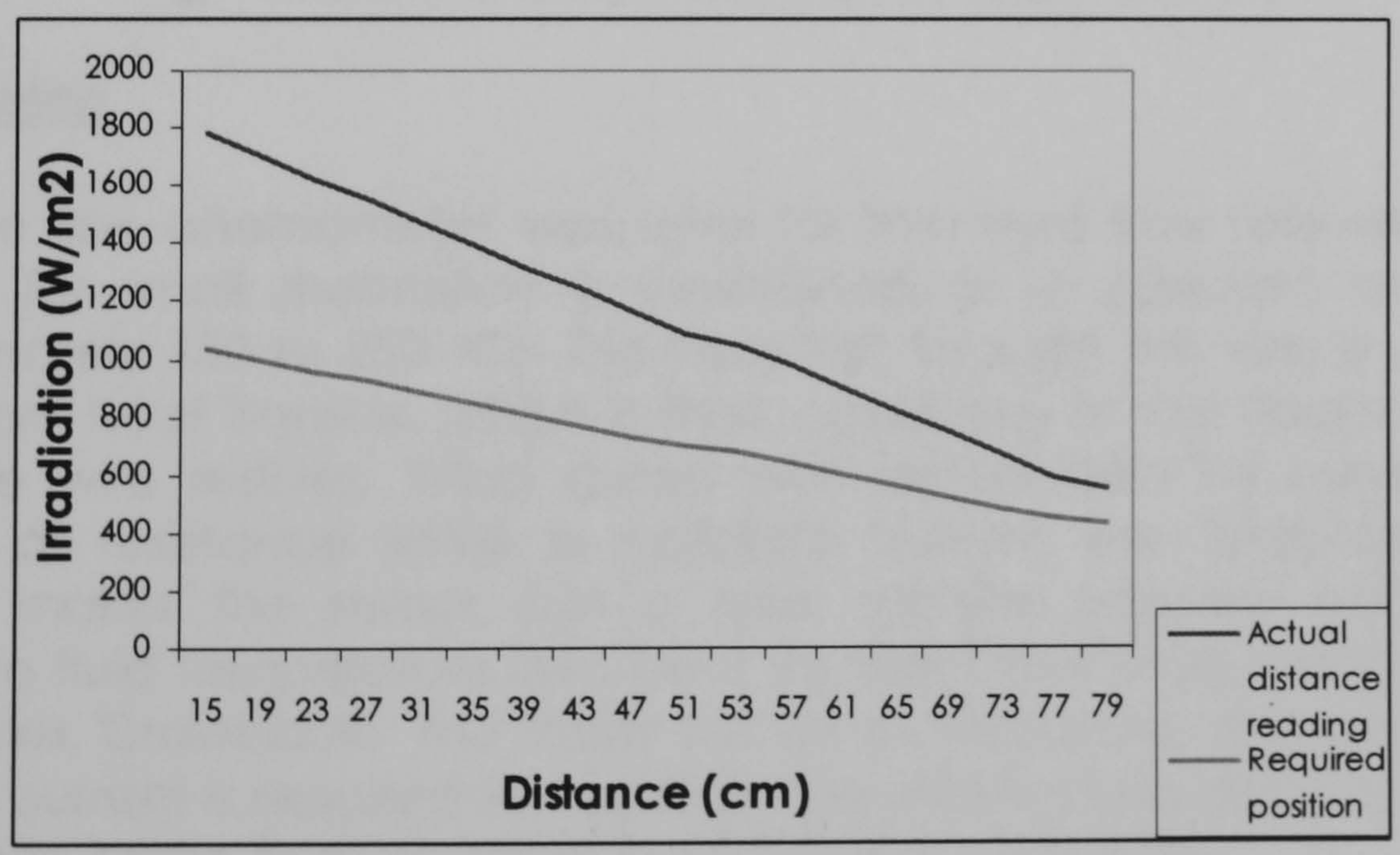

Figure 4.22: Solarimeter irradiation-distance calibration

4.19 The solarimeter couldn't be placed in the window (where the readings were required) as it would hinder the blind irradiated area.

Solarimeter Specifications: Part number: AWS solarimeter 187010B-03. Spectral range: 0.4 to 1.1 μm . Range: 0-200 W/m^2. Calibrated sensitivity 1.25 mV/(W/m^2). Response time <1s. Operating temperature range: -20°C to +40°C. Supply voltage 12Vdc. The solarimeter is fitted with a three core screened cable: blue=0V, red=+12 V supply, yellow=output.

Accuracy:
Using simulated solar light with uniform brightness in all directions the solarimeter reading has an accuracy of ±3%. In natural daylight conditions, the accuracy of the daily integrals of insulation are typically within ±5%.

Connection to logger:

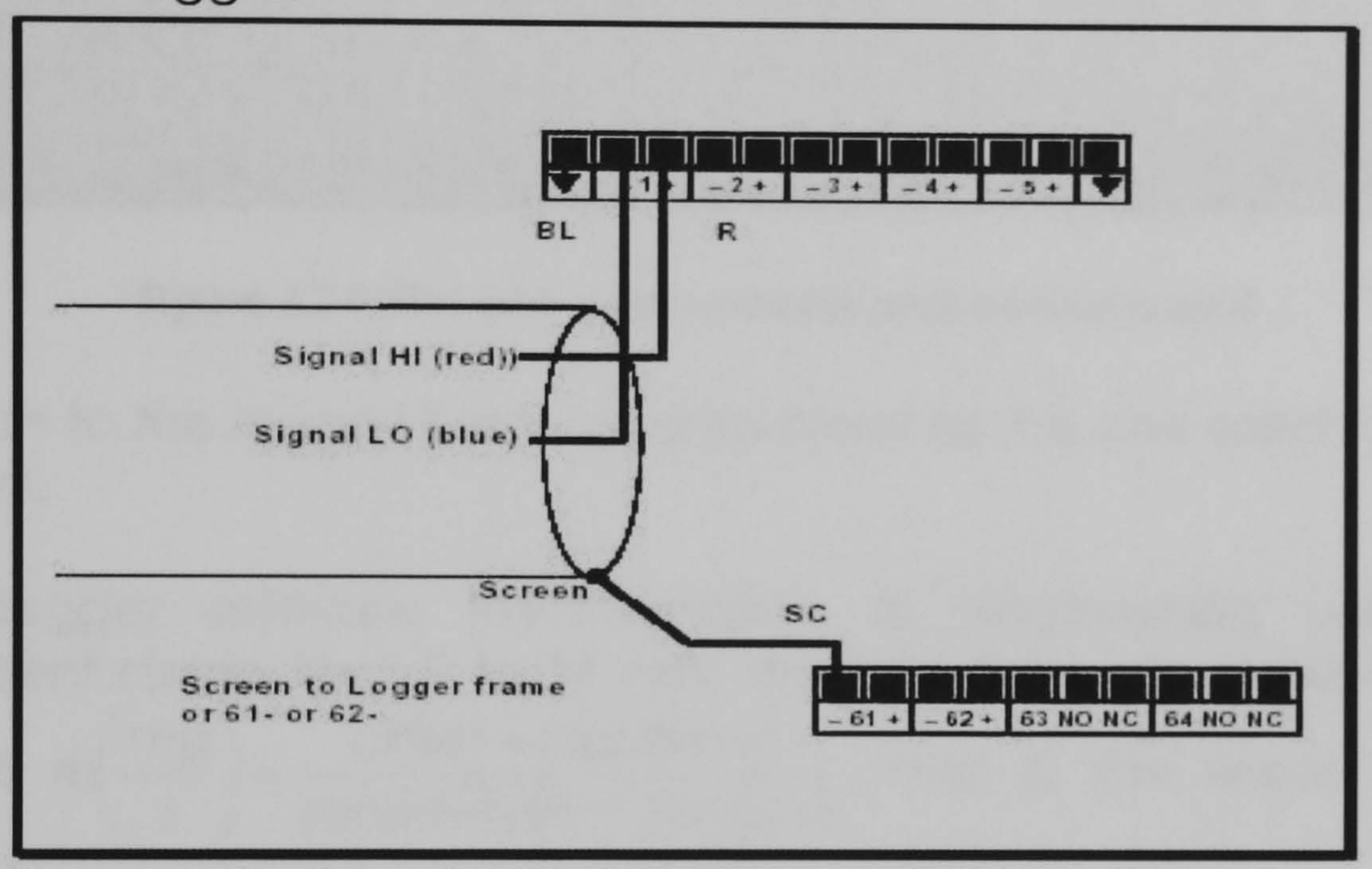

Figure 4.23: Solarimeter connection to logger (DeltaT)

Anemometer:

A hot wire fine anemometer was used for the mass flow rate readings. A thin wire (or small thermistor) is maintained at a constant temperature (approximately 150 to 250 °C). The heat loss through the wire is due to the convection heat transfer, which is then correlated to the steam velocity in which the wire resides. Wind speed was determined by measuring the variation of resistance while a constant current was maintained. This concept makes the sensor into a heat transfer element which is very sensitive to fluid temperature and heat transfer other than convection from the hot wire. Drawback: the faster the air moves across the anemometer, the more current is required to maintain the wire temperature, but the heat loss can also come from changes in ambient temperature.

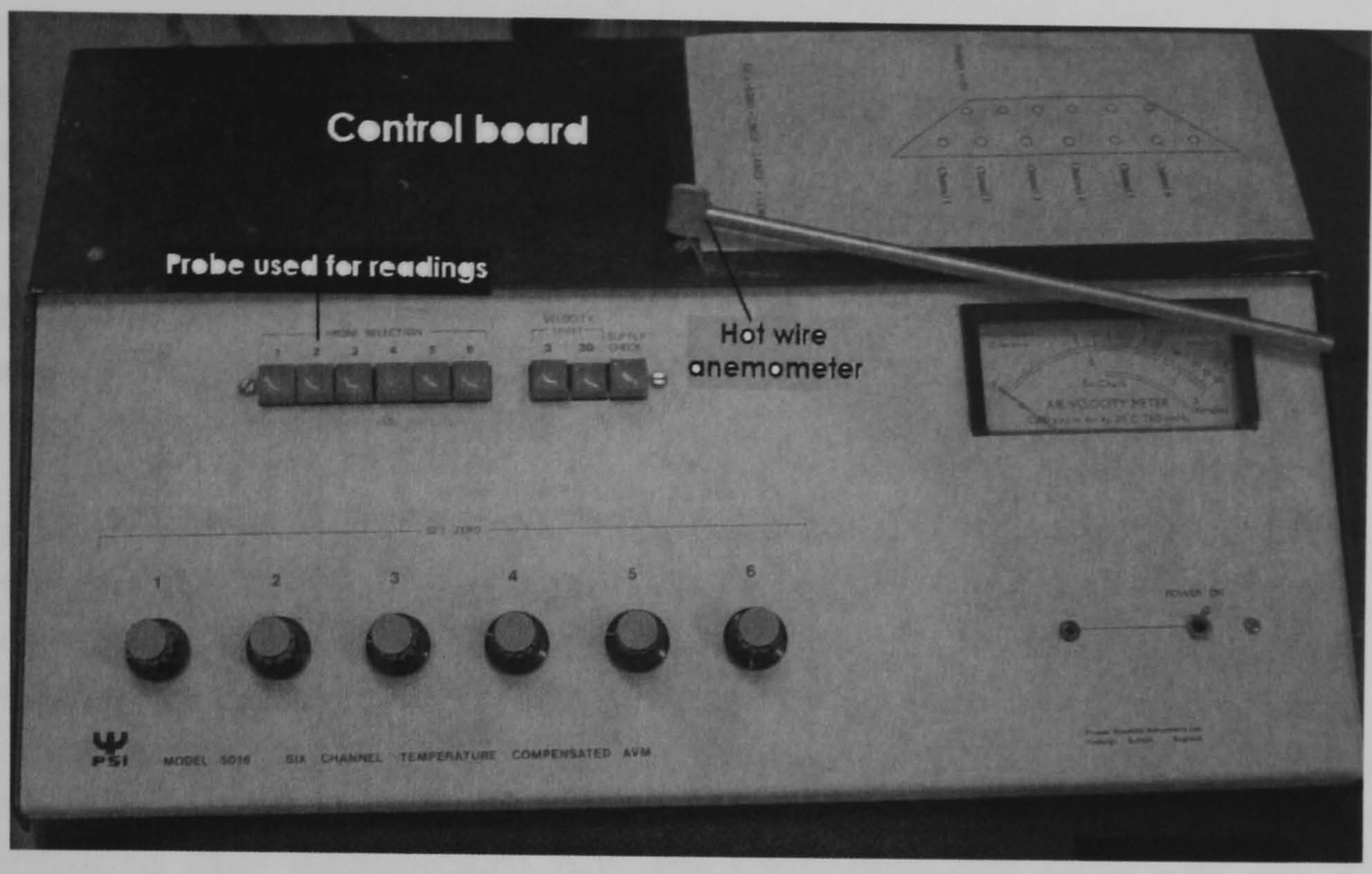

Figure 4.24: Hot wire anemometer and control board

Connection to the logger: Same arrangement as the one used for the heat fluxometers.

For the logger software transformation to engineering units with a measurement range from 0 to 64 m/s, the next linear conversion equation was used: $\dot{m}\left(\frac{mg}{s}\right) = \frac{offset + input(mV)}{sensitivity(mV/(mg/s)}$, that is, the linear conversion using factor and offset: $mg/s = \frac{-9638.4 + mV}{0.120}$. With a valid range of -17399.47 to 7799.46 mg/s.

The calibration of the anemometer is shown in appendix 4.E.

Simulation models

- Two main objectives were pursued when using the experimental apparatus for testing: PCM unit numerical model validation and system performance. The same rig was used for carrying out both experiments (labelled 1 and 2). Both testing schedules were performed according to an individual experimental design.

Experimental design

The objective of product development is to improve the performance features of the product relative to end user requirements and expectations (Ross 1995). User dissatisfaction with a product's performance increases as it deviates from a target value. Identifying known or expected sources of variability in the experimental units and reducing the effect of these sources of variability is one of the main aims of a designed experiment. In fact,

scientific research acquires meaning by assessing the relation between variables in terms of quantities or qualities. The two most elementary formal properties of every relation between variables are: 1) magnitude[4.20] (or size) and 2) reliability[4.21] (or truthfulness).

An effective set of experiments with an optimised set of control factors (design parameters specified to minimise the product sensitivity to noise) is extremely important for a robust performance assessment.

The experimental design space (or boundaries) are established by the factors included in an experiment and the set points (levels) at which they are evaluated. Approaches to specific experimental design spaces include: best-test-fix, one-factor-at-a-time, full factorial and orthogonal array (fractional factorials) experiments. In this work the Taguchi orthogonal array was the method selected, as it only requires a fraction of the full factorial combinations (the experiment has less runs) and the effect of each factor can be mathematically assessed independently of the effects of the other factors(Fowlkes and Creveling 1995).

Taguchi Orthogonal Array

The measured response of a design, in robust design, is referred to as the quality characteristic. The quality characteristic is the response that is measured at each treatment combination of the control factor and noise factors. In parameter design, an adequate selection of an effective characteristic to measure data is extremely important; as it should relate to the function itself and not to the symptoms of variability. (Fowlkes and Creveling 1995)

Taguchi robust design methods are set apart from traditional quality control procedures and industrial experimentation in:

1) The concept of quality loss function: It is loss due to functional variations. The greater the quality loss the lower the quality. Quality loss is a quadratic function of the deviation from a nominal value, and then the goal of quality improvement efforts should be to minimize the square deviations or variance around nominal specifications (StatSoftInc 1993)

2) The use of signal-to-noise (S/N) ratios: In order to avoid the necessity of having to model a large number of CFXNF (Control Factor X Noise Factor) interactions directly, the signal-to-noise ratio (S/N) is used to summarize the noise factor effects. The S/N ratio also helps reduce unnecessary complications due to interactions between the control factors. It also helps

---

4.20 Predict one based on the other

4.21 It says how probable it is that a similar relation would be found if the experiment was replicated with other samples drawn from the same population (we are interested in the sample only to the extend it can provide information about the population)

to achieve arithmetic additivity of the control factors while preserving information about the CFXNF interactions (Fowlkes and Creveling 1995)

3)The use of orthogonal arrays (OA) (StatSoftInc 1993): Orthogonal Arrays(OA) are a special set of Latin squares, constructed by Taguchi to lay out the product design experiments. Taguchi's OA analysis is used to produce the best parameters for the optimum design process, with the least number of experiments

Dr. Genichi Taguchi's approach to finding which factors affect a product in a Design of Experiments can dramatically reduce the number of trails required to gather necessary data. An orthogonal array selector can assist in determining how many trials are necessary, and the factor levels for each parameter[4.22] in each trial (Lohmeyer and Klepeiss 2001)

Number of Levels

Number of Parameters

	2	3	4	5
2	P=2, L=2	P=2, L=3	P=2, L=4	P=2, L=5
3	P=3, L=2	P=3, L=3	P=3, L=4	P=3, L=5
4	P=4, L=2	P=4, L=3	P=4, L=4	P=4, L=5
5	P=5, L=2	P=5, L=3	P=5, L=4	P=5, L=5
6	P=6, L=2	P=6, L=3	P=6, L=4	P=6, L=5
7	P=7, L=2	P=7, L=3	P=7, L=4	P=7, L=5
8	P=8, L=2	P=8, L=3	P=8, L=4	P=8, L=5
9	P=9, L=2	P=9, L=3	P=9, L=4	P=9, L=5
10	P=10, L=2	P=10, L=3	P=10, L=4	P=10, L=5
11	P=11, L=2	P=11, L=3		P=11, L=5
12	P=12, L=2	P=12, L=3		P=12, L=5
13	P=13, L=2	P=13, L=3		
14	P=14, L=2	P=14, L=3		
15	P=15, L=2	P=15, L=3		
16	P=16, L=2	P=16, L=3		
17	P=17, L=2	P=17, L=3		
18	P=18, L=2	P=18, L=3		
19	P=19, L=2	P=19, L=3		
20	P=20, L=2	P=20, L=3		
21	P=21, L=2	P=21, L=3		
22	P=22, L=2	P=22, L=3		
23	P=23, L=2	P=23, L=3		
24	P=24, L=2			
25	P=25, L=2			
26	P=26, L=2			
27	P=27, L=2			
28	P=28, L=2			
29	P=29, L=2			
30	P=30, L=2			
31	P=31, L=2			

THESE COMBINATIONS ARE NOT AVAILABLE – TRY RUNNING A SMALLER EXPERIMENT

Table 4.4: Taguchi Orthogonal Array's combination(Lohmeyer and Klepeiss 2001)

A commonly applied statistical treatment - The Analysis of Variance (ANOVA) - is used to analyse the results of the OA experiment in product design, and to determine how much variation each quality influencing factor has contributed. By studying the main effects of each of the factors, the general trends of the influence factors, towards the product, or process, can be characterised. The characteristics can be controlled, such that a lower, or a higher, value in a particular quality influencing factor produces the preferred result. Thus, the levels of influencing factors, to produce the best results, can be predicted (StatSoftInc 1993)

[4.22] A parameter is an independent variable that may influence the final product, whereas a level is a distinction within that parameter(StatSoftInc 1993).

Computer model validation, experiment 1

A simplified version of the latent heat storage system was tested to validate the computer model. The major benefit of this approach is that the results obtained can be applicable to broad classes of LHSS. An experiment labelled "Experiment 1" was designed regarding the model validation.

Experimental design:

All conditions (radiation flux, air temperature and material properties) were kept constant. The experiment was designed having as parameters (also called factors): The weather conditions, given by the Mexican 1) province and 2) season selected with 2 factor levels. The third parameter was time of the day (Day/Night). With these conditions an average temperature to be provided inside the rig was set and the solar simulator condition: ON/OFF.

Experiment 1
L4: 3 factors; all factors have 2 levels

Run	F1: Province	F2: Season	F3: Temp. Conditions
1	BC	Winter	1
2	BC	Summer	2
3	CH	Winter	2
4	CH	Summer	1

Table 4.5: Taguchi L4 for experiment 1

In order to take advantage of the testing, at the same time that the theoretical model results were assessed, two other aspects were looked at. 1) The LHSS charging behaviour during a winter and a summer day and a winter and a summer night in each province (an average temperature during the season representative day was applied). That is charging with and without radiation during cold and hot days and nights was appraised. This experiment was labelled "1-melting" 2) The LHSS discharging behaviour during winter and summer nights in each province placing the blind inside and outside the dwelling (using the lowest interior and exterior air temperatures). In previous research has been found that an exterior building element containing PCM can store slightly more energy than PCM contained in an interior LHSS. This is probably because it is better discharged at night, and next day is able to store more energy. This experiment was labelled "1-solidification"

For both experiments a Taguchi L4 was used.

Experiment 1
L4: 3 factors; all factors have 2 levels
For melting

Run	F1: Province	F2: Season	F3: Time of day	Average Temp	Lamp
1	BC	Winter	Day	17.22	ON
2	BC	Summer	Night	39.45	OFF
3	CH	Winter	Night	27.94	OFF
4	CH	Summer	Day	34.55	ON

Table 4.6: Taguchi L4, for experiment 1-melting

Experiment 1
L4: 3 factors; all factors have 2 levels
For solidification

Run	F1: Province	F2: Season	F3: Interior/Exterior Temp Cond	Lowest Temp	Lamp
1	BC	Winter	Interior	12.7	OFF
2	BC	Summer	Exterior	24.5	OFF
3	CH	Winter	Exterior	12	OFF
4	CH	Summer	Interior	28.8	OFF

Table 4.7: Taguchi L4 for experiment 1-solidification

Methodology

Capric Acid (Melting Temperature=23.5 °C) was the PCM selected to be used in this experiment. It was selected due to its stability, and the fact that it's melting temperature is within room thermal comfort range.

The aluminium tubes (also called cells) forming the blind had a section of 1.27cm x 2.54cm. The unit was intended to be thin in order to assure for thermal stability.

Time duration of the experiment: 5 hours is the time expected for the LHSS for a complete change of phase.

Testing proceedings:

- Storage PCM bottles were heated inside an oven above their fusion temperature, and poured in the liquid state into the aluminium tubes.
- Firstly a heating test was performed. The blind (LHSS) was cooled below the PCM solidification temperature (the experiment started with the PCM in the solid state).
- The heat exchanger connected to the chamber was set to the required melting temperature, and this heat was supplied inside the chamber by a constant air mass flow rate of 7g/s.
- Solar simulator (if required) was switched on
- Logger was started
- The conditions were kept constant for about 5 hours. The data was downloaded from the logger to the computer
- After 5 hours the logger was stopped.

- Then the cooling test was performed. The blind with the liquid PCM (melted from the previous test) allows the experiment to start with the PCM in liquid state
- The heat exchanger was set to the required fusion temperature to carry out one of the cooling tests; the same air mass flow rate was applied to deliver the cooling inside the chamber.
- Logger starts saving data for the new test
- The conditions were kept constant for about 5 hours. The data was downloaded from the logger to the computer
- All devices switched off

System performance, experiment 2:

The main purpose is to analyse the variables that affect the system thermal behaviour, in order to improve and/or optimize the system's operation. This experiment was labelled "Experiment 2".

Experimental design

Previous research findings on variables modifying the system's efficiency were brought together in this test to evaluate the effect that each one (and the interaction between them) had on the overall thermal performance of the LHSS.

- **Temperature ranges**: The weather conditions, given by the Mexican 1) province and 2) season provide 2 factors for this experiment. Irradiation values will be related to the temperature conditions selected.
- **PCM melting temperature:** to promote a more efficient behaviour as a heat storage unit. The case of multiple PCM cells and the case with all cells filled with the same PCM are compared. A range of melting points (multiple PCM) is useful because it extends the temperature range of the storage unit. Existing diurnal variations of temperature envisage the requirement of a range of melting temperatures. The attachment of multiple melting temperature PCM units, could help diminish the occurrence of slowing rate of core PCM melting.
- **PCM volume**: A greater PCM volume stores a larger amount of energy, but if the change of phase is not performed by the whole volume, (due to conditions lead by the volume) its effect is not straight forward
- **Surface container insulation:** For control over the rate of energy stored/released from a LHSS. The heat losses from the surface opposite the surface being heated for charging can be minimised by insulating that surface. If the energy stored is required in the interior, losses of the energy stored to the exterior could be minimized by insulating the surface facing the exterior.
- **Mass flow rate of HTF**: An important element determining the charging/discharging rate according to previous research. In the present

work its effect and interaction with other elements of the LHSS is evaluated.

- **Mode**: As the variables interactions and effect in the thermal behaviour of the unit differ during charging and discharging, the mode (heating/cooling) was considered an important variable.

Experiment 2
L8: 7 factors; all factors have 2 levels

Run	F1: Province	F2: Season	F3: PCM	F4: Cell thickness (in)	F5: Mass flow	F6: Insulation	F7:Mode
1	CH	Summer	Single (C-P)	1.5	Low	Insulation	Melting
2	CH	Summer	Single (C-P)	0.5	High	no-insulation	soldification
3	CH	Winter	Multiple (C-P,T,H)	1.5	Low	no-insulation	soldification
4	CH	Winter	Multiple (C-P,T,H)	0.5	High	Insulation	Melting
5	BC	Summer	Multiple (C-P,T,H)	1.5	High	Insulation	soldification
6	BC	Summer	Multiple (C-P,T,H)	0.5	Low	no-insulation	Melting
7	BC	Winter	Single (C-P)	1.5	High	no-insulation	Melting
8	BC	Winter	Single (C-P)	0.5	Low	Insulation	soldification

Table 4.8: Taguchi L7 for experiment 2

Approaches to system performance analysis

Energy stored/released

The objective is to determine the relation between the variation of energy stored/extracted with the variation of dependable variables as: Inlet air temperature, irradiation rates, PCM volume, and air flow rate. The cyclic behaviour of the LHSS can be illustrated by determining the temperature history of the charging process and the temperature dependence of the PCM total enthalpy[4.23] . A maximum energy stored can be obtained as the temperature of the PCM volume changes from a reference value to a maximum value. (Banaszek, Domanski et al. 1999)

Parameters such as accumulated energy, maximum energy storage capacity, charging ratio, temporal energy stored, total time of charging and discharging time changes of melted and solid phases of the medium in the whole unit, can be used to study the process of charging and discharging (Banaszek, Domanski et al. 1999)

Energy stored in the volume: $Q_{\max} = \rho V_{PCM} \Delta H(T_{\max,} T_{ref})$

Accumulated energy storage: $Q = \rho V_{PCM} \Delta H(T, T_{ref})$

Parametric studies included in this work assess the effects of the various design and operating conditions on the heat transfer process. The total energy stored can be correlated to the average output heat load.

4.23 The later was obtained with the DSC test

Encapsulated PCM insulated

The function of blinds in windows is to reduce solar radiation heat gains. In the present study blinds supplementary function as opaque interactive thermal storage system is evaluated. In experiment 2 aluminium blinds with/without insulation are compared to PCM blinds with/without insulation

In previous research transparent PCMs inside glass containers for its use in windows has been studied (Buddhi and Sharma 1999). Little work has been done regarding different PCM transmittance, which is crucial for its use in windows.

Also PCM contained in exterior building elements has been studied previously, but operating more as an insulator. Only a fraction of the energy stored during the day can be conducted to the interior, as the remaining fraction is lost (and probably at a faster rate, due to the larger temperature difference) to the exterior.

The difference between a PCM and a common thermal insulation system is that the latter always prevents the transfer of incoming/outgoing heat. That is, a PCM insulation system is more likely to prevent over/under heating by allowing heat to be stored/released as required.

System's efficiency

The overall efficiency is defined as the ratio between the enthalpy withdrawn from the unit during discharging and the enthalpy input during the process of the unit loading.

There are two ways of analysing the discharging performance of the PCM: by determining the amount of energy transferred to the cooling air or by determining the energy still stored in the PCM medium. In previous research has been found that at the end of discharging still 23% of the total energy remains in the PCM material.(Banaszek, Domanski et al. 1999)

Changing ratio: $$r_{CH} = \frac{Q}{Q_{\max}} = \frac{\Delta H(T, T_{ref})}{\Delta H(T_{\max}, T_{ref})}$$ **Equation 4.1**

Material investigation

An accurate determination of the PCM thermal properties and cyclic (charging/discharging) thermal behaviour is critical for the elements selection, design, performance and analysis of the LHSS.

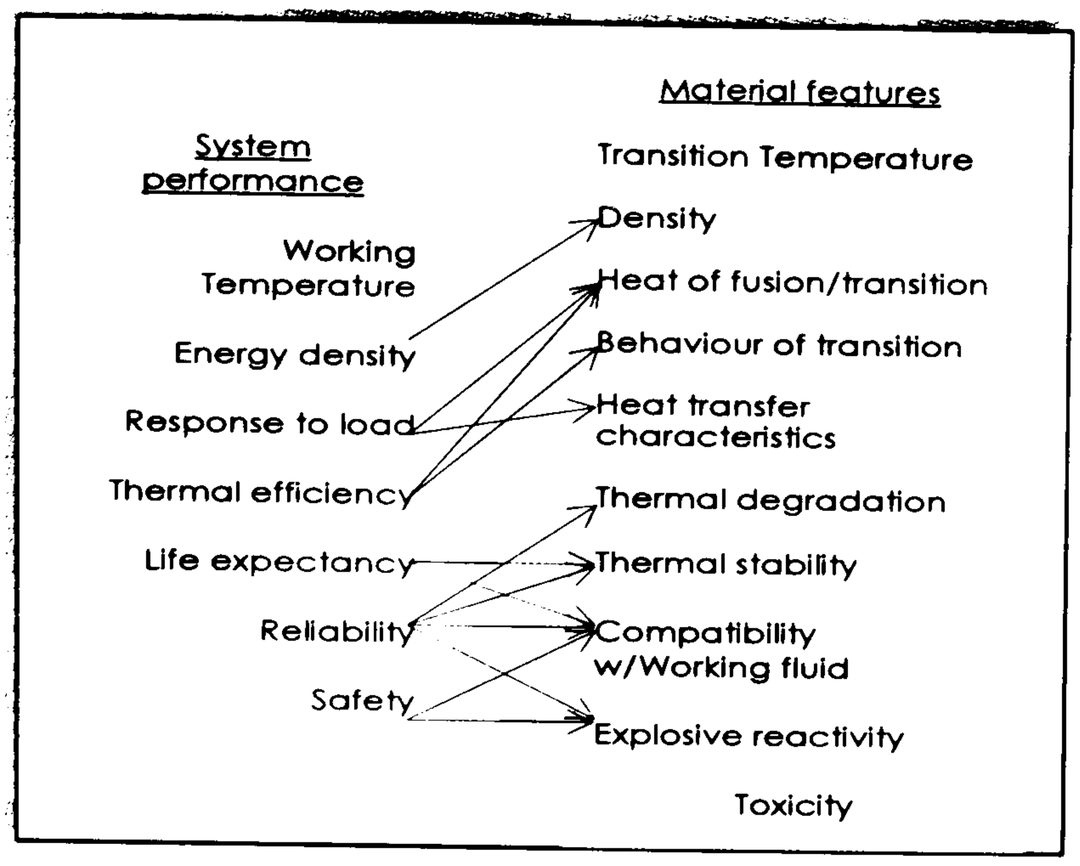

Figure 4.25 Material features and system performance correlation (Syed, Kumar et al. 1997)

The approaches to material investigation in this study are the following.

PCM selection criteria

As previously mentioned, the candidate PCM should have the following characteristics: i) melting temperature in the desired range, ii) high latent heat of fusion, high thermal conductivity, high density iii) thermal stability during repeated cycles; iv) low volume charge v) non-corrosive, non-toxic and non-flammable; vi) exhibit no Supercooling.

Compatibility of the PCM's melting temperature with the total of sunny periods in the day time is one of the critical issues in the PCM selection criteria (Esen, Durmu et al. 1998).

The melting temperature range chosen will depend on the climatic conditions imposed. According to EERE, the optimum melting temperature for a climate where the heating of buildings is the predominant requirement is between 18.3-22.2 °C and between 22.2-26.1 °C for climate where cooling is required(EERE 2003). A similar range for maintaining comfort indoor temperature was suggested by D. Feldman. For a heating climate a PCM melting temperature ranges between 17-23 °C and 24-27 °C in cooling climate (Feldman, Banu et al. 1995).

Peippo considered heating only by radiation and concluded that the optimal diurnal storage occurs with a melt temperature 1-3 °C above room temperature (Kauranen, Peippo et al. 1991). For this study charging by solar radiation is as well considered, but also the charging of the unit by internal heat gains (represented by the supplied air temperature to the room resultant from the TAS simulation). This mode of charging the unit shows the behaviour of the system on overcastted conditions.

Suitable PCM for Mexican weather operating temperature:

The PCM phase change temperature region must correspond to the intended operating temperature. Mexico has a predominantly cooling climate, although in the north during winter heating is required. The climatic ambient temperatures range from 7 to 42 °C in relation to the need for heating or cooling in buildings.

The table presented in appendix 2.C assisted in the selection of the PCMs used for testing the proposed storage blind system. The organic PCM group (fatty acids and paraffins) provides a range of material alternatives comprising melting temperatures within the required range. Complex lipids[4.24] additionally have the advantage of good crystallization and self-nucleation properties. Among materials with comparable melting temperatures and good crystallization and nucleation, those with the highest heats of fusion at affordable prices were selected.

In order to verify literature values pf the PCM properties, check for mixtures homogeneity and behaviour repeatability, thermal analysis was carried out.

Four PCM mixtures and two pure PCM materials were selected for a preliminary thermal analysis testing:

- Organic Hydrate Compound (Trimethylolethane-Urea-Water)
- Fatty acid Mixture (Capric-Lauric)
- Fatty acid Mixture (Capric-Myristic)
- Fatty acid Mixture (Capric-Palmitic)
- Fatty acid Mixture (Lauric-Myristic)
- Tetradecanol
- Paraffin hexadecane

According to the results of an experimental investigation (as it will be discussed later) the mixtures finally chosen for use in the rig test were: capric acid for experiment 1, Capric-Palmitic, Tetradecanol and paraffin hexadecane for experiments 2 and 3.

Melting/ freezing characteristics

Crystallization, supercooling, superheating, phase segregation:
A thorough perception of the charging/discharging process is required to improve a LHSS performance (Hernandez-Guerrero, Aceves et al. 1999). The fluctuation of the heat transfer mode and rate are given by the solid-liquid phase transition phenomenon (Banaszek, Domanski et al. 1999).

This section is concerned with the charging/discharging features of particular PCMs. Natural convection taking place within the melt due to the

---

4.24 Characteristically contain fatty acids and waxes

physics of specific LHSS and operation has not been studied in this work. Natural convection is not ascribed to solely intrinsic properties of a specific PCM, but rather to a correlation of the storage system operation and conditions imposed[4.25].

In the thermal analysis carried out by using differential scanning calorimetry (DSC) the melting/freezing characteristics of the PCMs were assessed.

In the case of solidification, the formation of solid nuclei and their growth are necessary for the crystallization to occur. The performance of the storage system deteriorates in cases where supercooling, or superheating occurs and no change of state takes place[4.26]. In those cases a nucleating agent has to be provided.

If the chemical composition of the material is altered due to the presence of phase segregation, thickening agents can hold the structure of the PCM together and so to reduce the segregation.

However, if any of these phenomena were detected in the PCMs studied those PCMs were considered unsuitable for the purposes of this work. Nevertheless further work on the chemistry of those materials can provide new alternatives as latent heat storage materials.

Thermal analysis[4.27]:

Differential scanning calorimetry was the technique used to determine the thermal properties of the selected PCMs. This method introduced by Perkin Elmer Co in 1964, is based on the computation of the inherent change in temperature or the development or absorption of heat of the sample as it goes through a transformation or reaction. These changes are identified relative to an unvarying reference material simultaneously undergoing the same temperature program. (Turi 1997)

DSC is configured to quantify the real amount of power (rate of heat flow in watts) concerned directly with the coupled thermal event, rather than its indirect effect, the plain change of temperature of the sample.

The power compensating DSC maintains the temperature difference between the sample pan and the reference pan very close to zero. The DSC setting utilizes software compensation to convert the temperature difference to heat flow based on prior calibration experiments. A heater is

---

4.25 i.e. The temperature difference between the wall and the melting point of the PCM can be important during convection mode of heat transfer in liquid.

4.26 In the case of super cooling, a liquid cooled below its freezing point, and in the case of super heating, a liquid heated above its boiling point.

4.27 A group of techniques in which a property of the sample is monitored against time or temperature while the temperature of the sample, in a specified atmosphere is programmed (Turi 1997)

driven in the appropriate sample or reference portion of the cell according to the imbalance detected by resistance thermometers placed into a bridge circuit.

The additional electrical power needed to keep the bridge circuit in equilibrium is proportional to the amount of heat needed to compensate for the changes in heat capacity of the sample and any heat evolved or absorbed by the processes that are taking place. The power is then integrated over the time of the thermal event to find out the associated thermal energy.(Turi 1997)

If additional power is supplied to the sample, the process is endothermic[4.28]. If it is supplied to the reference side, then the process is exothermic.

The DSC testing output is the energy-time diagram, also called thermogram (melting and freezing curves). With the information obtained it is possible to thermally characterise a material. With the form of the endothermic or exothermic peaks on the thermogram, it is possible to determine the melting/freezing point/ranges, the enthalpy of transitions (energy storage, heat of fusion and solidification), the rates of crystallization and reaction (sample purity), glass transition phenomena, nucleation of crystals (nucleation phenomena, degree of supercooling) and the thermal and oxidative stability. It is also possible to evaluate the heat capacity and thermal conductivity, as a function of temperature and with different proportions of mixtures to obtain phase diagrams. (Turi 1997)

DSC testing

TA instruments Modulated Differential Scanning Calorimeter[4.29] (MDSC) was the equipment used for the thermal analysis of the potential PCMs. This instrument has an accuracy of 1-2%. The DSC was calibrated with an indium standard for a thermal enthalpy and temperature / baseline. Mass balanced to ±0.1 mg. For heat capacity (error ± 0.008 kJ/mol) calibration an indium disc[4.30] was used.

Methodology:

4.28 The thermodynamic convention is that work performed on, energy supplied to, or heat input into the system by or from the surroundings is positive. Therefore power applied to the sample has a positive sign so that the integral yields a positive value of enthalpy change consistent with the endothermic process. (Turi 1997)

4.29 DSC is an analytical technique in which the difference in heat flow between a sample and an inert reference is measured (voltage difference measured by thermopiles) as a function of time and temperature in a controlled environment. MDSC is an extension of conventional DSC whereby an oscillatory (sine wave) perturbation is superimposed onto an underlying linear (isothermal or dynamic) temperature profile, this permits the measurement of heat capacity (reversing heat flow)

4.30 Enthalpy of fusion 3.296 kJ/mol, melting temperature 156.61 °C, error +/- 0.008 kJ/mol

The thermal analysis of the PCMs selected was carried out in two stages: a first preliminary testing of small samples of the PCM mixtures prepared, and a second testing with a sample of the total volume mixture prepared for the rig testing.

For the first test ten ml mixture samples were prepared for each of the selected mixtures by mixing the components in a round bottom flask heated in a heating mantle at approximately 60 °C and using a magnetic stirrer.

Once the mixture samples were ready, each mixture was stored in ten ml glass containers and kept in a fridge until the DSC test was carried out. The DSC tests were performed under atmospheric pressure and in a nitrogen atmosphere. The refrigerated PCMs to be tested were heated in an oven above their fusion temperature, and the liquid sample placed into the DSC aluminium pan. Pan samples of 5-15 mg were prepared[4.31] and weighed with a precision balance. The pan was sealed by using an hermetic pan sealer and introduced at room temperature into the DSC (some of the PCM samples were already in the solid state at this stage). The cooling accessory connected to the DSC was kept ON.

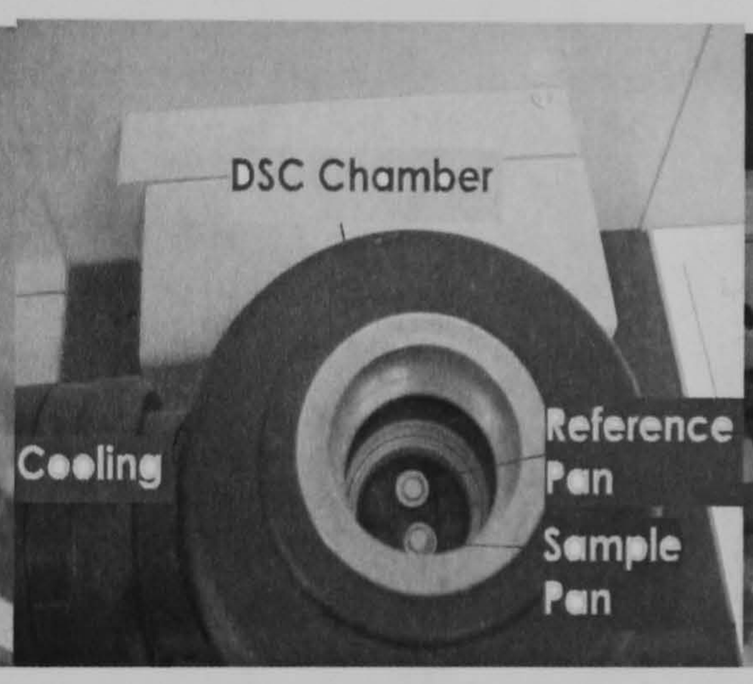

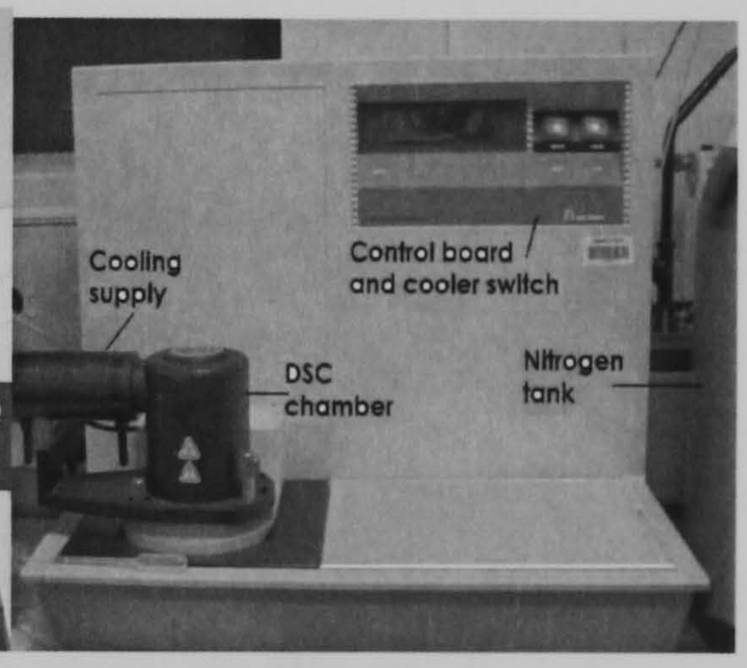

Figure 4.26: Hermetic pan sealer Figure 4.27: Reference and sample pans Figure 4.28: DSC

Method for segment conditions:

Conventional thermal analysis applies a programmed series of heating and cooling ramps with possible isothermal periods interspersed between them. These ramps have usually, but not necessarily, linear rates. The amplitude of the temperature difference signal is enlarged with increasing heating rate because the thermal event occurs in a shorter period of time. (Turi 1997).

These conditions varied slightly from sample to sample, according to the melting point expected (literature), but roughly the same method was followed for each sample:

[4.31] The dimensions of the open pan used were 7.2 mm diameter and 1.6 mm height with a maximum capacity of 50ml. The sealed pan used was 6.8 mm diameter and 2.6mm height with a capacity of 15 ml.

- Ramp 10 °C/min to -20°C
- Initial Temperature = -20°C
- Modulate +/- 1°C every 60 seconds
- Ramp 5°C/min to 40°C
- Isothermal 0.50 min
- Ramp 5°C/min to -20°C

Exploratory mixtures:

The results of the DSC showed:

Tetradecanol, Capric-Palmitic, and Capric-Myristic mixtures showed good repeatability, stability and had defined changes of phase with no phase separation, hysteresis or supercooling. The measurements were in good agreement with the majority of published values.

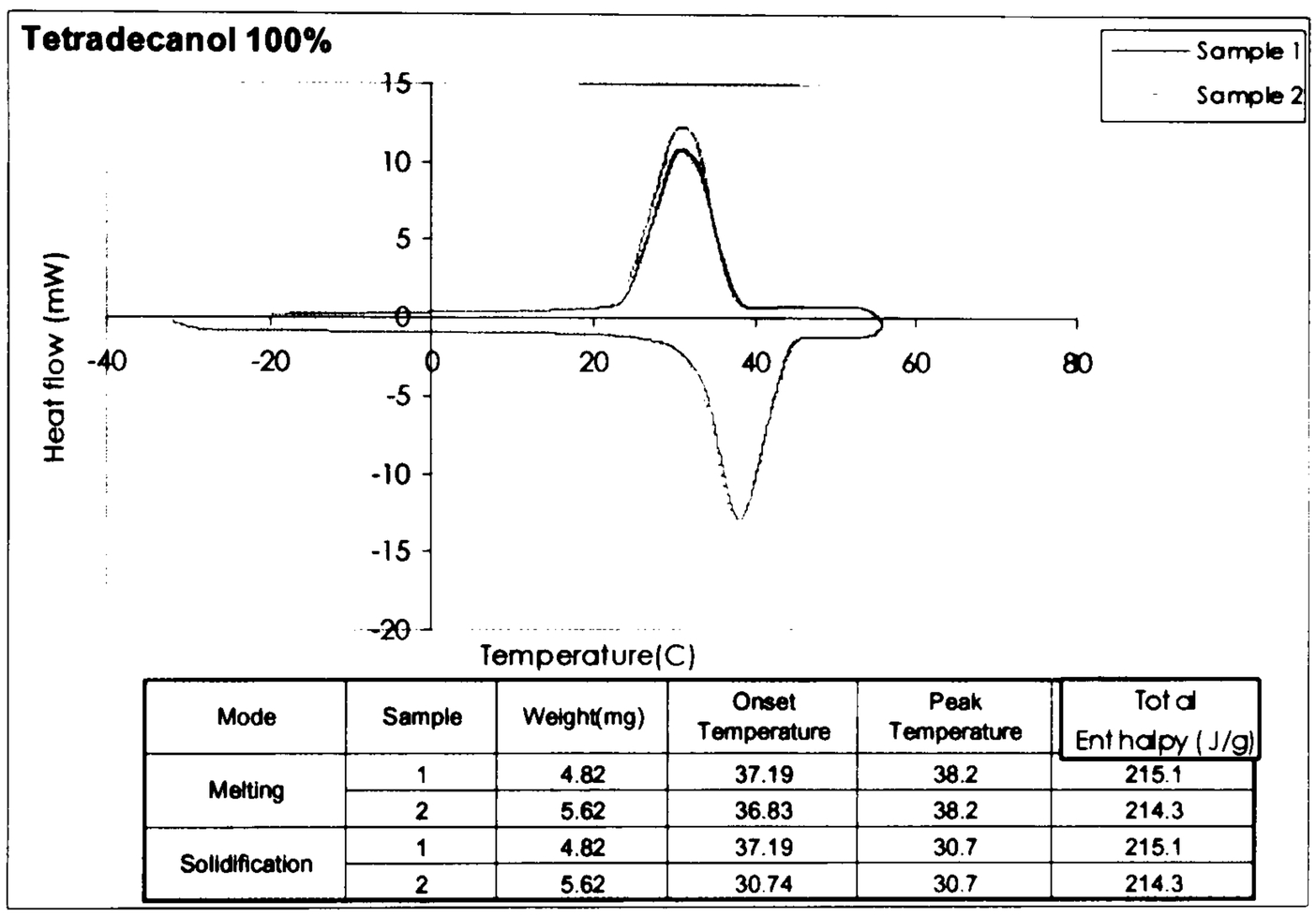

Mode	Sample	Weight(mg)	Onset Temperature	Peak Temperature	Total Enthalpy (J/g)
Melting	1	4.82	37.19	38.2	215.1
	2	5.62	36.83	38.2	214.3
Solidification	1	4.82	37.19	30.7	215.1
	2	5.62	30.74	30.7	214.3

Figure 4.29: DSC Tetradecanol, two samples

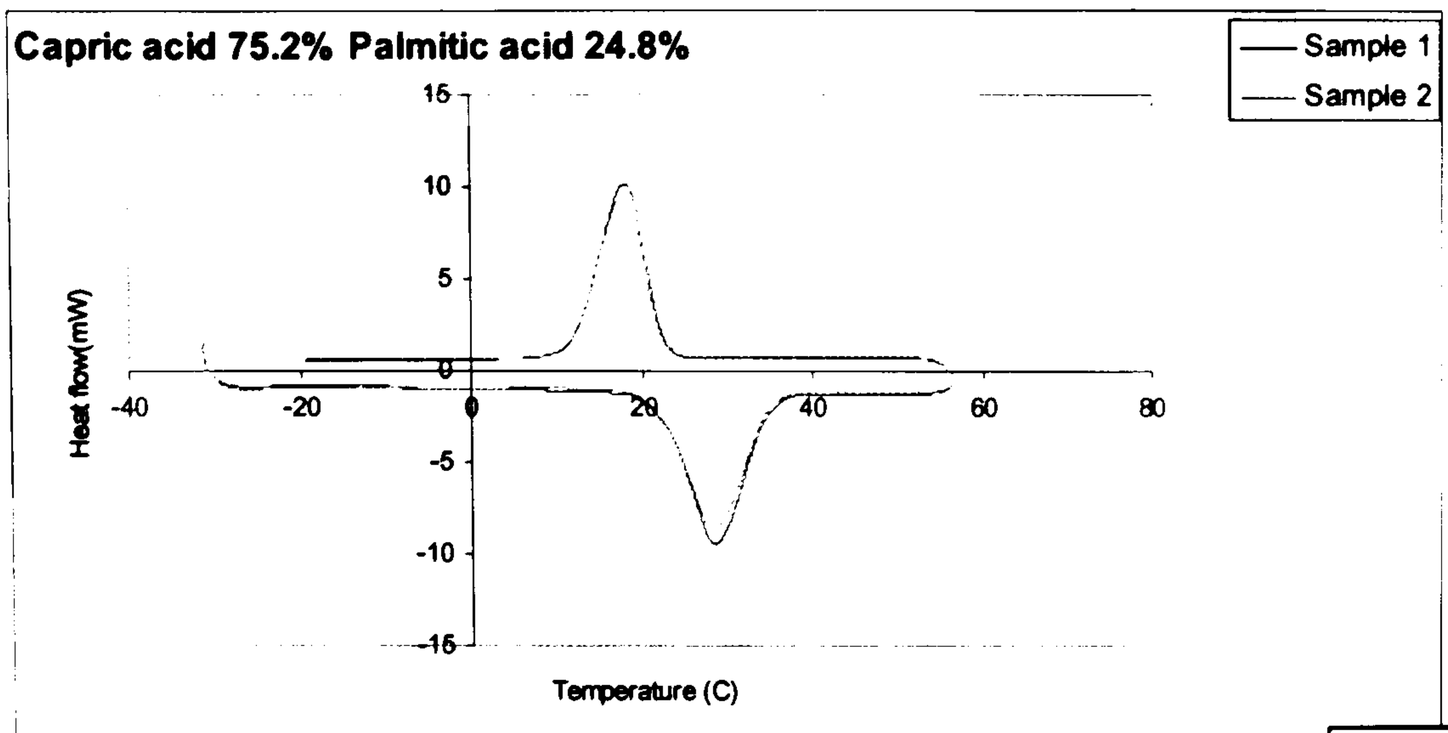

Mode	Sample	Weight(mg)	Onset Temperature	Peak Temperature	Total Enthalpy (J/g)
Melting	1	5.23	22.2	28.4	153.5
	2	4.37	21.89	28.32	170
Solidification	1	5.23	22.49	18.08	149.1
	2	4.37	22.33	17.88	164.3

Figure 4.30: DSC Capric-Palmitic Acid, two samples

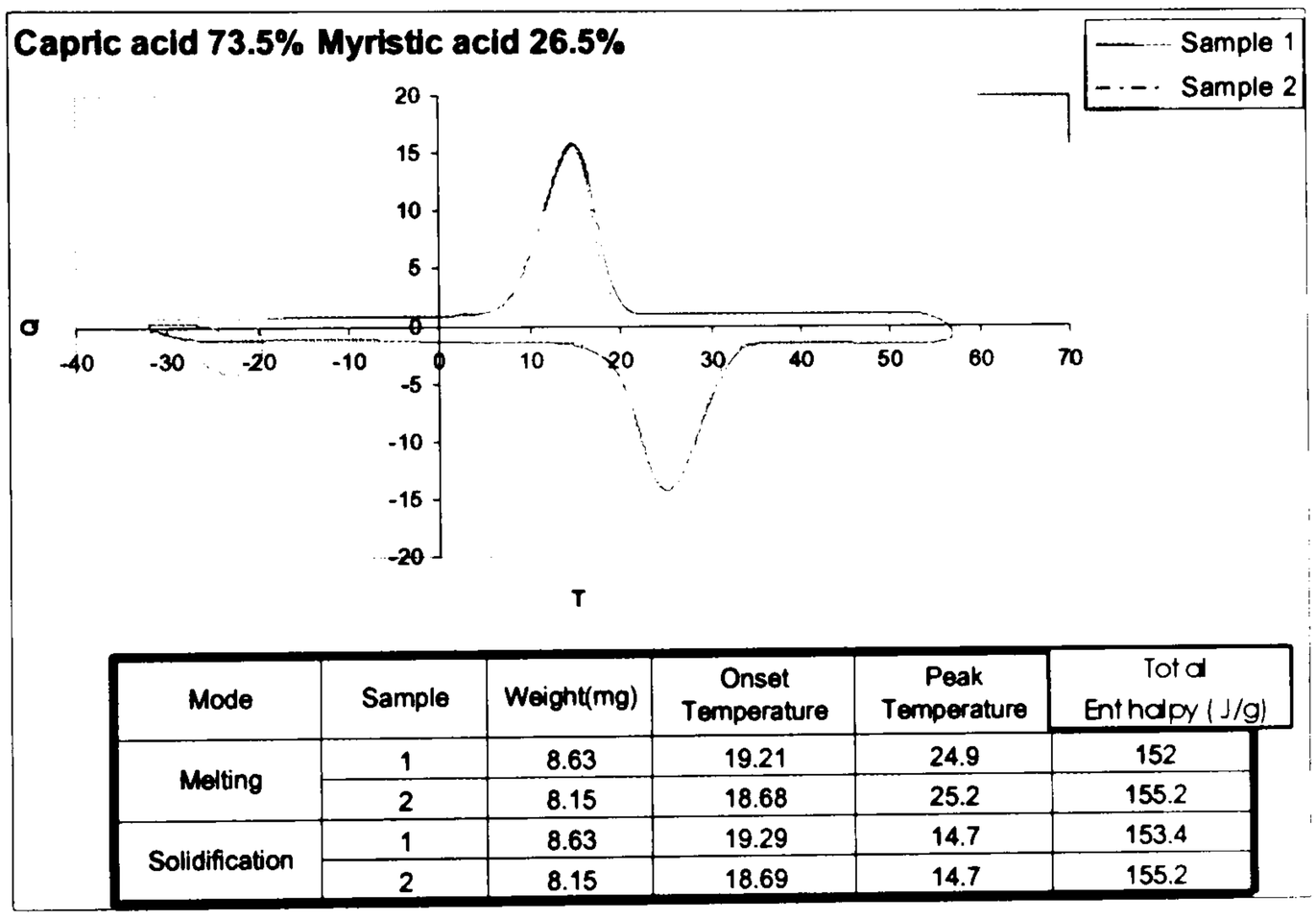

Mode	Sample	Weight(mg)	Onset Temperature	Peak Temperature	Total Enthalpy (J/g)
Melting	1	8.63	19.21	24.9	152
	2	8.15	18.68	25.2	155.2
Solidification	1	8.63	19.29	14.7	153.4
	2	8.15	18.69	14.7	155.2

Figure 4.31: DSC Capric-Myristic Acid, two samples

Lauric-Myristic and Capric-Lauric showed differences in enthalpy values between samples. This can be due to a difference in the sample composition between the samples, for being irregular mixtures (not having the same components between samples) or due to segregation.

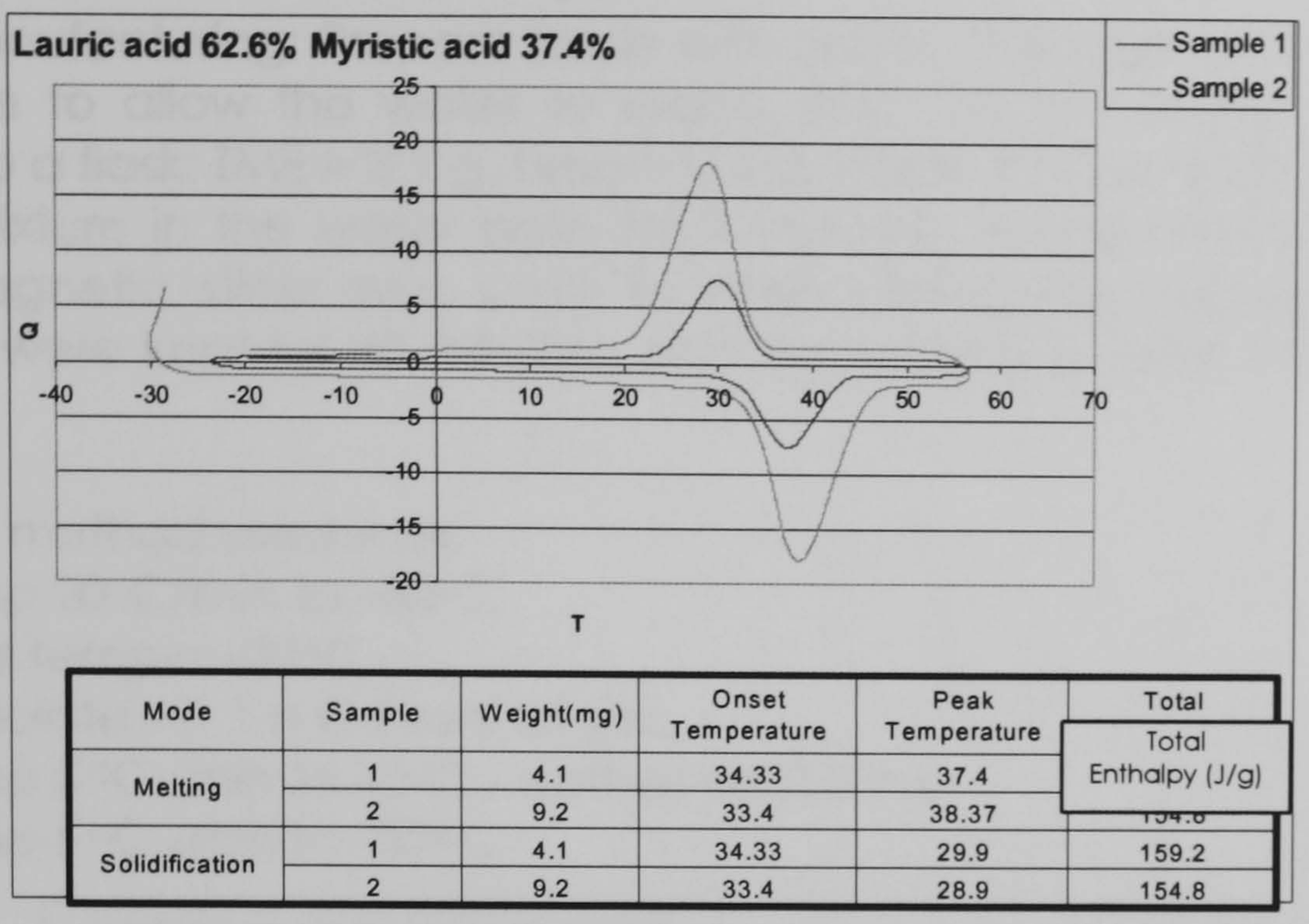

Mode	Sample	Weight(mg)	Onset Temperature	Peak Temperature	Total Enthalpy (J/g)
Melting	1	4.1	34.33	37.4	
	2	9.2	33.4	38.37	
Solidification	1	4.1	34.33	29.9	159.2
	2	9.2	33.4	28.9	154.8

Figure 4.32: DSC Lauric-Myristic Acid, two samples

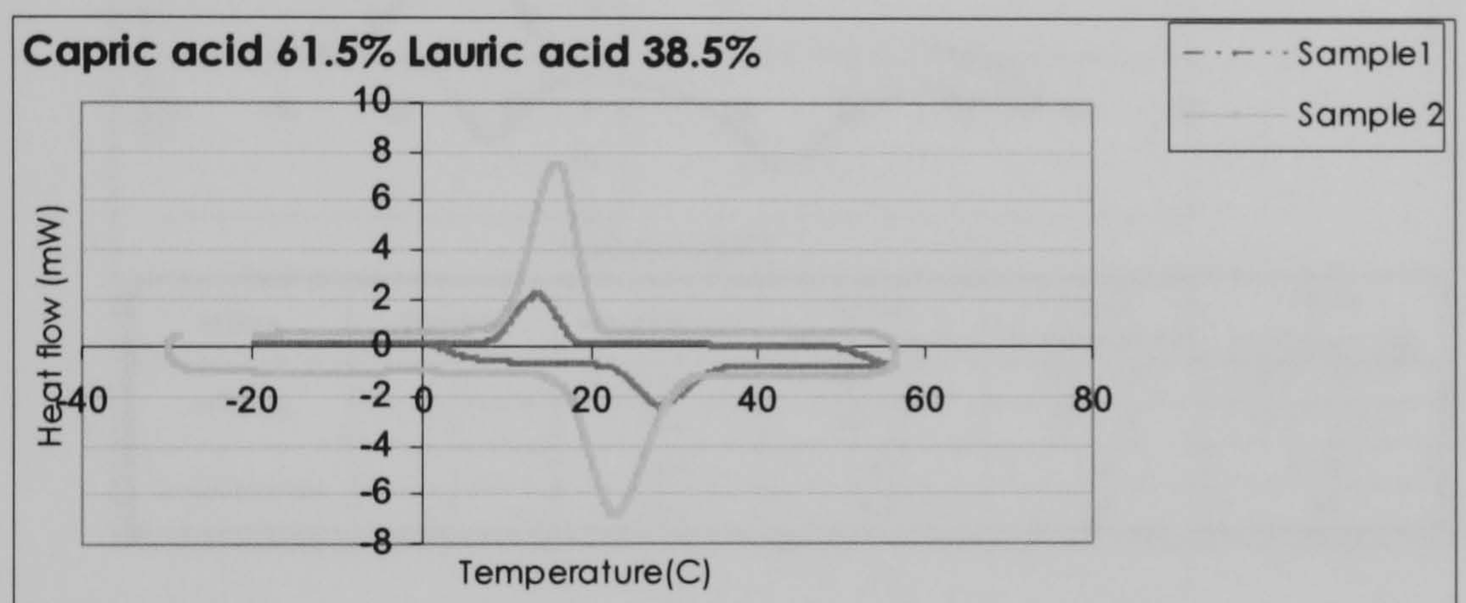

Mode	Sample	Weight(mg)	Onset Temperature	Peak Temperature	Total Enthalpy (J/g)
Melting	1	6.67	15.79	21.07	23.36
	2	4.01	17.1	22.83	136.3
Solidification	1	6.67	20.2	15.7	21.82
	2	4.01	20.2	16.07	137.6

Figure 4.33: DSC Capric-Lauric Acid, two samples

The Organic Hydrate Compound (Trimethylolethane[4.32]-Urea-Water) resulted in a totally amorphous evolution. A clear discontinuity in the base line indicates the presence of two different elements in the mixture with each different component changing phase at different temperatures.

[4.32] Trimethylolethane hydrate (TME) is a type of polyhydic alcohol with solid-solid phase transition of 81°C. The interesting part of it is that its phase transition temperature can be controlled between 13°C an 30°C by adding small amounts of urea. (L= 218 kJ/kg; density = 1gr/dm^3)

Mixture manufacturing: Prepare basin with water. The basin was heated by a hot plate to allow the water to reach 35°C. All the components were poured into a flask: TME = 3.1 g, Urea = 2.3 g, Water = 3.15 ml. Place the flask with the mixture in the water bath for 5 minutes. As the mixture started to melt a magnetic stirrer was used to keep mixing the components. The conditions were kept for 40 minutes, and the mixture poured into a sample flask.

MDSC: The method used was:

- Ramp 20°C/min to –30°C
- Initial temp = –30°C
- Modulate +/- 1 o C Every 60 sec
- Ramp 5 °C /min to 40°C - Isothermal 0.5 min
- Ramp 5 °C /min to -30 °C

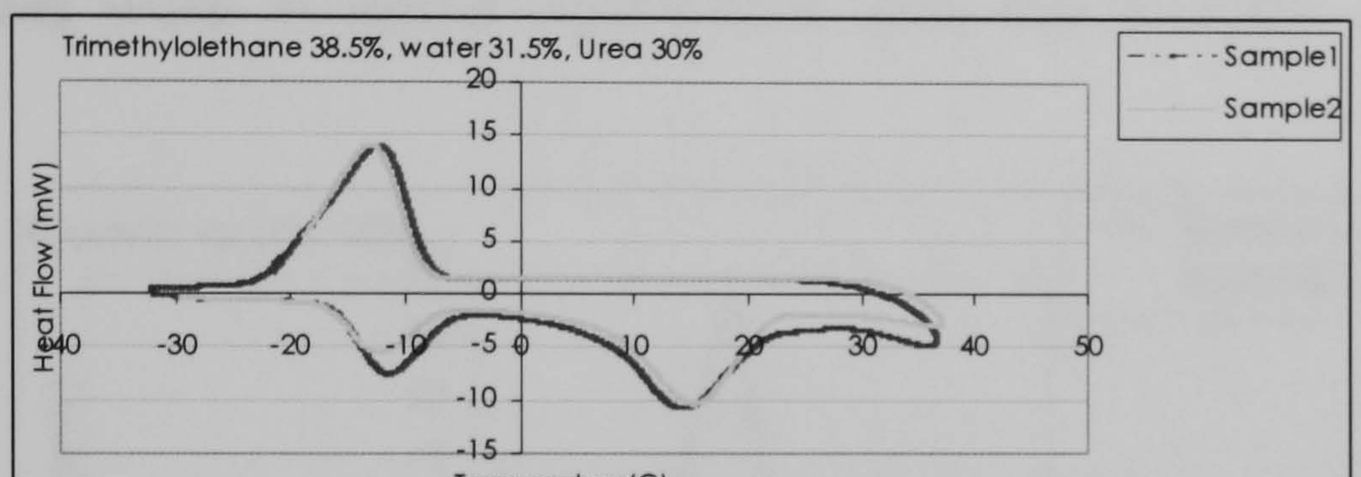

Mode	Sample	Weight(mg)	Onset Temperature	Peak Temperature	Total Enthalpy (J/g)
Melting	1	7.96	-18*, 2+	-10*, 15+	59.7*, 85.9+
	2	7.96	-18*, 2+	-11*, 16+	56.4*, 84.7+
Solidification	1	7.96	-8	-13	96.87
	2	7.96	-9.5	-15	99

Figure 4.34: DSC Trimethylolethane-Urea-water(* first transformation, + second transformation)

Two endothermic processes due to metastable-to-stable (amorphous to crystalline) transformations can be observed. These crystalline phases melt individually, generating two endothermic events. The onsets of the melting and freezing curves do not correspond due to the large superheating associated to the process. A reversible processes analogous to the original crystallization peaks will not occur.

After communication with other researchers, a new mixture of Trimethylolethane-Urea-Water mixed in a reduced temperature heating bath at 40 °C was made. The new DSC continued showing an amorphous change of phase. Phase segregation due to inherent properties of the components or set in the mixing procedure, preclude the mixture from showing sought behaviour. Hysteresis[4.33] associated with the induced temperature transition is observed.

4.33 The elastic portion of the material stores energy and returns it, and the viscous portion captures the energy and converts it to heat. Onsets of the melting and freezing

Final Mixtures:

Capric-Palmitic and Tetradecanol mixture were selected from the original group as they exhibited the sought behaviour. Capric-Myristic was not selected because it had a very close melting point to that of the Capric-Palmitic.

Additional material to be tested:

- Capric Acid (pure)
- Paraffin Hexadecane

As these are pure materials, their changes of phase were stable and clearly defined; reversibility and no supercooling are also shown. The measurements were in good agreement with the majority of published values.

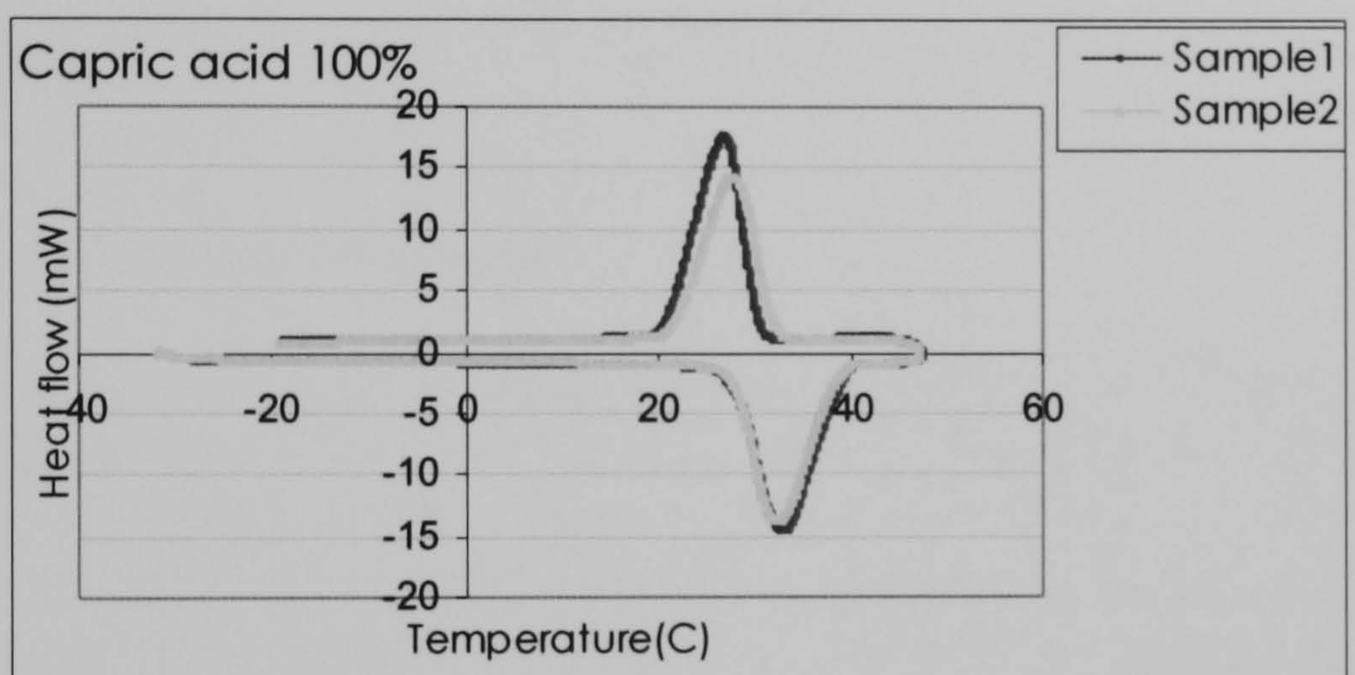

Mode	Sample	Weight(mg)	Onset Temperature	Peak Temperature	Total Enthalpy (J/g)
Melting	1	7.05	28.05	26.79	164.3
	2	6.4	28.01	32.19	160.5
Solidification	1	7.05	30.25	26.79	166.4
	2	6.4	31.61	27.62	160.6

Figure 4.35: DSC Pure Capric Acid

---

curves do not correspond. There would not be reversible process analogous to the original crystallization peaks.

CHAPTER V

RESULTS AND DISCUSSION

'The important thing in science is not so much to obtain new facts as to discover new ways of thinking about them." ...Sir Lawrence Bragg

PAGE NUMBERING AS ORIGINAL

Chapter V: Results and discussion

Previous experimental and numerical work on the heat transfer of the phase change phenomenon covers a range of geometries (flat, cylindrical, spherical) and a series of boundary conditions. Published work can also be found on the efficiency, long term behaviour and improvement of latent heat storage systems (LHSS) using PCMs. Also the effect on the system's performance using a variety of heat sources for the charging process in experimental studies as constant thermoelectric current and direct solar radiation have been studied.

Original aspects of this study include:

1) The application of simulated internal heat gains, temperature, irradiation and air changes per hour for the experimental and theoretical simulation. The data related to the magnitudes of these parameters was obtained by running a dynamic thermal simulation using the software TAS for a dwelling under Mexican like weather conditions.
2) The design and use of a large scale solar simulator constructed with Halogen lamps to reproduce irradiation fluxes.
3) The application of insulation in one face of the unit, as a mean for heat transfer rate control.
4) The non-linear temperature-enthalpy relation of the phase change materials used and their temperature dependent properties as heat capacity and thermal conductivity were experimentally obtained and are original contributions.
5) The numerical algorithm used in the program is based on the modified enthalpy formulation proposed by Voller and used by Zivkovic. Original

contribution of the computer model is the evaluation of the initial boundary condition according to given weather data as air temperature, irradiation and mass flow rate, and its application to the latent heat evolution calculation.

The experimental part of this work provided the means for the computer model validation of the Stefan problem (experiment 1), for the optimization and performance evaluation of the system proposed (experiment 2) and for an assessment of the impact of the application of the system proposed (experiment 3). The findings of these three experiments are discussed next.

Experiment 1: Computer model validation

The program was developed as a tool to evaluate the effect of the LHSS application to the provision of thermal comfort provided to a Mexican dwelling. If the weather conditions for other locations are known, it would also be possible to determine the feasibility of using the proposed LHSS in that location.

Recalling from chapter 4, the tests conditions imposed were as follows:

Experiment 1
L4: 3 factors; all factors have 2 levels
For melting

Run	F1: Province	F2: Season	F3: Time of day	Average Temp	Lamp
1	BC	Winter	Day	17.22	ON
2	BC	Summer	Night	39.45	OFF
3	CH	Winter	Night	27.94	OFF
4	CH	Summer	Day	34.55	ON

Table 5.1: Taguchi L4, for experiment 1-heating test (1h)

Experiment 1
L4: 3 factors; all factors have 2 levels
For solidification

Run	F1: Province	F2: Season	F3: Interior/Exterior Temp Cond	Lowest Temp	Lamp
1	BC	Winter	Interior	12.7	OFF
2	BC	Summer	Exterior	24.5	OFF
3	CH	Winter	Exterior	12	OFF
4	CH	Summer	Interior	28.8	OFF

Table 5.2: Taguchi L4 for experiment 1-cooling test (1c)

(where BC is Baja California and CH is Chiapas)
For practical purposes both experiments were conducted in sequence, that is, after a heating test a subsequent cooling test was carried out immediately. This was possible because the only changes required for the rig settings were related to cooling/heating loads and the lamp's radiation intensity.

As explained in chapter IV , this experiment had the double purpose of 1) Providing a means to assess the theoretical model, and 2)Evaluating the heat storage charging/discharging behaviour, with and without radiation

during cold and hot days and nights and during winter and summer nights in each province (using the lowest interior and exterior air temperatures).

Theoretical model assessment

Regarding the assessment of the theoretical model, the obtained temperature profile from the theoretical model was compared with the actual experimental temperatures obtained. Good agreement between the theoretical and experimental values was found, as can be observed in the following graphs of Figure 5.1to Figure 5.8

In most of the following graphs a less uniform temperature evolution can be observed in the theoretical model. This is due to the oscillations that arise from the numerical method utilised (as we can observe in Figure 5.1). That is, during the material's change of state the enthalpy method considers that the PCM temperature remains constant. This causes the numerical method to provide temperature profiles with a wavy pattern (as explained in the definition of the enthalpy formulation in chapter 2). The temperature difference between theoretical and experimental values can be due to differences between the actual material properties and the theoretical values assumed.

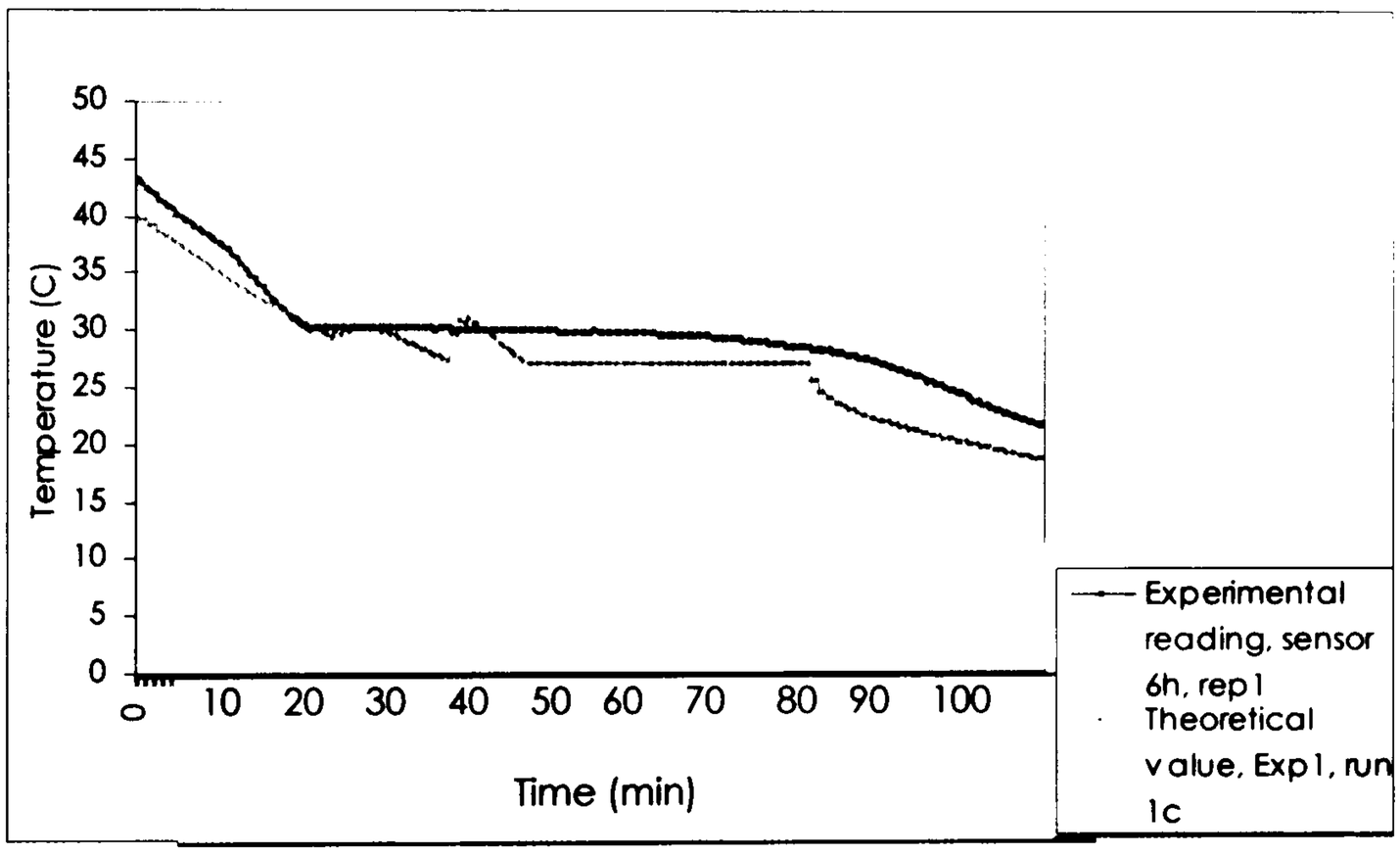

Figure 5.1: Temperature profile comparison, theoretical value (model) vs experimental data. Experiment 1, run 1c (cooling test)

A premature or delayed change of phase period, can be due to differences between actual position of the sensors and positions considered for the model.

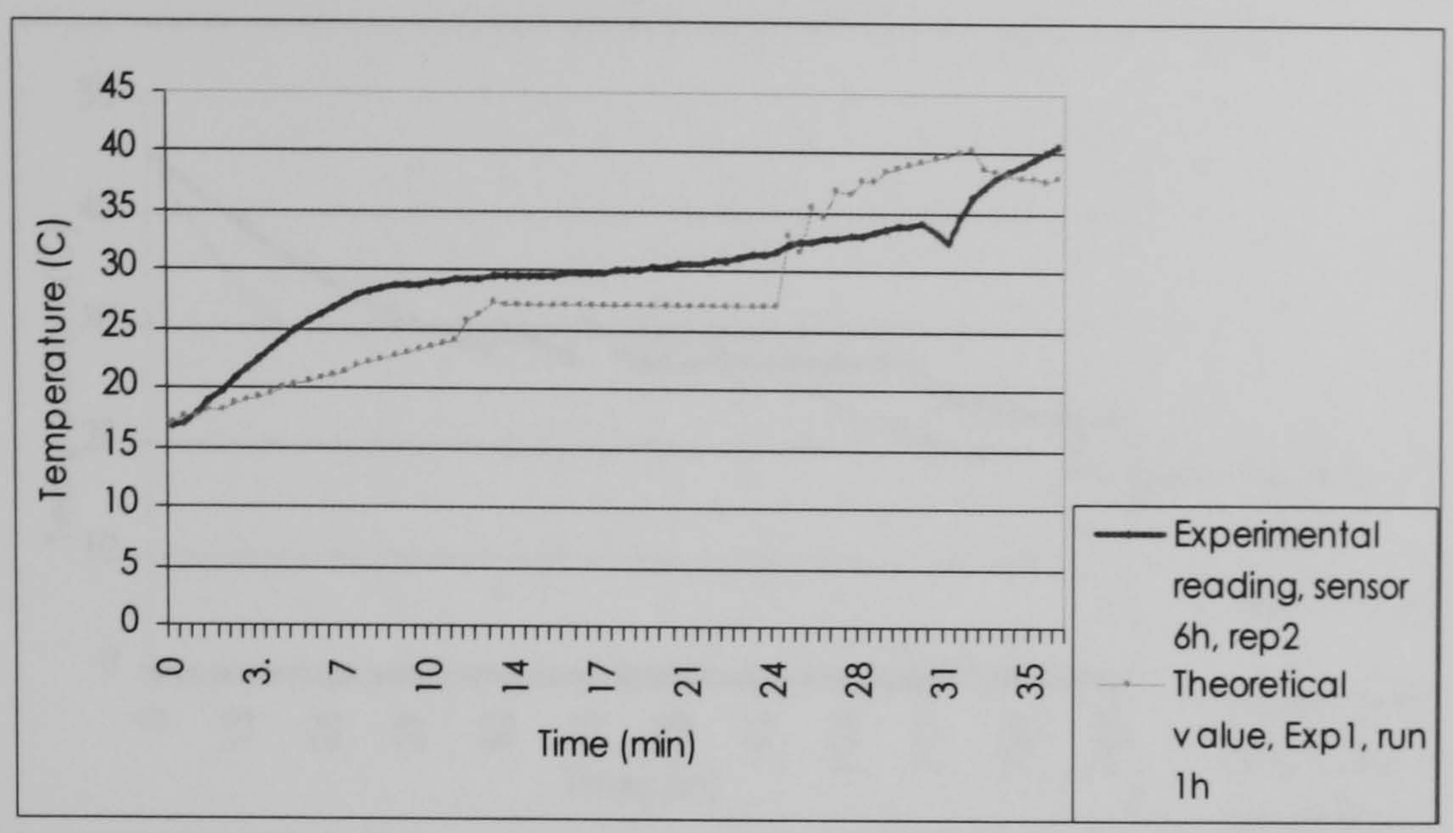

Figure 5.2: Temperature profile comparison, theoretical value (model) vs experimental data. Experimenta1, run 1h (heating test)

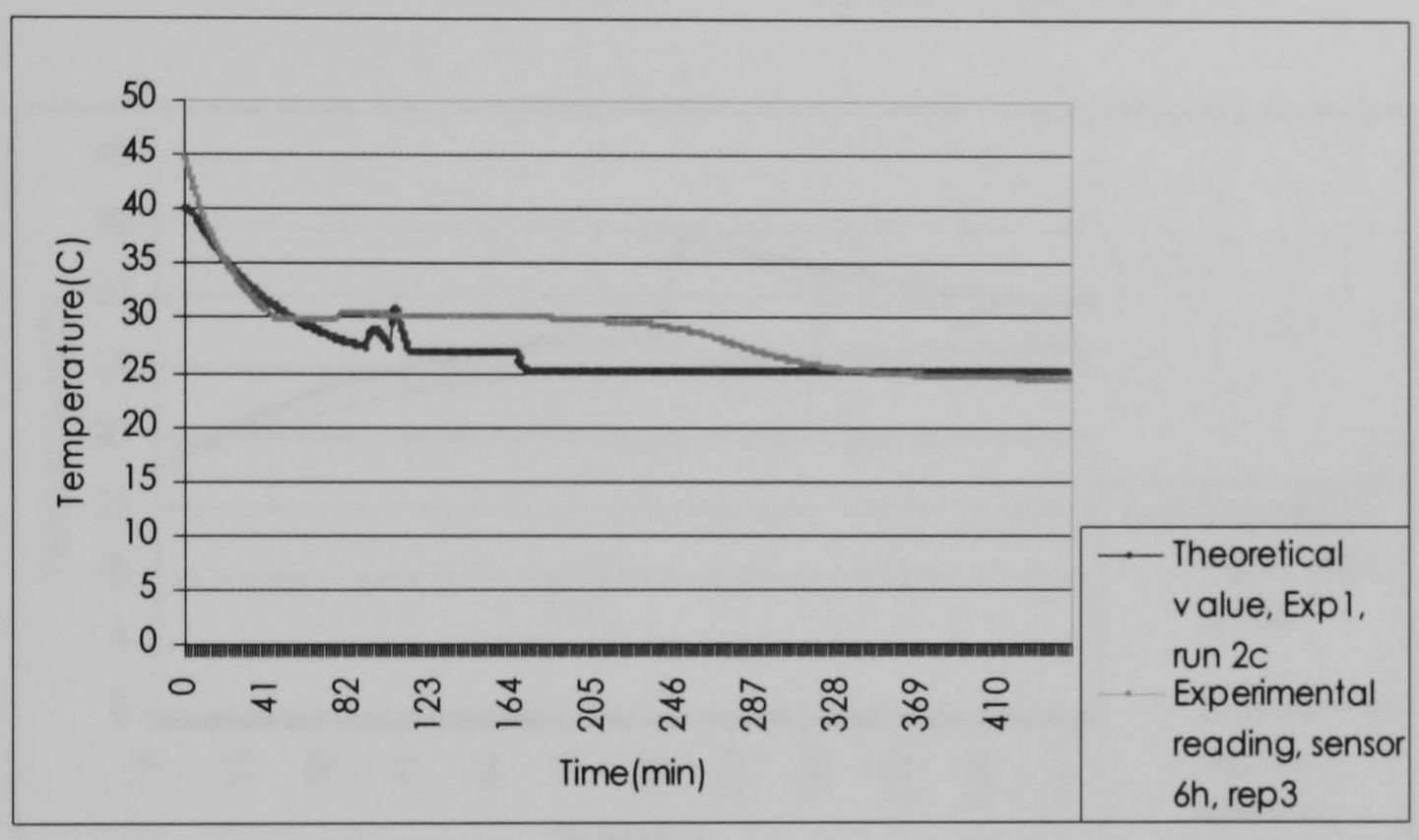

Figure 5.3: Temperature profile comparison, theoretical value (model) vs experimental data. Experimenta1, run 2c (cooling test)

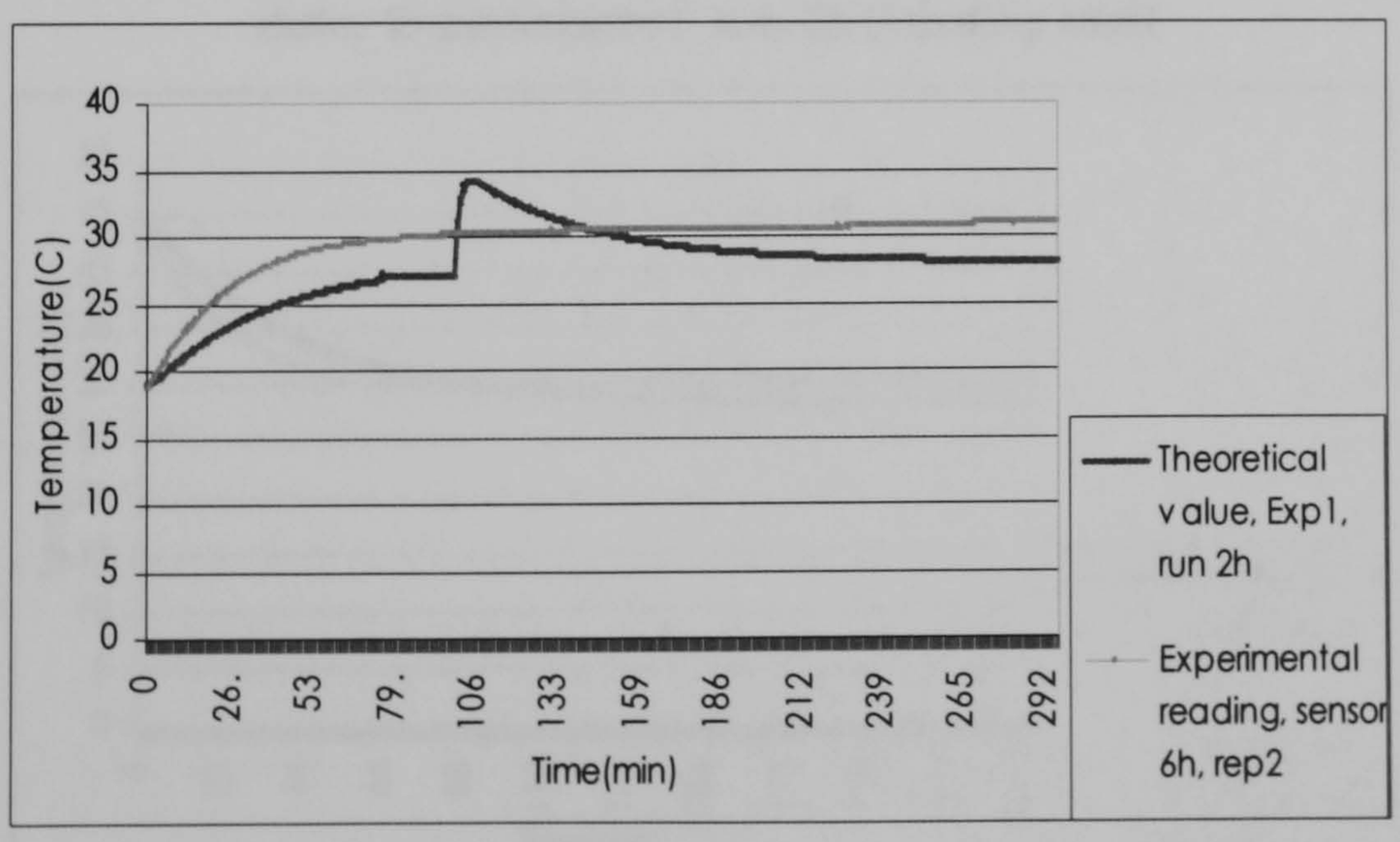

Figure 5.4: Temperature profile comparison, theoretical value (model) vs experimental data. Experimenta1, run 2h (heating test)

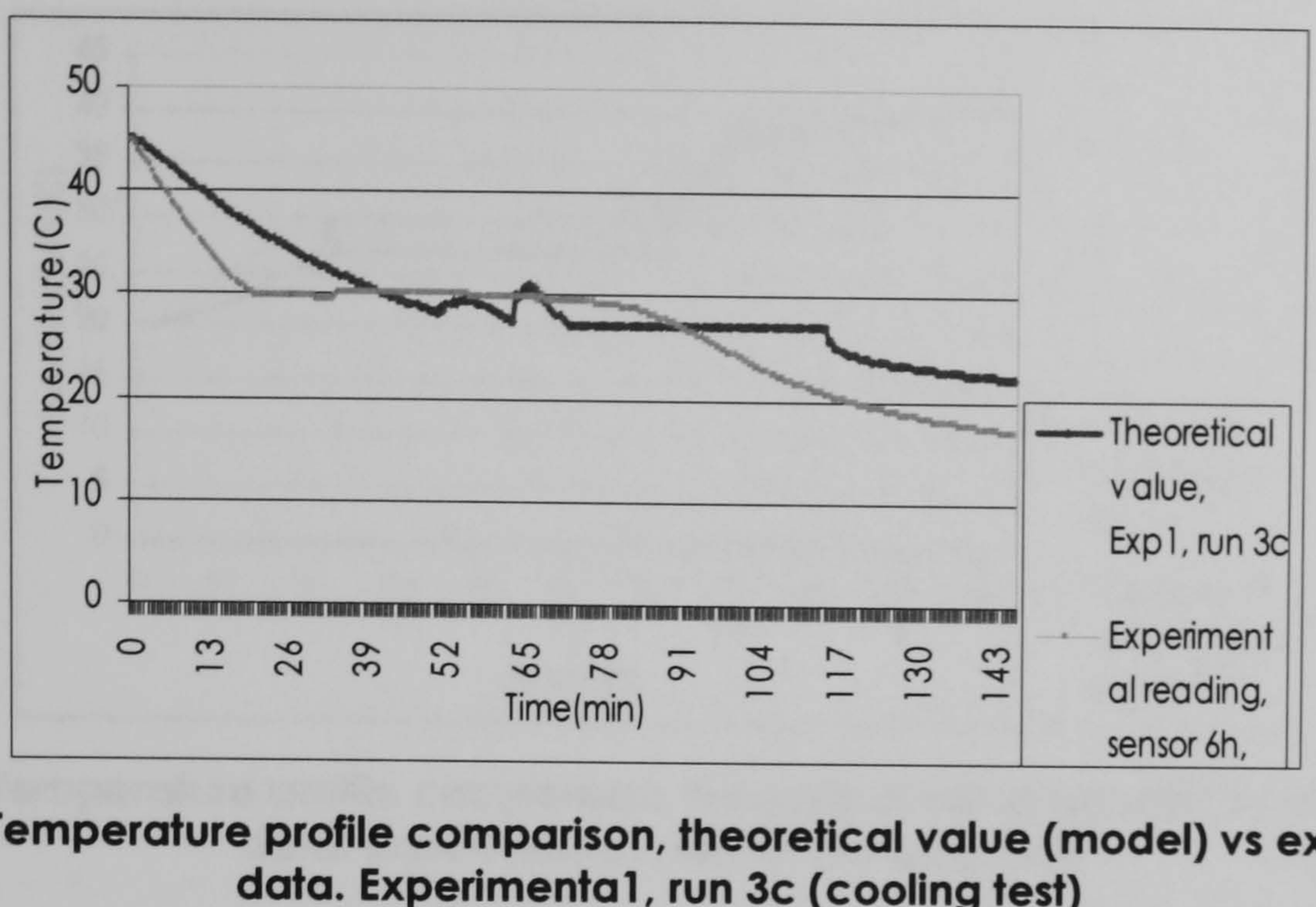

Figure 5.5: Temperature profile comparison, theoretical value (model) vs experimental data. Experimenta1, run 3c (cooling test)

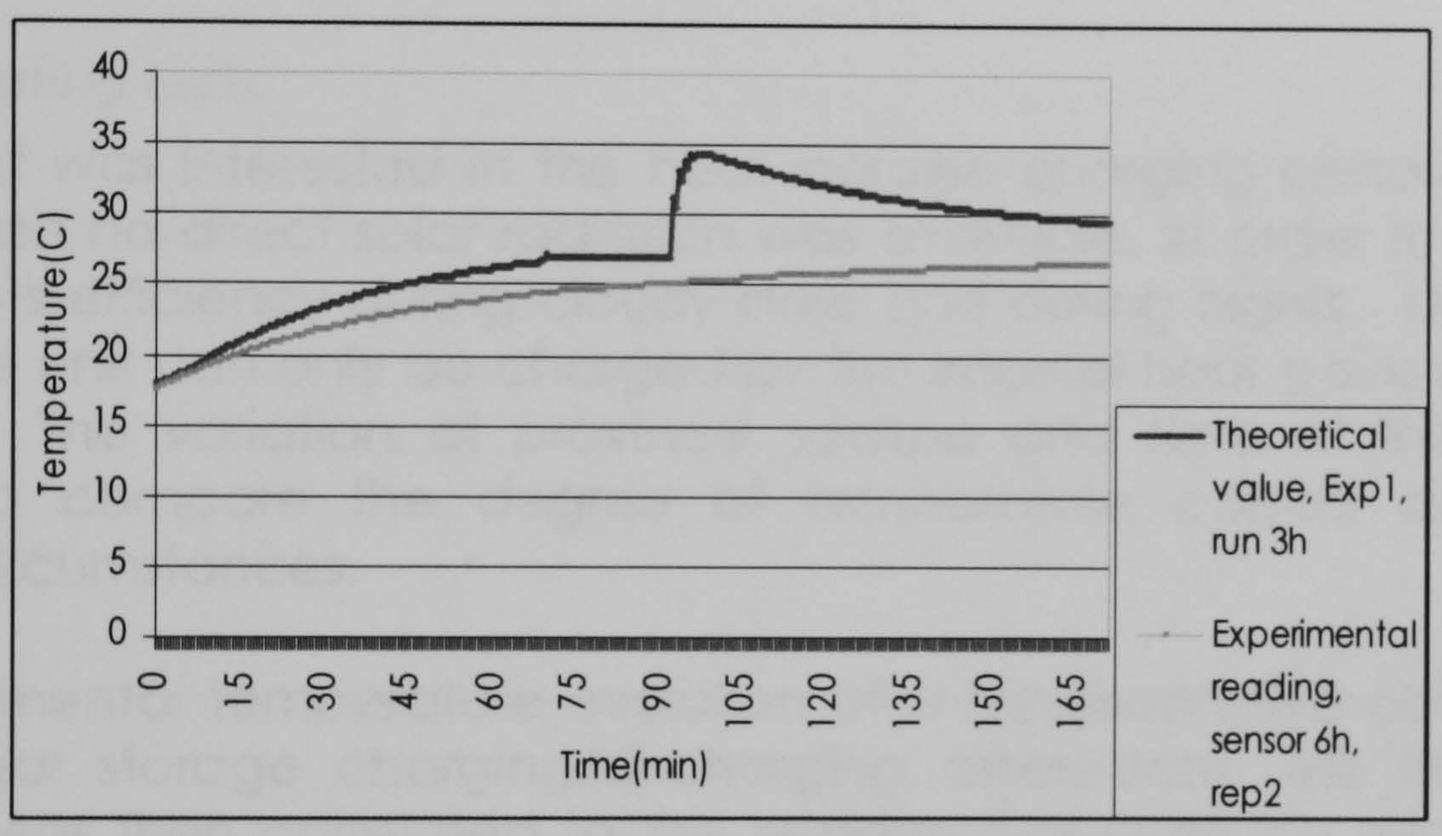

Figure 5.6: Temperature profile comparison, theoretical value (model) vs experimental data. Experimenta1, run 3h (heating test)

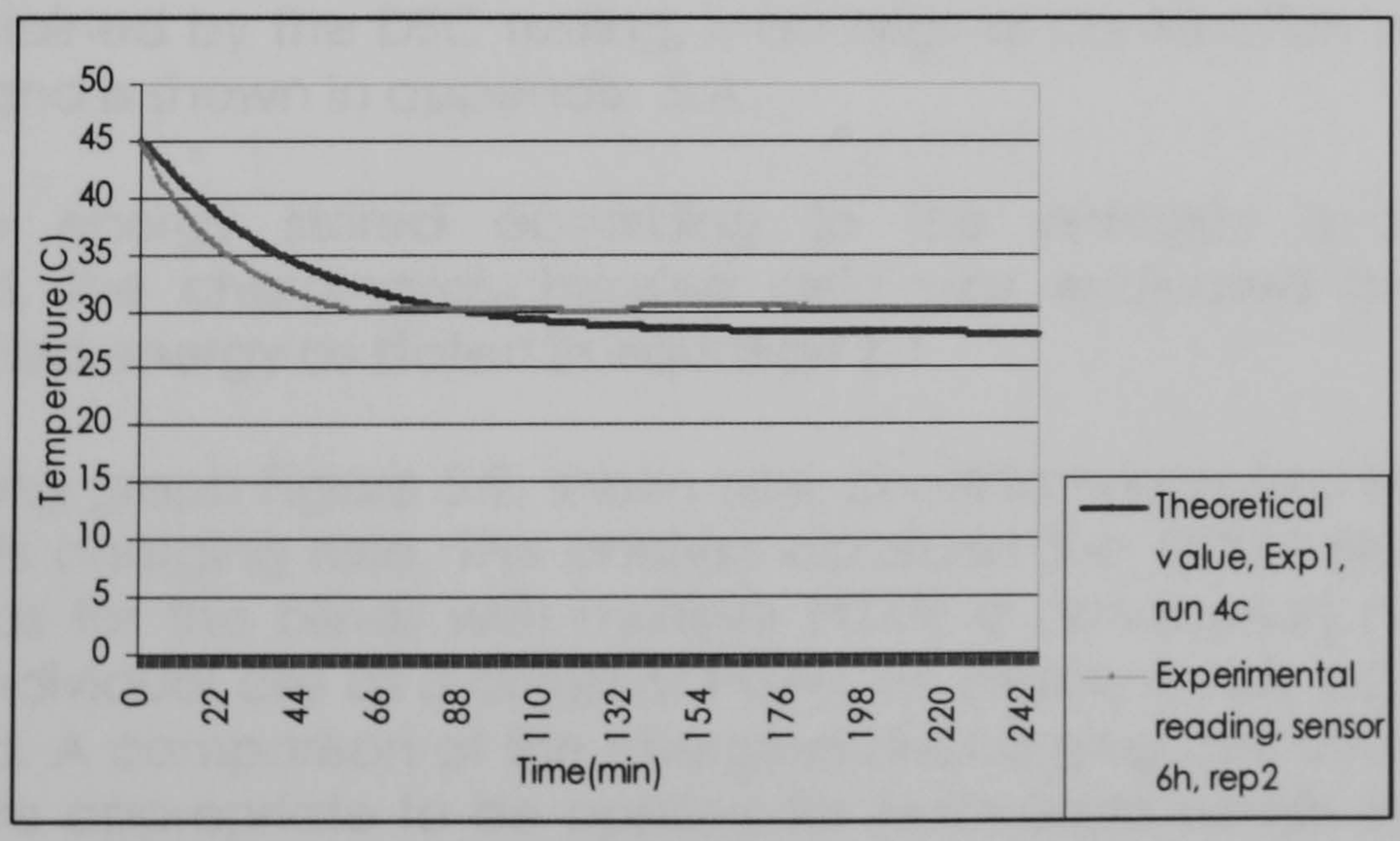

Figure 5.7: Temperature profile comparison, theoretical value (model) vs. experimental data. Experimenta1, run 4c (cooling test)

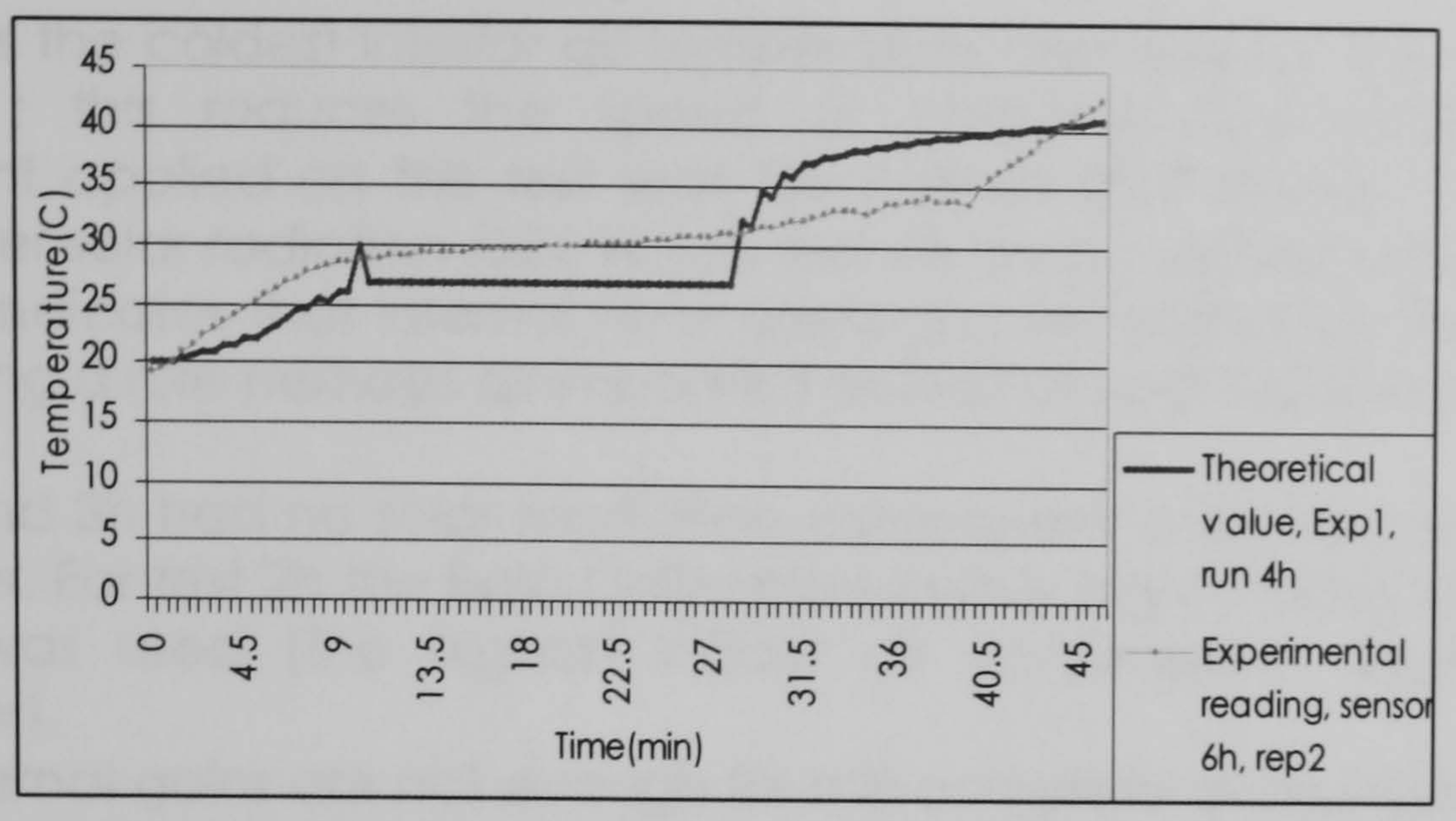

Figure 5.8: Temperature profile comparison, theoretical value (model) vs experimental data. Experimenta1, run 4h (heating test)

Heat storage charging/discharging behaviour

Heating tests

The project was interested in the heat storage charging behaviour of the system when no direct solar radiation was available, in order to determine the system's efficiency during cloudy days and during nights. During these periods the unit can only be charged by the internal heat gains and diffuse radiation. The variation of province, season and time of the day was applied to compare the degree of temperature control achieved in different circumstances.

The experimental temperature evolution of a representative cell was used for the heat storage charging/discharging assessment. This temperature evolution was then correlated to the temperature-enthalpy relationship to obtain the enthalpy evolution.
The temperature-enthalpy correlation used for the evaluation of the energy stored, obtained by the DSC testing, is an original contribution provided by this work, and is shown in appendix 5.A.

Once the energy stored according to the enthalpy evolution was calculated, the charging/discharging ratio was evaluated by using the accumulated energy as stated in equation 4.1

The following graph Figure 5.9, shows how conditions imposed on each test affected its charging rate. This analysis considers the PCM volume of one cell only, as for the blinds with multiple PCMs a comparison can only be done by individual cell as 3 different PCMs for different cells are contained in the blind. A comparison of the charging/discharging rate for a single cell seems more appropriate to be applied for both cases (single and multiple PCM tests).

Test 1h has the coldest interior air temperature imposed for the experiment (17.22°C) ; this reduces the speed of charging. The solar radiation component applied on this test was the highest (557 W/m^2), nevertheless with a lower solar radiation (324 W/m^2) test 4h had a slightly faster charging ratio. This indicates that internal heat gains can be critical on the charging rate, playing a role perhaps as important as that of solar irradiation.

Tests 2h and 3h had no solar irradiation component and their performance was poorer. For test 2h the Baja California summer night indoor temperature (39.4°C) was used (the highest indoor air temperature applied in the experiment).
That is, internal gains are not enough for the complete charging of the PCM (even though the resultant increase in internal air temperature is significant). Inclusively a low radiation location or season can be enough for a rapid charging of the unit, if the interior air temperature is not too low.

Test 3h has the lowest charging rate. In this test no solar irradiation was applied and the air temperature imposed was lower than the melting point(27.9 °C). Never the less, under these unfavourable circumstances 90% of the cell was charged.

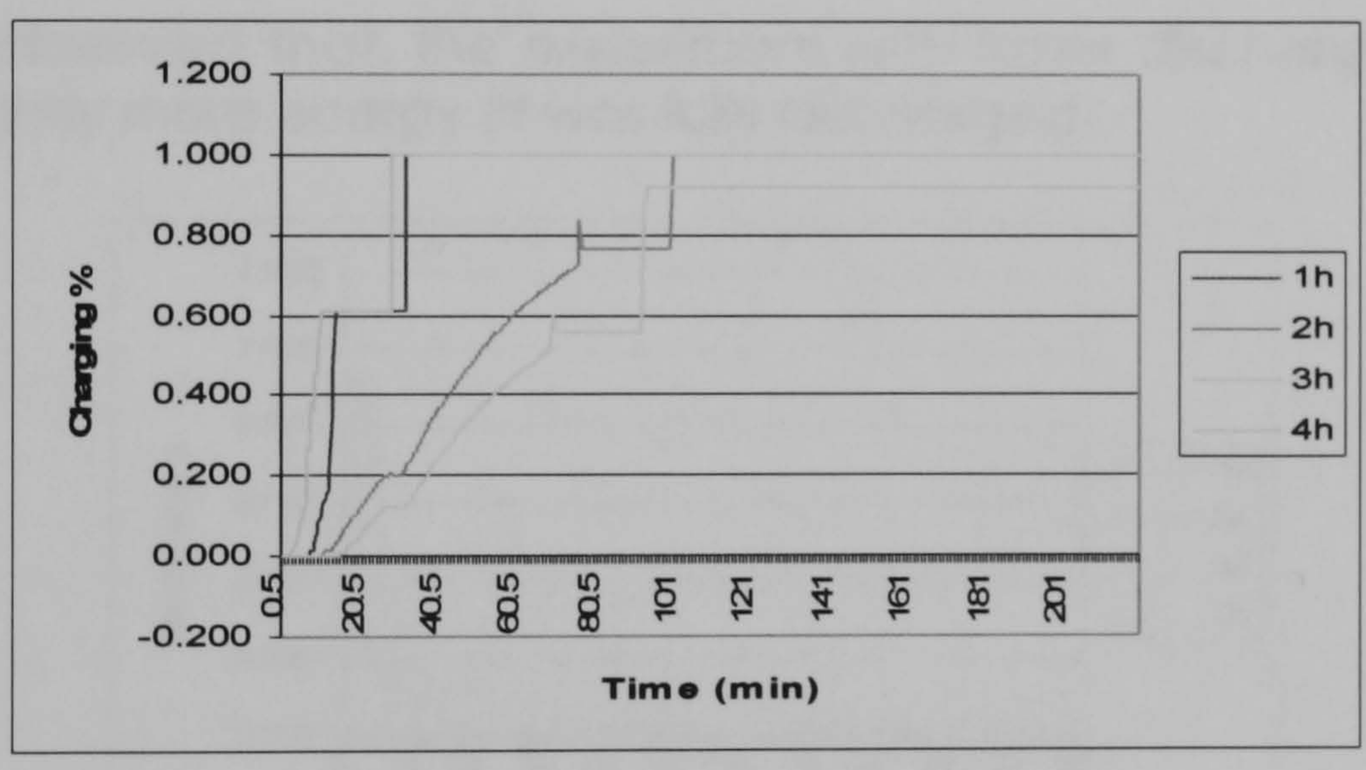

Figure 5.9: Charging rate for heating tests with/without radiation during cold/hot days/nights obtained by experimental temperature evolution.

Where the "h" in tests 1,2,3 and 4 means heating (charging) tests
One of the main aspects of interest was the role of the heat transfer mode on the charging of the unit. From observations of Figure 5.9, it can be concluded that charging the unit in a high air temperature environment without solar radiation has a slower charging rate than a winter day with low air temperatures but a high value of solar irradiation.

Cooling tests

The discharging rate of the heat stored is an important aspect of the system's efficacy. If the system is to operate as insulation only, it can be placed outside the building envelope to promote faster discharging.

However, it is not known if the amount of heat released is affected by the rapid discharging. Also the province and the season effects are evaluated to determine under which conditions the system performs better.

In order to carry out the cooling test, the unit was completely melted; even though for the previous condition tested it might have not been fully charged. The storage unit was removed from the chamber and placed in front of the solar simulator, which was turned on several minutes until the sensors inside the PCM read a temperature higher than the melting point. It was then replaced in the rig.

The fastest discharging rate was achieved in test 1c with the lowest air temperature (12.7 °C) and a medium air velocity. In that sequential order the tests with higher interior air temperature took longer to discharge. Although the larger mass flow rate for cooling was applied to the higher temperature tests, their discharging rate was smaller (see Figure 5.10).

From this we can conclude that the exterior lower temperatures during night either in summer or winter have a larger effect on the discharging ratio than the mass flow rate applied.

It was also observed that, the experiment with faster discharging rate also released slightly more energy (it was fully discharged).

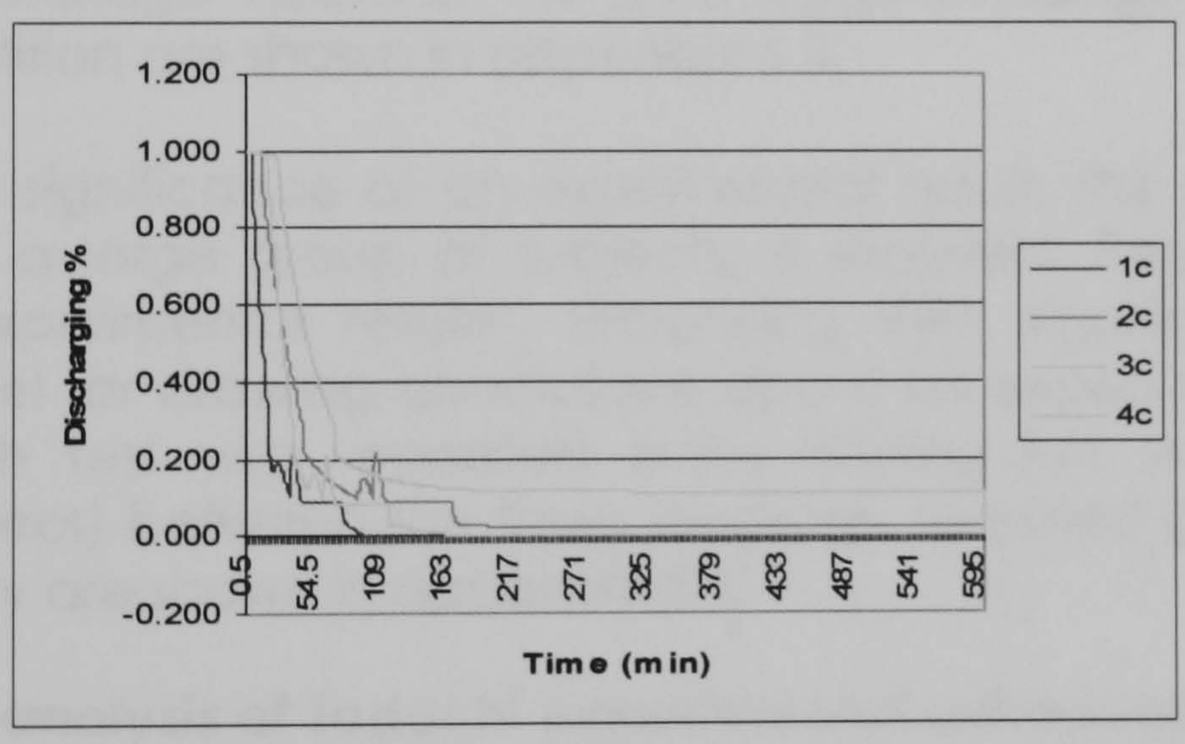

Figure 5.10: Discharging rate for cooling tests during cold winter and summer nights placing the blind inside/outside the envelope.

Where the "c" in tests 1,2,3 and 4 means cooling (discharging) tests

Placing the unit outside the building does promote faster discharging. But it is not possible to take advantage from the energy released from the unit. Placing the unit outside can be advantageous when the stored energy is not needed to heat the interior.

No particular advantage was found when discharging the unit under conditions typical for either of the provinces. Never the less, the more extreme conditions experienced in the Baja California region might provide slightly better performance systems.

Experiment 2

The main objective was to identify the factors that contributed to the system's operation optimisation. The variation of energy stored/extracted with the variation of dependable variables as: Inlet air temperature, irradiation rates, PCM volume, and air flow rate was determined The experimental design is shown in Table 5.3 The air mass flow rate was determined considering actual environmental conditions and experimental constrains. The inlet flow provided by the fan was limited to a range between 5 and 8 m/s.

Experiment 2
L8: 7 factors; all factors have 2 levels

Run	F1: Province	F2: Season	F3: PCM	F4: Cell Thickness (in)	F5: Mass flow	F6: Insulation	F7: Mode
1	CH	Summer	Single(C-P)	1.5	Low	Insulation	Cooling
2	CH	Summer	Single(C-P)	0.5	High	no-insulation	Heating
3	CH	Winter	Multiple(C-P,T,H)	1.5	Low	no-insulation	Heating
4	CH	Winter	Multiple(C-P,T,H)	0.5	High	Insulation	Cooling
5	BC	Summer	Multiple(C-P,T,H)	1.5	High	Insulation	Heating
6	BC	Summer	Multiple(C-P,T,H)	0.5	Low	no-insulation	Cooling
7	BC	Winter	Single(C-P)	1.5	High	no-insulation	Cooling
8	BC	Winter	Single(C-P)	0.5	Low	Insulation	Heating

Table 5.3: Experimental design, experiment 2

A summary of average values of the data logger readings for each sensor and each repetition are shown in appendix 5.B.

To improve the significance of an experimental result, the repetition of an experiment on a large group of subjects, is required. Repetition reduces variability in experimental results[1], increasing their significance and the confidence level for drawing conclusions about an experimental factor. In this work, each test was repeated twice finding just small differences (repeatability error) between the three readings. Selected graphs[2] showing the repeatability are shown in appendix 5.C.

Statistical analysis of Taguchi experimental orthogonal design.

The experimental work part 2 carried out for this project had the objective of assessing the effect of different design factors on the system's efficiency. In order to evaluate which factors might affect the average response of the system, and the factor's effect on variation. The experiment was designed according with a Taguchi orthogonal array. Orthogonal array is a method of setting up experiments that only requires a fraction of the full factorial combinations. The factors involved and the combinations of factors utilised for experiment 2 that result from this analysis are shown in Table 5.3.

---

[1] Experimental variation hides true factor effects
[2] Not all the graphs are shown due to the large space required to show them all.

Factors selection:

Temperature ranges and weather conditions to replicate: The behaviour of the unit when heating or cooling (F7: mode) was a crucial factor in defining the system, as the charging can be fairly different to the discharging patterns and behaviour. Two provinces at extreme latitudes and two seasons (winter-summer) defined the required temperature, mass flow, and irradiation. Detailed information on the temperatures, fluxes and type of PCM used for this test are shown in Table 5.4

The charging/discharging ratio, related to the material's properties helped to define other factors: PCM type. A series of PCM with varied melting points to extend the temperature range of the storage would make it possible to manipulate the rate of energy storage/release. The other factor to manipulate charging ratio is the presence/absence of insulation.

PCM volume: a greater volume stores a greater amount of energy, but if the change of phase is not performed by the whole volume its effect is not straight forward.

The mode, whether heating or cooling, was an additional factor.

With this information the Taguchi experimental design selected was L8, having 7 factors with 2 levels each.

Run	PCM	PCM Type	Province	Season	Cell thickness	Environ Interac	Mode	Interior Air Temp	Radiation at that time	PCM av. Temp C	Surface Tube T (C)	Inlet Air PRT (11,12) (C)	Outlet Air PRT (1,2,3,4 (C)	Chamber Air PRT (5-10) (C)	Exterior Air PRT (13,14) (C)	Anemometer mass flow (kg/s)	Maximum En. Stored (J)
1s	Single	(OP)	CH	Summer	1.5	Insulation	Solidfing	18.5	Off	26.2	25.37	18.14	20.16	19.53	25.59	5307	152648
2m	Single	(OP)	CH	Summer	0.5	No-ins	Melting	40	270	51.7	53.27	40.63	29.50	39.71	25.33	6800	146863
3m	Multiple	(OP, T, H)	CH	Winter	1.5	No-ins	Melting	34	306	43.1	47.78	33.35	49.76	32.32	26.86	5154	97232
4s	Multiple	(OP, T, H)	CH	Winter	0.5	Insulation	Solidfing	12	Off	27.4	26.9	12.0	15.3	12.6	23.6	6820	486110
5m	Multiple	(OP, T, H)	BC	Summer	1.5	Insulation	Melting	45	455	40.4	43.14	44.06	41.84	41.68	27.37	6715	175801
6s	Multiple	(OP, T, H)	BC	Summer	0.5	No-ins	Solidfing	24.5	Off	32.8	30.55	24.70	25.88	25.00	24.74	5265	543808
7s	Single	(OP)	BC	Winter	1.5	No-ins	Solidfing	9	Off	16.4	15.4	8.2	11.9	11.1	28.0	7509	556438
8m	Single	(OP)	BC	Winter	0.5	Insulation	Melting	22	520	31.5	32.87	22.07	25.32	22.63	25.09	5014	147439

Table 5.4: Experimental set up for experiment 2

Data obtained from the experimental work:

Logged data display the conditions under which the tests were actually carried out. These conditions depend on experimental complications, and on the interactive response of the heat storage system.

In Figure 5.11 chamber interior air temperatures of tests 2m and 5m seem to become nearly the same in the central part of the chamber. However, the inlet air temperature for test 2m was 40 °C, whilst that for test 5m was higher (44 °C). That is, the effect of the storage system interaction can be observed in test 5m which includes insulation, and the blind with multiple PCM cells (a larger range of melting temperatures allows a better modulation of the heat wave).

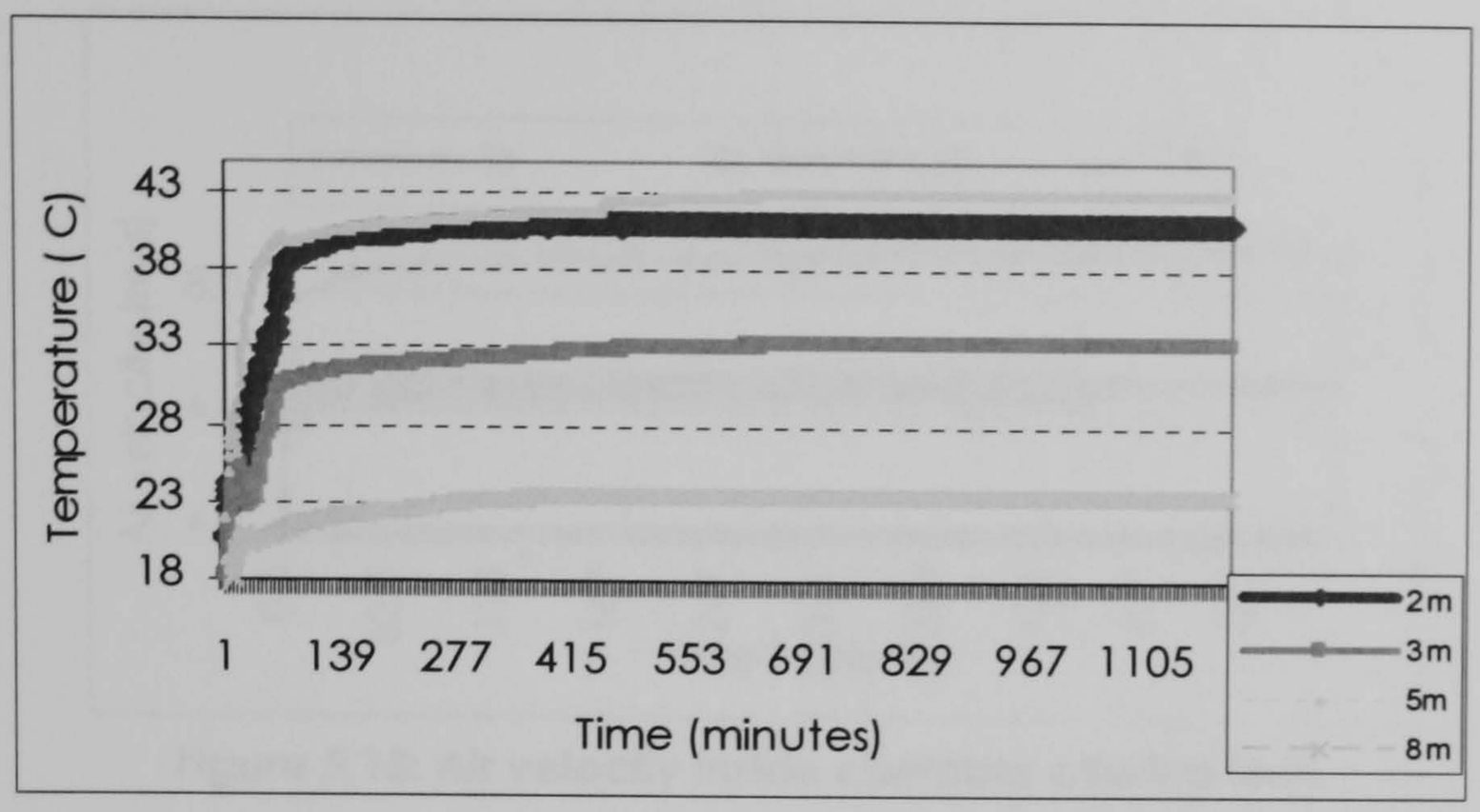

Figure 5.11: Chamber air temperature, heating test

Where the "m" in tests 1,2,3 and 4 means heating (charging) tests
The temperature applied to test 7s is slightly cooler than that for test 4s. This jointly with a larger cell volume on test 7s allows a slightly lower temperature on test 7s as can be observed in Figure 5.12

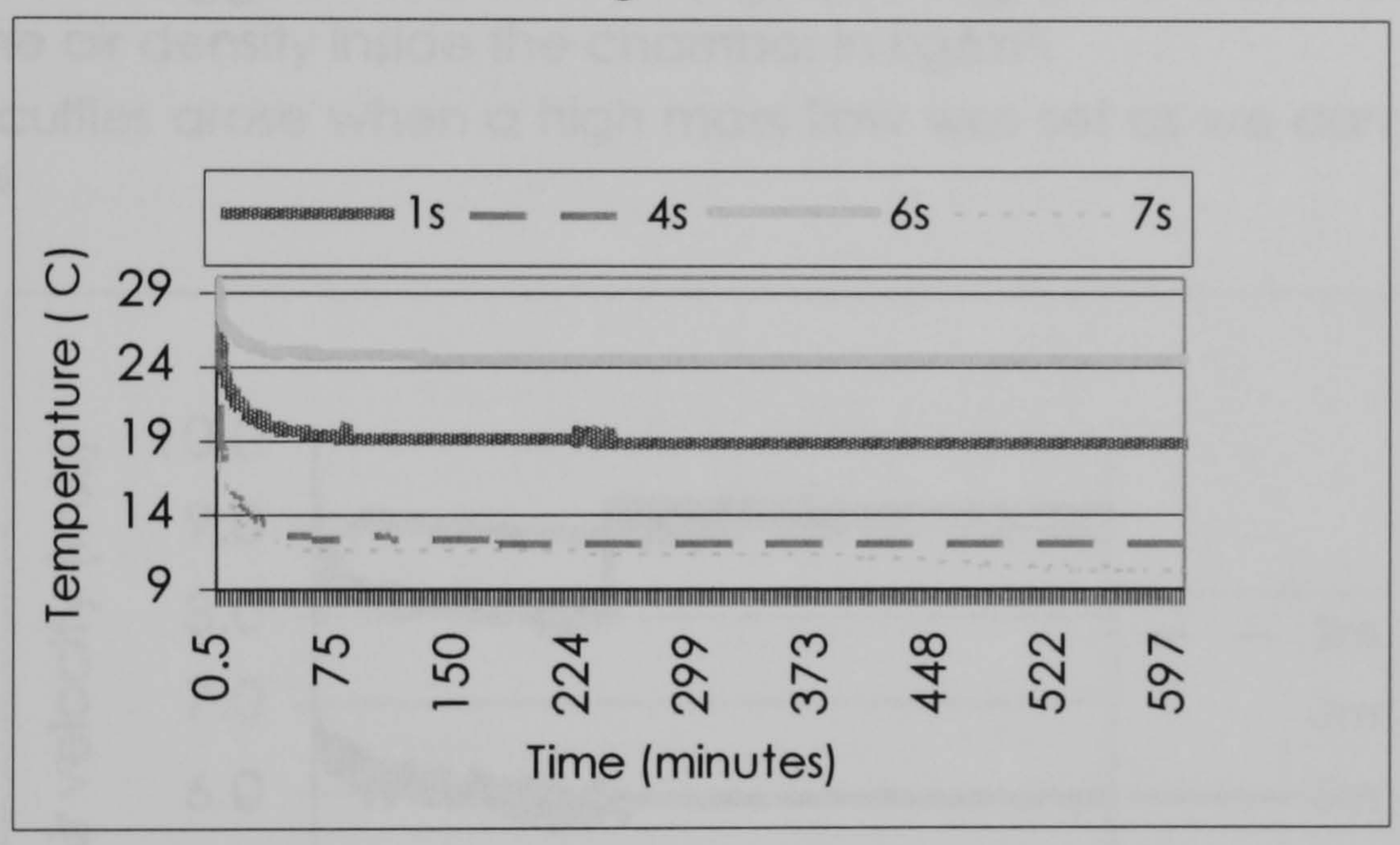

Figure 5.12: Chamber air temperature, cooling test

Where the "s" in tests 1,2,3 and 4 means cooling (discharging) tests
Air velocity applied for the experiments was set as high (between 8 and 8.5 m/s) and low (between 6 and 6.5 m/s). This was the feasible air mass flow range to be achieved with the available equipment, as this was the maximum air intake supplied from the fan. which is within comfort requirements (between 4 and 6 g/s). The difference in temperatures occurred due to experimental difficulties as we can observe in Figure 5.13 . The interaction between the effects of mass flow coupled with the rest of the test settings on the charging/discharging of the unit is an important aspect to attain charging/discharging control.

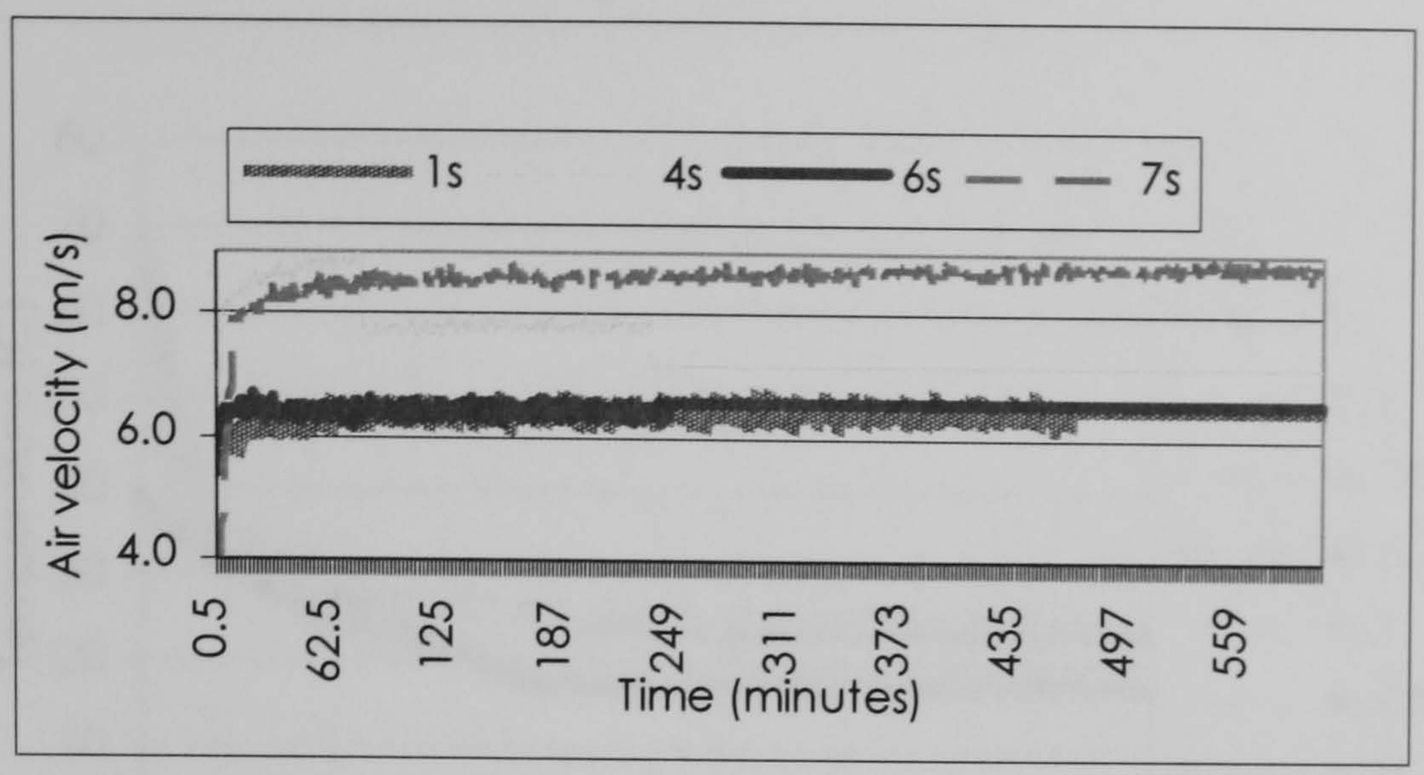

Figure 5.13: Air velocity inside chamber cooling tests

The air velocity was calculated from the logged mass flow according with the density of the air inside the chamber (corresponding to the air temperature applied inside the chamber). $V = \frac{\dot{m}}{A * \rho}$; where V is the velocity in m/s, $\dot{m}$ is the logged mass flow rate given in kg/s, A is the effective area, and ρ is the air density inside the chamber in kg/m^3.

Some difficulties arose when a high mass flow was set as we can observe in Figure 5.14

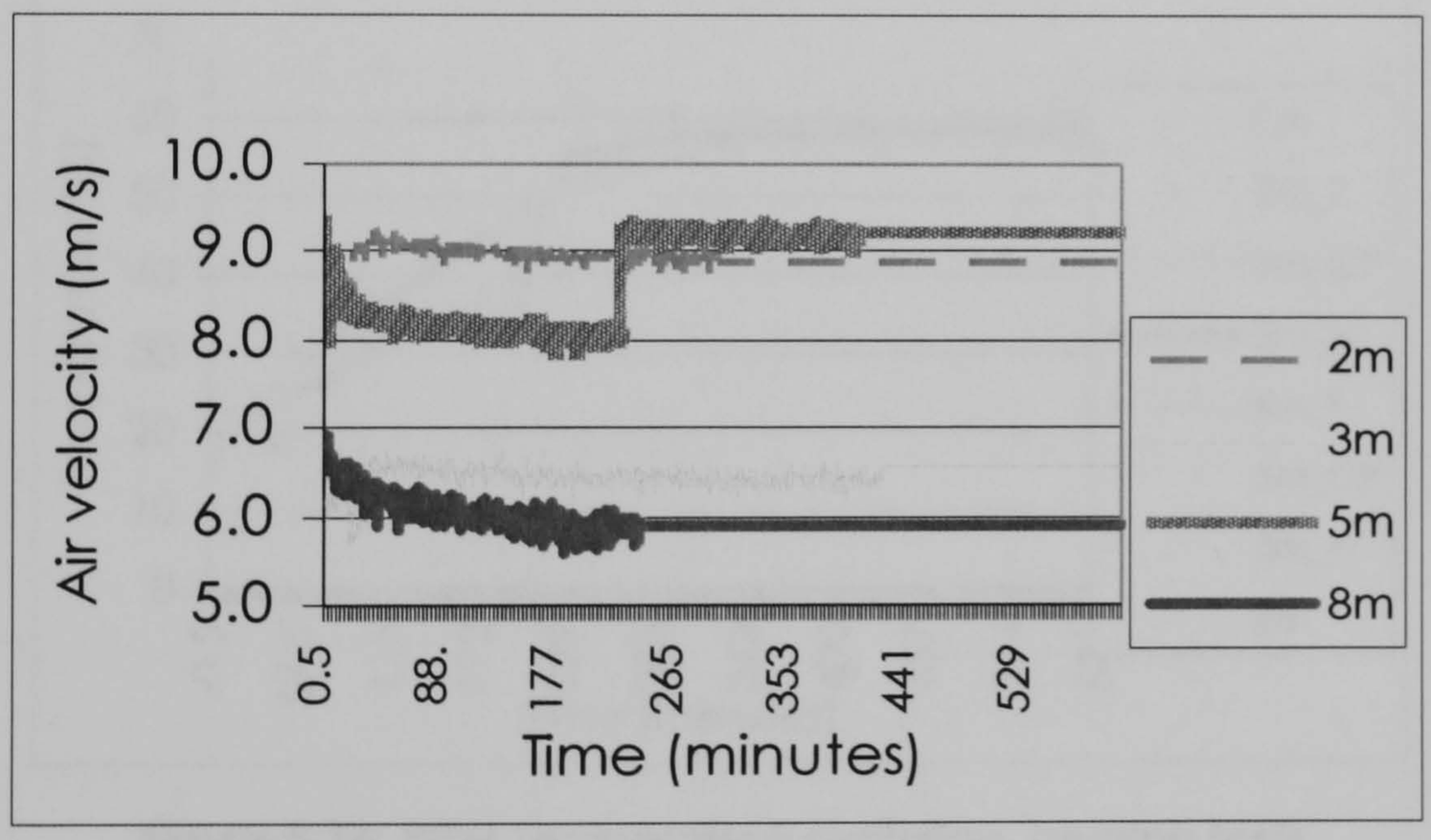

Figure 5.14: Air velocity inside chamber, heating tests

Temperature evolution of tests 1s and 4s is similar. Even though test 4s was set with a small volume, the fact that it contains multiple PCMs, and a high mass flow has an effect on the temperature evolution, as we can observe in Figure 5.15

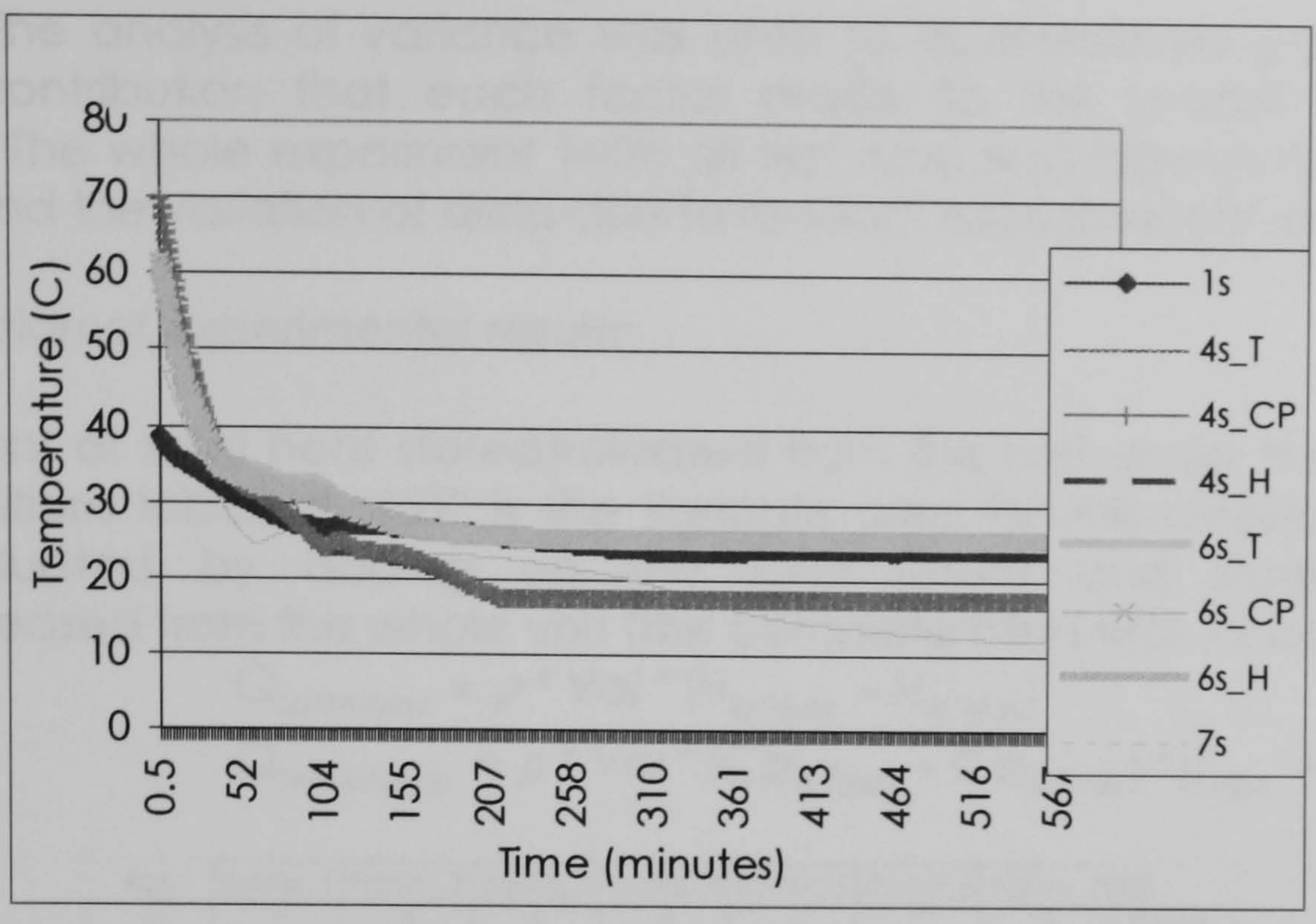

Figure 5.15: PCM temperature evolution, cooling tests

In test 2m the PCM has completely melted after 50 minutes, this was the test with the fastest charging rate. The other tests take around 2 hours to melt completely as we can observe in Figure 5.16

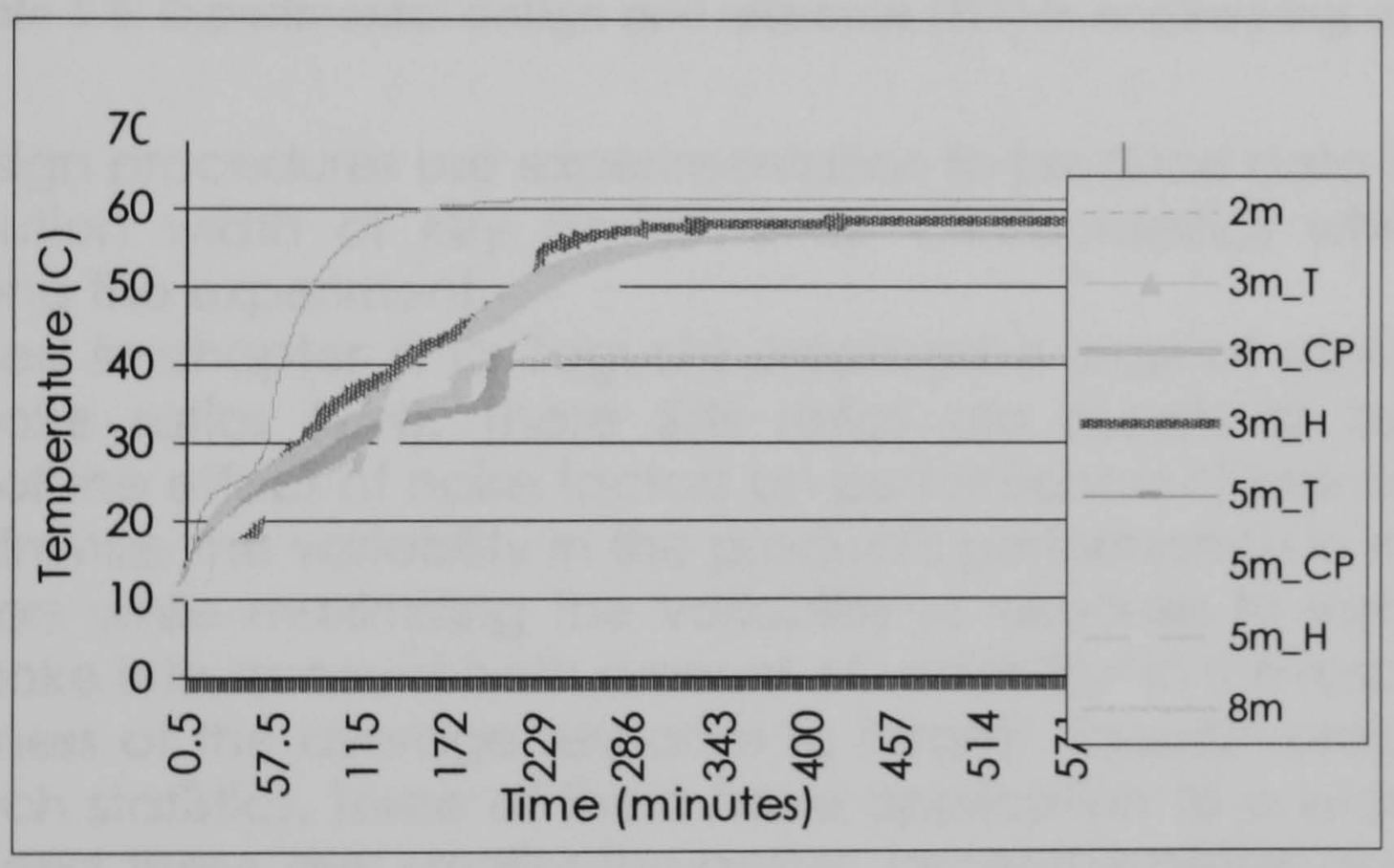

Figure 5.16: PCM temperature evolution, heating tests

Statistical analysis:

Statistical analysis was undertaken using a number of different statistical indicators. The results these analyses are shown in Table 5.7 and interpretation of the meaning of the indicators and their significance regarding the LHSS are discussed below.

ANOVA: The analysis of variance was used to quantitatively estimate the relative contribution that each factor made to the overall measured response. The whole experiment (with all test runs) was repeated 3 times in order to find the variation of data due to random experimental variability.

Interpretation of experimental results:

The amount of total heat stored/released from the unit under the different test conditions labelled "EST" is the variable used for this assessment. EST was evaluated by adding up the total latent and sensible heat stored/released from the whole unit (the complete blind with 12 cells).

$$Q_{LatentMax} = \rho * Vol * (H_{@Tmax} - H_{@Tmin})$$

$$Q_{SensibleMax} = \rho * Vol * (Cp_{@Tmax} - Cp_{@Tmin}) * (T_{max} - T_{min})$$

Run	Factor_1	Factor_2	Factor_3	Factor_4	Factor_5	Factor_6	Factor_7	EST
1s	2	2	1	2	1	1	2	152648.1
2m	2	2	1	1	2	2	1	175800.9
3m	2	1	2	2	1	2	1	543808.4
4s	2	1	2	1	2	1	2	146862.6
5m	1	2	2	2	2	1	1	556438.4
6s	1	2	2	1	1	2	2	97232.21
7s	1	1	1	2	2	2	2	486110.1
8m	1	1	1	1	1	1	1	147439.2

Table 5.5: Experimental design and response (EST) in engineering units

Robust design procedures use experimentation to produce data that define the distribution width of key performance characteristics while noise is active during the experiment.
As explained in chapter 4, Dr Taguchi proposed a class of statistics called signal-to-noise ratios (S/N). These S/N ratios are meant to be used as measures of the effect of noise factors on performance characteristics. We want to minimize the variability in the product's performance in response to noise factors while maximizing the variability in response to signal factors. S/N ratios take into account both amount of variability[3] in the response data and closeness of the average response to target[4]. Taguchi proposed over seventy such statistics. Three of them have application to a wide range of situations, and these are: smaller-the-better, larger-the-better and nominal-the best.

The adjusted mean square deviation of the average quality loss function actually accounts for sensitivity to noise. This is the key concept behind the S/N ratio. As the mean squared (the signal) increases and the variance

---

[3] There is interest in the effect of variation; Taguchi has created a transformation (S/N ratio) of the repetition data to another value which is a measure of the variation present.
[4] The S/N ratio is designed to separate the effects of noise on the response from the mean value of the response.

(the noise) decreases, the performance against the effects of noise is maximized while simultaneously the loss is minimized.
The particular response we were looking for whilst testing in this particular work was to maximize the energy stored/released; so the S/N ratio larger-the-better was used.
A distinguishing characteristic of the larger-the better type problem is that the desired value of the response is the largest number possible.

Statistical techniques for describing data distributions are key concepts for Robust Design; these include: mean, variance, standard deviation and the coefficient of variation.

The ANOVA (analysis of variance) is a computational technique that enables the engineer to quantitatively estimate the relative contribution each control factor makes to the overall measure response and express it as a percentage. In the Taguchi approach the ANOVA can be applied to two forms of data. First it can be applied to the data as measured in engineering units (as J in the case of energy stored) as shown in Table 5.5 . Second it can be applied to the data after it has been transformed into S/N ratios, as shown in Table 5.6.

With the given energy stored during each test, the data was transformed to the S/N ratios given for a larger the better type problem. In this work the software STATISTICA was used for the analysis of the robust design experiment. The S/N ratios were given in a column called Eta values.

Design Summary (estlar2.sta)

	F1	F2	F3	F4	F5	F6	F7	
	PROVINCE	SEASON	PCM	THICKNESS	M_FLOW	INSU	MODE	Eta
1	2	2	1	2	1	1	2	103.6738
2	2	2	1	1	2	2	1	104.9004
3	2	1	2	2	1	2	1	114.7089
4	2	1	2	1	2	1	2	103.3382
5	1	2	2	2	2	1	1	114.9083
6	1	2	2	1	1	2	2	99.7562
7	1	1	1	2	2	2	2	113.7347
8	1	1	1	1	1	1	1	103.3723

Table 5.6: Experimental design and S/N ratio (Eta)

In this case the central tendency of this Eta values was 107.29 (see Table 5.7). That is, this mean corresponds to the S/N ratios for a larger the better type problem. Sigma is the variance, which measures the width of a distribution of data about the mean value. STATISTICA calculates the variance as the sum of squared deviations about the mean divided by n-1. The standard deviation is also a measure of variability and is calculated as the square root of the variance.

Analysis of Variance (estlar2.sta)
Mean = 107.299 Sigma = 6.10764

Factor	SS	df	F	p
{1}PROVINCE	3.315444	1	0.021	0.909
{2}SEASON	17.74679	1	0.112	0.795
{3}PCM	6.178469	1	0.039	0.876
{4}THICKNES	158.9427	1	4.206	0.289
{5}M_FLOW	29.53143	1	0.186	0.741
{6}INSU	7.619788	1	0.048	0.863
{7}MODE	37.78841	1	0.238	0.711

Table 5.7: Analysis of variance experiment 2

ANOVA uses a mathematical technique known as the sum of squares (SS) to quantitatively examine the deviation of the control factor effect response averages from the overall experimental mean response. That is, the variation between the control factors.
In this case, the highest sum of squares is the thickness; this factor's power to reduce variation is strong. The lowest SS was the province.

The degrees of freedom describe how much information can be extracted from the experiment. The number of degrees of freedom needed to describe a factor effect is 1 less than the number of levels tested for that factor. In this case, L8 has a total of 7 degrees of freedom for the entire experiment, allocated to 7 columns of 2 levels, each column having 1 degree of freedom. Consequently, 1 degree of freedom is allowed for each fair (independent) comparison that can be made in the data.

The variance ratio (F) is used to test for the significance of factor effects. It is the ratio of the control factor effect variance, and the experimental error variance. For F>4 the control factor is strong, that is in these experiments the case of factor "thickness" is strong. The next significant factor effect is the mode, then the mass flow rate, then the season, then the insulation, then the PCM and finally the province.

The significance (p) of a relation between variables depends on the size of the sample[5]. The significance level calculated for each correlation is a primary source of information about the reliability of the correlation. The statistical significance of a result is an estimated measure of the degree to which it is "true" (in the sense of "representative of the population")[6]. More technically, the value of the p-level represents a decreasing index of the reliability of a result. The higher the p-level, the less we can believe that the observed relation between variables in the sample is a reliable indicator of the relation between the respective variables in the population. Specifically, the p-level represents the probability of error that is involved in

---

[5] The smaller the relation between variables, the larger the sample size is necessary to prove it significant.
[6]That is, there is strong evidence of a real factor effect.

accepting our observed result as valid, that is, as "representative of the population." In many areas of research, the p-level of .05 is customarily treated as a "border-line acceptable" error level. In this case it will be necessary to carry out alternative analysis to verify the actual significance of each factor effect.

How these statistical indicators relate to the system tested are now to be considered in more detail.

Surface plots:

The surface plots Figure 5.17 to Figure 5.21 display a surface representing a smoothed image of the data following one of the available transformation/fitting procedures. The available (in "statistica" software) 3D predefined Graphs Fitted Functions are: Linear Smooth, Quadratic Smooth, Least Squares, Negative Exp/Wght, Spline Smooth, Custom Function. In the plots presented the quadratic fitting was selected.

The following plot Figure 5.17 shows that the factor "mode" has a significant effect in summer, when the conditions for discharging (during cooling) are less favourable, and thus a lot more energy is stored (during heating)compared with the energy released. Energy stored during either winter or summer is large, but has similar value for both winter/summer therefore the season doesn't seem to have a large effect.

Surface plot raw data			
Test	Season	Mode	Est(J)
1	Summer	Solidifying	152648
2	Summer	Melting	175801
3	Winter	Melting	543808
4	Winter	Solidifying	146863
5	Summer	Melting	556438
6	Summer	Solidifying	97232
7	Winter	Solidifying	486110
8	Winter	Melting	147439

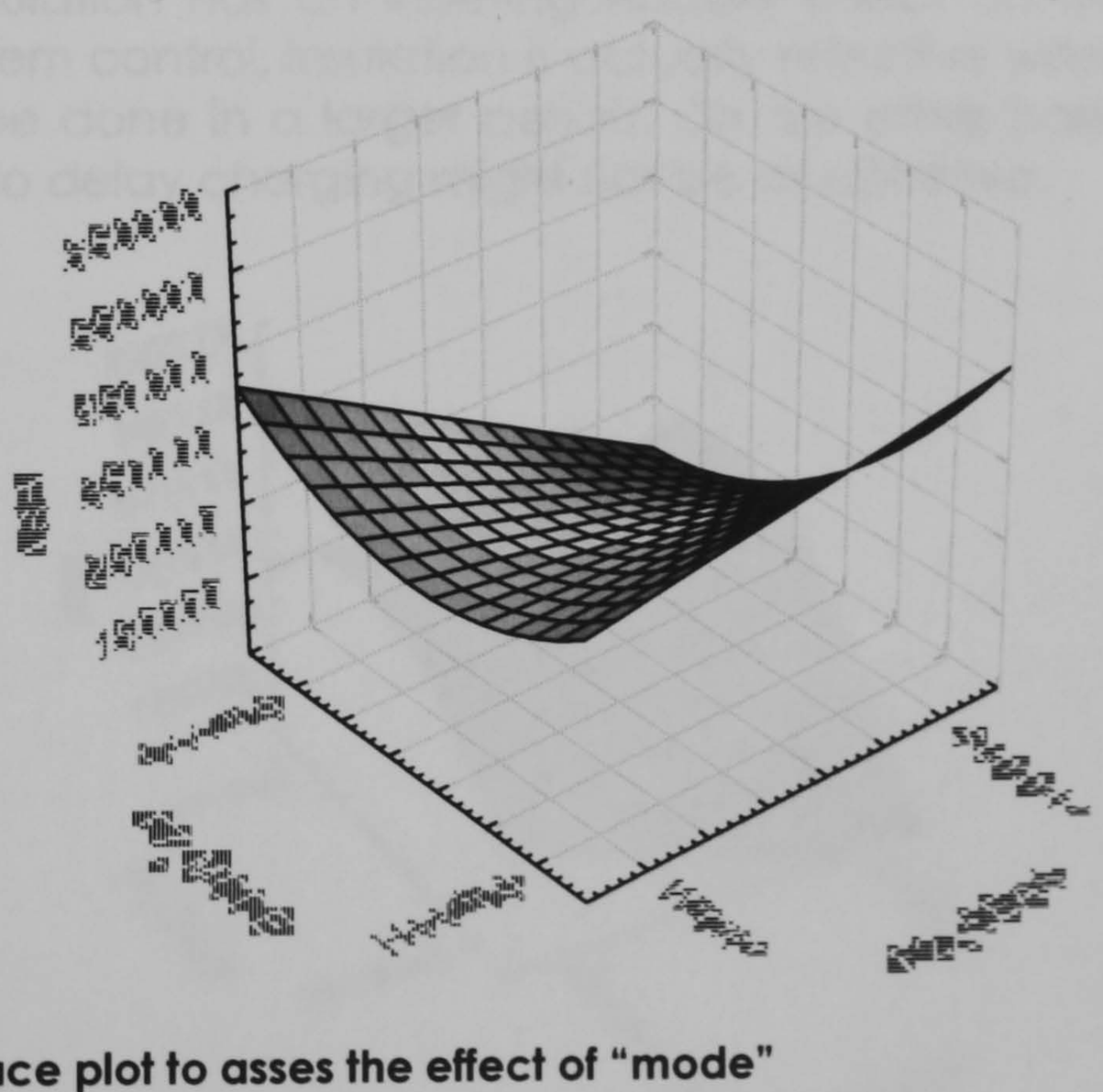

Figure 5.17: Surface plot to asses the effect of "mode"

In Figure 5.18 the effect of mass flow and mode on the energy stored/released are plotted. As mentioned before, less energy is released during the cooling tests (solidification), and this is especially clear for high

mass flow in comparison with the energy stored during the heating tests (melting) also with high mass flow. For low mass flow rate a similar amount of energy is stored as that released, so the effect of mass flow is less pronounced for low mass flow rates.

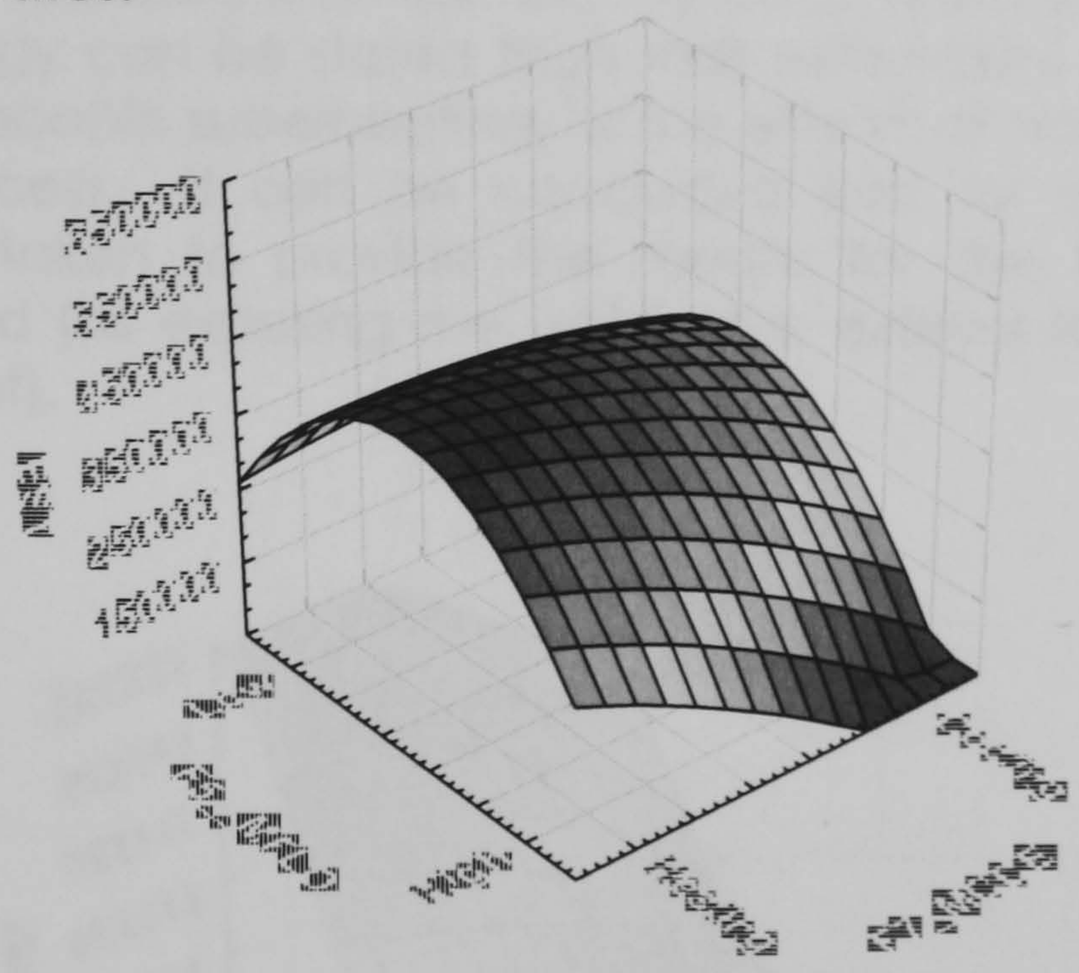

Surface plot raw data			
Test	Mode	Mass flow	Est(J)
1	Solidiying	Low	152648
2	Melting	High	175801
3	Melting	Low	543808
4	Solidiying	High	146863
5	Melting	High	556438
6	Solidiying	Low	97232
7	Solidiying	High	486110
8	Melting	Low	147439

Figure 5.18: Surface plot to asses the effect of mass flow during solidification

In Figure 5.19 the effect of insulation and mode on the energy stored/released are plotted. During cooling the presence of insulation is more noticeable, as the amount of energy released clearly drops. During heating the presence of insulation has an indistinguishable effect on the energy stored. That is, for system control, insulation is actually effective when the discharging requires to be done in a larger period. On the other hand the application of insulation to delay charging might not be as effective.

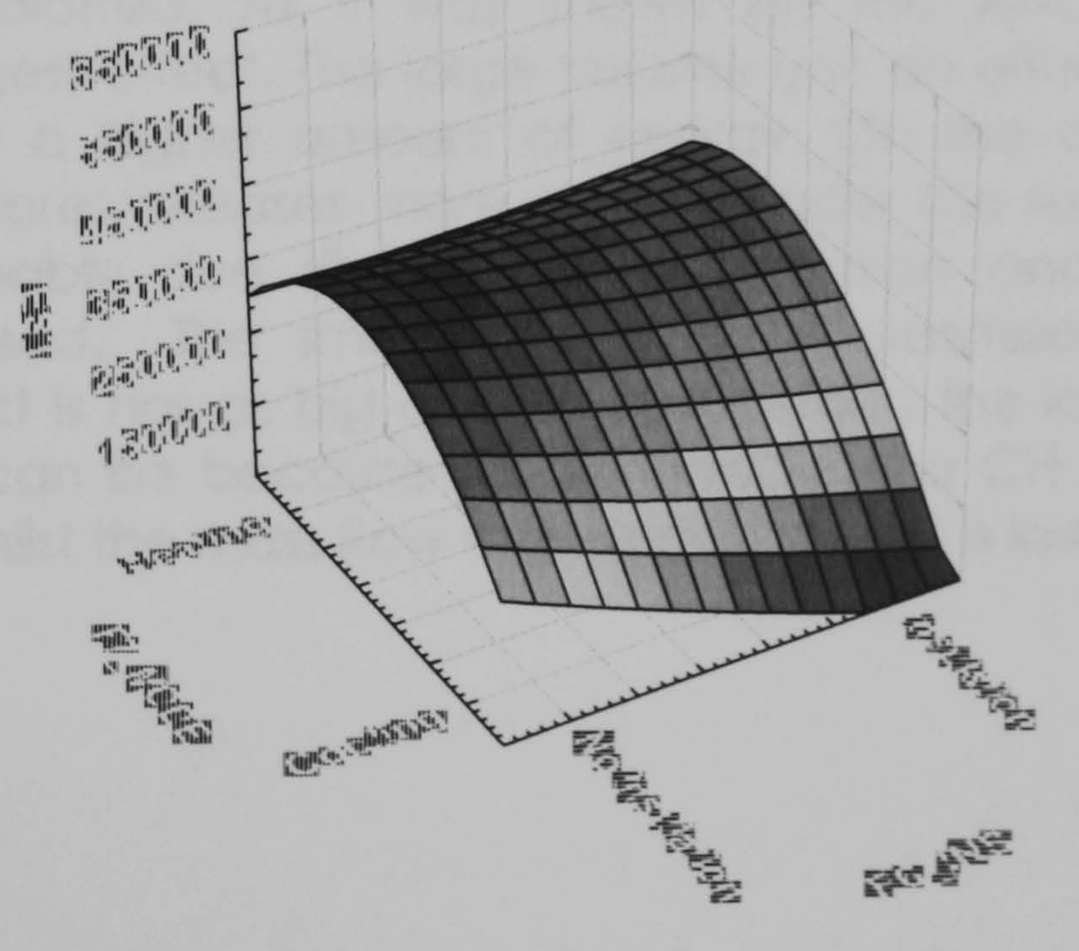

Surface plot raw data			
Test	Mode	Insulation	Est(J)
1	Solidifying	With	152648
2	Melting	without	175801
3	Melting	without	543808
4	Solidifying	With	146863
5	Melting	With	556438
6	Solidifying	without	97232
7	Solidifying	without	486110
8	Melting	With	147439

Figure 5.19: Surface plot to assess the effect of the presence of insulation

In Figure 5.20 the effect of volume (blind thickness) and mode on the energy stored/released are plotted. Here we can observe how large the

effect of the PCM volume on the energy stored and released is. The amount of energy stored and energy released by the large volume blind is much higher that that for the small volume blind. For the small blind the amount of energy stored and the energy released is similar. On the other hand in the large volume blind more energy can be stored than that withdrawn. This can be due either to some probable superheating, or the effects of natural convection delaying the process. It can be concluded that for large volume units care most be taken to provide the means for the total discharge of the energy stored (as exposing the unit to the exterior lower temperature conditions at night).

Surface plot raw data			
Test	Mode	Thickness	Est(J)
1	Solidifying	1.5"	152648
2	Melting	0.5"	175801
3	Melting	1.5"	543808
4	Solidifying	0.5"	146863
5	Melting	1.5"	556438
6	Solidifying	0.5"	97232
7	Solidifying	1.5"	486110
8	Melting	0.5"	147439

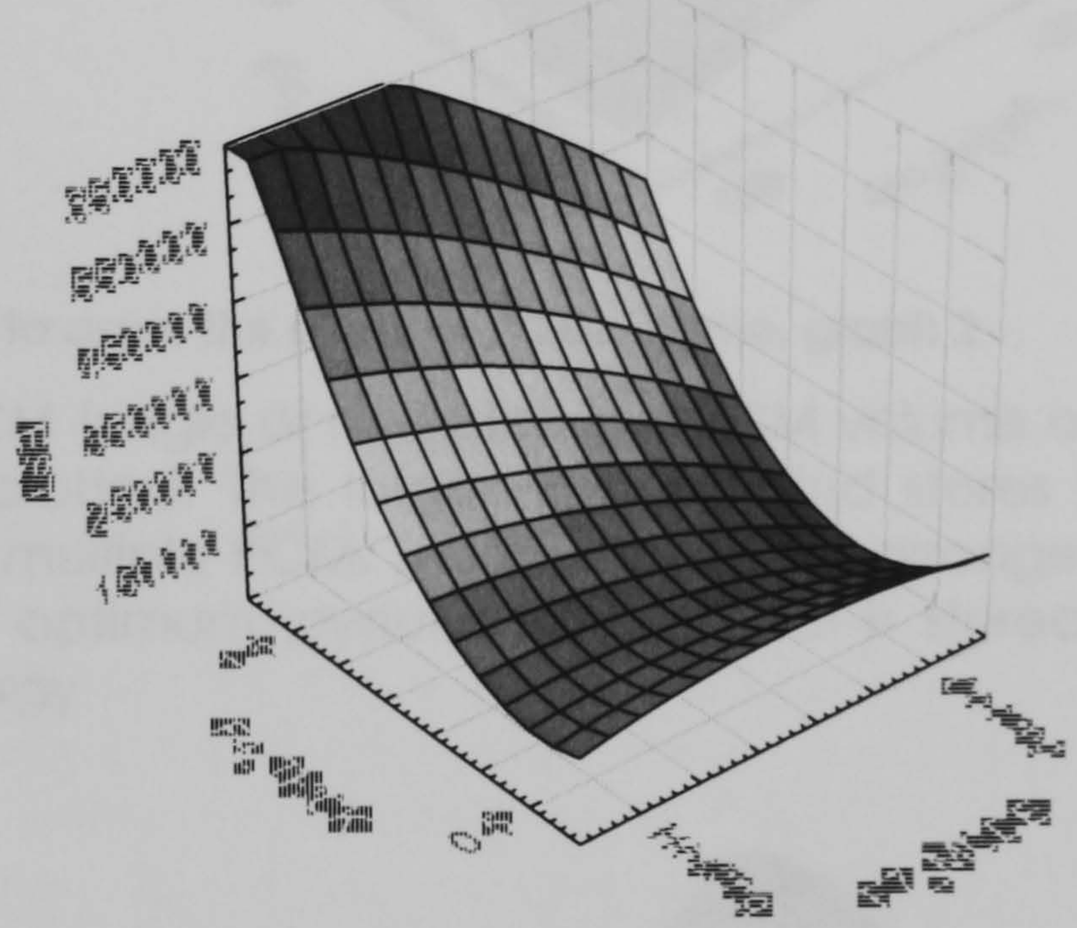

Figure 5.20: Surface plot to assess the effect of PCM volume

In Figure 5.21 the effect of volume (blind thickness) and province on the energy stored/released are plotted. As it was shown on the ANOVA, thickness is the factor with largest effect. The large volume unit on either of the provinces stores/ releases a higher amount of energy. On the other hand the large volume unit stores/releases more energy under the region BC weather conditions, probably due to the higher radiation and air temperature conditions imposed. The small volume unit stores/releases slightly more energy (the effect is not as big as that observed in the larger volume unit) in Chiapas. This can be because the settings for the CH tests include high mass flow rate, whilst the mass flow rate applied to BC is low.

Surface plot raw data			
Test	Province	Thickness	Est(J)
1	CH	1.5"	152648
2	CH	0.5"	175801
3	CH	1.5"	543808
4	CH	0.5"	146863
5	BC	1.5"	556438
6	BC	0.5"	97232
7	BC	1.5"	486110
8	BC	0.5"	147439

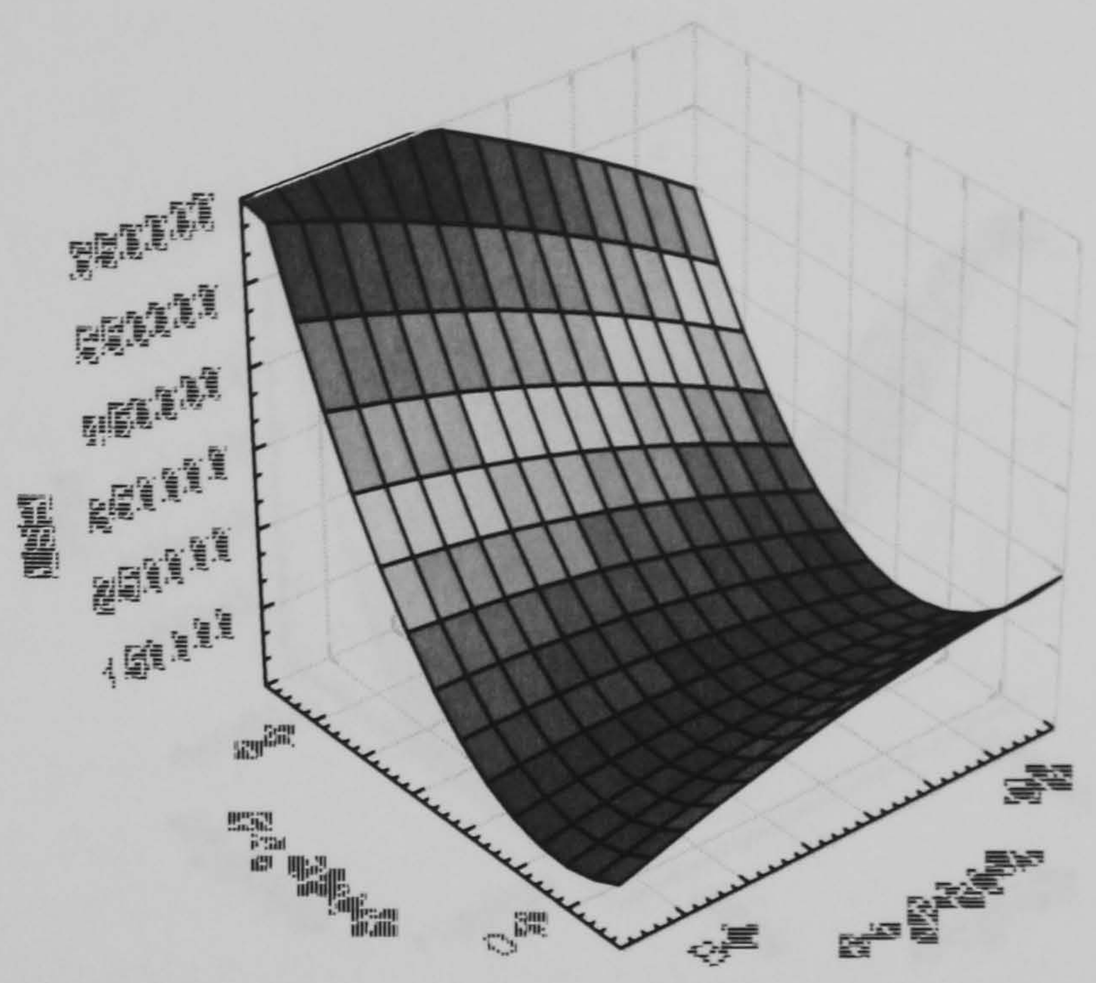

Figure 5.21: Surface plot to asses the effect of PCM volume, graph 2

In Figure 5.22 the effect of PCM (single or multiple) and PCM volume on the energy stored/released are plotted. The larger volume blind stores more energy either with a single or multiple PCM. The multiple PCM arrangement in a large volume unit is the optimum layout as more heat is stored. The single PCM unit stores less energy

Surface plot raw data			
Test	Thickness	PCM	Est(J)
1	1.5	Single	152648
2	0.5	Single	175801
3	1.5	Multiple	543808
4	0.5	Multiple	146863
5	1.5	Multiple	556438
6	0.5	Multiple	97232
7	1.5	Single	486110
8	0.5	Single	147439

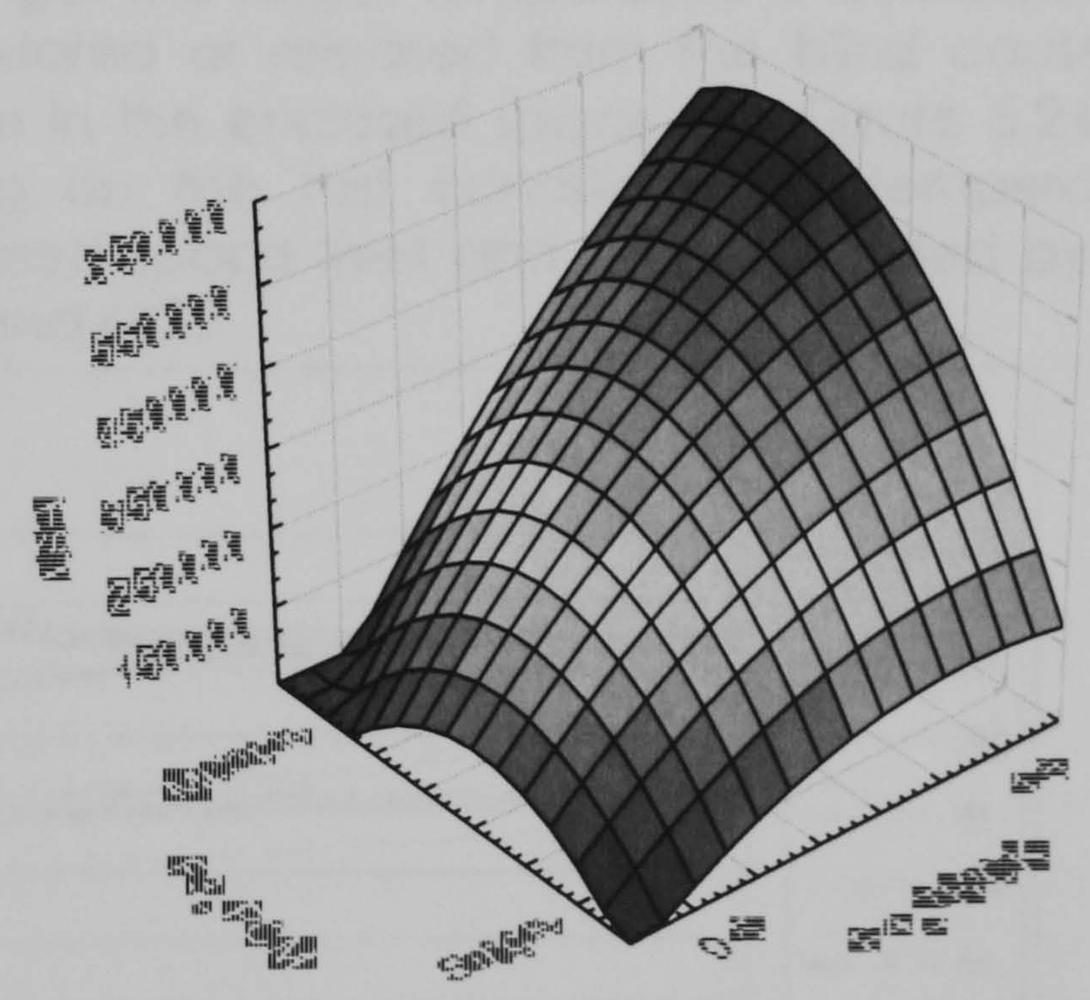

Figure 5.22: Surface plot to asses the effect of PCM type regarding PCM volume

In Figure 5.23 the effect of PCM (single or multiple) and mode (cooling or heating) on the energy stored/released are plotted. During cooling single PCM units released more heat. During heating multiple PCM units stored more energy. The multiple PCM unit during heating stores the highest amount of every overall

Surface plot raw data			
Test	PCM	Mode	Est(J)
1	Single	Solidifying	152648
2	Single	Melting	175801
3	Multiple	Melting	543808
4	Multiple	Solidifying	146863
5	Multiple	Melting	556438
6	Multiple	Solidifying	97232
7	Single	Solidifying	486110
8	Single	Melting	147439

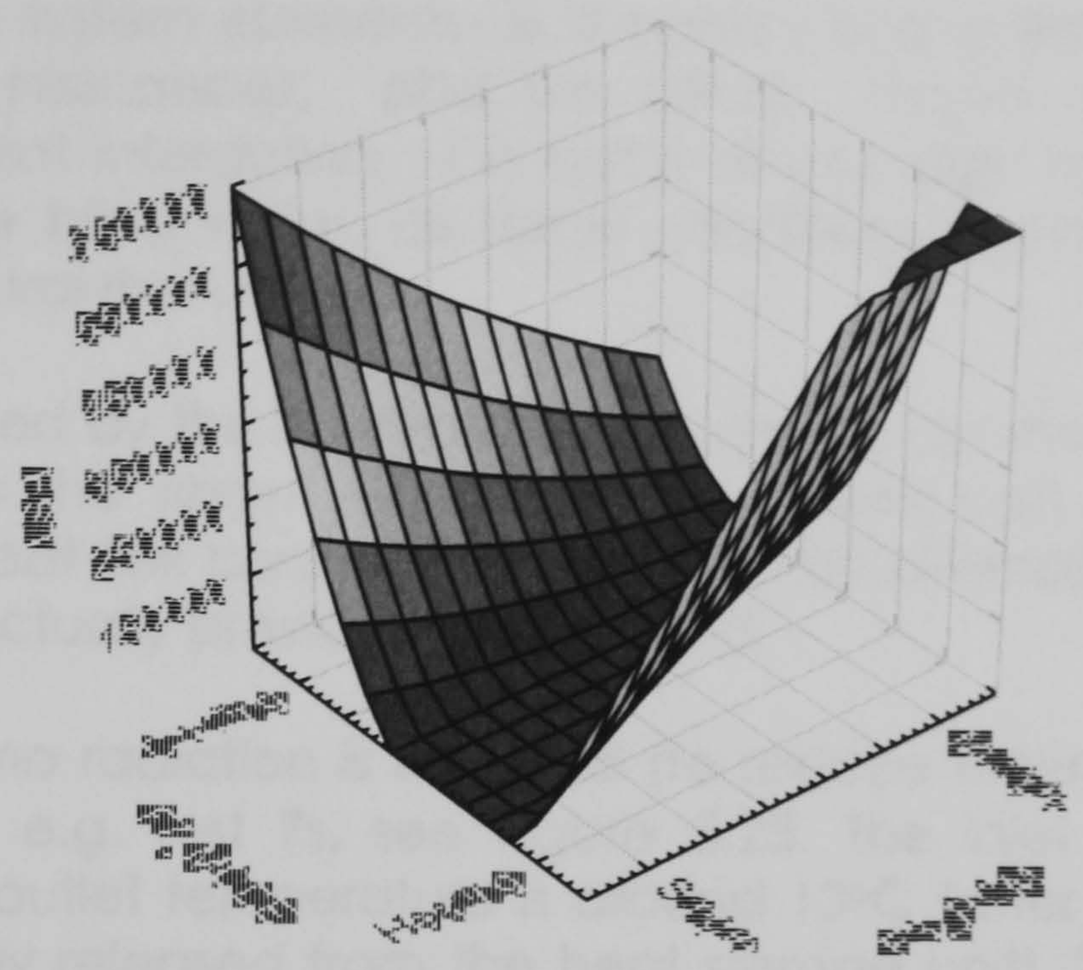

Figure 5.23: Surface plot to assess the effect of PCM type regarding the mode

,

Effect of heat flux from the blind on air temperature

The main objective of the passive system for temperature modulation proposed in this project is to maintain the temperature of the enclosed room within a comfortable range. The target temperature is considered to be 24°C. The energy that is stored or released from the blind causes a change of the air temperature in the enclosed space. On Figure 5.24 we can observe that depending on the test conditions the temperature difference between the enclosed space inlet and outlet provided by the system varied between 0.1°C and 6°C.

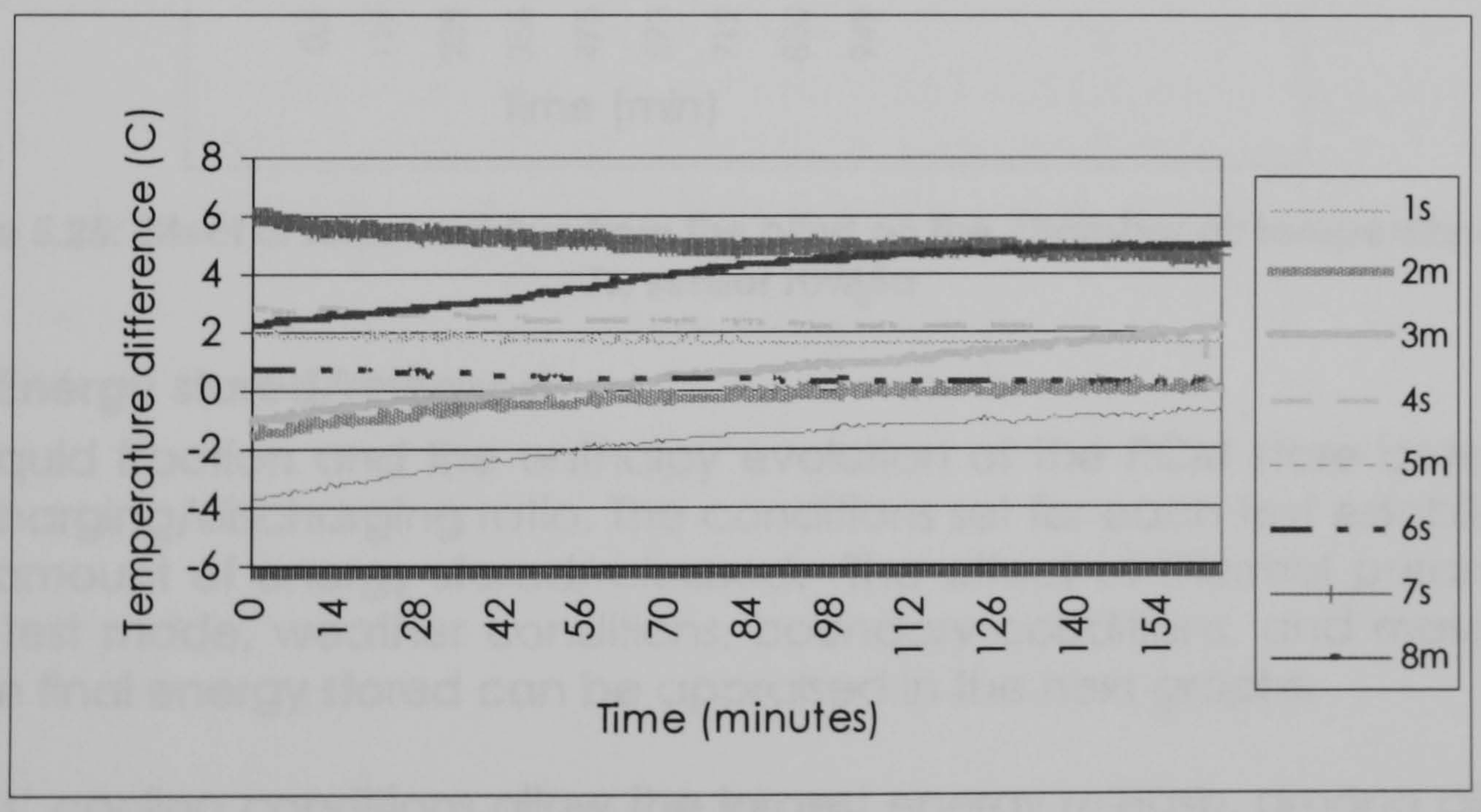

Figure 5.24: Difference between inlet and outlet air temperature for different tests

These temperature differences are attained due to the imposed conditions on each test: irradiation, mass flow rate and temperature of air supplied in

the chamber, properties of the system elements as thermal conductivities, convection coefficients, heat resistances; and the blinds stored and released sensible and latent heat interaction. On each of the eight tests carried out the response of the blind varies, as some conditions imposed allow for more temperature control than others.

How does the heat flux generated by the thermal storage system aid the air temperature to move towards the target temperature? These can be evaluated by comparing the heat flux contribution provided by alternative sources and the final heat flux actually provided by the blind.

We can observe a test where no radiation is imposed (to reduce external assistance from other sources) e.g. test 7s, see Figure 5.25. The inlet air temperature is 9 °C, whilst the outlet temperature is around 13°C (after air has been heated by the energy released from the heat storage unit). This temperature increment is due to the release of the energy stored in the unit, as no other source of heat is present and the chamber is completely insulated.

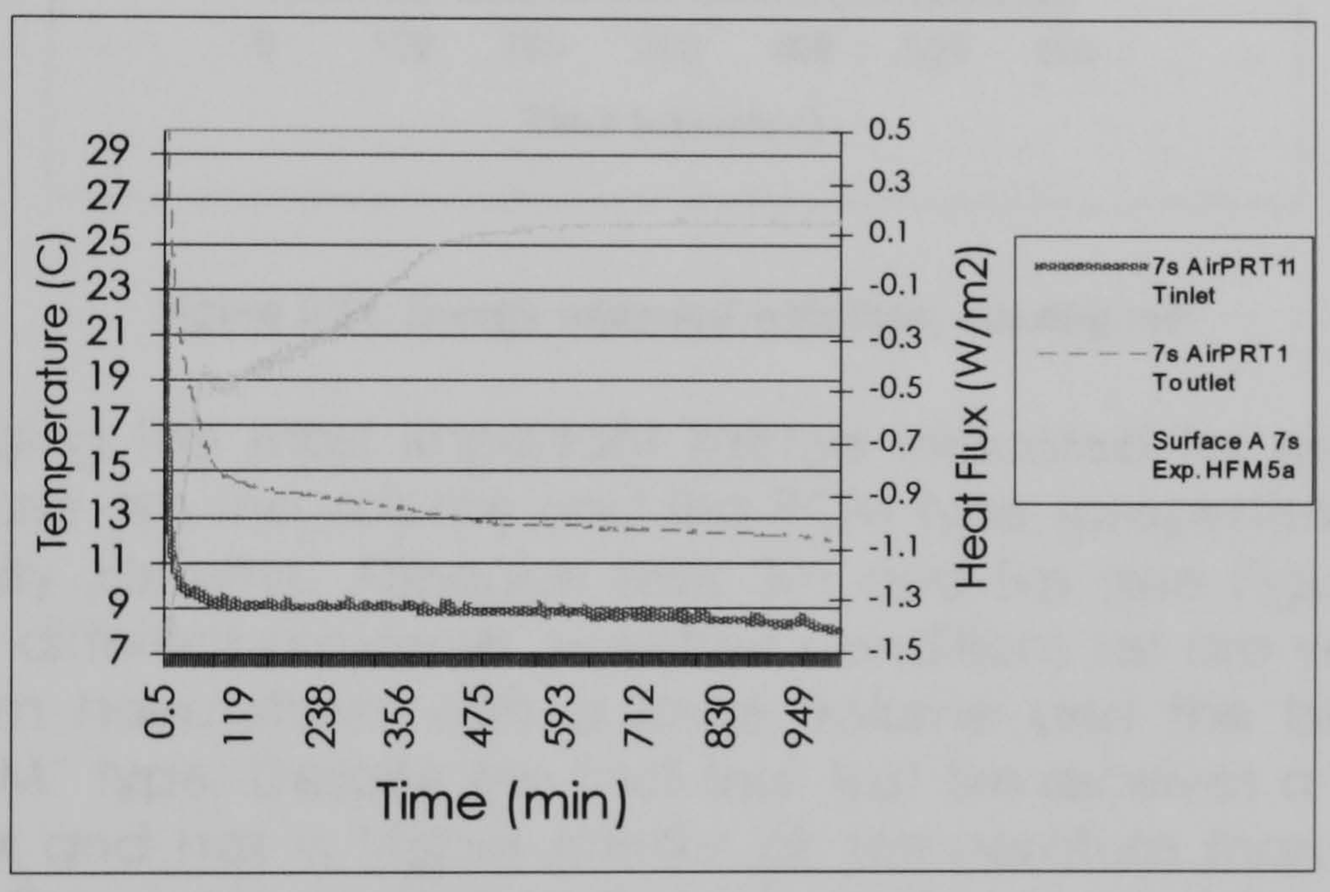

Figure 5.25: Effect of total heat flux from the blind on the chamber air temperature, test 7s, sensor HFM5a

Energy stored/released

The liquid fraction and the enthalpy evolution of the PCM store determine the charging/discharging ratio. The conditions set for each test establish the final amount of energy stored/released. The effect of thermal parameters (e.g. test mode, weather conditions, boundary conditions, and mass flow) on the final energy stored can be appraised in the next graphs.

Test 7s' cooling conditions allow the largest energy release, among all tests, see Figure 5.26. In this case for Baja California, winter reaches a colder temperature than in Chiapas, thus a larger temperature difference allows for a larger amount of heat being released. Additionally, the mass flow rate of the air entering the enclosed space was set to high value. The single CP

storage blind was fully charged. This blind was large, volume 2, and the heat was released from it during a period of more than 5 hours.

Although test 4s also had a low cooling temperature (indoor temperature), the blind was of small volume, and air mass flow rate was low, consequently its energy content was smaller, and it was released in a shorter time of 1.3 hrs.

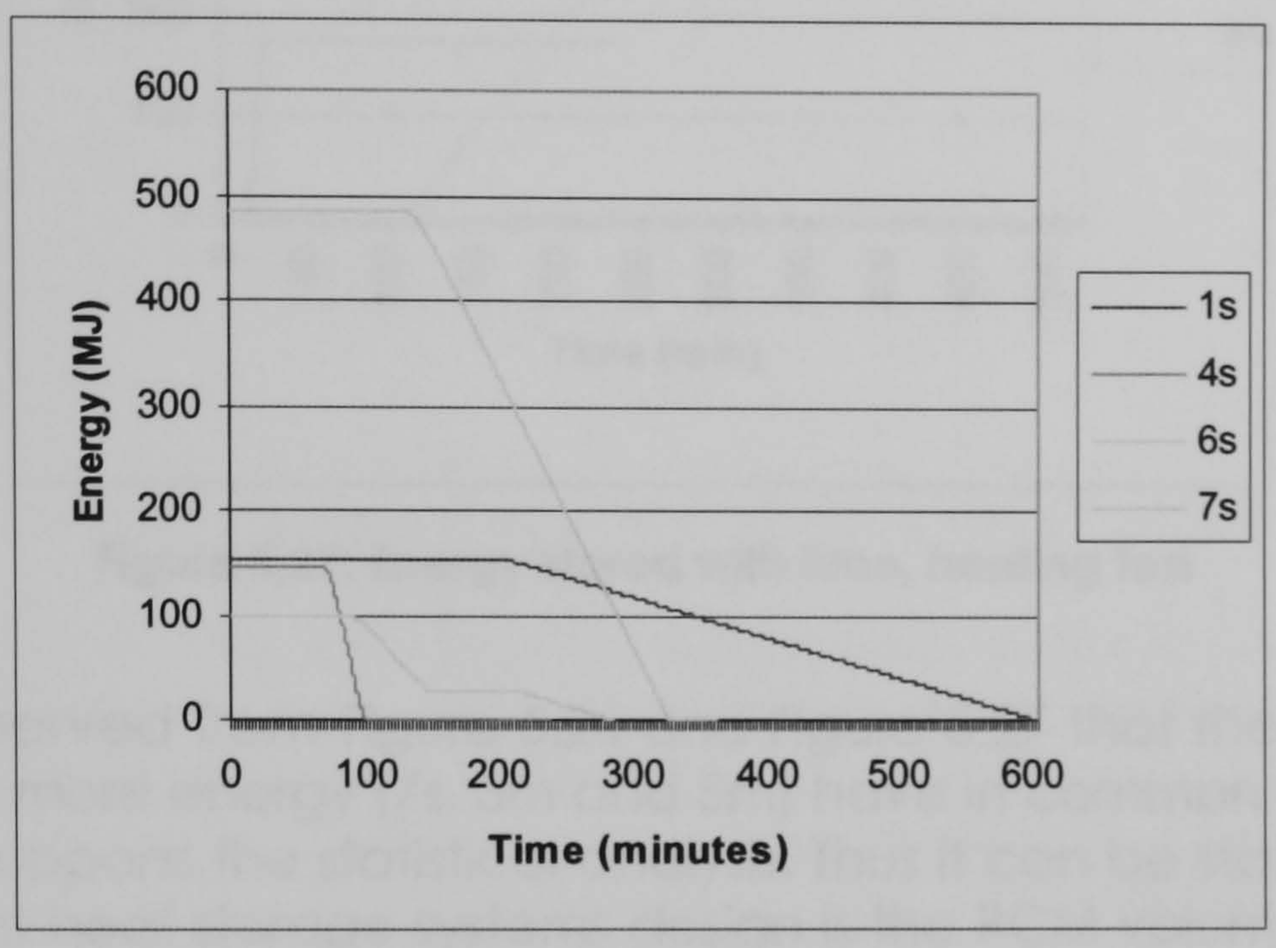

Figure 5.26: Energy released with time, cooling test

During charging the most important factors indicated for greater energy storage/release are the volume and the PCM type (properties: latent heat, heat capacity ,density). Although tests 3m and 5m (see Figure 5.27), are representing different provinces (weather conditions set are very different), both of them have stores with a large volume and the blind is of the "multiple PCM" type. Despite the fact that test 5m receives a more intense radiation flux and has a higher interior air temperature than test 3m, the higher mass flow rate, causing higher energy losses on the surface facing the chamber, and the presence of insulation (on the surface facing the solar simulator) on test 5m cause a longer charging time (8.25 hrs vs 6 hrs charging time for test 3m).

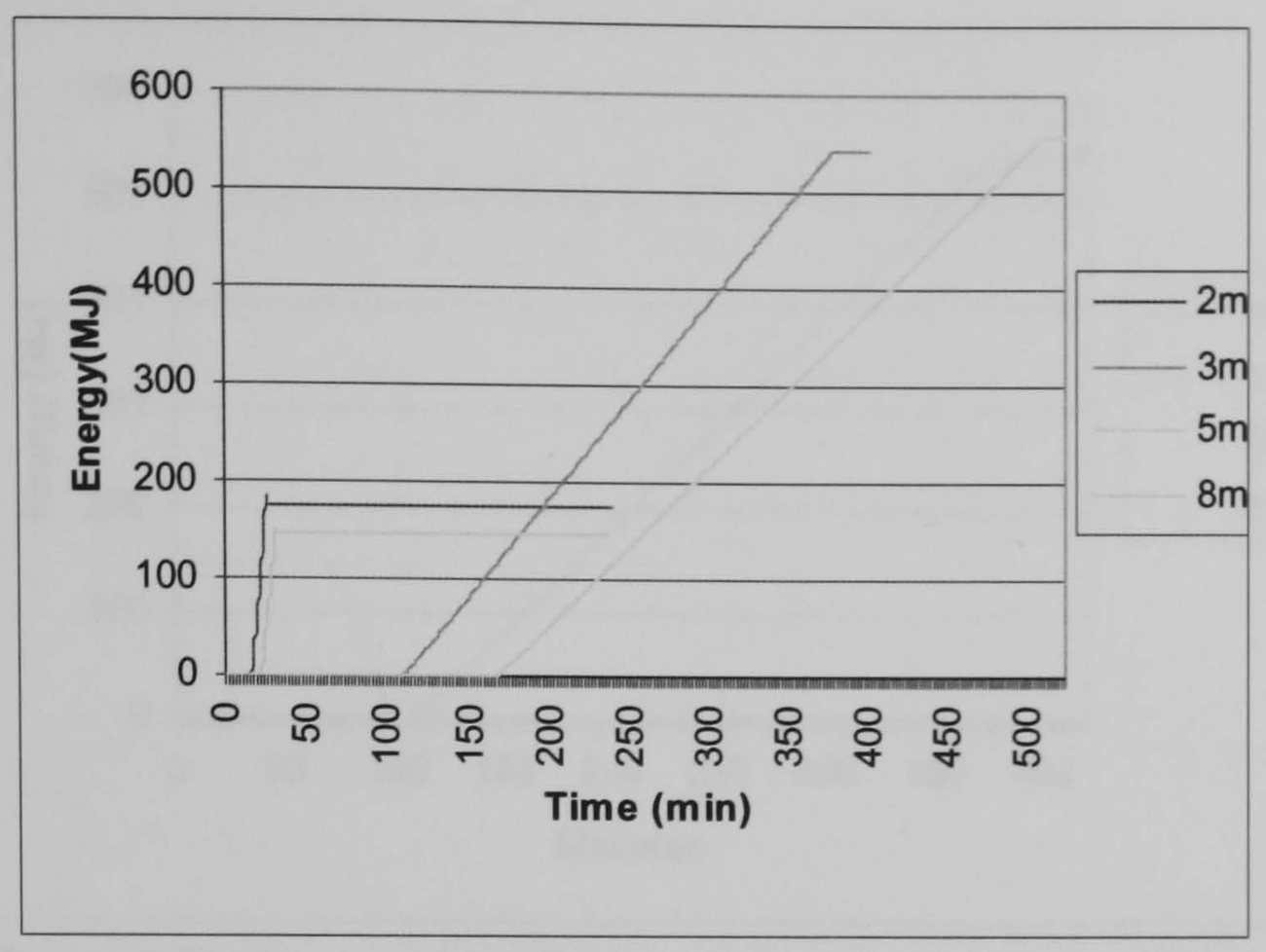

Figure 5.27: Energy stored with time, heating test

It can be observed from Figure 5.26 and Figure 5.27 that the 3 tests storing and releasing more energy (7s, 3m and 5m) have in common being of large volume. This supports the statistical analysis. Thus it can be stated that a key factor in latent heat storage systems design is the PCM volume. As it is now mentioned that the major factor contributing to the large energy storage/release in tests 7s, 3m and 5m is the volume; in the following analysis only other outstanding aspects will be pointed out.

Figure 5.28 shows the energy stored/released evolution for tests under winter conditions. During winter tests 3m and 7s provide the highest energy storage/release. These tests take between 5 and 6 hours for a complete change of phase, whilst the small volume tests take between 0.5 to 1.6 hrs to change state. These tests have in common that neither of them has insulation (besides that these tests are of large volume), whilst tests 4s and 8m do have insulation. The low temperatures prevailing in winter (compared to summer conditions) make it necessary to take advantage of all driving potentials to transfer the heat from or to external sources for charging, and discharging. That is, insulation of the blinds is not recommended to be used under winter conditions.

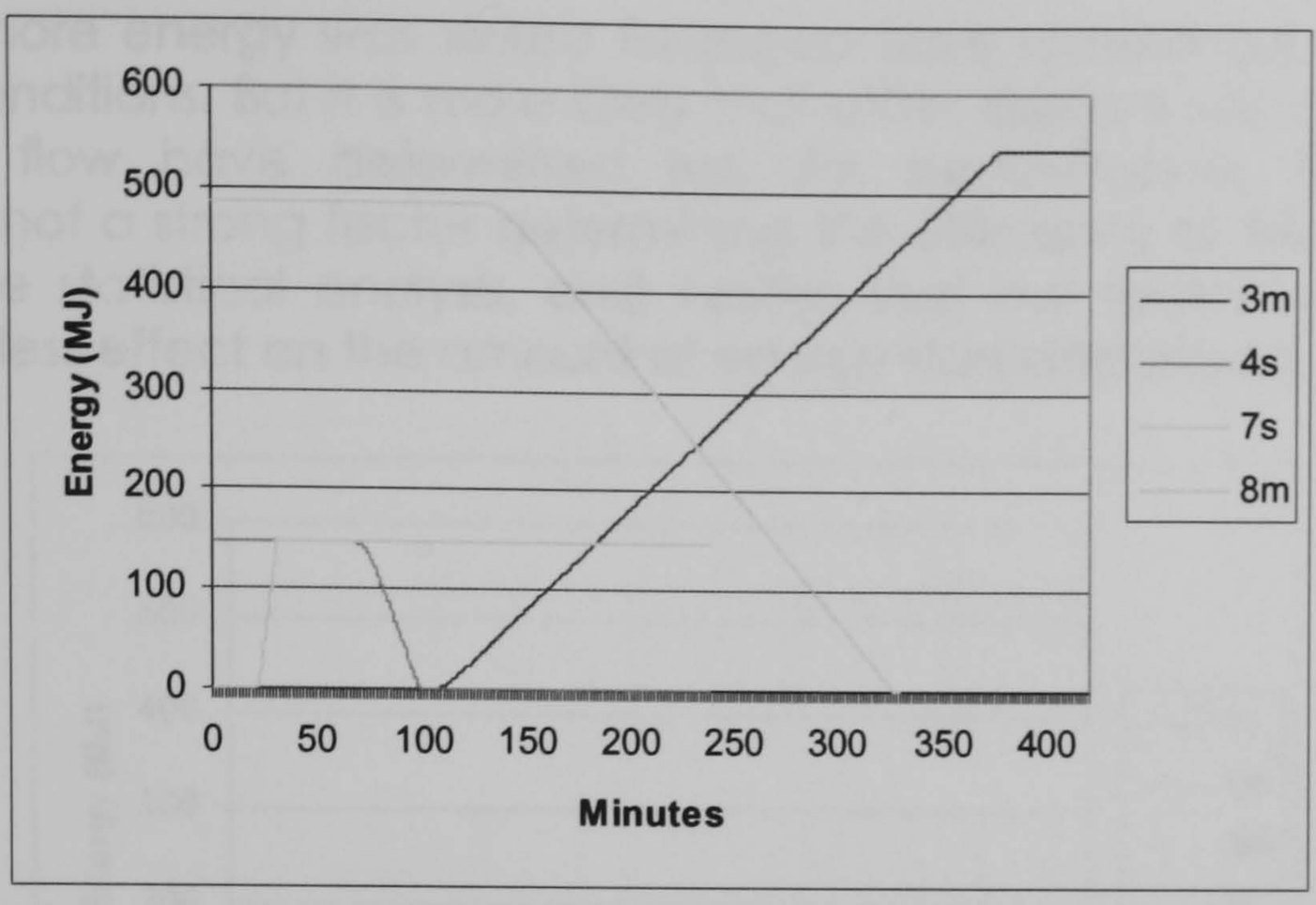

Figure 5.28: Energy stored/released under winter conditions

Figure 5.29 shows the energy stored/released evolution for tests under summer conditions. During summer, test 1s has a large volume and from the start of the test has already in store more heat than its counterpart (test 6s). Although in test 1s the mild weather conditions are imposed (CH), as insulation facing the window is present, the losses to the exterior are reduced; thus the longer discharging time. This supports the statistical analysis. Thus it can be stated that for system control, insulation is in fact favourable when energy needs to be released in a longer period.

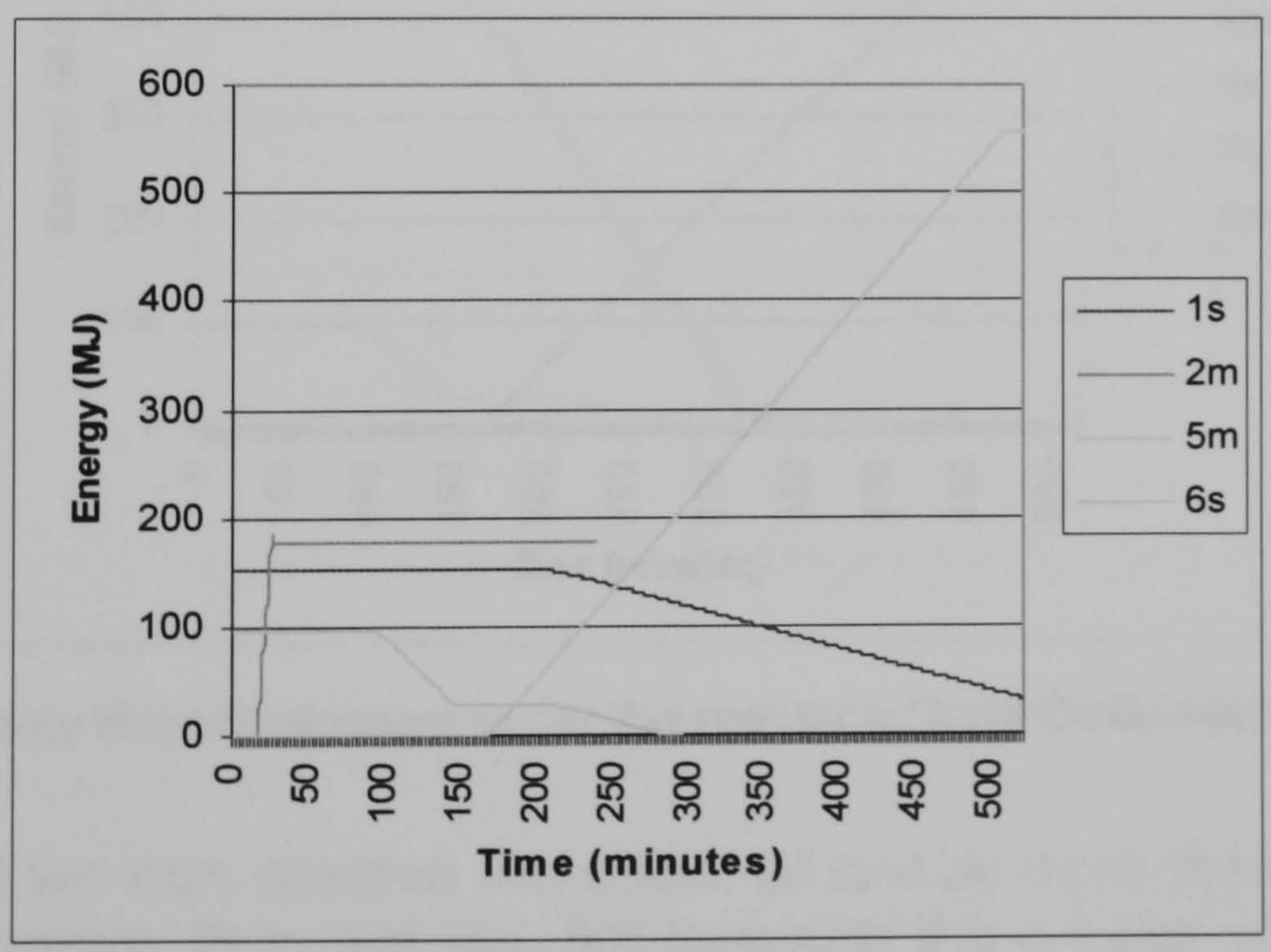

Figure 5.29: Energy stored/released under summer conditions

It is difficult to determine under which province the storage unit performed better from the results of the tests as illustrated in Figure 5.26 to Figure 5.29. In Figure 5.30 and Figure 5.31 we observe again that two out of the three tests

on which more energy was stored /released were carried out with the BC weather conditions. But it is more likely that other aspects such as thickness and mass flow have determined test 3m performance. The regional province is not a strong factor determining the efficiency of the system. This supports the statistical analysis, and verifies that the factor province is a factor with less effect on the amount of energy stored/released.

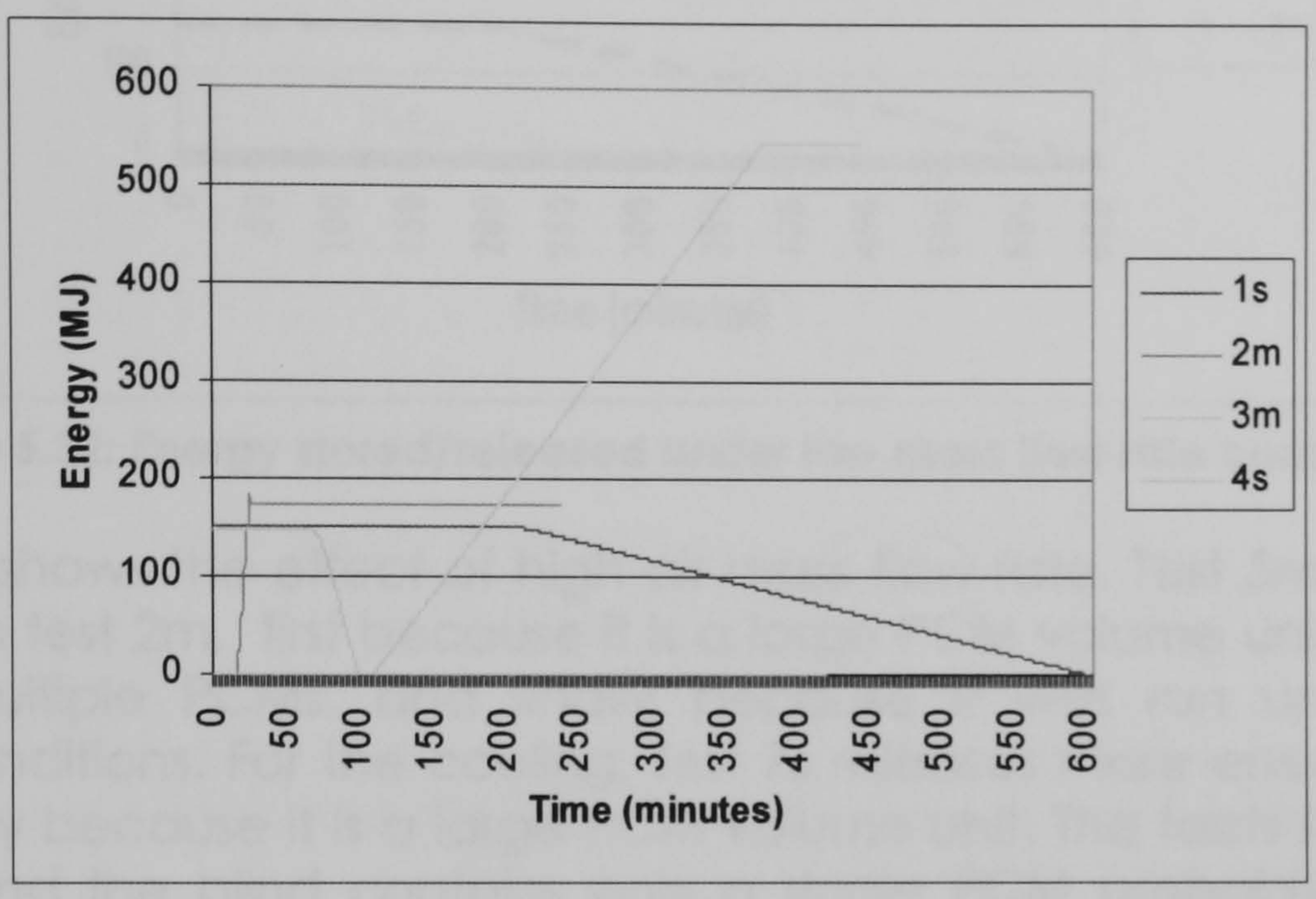

Figure 5.30: Energy stored/released under the province "Chiapas" test conditions.

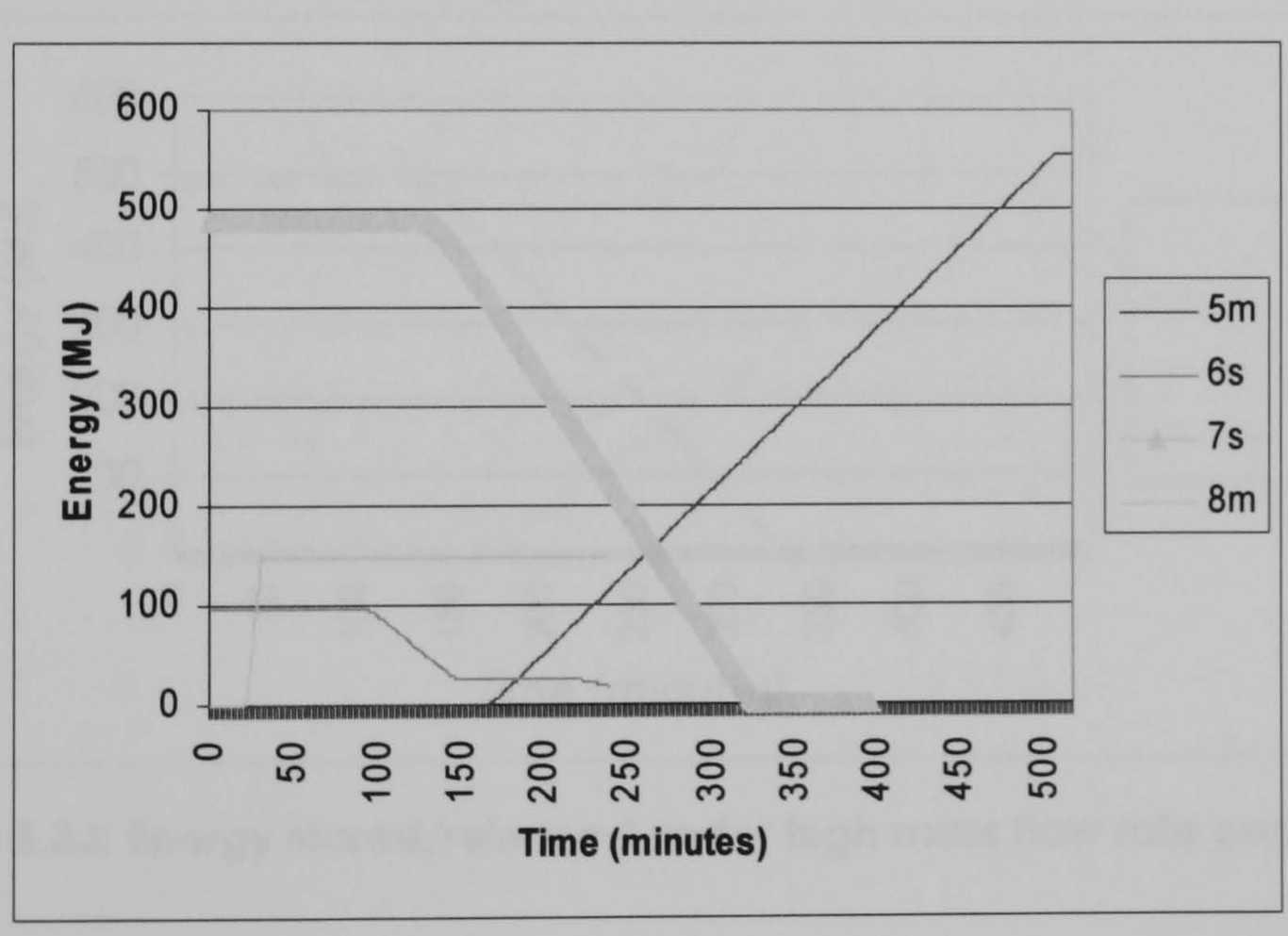

Figure 5.31: Energy stored/released under the province "Baja California" test conditions.

In Figure 5.32 we can observe the effect of low air mass flow rate. Test 3m stores more energy than test 8m first because it is a large volume blind, it has no insulation (recall that for heating the presence of insulation on the surface facing the heat source with a low mass flow rate applied on the surface facing the chamber delays the charging) and finally because it has multiple PCMs. As all these factors might be determining test 3m performance, it is likely that low air mass flow rate effect is small.

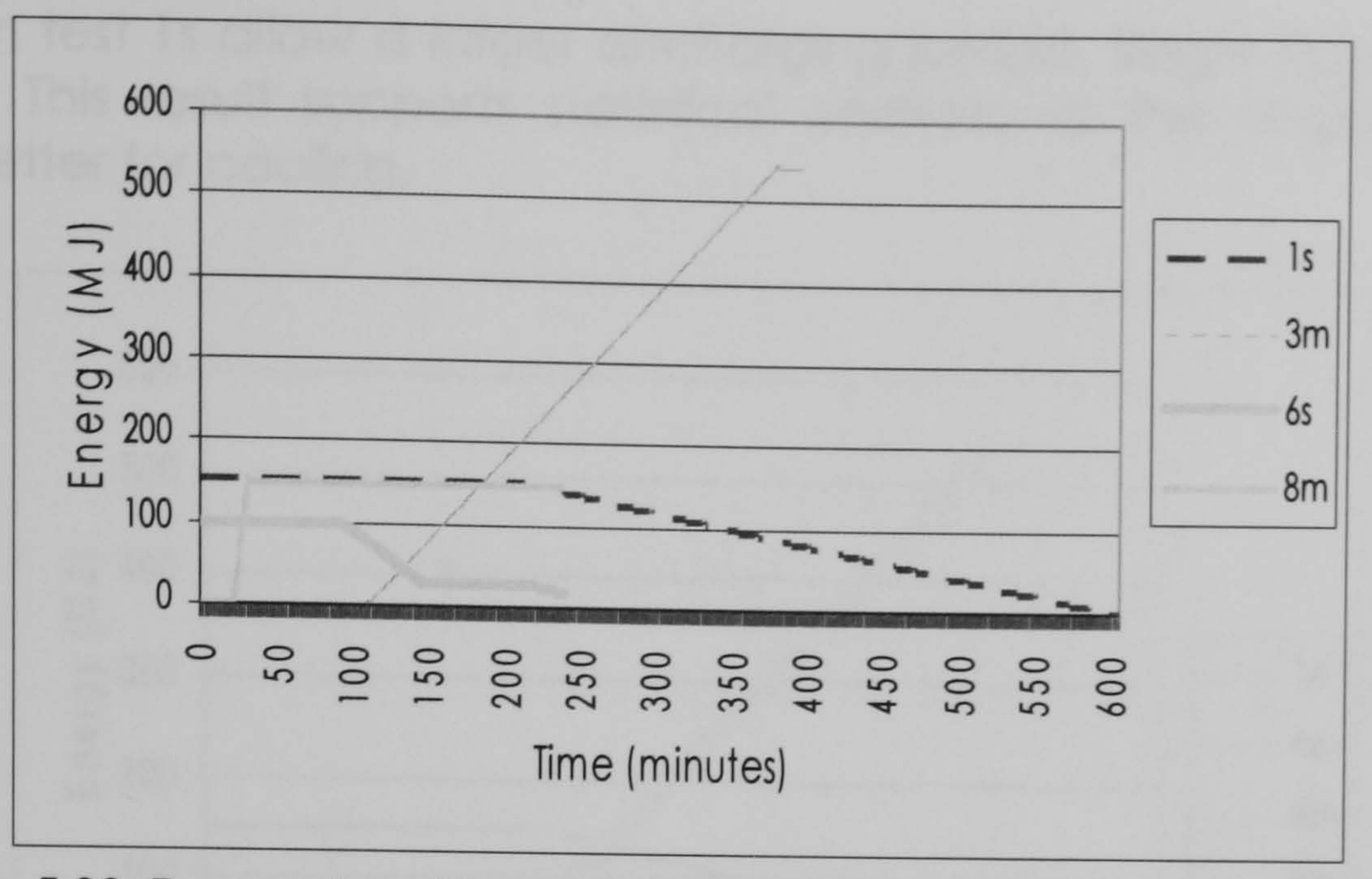

Figure 5.32: Energy stored/released under low mass flow rate conditions.

Figure 5.33 shows the effect of high air mass flow rate. Test 5m stores more energy than test 2m, first because it is a large PCM volume unit, because it contains multiple PCMs, and finally because it was run under the BC weather conditions. For the cooling, test 7s releases more energy than test 4s first mainly because it is a large PCM volume unit. The facts that it has no insulation and the blind contains only a single PCM probably play a less significant role on the final energy stored.

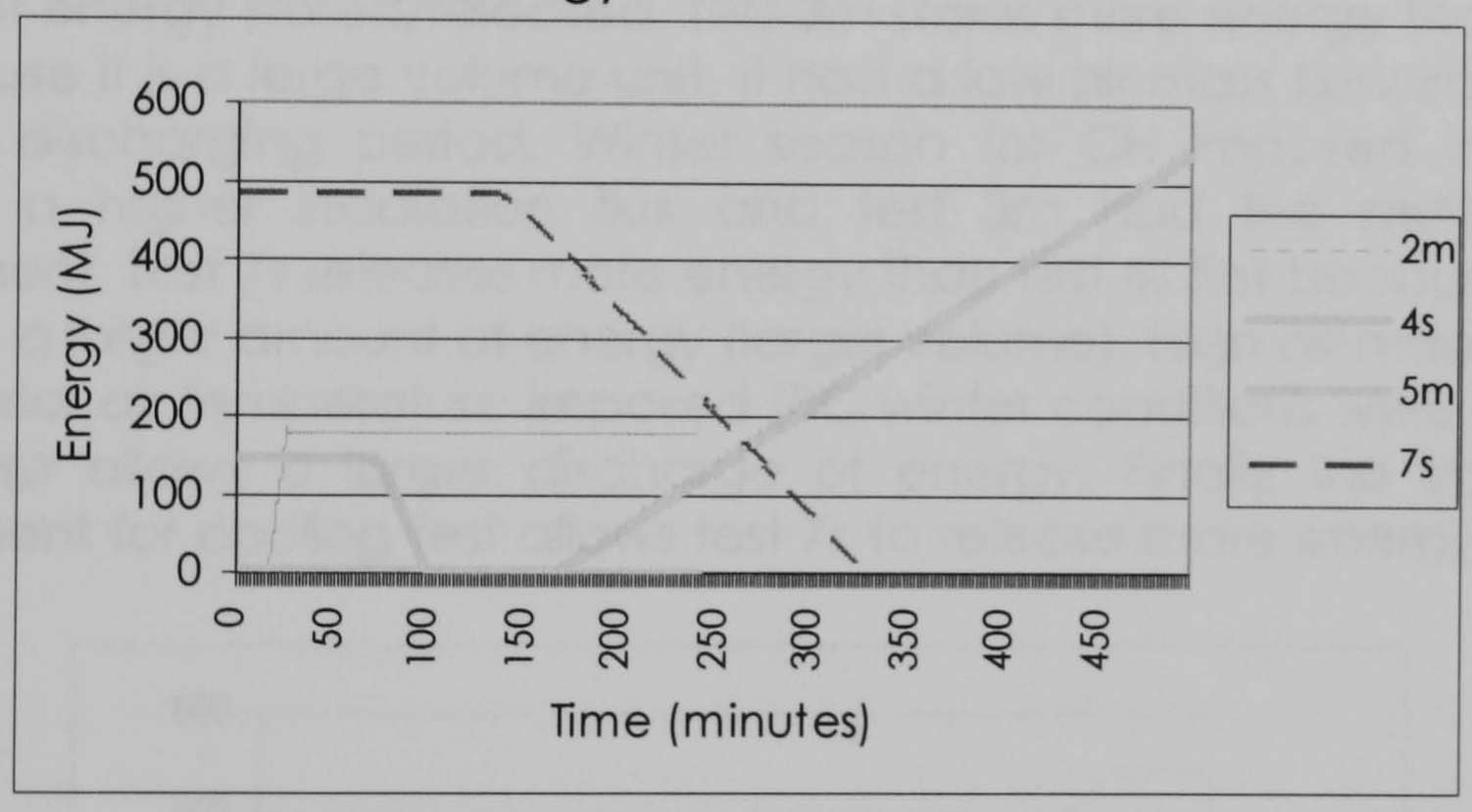

Figure 5.33: Energy stored/released under high mass flow rate conditions

In Figure 5.34 we can observe the effect of insulation on the amount of energy stored/released. Test 5m stores more energy than test 8m first because it is a large PCM volume unit. Test 5m is supplied with air at high temperature with high mass flow, that is, the larger temperature difference between the air and the blind (which PCM starts the test on the solid state) allows a larger storage. Test 5m had summer weather conditions (larger interior air temperature due to internal heat gains were imposed), compared to the test 8m winter conditions. Finally test 5m used multiple PCM blind. Test 1s releases more energy compared to test 4s first because it has large PCM volume. The low mass flow (of a larger air temperature)

imposed on test 1s allow a larger discharging period. Single PCM was used on test 1s. This result supports statistical analysis, as the single PCM unit performs better for cooling.

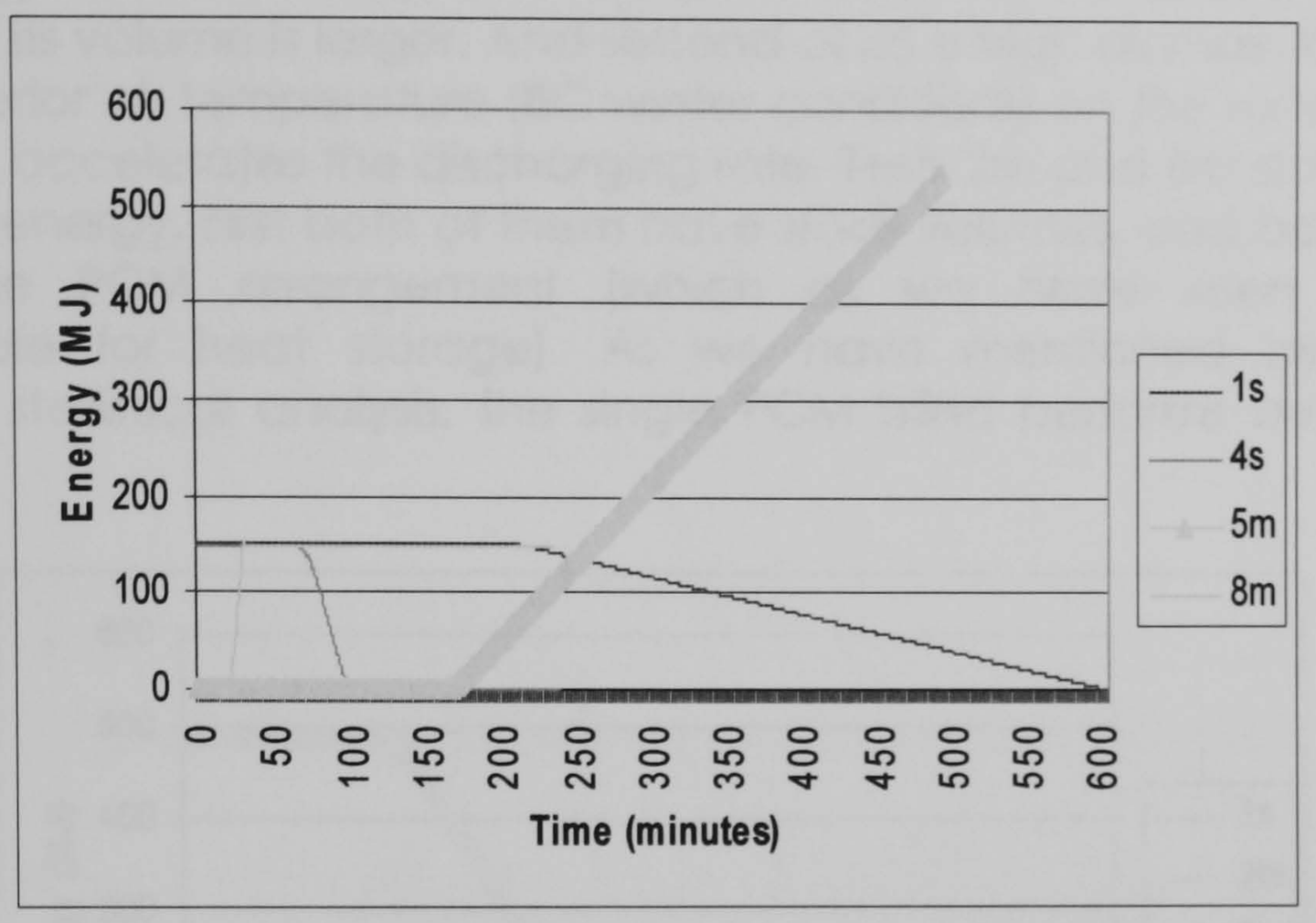

Figure 5.34: Energy stored/released with insulation on the blind.

In Figure 5.35 we can observe the effect of having no insulation on the amount of energy stored/released. Test 3m stores more energy than test 2m first because it is a large volume unit. It had a low air mass flow imposed for a longer discharging period. Winter season for CH imposed in test 3m provided a higher irradiation flux and test 3m had the multiple PCM arrangement. Test 7s releases more energy than test 6s first because the test starts with a larger amount of energy (larger volume). High air mass flow of a lower interior air temperature imposed (BC winter conditions were imposed) test 7s also allows a larger discharge of energy. Finally the single PCM arrangement for cooling test allows test 7s to release more energy than test 4s

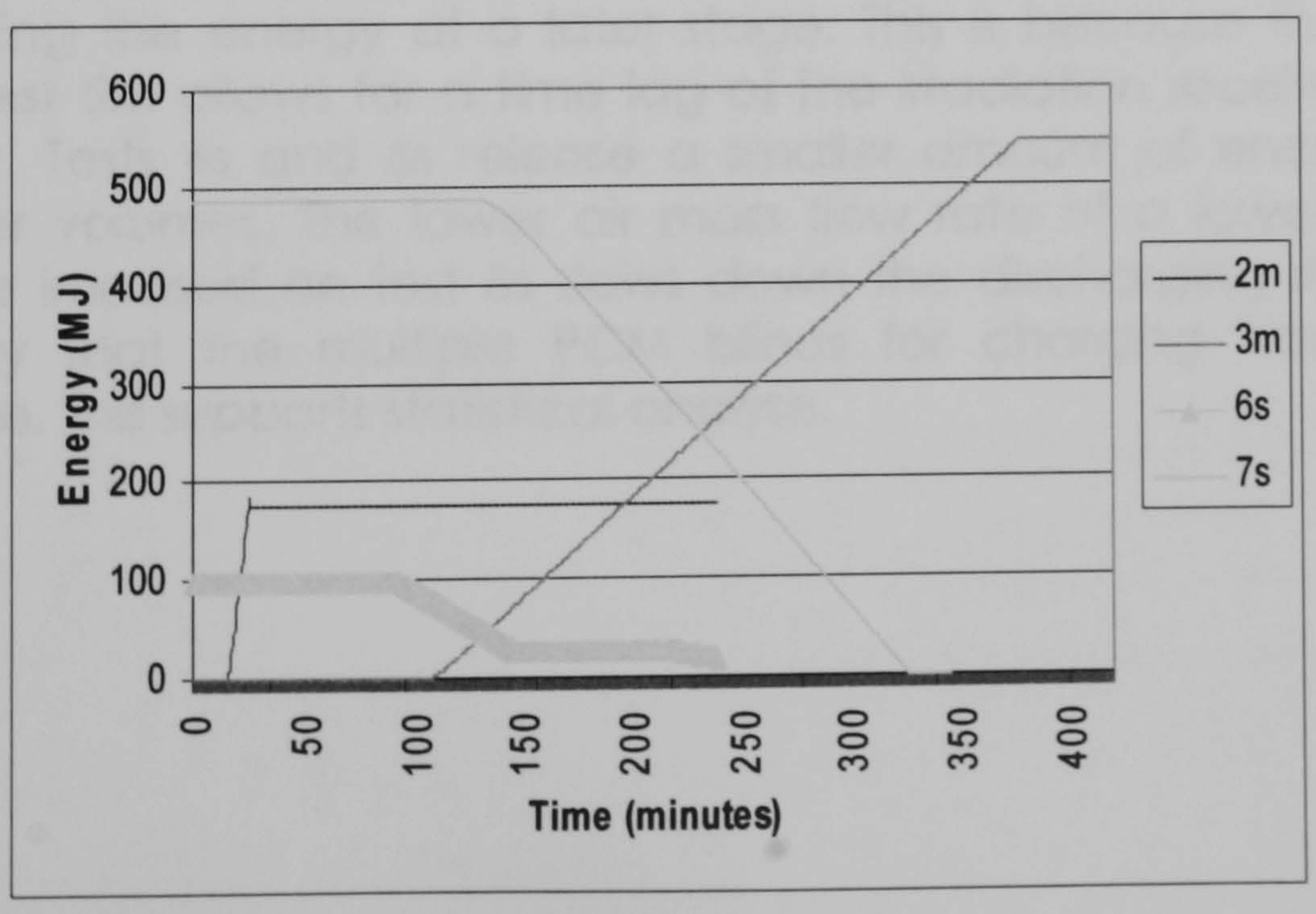

Figure 5.35: Energy stored/released without insulation

In Figure 5.36 we can observe the effect of the single PCM blind arrangement on the amount of energy stored/released. Test 7s releases more energy than test 1s, but the main point here is that it does it in a shorter period. First its volume is larger. And second of all a high air mass flow rate of a lower interior air temperature (BC winter conditions) on the surface facing the interior, accelerates the discharging rate. Tests 2m and 8m store a similar amount of energy. First both of them have small volumes, and both of them have single PCM arrangement (which as we have seen before is unfavourable for heat storage). As we have mentioned before, and supporting statistical analysis, the single PCM blind performs better during cooling.

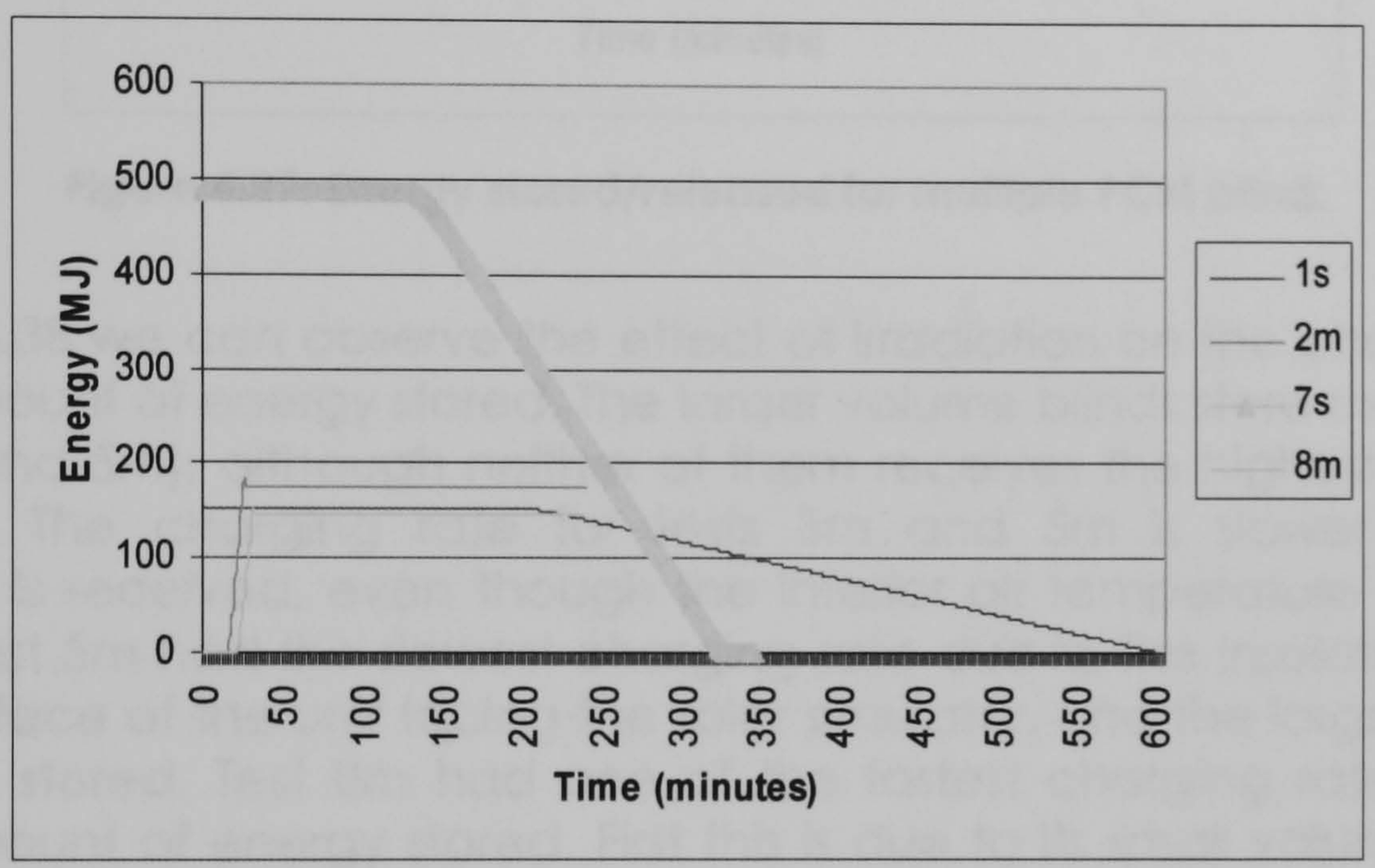

Figure 5.36: Energy stored/released for tests with single PCM blind (C-P).

In Figure 5.37 we can observe the effect of the multiple PCM blind arrangement on the amount of energy stored/released. Tests 3m and 5m store a large amount of energy (both are of large PCM volume) but test 5m starts releasing the energy at a later stage. This is because the insulation present in test 5m allows for a time lag of the irradiation received through the window. Tests 4s and 6s release a smaller amount of energy as they have smaller volumes. The lower air mass flow rate of a lower interior air temperature imposed on test 6s slows down the discharging rate. Overall we can say that the multiple PCM blinds for charging have a good performance. This supports statistical analysis.

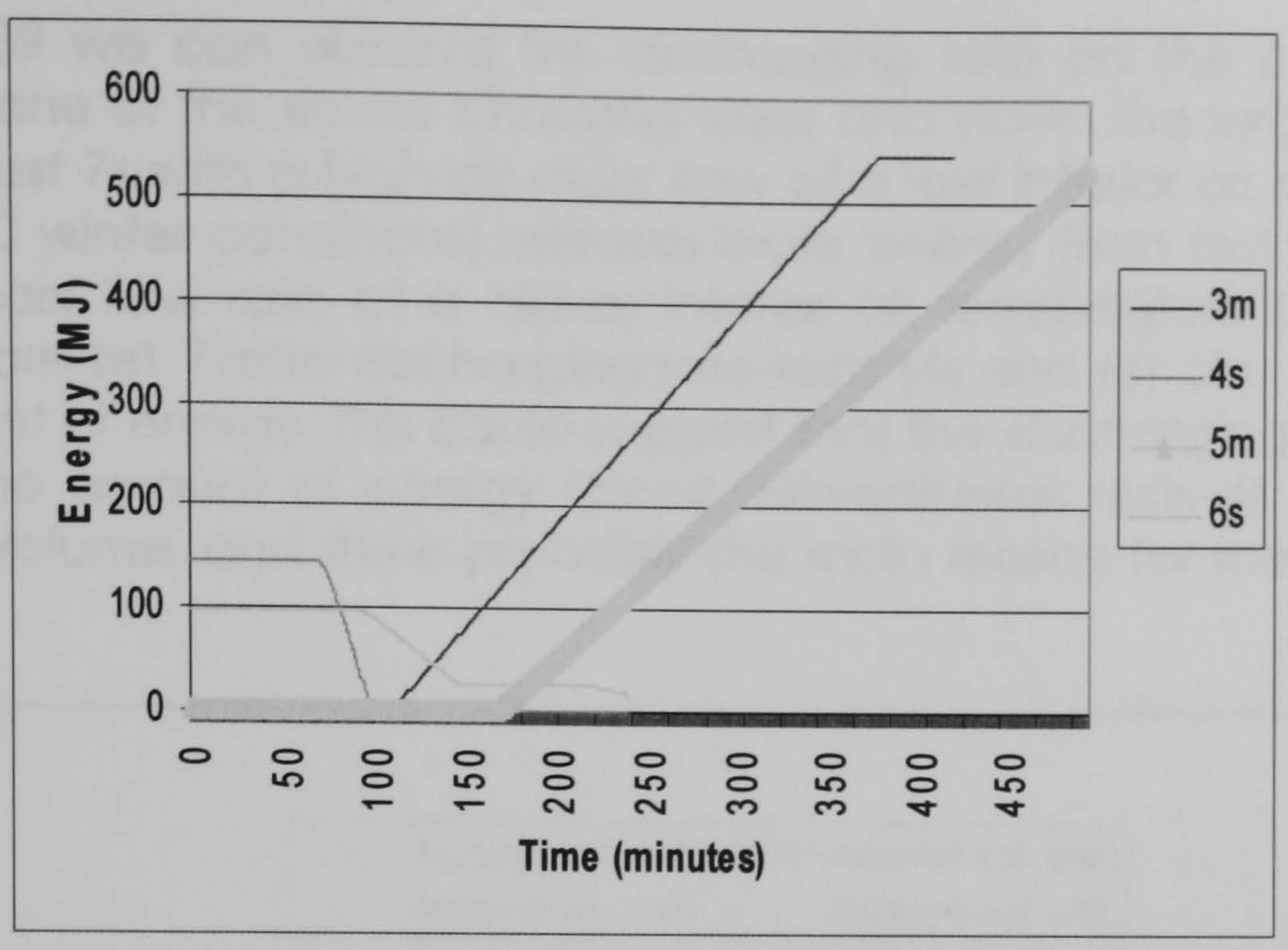

Figure 5.37: Energy stored/released for multiple PCM blind.

In Figure 5.38 we can observe the effect of irradiation on the charging tests on the amount of energy stored. The larger volume blinds store more energy (test 3m and 5m), although neither of them receives the highest irradiation (test 8m). The charging rate for tests 3m and 5m is slower (as lower irradiation is received, even though the interior air temperature imposed is higher). Test 5m had the slowest charging rate due to the insulation placed on the surface of the unit facing the solar simulator, and the largest amount of energy stored. Test 8m had one of the fastest charging rates and the lowest amount of energy stored. First this is due to its small volume. Low air mass flow rate of a relatively mild interior air temperature (BC winter conditions, 22°C), the fact that the surface facing the solar simulator had insulation and that the single PCM arrangement was used made this test to have a poor performance. We can conclude that the amount of irradiation applied in the unit is important but not definite to determine the final energy stored in the unit.

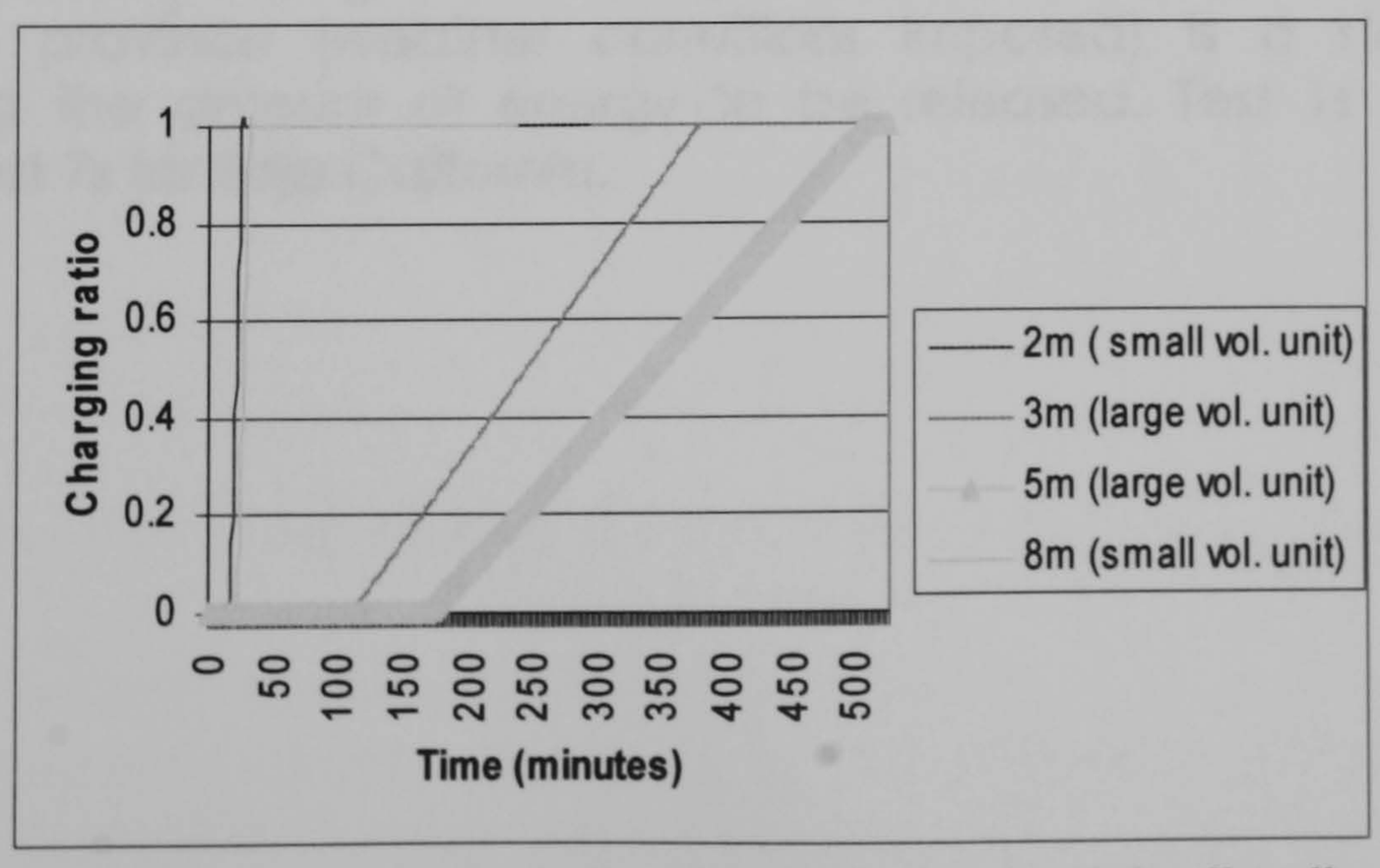

Figure 5.38: Charging ratio for tests using the solar simulator (heating tests).

In Figure 5.39 we can observe the discharging rate on the cooling tests. Test 7s had one of the slower charging rates and stores the largest amount of energy. Test 7s with a high air mass flow of a low interior air temperature imposed (BC winter conditions) releases more energy than test 4s for which a low air mass flow rate of a higher interior air temperature (CH summer conditions) are set. Faster discharging rate tests (4s and 6s) also discharge a lower amount of energy. This could suggest that the discharging rate has an effect on the amount of energy stored. Nevertheless tests 4s and 6s also have small volume, and this is probably the main reason for the low energy storage.

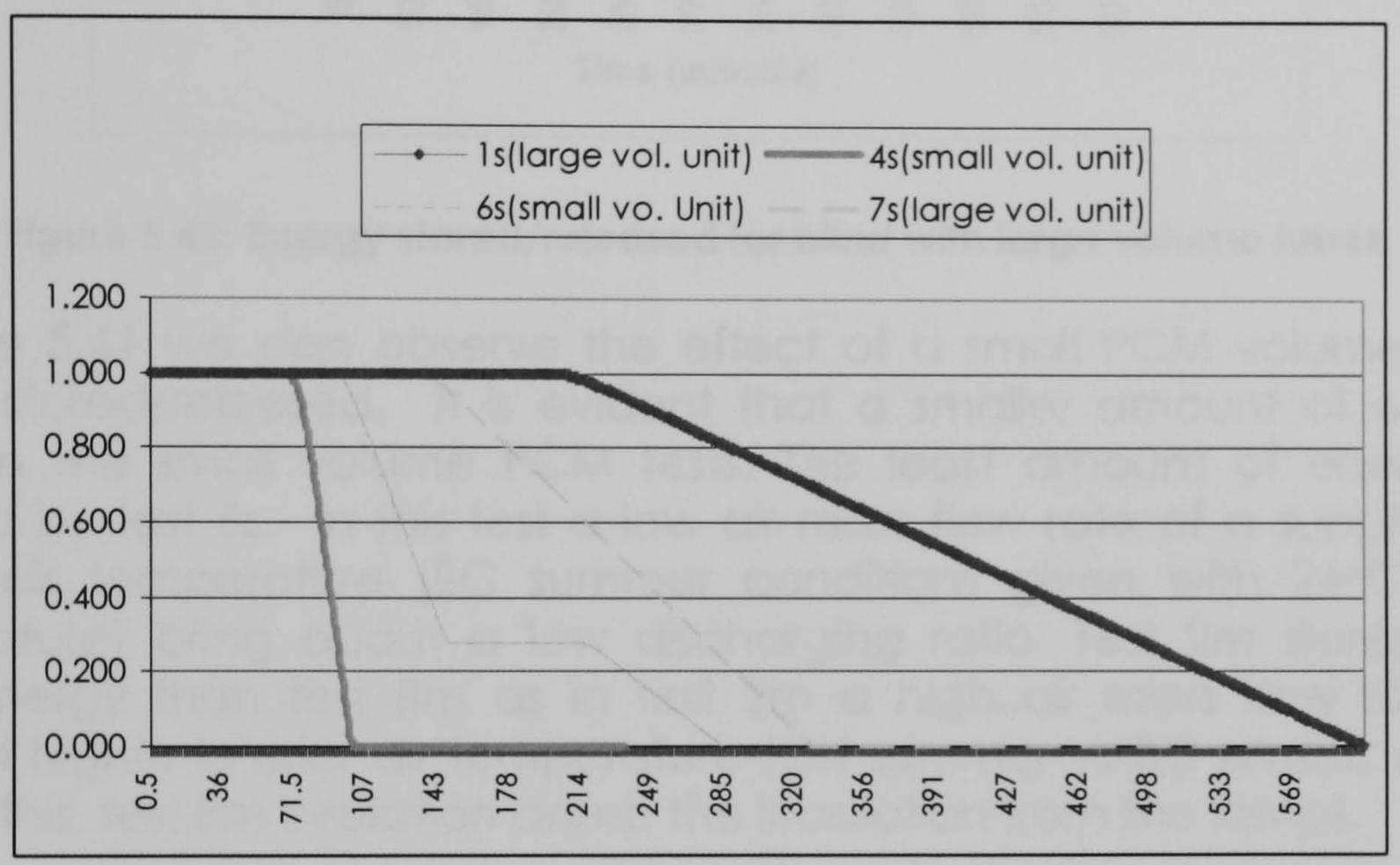

Figure 5.39: Diascharging ratio for cooling tests

In Figure 5.40 we can observe the effect of a large PCM volume on the energy stored/released. The geometric parameter determining the thermal behaviour of the system is the volume of PCM available for energy storage or release. We can observe that the tests with larger volume store more energy, for both heating and cooling conditions. Test 1s is the exception where the province (weather conditions imposed) is a strong factor determining the amount of energy to be released. Test 1s was set for Chiapas, test 7s for Baja California.

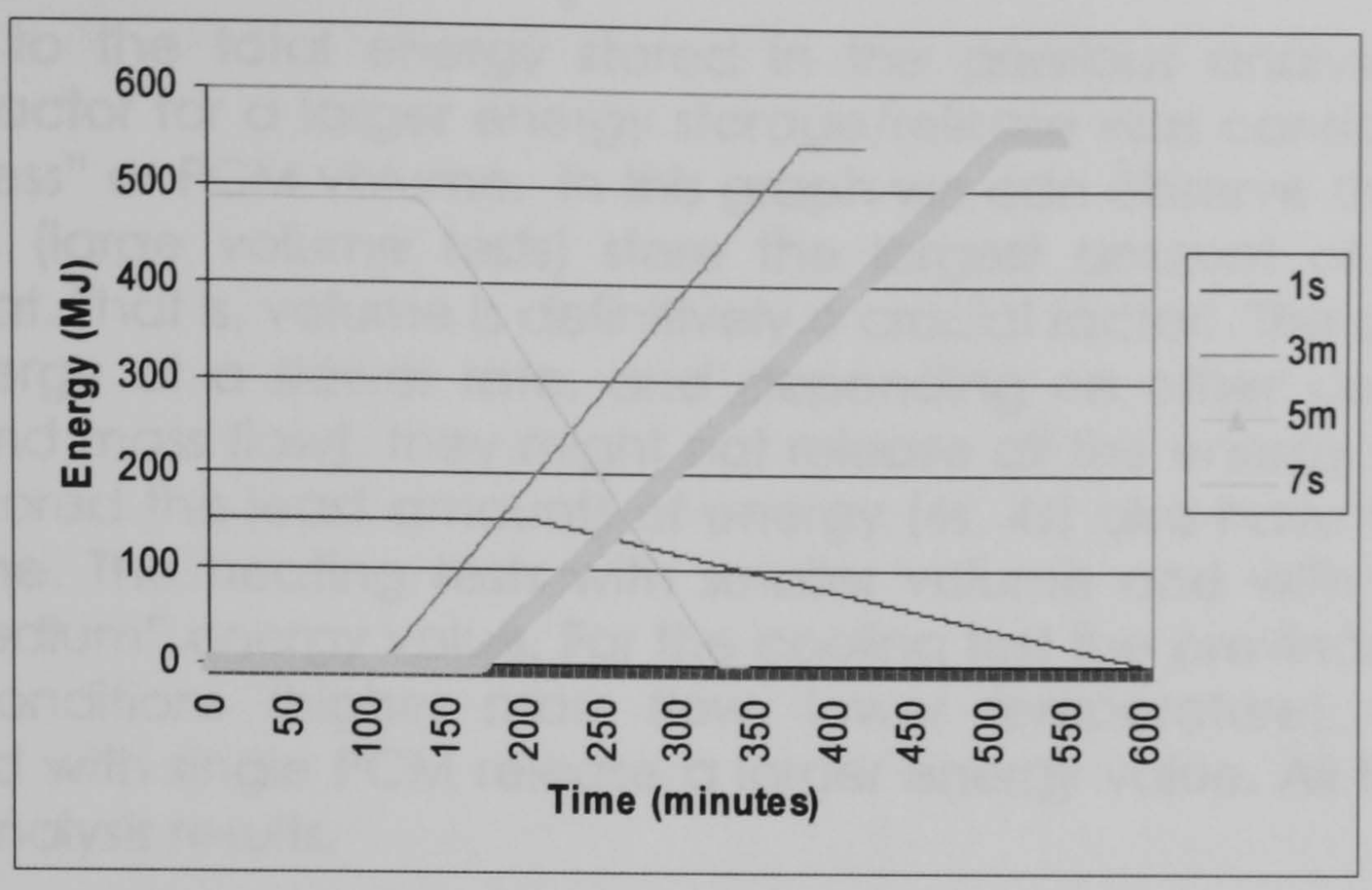

Figure 5.40: Energy stored/released for blind with large volume tubes.

In Figure 5.41 we can observe the effect of a small PCM volume on the energy stored/released. It is evident that a smaller amount of energy is stored in the small volume PCM tests. The least amount of energy was released by test 6s. In this test a low air mass flow rate of a supplied mild interior air temperature (BC summer conditions given with 24°C interior temperature) bring about a low discharging ratio. Test 2m stores slightly more energy than test 8m as in test 2m a high air mass flow rate of a supplied higher interior air temperature (CH summer vs BC winter) applied. Besides this, test 8m insulation damp the irradiation from the lamps.

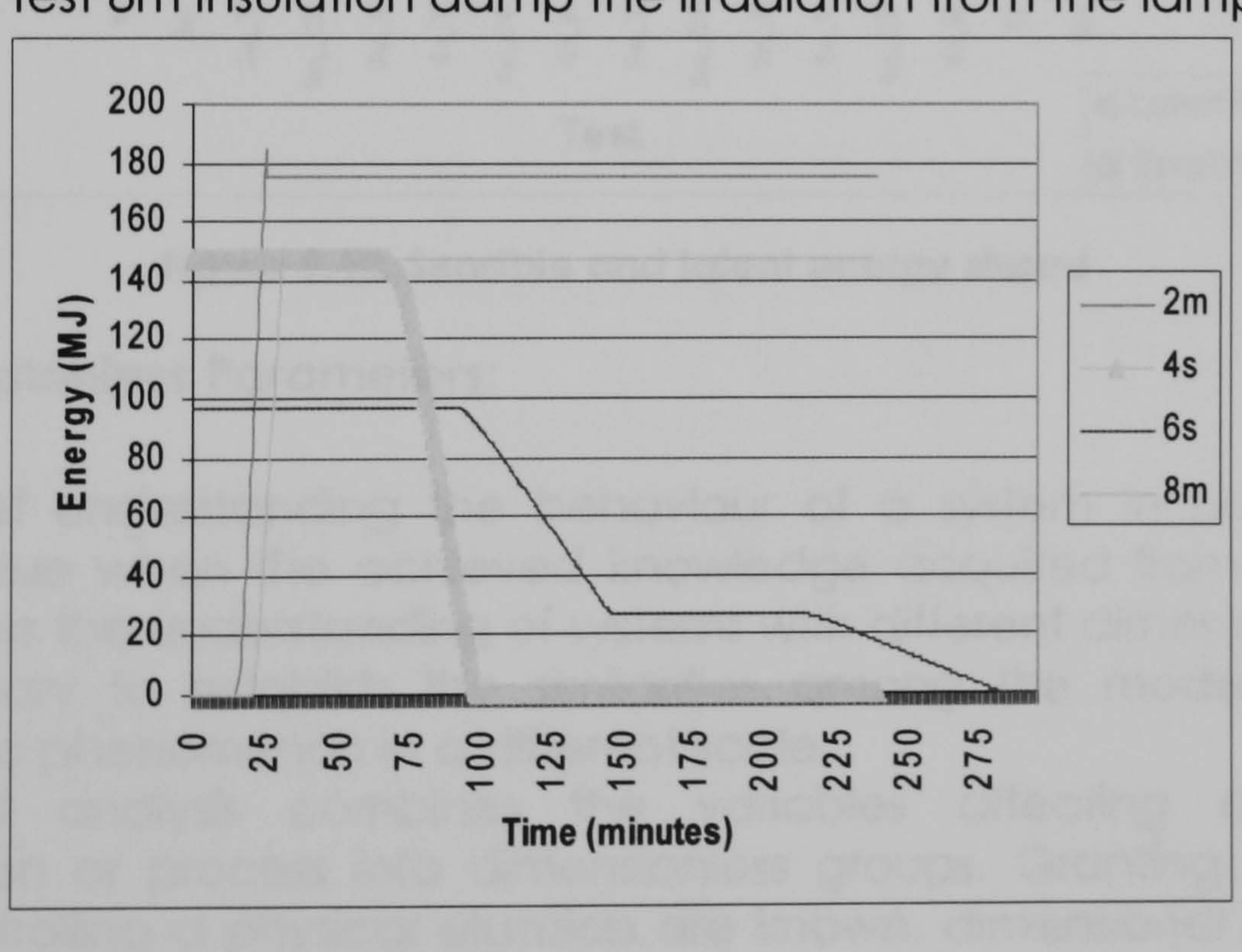

Figure 5.41: Energy stored/released for blind with small volume tubes

Latent energy storage contribution.

From the following graph (Figure 5.42) the potential of latent energy, compared to sensible storage can be appreciated.

According to the total energy stored in the previous analysis the most important factor for a larger energy storage/release was considered to be the "thickness" or PCM volume. In this graph we can observe that tests 3m, 5m and 7s (large volume tests) store the largest amount of latent and sensible heat. That is, volume is definitively a crucial factor. The cooling tests release energy at a slower rate, and depending on other conditions (as province and mass flow), they might not release all the energy stored. The tests that stored the least amounts of energy (6s, 4s) also have the smallest PCM volume. The heating tests with smaller volume and with single PCM store a "medium" energy value. For the cooling test the province with more extreme conditions (higher mass flow, lower temperature), with larger volume and with single PCM release a larger energy value. All this supports statistical analysis results.

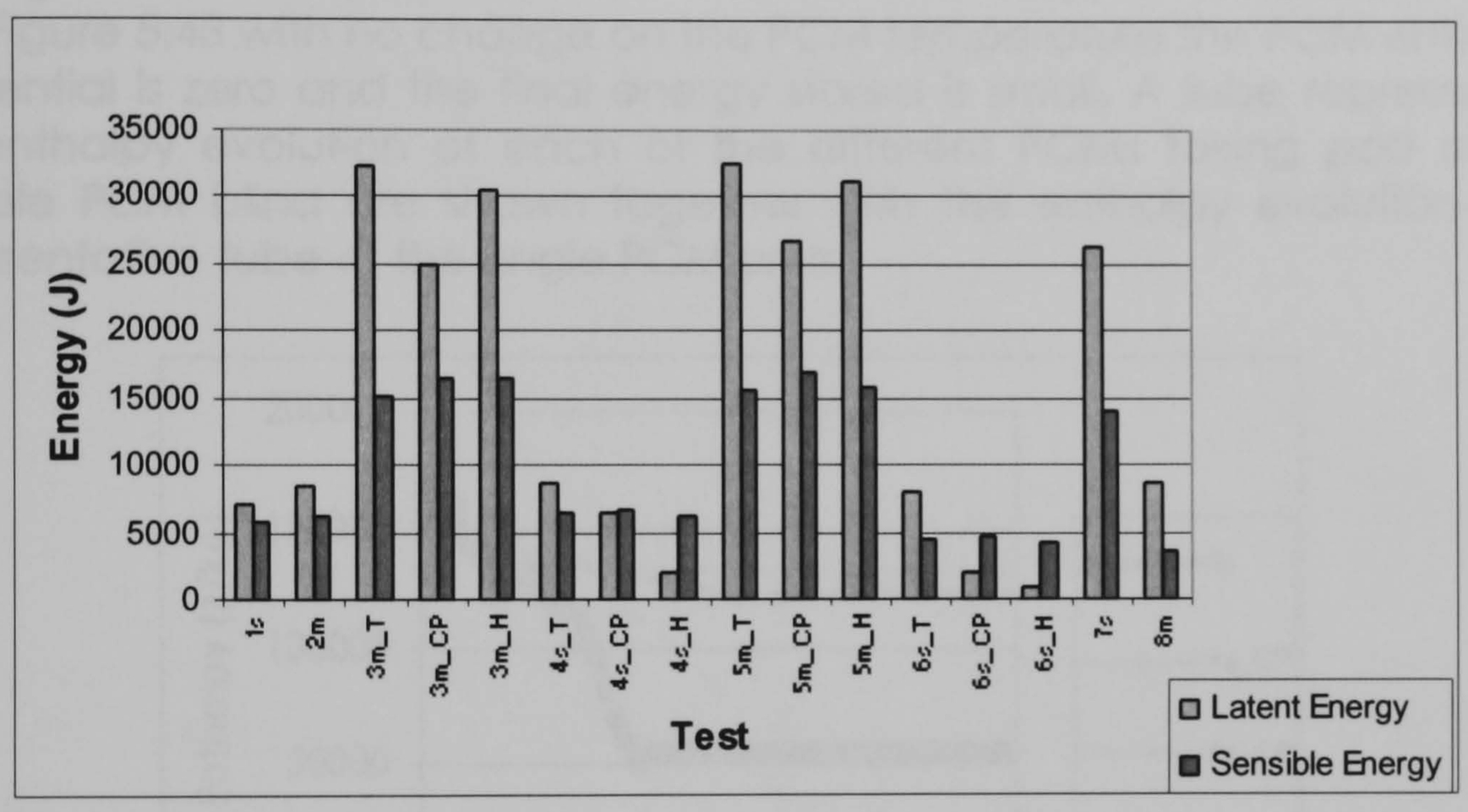

Figure 5.42: Sensible and latent energy stored

Dimensionless Parameters:

The utility of understanding the behaviour of a system in particular has genuine value when the achieved knowledge acquired from that "one" system allows the understanding of systems with different dimensions. For this it is necessary to establish the similarities among the models that can replicate the phenomenon in a different scale.

Dimensional analysis combines the variables affecting a particular phenomenon or process into dimensionless groups. Granting that all the factors controlling a physical situation are known, dimensional analysis is a method by which this knowledge may be useful for planning experiments and interpreting the data obtained.

Dimensionless combinations are helpful in interpreting data where two or more factors have been varied in different experiments.

Following the properties involved in the dimensionless parameters definitions are described:

Enthalpy[7]:
The enthalpy was evaluated by fitted equations for the experimental temperatures. The temperature-enthalpy correlation obtained from the DSC test was applied to the temperature evolution of the PCM under the tests conditions. The evolution of the enthalpy differential on each specific test is a sign of the material's potentiality as heat storage mean under those circumstances. When stable conditions are reached inside the chamber (no more heat is being transferred) the temperature differential that allowed for an enthalpy differential fade away, and no more energy is being either stored or released. Test 6s reaches stable conditions fairly soon. Although it's latent (hidden) heat is there, and stays at a constant value (see Figure 5.43 with no change on the PCM temperature the PCM enthalpy differential is zero and the final energy stored is small. A tube representing the enthalpy evolution of each of the different PCMs taking part of the multiple PCM blind are shown together with the enthalpy evolution of a representative tube of the single PCM units.

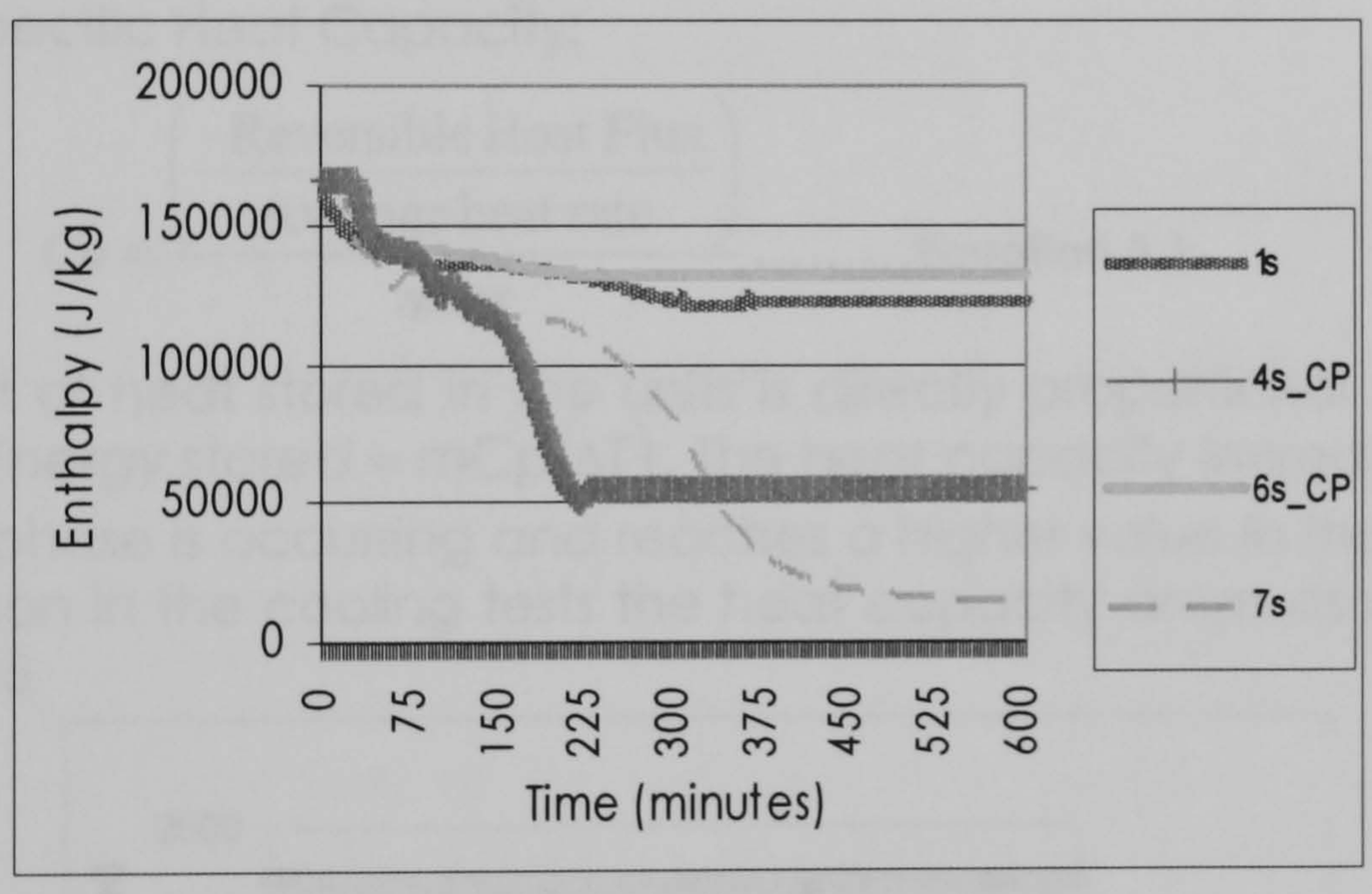

Figure 5.43: Enthalpy evolution, cooling tests

In Figure 5.44 a similar situation to test 6s occurs in tests 2m and 8m. Stable conditions reached sooner maintain the PCM temperature on a constant value, for which the enthalpy differential is zero.

---

[7] Known as heat content. Latent heat of transformation: is the specific enthalpy change associated with a phase transition of a substance at constant temperature and pressure. Latent heat of freezing of a quantity of liquid at its freezing point is the heat given up to its surroundings when it freezes. Latent heat of fusion is the heat required to melt it.

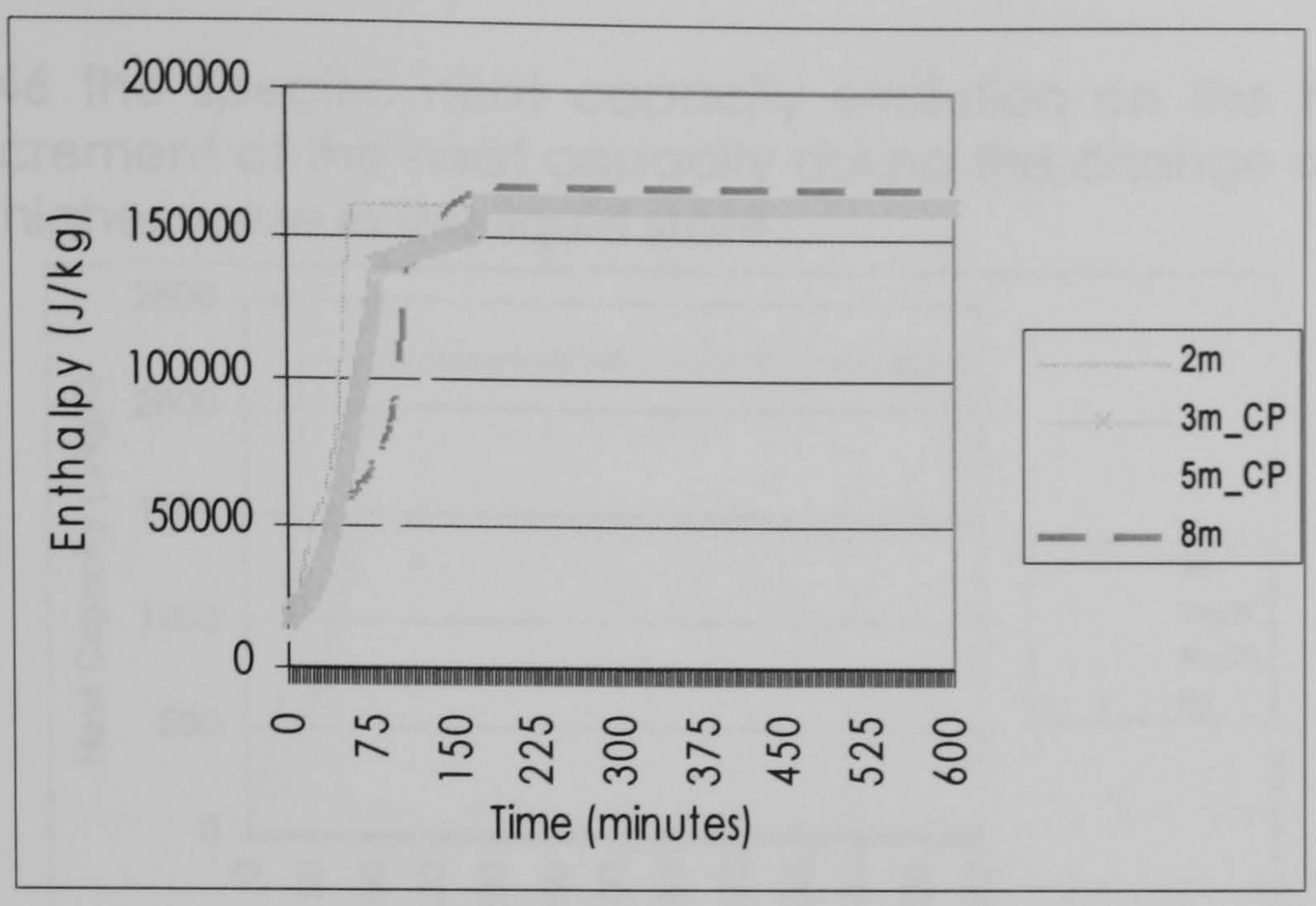

Figure 5.44:Enthalpy evolution, heating tests

Specific Heat Capacity[8]: The specific heat capacity was evaluated by fitted equations for the experimental temperatures, following the specific heat capacity evolution obtained from MDSC data:

- Specific Heat Capacity:

$$Cp = \frac{\left(\frac{\text{- Reversible Heat Flux}}{\text{Average heat rate}}\right)}{mass} \quad \text{.....Equation 5.1}$$

The amount of heat stored in the units is directly proportional to their heat capacity ($Energy\ stored = mCp(\Delta T)$. The heat capacity increases whilst the change of phase is occurring and reaches a higher value in the liquid state. For this reason in the cooling tests the heat capacity drops as can be seen in Figure 5.45

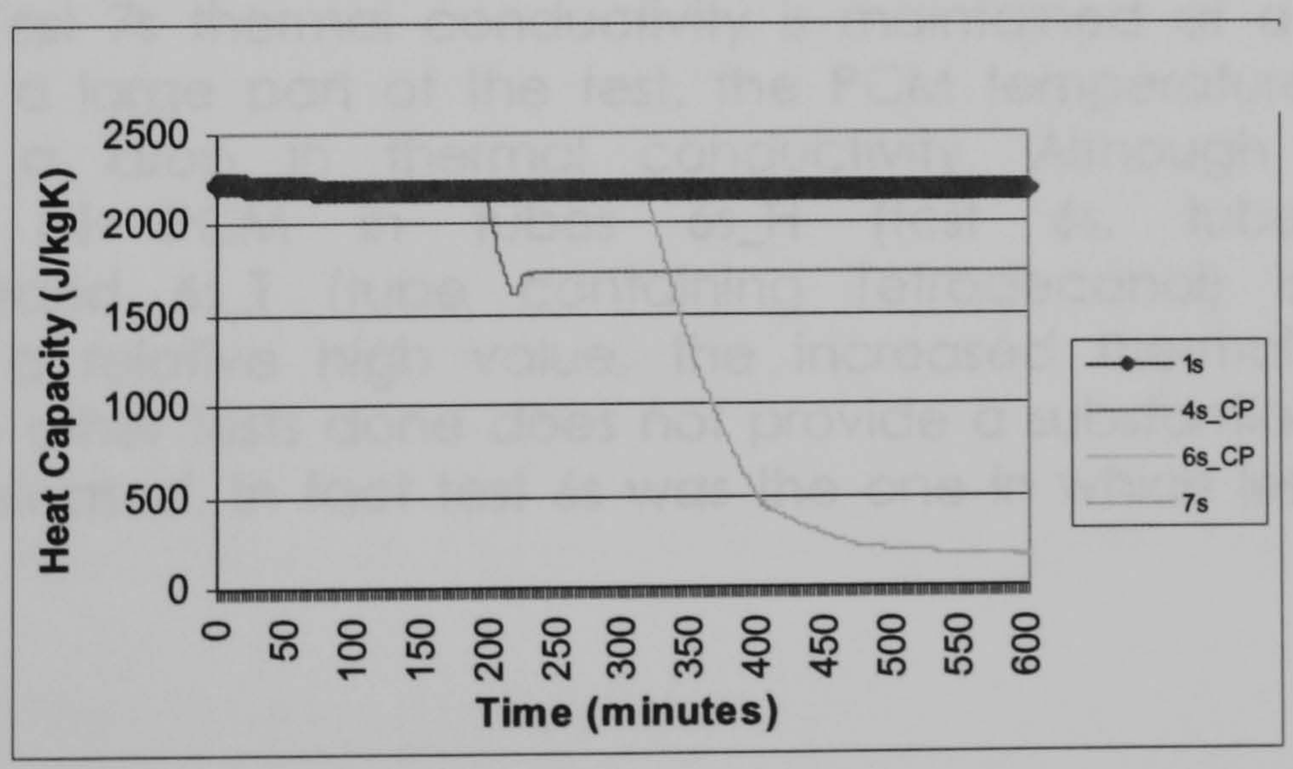

Figure 5.45:Specific heat capacity evolution, cooling tests

---

[8] It is the amount of heat required to change the temperature of one kg of a substance by one degree.

In Figure 5.46 the specific heat capacity evolution on the heating tests shows the increment of the heat capacity during the change of phase until it reaches a higher value in the liquid state.

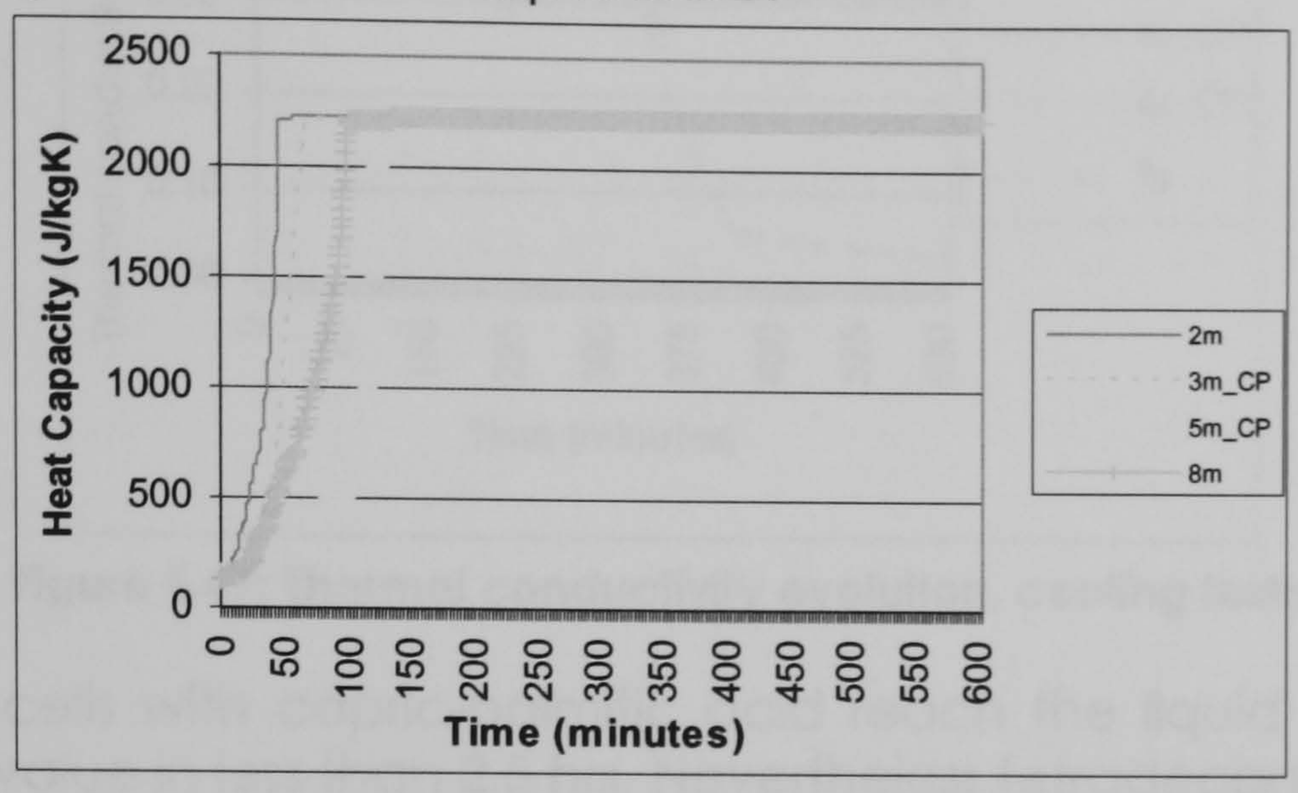

Figure 5.46: Specific heat capacity evolution, heating tests

Thermal conductivity[9]: The thermal conductivity was evaluated by fitted equations for the experimental temperatures, following the thermal conductivity evolution obtained from MDSC data:

$$k = \frac{8LCp_{apparent}^{2}}{Cp_{specific} * m * \phi^{2} * p} \quad \text{.....Equation 5.2}$$

Heat transferred by conduction is directly proportional to the material's thermal conductivity ($Q_{cond} = \frac{k\Delta T}{L}$). This property is temperature dependent and has a higher value in the liquid state. We can observe the evolution of the thermal conductivity under the imposed conditions for each test in Figure 5.47. Test 7s thermal conductivity is maintained at a relative high value during a large part of the test, the PCM temperature hasn't drop enough for a drop in thermal conductivity. Although the thermal conductivity of PCM in tubes 6s_H (test 6s, tube containing Hexadecane)and 6s_T (tube containing Tetradecanol) is maintained constant at a relative high value, the increased thermal conductivity compared to other tests done does not provide a substantial increment in the energy released. In fact test 6s was the one in which less energy was released.

---

[9] The property of a material that describes the rate at which heat will be conducted through a unit area of material for a given driving force.

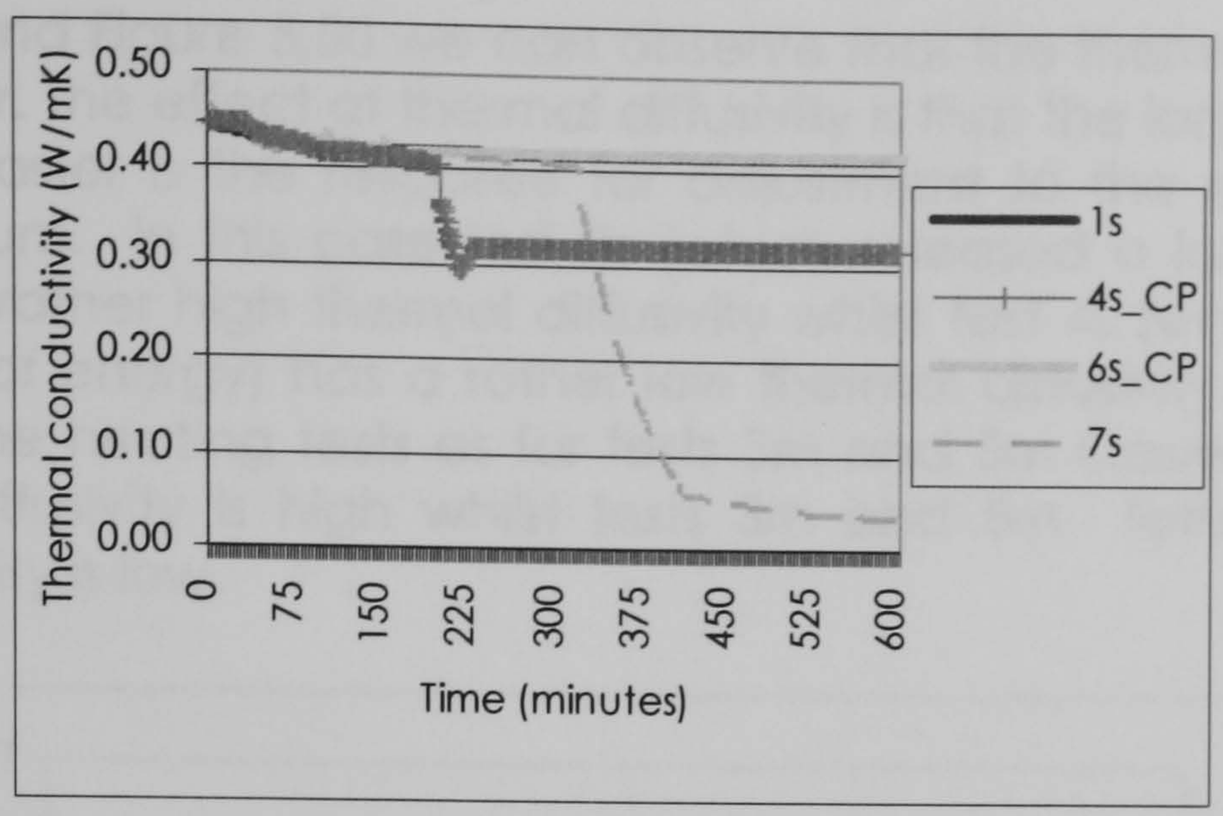

Figure 5.47: Thermal conductivity evolution, cooling tests

All the blind cells with capric-palmitic acid reach the liquid state thermal conductivity value in less than 2.5 hrs. Nevertheless tetradecanol cells in tests 5m (formed with multiple PCM cells) take more than 3 hours to reach their thermal conductivity peak value. The thermal conductivity for the Tetradecanol is smaller than that for Hexadecanol or Capric-Palmitic acid mixture . Nevertheless test 5m was the test which stored the largest amount of energy. That is, as mentioned for the cooling tests, improvement on the thermal conductivity of the PCM hasn't provide a larger thermal energy storage, as many other factors are involved which might be more critical.

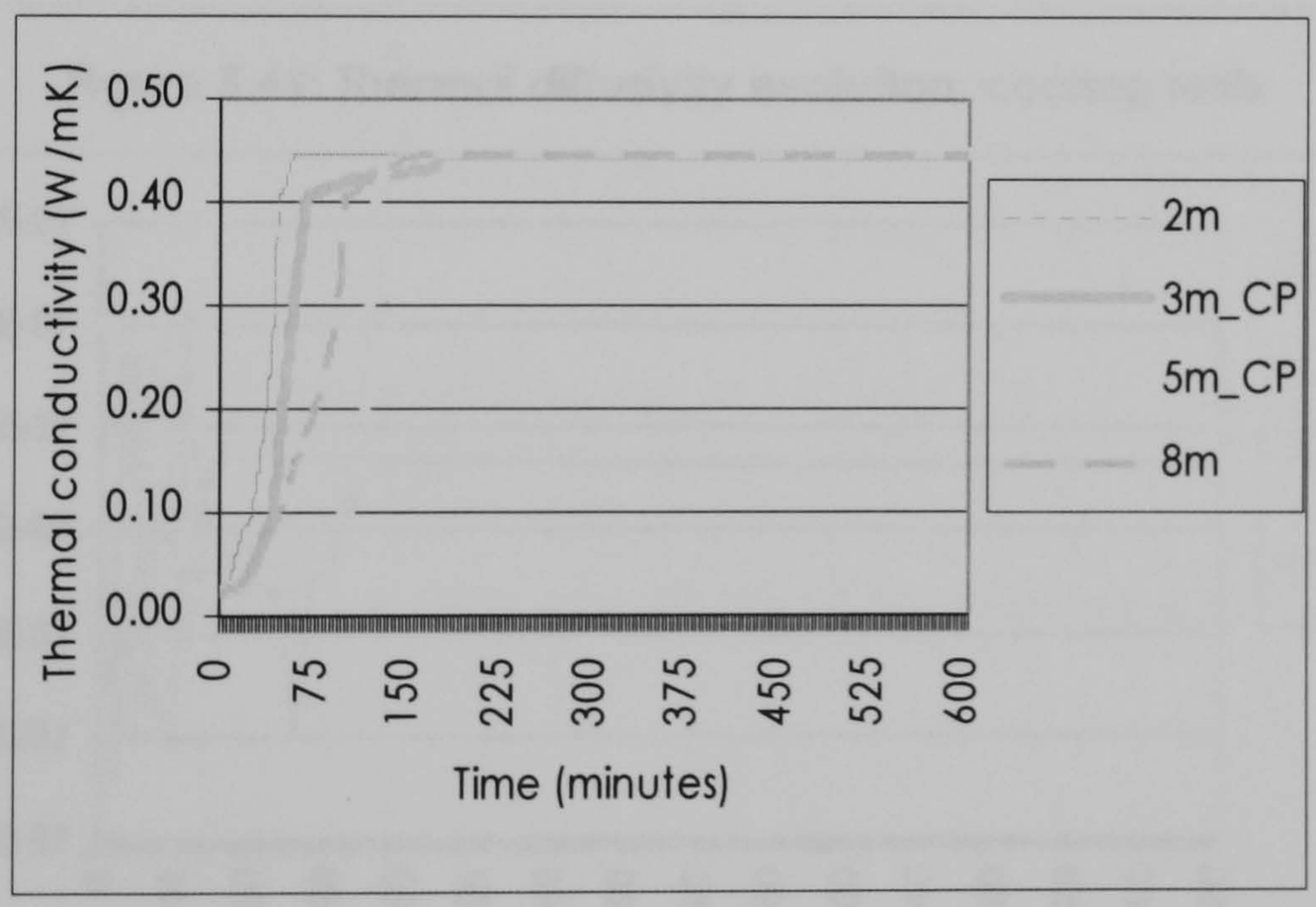

Figure 5.48:Thermal conductivity evolution, heating tests

Thermal diffusivity: [10]It was calculated as follows:

$$\alpha = \frac{k}{\rho Cp}$$

---

[10] Measures the ability of a material to conduct thermal energy relative to its ability to store thermal energy

In Figure 5.49 and Figure 5.50 we can observe that the thermal diffusivity for all tests is similar. The effect of thermal diffusivity is that the larger the thermal diffusivity the faster is the response for adjustment to the environment to reach equilibrium. In this case test 7s (which released a large amount of energy) has a rather high thermal diffusivity whilst test 4s (which released a small amount of energy) has a rather low thermal diffusivity. This relation is less clear on the heating tests as for tests 3m and 5m Capric-Palmitic cells the thermal diffusivity is high whilst tests 3m and 5m Tetradecanol cells thermal diffusivity is low.

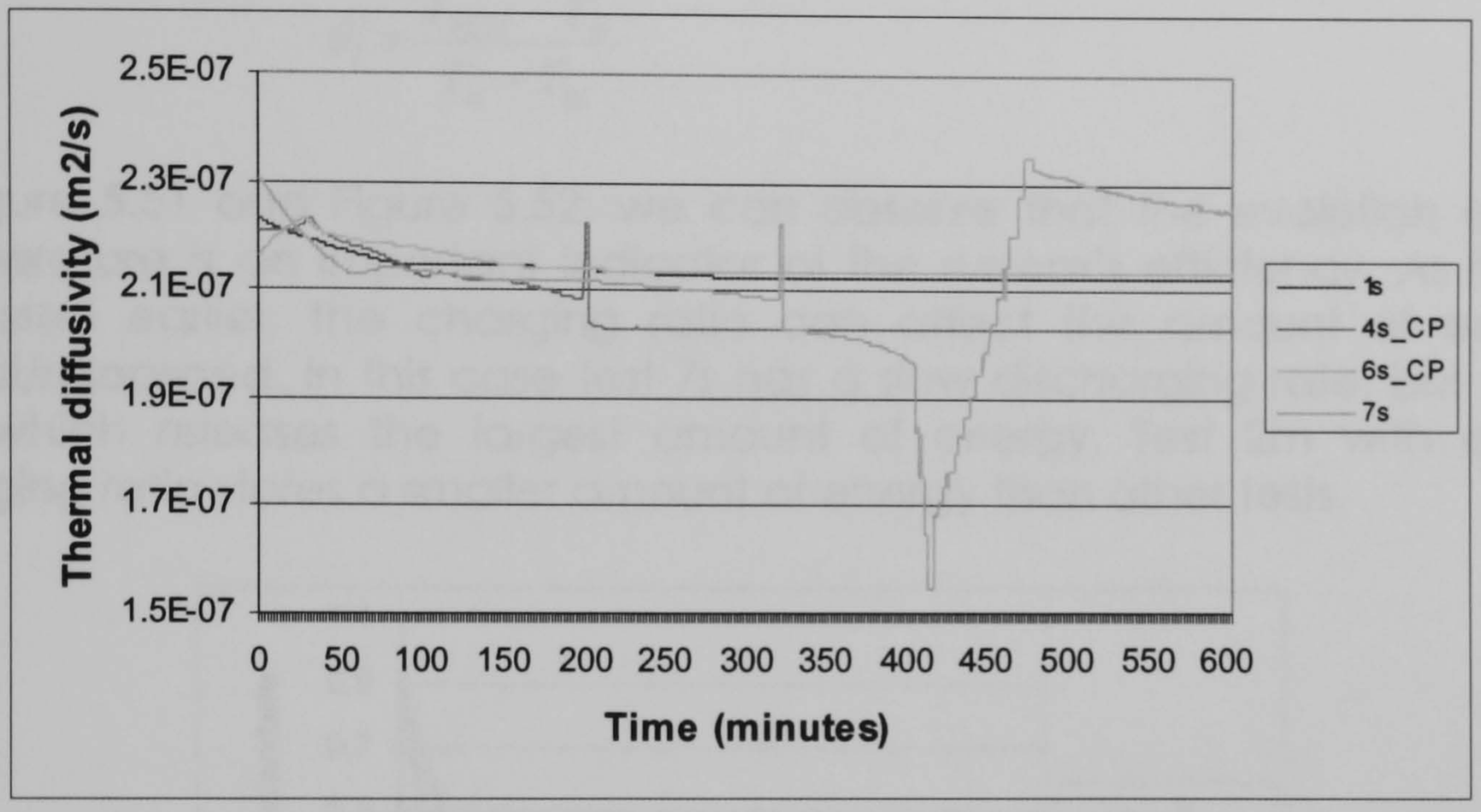

Figure 5.49: Thermal diffusivity evolution, cooling tests

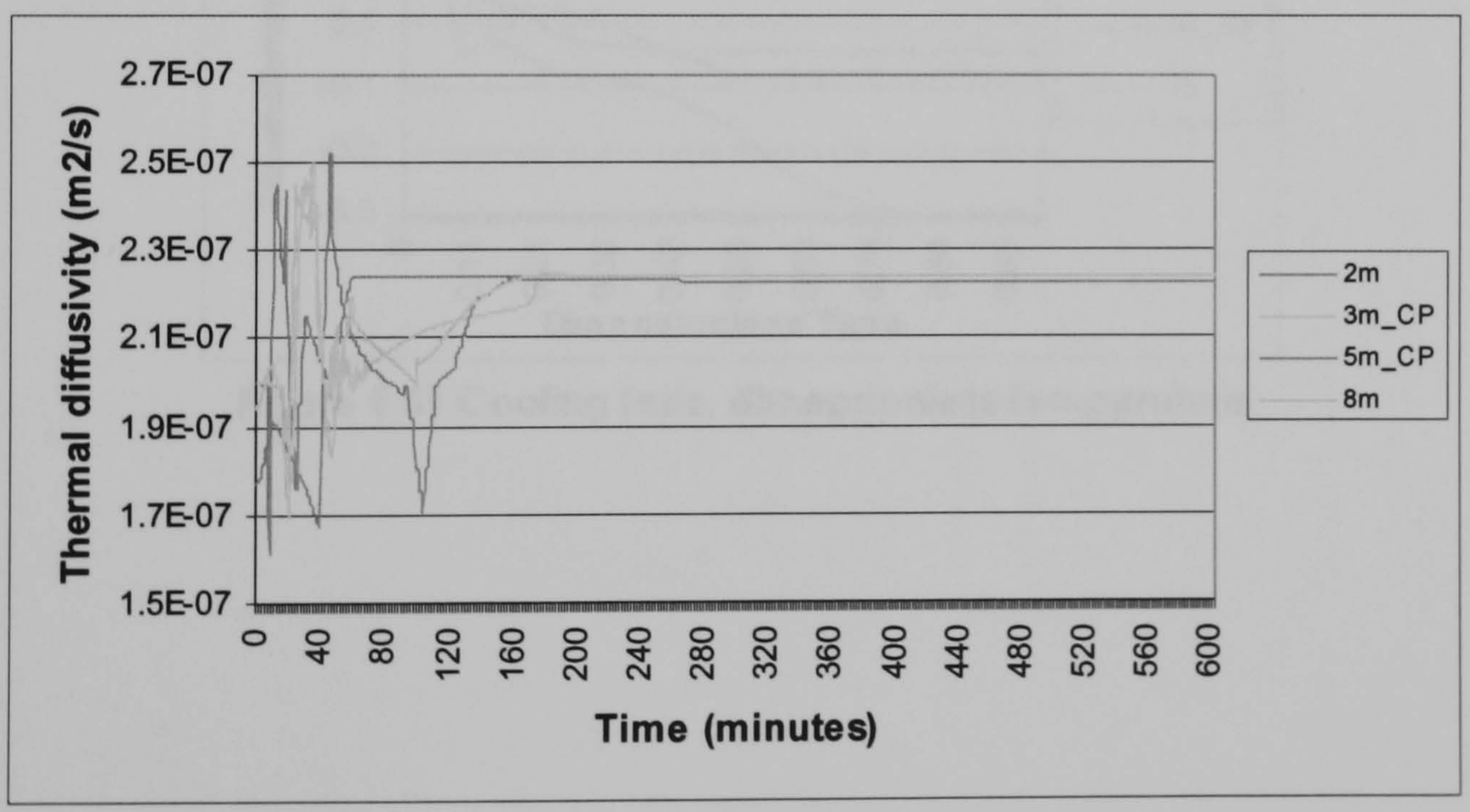

Figure 5.50: Thermal diffusivity evolution, heating tests

For the present study, the next ***dimensionless parameters*** are defined:

Dimensionless ***time***:

$$\tau = \frac{\text{Time elapsed at iteration}}{\text{Total test duration}}$$

Dimensionless ***temperature***:

- For cooling tests:

$$\theta_s = \frac{T_m - T_{PCM}}{T_m - T_{ini}}$$

- For heating tests:

$$\theta_l = \frac{T_{PCM} - T_m}{T_m - T_{ini}}$$

In Figure 5.51 and Figure 5.52, we can observe that the evolution of the temperature is an important indicator of the system's efficiency. As it was discussed earlier, the charging ratio can affect the amount of energy stored/releasaed. In this case test 7s has a slow discharging rate, but is the test which releases the largest amount of energy. Test 2m with a fast charging ratio stores a smaller amount of energy than other tests.

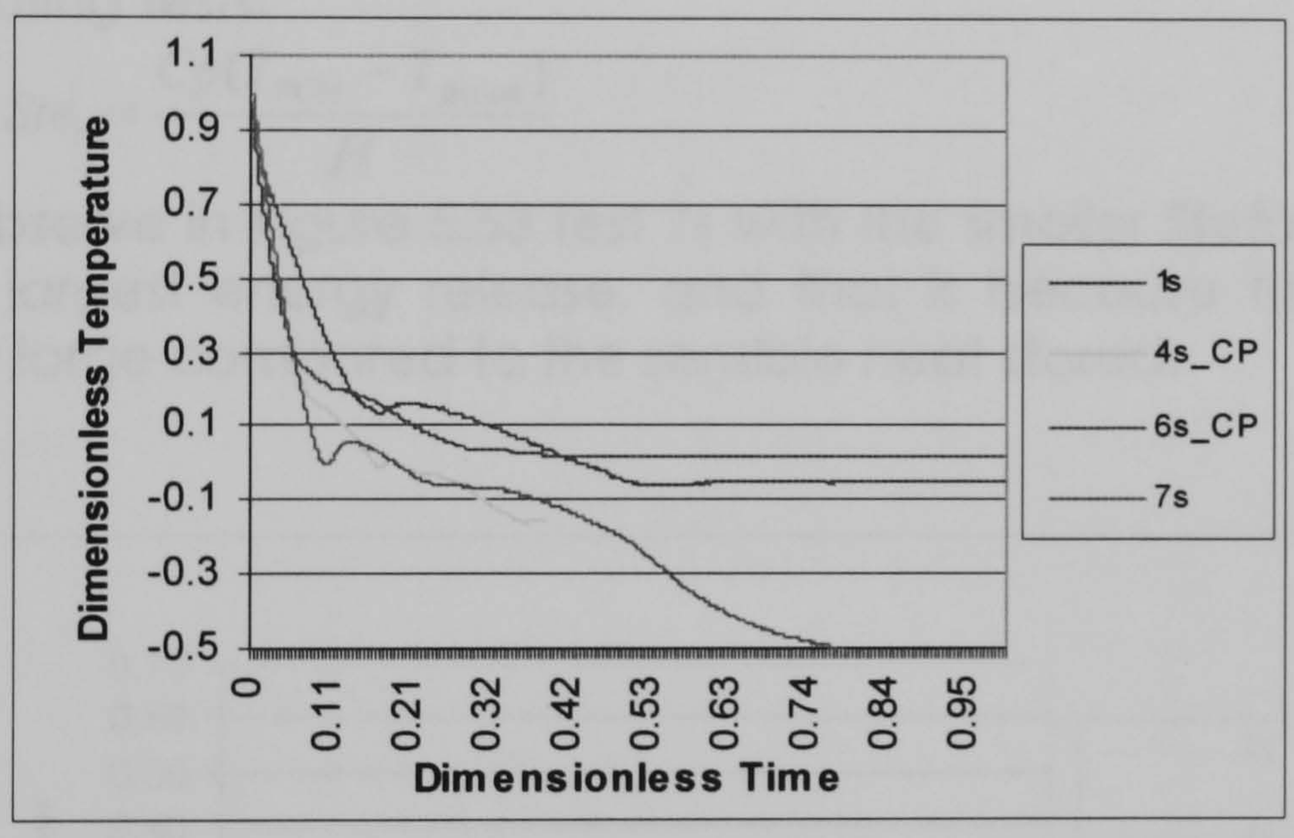

Figure 5.51 Cooling tests, dimensionless temperature

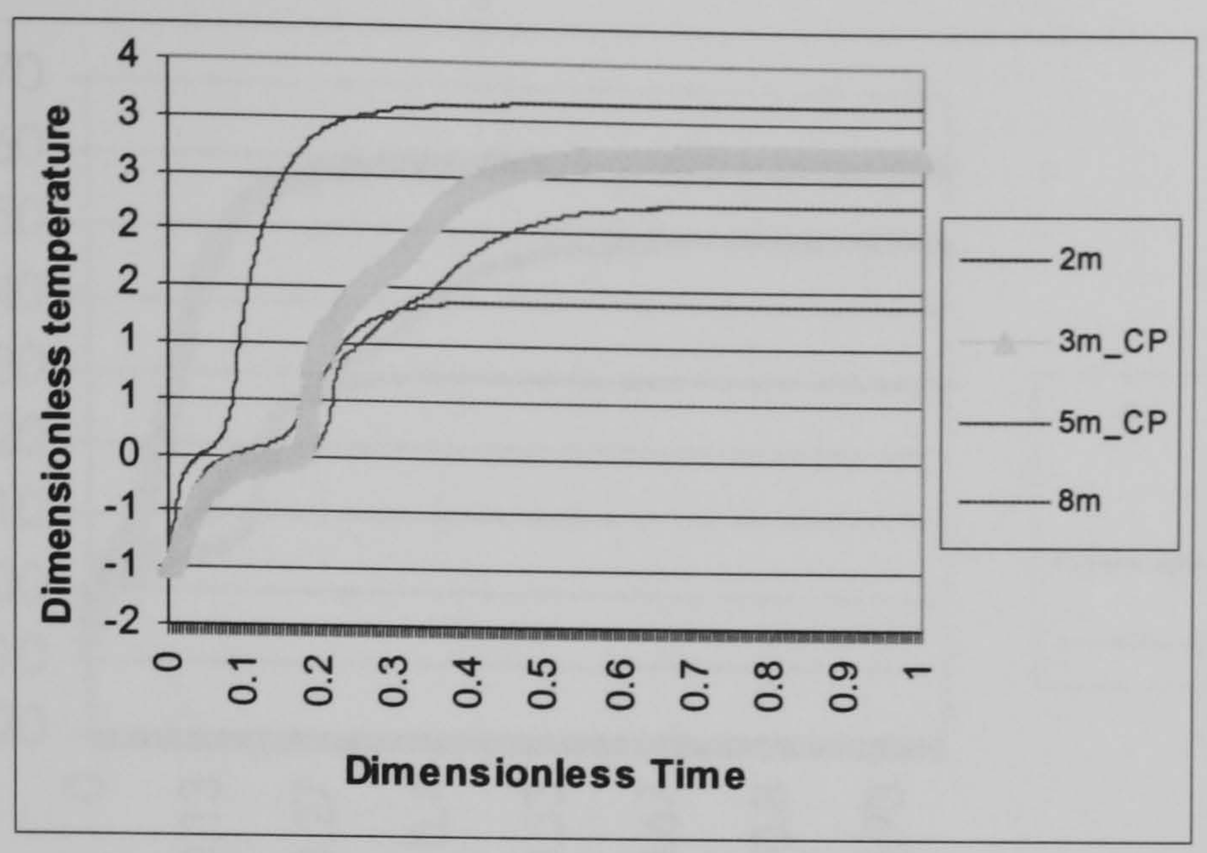

Figure 5.52: Heating tests, dimensionless temperature

Stefan Number: Is the ratio of sensible heat to latent heat

- For cooling tests:

$$Ste_s = \frac{Cp(T_{PCM} - T_m)}{H}$$

- For heating tests:

$$Ste_l = \frac{Cp(T_{PCM} - T_{fusion})}{H}$$

As we can observe in Figure 5.53 test 7s with the smaller Stefan number has allowed the largest energy release, and that is because the latent heat stored is fairly large compared to the sensible heat stored.

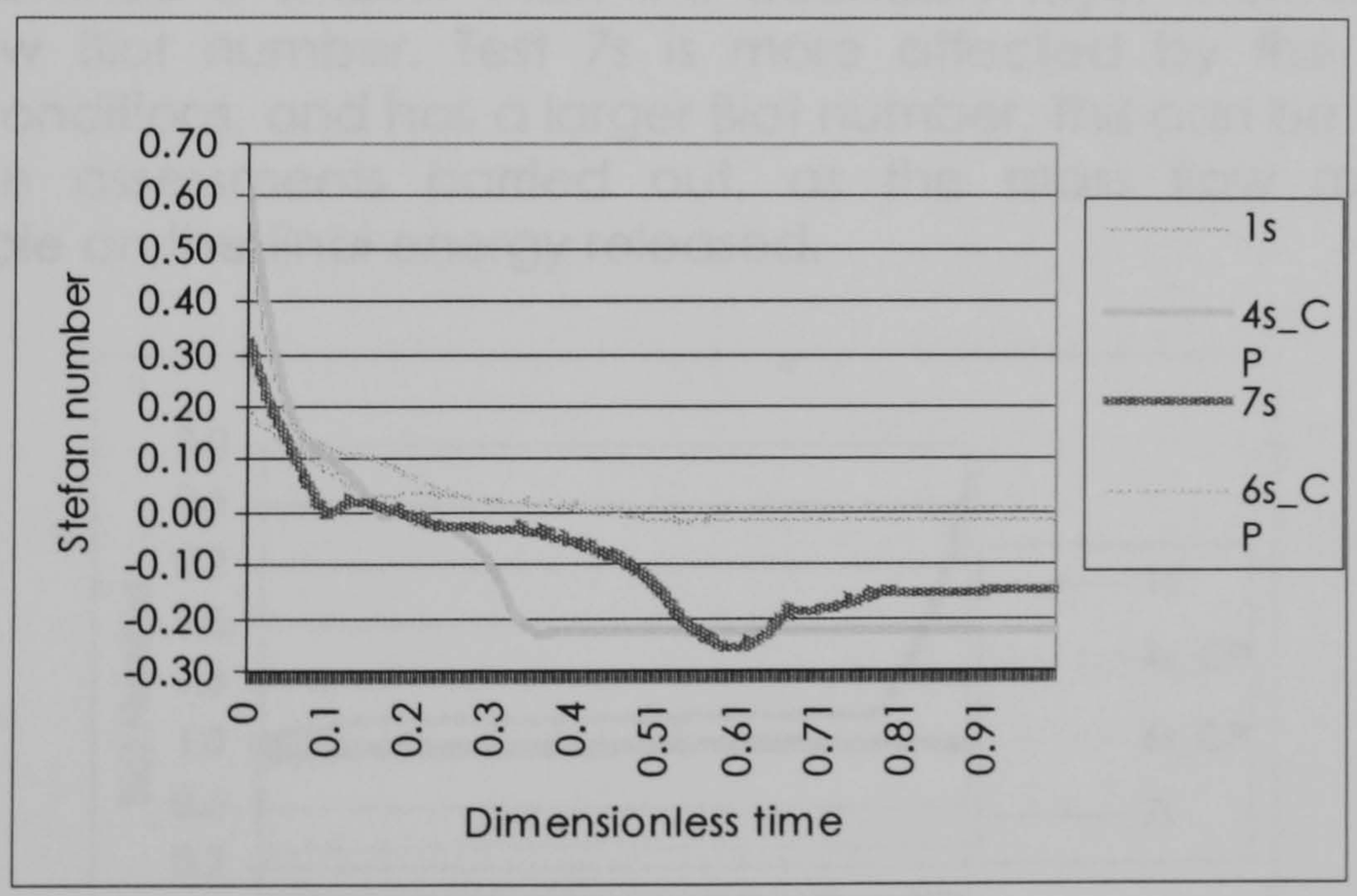

Figure 5.53: Stefan number response time for the solidification.

In Figure 5.54 we can also observe that test 5m with the largest amount of energy stored has the smaller Stefan number. For test 2m, one of the tests which stored a small amount of energy the Stefan number is the largest.

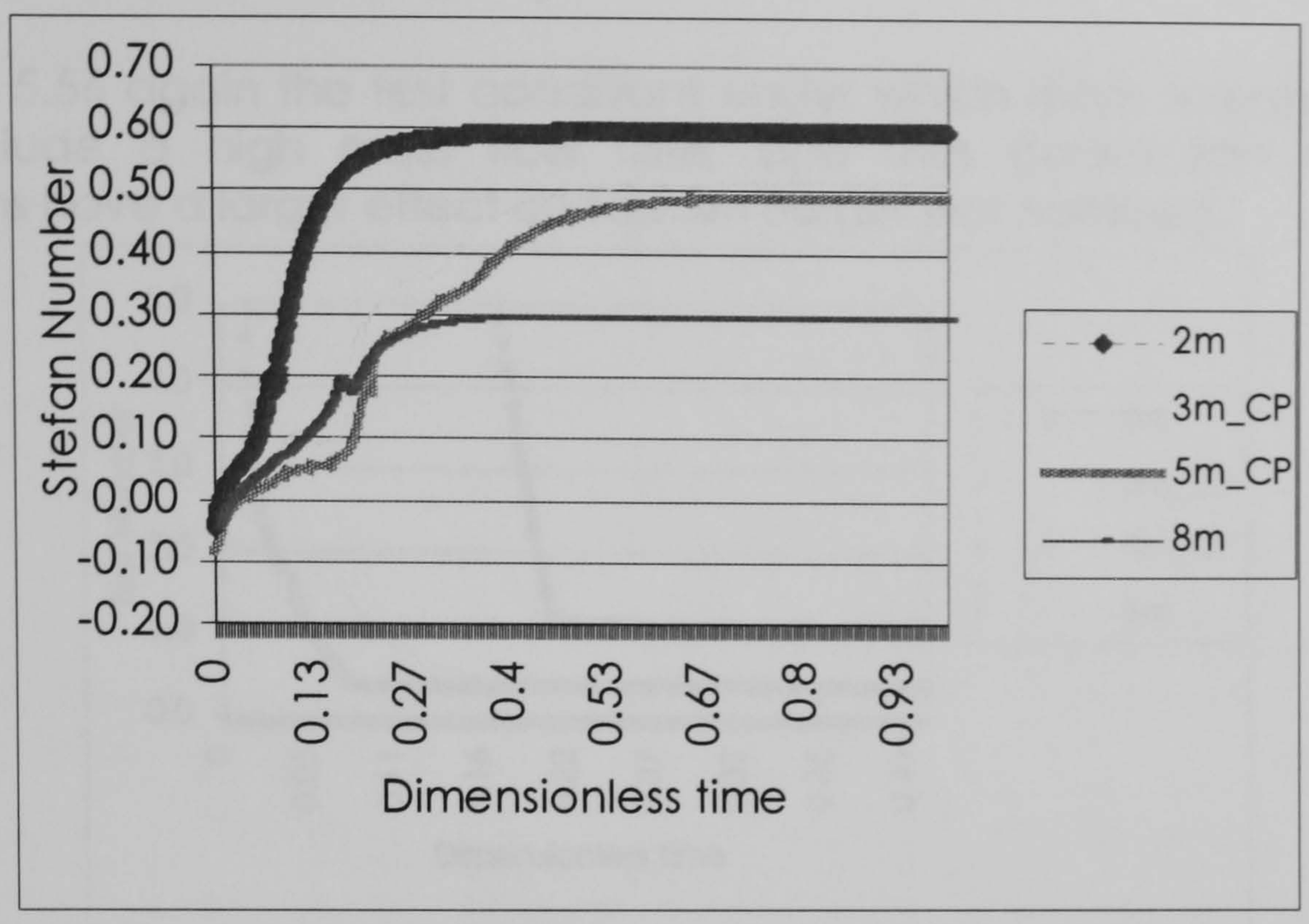

Figure 5.54:Stefan number response time for the heating

Biot Number: Is the ratio of the internal thermal resistance of a solid to the boundary layer thermal resistance. It provides a measure of the temperature drop in the solid relative to the temperature difference between the surface and the fluid. It relates the heat transfer resistance inside and at the surface of a body

$$Bi = \frac{h * dx}{k}$$

In Figure 5.55 we can observe that in test 6s Capric-Palmitic cell the internal thermal resistance is smaller than the boundary layer thermal resistance giving a low Biot number. Test 7s is more affected by the convection boundary conditions, and has a larger Biot number. This can be verified with the previous assessments carried out, as the mass flow rate plays a significant role on the final energy released.

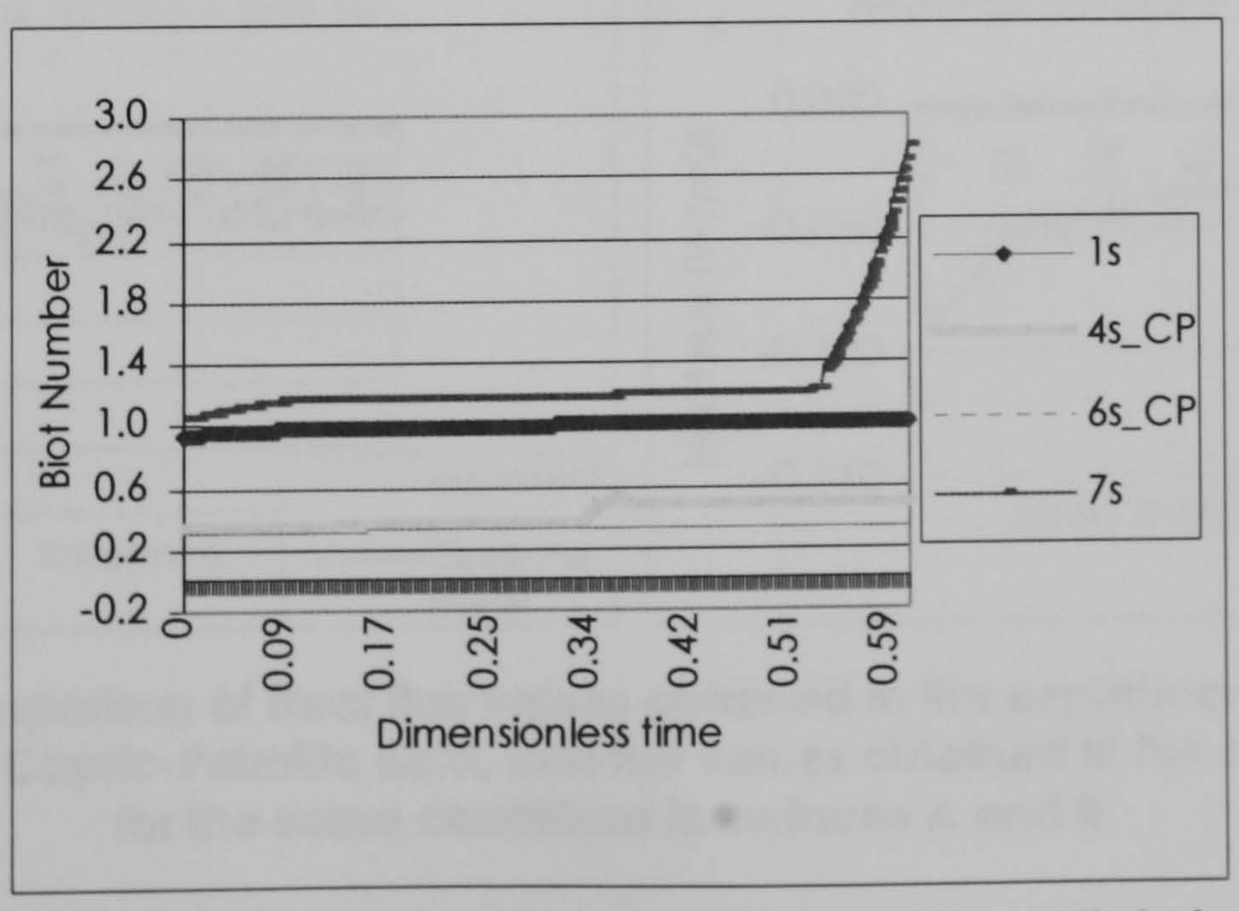

Figure 5.55: Heat resistance inside and at the surface of the unit during solidification.

In Figure 5.56 again the test conditions under which more energy is stored (5m) include a high mass flow rate, and thus convection boundary conditions have a larger effect on test 5m (larger Biot number)

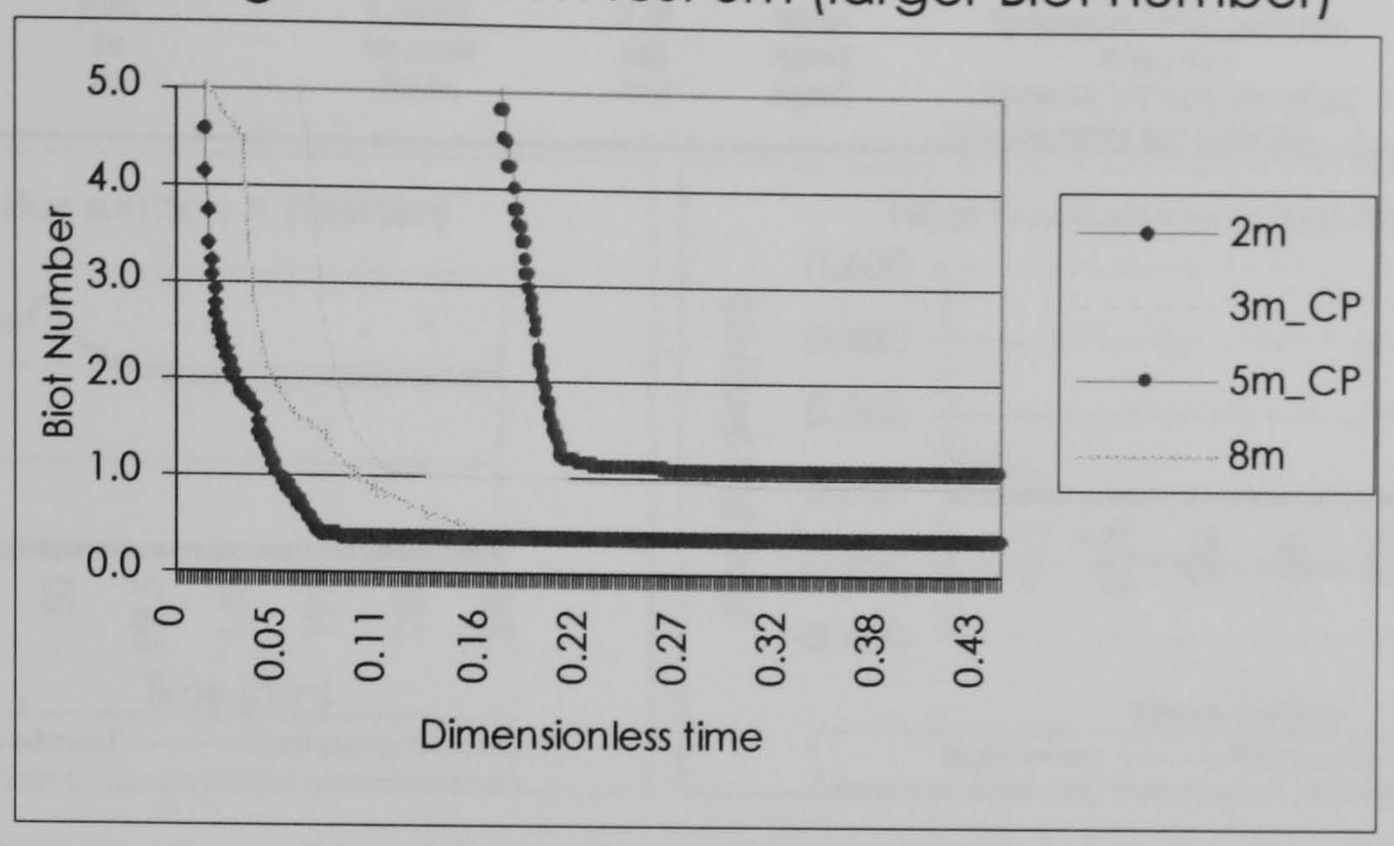

Figure 5.56: Heat transfer resistance inside and at the surface of the unit during heating

Theoretical model assessment

Experimental heat flux values for this experiment were compared with the computer model results, in order to validate the code. As it can be observed in the following graphs good agreement between the computer model and experimental values was found:

Test	1s	Melting Temp	24	C	Initial PCM Temp	38.56	C
Mode	cooling	Enthalpy	153000	J/kg	Surface A intial T	38.06	C
Replica	2	Cp, liquid	2155	J/kgK	Test duration	27900	sec
PCM	Single C-P	Cp, solid	1830	J/kgK	Irradiation	lamps off	W/m2
Temp sensor surf A	EB1	k, solid	0.17	W/mK	Tube depth	0.0381	m
Temp sensor surf B	EB4	k, liquid	0.45	W/mK	Barometric Pressure of day	1005	Pa
HF sensor surf A	4a	Ro, solid	886	kg/m3	Mass flow	5.3	g/s
HF sensor surf B	4b	Ro liq	910	kg/m3	Temp Air chamber (average)	19.5	C
Time interval	30 sec				Temp Exterior air (average)	25.6	C

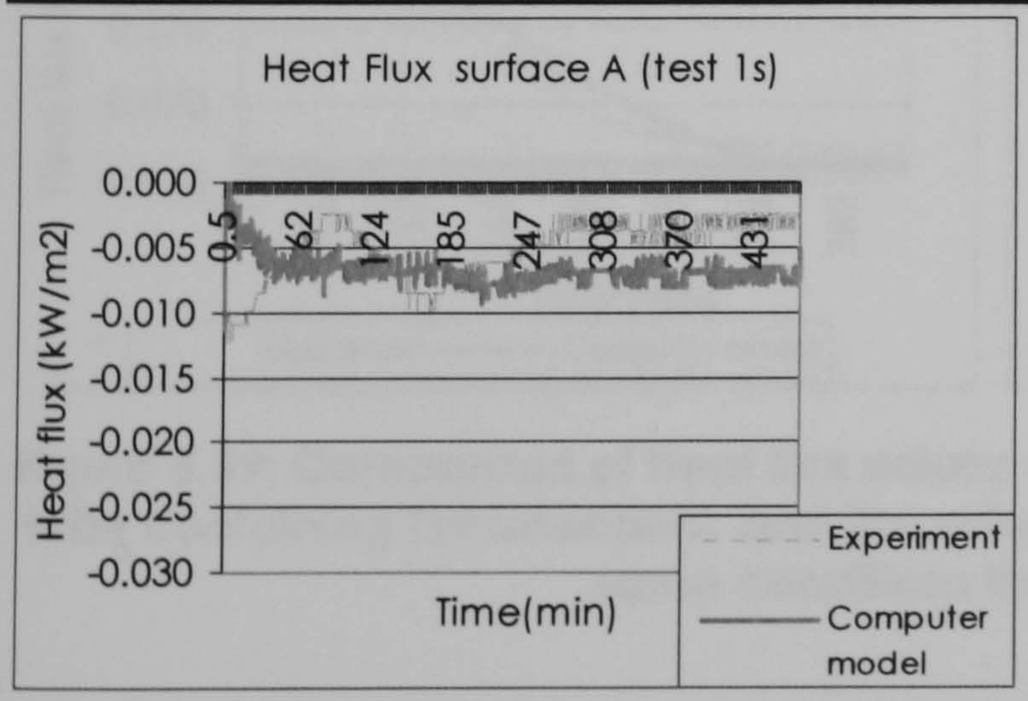

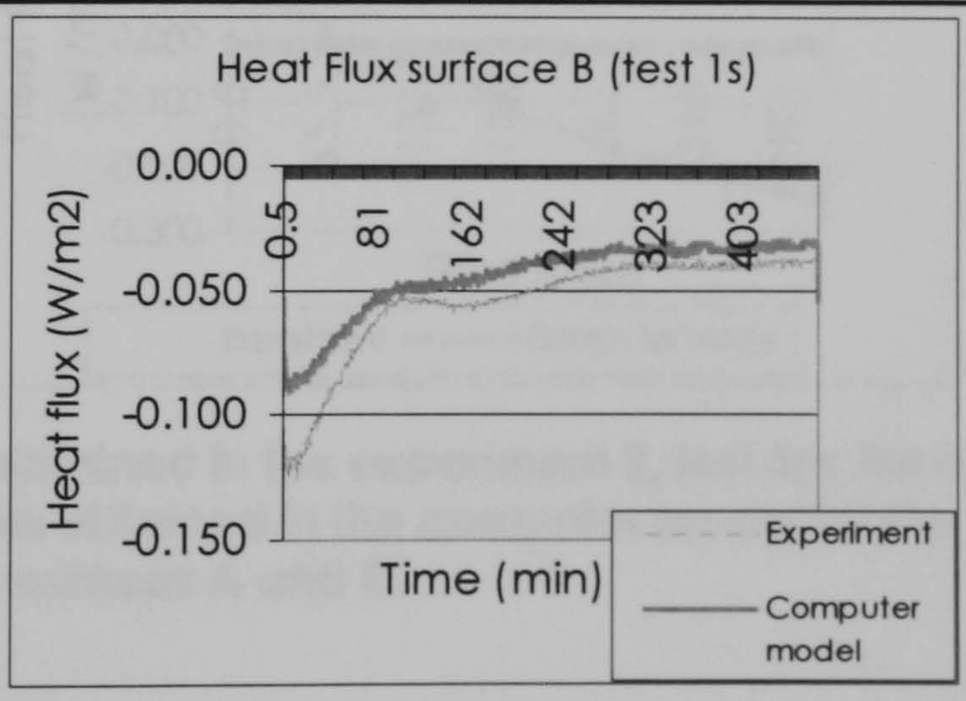

Figure 5.57: Comparison of Heat flux values obtained in the experiment 2, test 1s for a tube containing Capric-Palmitic acid, and the values obtained in the computer model for the same conditions in surfaces A and B.

Test	2m	Melting Temp	24	C	Initial PCM Temp	12.81	C
Mode	heating	Enthalpy	153000	J/kg	Surface A intial T	15.72	C
Replica	2	Cp, liquid	2155	J/kgK	Test duration	17760	sec
PCM	Single C-P	Cp, solid	1830	J/kgK	Irradiation	384	W/m2
Temp sensor surf A	EB2	k, solid	0.17	W/mK	Tube depth	0.0127	m
Temp sensor surf B	EB5	k, liquid	0.45	W/mK	Barometric Pressure of day	1011	Pa
HF sensor surf A	6a	Ro, solid	886	kg/m3	Mass flow	6.8	g/s
HF sensor surf B	5b	Ro liq	910	kg/m3	Temp Air chamber (average)	39.7	C
					Temp Exterior air (average)	25.3	C

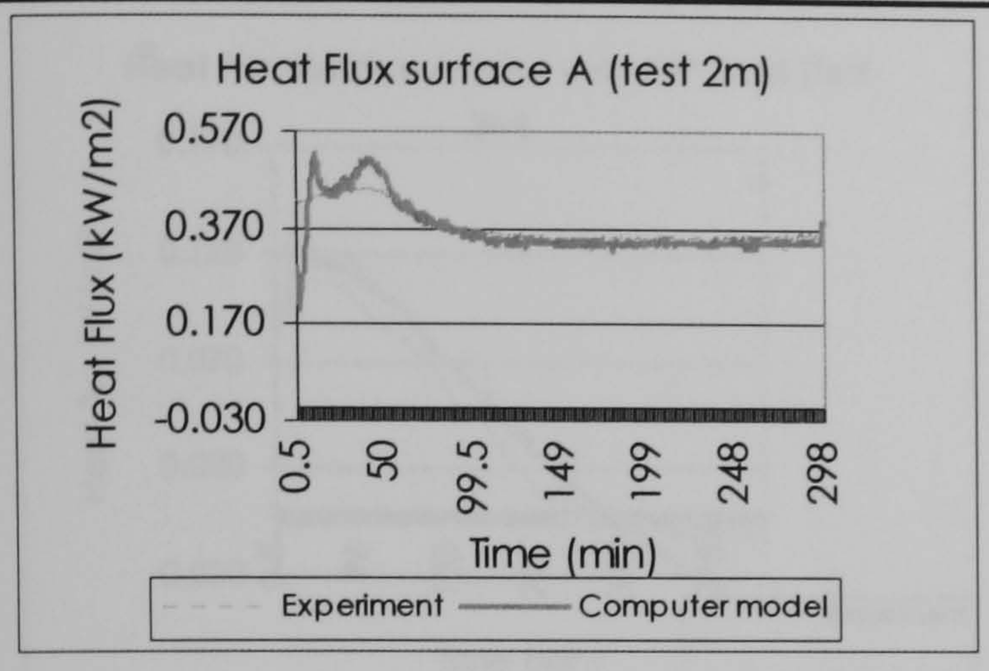

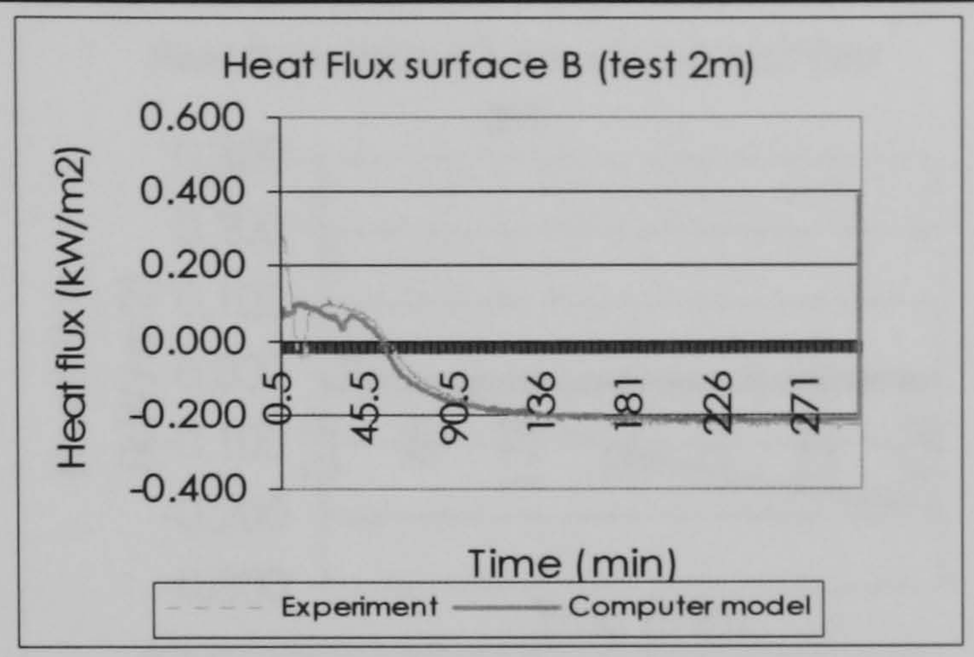

Figure 5.58: Comparison of Heat flux values obtained in the experiment 2, test 2m for a tube containing Capric-Palmitic acid, and the values obtained in the computer model for the same conditions in surfaces A and B.

		For a tube with Tetradecanol					
Test	3m	Melting Temp	34	C	Initial PCM Temp	13.18	C
Mode	heating	Enthalpy	205000	J/kg	Surface A intial T	13.8	C
Replica	2	Cp, liquid	2200	J/kgK	Test duration	25320	sec
PCM	Multiple (T,CP,H)	Cp, solid	1800	J/kgK	Irradiation	402	W/m2
Temp sensor surf A	EB1	k, solid	0.13	W/mK	Tube depth	0.0381	m
Temp sensor surf B	EB4	k, liquid	0.45	W/mK	Barometric Pressure of day	1023	Pa
HF sensor surf A	HF4a	Ro, solid	823	kg/m3	Mass flow	5.154	g/s
HF sensor surf B	HF4b	Ro liq	850	kg/m3	Temp Air chamber (average)	32.3	C
					Temp Exterior air (average)	26.9	C

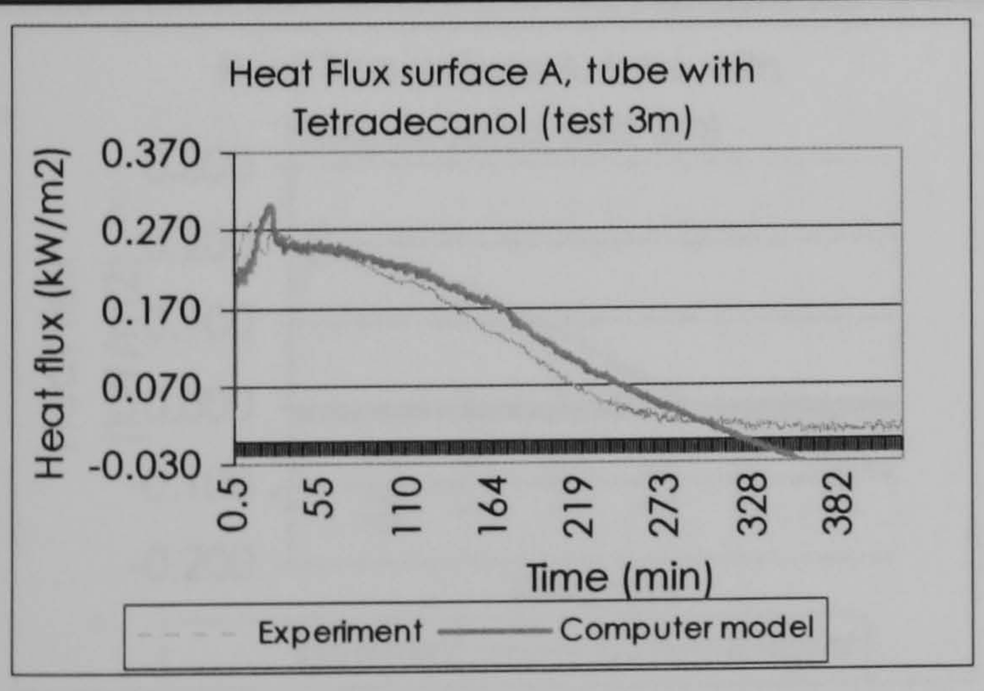

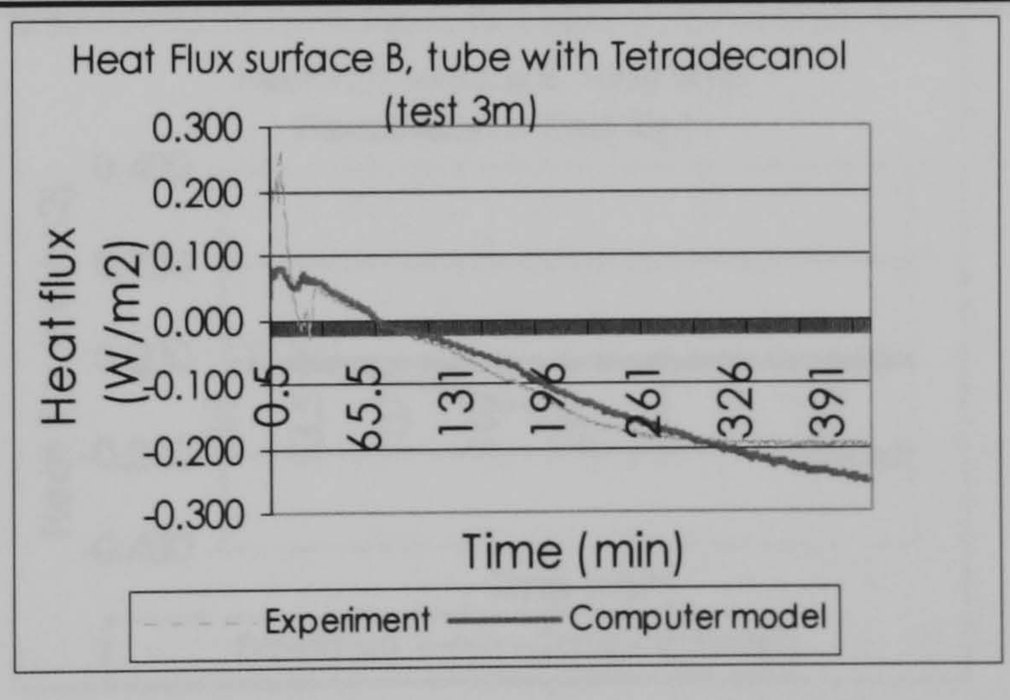

Figure 5.59: Comparison of Heat flux values obtained in the experiment 2, test 3m for a tube containing Tetradecanol, and the values obtained in the computer model for the same conditions in surfaces A and B.

		For a tube with Capric-Palmitic Acid					
Test	3m	Melting Temp	24	C	Initial PCM Temp	13.13	C
Mode	heating	Enthalpy	153000	J/kg	Surface A intial T	13.95	C
Replica	2	Cp, liquid	2155	J/kgK	Test duration	25320	sec
PCM	Multiple (T,CP,H)	Cp, solid	1830	J/kgK	Irradiation	402	W/m2
Temp sensor surf A	EB2	k, solid	0.17	W/mK	Tube depth	0.0381	m
Temp sensor surf B	EB5	k, liquid	0.45	W/mK	Barometric Pressure of day	1023	Pa
HF sensor surf A	HF5a	Ro, solid	886	kg/m3	Mass flow	5.154	g/s
HF sensor surf B	HF5b	Ro liq	910	kg/m3	Temp Air chamber (average)	32.3	C
					Temp Exterior air (average)	26.9	C

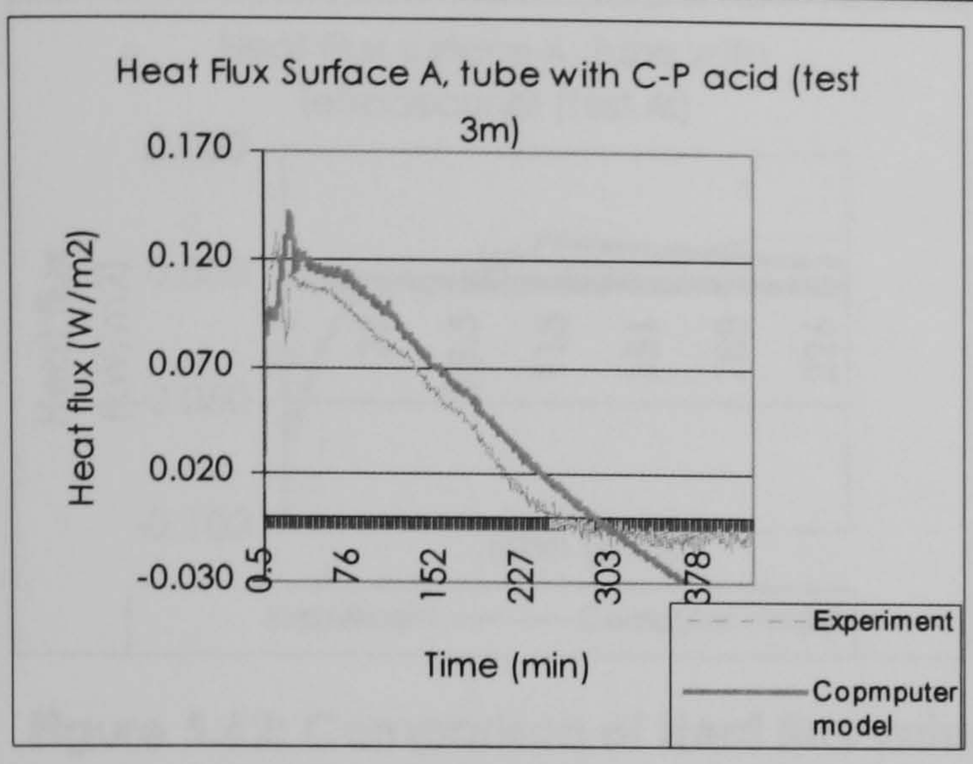

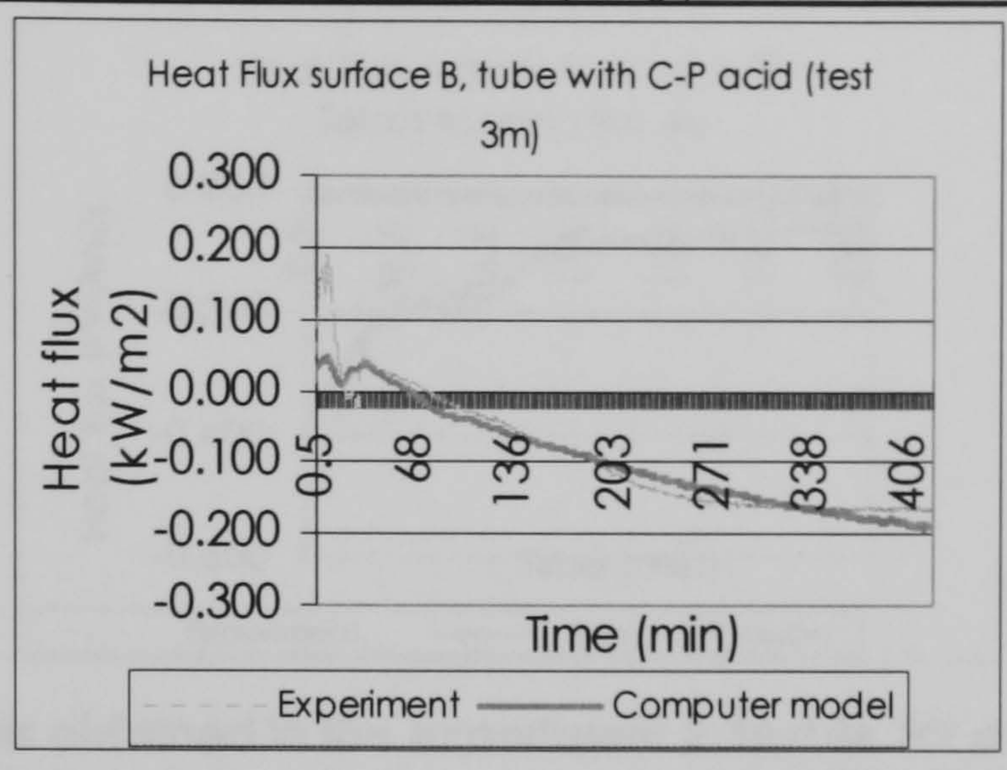

Figure 60: Comparison of Heat flux values obtained in the experiment 2, test 3m for a tube containing Capric-Palmitic acid, and the values obtained in the computer model for the same conditions in surfaces A and B.

		For a tube with Hexadecanol					
Test	3m	Melting Temp	20	C	Initial PCM Temp	13.2	C
Mode	heating	Enthalpy	236000	J/kg	Surface A intial T	13.95	C
Replica	2	Cp, liquid	2220	J/kgK	Test duration	25320	sec
PCM	Multiple (T,CP,H)	Cp, solid	1750	J/kgK	Irradiation	402	W/m2
Temp sensor surf A	EB3	k, solid	0.15	W/mK	Tube depth	0.0381	m
Temp sensor surf B	EB6	k, liquid	0,45	W/mK	Barometric Pressure of day	1023	Pa
HF sensor surf A	HF6a	Ro, solid	830	kg/m3	Mass flow	5.154	g/s
HF sensor surf B	HF6b	Ro liq	870	kg/m3	Temp Air chamber (average)	32.3	C
					Temp Exterior air (average)	26.9	C

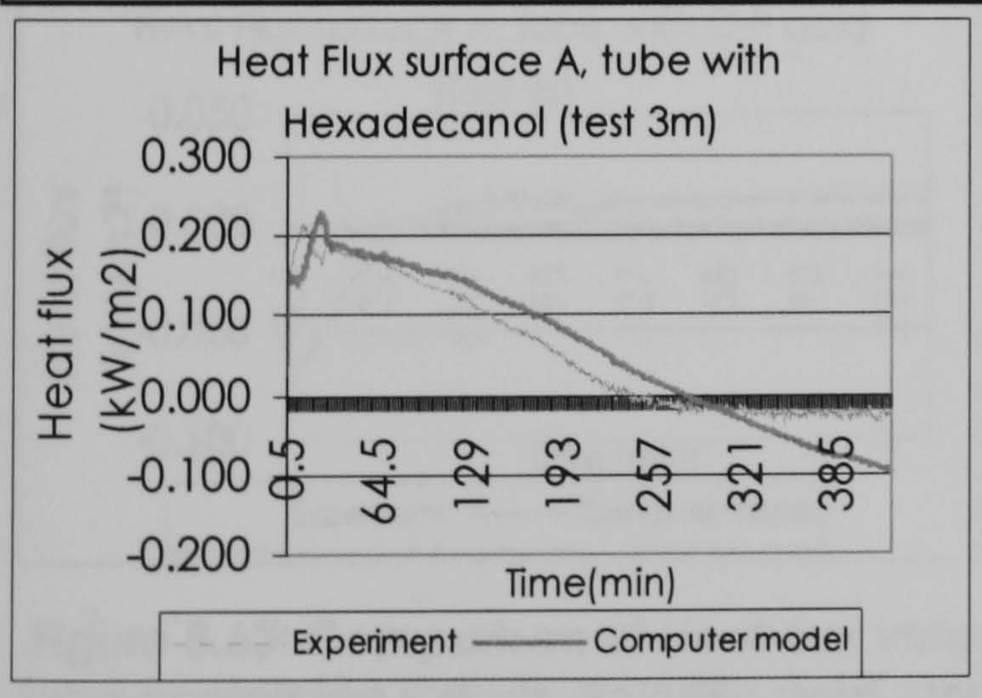

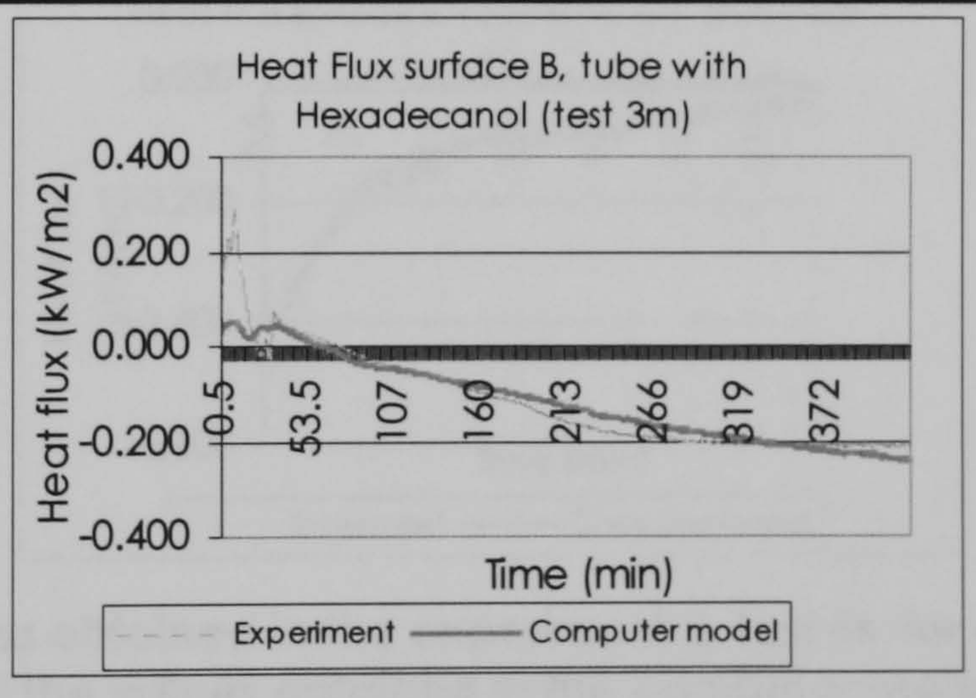

Figure 5.61: Comparison of Heat flux values obtained in the experiment 2, test 3m for a tube containing Hexadecanol, and the values obtained in the computer model for the same conditions in surfaces A and B.

		For a tube with Tetradecanol					
Test	4s	Melting Temp	34	C	Initial PCM Temp	70.64	C
Mode	cooling	Enthalpy	205000	J/kg	Surface A intial T	68.4	C
Replica	2	Cp, liquid	2200	J/kgK	Test duration	14130	sec
PCM	Multiple (T,CP,H)	Cp, solid	1800	J/kgK	Irradiation	lamps off	W/m2
Temp sensor surf A	EB1	k, solid	0.13	W/mK	Tube depth	0.0127	m
Temp sensor surf B	EB4	k, liquid	0.45	W/mK	Barometric Pressure of day	1001	Pa
HF sensor surf A	HF5a (4a failed)	Ro, solid	823	kg/m3	Mass flow	6.92	g/s
HF sensor surf B	HF4b	Ro liq	850	kg/m3	Temp Air chamber (average)	12.6	C
					Temp Exterior air (average)	23.6	C

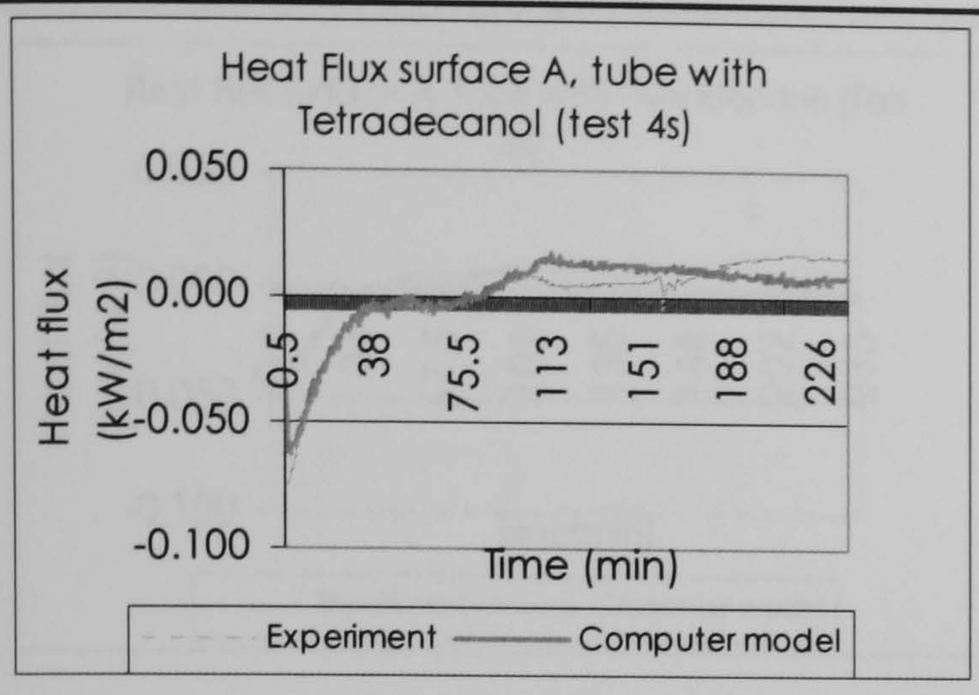

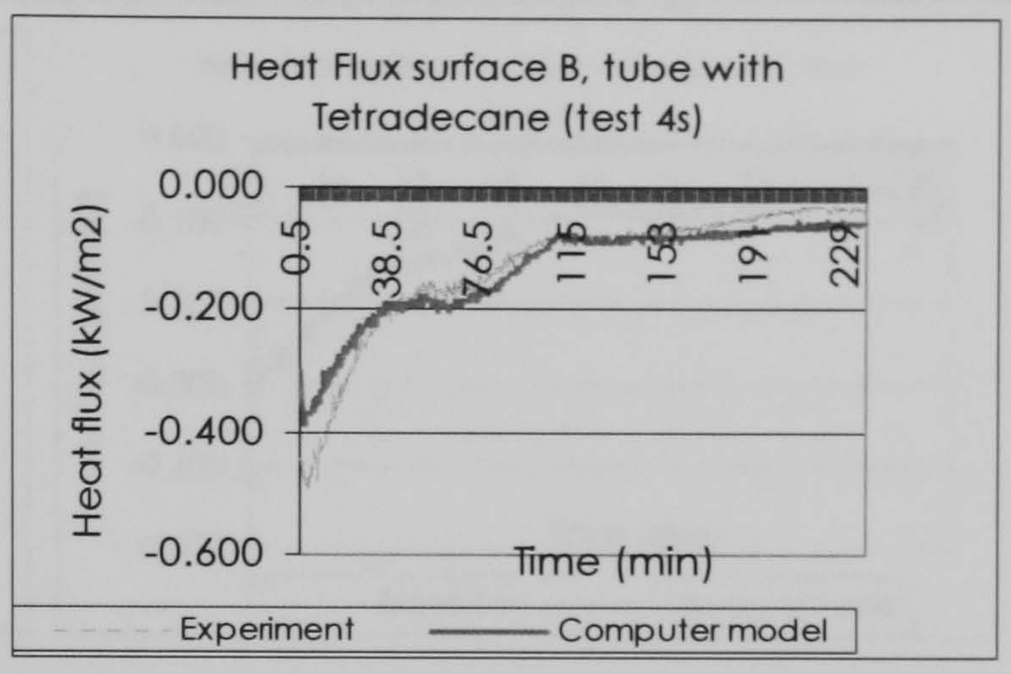

Figure 5.62: Comparison of Heat flux values obtained in the experiment 2, test 4s for a tube containing Tetradecanol, and the values obtained in the computer model for the same conditions in surfaces A and B.

		For a tube with Capric-Palmitic Acid					
Test	4s	Melting Temp	32	C	Initial PCM Temp	70	C
Mode	cooling	Enthalpy	153000	J/kg	Surface A intial T	67.52	C
Replica	2	Cp, liquid	2155	J/kgK	Test duration	14130	sec
PCM	Multiple (T,CP,H)	Cp, solid	1830	J/kgK	Irradiation	lamps off	W/m2
Temp sensor surf A	EB2	k, solid	0.17	W/mK	Tube depth	0.0127	m
Temp sensor surf B	EB5	k, liquid	0.45	W/mK	Barometric Pressure of day	1001	Pa
HF sensor surf A	HF5a	Ro, solid	886	kg/m3	Mass flow	6.92	g/s
HF sensor surf B	HF4b (5b failed)	Ro liq	910	kg/m3	Temp Air chamber (average)	12.6	C
					Temp Exterior air (average)	23.6	C

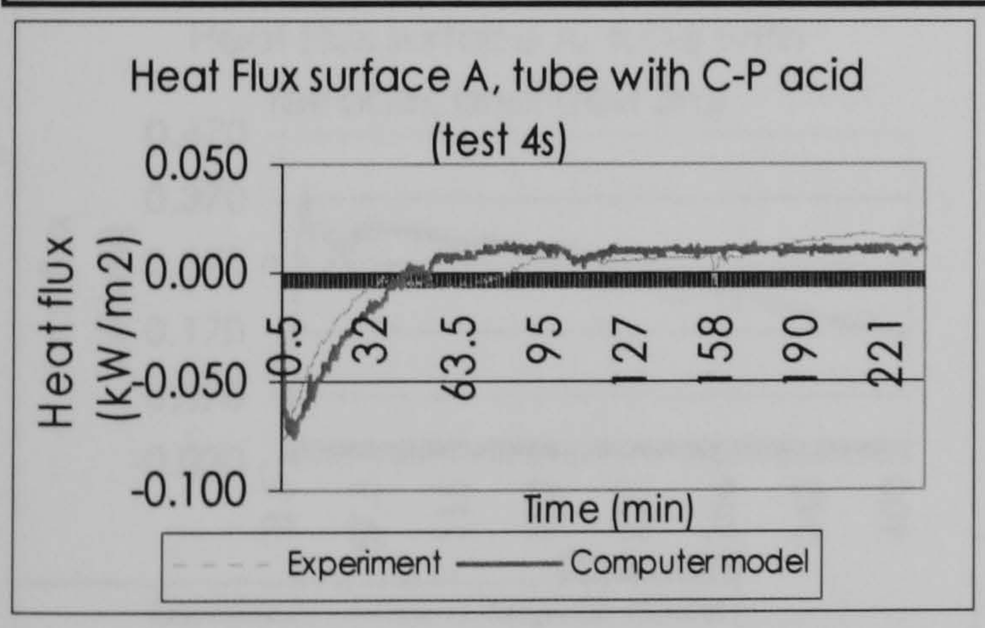

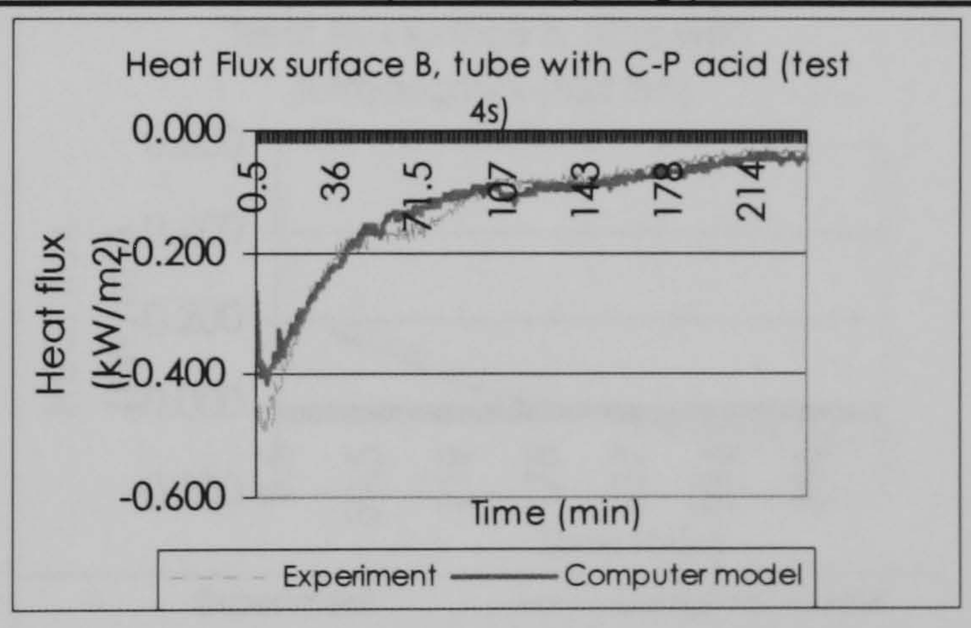

Figure 5.63: Comparison of Heat flux values obtained in the experiment 2, test 4s for a tube containing Capric-Palmitic acid, and the values obtained in the computer model for the same conditions in surfaces A and B.

		For a tube with Hexadecanol				
Test	4s	Melting Temp	23	C	Initial PCM Temp	68.9 C
Mode	cooling	Enthalpy	236000	J/kg	Surface A intial T	67.12 C
Replica	2	Cp, liquid	2220	J/kgK	Test duration	14130 sec
PCM	Multiple (T,CP,H)	Cp, solid	1750	J/kgK	Irradiation	lamps off W/m2
Temp sensor surf A	EB3	k, solid	0.15	W/mK	Tube depth	0.0127 m
Temp sensor surf B	EB6	k, liquid	0,45	W/mK	Barometric Pressure of day	1001 Pa
HF sensor surf A	HF5a (6a failed)	Ro, solid	830	kg/m3	Mass flow	6.92 g/s
HF sensor surf B	HF6b	Ro liq	870	kg/m3	Temp Air chamber (average)	12.6 C
					Temp Exterior air (average)	23.6 C

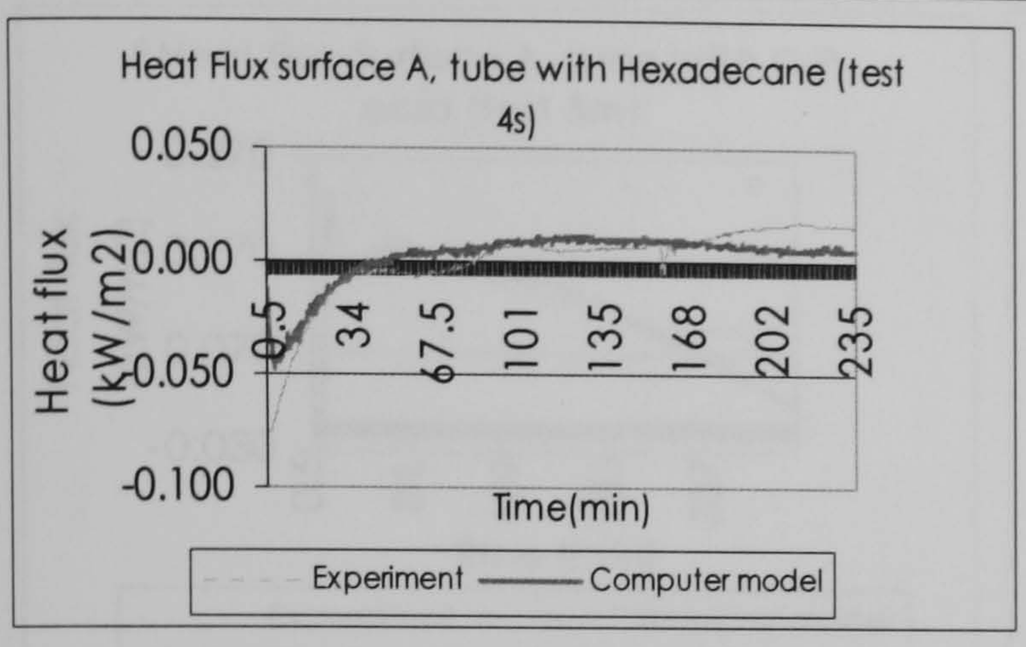

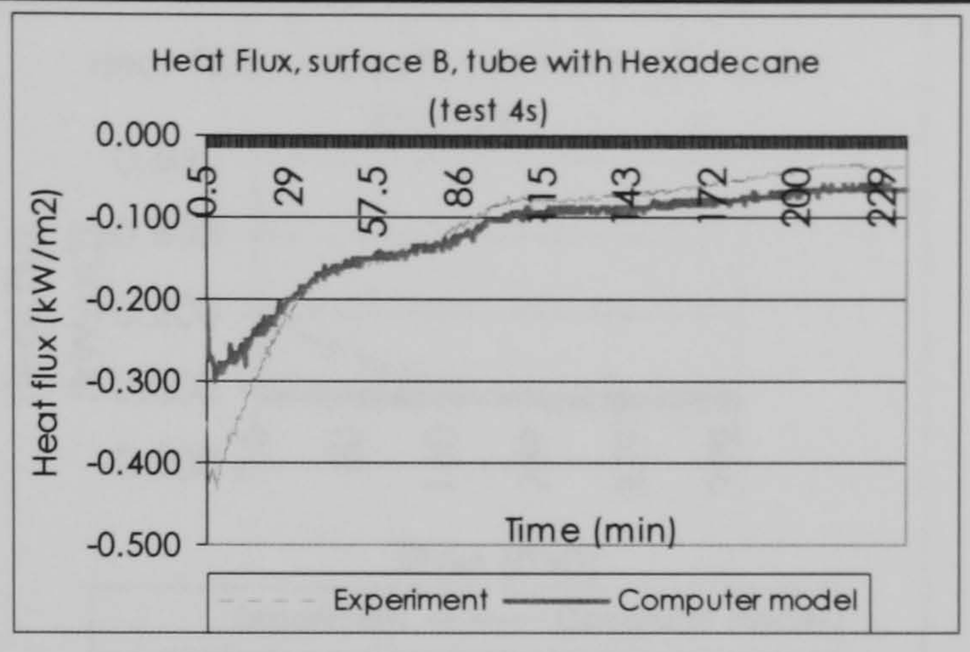

Figure 5.64: Comparison of Heat flux values obtained in the experiment 2, test 4s for a tube containing Hexadecane, and the values obtained in the computer model for the same conditions in surfaces A and B.

		For a tube with Tetradecanol				
Test	5m	Melting Temp	34	C	Initial PCM Temp	11.31 C
Mode	heating	Enthalpy	205000	J/kg	Surface A intial T	11.86 C
Replica	2	Cp, liquid	2200	J/kgK	Test duration	24360 sec
PCM	Multiple (T,CP,H)	Cp, solid	1800	J/kgK	Irradiation	729 W/m2
Temp sensor surf A	EB1	k, solid	0.13	W/mK	Tube depth	0.0381 m
Temp sensor surf B	EB4	k, liquid	0.45	W/mK	Barometric Pressure of day	1013 Pa
HF sensor surf A	HF4a	Ro, solid	823	kg/m3	Mass flow	6.715 g/s
HF sensor surf B	HF4b	Ro liq	850	kg/m3	Temp Air chamber (average)	41.7 C
					Temp Exterior air (average)	27.4 C

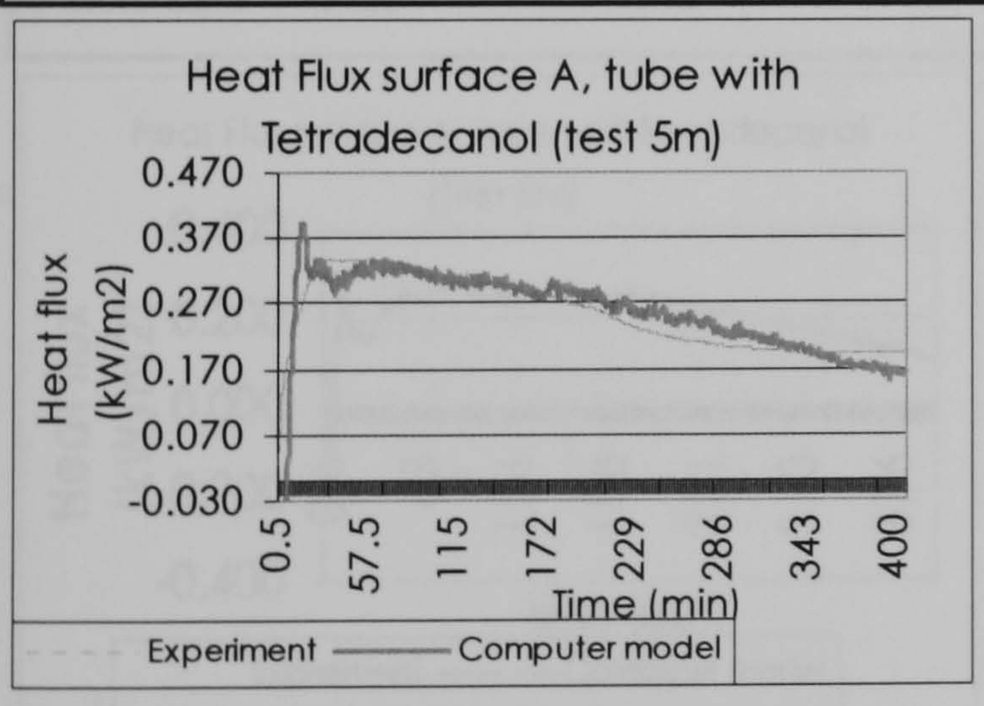

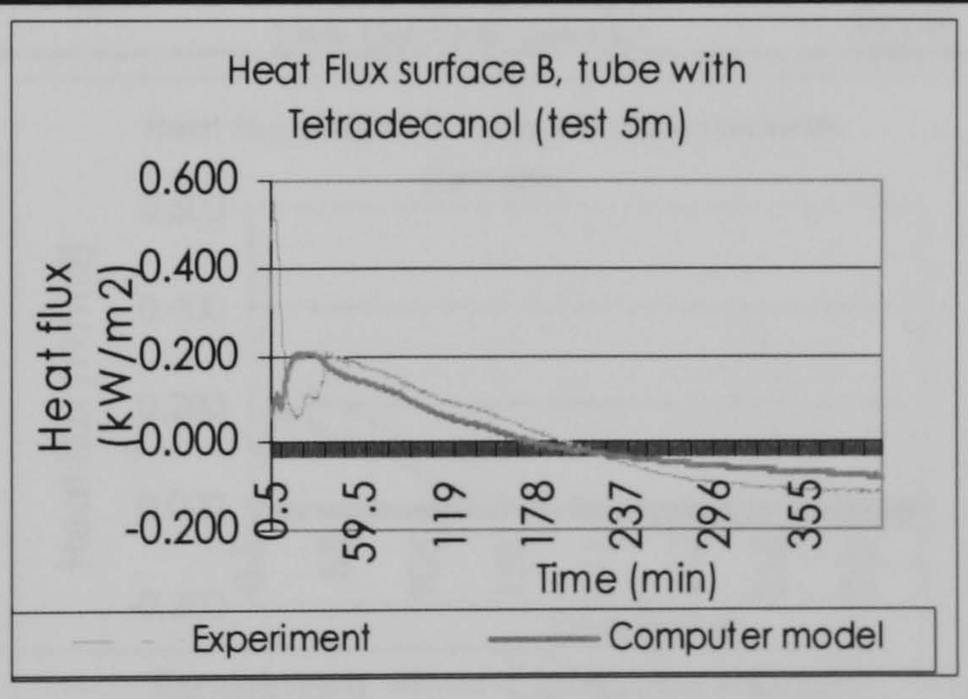

Figure 5.65: Comparison of Heat flux values obtained in the experiment 2, test 5m for a tube containing Tetradecanol, and the values obtained in the computer model for the same conditions in surfaces A and B.

		For a tube with Capric-Palmitic Acid				
Test	5m	Melting Temp	24	C	Initial PCM Temp	11.19 C
Mode	heating	Enthalpy	153000	J/kg	Surface A intial T	12.08 C
Replica	2	Cp, liquid	2155	J/kgK	Test duration	24360 sec
PCM	Multiple (T,CP,H)	Cp, solid	1830	J/kgK	Irradiation	729 W/m2
Temp sensor surf A	EB2	k, solid	0.17	W/mK	Tube depth	0.0381 m
Temp sensor surf B	EB5	k, liquid	0.45	W/mK	Barometric Pressure of day	1013 Pa
HF sensor surf A	HF5a	Ro, solid	886	kg/m3	Mass flow	6.715 g/s
HF sensor surf B	HF5b	Ro liq	910	kg/m3	Temp Air chamber (average)	41.7 C
					Temp Exterior air (average)	27.4 C

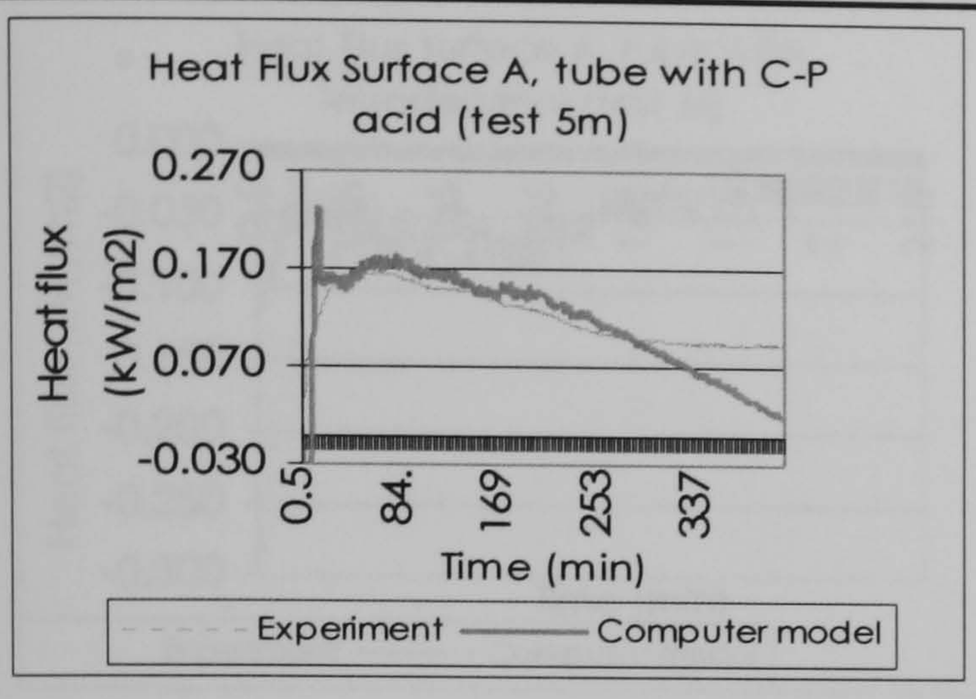

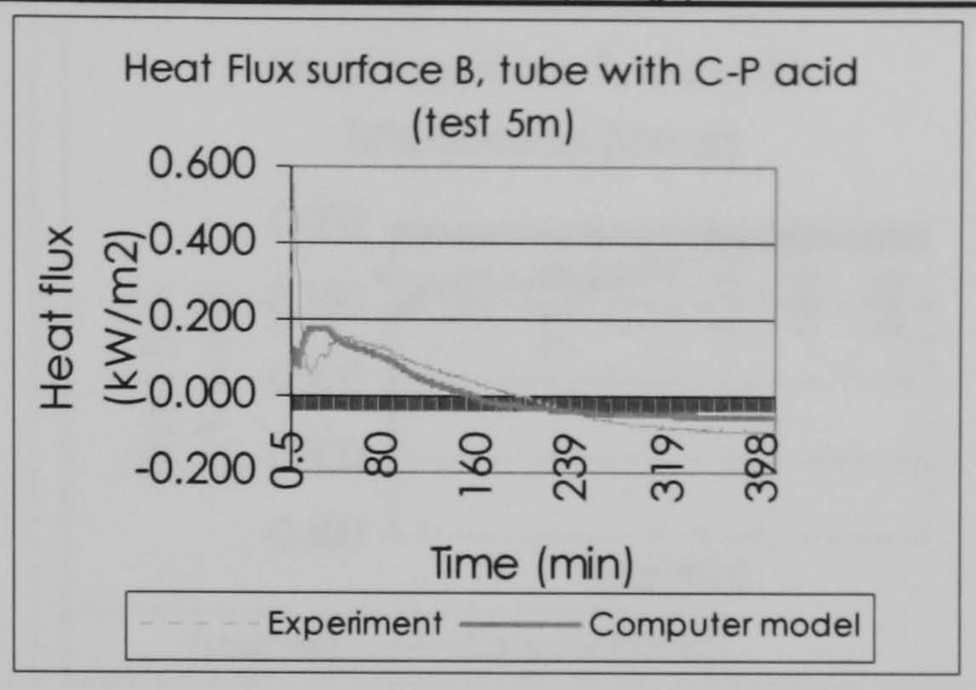

Figure 5.66: Comparison of Heat flux values obtained in the experiment 2, test 5m for a tube containing Capric-Palmitic acid, and the values obtained in the computer model for the same conditions in surfaces A and B.

		For a tube with Hexadecanol				
Test	5m	Melting Temp	17.5	C	Initial PCM Temp	11.46 C
Mode	heating	Enthalpy	236000	J/kg	Surface A intial T	12.16 C
Replica	2	Cp, liquid	2220	J/kgK	Test duration	24360 sec
PCM	Multiple (T,CP,H)	Cp, solid	1750	J/kgK	Irradiation	729 W/m2
Temp sensor surf A	EB3	k, solid	0.15	W/mK	Tube depth	0.0381 m
Temp sensor surf B	EB6	k, liquid	0,45	W/mK	Barometric Pressure of day	1013 Pa
HF sensor surf A	HF6a	Ro, solid	830	kg/m3	Mass flow	6.715 g/s
HF sensor surf B	HF6b	Ro liq	870	kg/m3	Temp Air chamber (average)	41.7 C
					Temp Exterior air (average)	27.4 C

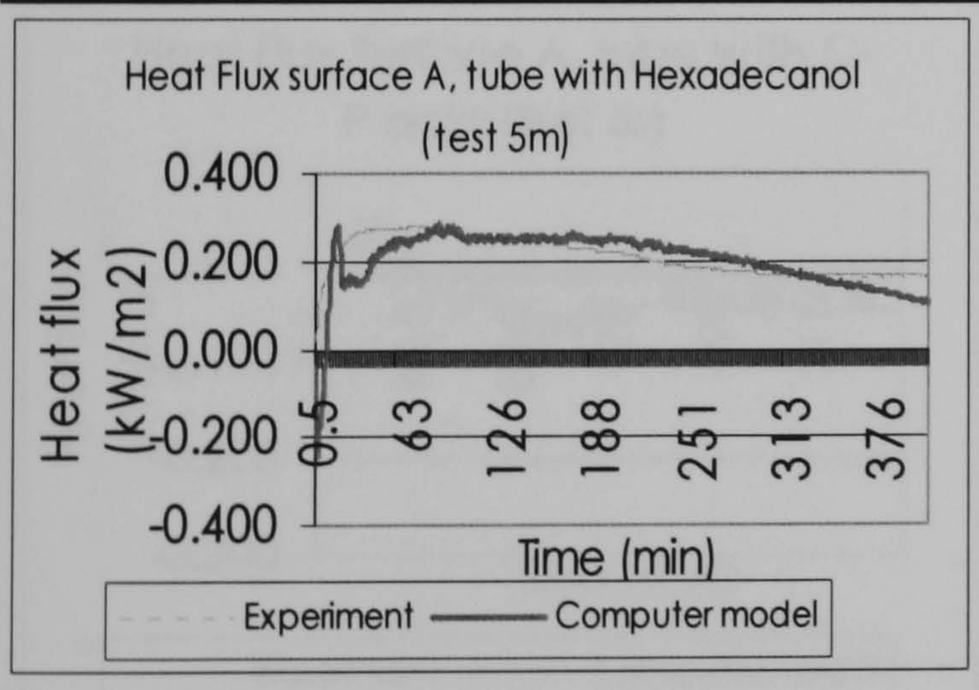

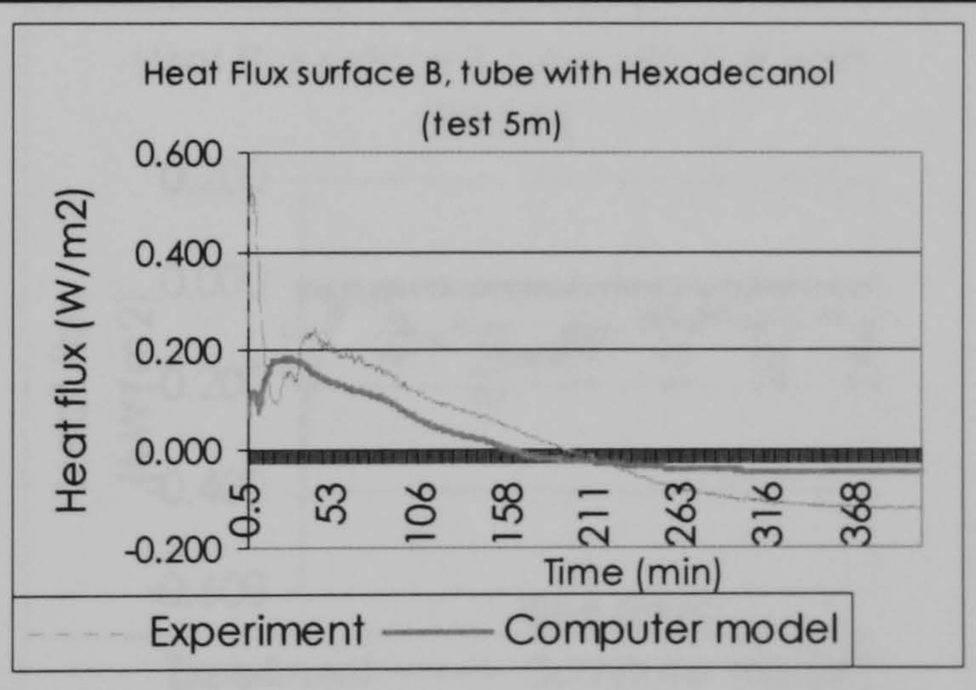

Figure 5.67: Comparison of Heat flux values obtained in the experiment 2, test 5m for a tube containing Hexadecanol, and the values obtained in the computer model for the same conditions in surfaces A and B.

		For a tube with Tetradecanol					
Test	6s	Melting Temp	34	C	Initial PCM Temp	62.4	C
Mode	cooling	Enthalpy	205000	J/kg	Surface A intial T	58.4	C
Replica	3	Cp, liquid	2200	J/kgK	Test duration	14790	sec
PCM	Multiple (T,CP,H)	Cp, solid	1800	J/kgK	Irradiation	lamps off	W/m2
Temp sensor surf A	EB1	k, solid	0.13	W/mK	Tube depth	0.0127	m
Temp sensor surf B	EB4	k, liquid	0.45	W/mK	Barometric Pressure of day	1019	Pa
HF sensor surf A	HF4a	Ro, solid	823	kg/m3	Mass flow	5.265	g/s
HF sensor surf B	HF4b	Ro liq	850	kg/m3	Temp Air chamber (average)	25	C
					Temp Exterior air (average)	24.7	C

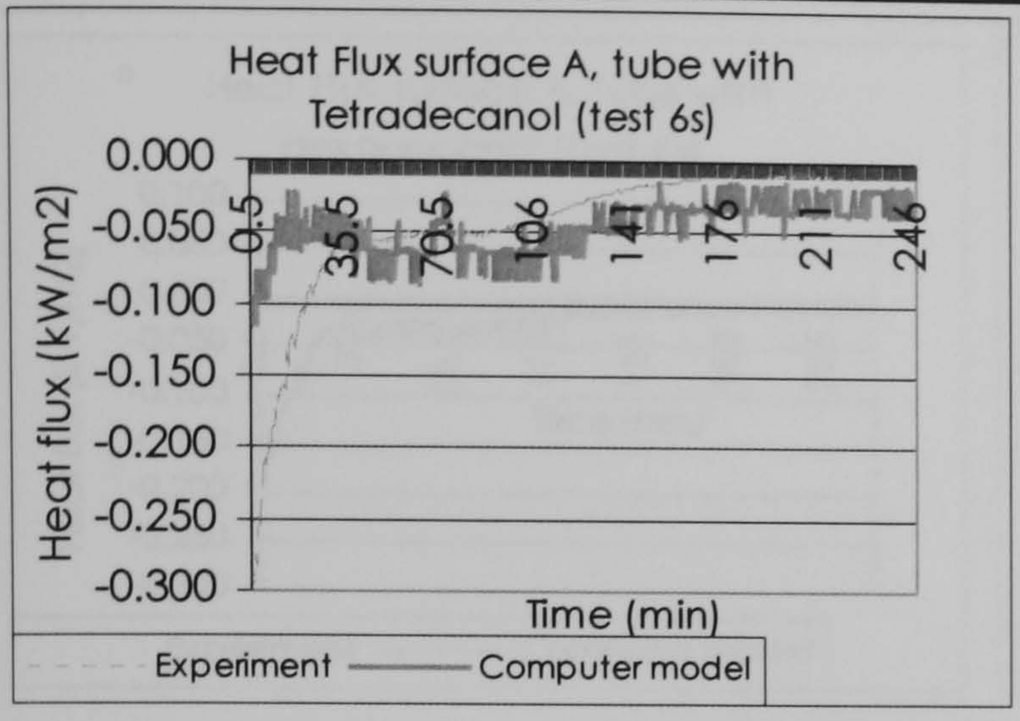

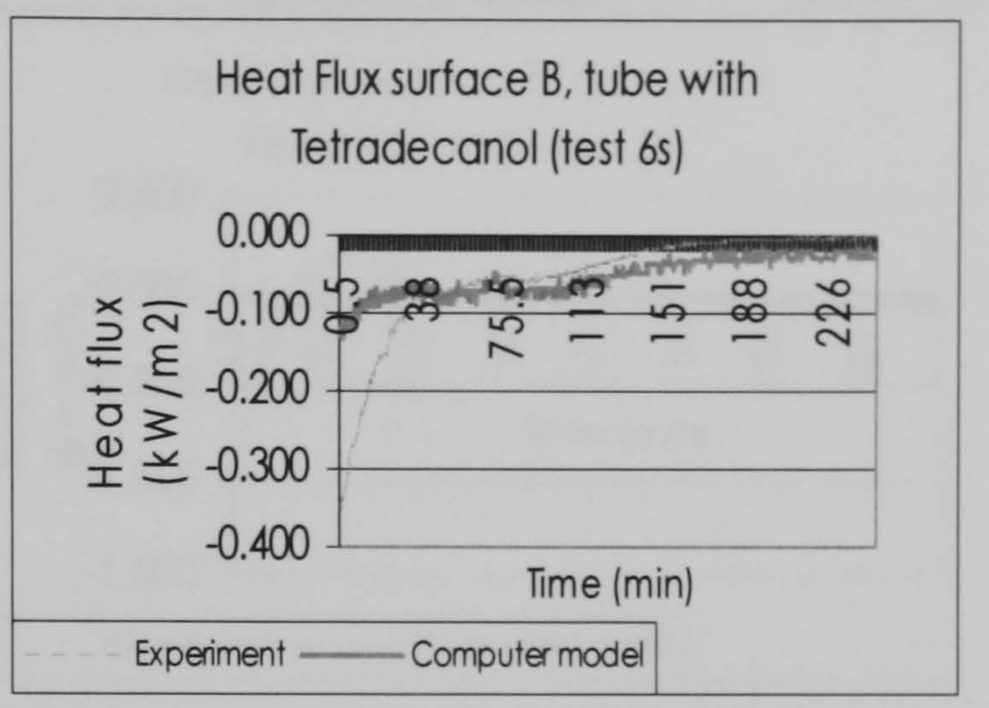

Figure 5.68: Comparison of Heat flux values obtained in the experiment 2, test 6s for a tube containing Tetradecanol, and the values obtained in the computer model for the same conditions in surfaces A and B.

		For a tube with Capric-Palmitic Acid					
Test	6s	Melting Temp	26	C	Initial PCM Temp	61.36	C
Mode	cooling	Enthalpy	153000	J/kg	Surface A intial T	57.3	C
Replica	3	Cp, liquid	2155	J/kgK	Test duration	14790	sec
PCM	Multiple (T,CP,H)	Cp, solid	1830	J/kgK	Irradiation	lamps off	W/m2
Temp sensor surf A	EB2	k, solid	0.17	W/mK	Tube depth	0.0127	m
Temp sensor surf B	EB5	k, liquid	0.45	W/mK	Barometric Pressure of day	1019	Pa
HF sensor surf A	HF5a	Ro, solid	886	kg/m3	Mass flow	5.265	g/s
HF sensor surf B	HF5b	Ro liq	910	kg/m3	Temp Air chamber (average)	25	C
					Temp Exterior air (average)	24.7	C

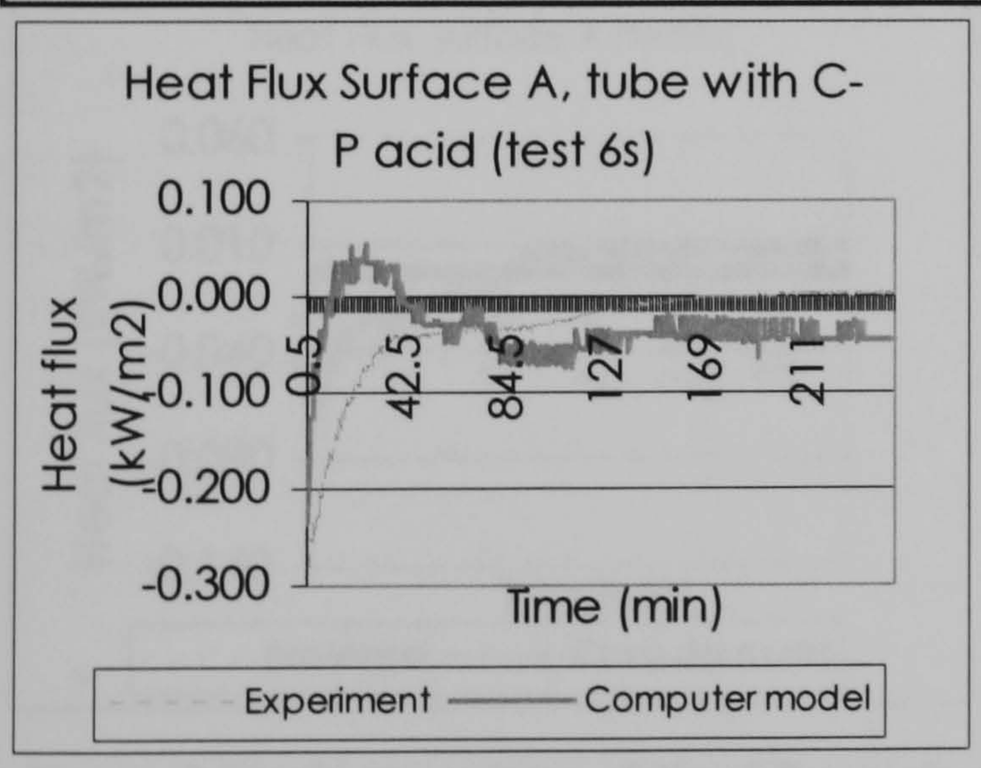

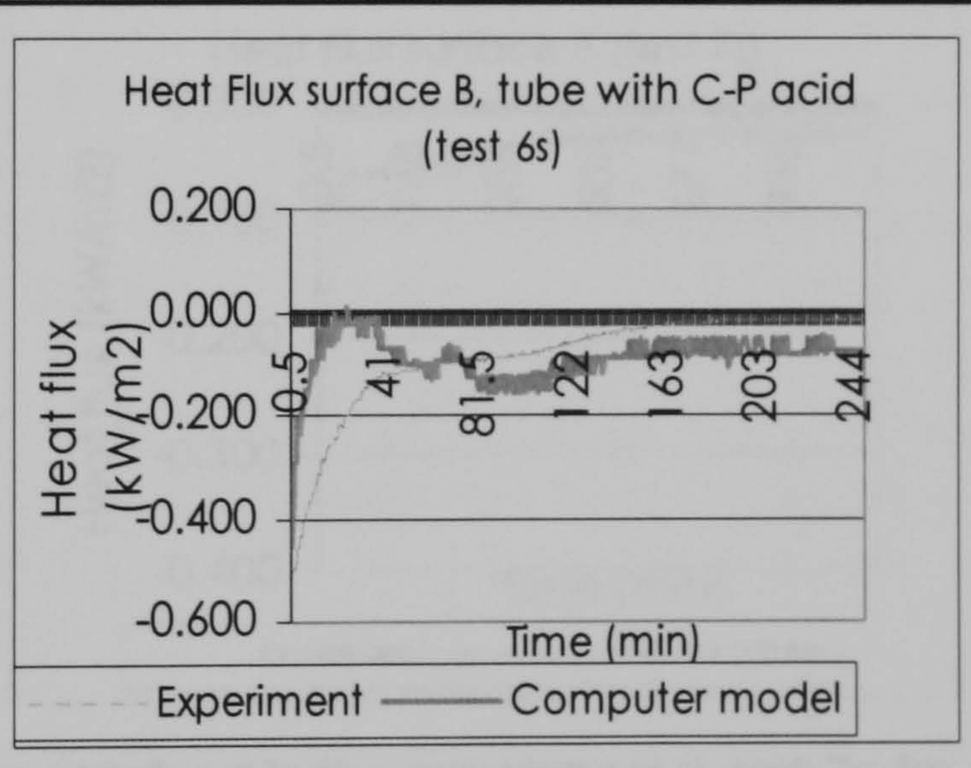

Figure 5.69: Comparison of Heat flux values obtained in the experiment 2, test 6s for a tube containing Capric-Palmitic acid, and the values obtained in the computer model for the same conditions in surfaces A and B.

		For a tube with Hexadecanol						
Test	6s	Melting Temp		25.5	C	Initial PCM Temp	59.4	C
Mode	cooling	Enthalpy		236000	J/kg	Surface A intial T	56.2	C
Replica	3	Cp, liquid		2220	J/kgK	Test duration	14790	sec
PCM	Multiple (T,CP,H)	Cp, solid		1750	J/kgK	Irradiation	lamps off	W/m2
Temp sensor surf A	EB3	k, solid		0.15	W/mK	Tube depth	0.0127	m
Temp sensor surf B	EB6	k, liquid	0,45		W/mK	Barometric Pressure of day	1019	Pa
HF sensor surf A	HF6a	Ro, solid		830	kg/m3	Mass flow	5.265	g/s
HF sensor surf B	HF6b	Ro liq		870	kg/m3	Temp Air chamber (average)	25	C
						Temp Exterior air (average)	24.7	C

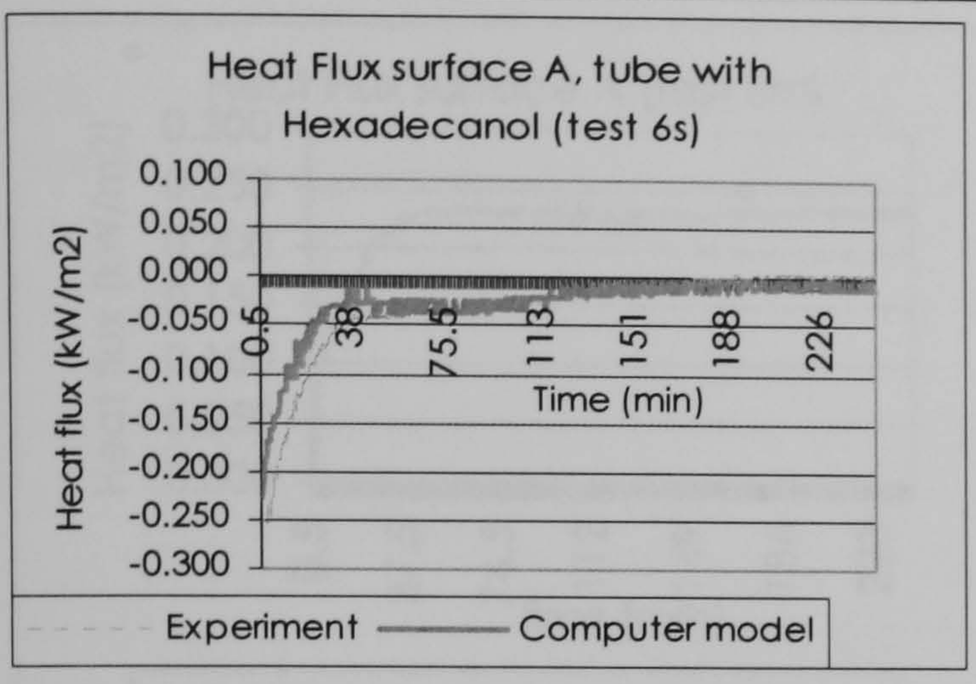

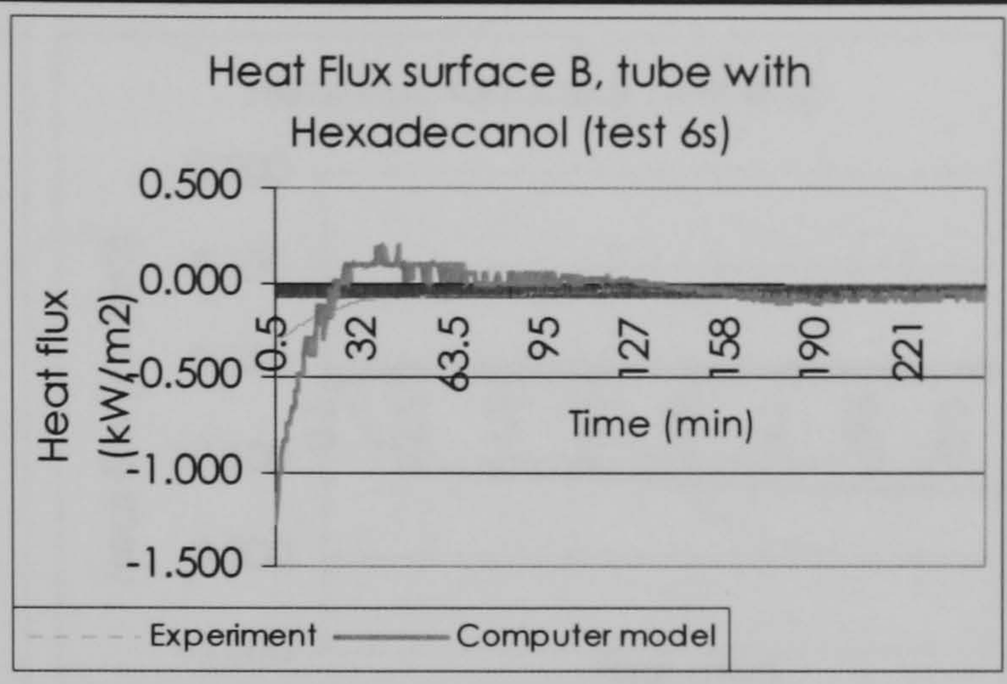

Figure 5.70: Comparison of Heat flux values obtained in the experiment 2, test 6s for a tube containing Hexadecanol, and the values obtained in the computer model for the same conditions in surfaces A and B.

Test	7s		Melting Temp	23.5	C	Initial PCM Temp	48.2	C
Mode	cooling		Enthalpy	153000	J/kg	Surface A intial T	44.9	C
Replica	3		Cp, liquid	2155	J/kgK	Test duration	60,180	sec
PCM	Single C-P		Cp, solid	1830	J/kgK	Irradiation	lamps off	W/m2
Temp sensor surf A	EB2		k, solid	0.17	W/mK	Tube depth	0.0381	m
Temp sensor surf B	EB5		k, liquid	0.45	W/mK	Barometric Pressure of day	1019	Pa
HF sensor surf A	5a		Ro, solid	886	kg/m3	Mass flow	7.509	g/s
HF sensor surf B	5b		Ro liq	910	kg/m3	Temp Air chamber (average)	11.1	C
Time interval	30	sec				Temp Exterior air (average)	28	C

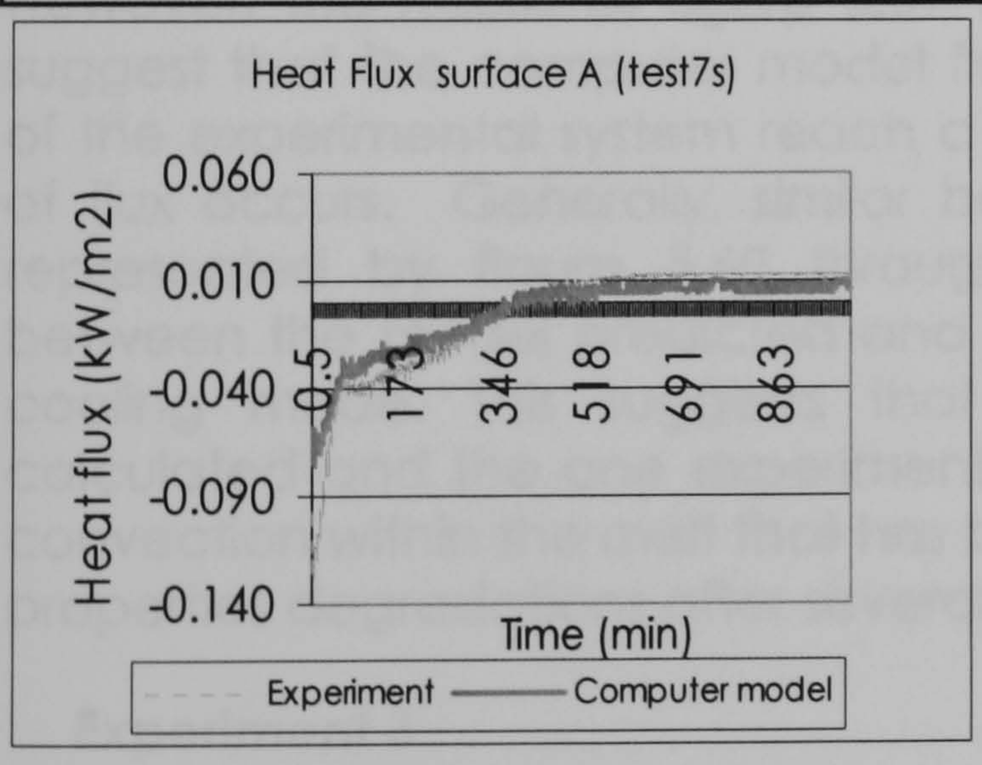

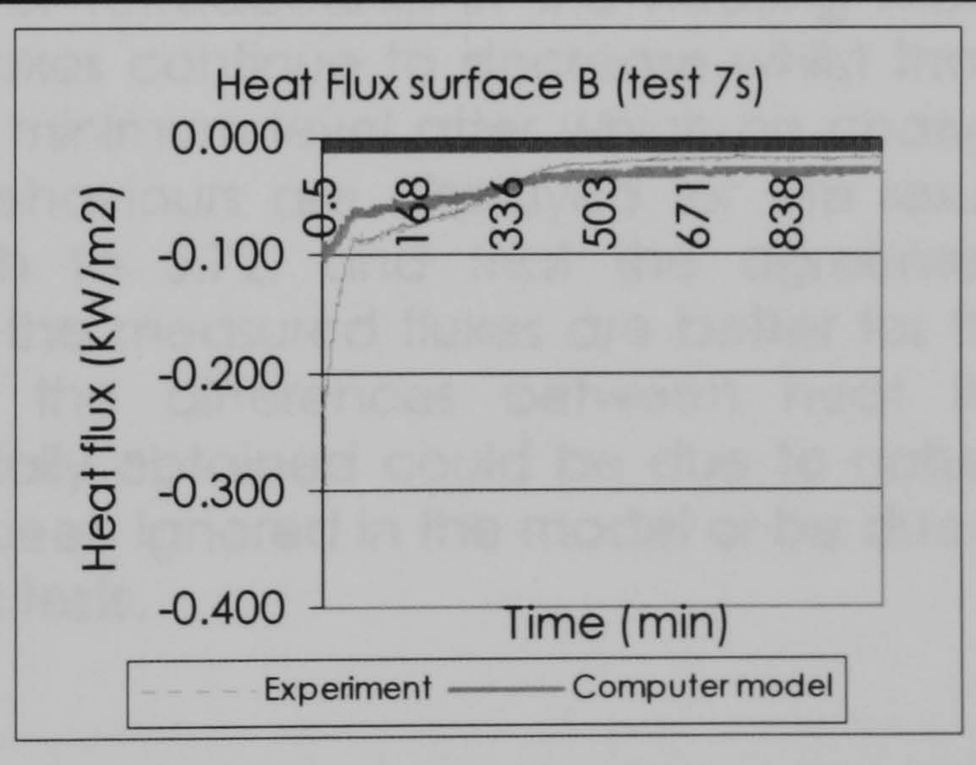

Figure 5.71: Comparison of Heat flux values obtained in the experiment 2, test 7s for a tube containing Capric-Palmitic acid, and the values obtained in the computer model for the same conditions in surfaces A and B.

Test	8m	Melting Temp	25	C	Initial PCM Temp	12.9	C
Mode	heating	Enthalpy	153000	J/kg	Surface A intial T	13.27	C
Replica	2	Cp, liquid	2155	J/kgK	Test duration	14280	sec
PCM	Single C-P	Cp, solid	1830	J/kgK	Irradiation	754	W/m2
Temp sensor surf A	EB2	k, solid	0.17	W/mK	Tube depth	0.0127	m
Temp sensor surf B	EB5	k, liquid	0.45	W/mK	Barometric Pressure of day	1014	Pa
HF sensor surf A	6a	Ro, solid	886	kg/m3	Mass flow	5.014	g/s
HF sensor surf B	5b	Ro liq	910	kg/m3	Temp Air chamber (average)	22.6	C
					Temp Exterior air (average)	25.1	C

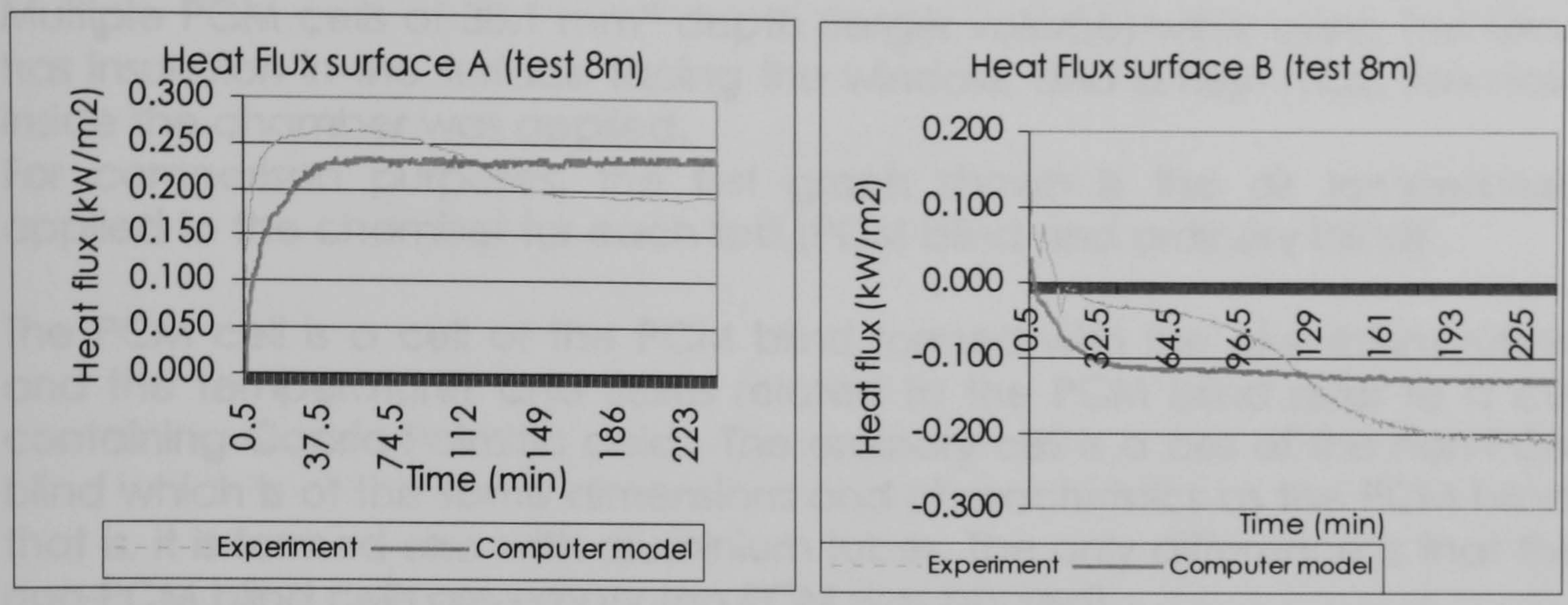

Figure 5.72: Comparison of Heat flux values obtained in the experiment 2, test 8m for a tube containing Capric-Palmitic acid, and the values obtained in the computer model for the same conditions in surfaces A and B.

From the previous graphs of Figure 5.57 to Figure 5.72 it can be concluded that good agreement exists between the computer model and experimental data. For the capric-palmitic acid results of fig's 5.57 and 5.58 very good agreement occurred between the modelled heat fluxes and those for the measured systems in both the heating and cooling modes. However, the results of figure 5.59 for tetradecanol in the heating mode suggest that the computer model fluxes continue to decrease whilst those of the experimental system reach a minimum level after which no change of flux occurs. Generally, similar behaviours are displayed for the results represented by figure 5.60 through to 5.72, and that the agreement between the model predicted and the measured fluxes are better for the cooling mode. This suggests that the differences between heat flux calculated and the one experimentally obtained could be due to natural convection within the melt that has been ignored in the model or be due to properties degradations after several tests.

Experiment 3

In order to evaluate the impact of the blind on interior air temperature control, an experiment comparing the results obtained in experiment 2 (using the blind) and an experiment run without the blind has been used for comparison purposes.

Experiment 2 test 5 for charging and test 7 for discharging were identified as the trials gathering the most favourable factor's values contributing to an optimised system. For this reason only the comparison between test 5 and 7

with and without blind is shown in this report. Never the less, the comparison values for the rest of the tests are also available.

Test 5

This test was set up with the Baja California (BC) summer weather conditions. Multiple PCM cells of 38.1 mm" depth (larger volume) were used. The blind has insulation in the surface facing the window, and a high mass flow rate inside the chamber was applied.
For comparison purposes, the first graph shown is the air temperature applied to the chamber for each test (PCM blind and ordinary blind).

The PCM cell is a cell of the PCM blind formed with the aluminium tubes, and the temperatures and fluxes related to the PCM blind refer to a cell containing Capric-Palmitic acid. The ordinary cell is a cell of the non-PCM blind which is of the same dimensions and characteristics as the PCM blind, that is, it is formed also with aluminium tubes. The only difference is that the non-PCM blind cells are empty (no PCM was poured).

The reason why the conditions inside the chamber with the PCM blind were compared to a non-PCM blind condition instead of no blind at all was to have present the effect of the opaque element. The aluminium tubes forming the blind have sensible heat that is an additional effect to the sensible and latent PCM heat storage. Besides, the blind element (with/without PCM) absorbs and reflects radiation.

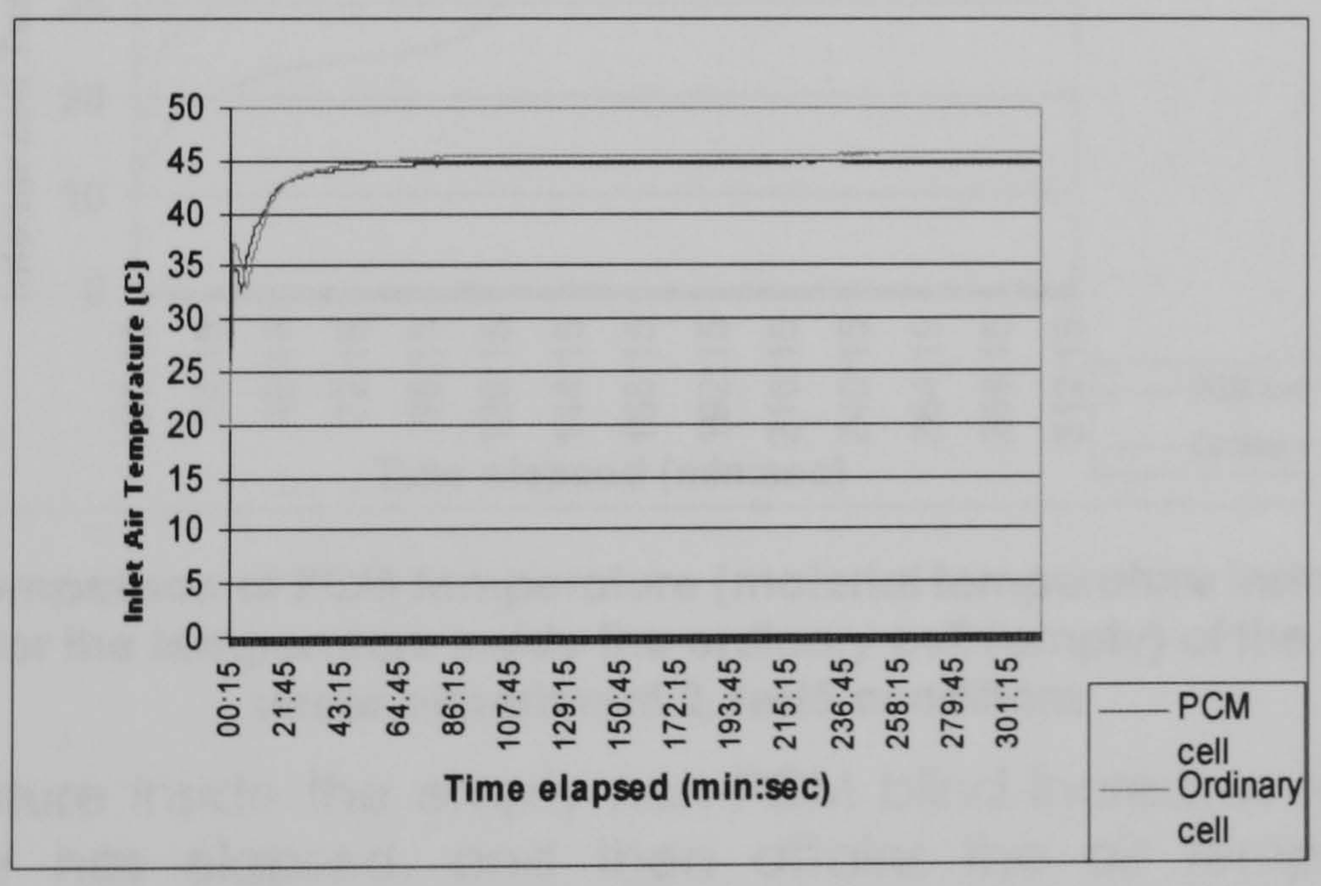

Figure 5.73: Comparison of the Inlet air temperature supplied for a PCM cell and ordinary cell test chamber under experiment 2, test 5 conditions

The external surface temperature is a result of the irradiated heat, the lower inlet air temperature supplied, and the heat absorbed during the change of phase:

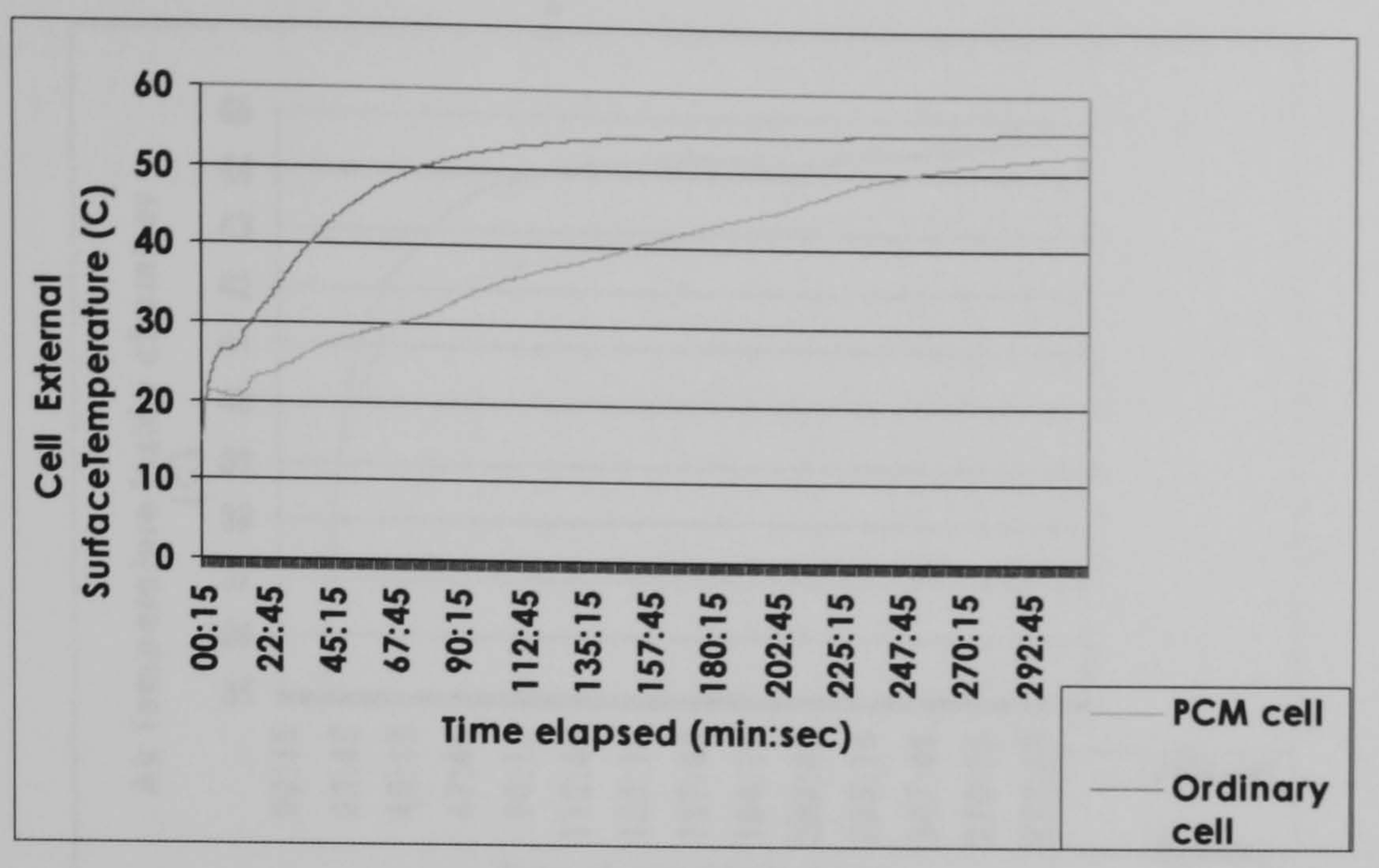

Figure 5.74: Comparison of the external surface temperature of the PCM blind cell and the non-PCM blind of the ordinary cell under experiment 2, test 5 conditions

The temperature of the PCM contained in the cell is an indication of the rate and amount of energy stored by the system under determined conditions:

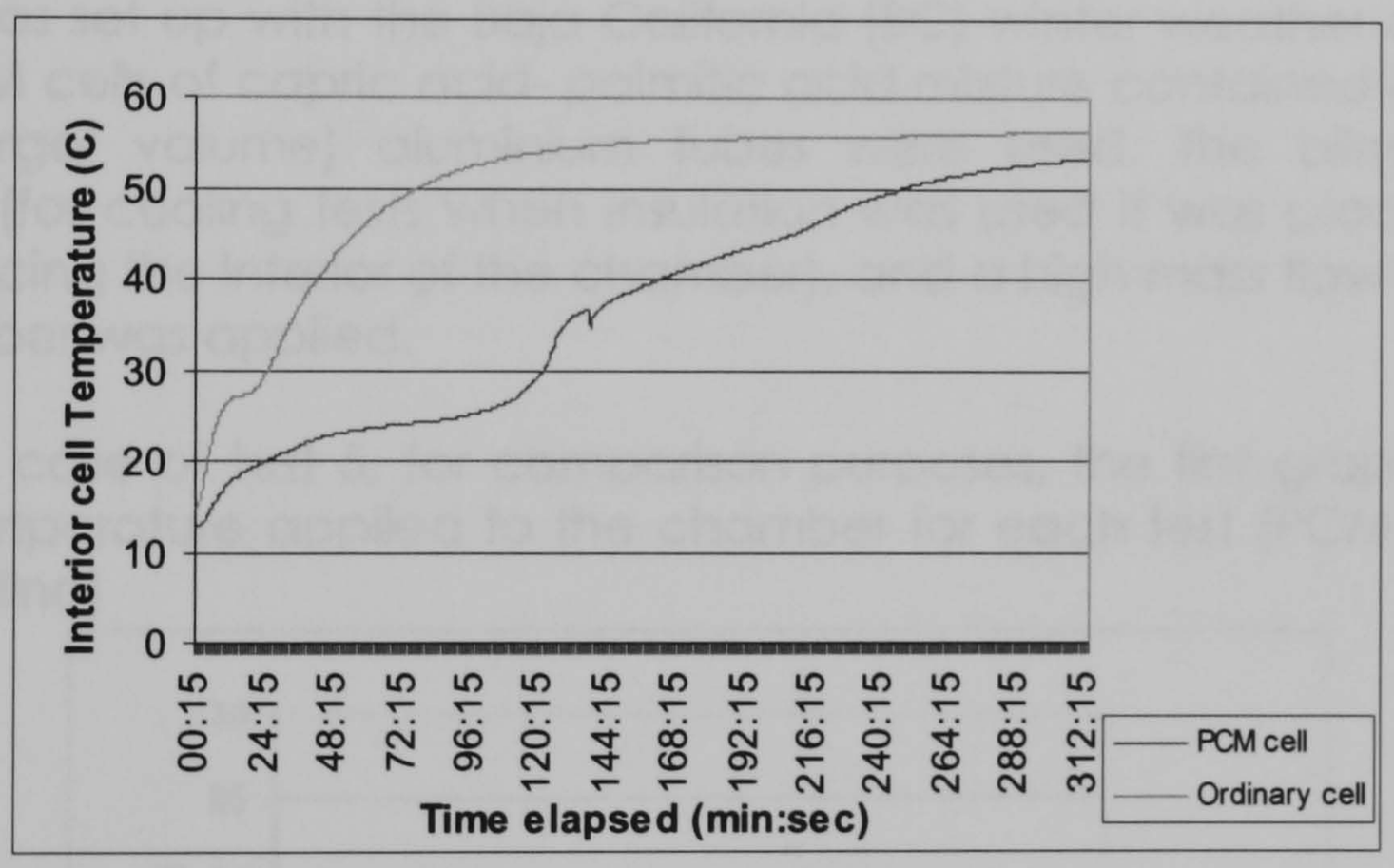

Figure 5.75: Comparison of PCM temperature (material temperature inside the cell)for a PCM cell and for the temperature inside the ordinary cell (empty) of the non-PCM blind under experiment 2, test5 conditions

The temperature inside the empty non-PCM blind increases rapidly before half an hour has elapsed, and then attains the air temperature after approximately one hour has elapsed. However the PCM temperature remains at a nearly constant level for nearly 2 hours while it changes phase (absorbing heat).

The comparison between the air temperature inside the chamber with the PCM cell and with the ordinary cell, provide information on the temperature modulation achieved by using the LHSS:

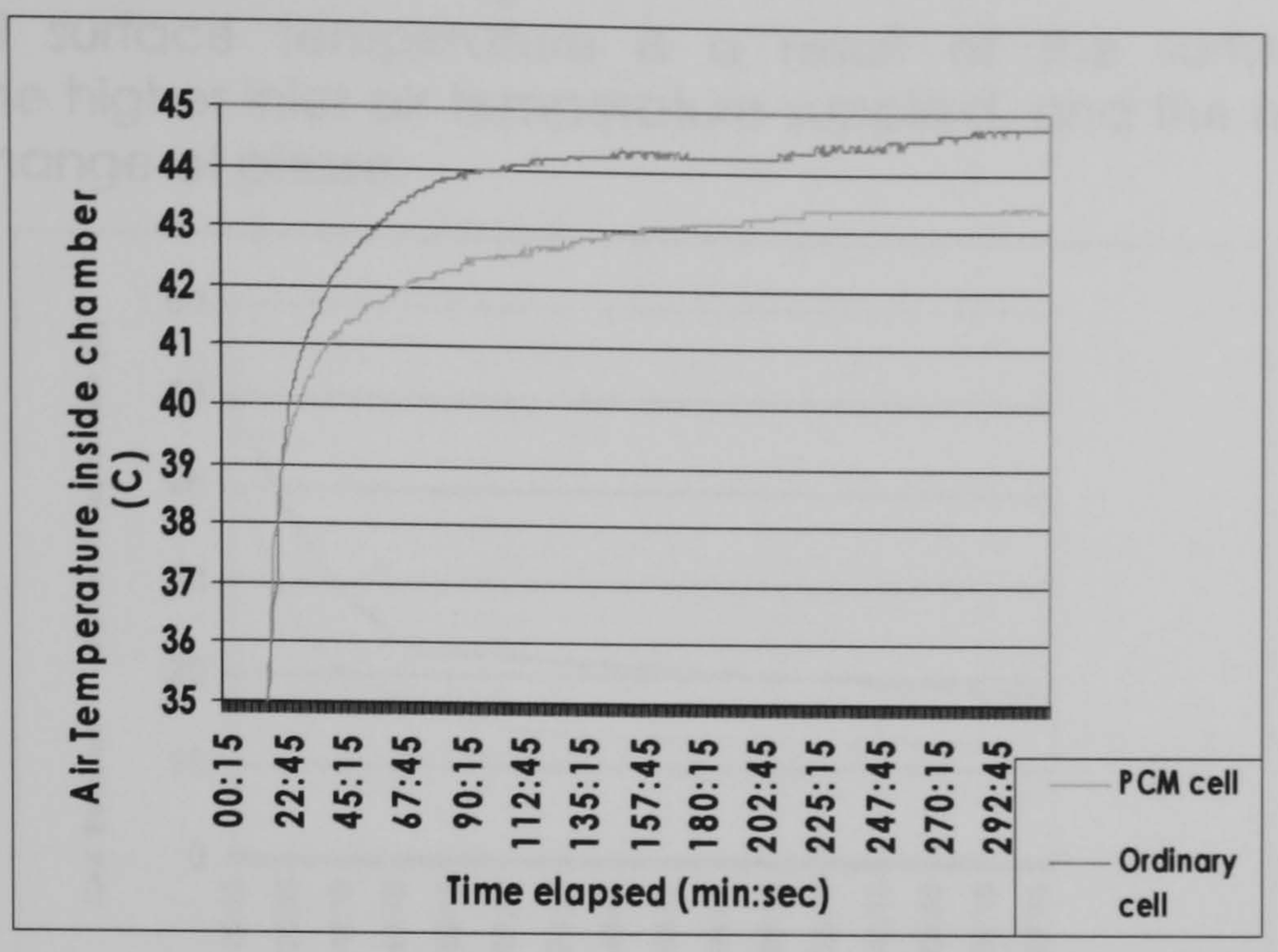

Figure 5.76: Comparison between the air temperature inside the chamber for the PCM cell and the ordinary cell under experiment 2 test 5 conditions

Test 7

This test was set up with the Baja California (BC) winter weather conditions. Single PCM cells of capric acid- palmitic acid mixture contained in 38.1 mm depth (larger volume) aluminium tubes were used. The blind had no insulation (for cooling tests when insulation was used it was placed on the surface facing the interior of the chamber), and a high mass flow rate inside the chamber was applied.

As for the case of test 5, for comparison purposes, the first graph shown is the air temperature applied to the chamber for each test (PCM blind and ordinary blind)

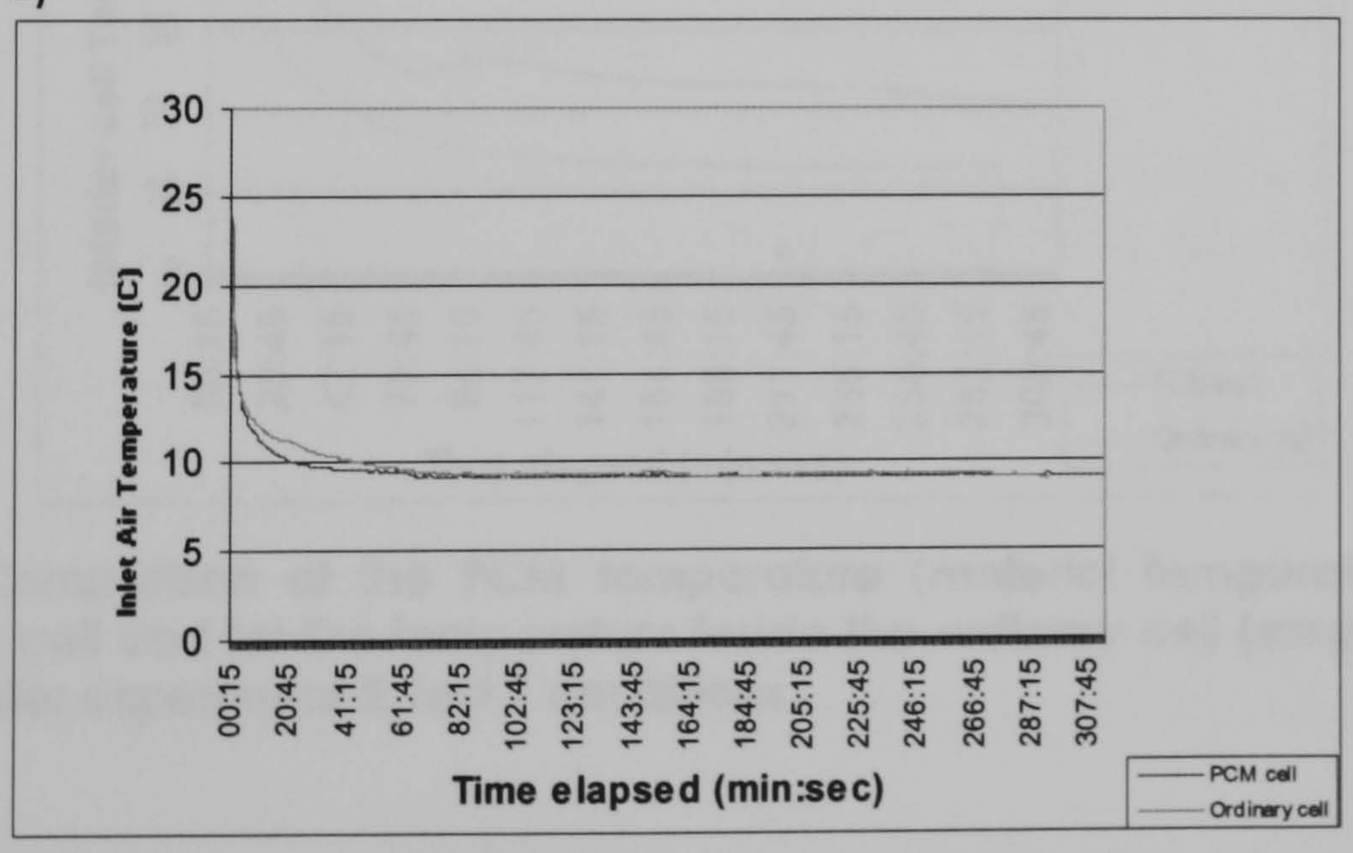

Figure 5.77: Comparison of the Inlet air temperature supplied for a PCM cell and ordinary cell test chamber under experiment 2, test 7 conditions

The external surface temperature is a result of the surface radiative properties, the higher inlet air temperature supplied, and the heat released during the change of phase:

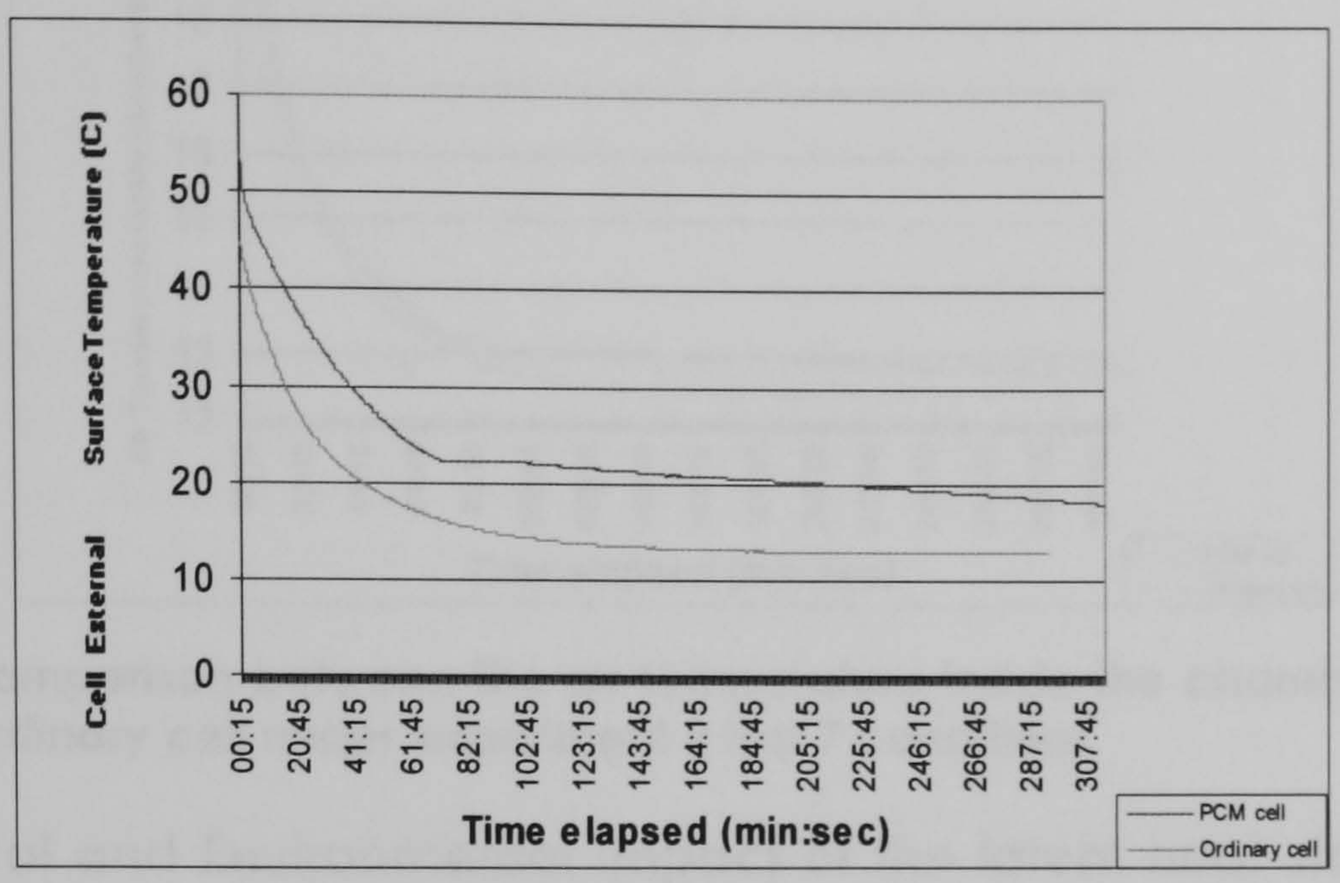

Figure 5.78: Comparison of the external surface temperature of the PCM blind cell and the ordinary cell, in the non-PCM blind under experiment 2, test 7 conditions

The temperature of the PCM contained in the cell is an indication of the rate and amount of energy released by the system under determined conditions:

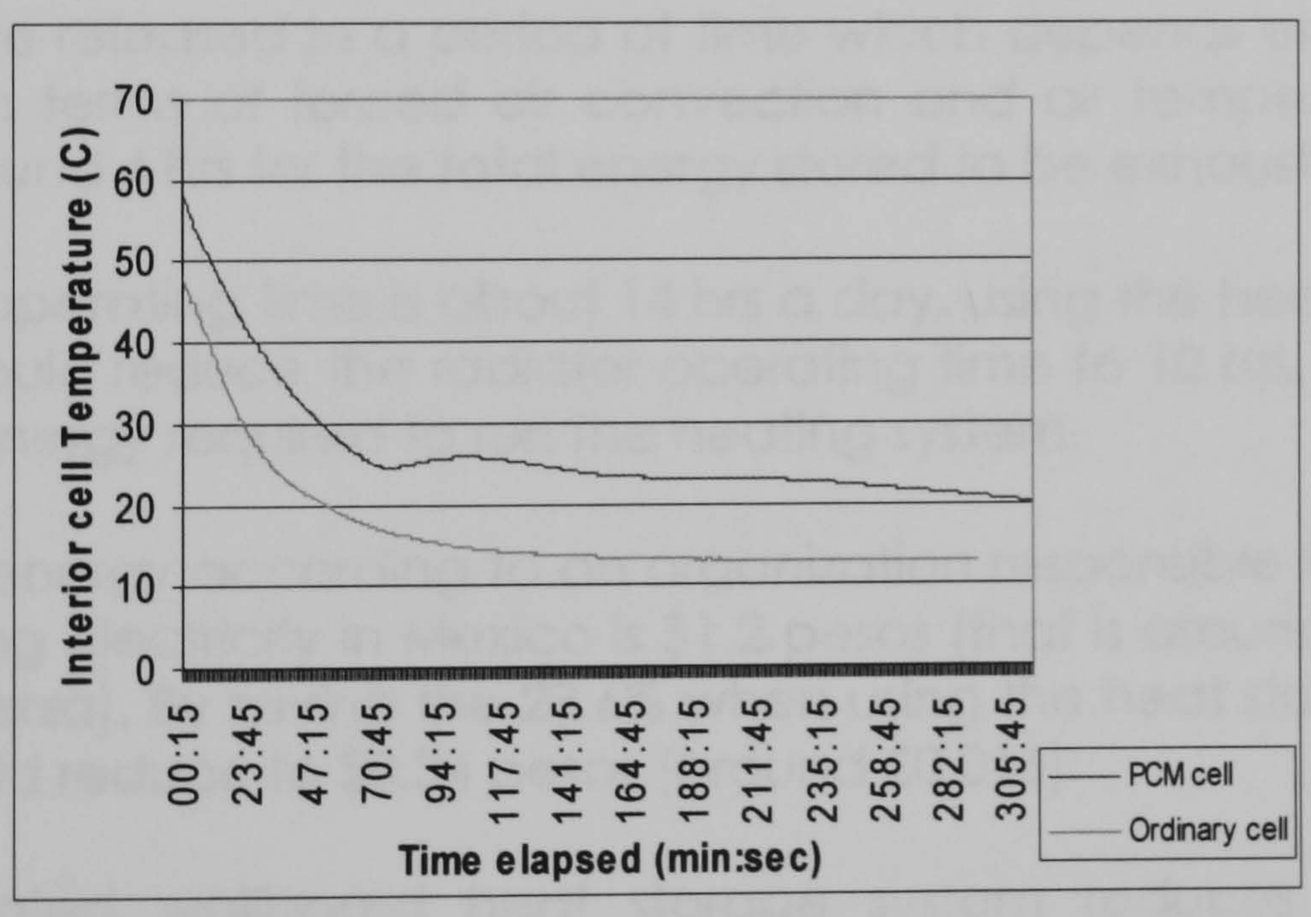

Figure 5.79: Comparison of the PCM temperature (material temperature inside the cell)for a PCM cell and for the temperature inside the ordinary cell (empty) of the non-PCM blind under experiment 2, test 7 conditions

The comparison between the air temperature inside the chamber with the PCM cell and with the ordinary cell, provide information on the temperature modulation achieved by using the LHSS:

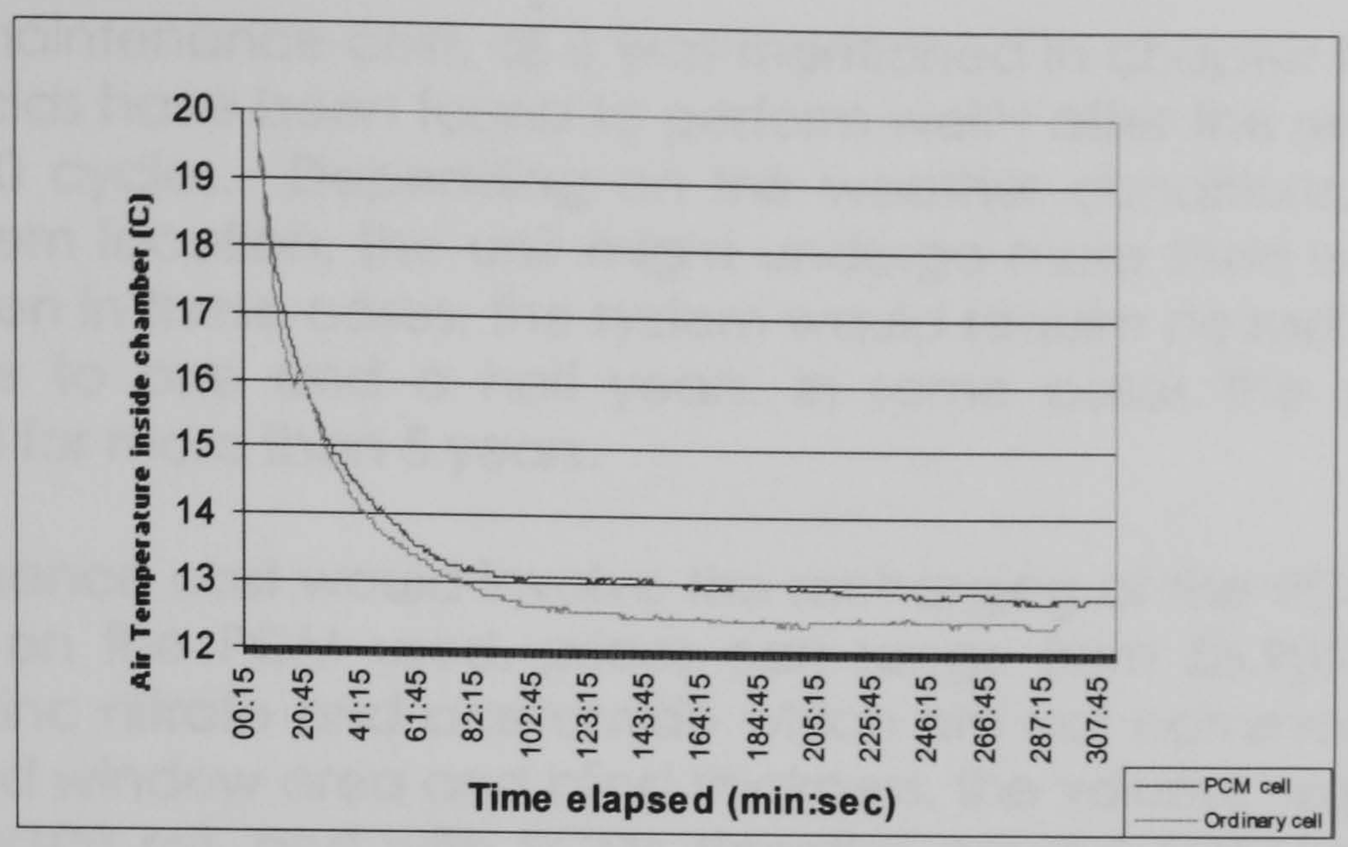

Figure 5.80: Comparison between the air temperature inside the chamber for the PCM cell and the ordinary cell under experiment 2 test 7 conditions

Economical and Environmental Impact of the latent heat storage system proposed

As explained in chapter four regarding the system's real contribution to thermal loads, a fully charged real size blind unit stores around 3200 kJ, being able to release nearly 400 W. That is more than 1/3 of the load of an operating radiator sized for a room (1kW)[11].

The 400 W are released in a period of time which depends on the external conditions (in terms of forced air convection and air temperature), but it can take around 4 hrs for the total energy stored to be exhausted[12].

If a radiator operating time is about 14 hrs a day, using the heat storage unit proposed would reduce the radiator operating time to 10 hrs. That is, 28.6% of the total energy required to run the heating system.

The price of energy according to an organization responsible for distributing and marketing electricity in Mexico is $1.2 pesos (that is around £0.0568) per kWh(Luz y fuerza). By saving the 28.6% when using the heat storage unit, this amount would reduce to $0.34 pesos (around £0.016)

An impregnated wallboard heat storage system reduces the auxiliary heating energy by 15% in temperate weather conditions (Kelly 1999). The storage system proposed here is therefore more effective reducing the heating system total load by almost the two times that of a wallboard.

---

[11] Other heating systems consume around the same amount of energy, i.e. air heaters consume around 1.3 kW

[12] Recall that however, according to the prevailing conditions inside the room, the unit might not be fully charged or fully discharged; nevertheless the system seems attractive from the point of view of energy and economy savings.

About the maintenance cost, as it was mentioned in chapter four, paraffins and fatty acids have been found to perform well[13] after the recommended 1000 to 2000 cycles. Depending on the weather conditions, and on the storage system location, the unit might undergo more than one cycle per day. But even in these cases, the system would require no maintenance for at least one to one and a half years. In some cases the system might perform well for more than 5 years.

The maintenance cost would involve the recharging of the PCM in the unit. Depending on the PCM used, prices can range from £8.90/kg to £58/kg (excluding zinc nitrate and acetamide which are not commonly used). For the proposed window area and blind thickness, the volume required for one blind is $6.35x10^{-3}$ m^3, and with PCMs densities around 1500 kg/m^3 the refill cost ranges from £80 to nearly £500.

If in one month approximately 300 kWh are consumed (average dwelling heating load during winter in BC), that is $420 pesos paid per month (around £20), the PCM refilling cost payback period can range from 4 months to 2 years. If the refilling is required in between 1 to 5 years, the investment is cost-effective.

Regarding thermal comfort, according to the experimental work carried out, the maximum air temperature can be reduced by up to 6°C due to the absorption of the heat gains by the storage unit. This provides a significant enhancement in thermal comfort. One person can feel cold/hot even within 2°C difference.

CO_2 emissions: It is essential to save energy and reduce or restrain the CO_2 production, firstly in order to assure the provision of fuel for further generations, next for the ecological impact of the CO_2 on the climate change (global warming). The idea is to keep the concentration below 550 ppm[14]. Nevertheless, the CO2 concentration on the atmosphere is going to increase the next two centuries, even restricting the CO_2 emissions.

Mexico contributes to around 2% of the world's Green House Gases emissions (GHG)[15]. It is ranked within the first 15 countries with the highest GHG emissions in the world. If Mexico keeps this trend by 210 will be emitting twice as much as it is emitting now. (Pardo 2000)

---

[13] That is, to have small variations of melting point and enthalpy values.
[14] Parts per million
[15] The GHG are: CO2, CH4, NOx,CO, volatile organic compounds, SO2

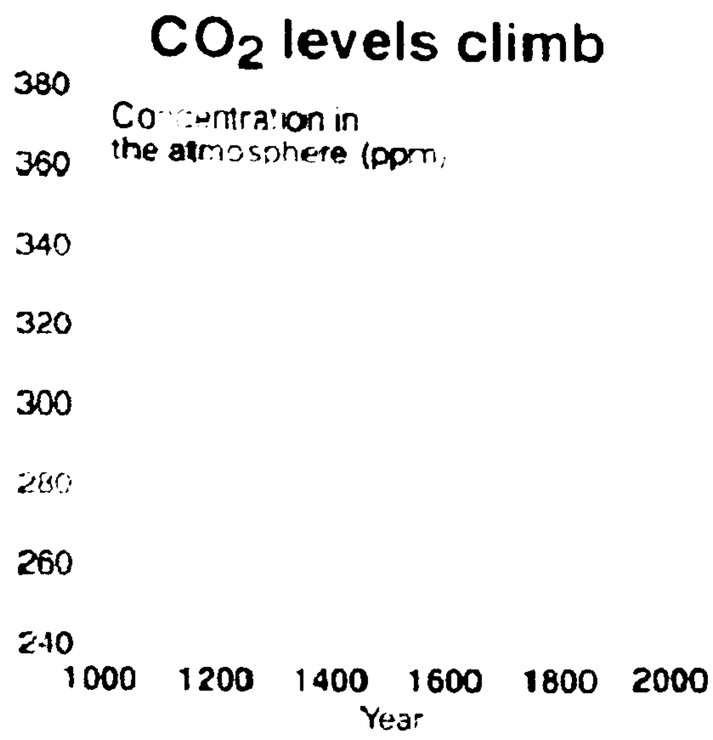

Figure 5.81:CO_2 levels climb (Barker 2004)

Buildings are high consumers of energy from their construction, their operation and their destruction, and therefore have a considerable impact on our environment. The use of solar energy in dwellings has great potential for reducing energy consumption and CO_2 emissions.
Indirect emissions associated with the utilization of electricity have an important part in this sector[16]. Private and public services, including domestic sectors accounted for nearly 40% of the total CO_2 emissions in 1990 in USA.(Joosen and Blok 2001)

By using passive means to heat and cool buildings for thermal comfort the CO_2 emissions can definitively be decreased.

---

[16] CO2 is a gas that is produced by the combustion of fuels containing carbon. The emissions vary according to the amount of carbon in the fuel. CO2 emissions depend on the fuel and not on the combustion technology. (Pardo 2000)

Appendix 5.A: Temperature-enthalpy correlations obtained by DSC testing

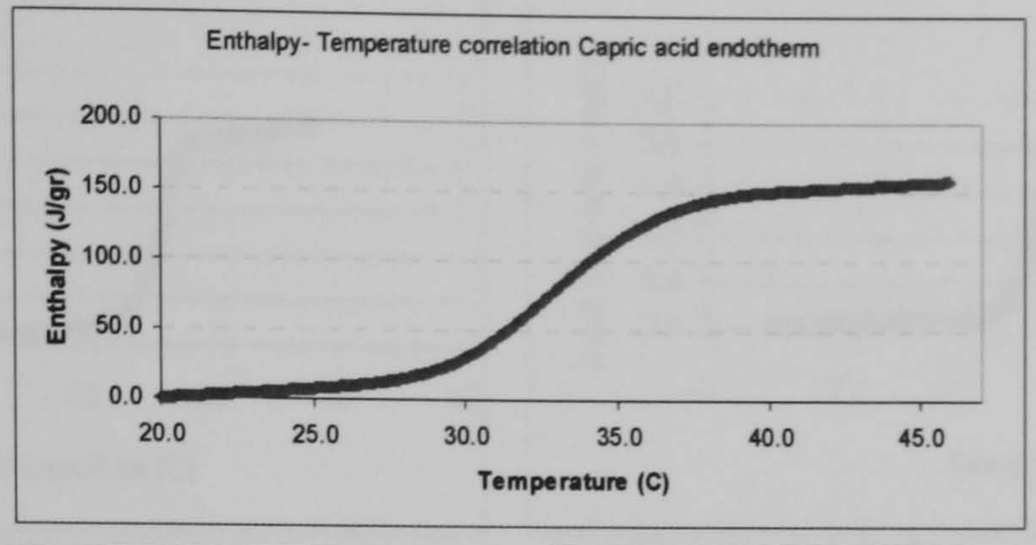

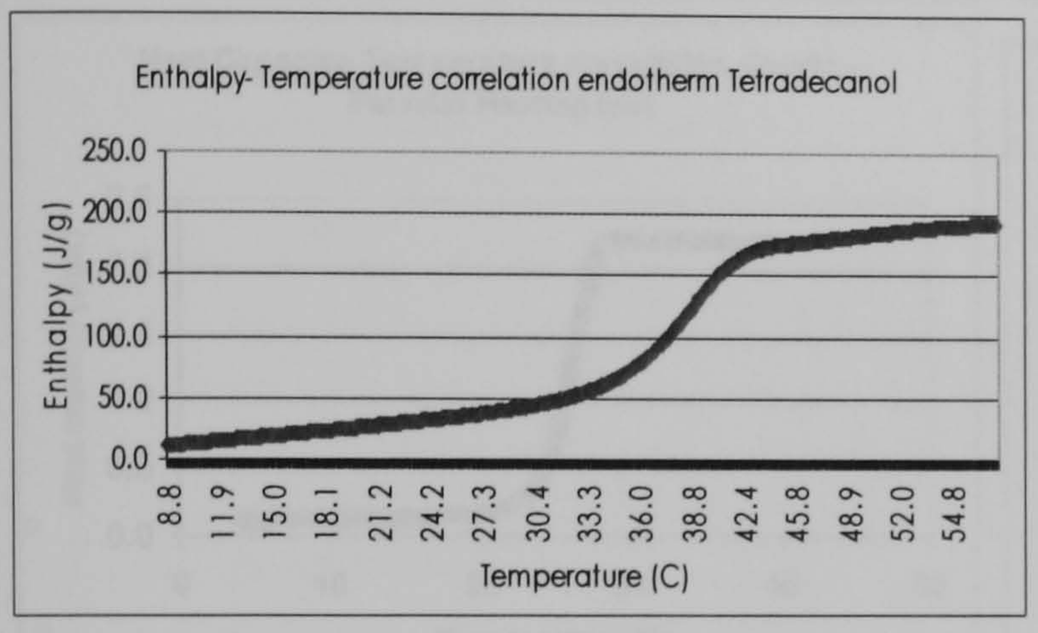

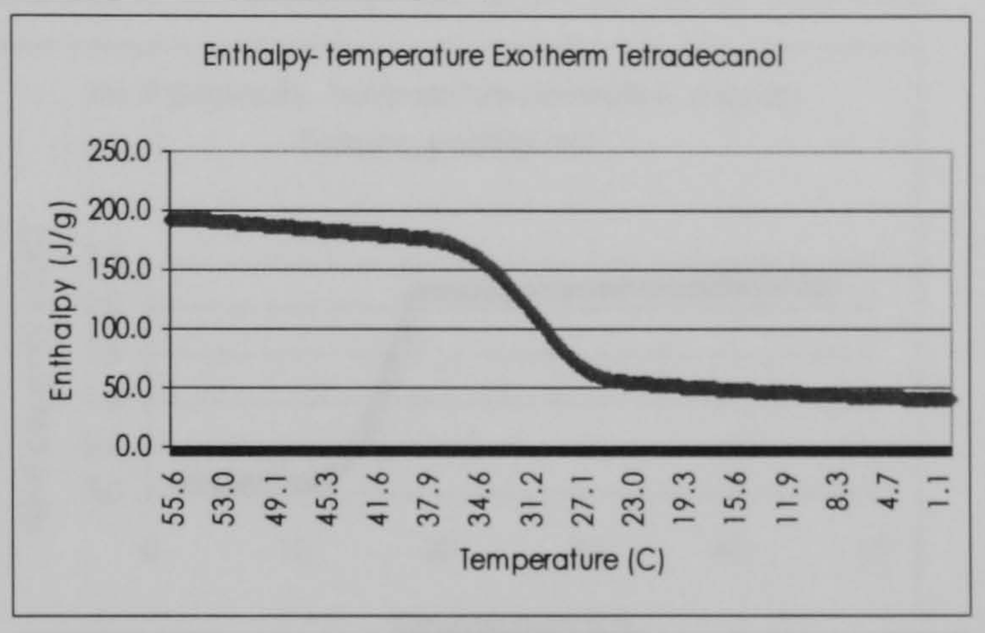

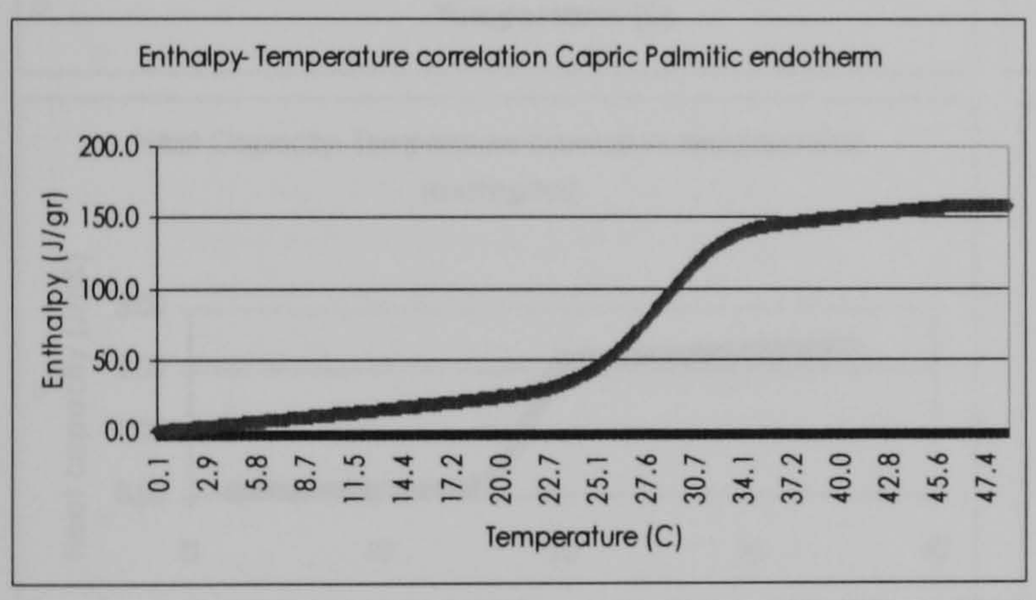

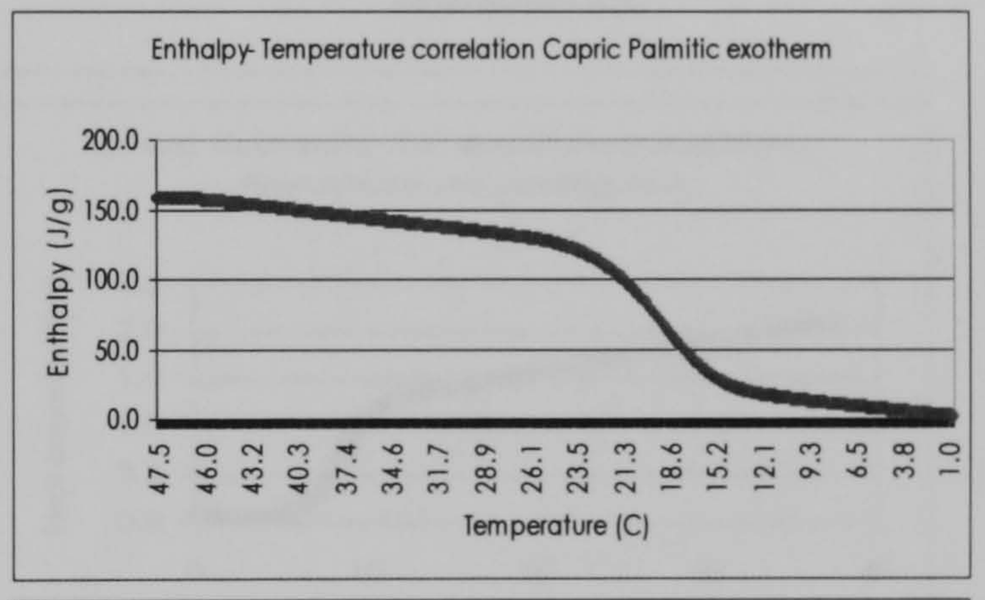

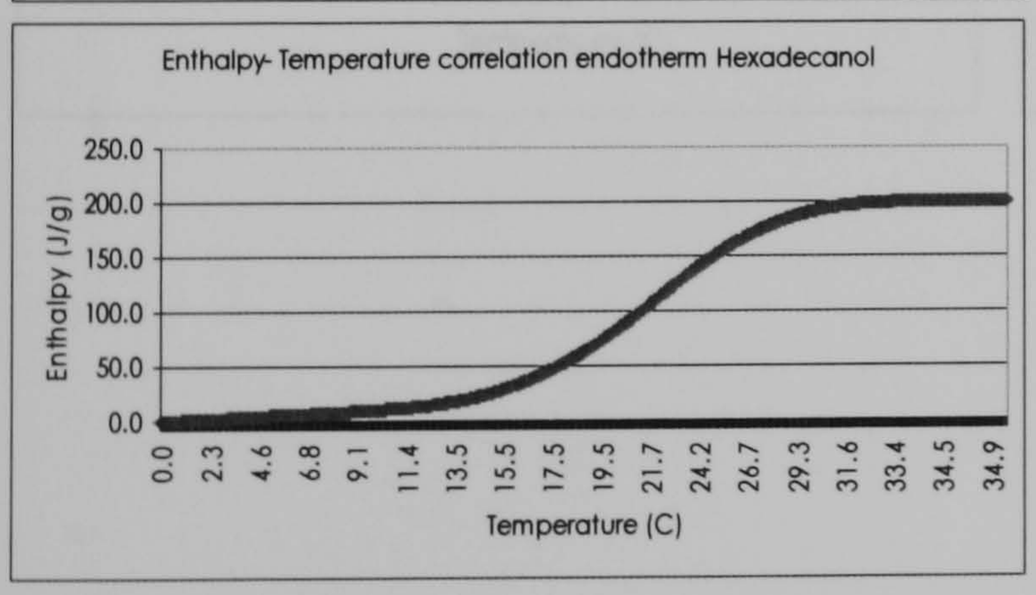

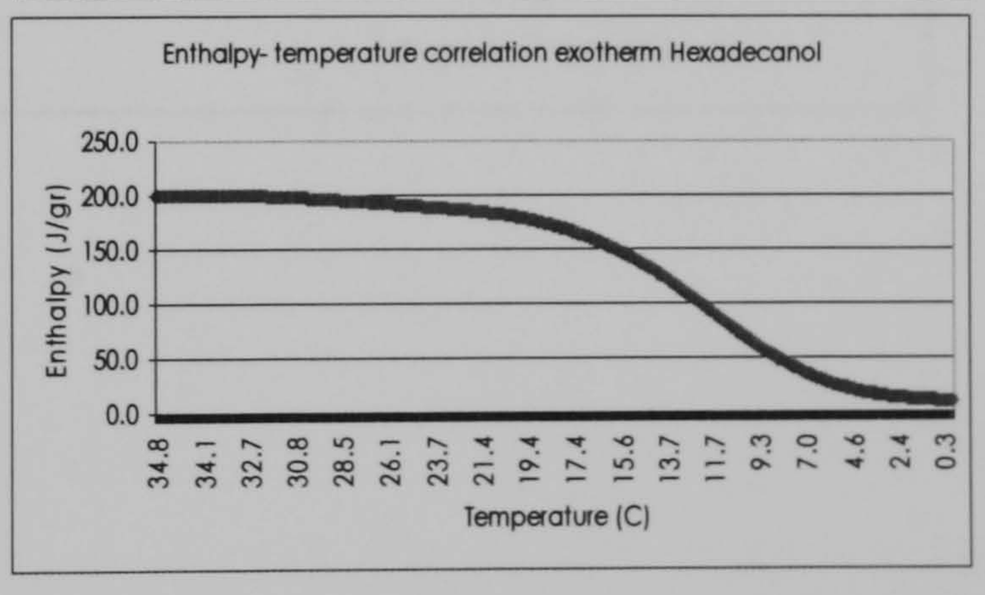

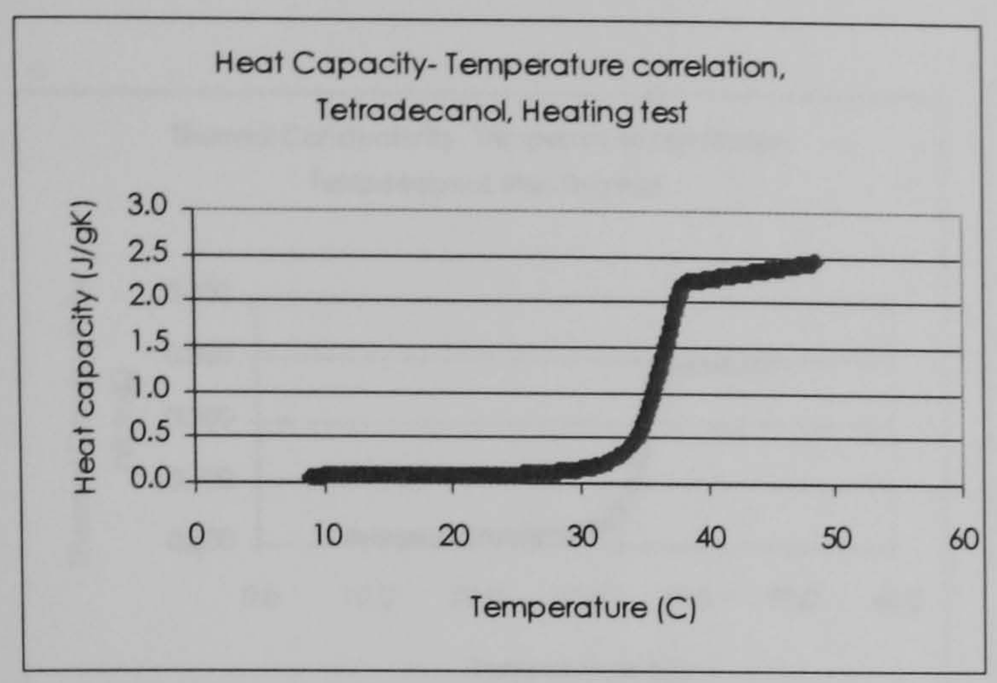
Heat Capacity- Temperature correlation,
Tetradecanol, Heating test
Heat capacity (J/gK)
3.0
2.5
2.0
1.5
1.0
0.5
0.0
0
10
20
30
40
50
60
Temperature (C)

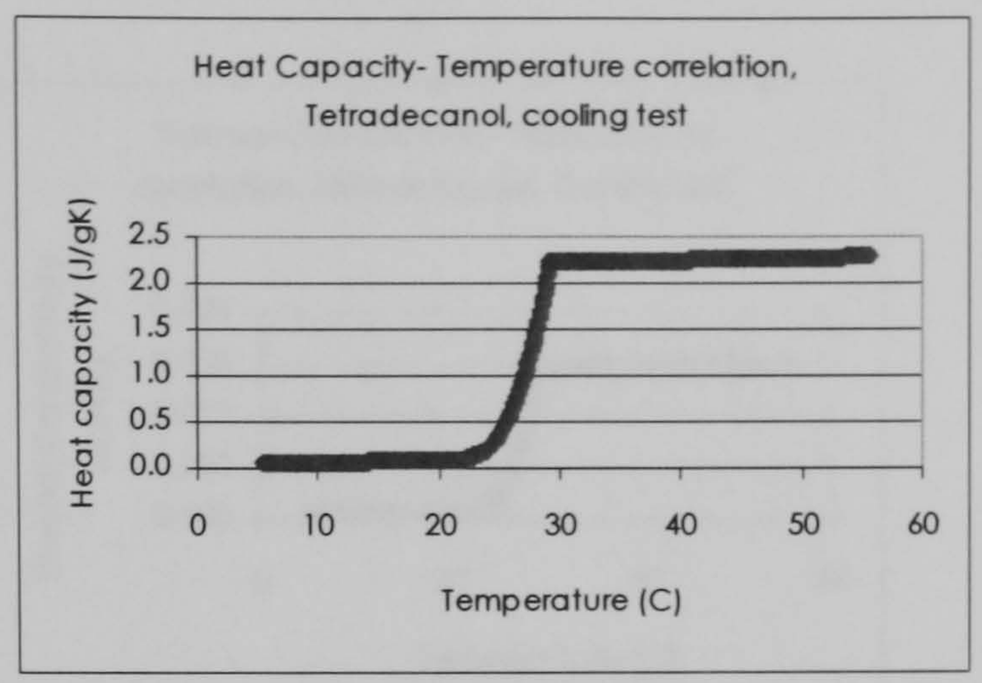
Heat Capacity- Temperature correlation,
Tetradecanol, cooling test
Heat capacity (J/gK)
2.5
2.0
1.5
1.0
0.5
0.0
0
10
20
30
40
50
60
Temperature (C)

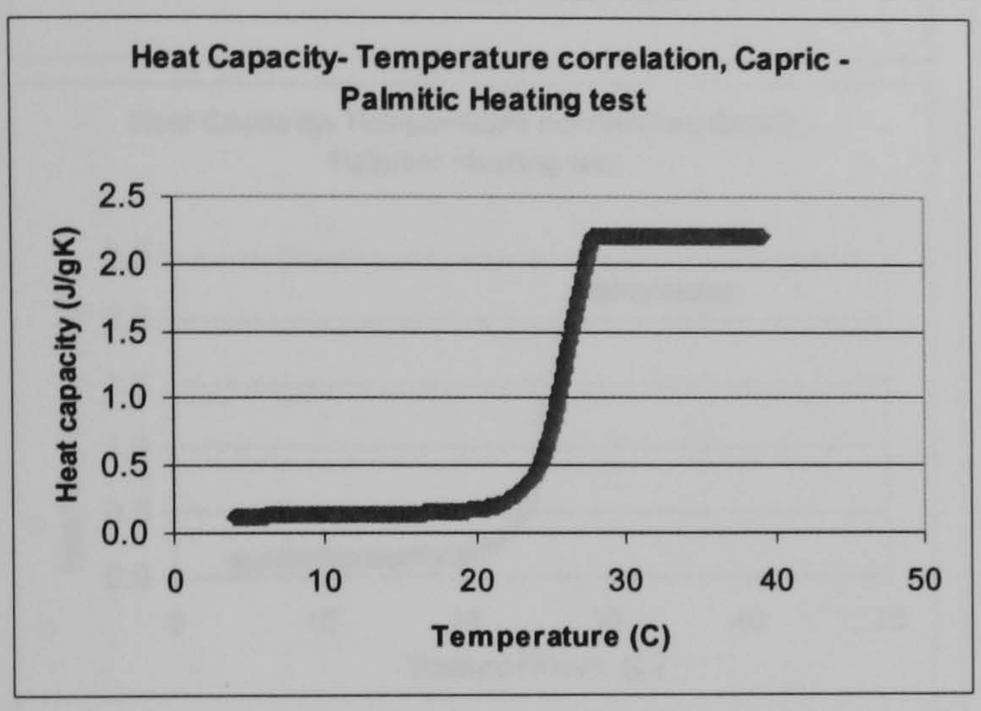
Heat Capacity- Temperature correlation, Capric -
Palmitic Heating test
Heat capacity (J/gK)
2.5
2.0
1.5
1.0
0.5
0.0
0
10
20
30
40
50
Temperature (C)

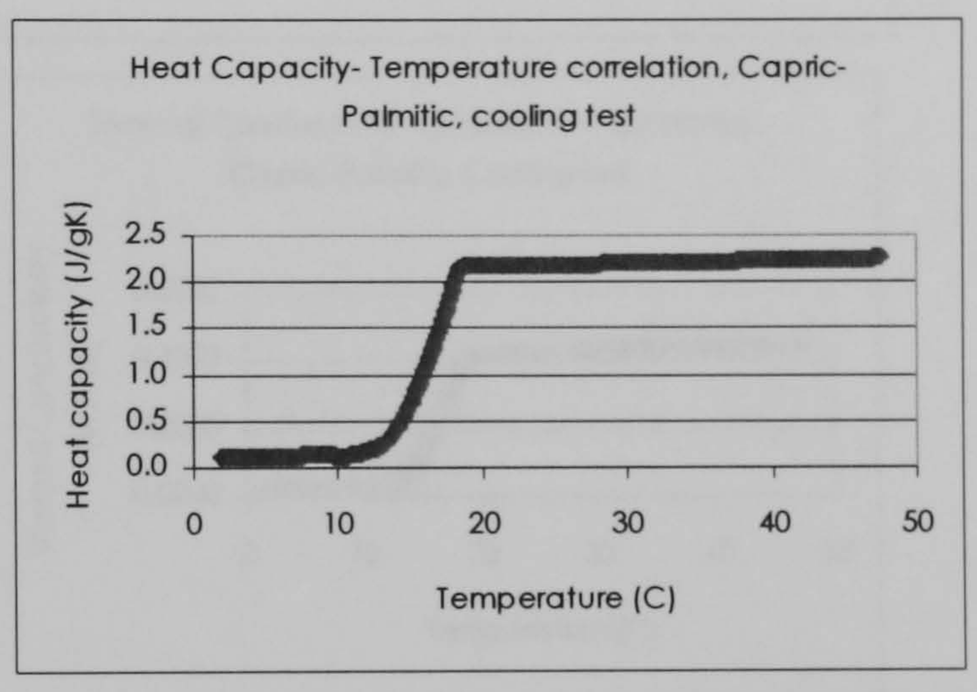
Heat Capacity- Temperature correlation, Capric-
Palmitic, cooling test
Heat capacity (J/gK)
2.5
2.0
1.5
1.0
0.5
0.0
0
10
20
30
40
50
Temperature (C)

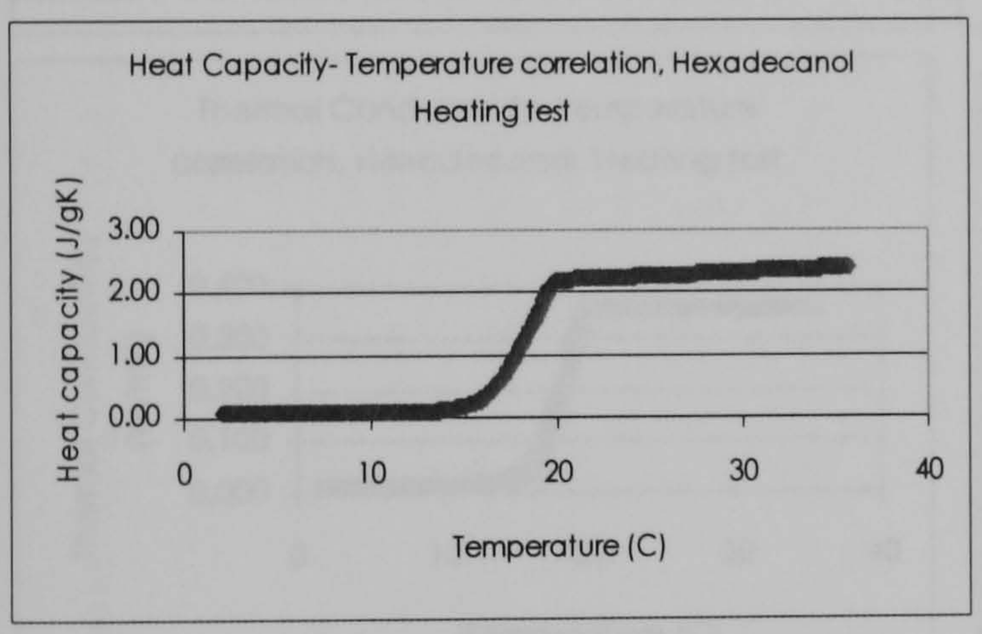
Heat Capacity- Temperature correlation, Hexadecanol
Heating test
Heat capacity (J/gK)
3.00
2.00
1.00
0.00
0
10
20
30
40
Temperature (C)

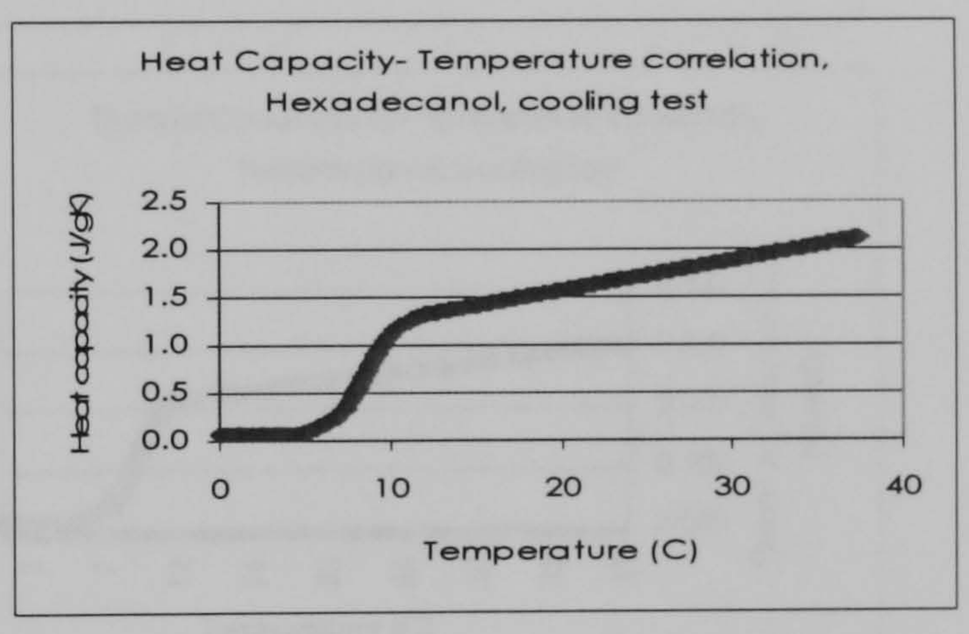
Heat Capacity- Temperature correlation,
Hexadecanol, cooling test
Heat capacity (J/gK)
2.5
2.0
1.5
1.0
0.5
0.0
0
10
20
30
40
Temperature (C)

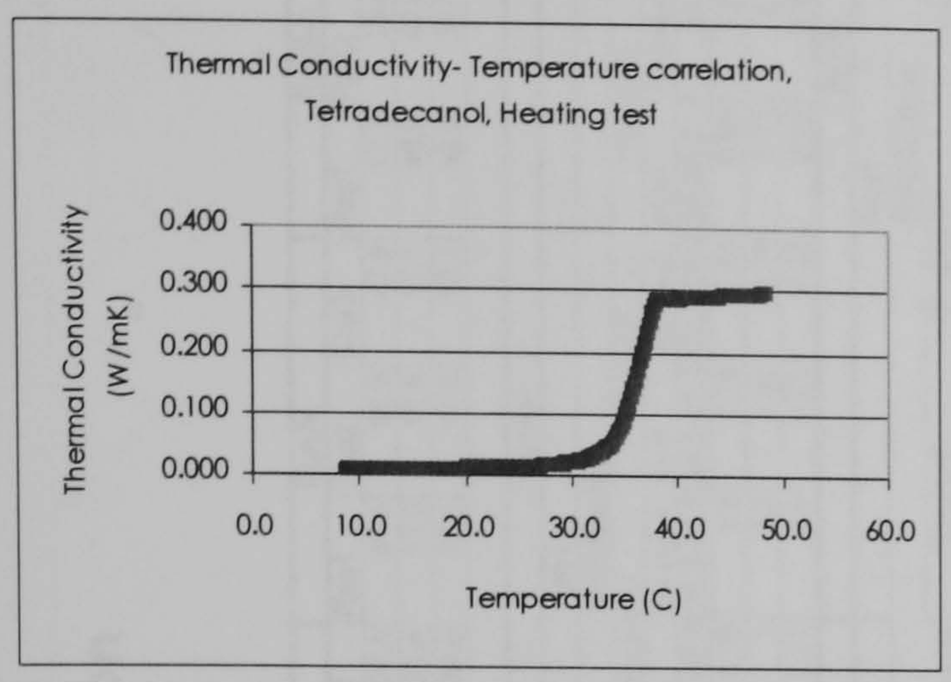
Thermal Conductivity- Temperature correlation, Tetradecanol, Heating test
Thermal Conductivity (W/mK)
0.400
0.300
0.200
0.100
0.000
0.0
10.0
20.0
30.0
40.0
50.0
60.0
Temperature (C)

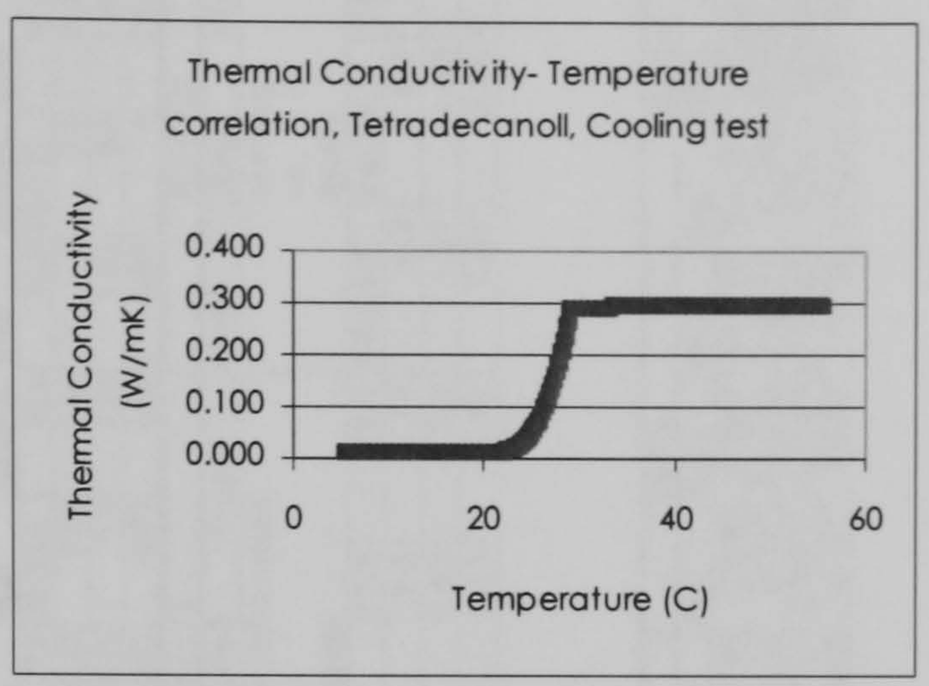
Thermal Conductivity- Temperature correlation, Tetradecanoll, Cooling test
Thermal Conductivity (W/mK)
0.400
0.300
0.200
0.100
0.000
0
20
40
60
Temperature (C)

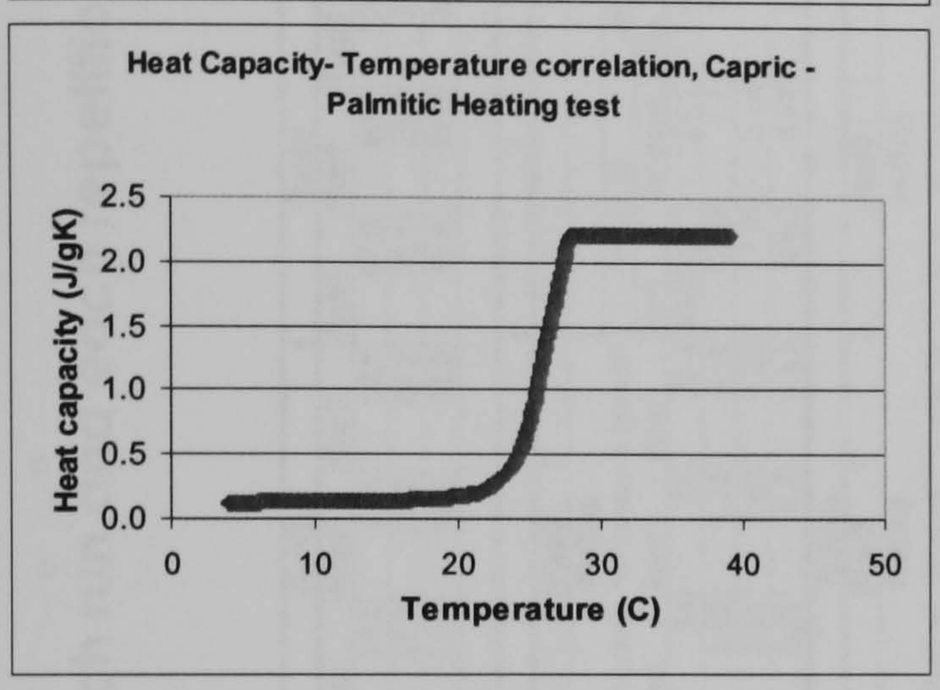
Heat Capacity- Temperature correlation, Capric - Palmitic Heating test
Heat capacity (J/gK)
2.5
2.0
1.5
1.0
0.5
0.0
0
10
20
30
40
50
Temperature (C)

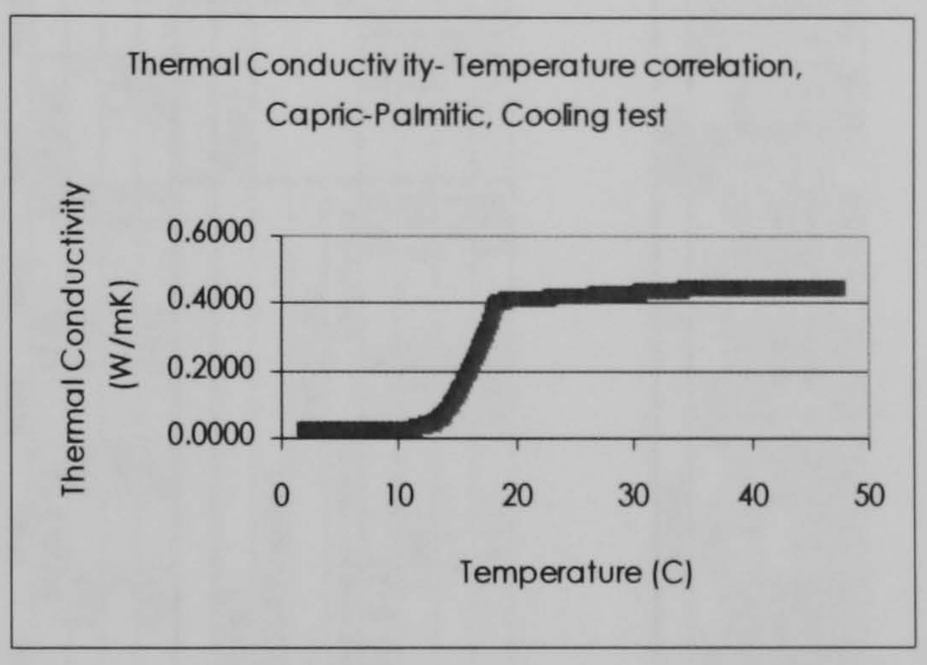
Thermal Conductivity- Temperature correlation, Capric-Palmitic, Cooling test
Thermal Conductivity (W/mK)
0.6000
0.4000
0.2000
0.0000
0
10
20
30
40
50
Temperature (C)

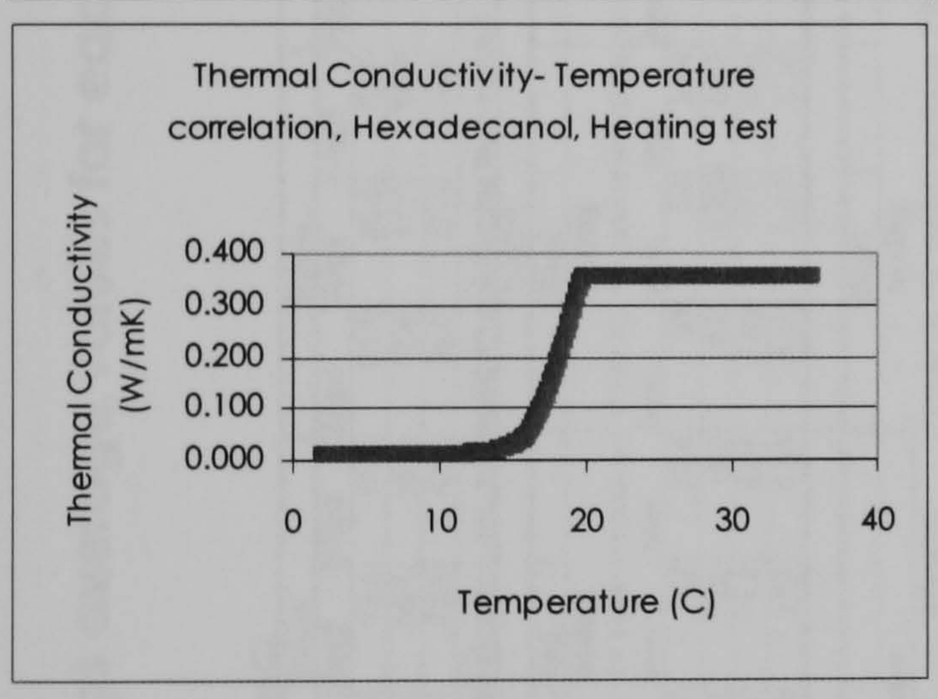
Thermal Conductivity- Temperature correlation, Hexadecanol, Heating test
Thermal Conductivity (W/mK)
0.400
0.300
0.200
0.100
0.000
0
10
20
30
40
Temperature (C)

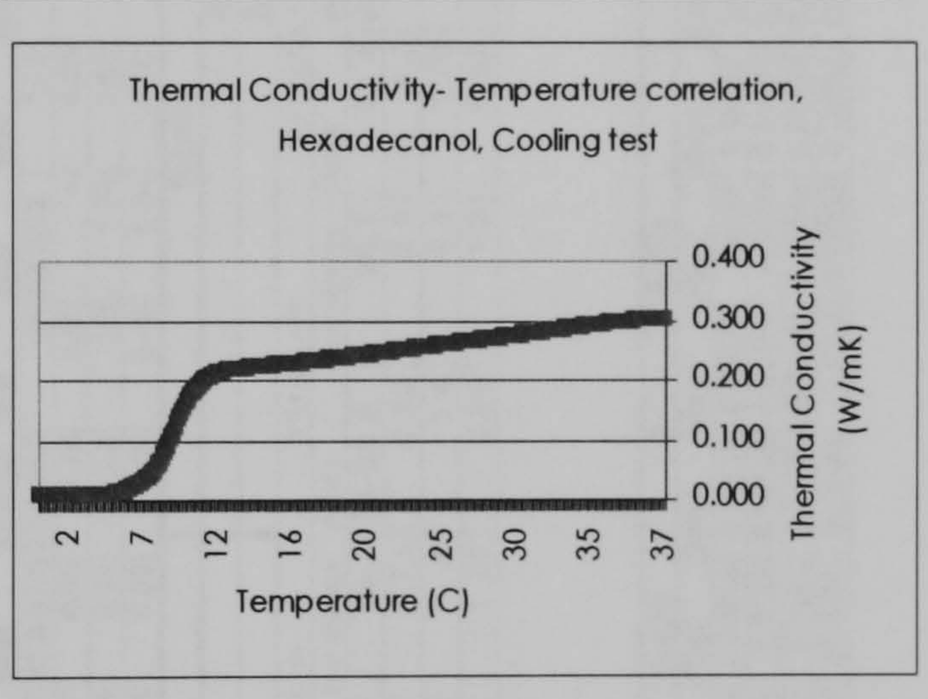
Thermal Conductivity- Temperature correlation, Hexadecanol, Cooling test
0.400
0.300
0.200
0.100
0.000
Thermal Conductivity (W/mK)
2
7
12
16
20
25
30
35
37
Temperature (C)

Appendix 5.B: Data logger readings average values for each run and each repetition

INTERNAL BLINDS

Average value for all the 12 tubes (Internal Blind Temperature in degC)

	Run1s			Run2m			Run3m			Run4s			Run5m			Run6s			Run7s			Run8m		
	Rep1	Rep2	Rep3	Rep1	Rep2	Rep3	Rep1	Rep2	Rep3	Rep1	Rep2	Rep3	Rep1	Rep2	Rep3	Rep1	Rep2	Rep3	Rep1	Rep2	Rep3	Rep1	Rep2	Rep3
initial val	59.1	38.9	47.4	18.6	12.9	14.7	15.6	13.2	11.1	65.1	69.9	73.4	13.1	11.4	12.5	57.0	60.0	123.8	51.9	56.9	47.9	12.1	13.0	13.6
final val	23.3	23.8	22.9	61.3	61.3	60.3	57.8	55.1	55.2	17.5	17.7	17.7	51.7	54.7	54.3	25.1	25.5	25.4	13.0	12.0	11.7	40.9	40.6	40.6
average	27.3	26.2	26.2	53.3	51.7	51.6	50.3	43.1	42.7	25.9	27.4	26.1	41.9	40.4	42.3	30.4	31.0	32.8	17.5	17.5	16.4	32.3	31.5	32.8

Taking one tube as model (representing all the tubes) to determine the change of state period (starting time, end, and length) the next tube has been selected:

	Run1s			Run2m			Run3m									Run4s								
	Rep1	Rep2	Rep3	Rep1	Rep2	Rep3		Rep1			Rep2			Rep3		Rep1						Rep2		
Mode		Solidification			Melting			Melting			Melting			Melting			Solidification							
PCM		CP			CP		"T"(1,4,7,10)	"CP" (2,5,8,11	"H"(3,6,9,12)	"T"(1,4,7,10)	"CP" (2,5,8,11	"H"(3,6,9,12)	"T"(1,4,7,10)	"CP" (2,5,8,11	"H"(3,6,9,12)	"T"(1,4,7,10)		"CP" (2,5,8,11)		"H"(3,6,9,12)		"T"(1,4,7,10)		"CP" (2...)
Tube		Blind5e			Blind5e		Blind1	Blind2	Blind3	Blind1	Blind2	Blind3	Blind1	Blind2	Blind3	Blind1	2nd change	Blind2	2nd change	Blind3	2nd change	Blind1	2nd change	Blind2
Tchange st	24	23.9	23.9	24	24	24	34	24	20.4	34	24	20.4	34	24	20.4	33-35.5	23.5	31.5-32.5	23.5-24.5	31.5-32.5	22.5-23.5	33-35.5	23.5	31.5-32.5
Reached (h	6.45	5.1	5.4	0.22	0.31	0.3	1.82	1.02	0.2	2.2	1.23	0.18	2.55	1.22	0.18	0.75	1.7	0.79	1.6	0.75	1.65	0.66	1.72	0.83
Maint.until(	10.63	7.7	8.3	0.42	0.5	0.5	2.15	1.4	0.54	2.63	1.71	0.53	2.81	1.62	0.59	1.2	2.14	1	2.2	0.96	2.16	1.21	2.2	1
Change du	4.18	2.6	2.9	0.2	0.19	0.2	0.33	0.38	0.34	0.43	0.48	0.35	0.26	0.4	0.41	0.45	0.44	0.21	0.6	0.21	0.51	0.55	0.48	0.17

	Run4s				Run4s						Run5m									Run6s					
	Rep2				Rep3						Rep1			Rep2			Rep3			Rep1					
Mode	Solidification				Solidification						Melting			Melting			Melting			Solidification					
PCM	"CP" (2,5,8,11		"H"(3,6,9,12)		"T"(1,4,7,10)		"CP" (2,5,8,11)		"H"(3,6,9,12)		"T"(1,4,7,10)	"CP" (2,5,8,11	"H"(3,6,9,12)	"T"(1,4,7,10)	"CP" (2,5,8,11	"H"(3,6,9,12)	"T"(1,4,7,10)	"CP" (2,5,8,11	"H"(3,6,9,12)	"T"(1,4,7,10)		"CP" (2,5,8,11)		"H"(3,6,9,12)		
Tube	2nd change	Blind3	2nd change	Blind1	2nd change	Blind2	2nd change	Blind3	2nd change	Blind1	Blind2	Blind3	Blind1	Blind2	Blind3	Blind1	Blind2	Blind3	Blind1	2nd change	Blind2	2nd change	Blind3	2nd change
Temp chan	23.5-24.5	31.5-32.5	22.5-23.5	33-35.5	23.5	31.5-32.5	23.5-24.5	31.5-32.5	22.5-23.5	34	23.5-25	17.5	34	23.5-25	17.5	34	23.5-25	17.5	33-35.5	26.5	31.5	25.5-27	31.5	25.5
Reached at	1.65	0.81	1.71	0.65	1.8	0.85	1.7	0.85	1.76	2.85	1	0.25	2.63	1.15	0.25	2.5	1	0.22	0.51	2.43	1	2.3	0.96	2.52
Maintained	2.2	0.93	2.23	1.2	2.31	1	2.3	0.94	2.3	3.3	1.84	0.83	3	1.82	0.78	2.9	1.74	0.75	1.2	2.92	1.53	3.3	1.48	3.4
Change du	0.55	0.12	0.52	0.55	0.51	0.15	0.6	0.09	0.54	0.45	0.84	0.58	0.37	0.67	0.53	0.4	0.74	0.53	0.69	0.49	0.53	1	0.52	0.88

	Run6s						Run6s						Run7s			Run8m		
	Rep2						Rep3						Rep1	Rep2	Rep3	Rep1	Rep2	Rep3
Mode	Solidification						Solidification						Solidification			Melting		
PCM	"T"(1,4,7,10)		"CP" (2,5,8,11)		"H"(3,6,9,12)		"T"(1,4,7,10)		"CP" (2,5,8,11)		"H"(3,6,9,12)		CP			CP		
Tube	Blind1	2nd change	Blind2	2nd change	Blind3	2nd change	Blind1	2nd change	Blind2	2nd change	Blind3	2nd change	Blind5e			Blind5e		
Temp chan	33-35.5	26.5	31.5	25.5-27	31.5	25.5	33-35.5	26.5	31.5	25.5-27	31.5	25.5	23.5	23.5	23.5	24-26.5	24-26.5	24-26.5
Reached at	0.57	2.64	1.08	2.41	1.05	2.71	0.62	2.8	1.2	2.56	1.13	2.88	2.27	2.5	2.17	0.7	0.7	0.67
Maintained	1.71	3.4	1.62	3.53	1.6	4	1.4	4.1	1.75	4.1	1.68	4.1	3.5	3.63	3.3	1.57	1.56	1.53
Change du	1.14	0.76	0.54	1.12	0.55	1.29	0.78	1.3	0.55	1.54	0.55	1.22	1.23	1.13	1.13	0.87	0.86	0.86

HEAT FLUXOMETERS

Average value for all front HF (4a,5a,6a) in kW/m2

	Run1s			Run2m			Run3m			Run4s			Run5m			Run6s			Run7s			Run8m		
	Rep1	Rep2	Rep3	Rep1	Rep2	Rep3	Rep1	Rep2	Rep3	Rep1	Rep2	Rep3	Rep1	Rep2	Rep3	Rep1	Rep2	Rep3	Rep1	Rep2	Rep3	Rep1	Rep2	Rep3
initial val	-0.04065	-0.00813	-0.0252	-0.21016	-0.11179	-0.27398	0.0126	0.02236	0.03211	0.03476	0.0248	0.02927	0.01951	0.0187	0.01382	0.23293	0.24268	0.28049	-0.1939	-0.1687	-0.14106	-0.02927	-0.02073	-0.01707
final val	-0.00285	-0.00407	-0.00163	-0.29085	-0.28293	-0.22805	-0.01463	-0.0065	-0.00569	-0.00793	-0.0065	-0.00691	0.14878	0.15	0.14797	0.00244	-0.00122	-0.00122	0.0187	0.01748	0.02033	-0.2061	-0.19268	-0.19146
average	-0.00682	-0.00469	-0.00561	-0.19736	-0.17147	-0.25701	0.02842	0.0663	0.06769	-0.00043	-0.00154	-0.00154	0.18053	0.19636	0.18618	0.03209	0.03382	0.03177	-0.00776	-0.01039	-0.00723	-0.2321	-0.22269	-0.20781
Total Ac.	-10.38	-4.36282	-7.46415	-120.191	-102.022	-154.46	39.4516	55.8902	58.1443	-0.2128	-0.72358	-0.78653	202.731	159.247	175.192	14.2793	14.678	15.0293	-15.561	-20.839	-14.498	-118.834	-105.776	-111.18

Average value for all back HF (4b,5b,6b) in kW/m2

	Run1s			Run2m			Run3m			Run4s			Run5m			Run6s			Run7s			Run8m		
	Rep1	Rep2	Rep3	Rep1	Rep2	Rep3	Rep1	Rep2	Rep3	Rep1	Rep2	Rep3	Rep1	Rep2	Rep3	Rep1	Rep2	Rep3	Rep1	Rep2	Rep3	Rep1	Rep2	Rep3
initial val	-0.22683	-0.06789	-0.13171	-0.04187	-165.237	-0.04024	-0.00528	0.0122	0.01789	0.04878	0.02967	0.02195	0.05813	0.18577	0.25447	-0.33049	-0.34431	-0.38577	-0.26057	-0.18354	-0.2248	-0.01016	-0.01179	-0.0126
final val	-0.02886	-0.03862	-0.03293	-0.23232	-0.21402	0.13455	-0.18821	-0.19024	-0.18862	-0.00244	-0.00325	0	-0.1122	-0.07927	-0.07764	-0.00854	-0.00813	-0.00813	-0.0187	-0.01768	-0.01789	0.06789	0.06504	0.06585
average	-0.05564	-0.053	-0.05512	-0.12628	-0.09677	0.09092	-0.13784	-0.10477	-0.10072	0.00681	0.00336	0.00339	-0.03284	0.00861	-0.00095	-0.05827	-0.06078	-0.0518	-0.04692	-0.04706	-0.04626	0.03619	0.03487	0.03742
Total Ac.	-84.7373	-49.2876	-73.3051	-76.9061	-57.4809	54.6411	-191.317	-88.3236	-86.5183	3.52073	1.57967	1.69916	-114.314	6.98333	-0.89187	-27.9106	-29.298	-31.15	-94.0683	-94.3482	-92.7435	18.5268	16.5618	20.0187

EXTERNAL BLINDS

Average value for all the 6 tubes (External Blind Temperature, in deg C)

	Run1s			Run2m			Run3m			Run4s			Run5m			Run6s			Run7s			Run8m		
	Rep1	Rep2	Rep3	Rep1	Rep2	Rep3	Rep1	Rep2	Rep3	Rep1	Rep2	Rep3	Rep1	Rep2	Rep3	Rep1	Rep2	Rep3	Rep1	Rep2	Rep3	Rep1	Rep2	Rep3
initial val	56.2	37.6	45.4	19.4	14.9	15.1	15.8	13.8	11.9	61.5	66.2	69.5	13.7	12.5	14.2	53.3	56.1	57.6	48.6	53.6	44.1	12.5	13.3	13.9
final val	22.8	23.2	22.5	61.8	61.8	60.9	57.6	54.9	55.1	17.3	17.6	17.6	52.2	55.3	54.8	25.0	25.4	25.4	13.0	12.0	11.8	41.3	40.9	40.8
average	26.4	25.4	25.4	54.8	53.3	53.2	51.4	47.8	44.7	25.4	26.9	26.6	43.9	43.1	45.0	29.7	30.3	30.6	16.5	16.5	15.4	33.7	32.9	33.3

AIR PLATINIUM RESISTANCE THERMOMETERS

Average value for all Inlet Air PRT (11,12) in deg C

	Run1s			Run2m			Run3m			Run4s			Run5m			Run6s			Run7s			Run8m		
	Rep1	Rep2	Rep3	Rep1	Rep2	Rep3	Rep1	Rep2	Rep3	Rep1	Rep2	Rep3	Rep1	Rep2	Rep3	Rep1	Rep2	Rep3	Rep1	Rep2	Rep3	Rep1	Rep2	Rep3
initial val	25.5	25.5	24.9	25.8	29.6	22.4	13.7	15.7	18.6	19.6	23.9	23.3	30.8	29.8	33.7	24.6	25.7	26.9	11.1	24.2	11.9	13.6	16.2	16.2
final val	18.7	18.0	18.0	41.8	41.4	40.9	37.3	33.7	33.7	11.7	11.7	11.9	40.9	44.8	44.5	24.2	24.6	24.5	9.0	7.9	8.1	22.5	22.6	22.4
average	18.9	18.1	18.1	41.4	40.6	40.4	36.8	33.4	33.2	11.9	12.0	12.2	40.6	44.1	44.3	24.4	24.6	24.7	9.1	8.8	8.2	22.0	22.1	21.9

Average value for all Outlet AirPRT (1,2,3,4) in deg C

	Run1s			Run2m			Run3m			Run4s			Run5m			Run6s			Run7s			Run8m		
	Rep1	Rep2	Rep3	Rep1	Rep2	Rep3	Rep1	Rep2	Rep3	Rep1	Rep2	Rep3	Rep1	Rep2	Rep3	Rep1	Rep2	Rep3	Rep1	Rep2	Rep3	Rep1	Rep2	Rep3
initial val	34.5	32.0	33.0	28.4	22.3	22.5	19.7	18.2	15.1	28.2	33.9	32.5	21.4	21.5	24.2	32.7	33.8	35.4	19.7	29.9	18.9	21.1	22.6	24.1
final val	20.1	19.6	19.6	41.7	30.9	30.4	29.5	55.6	27.2	13.8	13.9	14.0	40.9	43.9	43.7	24.3	24.7	24.7	12.7	11.5	11.2	27.7	27.8	27.2
average	20.7	20.2	20.1	40.5	29.5	29.3	28.2	49.8	42.2	15.0	15.3	15.5	39.7	41.8	42.5	25.1	25.5	25.9	13.1	13.0	11.9	25.4	25.3	25.2

Average value for all Chamber AirPRT(5-10) in deg C

	Run1s			Run2m			Run3m			Run4s			Run5m			Run6s			Run7s			Run8m		
	Rep1	Rep2	Rep3	Rep1	Rep2	Rep3	Rep1	Rep2	Rep3	Rep1	Rep2	Rep3	Rep1	Rep2	Rep3	Rep1	Rep2	Rep3	Rep1	Rep2	Rep3	Rep1	Rep2	Rep3
initial val	29.8	28.6	29.0	24.8	19.3	18.1	15.3	16.9	16.1	28.8	33.2	33.5	20.2	20.8	24.5	31.9	32.8	34.2	17.7	27.7	17.7	14.4	16.2	17.0
final val	19.8	19.2	19.3	41.7	41.3	40.8	36.5	33.5	33.6	12.2	12.3	12.5	40.0	43.4	43.2	24.2	24.6	24.6	12.3	11.1	10.8	23.5	23.7	23.5
average	20.1	19.5	19.6	40.7	39.7	39.5	35.4	32.3	32.3	12.9	12.6	13.3	39.1	41.7	42.4	24.6	24.9	25.0	12.4	12.2	11.1	22.6	22.6	22.6

Average value for all Exterior AirPRT(13,14) in deg C

	Run1s			Run2m			Run3m			Run4s			Run5m			Run6s			Run7s			Run8m		
	Rep1	Rep2	Rep3	Rep1	Rep2	Rep3	Rep1	Rep2	Rep3	Rep1	Rep2	Rep3	Rep1	Rep2	Rep3	Rep1	Rep2	Rep3	Rep1	Rep2	Rep3	Rep1	Rep2	Rep3
initial val	25.4	25.5	25.7	23.6	24.5	23.9	26.1	25.4	26.6	23.4	23.9	24.1	26.3	27.2	27.6	23.0	24.0	24.7	28.5	27.4	27.0	24.1	24.4	24.9
final val	25.1	25.5	25.9	25.1	25.5	25.0	27.0	27.1	27.6	23.8	23.9	24.2	27.6	27.7	27.0	23.1	24.4	24.8	28.9	26.9	28.4	25.1	25.1	24.5
average	25.6	25.6	26.0	24.8	25.3	24.9	26.9	26.9	27.1	23.7	23.6	24.2	26.9	27.4	27.6	23.6	24.1	24.7	28.8	27.5	28.0	24.9	25.1	24.8

Appendix 5.C: Experiment 2 Repeatability

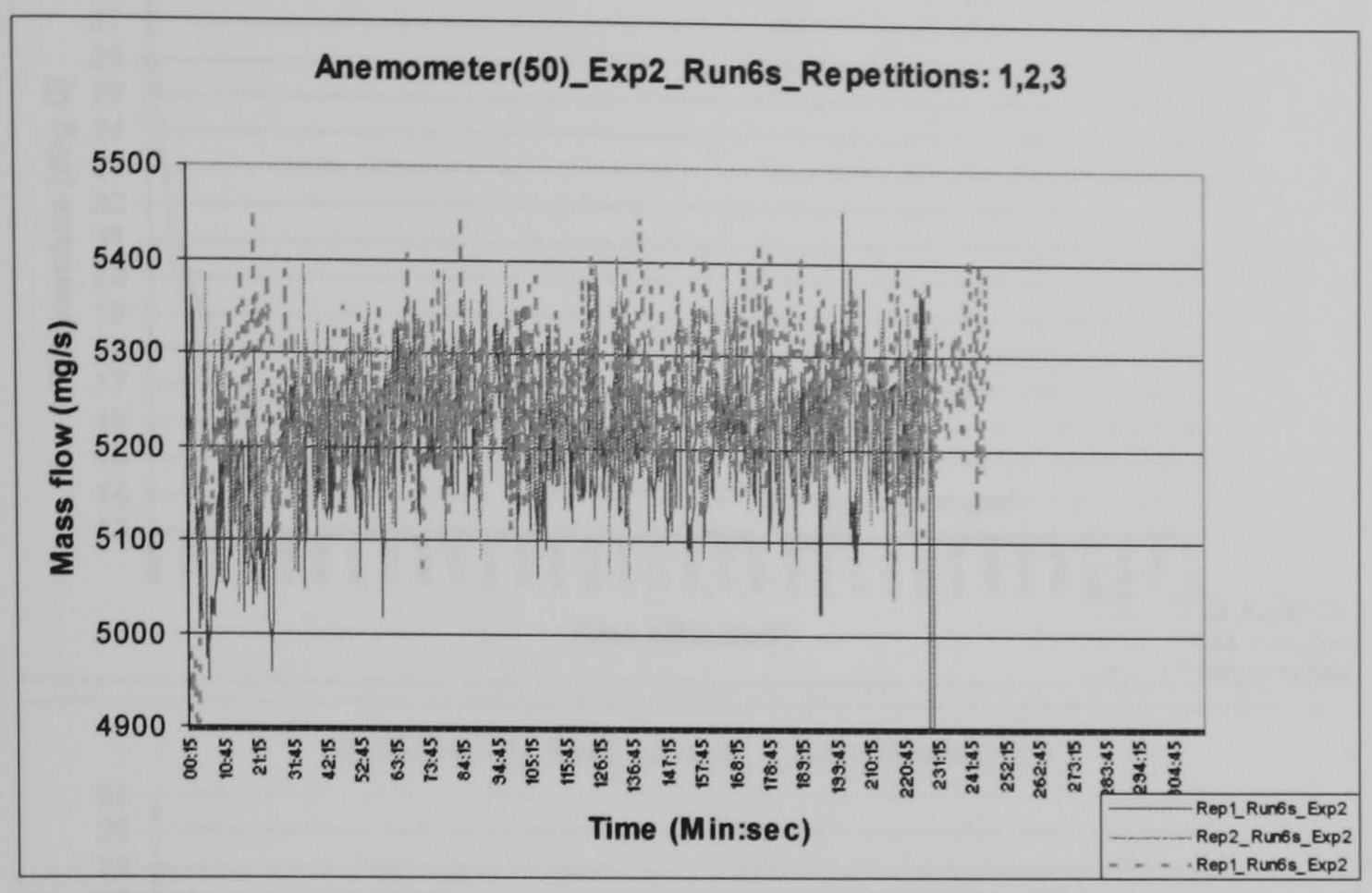

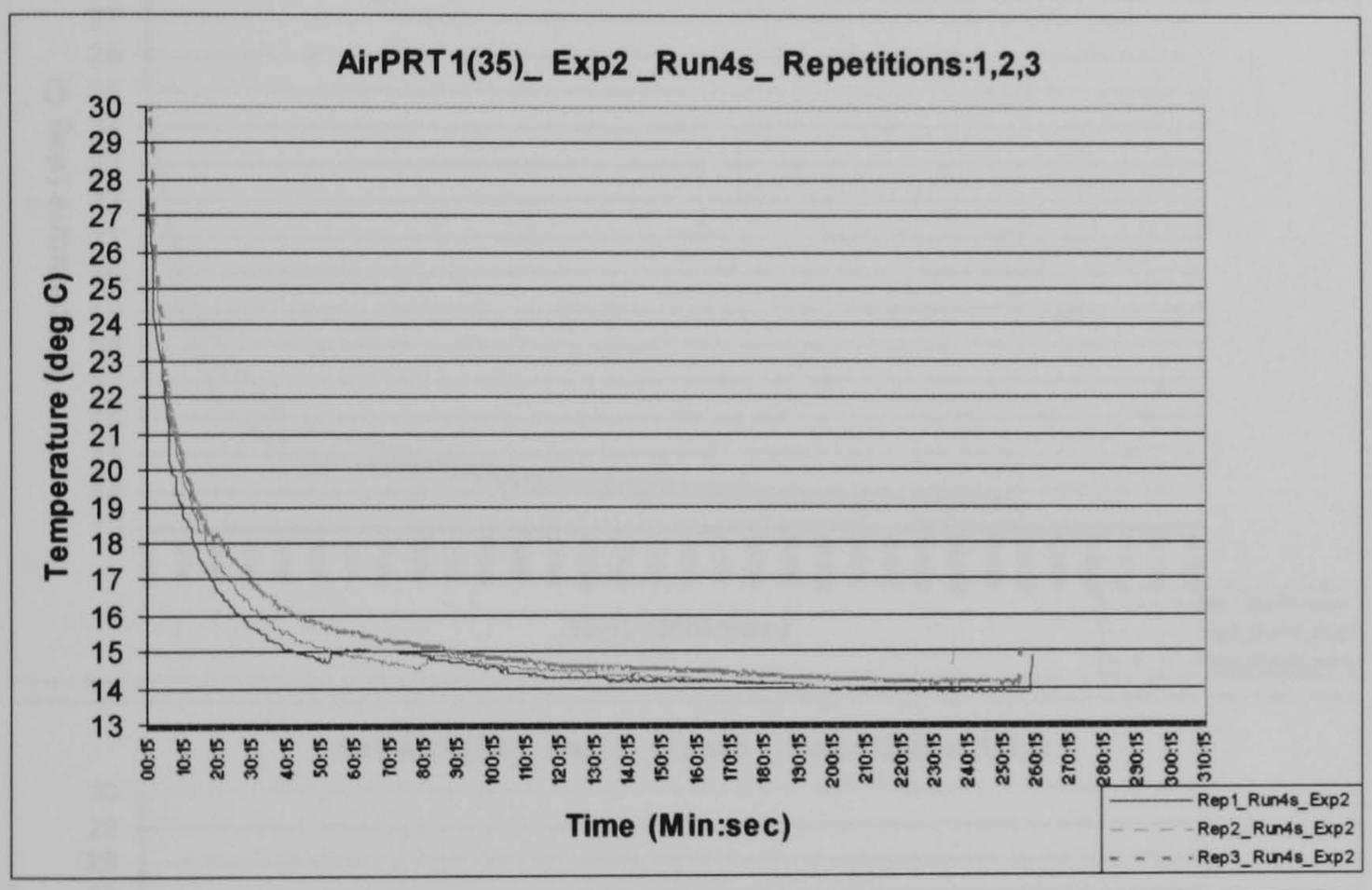

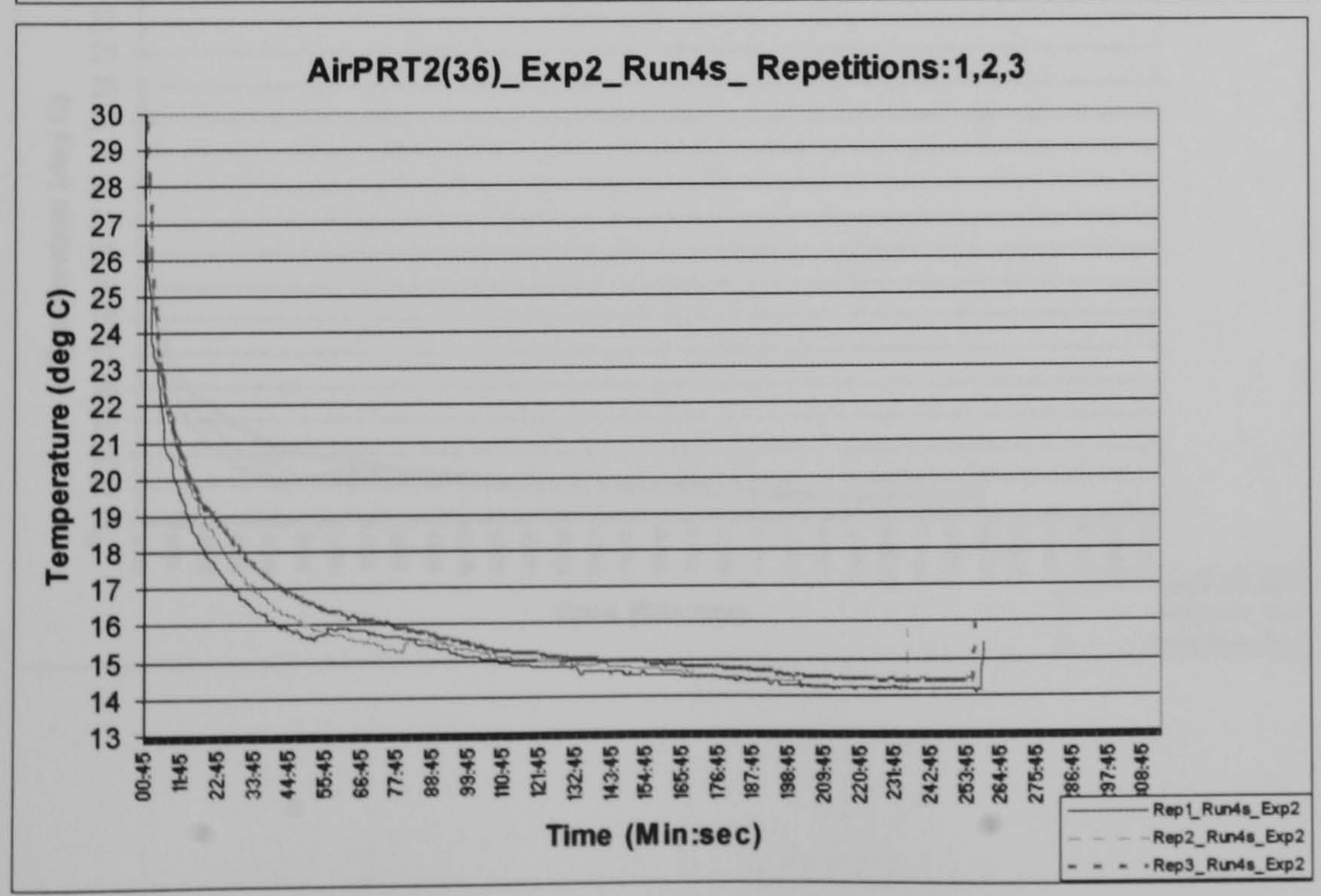

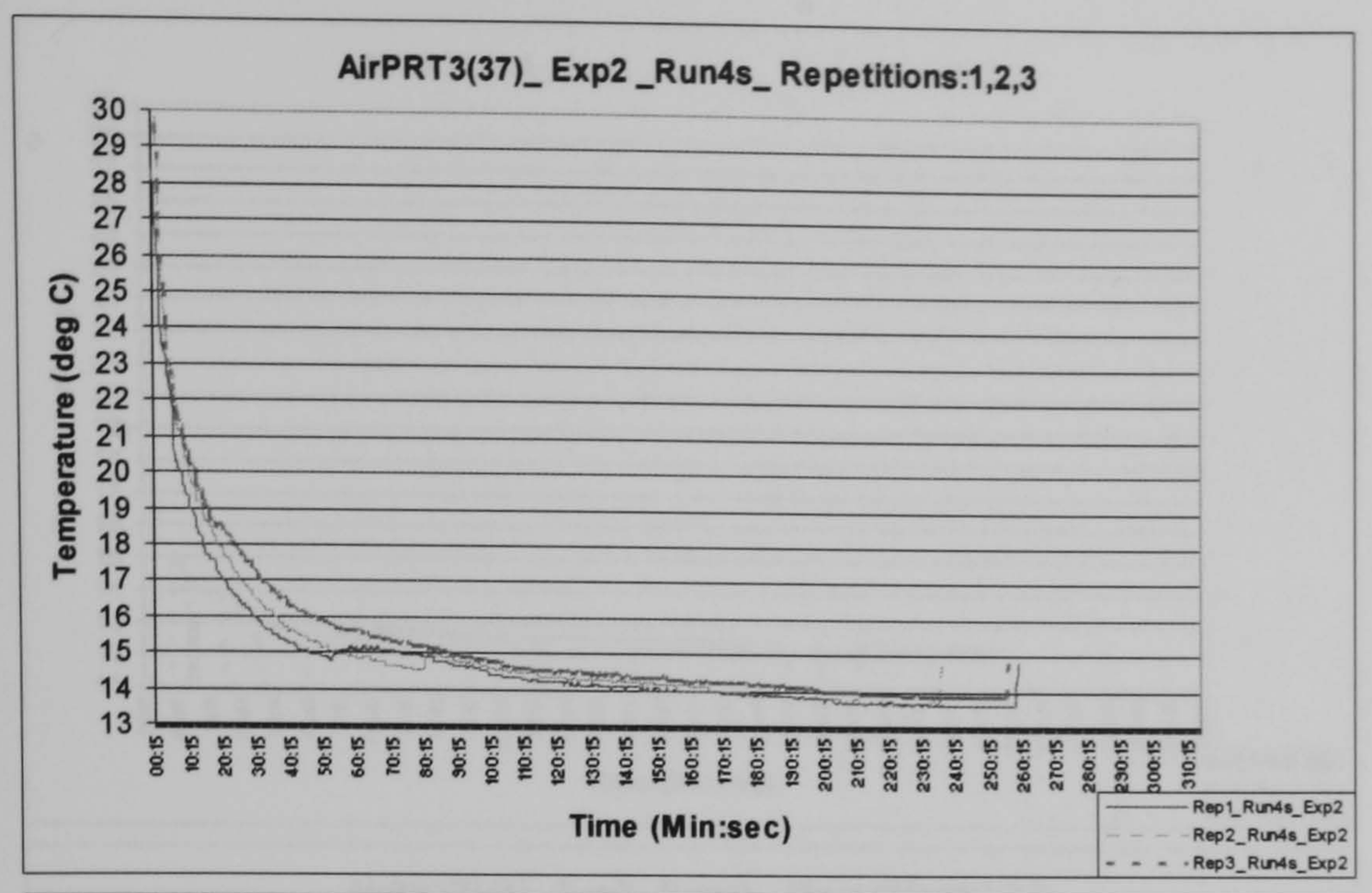
AirPRT3(37)_ Exp2 _Run4s_ Repetitions:1,2,3
Temperature (deg C)
Time (Min:sec)
Rep1_Run4s_Exp2
Rep2_Run4s_Exp2
Rep3_Run4s_Exp2

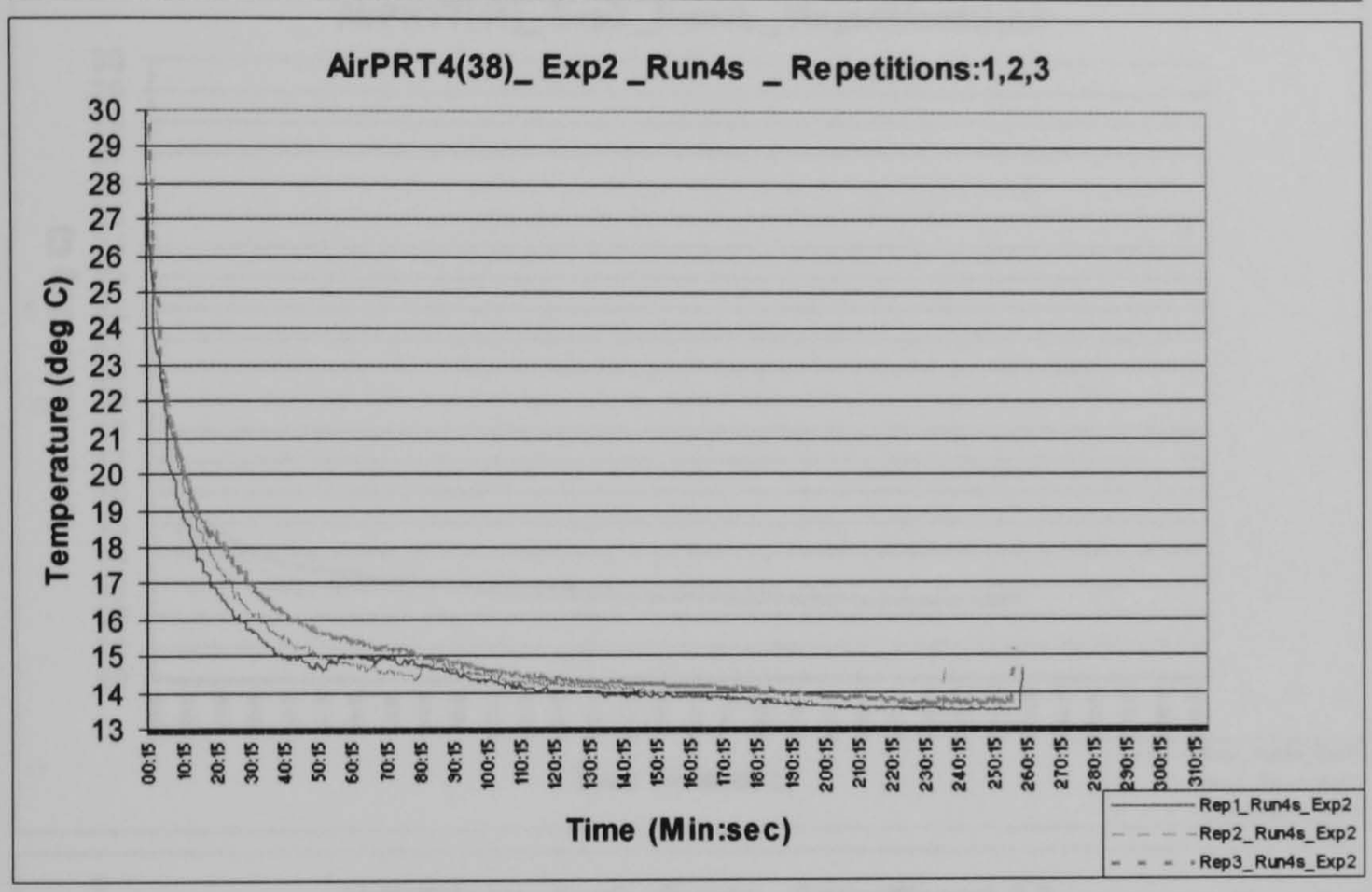
AirPRT4(38)_ Exp2 _Run4s _ Repetitions:1,2,3
Temperature (deg C)
Time (Min:sec)
Rep1_Run4s_Exp2
Rep2_Run4s_Exp2
Rep3_Run4s_Exp2

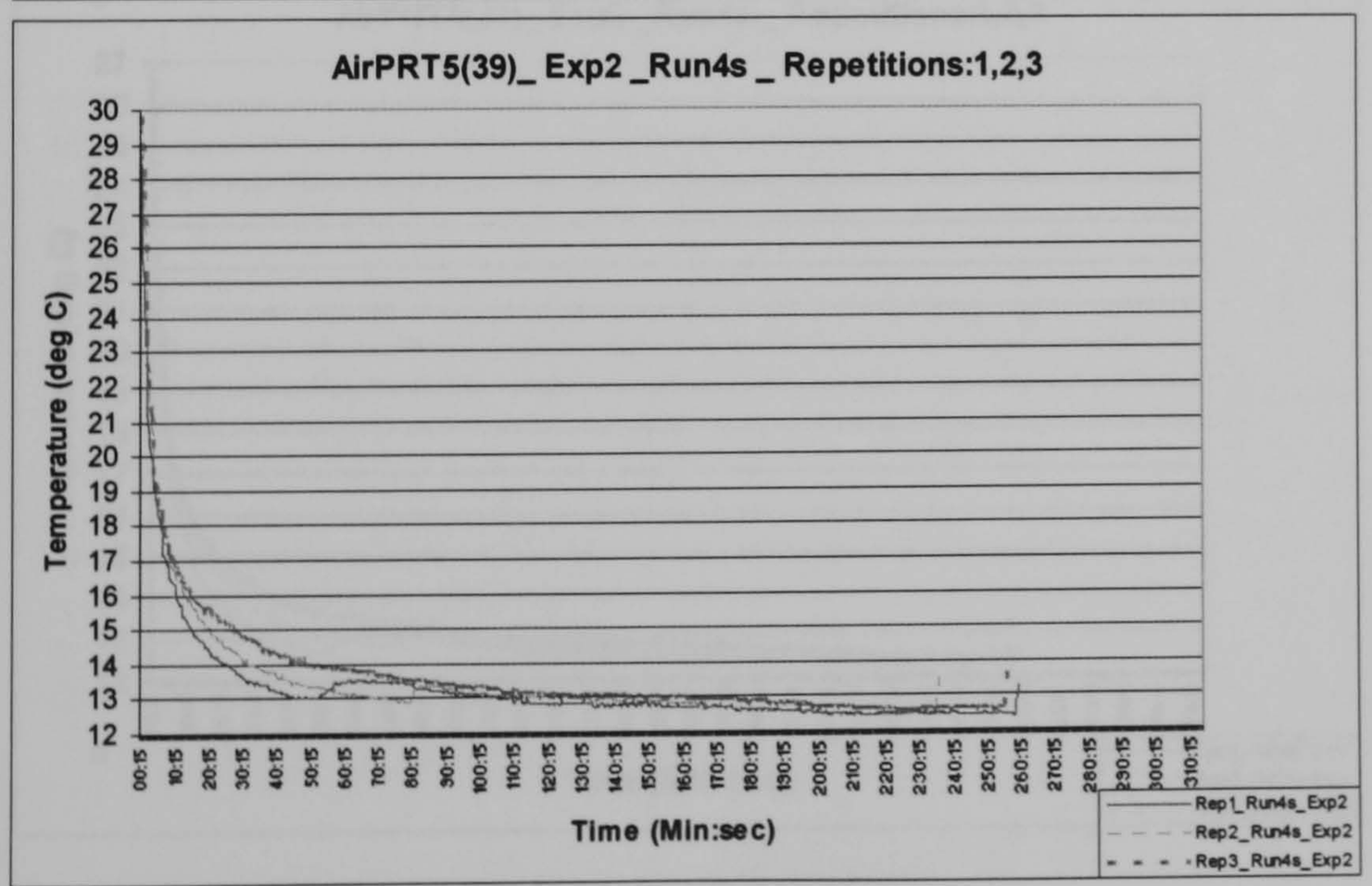
AirPRT5(39)_ Exp2 _Run4s _ Repetitions:1,2,3
Temperature (deg C)
Time (Min:sec)
Rep1_Run4s_Exp2
Rep2_Run4s_Exp2
Rep3_Run4s_Exp2

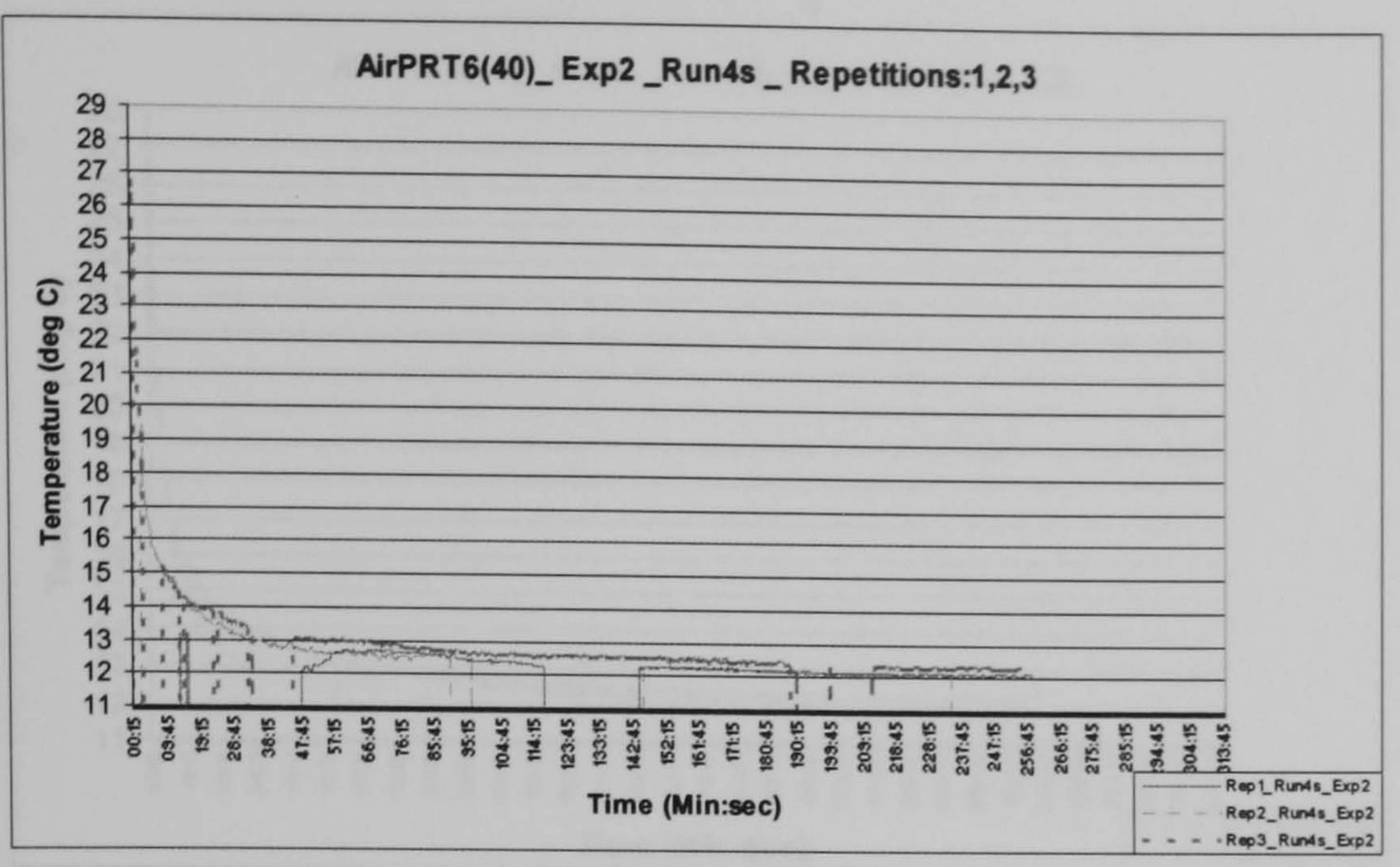
AirPRT6(40)_ Exp2 _Run4s _ Repetitions:1,2,3
Temperature (deg C)
Time (Min:sec)
Rep1_Run4s_Exp2
Rep2_Run4s_Exp2
Rep3_Run4s_Exp2

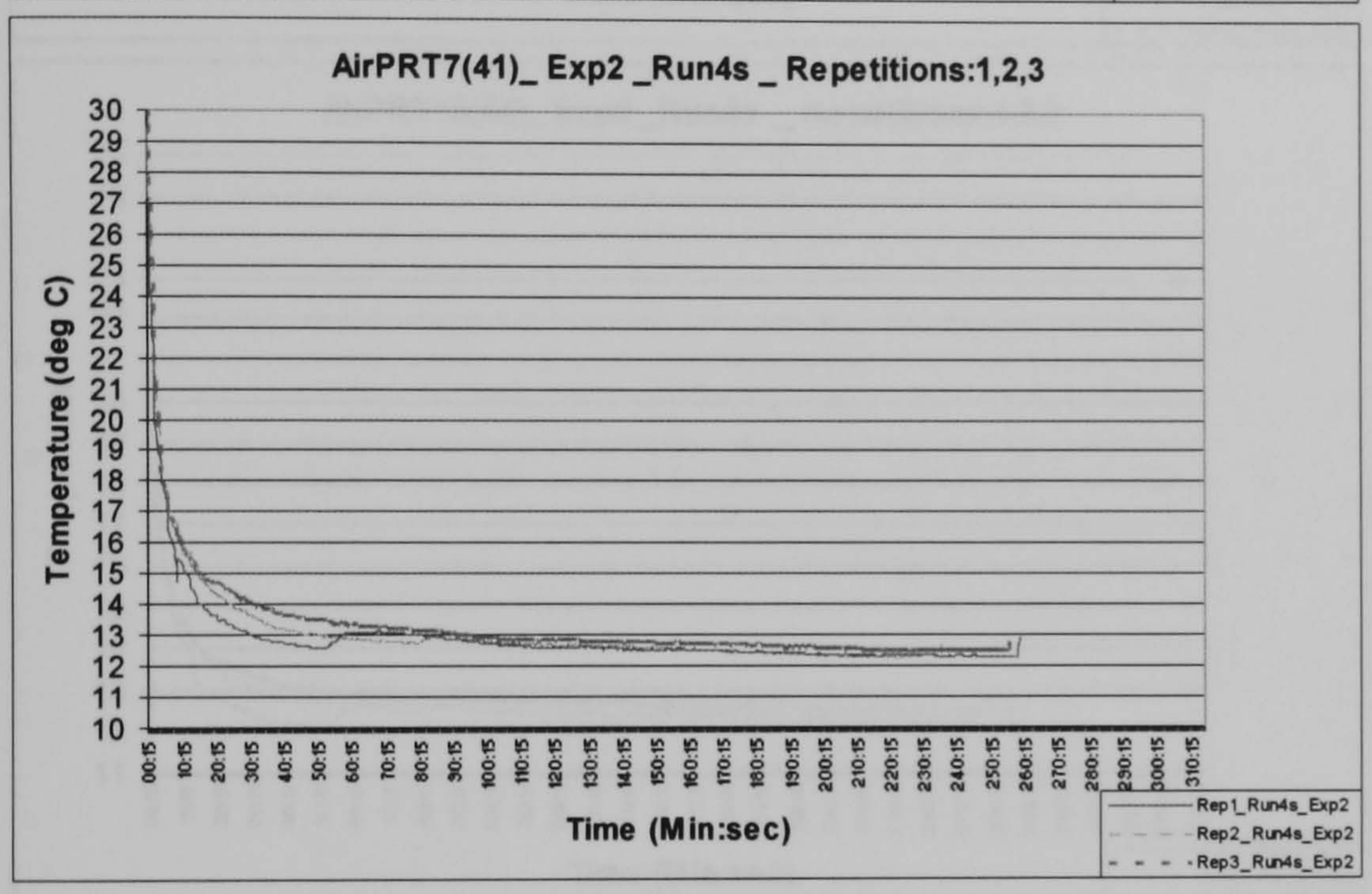
AirPRT7(41)_ Exp2 _Run4s _ Repetitions:1,2,3
Temperature (deg C)
Time (Min:sec)
Rep1_Run4s_Exp2
Rep2_Run4s_Exp2
Rep3_Run4s_Exp2

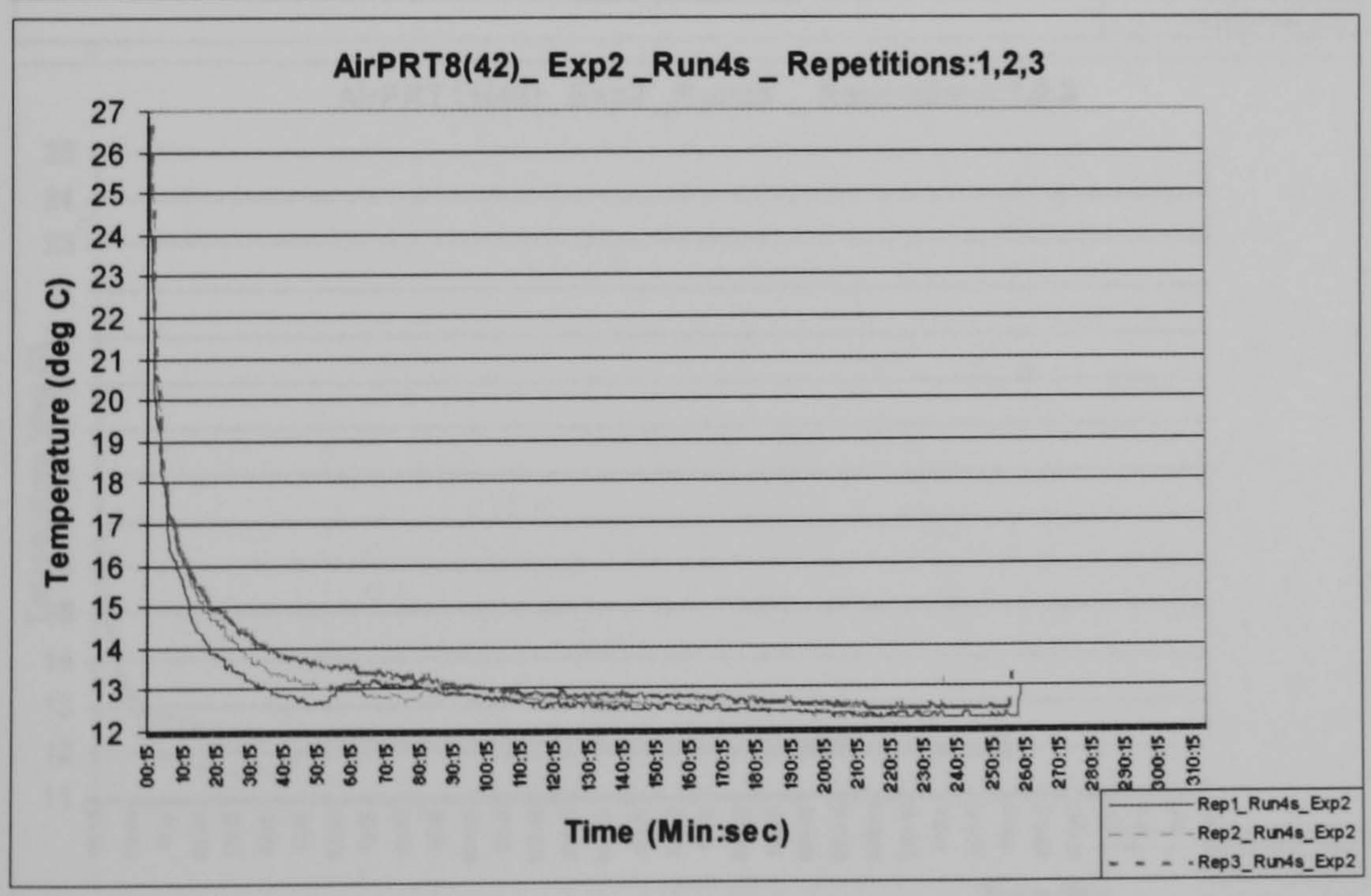
AirPRT8(42)_ Exp2 _Run4s _ Repetitions:1,2,3
Temperature (deg C)
Time (Min:sec)
Rep1_Run4s_Exp2
Rep2_Run4s_Exp2
Rep3_Run4s_Exp2

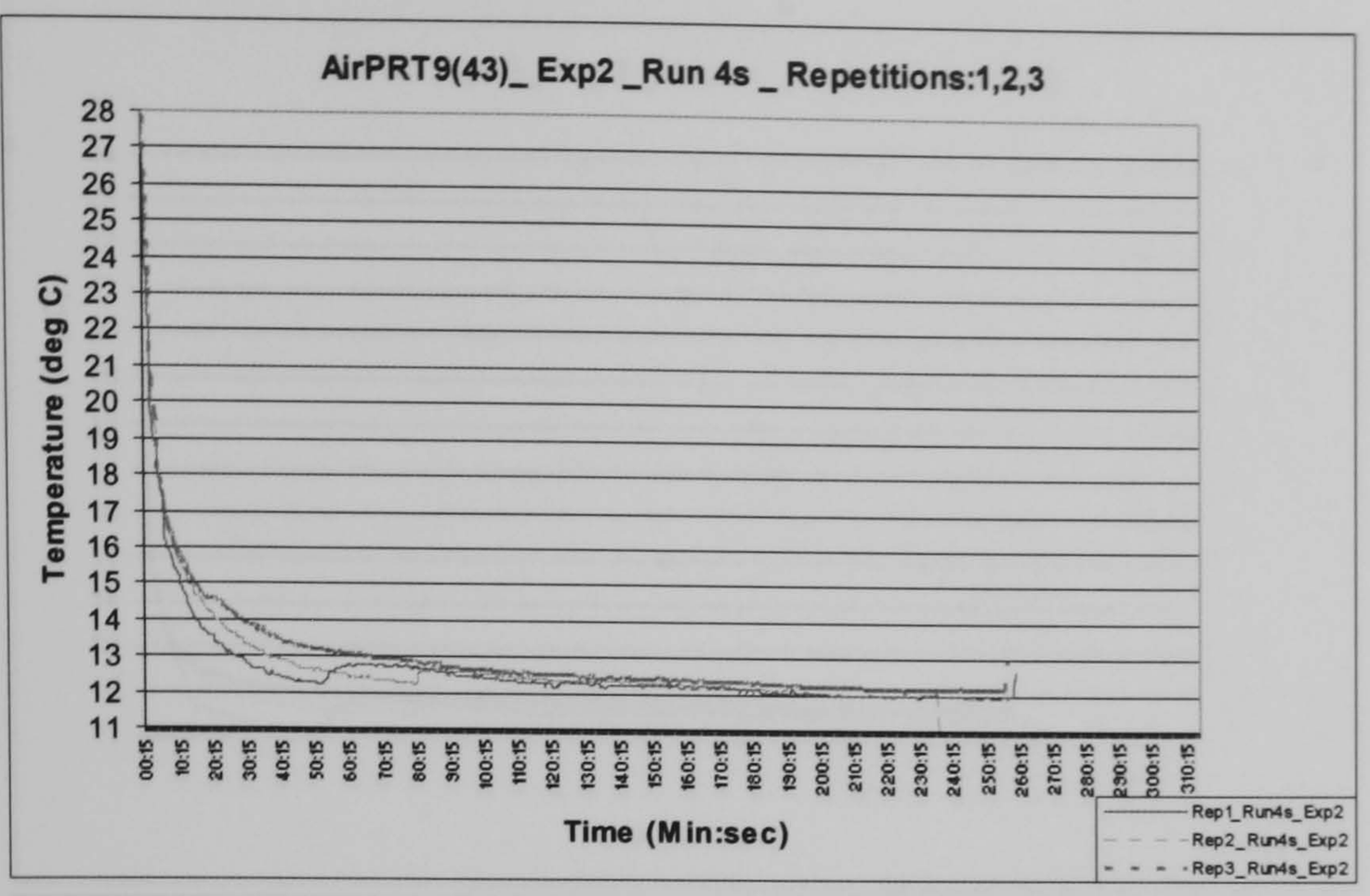
AirPRT9(43)_ Exp2 _Run 4s _ Repetitions:1,2,3
Temperature (deg C)
Time (Min:sec)
Rep1_Run4s_Exp2
Rep2_Run4s_Exp2
Rep3_Run4s_Exp2

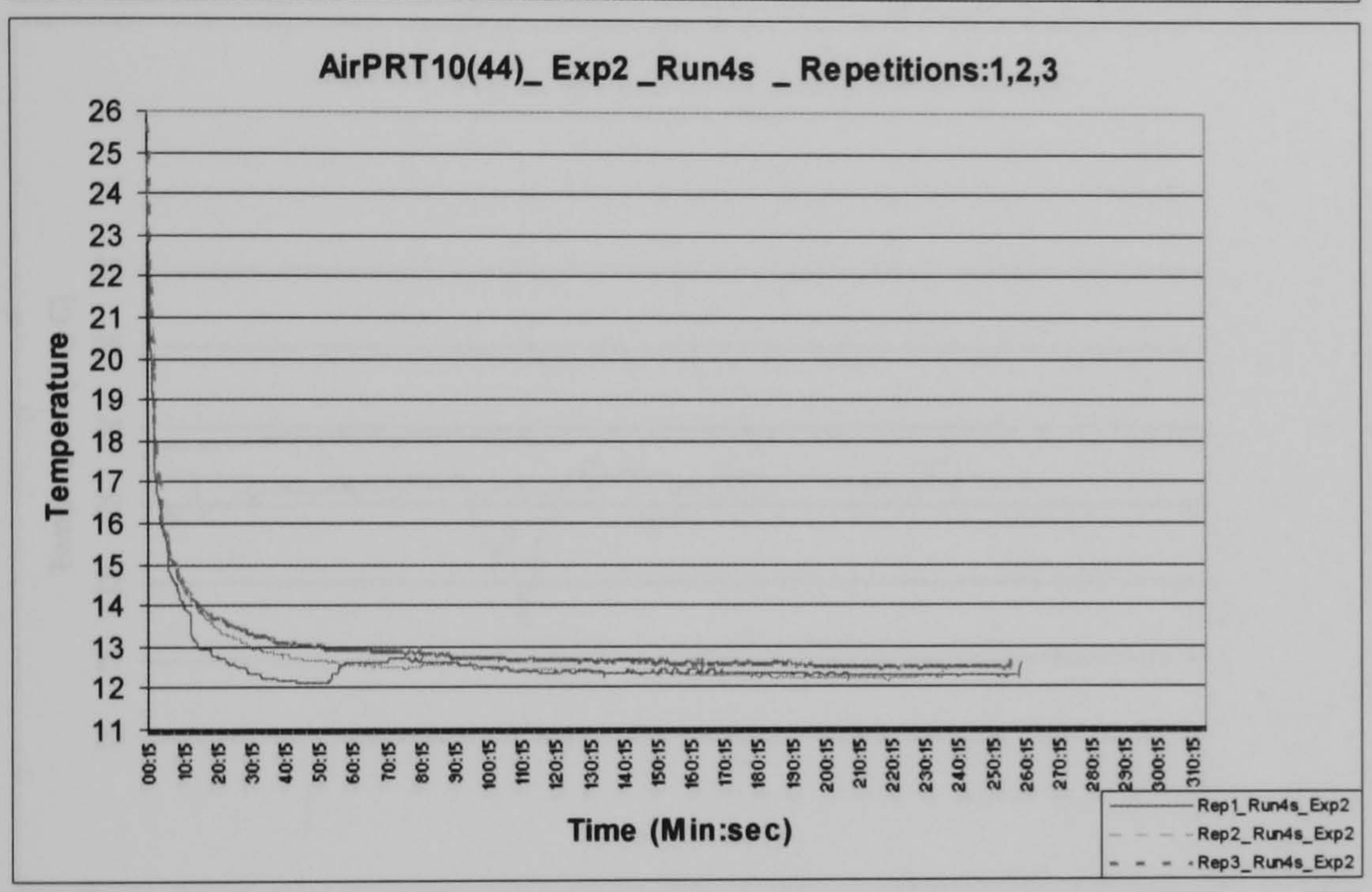
AirPRT10(44)_ Exp2 _Run4s _ Repetitions:1,2,3
Temperature
Time (Min:sec)
Rep1_Run4s_Exp2
Rep2_Run4s_Exp2
Rep3_Run4s_Exp2

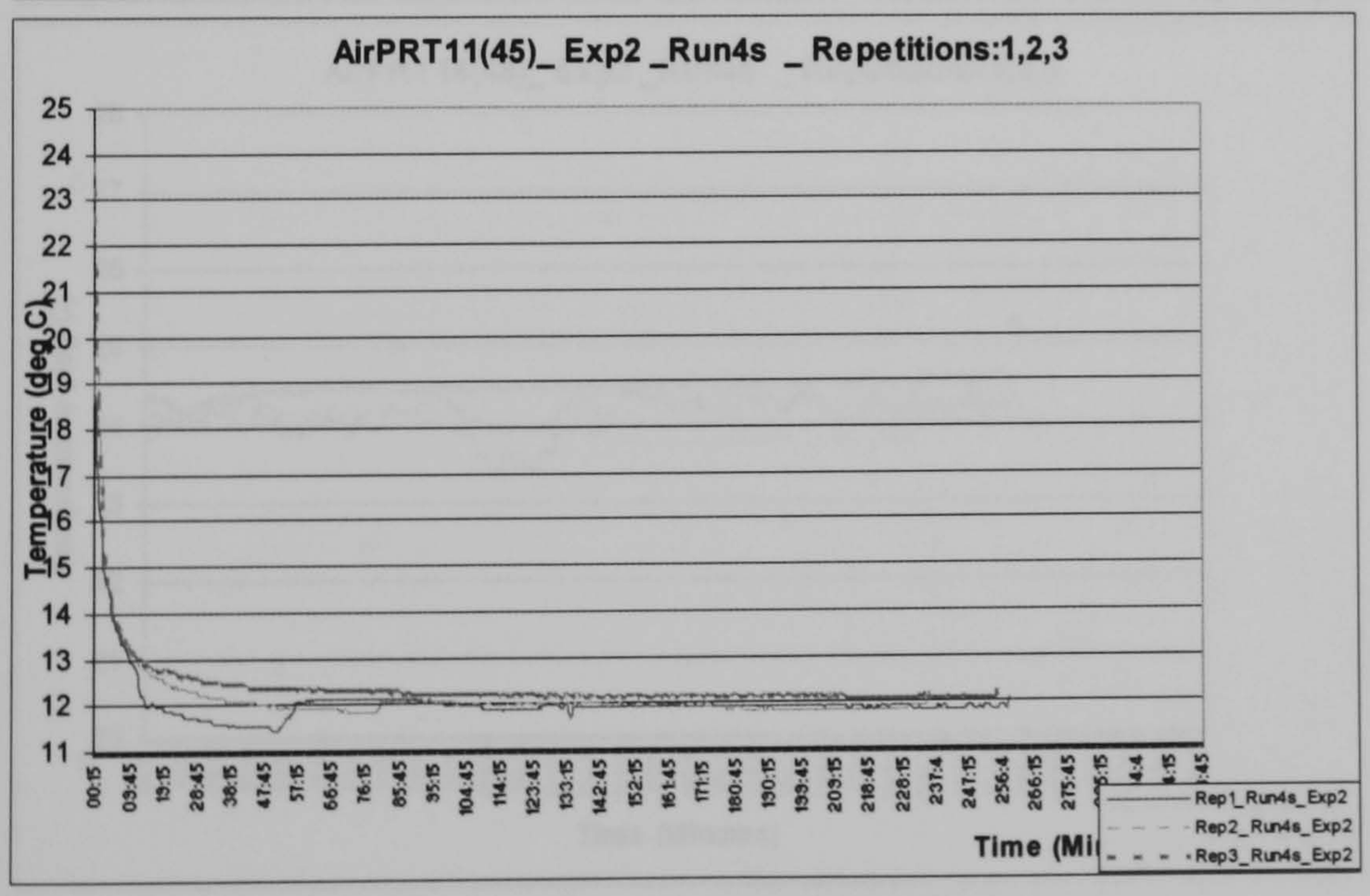
AirPRT11(45)_ Exp2 _Run4s _ Repetitions:1,2,3
Temperature (deg C)
Time (Mi
Rep1_Run4s_Exp2
Rep2_Run4s_Exp2
Rep3_Run4s_Exp2

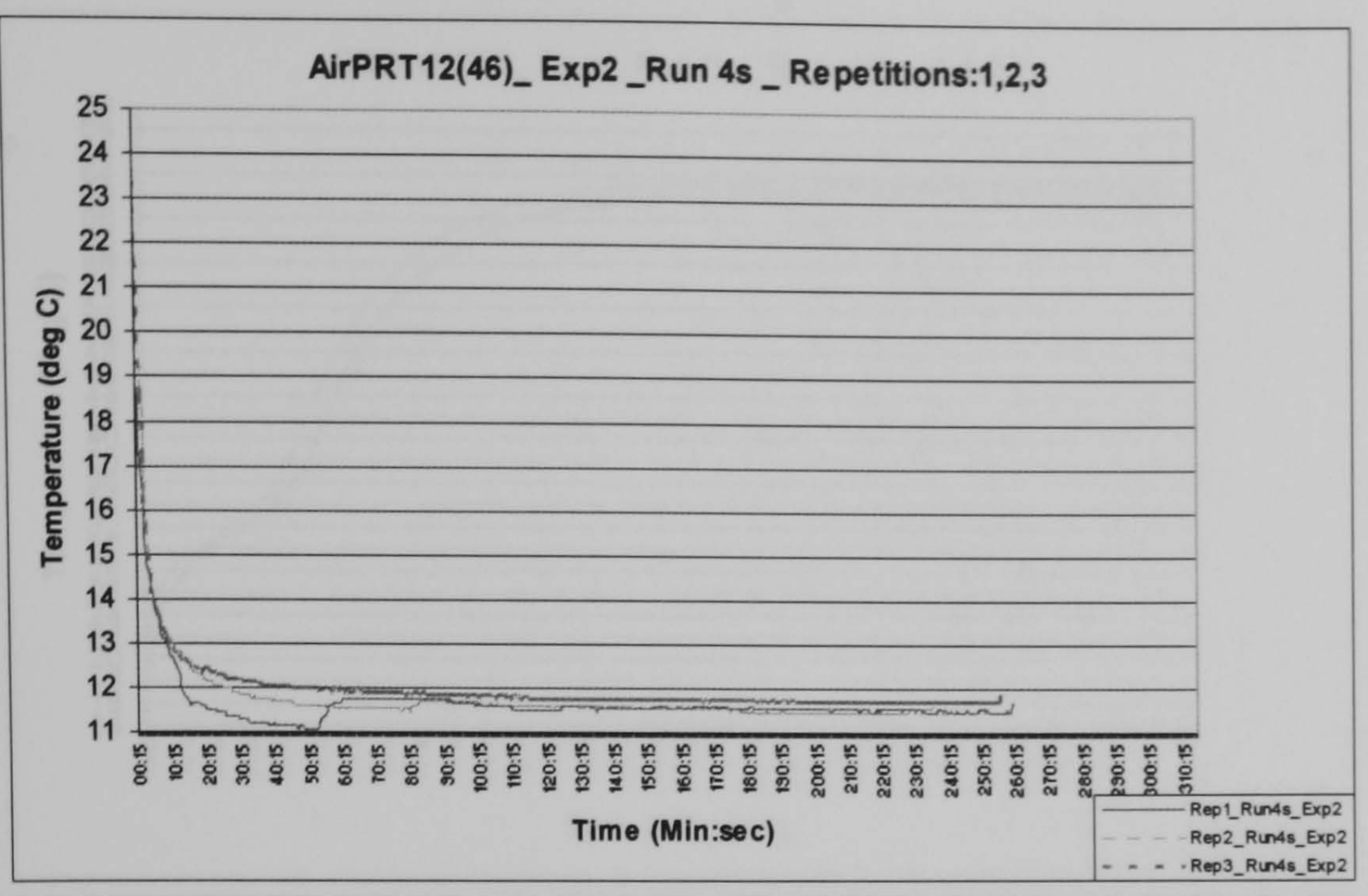
AirPRT12(46)_ Exp2 _Run 4s _ Repetitions:1,2,3
Temperature (deg C)
25
24
23
22
21
20
19
18
17
16
15
14
13
12
11
00:15
10:15
20:15
30:15
40:15
50:15
60:15
70:15
80:15
90:15
100:15
110:15
120:15
130:15
140:15
150:15
160:15
170:15
180:15
190:15
200:15
210:15
220:15
230:15
240:15
250:15
260:15
270:15
280:15
290:15
300:15
310:15
Time (Min:sec)
Rep1_Run4s_Exp2
Rep2_Run4s_Exp2
Rep3_Run4s_Exp2

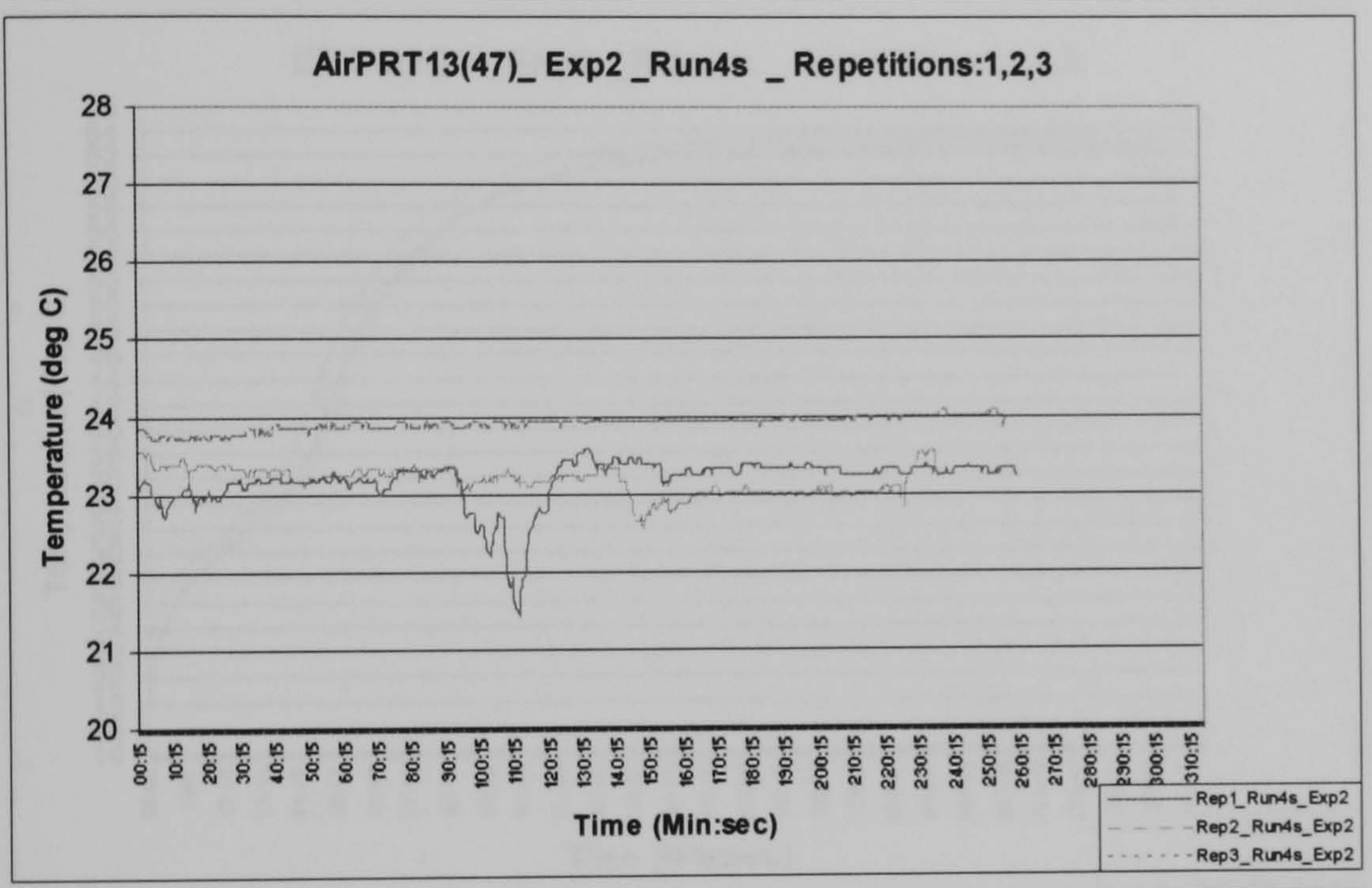
AirPRT13(47)_ Exp2 _Run4s _ Repetitions:1,2,3
Temperature (deg C)
28
27
26
25
24
23
22
21
20
00:15
10:15
20:15
30:15
40:15
50:15
60:15
70:15
80:15
90:15
100:15
110:15
120:15
130:15
140:15
150:15
160:15
170:15
180:15
190:15
200:15
210:15
220:15
230:15
240:15
250:15
260:15
270:15
280:15
290:15
300:15
310:15
Time (Min:sec)
Rep1_Run4s_Exp2
Rep2_Run4s_Exp2
Rep3_Run4s_Exp2

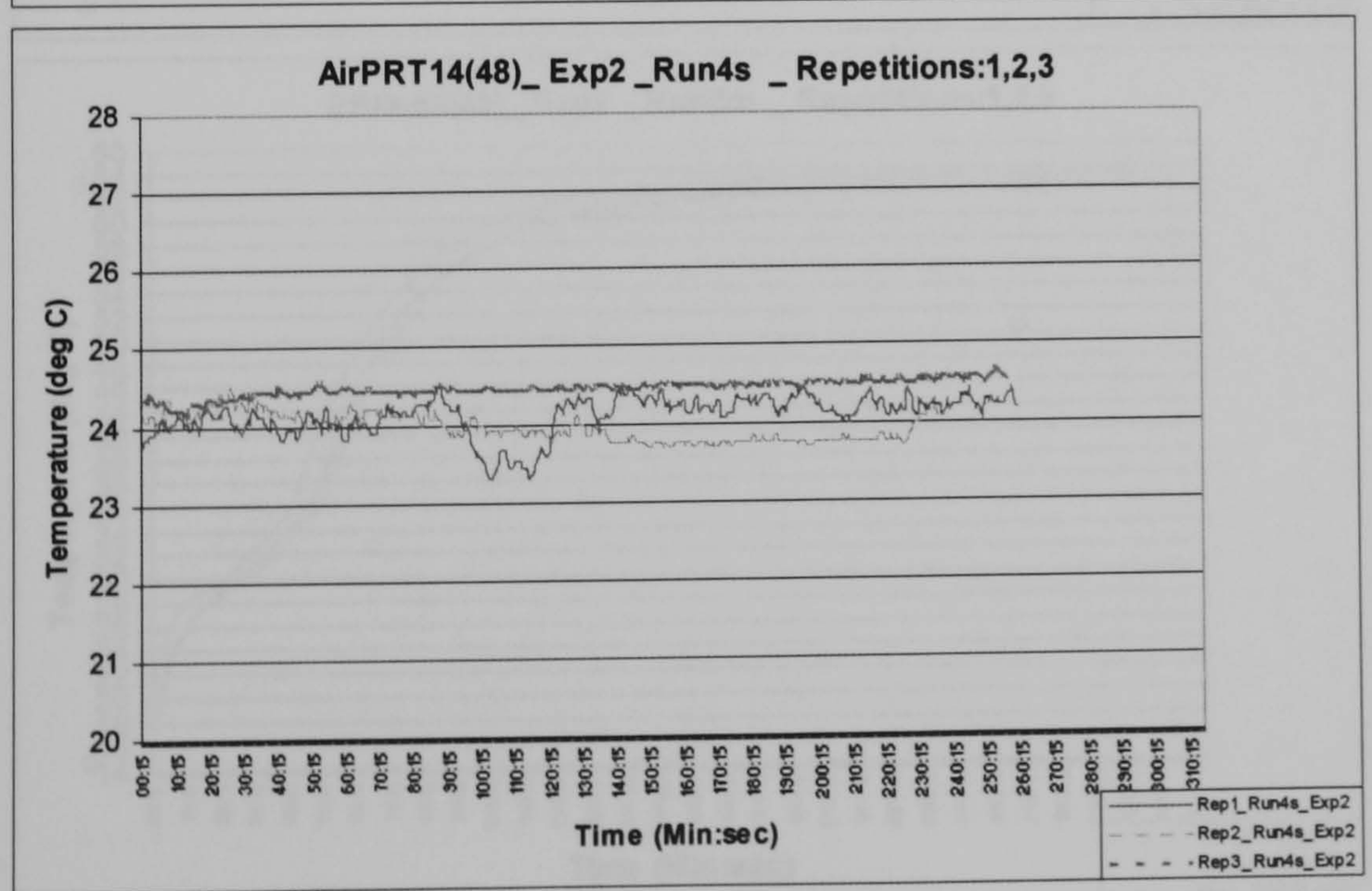
AirPRT14(48)_ Exp2 _Run4s _ Repetitions:1,2,3
Temperature (deg C)
28
27
26
25
24
23
22
21
20
00:15
10:15
20:15
30:15
40:15
50:15
60:15
70:15
80:15
90:15
100:15
110:15
120:15
130:15
140:15
150:15
160:15
170:15
180:15
190:15
200:15
210:15
220:15
230:15
240:15
250:15
260:15
270:15
280:15
290:15
300:15
310:15
Time (Min:sec)
Rep1_Run4s_Exp2
Rep2_Run4s_Exp2
Rep3_Run4s_Exp2

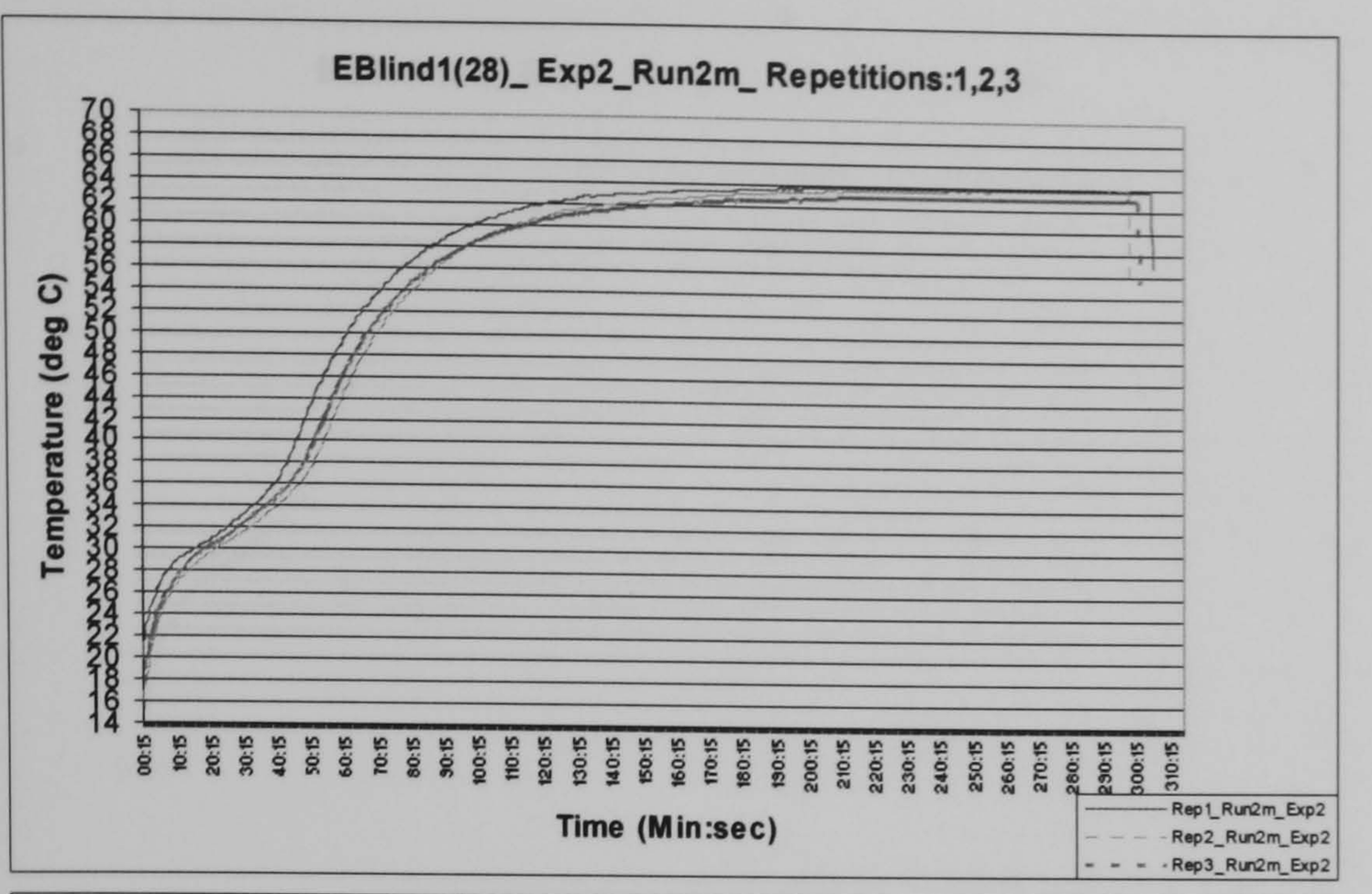
EBlind1(28)_ Exp2_Run2m_ Repetitions:1,2,3
Temperature (deg C)
Time (Min:sec)
Rep1_Run2m_Exp2
Rep2_Run2m_Exp2
Rep3_Run2m_Exp2

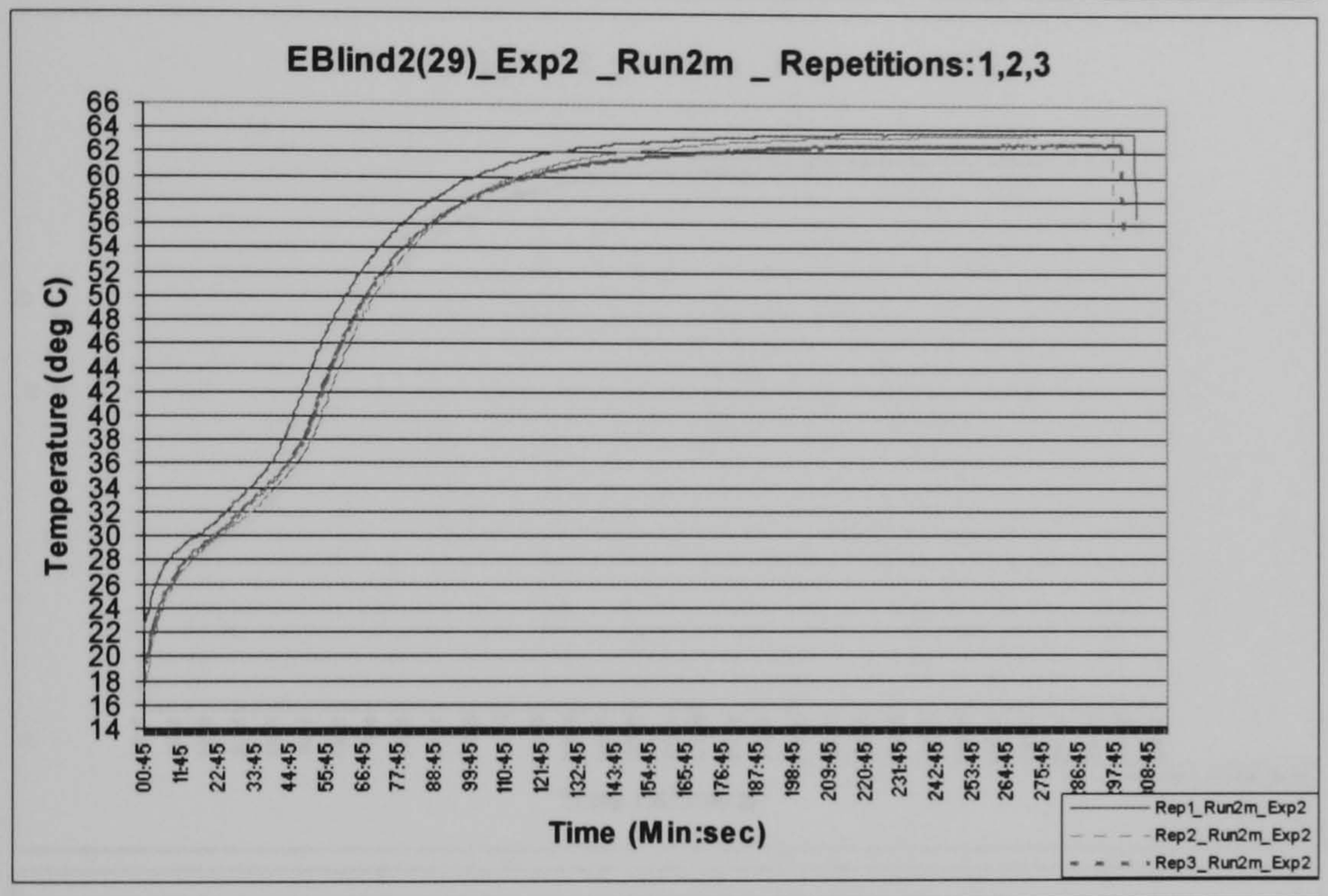
EBlind2(29)_Exp2 _Run2m _ Repetitions:1,2,3
Temperature (deg C)
Time (Min:sec)
Rep1_Run2m_Exp2
Rep2_Run2m_Exp2
Rep3_Run2m_Exp2

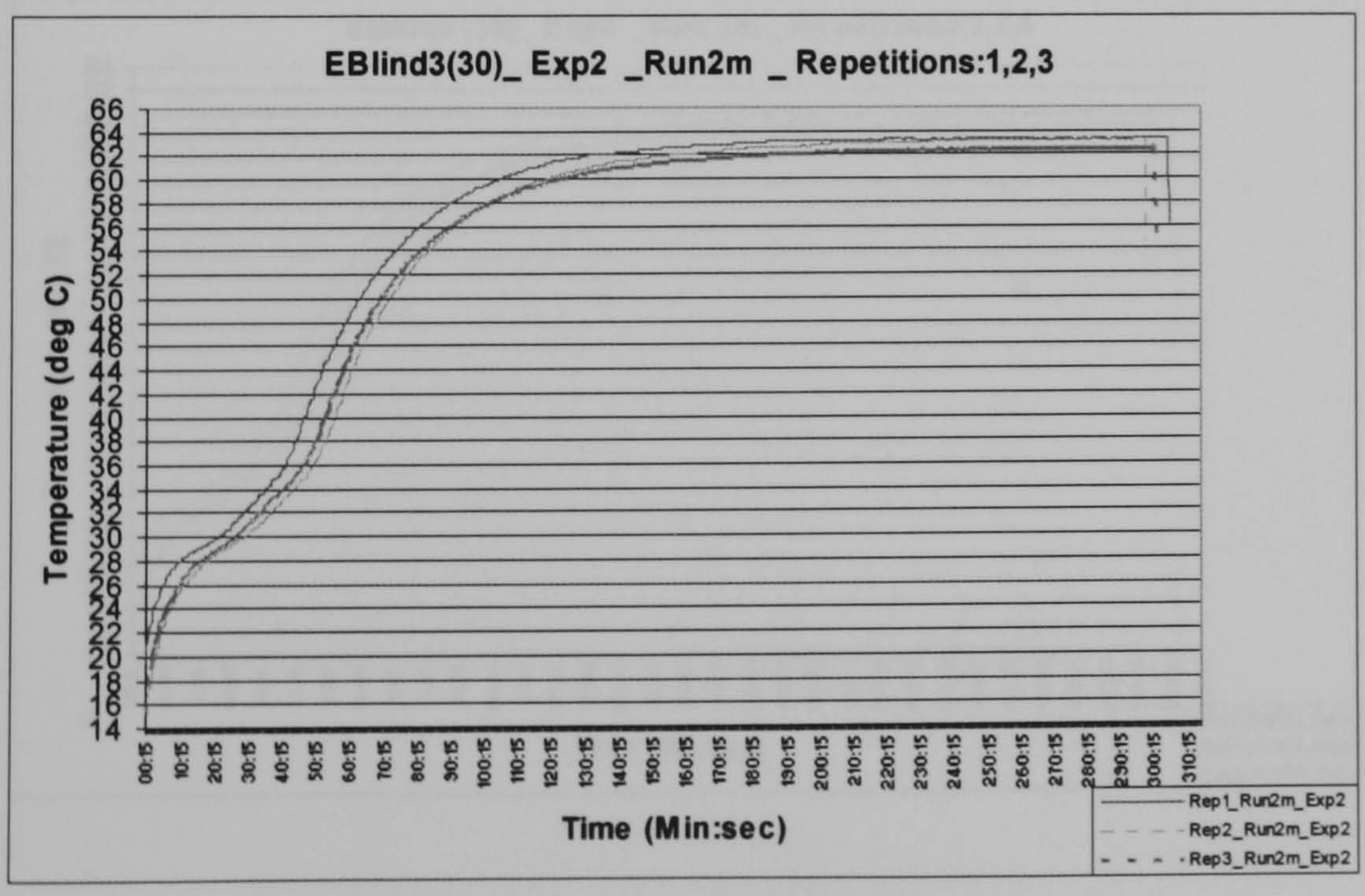
EBlind3(30)_ Exp2 _Run2m _ Repetitions:1,2,3
Temperature (deg C)
Time (Min:sec)
Rep1_Run2m_Exp2
Rep2_Run2m_Exp2
Rep3_Run2m_Exp2

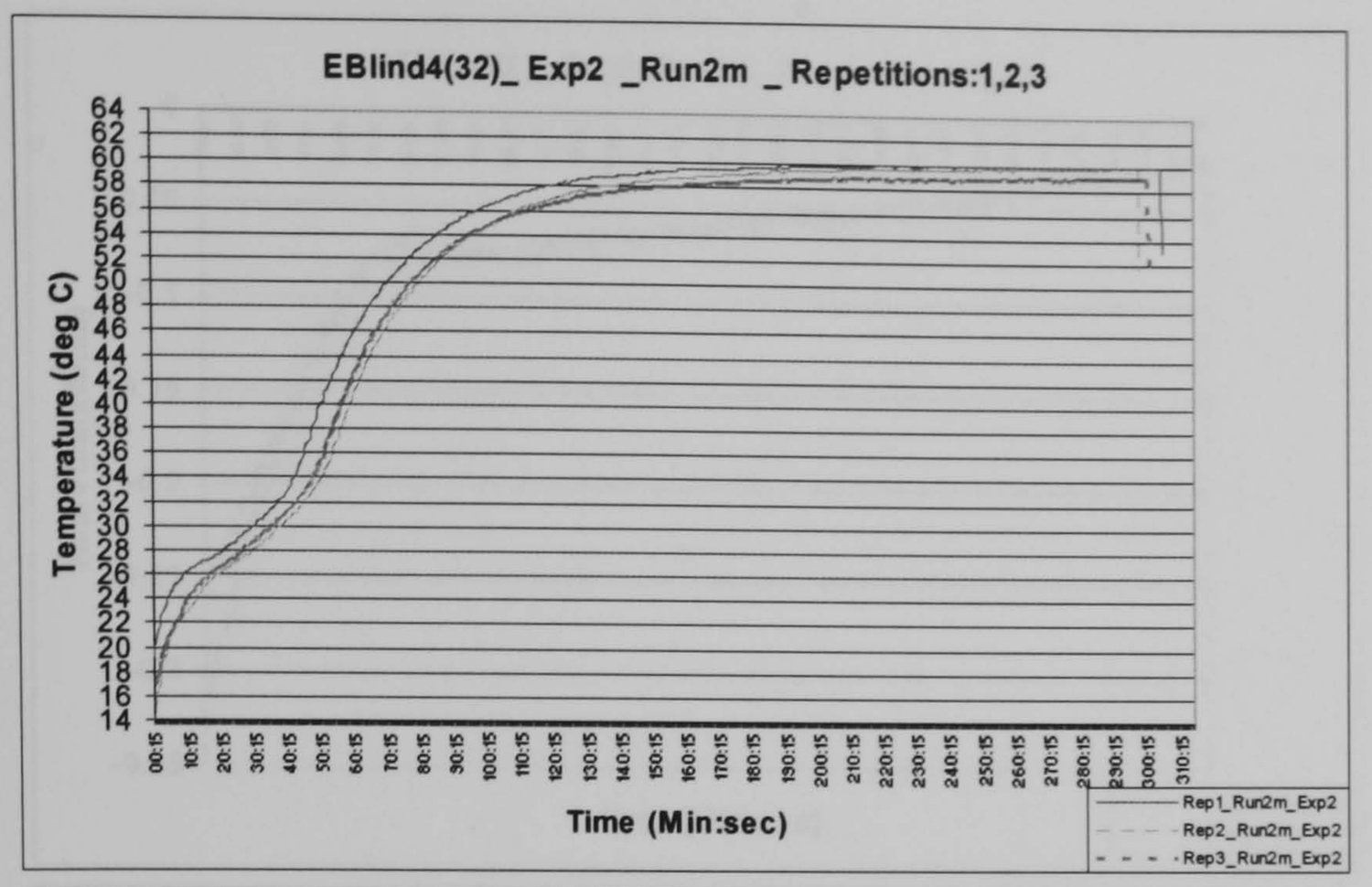
EBlind4(32)_ Exp2 _Run2m _ Repetitions:1,2,3
Temperature (deg C)
Time (Min:sec)
Rep1_Run2m_Exp2
Rep2_Run2m_Exp2
Rep3_Run2m_Exp2

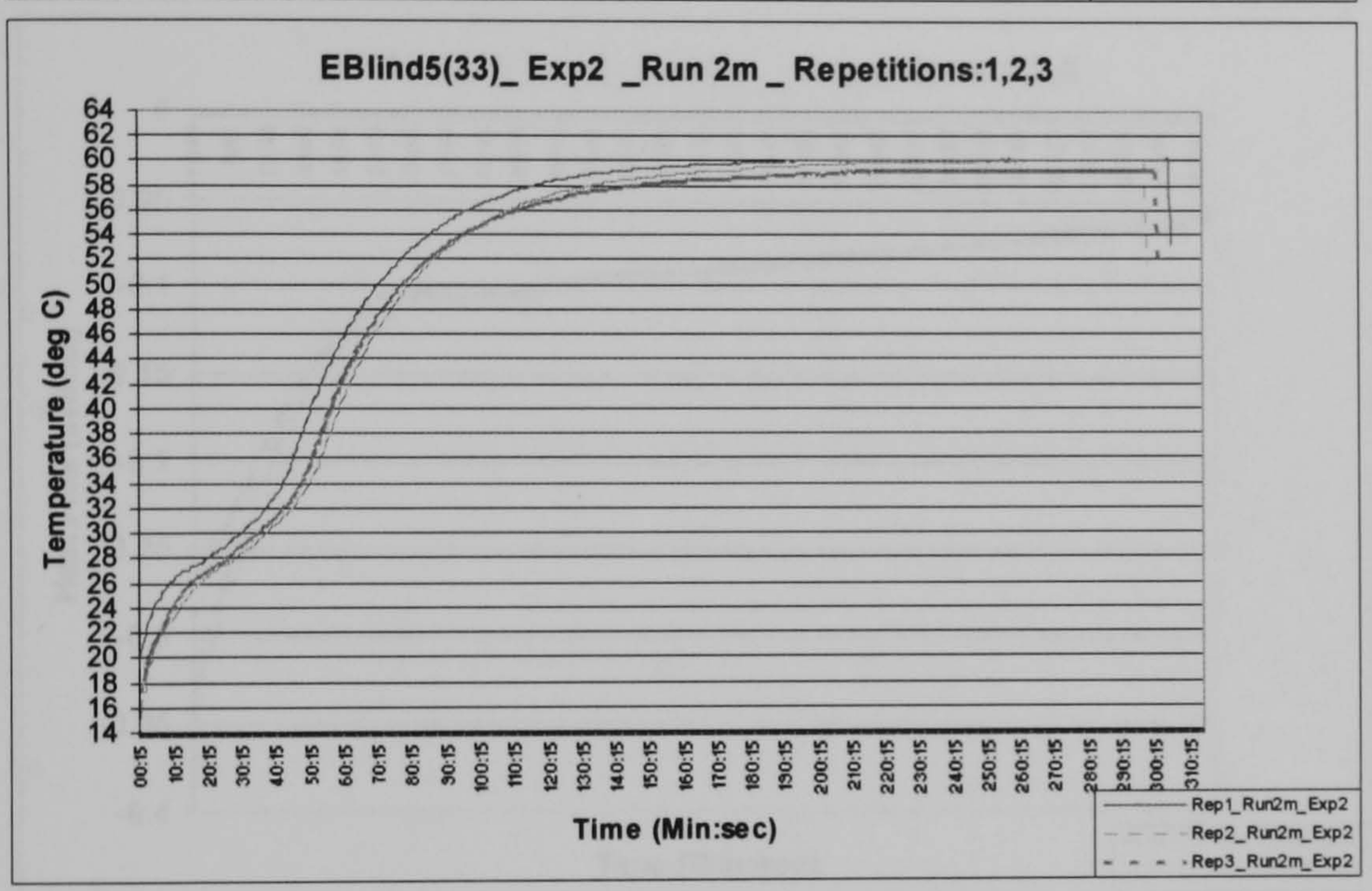
EBlind5(33)_ Exp2 _Run 2m _ Repetitions:1,2,3
Temperature (deg C)
Time (Min:sec)
Rep1_Run2m_Exp2
Rep2_Run2m_Exp2
Rep3_Run2m_Exp2

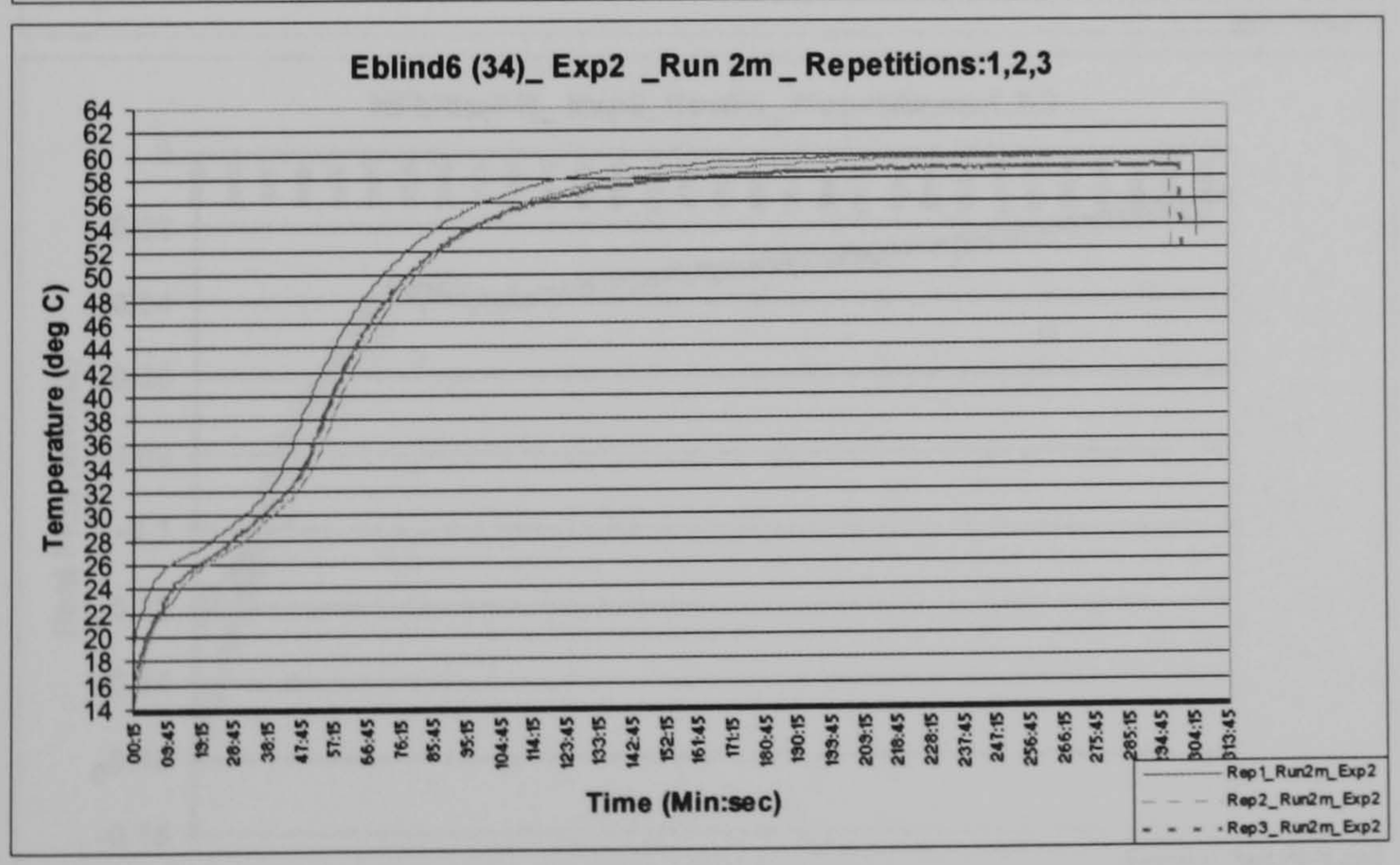
Eblind6 (34)_ Exp2 _Run 2m _ Repetitions:1,2,3
Temperature (deg C)
Time (Min:sec)
Rep1_Run2m_Exp2
Rep2_Run2m_Exp2
Rep3_Run2m_Exp2

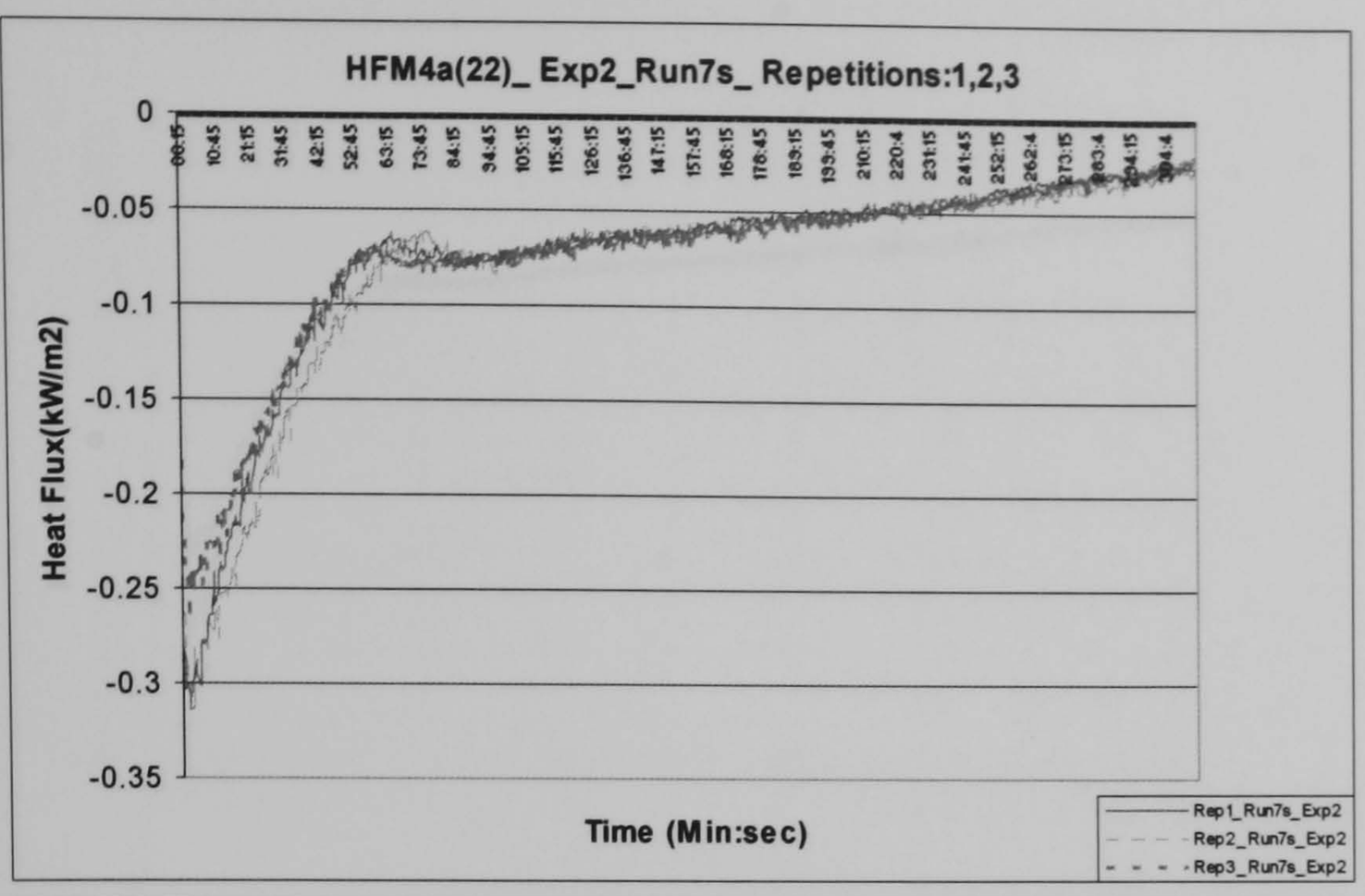
HFM4a(22)_ Exp2_Run7s_ Repetitions:1,2,3
Heat Flux(kW/m2)
0
-0.05
-0.1
-0.15
-0.2
-0.25
-0.3
-0.35
00:15
10:45
21:15
31:45
42:15
52:45
63:15
73:45
84:15
94:45
105:15
115:45
126:15
136:45
147:15
157:45
168:15
178:45
189:15
199:45
210:15
220:4
231:15
241:45
252:15
262:4
273:15
283:4
294:15
304:4
Time (Min:sec)
Rep1_Run7s_Exp2
Rep2_Run7s_Exp2
Rep3_Run7s_Exp2

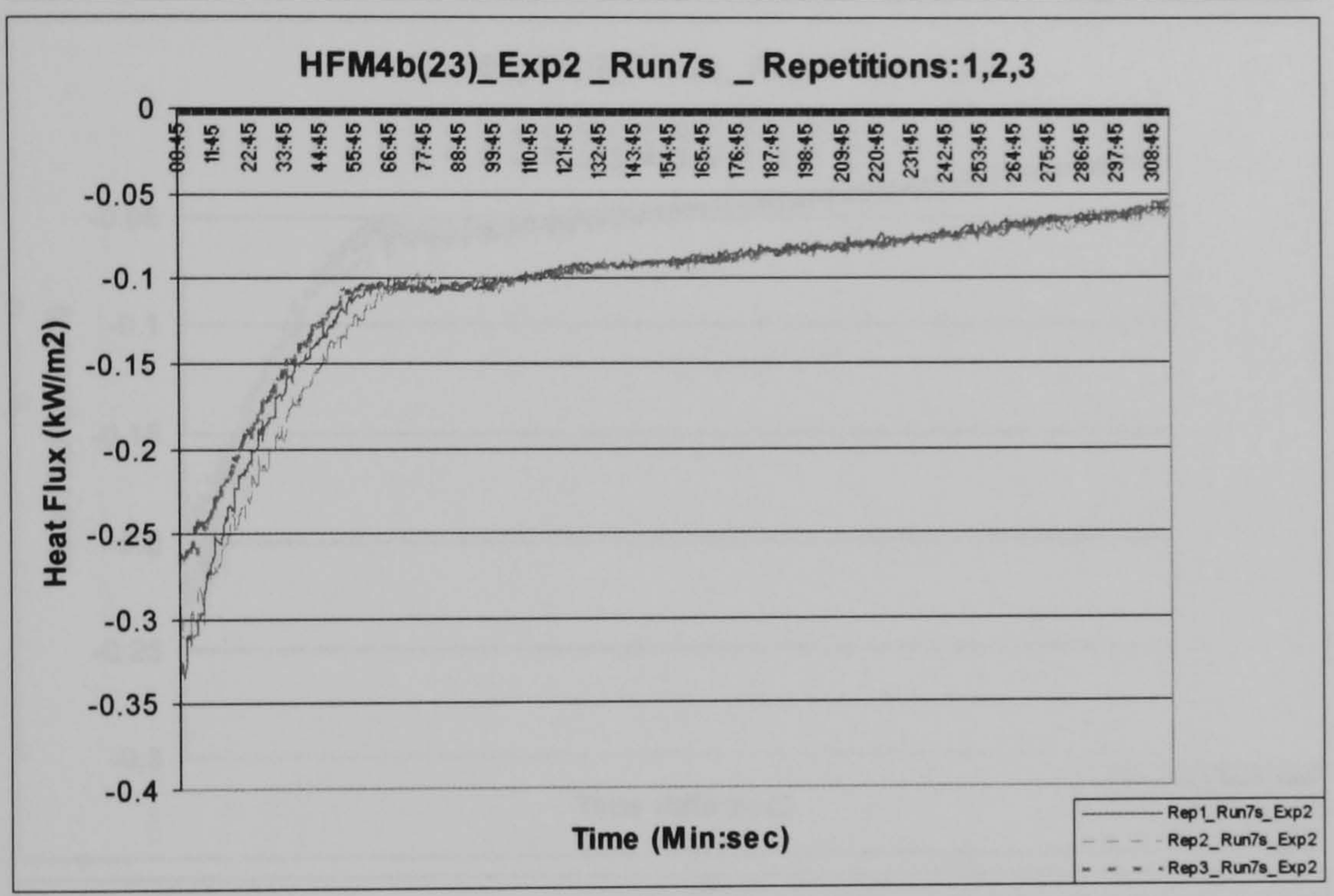
HFM4b(23)_Exp2 _Run7s _ Repetitions:1,2,3
Heat Flux (kW/m2)
0
-0.05
-0.1
-0.15
-0.2
-0.25
-0.3
-0.35
-0.4
00:45
11:45
22:45
33:45
44:45
55:45
66:45
77:45
88:45
99:45
110:45
121:45
132:45
143:45
154:45
165:45
176:45
187:45
198:45
209:45
220:45
231:45
242:45
253:45
264:45
275:45
286:45
297:45
308:45
Time (Min:sec)
Rep1_Run7s_Exp2
Rep2_Run7s_Exp2
Rep3_Run7s_Exp2

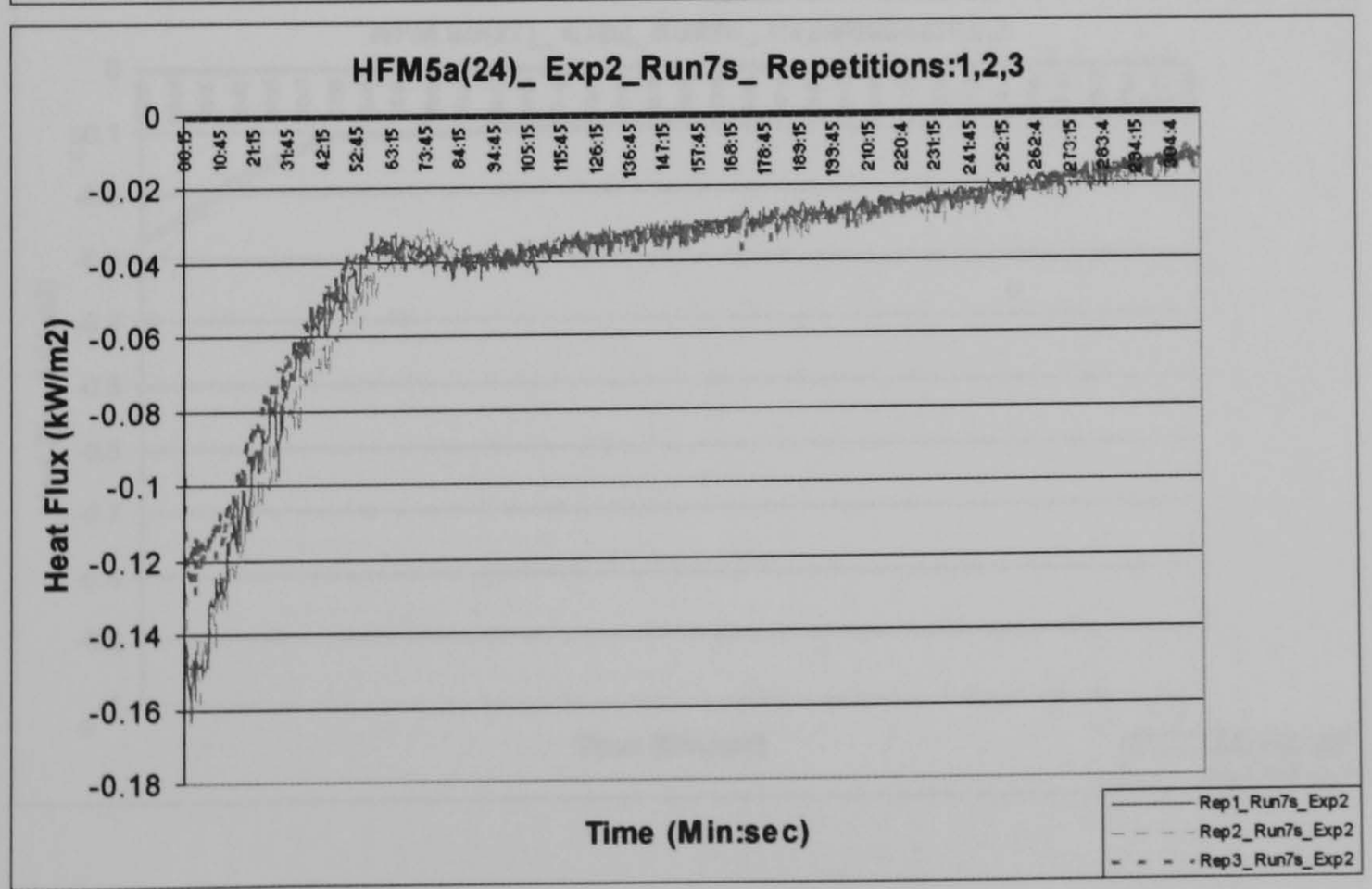
HFM5a(24)_ Exp2_Run7s_ Repetitions:1,2,3
Heat Flux (kW/m2)
0
-0.02
-0.04
-0.06
-0.08
-0.1
-0.12
-0.14
-0.16
-0.18
00:15
10:45
21:15
31:45
42:15
52:45
63:15
73:45
84:15
94:45
105:15
115:45
126:15
136:45
147:15
157:45
168:15
178:45
189:15
199:45
210:15
220:4
231:15
241:45
252:15
262:4
273:15
283:4
294:15
304:4
Time (Min:sec)
Rep1_Run7s_Exp2
Rep2_Run7s_Exp2
Rep3_Run7s_Exp2

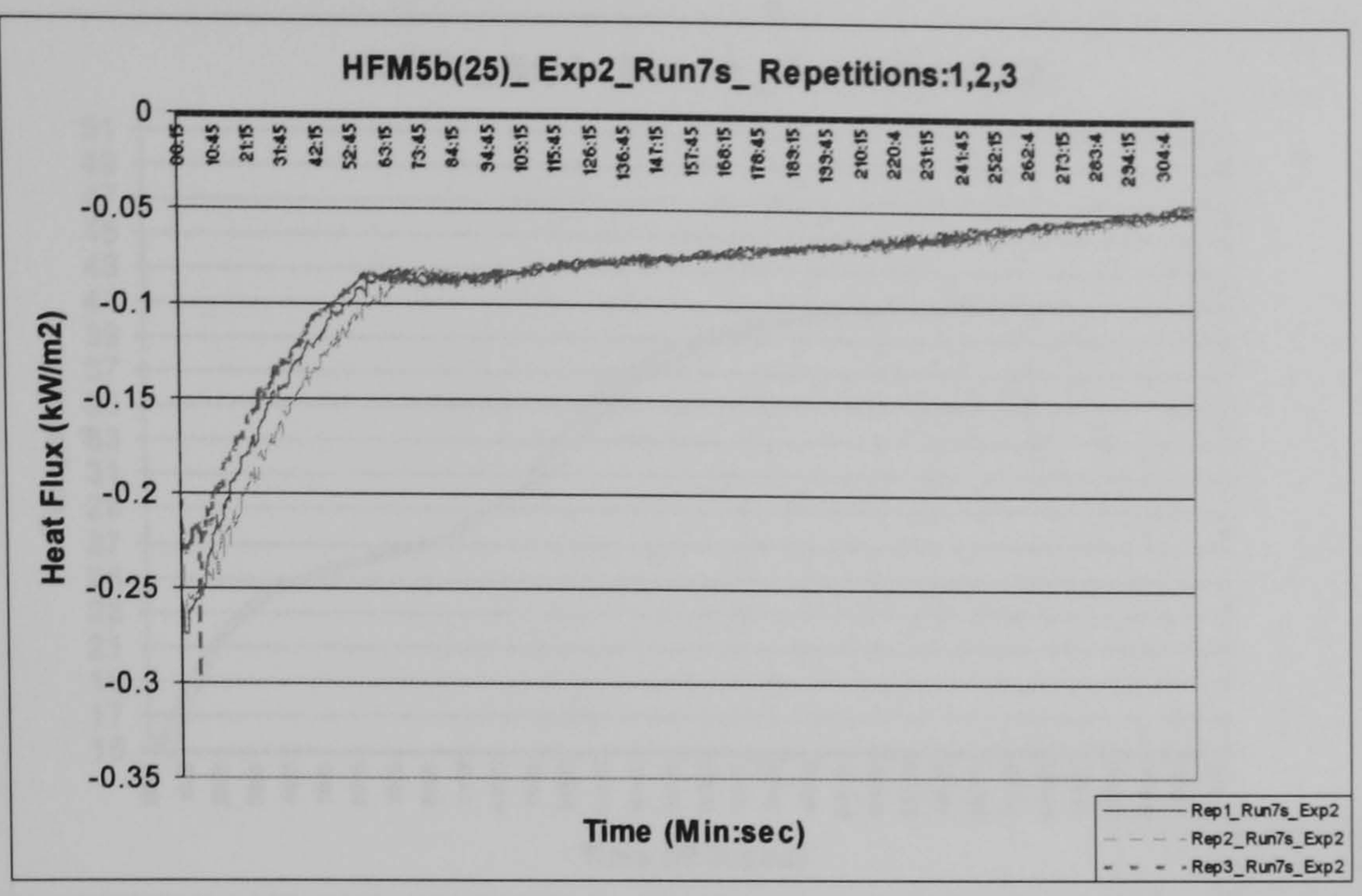
HFM5b(25)_ Exp2_Run7s_ Repetitions:1,2,3
Heat Flux (kW/m2)
0
-0.05
-0.1
-0.15
-0.2
-0.25
-0.3
-0.35
00:15
10:45
21:15
31:45
42:15
52:45
63:15
73:45
84:15
94:45
105:15
115:45
126:15
136:45
147:15
157:45
168:15
178:45
189:15
199:45
210:15
220:4
231:15
241:45
252:15
262:4
273:15
283:4
294:15
304:4
Time (Min:sec)
Rep1_Run7s_Exp2
Rep2_Run7s_Exp2
Rep3_Run7s_Exp2

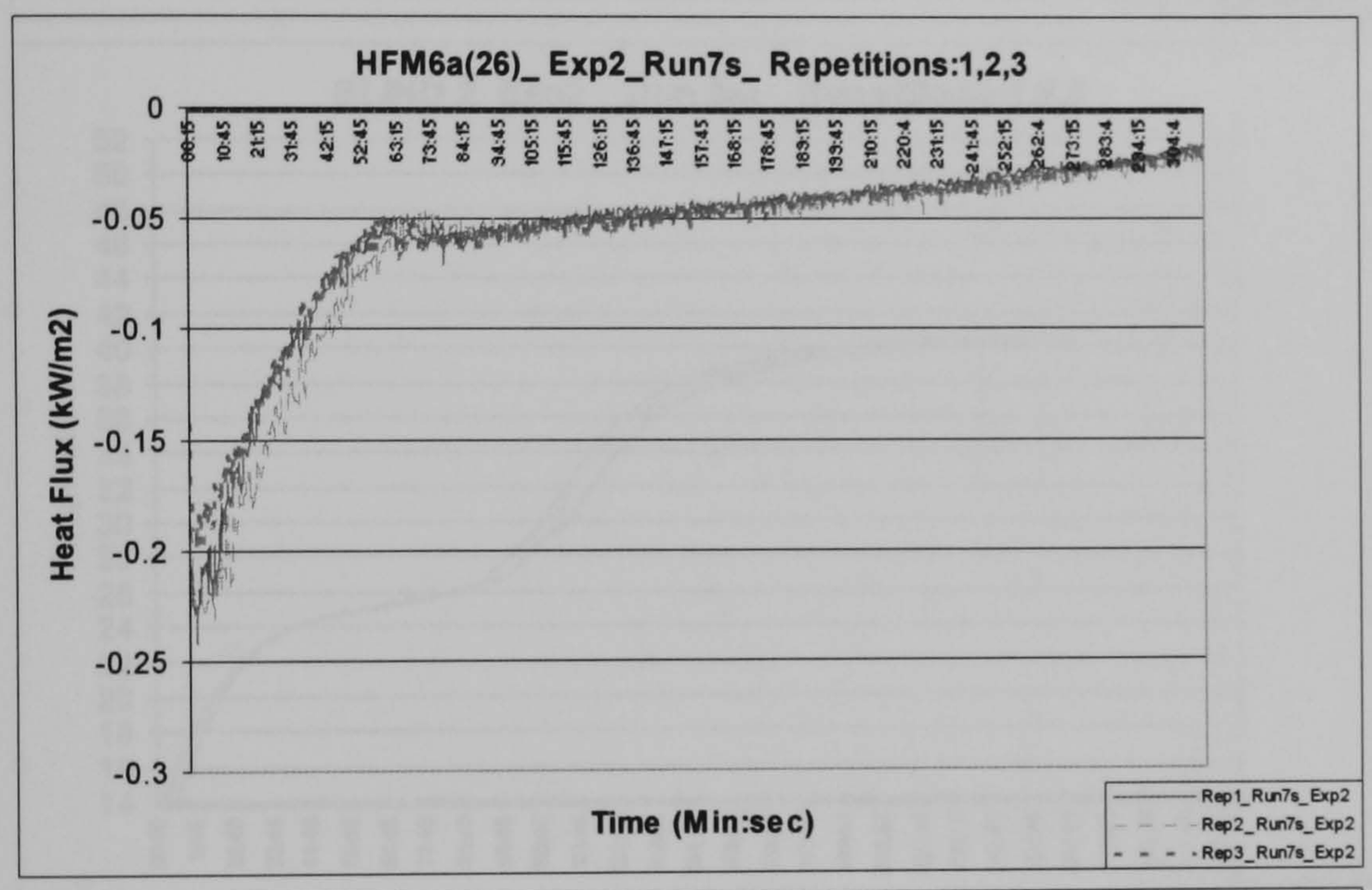
HFM6a(26)_ Exp2_Run7s_ Repetitions:1,2,3
Heat Flux (kW/m2)
0
-0.05
-0.1
-0.15
-0.2
-0.25
-0.3
00:15
10:45
21:15
31:45
42:15
52:45
63:15
73:45
84:15
94:45
105:15
115:45
126:15
136:45
147:15
157:45
168:15
178:45
189:15
199:45
210:15
220:4
231:15
241:45
252:15
262:4
273:15
283:4
294:15
304:4
Time (Min:sec)
Rep1_Run7s_Exp2
Rep2_Run7s_Exp2
Rep3_Run7s_Exp2

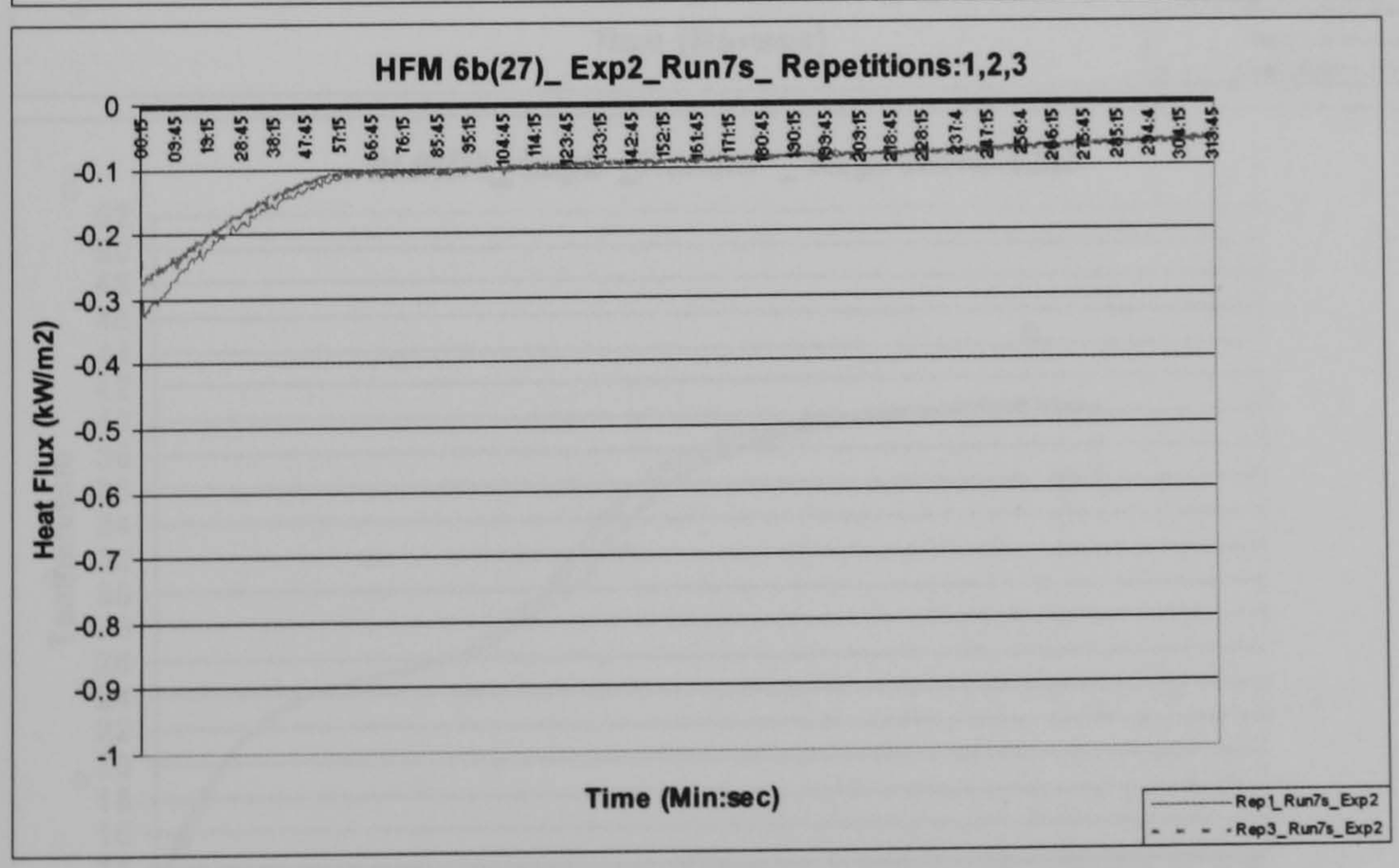
HFM 6b(27)_ Exp2_Run7s_ Repetitions:1,2,3
Heat Flux (kW/m2)
0
-0.1
-0.2
-0.3
-0.4
-0.5
-0.6
-0.7
-0.8
-0.9
-1
00:15
09:45
19:15
28:45
38:15
47:45
57:15
66:45
76:15
85:45
95:15
104:45
114:15
123:45
133:15
142:45
152:15
161:45
171:15
180:45
190:15
199:45
209:15
218:45
228:15
237:4
247:15
256:4
266:15
275:45
285:15
294:4
304:15
313:45
Time (Min:sec)
Rep1_Run7s_Exp2
Rep3_Run7s_Exp2

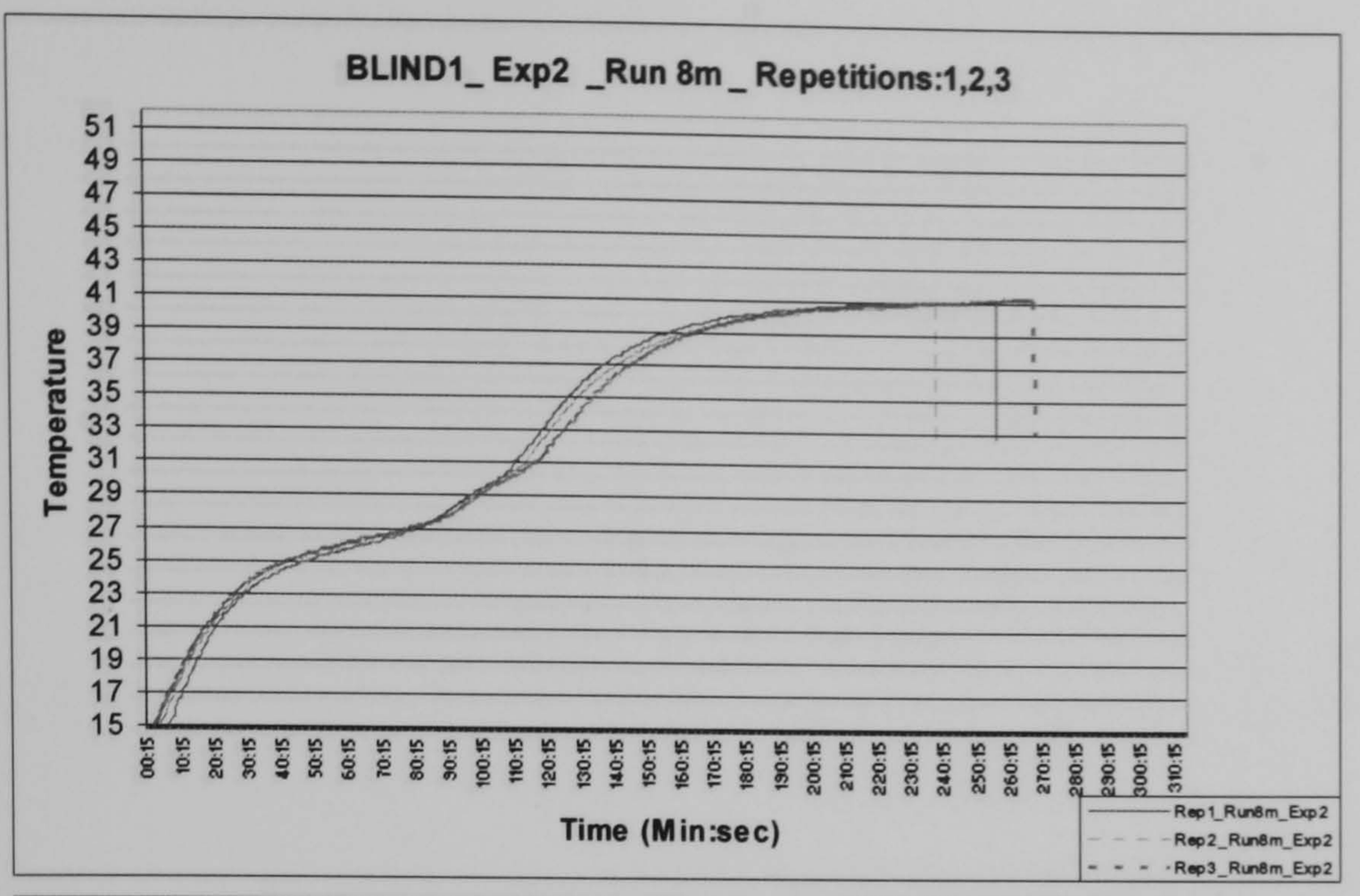
BLIND1_ Exp2 _Run 8m _ Repetitions:1,2,3
Temperature
Time (Min:sec)
Rep1_Run8m_Exp2
Rep2_Run8m_Exp2
Rep3_Run8m_Exp2

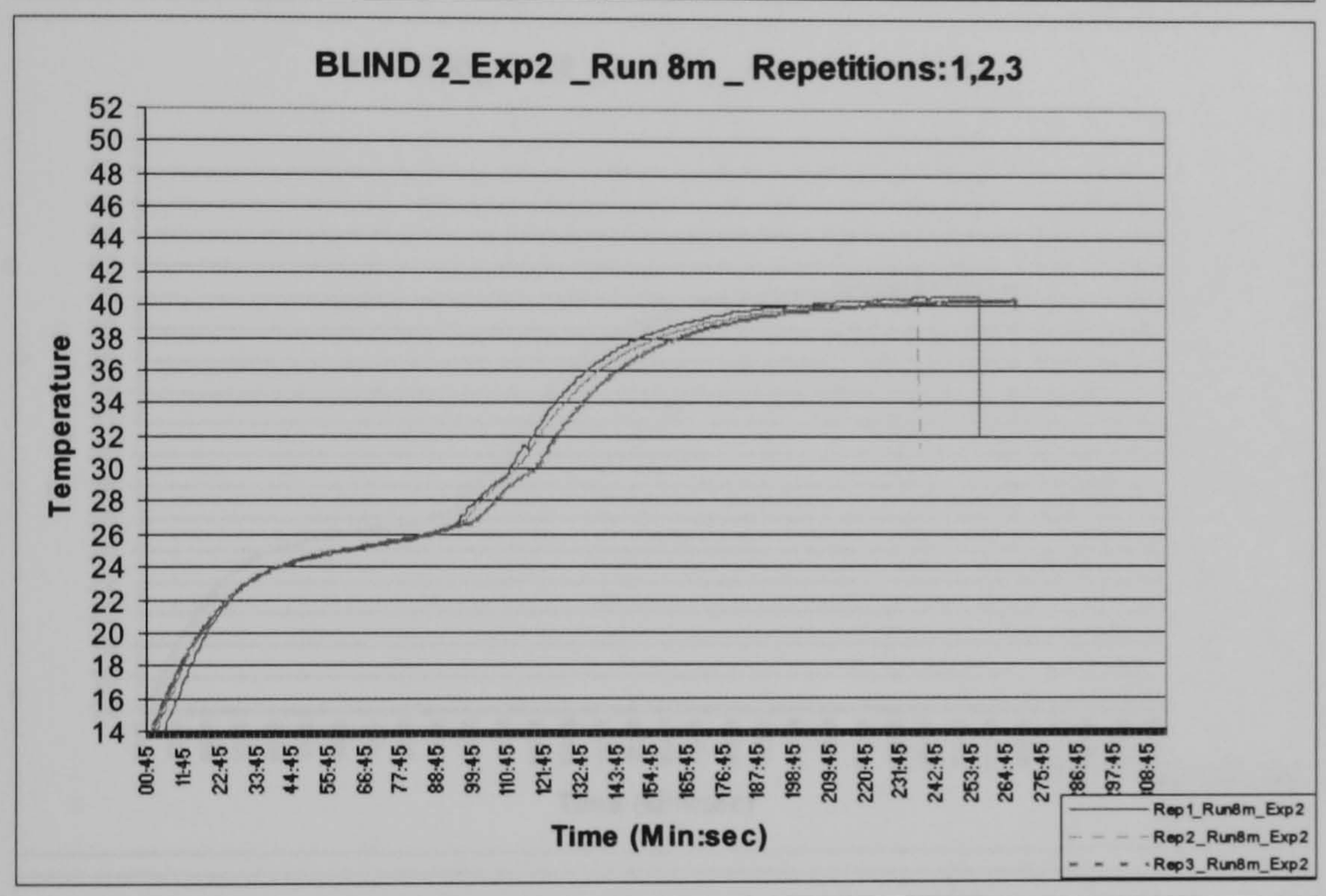
BLIND 2_Exp2 _Run 8m _ Repetitions:1,2,3
Temperature
Time (Min:sec)
Rep1_Run8m_Exp2
Rep2_Run8m_Exp2
Rep3_Run8m_Exp2

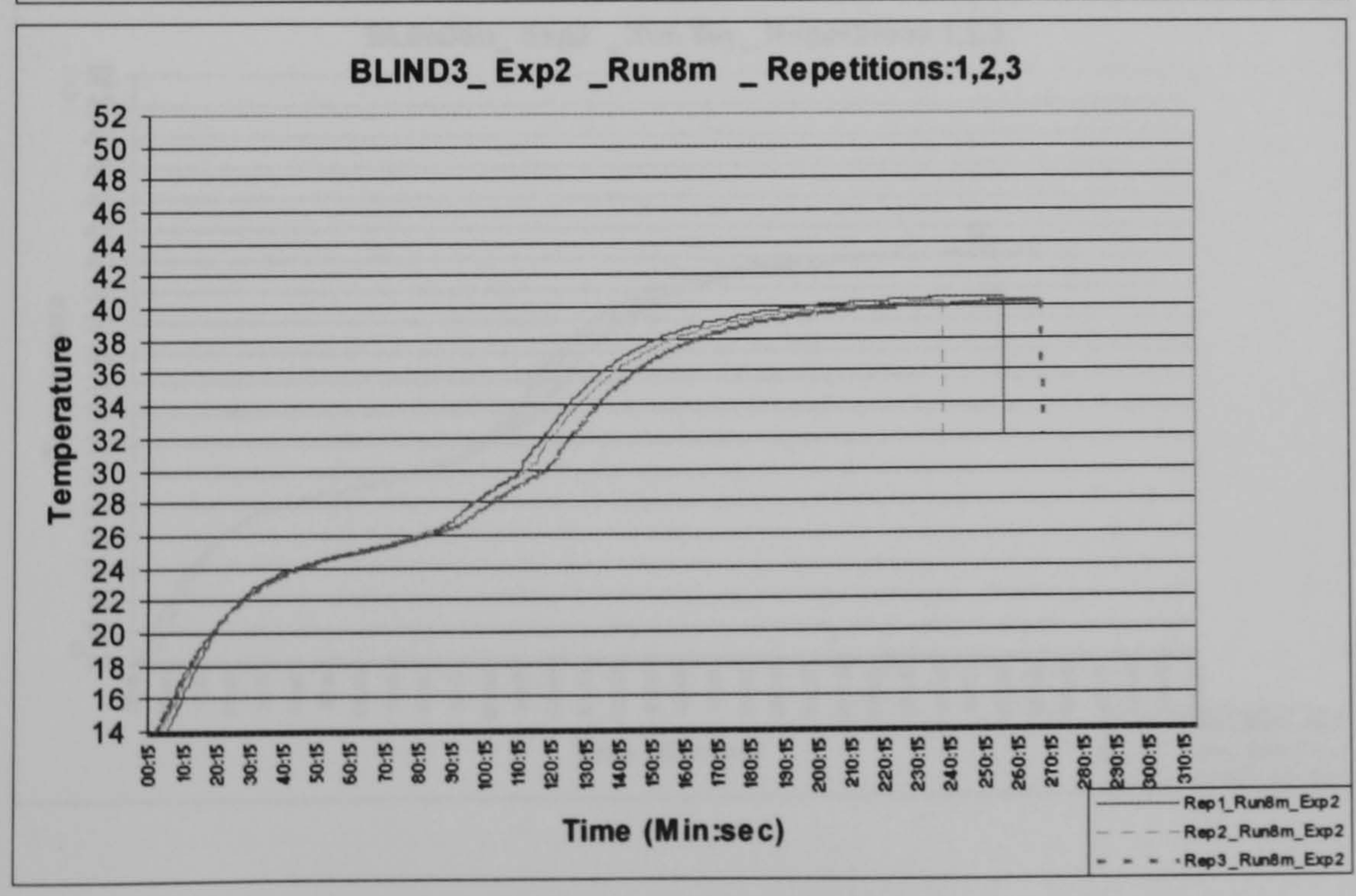
BLIND3_ Exp2 _Run8m _ Repetitions:1,2,3
Temperature
Time (Min:sec)
Rep1_Run8m_Exp2
Rep2_Run8m_Exp2
Rep3_Run8m_Exp2

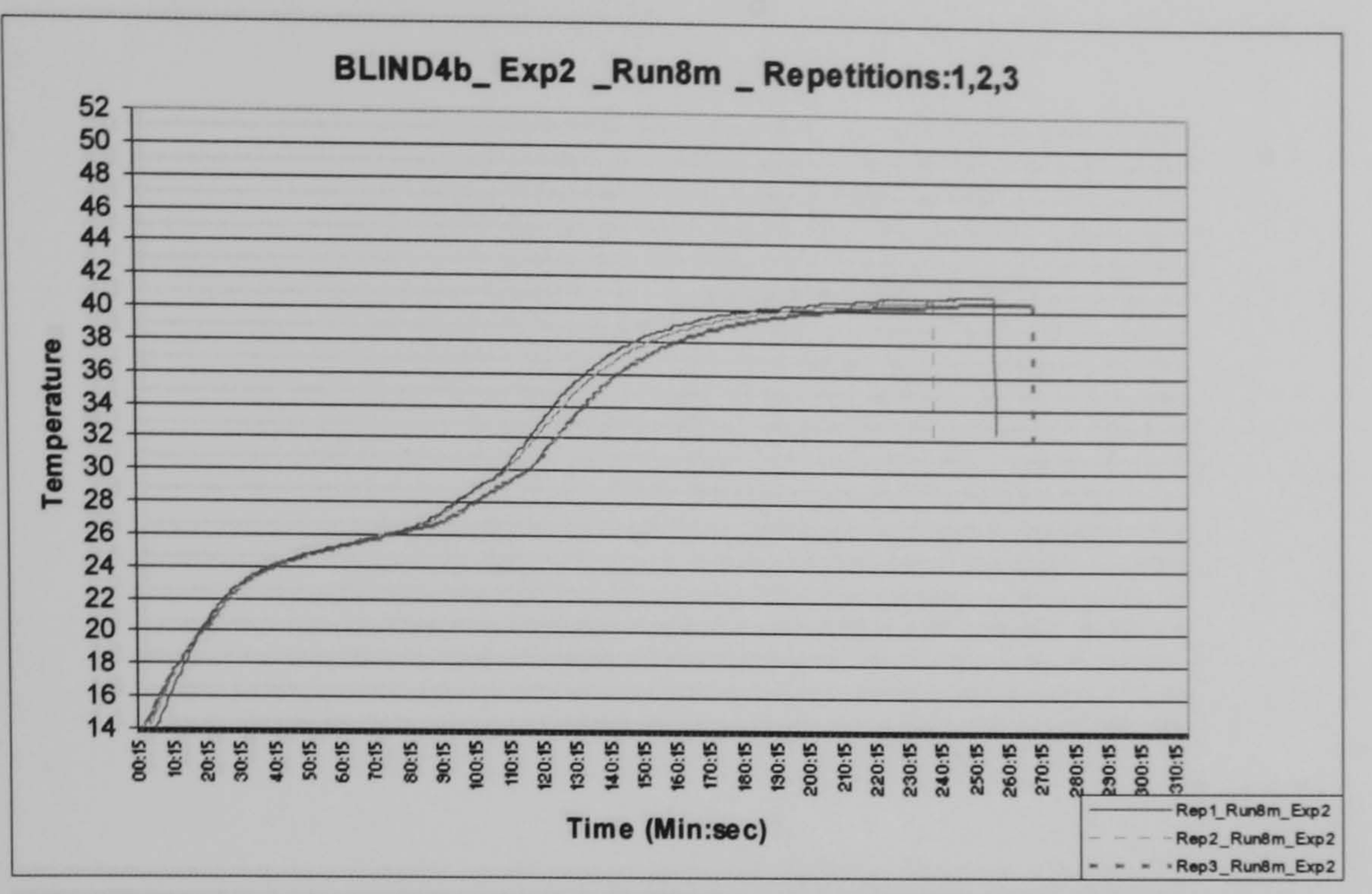
BLIND4b_ Exp2 _Run8m _ Repetitions:1,2,3
Temperature
Time (Min:sec)
Rep1_Run8m_Exp2
Rep2_Run8m_Exp2
Rep3_Run8m_Exp2

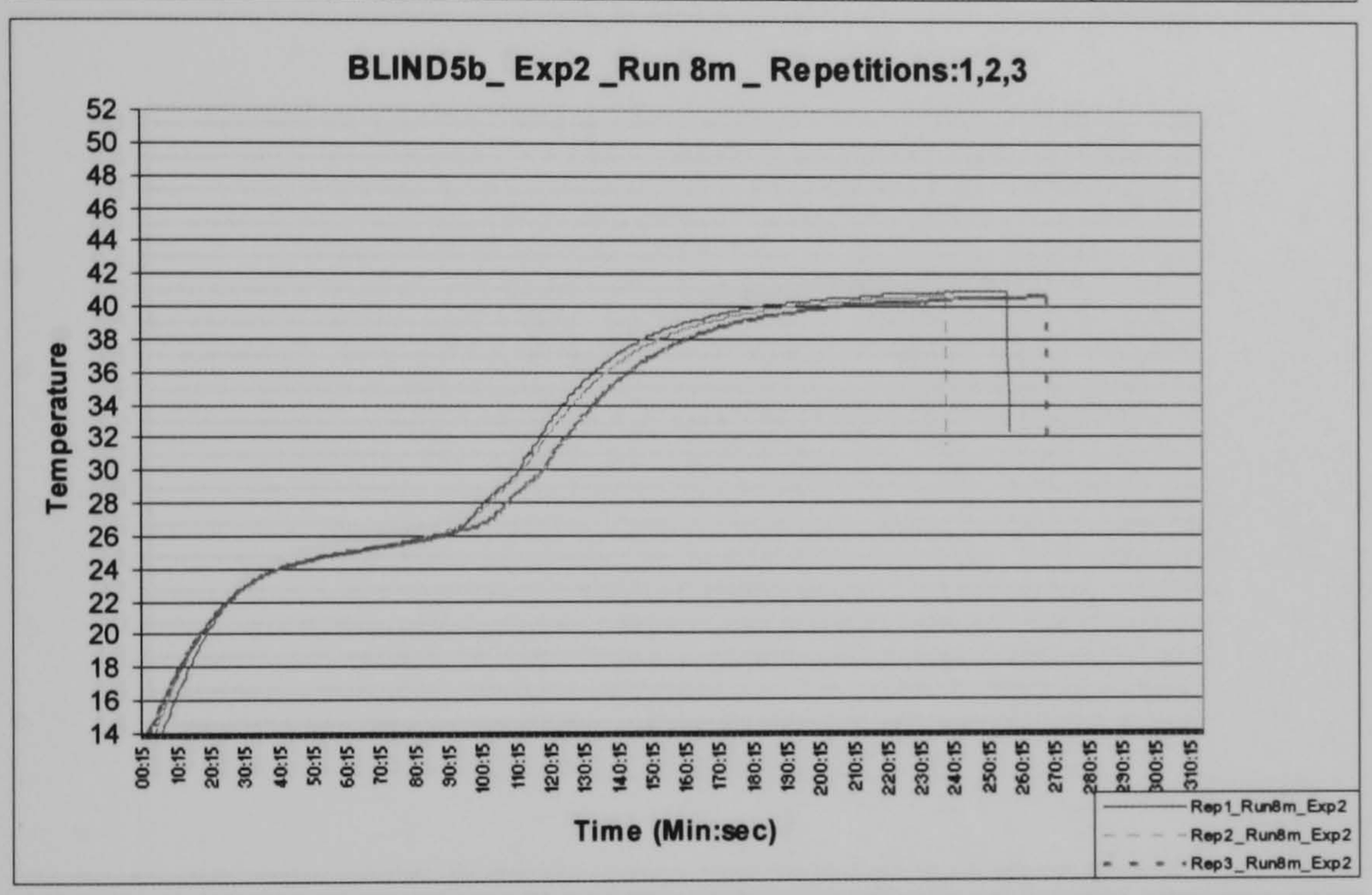
BLIND5b_ Exp2 _Run 8m _ Repetitions:1,2,3
Temperature
Time (Min:sec)
Rep1_Run8m_Exp2
Rep2_Run8m_Exp2
Rep3_Run8m_Exp2

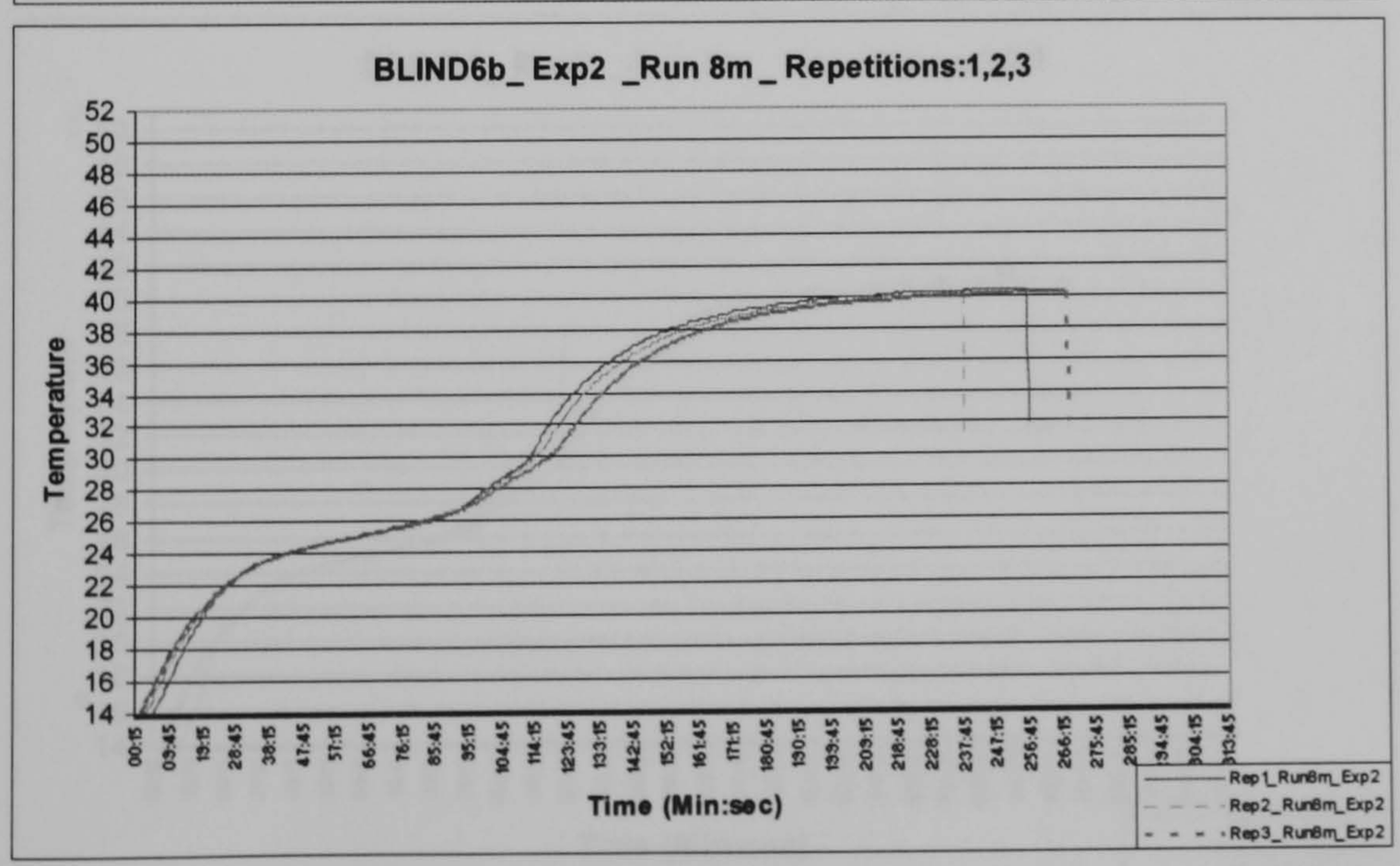
BLIND6b_ Exp2 _Run 8m _ Repetitions:1,2,3
Temperature
Time (Min:sec)
Rep1_Run8m_Exp2
Rep2_Run8m_Exp2
Rep3_Run8m_Exp2

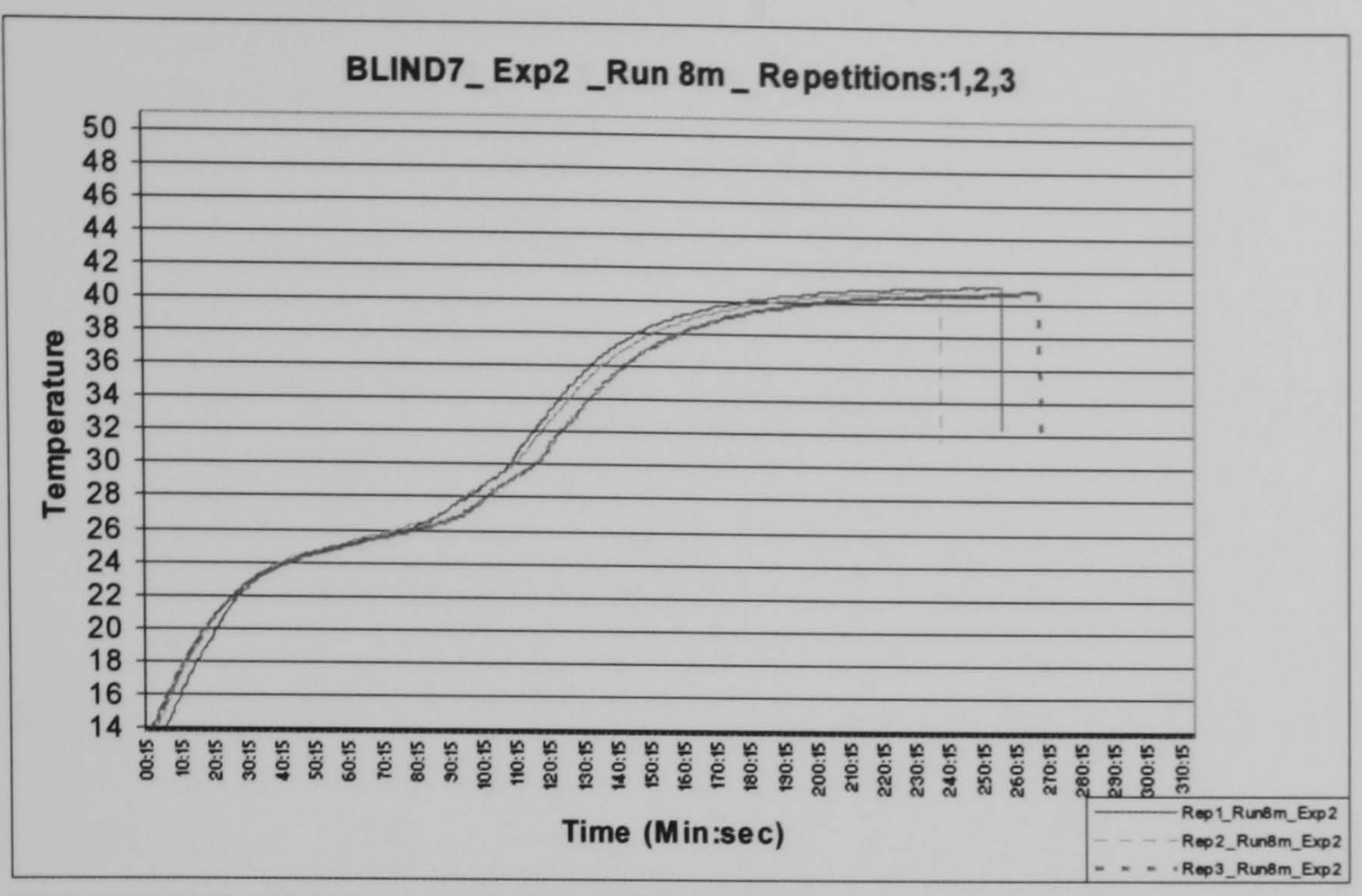
BLIND7_ Exp2 _Run 8m _ Repetitions:1,2,3
Temperature
50
48
46
44
42
40
38
36
34
32
30
28
26
24
22
20
18
16
14
00:15
10:15
20:15
30:15
40:15
50:15
60:15
70:15
80:15
90:15
100:15
110:15
120:15
130:15
140:15
150:15
160:15
170:15
180:15
190:15
200:15
210:15
220:15
230:15
240:15
250:15
260:15
270:15
280:15
290:15
300:15
310:15
Time (Min:sec)
Rep1_Run8m_Exp2
Rep2_Run8m_Exp2
Rep3_Run8m_Exp2

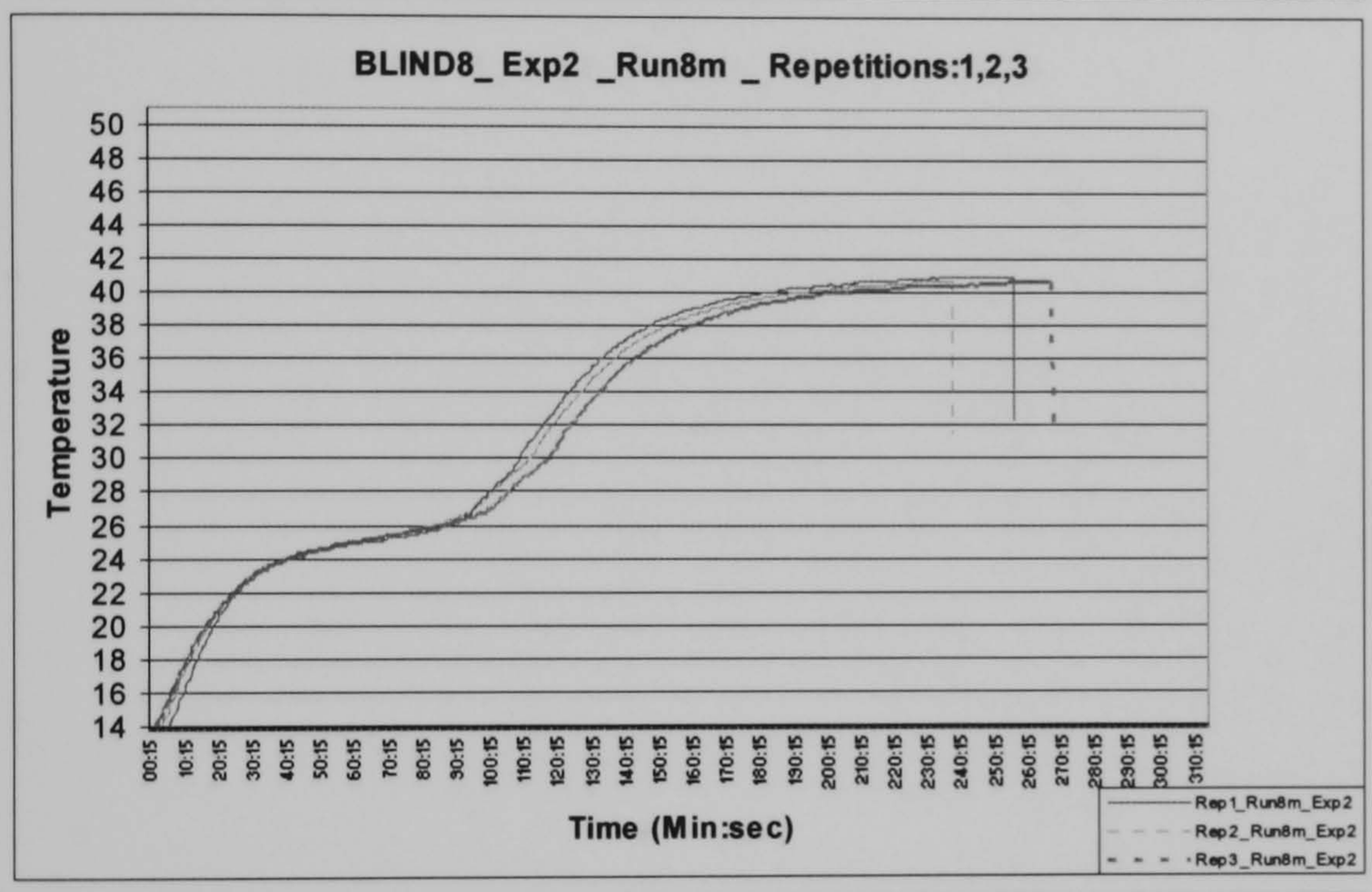
BLIND8_ Exp2 _Run8m _ Repetitions:1,2,3
Temperature
50
48
46
44
42
40
38
36
34
32
30
28
26
24
22
20
18
16
14
00:15
10:15
20:15
30:15
40:15
50:15
60:15
70:15
80:15
90:15
100:15
110:15
120:15
130:15
140:15
150:15
160:15
170:15
180:15
190:15
200:15
210:15
220:15
230:15
240:15
250:15
260:15
270:15
280:15
290:15
300:15
310:15
Time (Min:sec)
Rep1_Run8m_Exp2
Rep2_Run8m_Exp2
Rep3_Run8m_Exp2

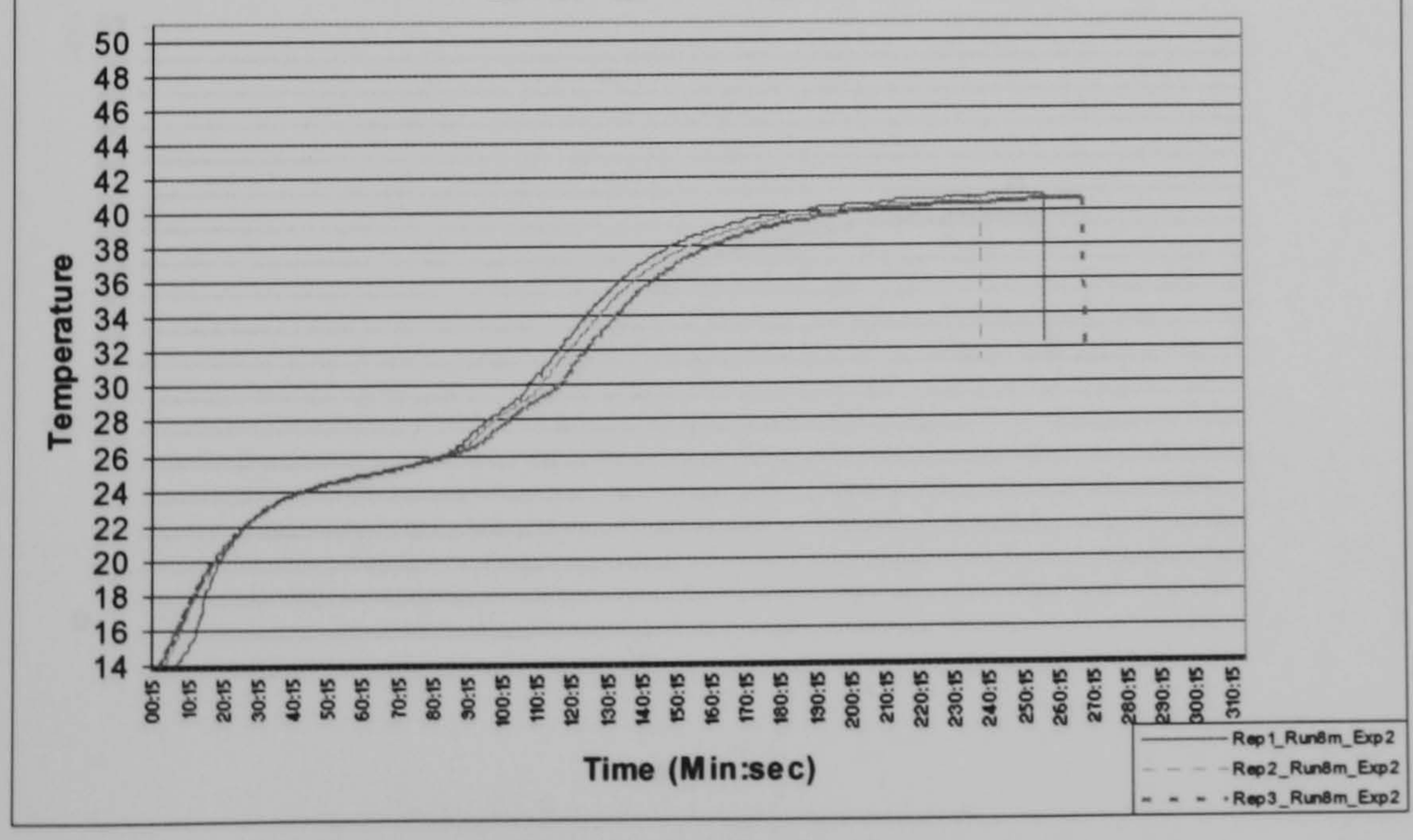
BLIND9_ Exp2 _Run 8m _ Repetitions:1,2,3
Temperature
50
48
46
44
42
40
38
36
34
32
30
28
26
24
22
20
18
16
14
00:15
10:15
20:15
30:15
40:15
50:15
60:15
70:15
80:15
90:15
100:15
110:15
120:15
130:15
140:15
150:15
160:15
170:15
180:15
190:15
200:15
210:15
220:15
230:15
240:15
250:15
260:15
270:15
280:15
290:15
300:15
310:15
Time (Min:sec)
Rep1_Run8m_Exp2
Rep2_Run8m_Exp2
Rep3_Run8m_Exp2

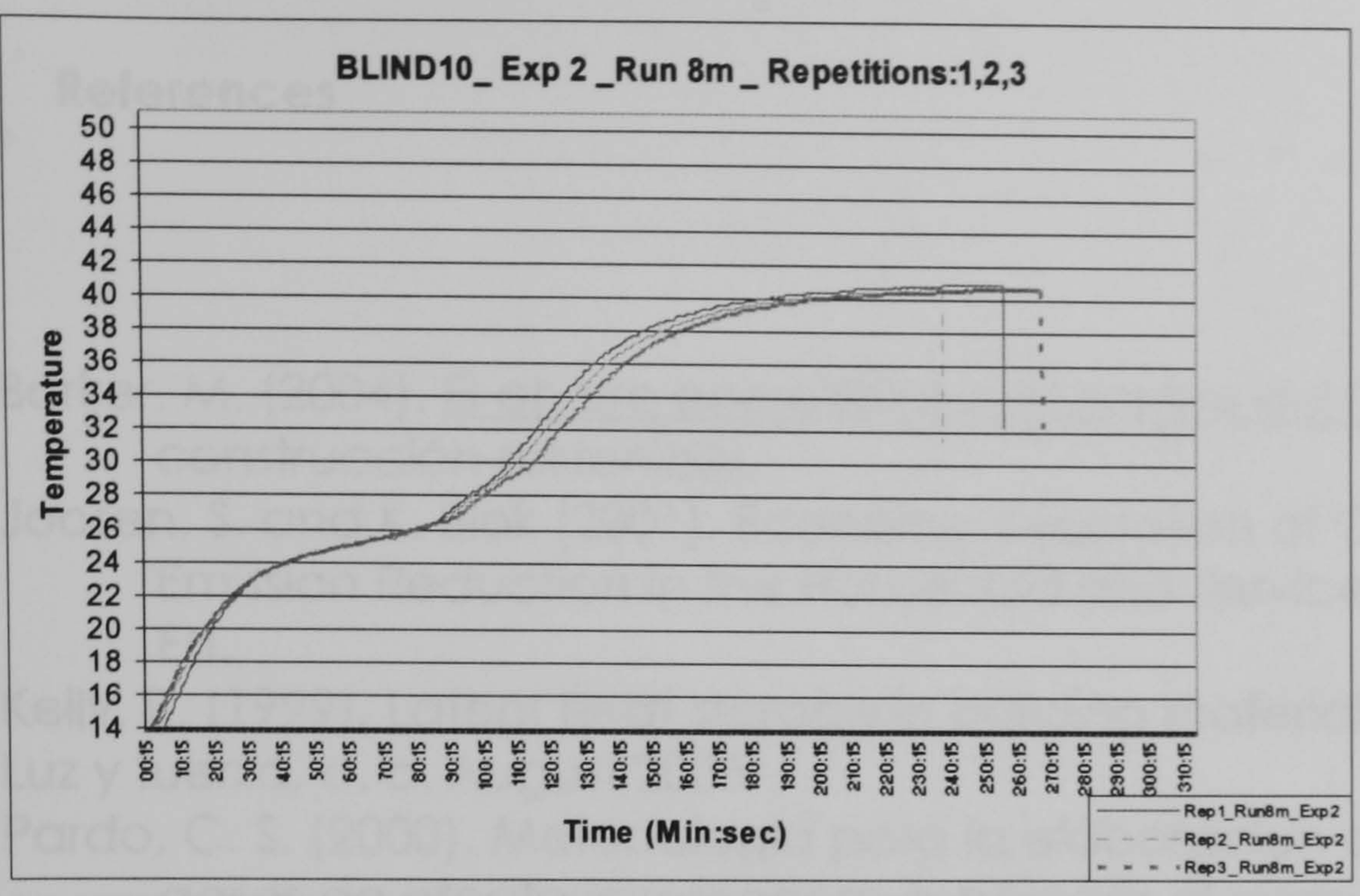
BLIND10_ Exp 2 _Run 8m _ Repetitions:1,2,3
Temperature
50
48
46
44
42
40
38
36
34
32
30
28
26
24
22
20
18
16
14
00:15
10:15
20:15
30:15
40:15
50:15
60:15
70:15
80:15
90:15
100:15
110:15
120:15
130:15
140:15
150:15
160:15
170:15
180:15
190:15
200:15
210:15
220:15
230:15
240:15
250:15
260:15
270:15
280:15
290:15
300:15
310:15
Time (Min:sec)
Rep1_Run8m_Exp2
Rep2_Run8m_Exp2
Rep3_Run8m_Exp2

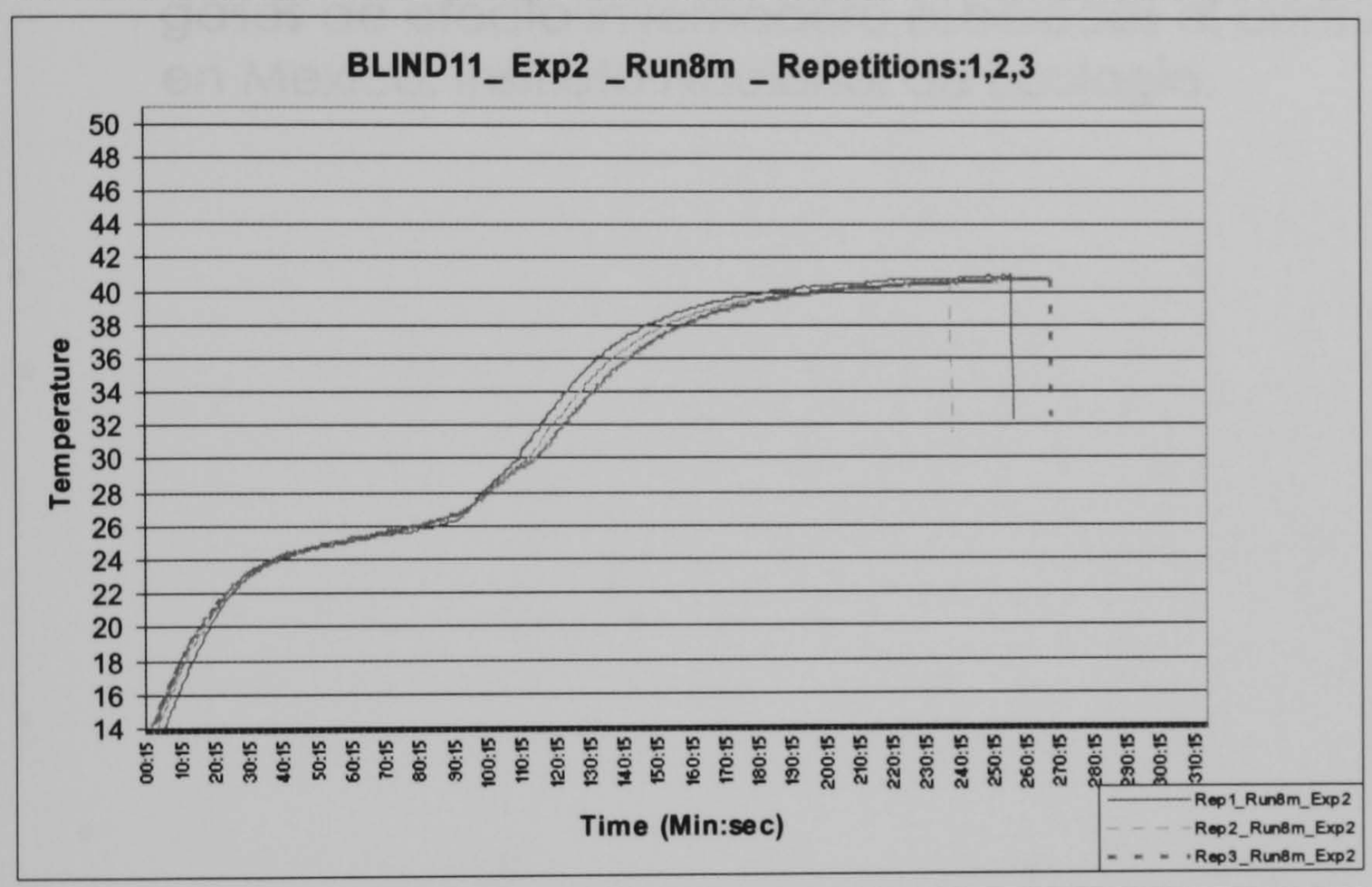
BLIND11_ Exp2 _Run8m _ Repetitions:1,2,3
Temperature
50
48
46
44
42
40
38
36
34
32
30
28
26
24
22
20
18
16
14
00:15
10:15
20:15
30:15
40:15
50:15
60:15
70:15
80:15
90:15
100:15
110:15
120:15
130:15
140:15
150:15
160:15
170:15
180:15
190:15
200:15
210:15
220:15
230:15
240:15
250:15
260:15
270:15
280:15
290:15
300:15
310:15
Time (Min:sec)
Rep1_Run8m_Exp2
Rep2_Run8m_Exp2
Rep3_Run8m_Exp2

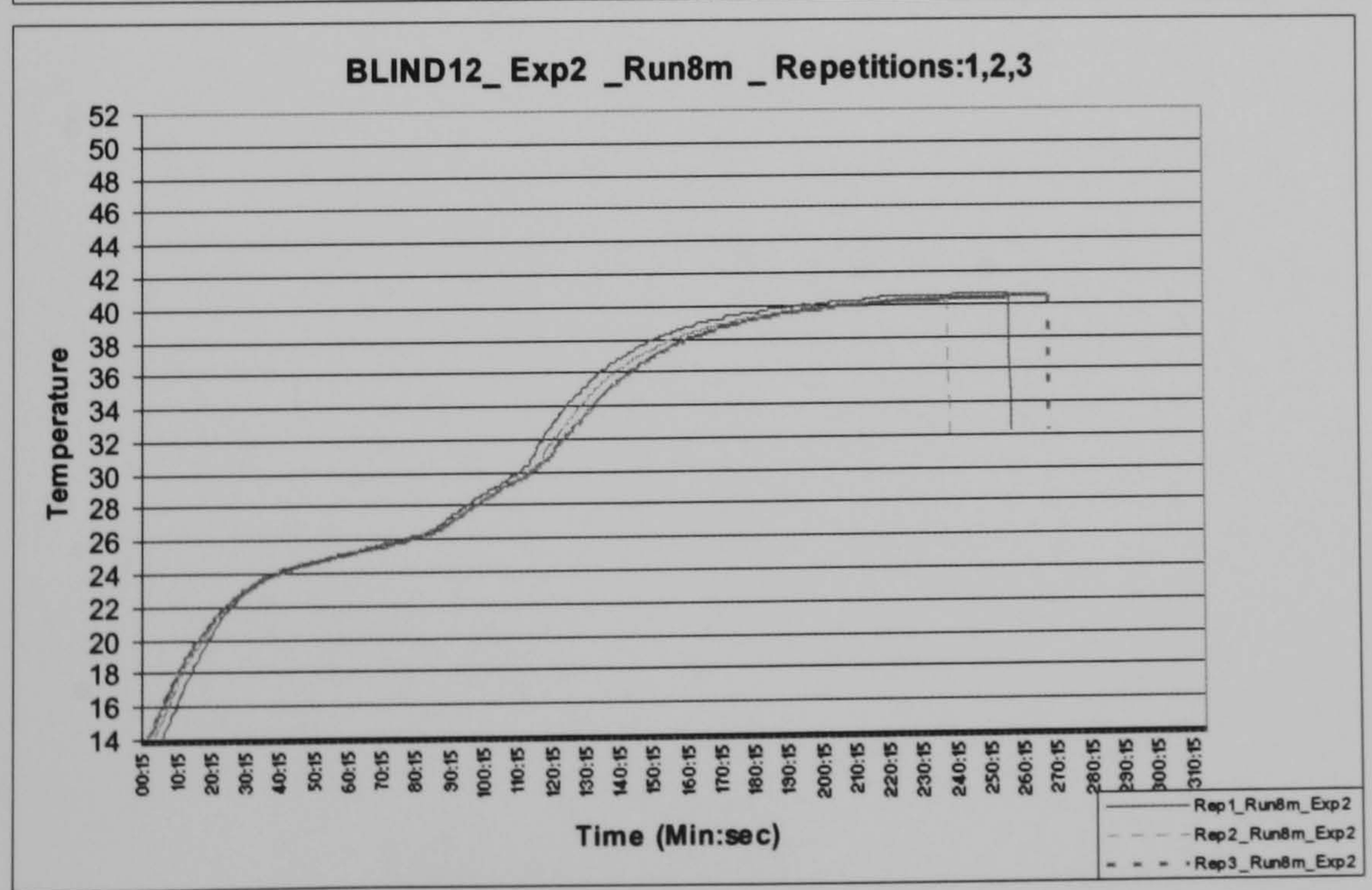
BLIND12_ Exp2 _Run8m _ Repetitions:1,2,3
Temperature
52
50
48
46
44
42
40
38
36
34
32
30
28
26
24
22
20
18
16
14
00:15
10:15
20:15
30:15
40:15
50:15
60:15
70:15
80:15
90:15
100:15
110:15
120:15
130:15
140:15
150:15
160:15
170:15
180:15
190:15
200:15
210:15
220:15
230:15
240:15
250:15
260:15
270:15
280:15
290:15
300:15
310:15
Time (Min:sec)
Rep1_Run8m_Exp2
Rep2_Run8m_Exp2
Rep3_Run8m_Exp2

References

Barker, M. (2004). El ahorro energético y el control del CO2. Hacia una construcción sostenible.

Joosen, S. and K. Blok (2001). Economic Evaluation of Carbon Dioxide Emission Reduction in the Household and Services Sectors in the EU.

Kelly, R. (1999). Latent heat storage in building materials.

Luz y fuerza, d. c. August 2005

Pardo, C. S. (2000). Metodologia para la elaboracion del inventario de gases de efecto invernadero asociados al consumo de energia en Mexico, Instituto Nacional de Ecologia.

Chapter VI

Summary, Conclusions and Further work

Chapter VI: Summary, Conclusions and Further work

Heat storage has gained much attention in the last few decades, as a means to respond to the requirements for improved energy efficiency and the need to reduce fossil fuel exploitation and CO_2 production in providing thermal comfort in buildings.

Promising renewable energy sources in Mexico, and in this case specifically the use of solar radiation, make viable alternative to fossil fuels as sources of energy. One main difficulty in the utilization of solar energy is that due to its intermittent availability usually it must be stored to respond to the energy demand, e.g. when electrical supply is scarce.

In previous studies it has been found that in Mexico during the dry season large amounts of heat are stored in the fabric of buildings. This illustrates the actual possibility of a substantial contribution by heat storage systems in answering to the thermal needs regarding human comfort, without the excessive use of external energy sources.

The objective of this study was to evaluate the impact of thermal energy storage in dwellings under Mexican climatic conditions. Traditional vernacular architecture with its ancient wisdom provided enlightenment on the role of mass transfer in heat storage. The significant contribution of latent heat storage that was discerned prompted the study of a solar-thermal storage system using Phase Change Materials.

Adobe:

Adobe buildings have been used traditionally in the rural areas of Mexico with great structural and thermal success due to its weight bearing properties, its elastic capacity and its large thermal mass. The moisture content within these structures with its inherent hydration/dehydration processes has a dual role of providing a means for latent heat storage and as an agent causing wall deteriorating, due to shrinkage, thermal expansion and erosion.

Due to its hydrogen bonding in the liquid state, water as a thermal storage medium presents advantages over other phase change materials. Water absorbs and releases more latent heat than a number of substances; moreover, water is non-corrosive, non-toxic and is an inert chemical substance.

The effect of moisture content and moisture transport on the latent heat storage of these structures has not been studied before, and its study was undertaken in this project.

Sensible and latent energy transfers require a heat source or sink for setting up a temperature difference which would trigger heat and mass transfer, an increased heat capacity and a change of phase.

Existing coupled heat and mass transfer software modelling building construction elements consider in most cases that the latent heat effect is negligible and do not depend very sensitively on the precise values of the heat conductivities.

In this study, moisture movement within adobe constructions was assessed by simulations carried out using a commercial one-dimensional software called WUFI.
During the daytime irradiation hours the water vapour contained in the wall changes phase and releases the latent heat for vaporization, reducing the amount of moisture contained. Latent heat stored would be correspondingly released. Later in the evening, when the interior moisture conditions start to increase and water vapour condenses within the wall structure, the moisture content of the wall starts to increase, and heat energy will be stored again.

The weather conditions were found to be the most definite factors on the final moisture content distribution within adobe walls but unfortunately these parameters are outside the reach of designer adjustment. The first thing to consider for water-vapour control is the thermal resistance of the material (and therefore the thermal conductivity) and the initial moisture content. Temperature dependent thermal conductivity substances must be modelled having a heat flux greatly affected by changes in moisture content. Nevertheless this could not be observed in the software used.

Wall thickness, orientation, hygrothermal conditions, interior moisture load, vapour diffusion thickness and radiation (absorption-emission values) had a lesser effect, in the order listed. Surface coatings showed little effect on the final water movement within the wall. However, an initial assumed moisture content considers that the wall has already absorbed water, probably even by rain, the absorption of which depends on the surface coating.

It was not possible to determine the influence of the building components on the room climate by virtue of contained moisture within the building elements, and temperature modulation with the existing software. In this work it is proposed that this software would be improved by taking into account the latent heat storage/release due to the contained water's change of phase in the heat transfer calculations.

To achieve this aim, the code for the computational model for latent heat evolution proposed for phase change materials could be adapted to the WUFI. With the material surface temperature (initial boundary value), obtained with the heat flux balance on the boundary, and with the water

vapour temperature profile obtained from the WUFI coupled heat and mass transfer, the temperature coefficients for the nodes are formed. The finite differences could then be solved to determine liquid fractions (amount of water changing state). Then the energy stored would be calculated using the temperature-water vapour correlation. When the material has completely dried out or is completely saturated, according to the interactive weather conditions, the cycle starts again.

Environmental impact: Adobe constructions allow the reduction of CO_2 production as the bricks are sun dried and not fired. When adobe walls are eventually demolished they produce fewer environmental problems than ordinary buildings because they are basically unfired earth or clay. The high thermal mass and latent heat storage properties of adobe walls allow the modulation of the heat wave generated by diurnal variations of ambient temperature and solar irradiation by passive means, reducing the size of heating and cooling power required.

Adobe remains a largely rural expression of traditional building due to the hugely variable properties of clays in terms of structural performance prediction (due to the variable content of organic matter related to the location of the source of the clay).

In non-adobe structures, heat storage systems that are independent of the structural elements are welcomed. These systems offer the possibility to be applied to existing buildings as well as new constructions. That is the case that is being adopted for the heat storage system developed and assessed in this work.

PCMs:

Phase change materials (PCMs) undergo a change of state by absorbing and releasing heat at, or in a region about, their melting temperatures in a generally isothermal process. With the correct choice of PCM the indoor temperature may be maintained within a small range appropriate for human comfort.

The advantage that latent heat storage systems have over other heat storage systems is their large range of operating temperatures, low price availability, reduced ecological load, low maintenance requirements, negligible CO_2 emissions, noiseless operation, they have no requirements for mechanical or electrical systems, and they operate effectively with solar energy as a heat source.

According to previous research the amount of energy and the rate at which it can be passively absorbed and released is influenced by the PCM thermal conductivity (and diffusivity), air velocity, PCM latent heat of fusion, melt temperature (or the temperature range over which the melt occurs),

and PCM specific heat. In this study, these factors were integrated in an experimental design, and tested. Their interaction identified means for the system's optimisation under the different conditions imposed. The unit modelled was designed to improve the aspects of the design that have been shown in previous research to influence the performance of heat storage units.

Design of energy storage systems is in general case-specific, as the regional variations (temperature differentials), methods of construction (heat losses and gains of materials used, size of the building and room distribution) and occupancy schedules play a crucial role in the performance of the system. Also, depending on the type of application, the rate of heat storage might need to be enhanced either for charging, discharging or both.

Experimental work to assess heat storage systems feasibility can be expensive and time consuming. In order to allow the assessment of other similar heat storage systems, a computational model for the thermal behaviours of phase change materials (moving boundary problem) was developed. The model was based on imposed constant boundary conditions to develop the temperature and enthalpy evolution of the PCM.

The heat storage unit was exposed to simulated solar radiation. An independent calculation evaluated the air temperature that the inside of the chamber reached with the given radiation received (sol-air temperature). The condition for the moving boundary problem imposed at the irradiated wall was that of convection. The edges of the unit were insulated.
With this methodology the heat transfer flux into and out of the unit could be calculated and compared with experimental data.

Original aspects of this part of the study included:

1) The application of authentic internal heat gains, temperature, irradiation and air changes per hour for the climatic regions studied for both the experimental investigation and theoretical simulation.
2) The design and use of a large-scale solar simulator constructed with halogen lamps to reproduce irradiation fluxes (flux applied on the surface of the thermal storage unit and experimental chamber).
3) The application of insulation on one face of the unit, as a means for heat transfer rate control.
4) A DSC was used to obtain the non-linear temperature-enthalpy relation of the PCM materials and the temperature dependent properties, such as heat capacity and thermal conductivity. Also the PCM stability was tested with the DSC
5) Evaluation of the latent heat evolution by the modified enthalpy formulation with initial boundary condition set according to local weather data.

PCM Numerical analysis

Enhanced modelling and understanding of the phenomenon of melting and solidification is essential for future industrial development and for modelling natural processes. In this project solid-liquid phase change applied to latent heat storage was of particular interest.

In this project a mathematical model for specific systems, designed to be applied under Mexican-like weather conditions, was intended to provide a tool to analyze the feasibility of a latent storage system in view of regional climatic variations. This original research approach to the application of thermal storage for climatic regions in Mexico was the basis for this project.

Considerable literature is available regarding the experimental and numerical research of the phase change phenomenon. However, for the first time the main factors for promoting system's optimization are gathered in a single comparison study. The effects of individual factors on the efficiency of a thermal storage system and its contribution to energy saving was evaluated by running computer model simulations under different sets of climatic conditions.

Among the various approaches for solution of the Stephan problem, the enthalpy method was selected due to the physics of the solid-liquid phase transition. A paraffin was included as one of the PCM's in this study. The interface between the solid and liquid phases during melting and solidification is not clearly defined in paraffins and so a mushy zone model was adopted to describe the region where phase change was occurring.

Good agreement between the theoretical predictions and experimental data was found for the single cell latent heat stores. The small temperature differences that did occur between theoretical and experimental values could be due to differences between the actual material properties and the theoretical values. A premature or delayed change of phase period could be due to differences between the actual position of the sensors in the experiments and the positions considered for the model.

The chosen system was shown to be suitable for operating under the simulated Mexican climatic conditions imposed. A fully charged paraffin hexadecane cell unit was able to store approximately 11kJ of latent heat energy and around 5 kJ of sensible energy in a charging period of 3.5 hours. The consequent time lag in the internal air temperature in the experimental chamber indicates that the system provides a comfortable interior temperature when the exterior temperature and irradiation are at their peak. Additionally it was demonstrated that the subsequent release of the stored energy was adequate to compensate for the fall in the exterior temperature following the peak.

PCM Experiments

Three experiments were carried out to achieve the objectives considered for this work. Experiment one for the computer model validation. Experiment two for the optimization and performance evaluation of the system proposed. Experiment three for an assessment of the impact of the application of the system proposed.

The proposal was a storage element that constituted internal blinds in windows. This location takes advantage of incident solar radiation, and provides at the same time the opportunity to vary the mass flow rate of the heat transfer fluid (air) without the use of additional electro-mechanical means.
The experimental unit consisted of a single and a series of encapsulated PCMs contained in aluminium tubes (aluminium to improve thermal conductivity between the external environment and the contained pcm). The tubes form a blind which acts as a heat exchanger with the atmospheric air as the working fluid as well as experiencing direct thermal irradiation.

Experiment 1: An additional objective besides the computer model validation was the assessment of the heat storage charging/discharging behaviours, with and without radiation during cold and hot days and nights and during winter and summer nights in each province (using the lowest interior and exterior air temperatures that are likely to occur).

During cloudy days and during nights the unit can only be charged by internal heat gains and diffuse radiation. According to the results of the laboratory experiments internal heat gains can be critical on the charging rate, playing a role perhaps as important as that of direct radiation (the absence of which definitively reduces charging rate). Charging the unit in a summer day without direct solar radiation showed a slower charging rate than a winter day with a high irradiation.

Operating the unit as insulation only (placed on the exterior layer of the building envelope) was tested as it was thought to promote faster discharging of the thermal storage unit. It was not known if the amount of heat released was affected by the rapid discharging of the unit. From this we can conclude that the exterior lower temperatures during the night either in summer or winter have a larger effect on the discharging ratio than the air flow velocity applied to it. Additionally it was observed that, the experiment with faster discharging rate also released slightly more energy. Placing the unit outside can be advantageous when the stored energy is not needed to heat the interior.

Experiment 2: Two Mexican provinces at extreme latitudes and two seasons (winter-summer) defined the required temperature, mass flow, and irradiation. The main objective was to identify the interaction between factors that contributed to the system's operation optimization as are: temperature ranges; PCM melting temperature; PCM volume; surface container insulation; mass flow rate of HTF; mode(heating-cooling). The liquid Fraction and the enthalpy evolution determine the charging/discharging ratio.

PCM volume was shown to be the most important factor determining the system performance. Larger volume blinds store and release more energy than small volume blinds, although for the Taguchi matrix for charging none of the large volume blinds received the highest irradiation. Less energy than expected was withdrawn for both large and small volumes; this could be due either to superheating, or the effects of natural convection delaying the process. It can be concluded that especially for large volume units care most be taken to provide the means for the total discharge of the energy stored (such as exposing the unit to the exterior lower temperature conditions at night).

It is also clear from the results that the cooling (discharging) mode is less efficient than the heating (charging) mode and requires additional elements to boost it; especially when the conditions for discharging during summer are less favorable,

Air mass flow rate plays a significant role on the energy release. During heating high mass flow rates enhanced energy charging, but not so in the discharging process. The statistical analysis suggested that the low mass flow rate has little effect on the performance of the unit.

The season defines the parameters that the unit will experience. The cooling tests released energy at a slower rate than the absorption for the heating tests, and depending on the imposed conditions (mass flow, season and province), the units did not release all the energy stored without additional boosting elements. These boosting elements depend on the conditions imposed and on the charging/discharging rates required. Next the effects of some of these elements are summarised.

Insulation on the storage unit surface facing the window (to reduce heat gains from the heat source and heat losses from the blind to the exterior) clearly reduces the energy released (losses to the exterior) during cooling. For melting the presence of insulation delays the charging, but provides a less effective barrier than for the cooling mode. Nevertheless the delay is observed even though high interior temperatures and mass flow rates are applied. That is, for system control, insulation is actually effective when the discharging is required to occur over a longer period. The application of insulation to delay charging is not as effective.

The hypothesis that the multiple PCM cells blind could improve system performance was found to be true for the charging process, that is, during heating multiple PCM units stored more energy than units containing a single PCM. During cooling single PCM units released more heat (single PCM unit performs better for cooling). The larger volume blind stores more energy either with a single or multiple PCM. The multiple PCM arrangement in a large volume unit is the optimum configuration as more heat is stored.

Regarding the province; the large volume units stored/ released a higher amount of energy in both of the provinces considered. The large volume unit stored/released more energy under the region BC weather conditions. The small volume unit performed better in Chiapas. This could be because the settings for the CH tests include high mass flow rate, whilst the mass flow rate applied to BC is low. The irradiation value applied is important but not definite to determine the final energy stored in the unit.

Regarding the thermal conductivity of the PCM as a detrimental factor of latent heat storage system's performance, the question is raised on to which extent it influences system's performance. Slightly higher thermal conductivity PCM's did not show show a significant effect on the amount of thermal energy stored. The larger quantity of thermal energy storage found in tests was rather attributed to a combination of the various factors involved such as insulation, mass flow, weather conditions, etc. Further work on higher thermal conductivity materials is required to determine to what extent its effect is important.

Extended discharging time for the unit application during winter in Baja California (BC) can be attained by using a non-insulated single PCM blind and by applying high mass flow. During summer extended charging times can be achieved by using a non-insulated multiple PCM blind and by applying high air mass flow. In the case of Chiapas the unit performs more efficiently in winter. For discharge enhancement during summer in Chiapas (CH) an insulated single PCM blind can be used with a low mass flow rate. Finally Chiapas summer charging time can be improved by applying a high air mass flow rate, and a multiple PCM blind with insulation.

The tests that stored the least amount of energy also had the smallest PCM volume. The melting tests with smaller volume and with single PCM store a "medium" energy content value. For the cooling test the province with more extreme conditions (higher mass flow, lower temperature), with larger volume and with single PCM released a larger amount of energy.

All these results support the statistical analysis.

Theoretical model: good agreement between the computer model and experimental values was found. The differences between heat flux calculated and the one experimentally obtained can be due to natural

convection within the melt that have been ignored in the model, or properties degradation after several tests.

Experiment 3: In order to evaluate the impact of the blind on interior air temperature control, an experiment comparing the results obtained in experiment 2 (using the blind) and an experiment run without the blind has been used for comparison purposes. Depending on the test conditions the temperature difference provided by the system varies between 0.1°C and 6°C.

Impact of the latent heat storage system proposed: The storage system proposed here is more effective than other latent heat storage systems using PCMs. That is for example the case when comparing this system with PCM wallboards, which are gypsum host matrixes soaked in PCM and used as wall latent heat storage elements in buildings. The latent heat storage system proposed here reduces the heating system by almost the two times that of a wallboard. That is, 28.6% vs 15% of the total energy required to operate the heating system.

No system maintenance of the storage unit will be required for at least one to one and a half years. In some cases the systems might perform well for more than 5 years. PCM refilling cost payback period can range from 4 months to 2 years. If the refilling is required in between 1 to 5 years, the investment seems cost-effective.

By using passive means to heat and cool buildings for thermal comfort the CO_2 emissions are definitively decreased.

Further work

A series of further experimental tests to better understand the effects of different modes of heat transfer on the final energy stored of a PCM blind could improve accuracy on the assessment of system location feasibility.

Examples of such tests could be a calorimeter type test, in which the difference in electrical heat generation required to keep two different rooms, one with the PCM blind, the other with an ordinary blind, at the same temperature should directly give the amount of energy that went into and out of the storage in the PCM. Also a PCM unit energy balance for the both rooms might include the heat loads by infiltration, heat generated inside the room, air conditioning, wind, and PCM. The difference between the heat conducted on one side and the heat convected on the other, is equated to energy storage in the PCM.

Solidification under constant temperature: Study of solidification (freezing) in rectangular enclosure: It is important to know which mode of heat transfer is predominant through the solidification process in order to better understand

the phenomenon and provide better means to control it. A test could be devised that consisted of the PCM contained in plexiglass tubes. One vertical wall could be cooled isothermally by a cold plate, while the others were adiabatic, and used plexiglass transparent sheet for visualisation. External water/air flows for cooling. Different wall temperatures could be tested. The horizontal and vertical temperature distributions of the material in the PCM unit could then be measured using a grid of thermocouples. The solid liquid interface advancement could be photographed at various time points.

Melting/solidification under a constant temperature heat source or sink: with this test a stronger convection in the liquid, could be achieved. One vertical wall would be maintained at a temperature higher than the fusion temperature while the opposite wall would be cooled. For these experiments the effects of parameters such as cold wall temperature and initial liquid superheat could be evaluated.

Effect of heat extraction at constant heat rate on the mass fraction solidified: A variation of the experiment just described would be to cool the vertical aluminum wall under constant heat rate conduction (instead of temperature). The remaining walls would be adiabatic to reduce heat gains from surroundings and a removable piece of polystyrene could be placed in a window for observation.

Relevance of PCM optical transmittance for transparent building elements: In order to carry out an experiment to study the transmittance of solar radiation of the PCM to be employed a specific experiment would have to be set up. The material must be placed among transparent walls (glass) so as to measure the radiation received and the radiation transmitted to the other side. The lateral sides of the container must be highly reflective to avoid transmission of radiation to the side. A control experiment must be constructed to compare values of transmitted radiation though PCM unit. The effects of temperature (phase) and thickness on transmittance could be studied.

Regarding the computational model for latent heat evolution, as it was mentioned earlier, it would be very interesting to include it in the coupled heat and mass transfer model, in order to obtain a more realistic approach to heat losses and gains for porous systems when latent heat storage is accounted for regarding moisture evaporation and condensation.

Modeling the phase change using finite element could also give a more detailed insight on the phenomenon, as there it is possible to isolate elements and assess the outcome under different conditions.